



Scenarios of Large-Scale Solar Integration with Wind in Morocco : Impact of Storage, Cost, Spatio-Temporal Complementarity and Climate Change

Ayat-Allah Bouramdane

► To cite this version:

Ayat-Allah Bouramdane. Scenarios of Large-Scale Solar Integration with Wind in Morocco : Impact of Storage, Cost, Spatio-Temporal Complementarity and Climate Change. Physics [physics]. Institut Polytechnique de Paris, 2021. English. NNT : 2021IPPAX083 . tel-03518906

HAL Id: tel-03518906

<https://theses.hal.science/tel-03518906>

Submitted on 10 Jan 2022

HAL is a multi-disciplinary open access archive for the deposit and dissemination of scientific research documents, whether they are published or not. The documents may come from teaching and research institutions in France or abroad, or from public or private research centers.

L'archive ouverte pluridisciplinaire **HAL**, est destinée au dépôt et à la diffusion de documents scientifiques de niveau recherche, publiés ou non, émanant des établissements d'enseignement et de recherche français ou étrangers, des laboratoires publics ou privés.



INSTITUT
POLYTECHNIQUE
DE PARIS

NNT : 2021IPPAX083

Thèse de doctorat



Scenarios of Large-Scale Solar Integration with Wind in Morocco: Impact of Storage, Cost, Spatio-Temporal Complementarity and Climate Change

Thèse de doctorat de l'Institut Polytechnique de Paris
préparée à l'École Polytechnique

École doctorale n°626: École Doctorale de l'Institut Polytechnique de Paris (ED IP Paris)
Spécialité de doctorat: Mécanique des fluides et des solides, acoustique.

Thèse présentée et soutenue à Palaiseau, le 20 Octobre 2021, par

AYAT-ALLAH BOURAMDANE

Composition du Jury :

Riwal PLOUGONVEN Professeur Ecole Polytechnique, LMD	Président du Jury
Olivier BOUCHER Directeur de recherche CNRS, IPSL	Rapporteur
Philippe QUIRION Directeur de recherche CNRS, CIRED	Rapporteur
Anna CRET Professeur Paris Dauphine, Chaire Economie du Climat	Examinatrice
Hiba OMRANI Ingénieure-Chercheuse, EDF	Examinatrice
Mohamed RHAIHAT Chef de Projet OCP, UM6P Présentant du financeur MED-OCEAN	Examineur
Philippe DROBINSKI Directeur de recherche CNRS, LMD	Directeur de thèse
Alexis TANTET Professeur Assistant Ecole Polytechnique, LMD	Co-encadrant

Dedication

To my parents, mima and tati Nezha for their unconditional love, encouragement and continued support in all stages of my life.

*We are drowning in information but
starved for knowledge.*

John Naisbitt

Acknowledgements

First and foremost, to his eternal divine light, who gives me the patience, the power and the determination to pursue my dreams and goals. Thanks.

I spent three years, as a PhD student at the Laboratory of Dynamic Meteorology (LMD) of Ecole Polytechnique in Palaiseau, France. This work was conducted in the framework of the Energy4Climate Interdisciplinary Center (E4C) of Institut Polytechnique de Paris and Ecole des Ponts ParisTech, supported by MED-OCEAN research contract. This research leading to these results has received funding from the Moroccan company MED-OCEAN through a PhD scholarship.

I would like to thank the following people who contributed in one way or another to the successful accomplishment of this thesis.

First, I would like to express my sincere gratitude to Dr. Mustapha Aziz, CEO of MED-OCEAN, for funding my thesis. I also thank you for your unfailing support in all stages of this thesis. It is greatly appreciated. My sincere thanks also go to Mr. Gabriel Acharian and Mr. Hamid El Gamali, may his soul rest in peace, who supported me greatly and were always willing to help me in my administrative queries. To all who gave a hand, I say thank you very much.

I would like to acknowledge all members of the jury for agreeing to read the manuscript and to participate in the defense of this thesis. I particularly thank Mr. Olivier Boucher and Mr. Philippe Quirion for taking the time to review my thesis manuscript and to provide constructive comments. I also appreciate the questions of Mr. Riwal Plougonven, Ms. Anna Creti, Ms. Hiba Omrani and Mr. Mohamed Rhaihat.

I also wish to thank Ms. Nadège Ollier, Mr. Vincent Bourdin and Ms. Anne Migan for their time and for giving me a valuable support before my thesis defense that helped me to make it such a special event.

I would like to acknowledge the National Office of Electricity (ONE) in Morocco, particularly Mr. Mohammed Bouramtane and Mr. Abdelghani Hammadia, for our discussion and for providing me the regional hourly demand data.

I would like to thank Philippe Drobinski and Alexis Tantet for the supervision.

I think particularly to Riwal Plougonven who supported and encouraged me when the road got tough. Your support gave me strength when I needed it most. Thank you very much for your kindness, time and help.

Many thanks to the doctoral school team—particularly Mr. Emmanuel Fullenwarth, Mr. Aurelien Arnoux and Ms. Audrey Lemarechal—and all the LMD administrative team for their kindness and help. I would also like to thank all the doctoral students and the post-docs or the interns at LMD for the moments spent with you. I wish you all the best for the future!

Thanks Ecole Polytechnique for this opportunity in which I have developed myself. Undoubtedly, it has been one of the best station in my life.

There are many other people who encouraged me throughout my years of study. I think particularly to Mr. Abdelaali Koubaiti. Thank you for the keen interest to complete this thesis successfully.

I would like to thank Josias and Mohammed for giving me a reason to take a break and talk about anything other than research (well, other than my thesis!!). Thanks also to Andreas and Christophe for their kindness and compassion. Thanks to all my family members and friends!

Soufiane, you always make me feel special and appreciate me for who I am. I thank you and thank the fate that has put you back on my path. You are all that Annabelle needs and the one she wants to be with. Thank you for being mine (le plus et le moins sont évidents!).

Lastly, but the most importantly, my thanks go to my wonderful parents, mima and tati Nezha who have always supported me (since day one!). I cannot thank you enough. This thesis wouldn't have been completed without your continuous support and love. Thank you for your unceasing encouragements and for pushing me further than I thought I could go. I love you more than words can say. I still can't believe that mima is died. I know you are in a much better place. I miss you and need you mima but your spirit and strength live on in each of us. I wish you could have been here with me, now. I hope I have made you proud. Love you mima, rest in peace, I'll never forget you.



Résumé de la Thèse

Le monde est actuellement à un tournant de son avenir énergétique avec un choix crucial pour son future mix électrique: par quoi remplacer la production fossile et les réacteurs nucléaires après leur fermeture dans les décennies qui arrivent? Faut-il améliorer la production de ces sources ou faut-il progressivement aller vers un mix 100% renouvelable (RE)? Le choix d'un mix électrique RE en considérant prioritairement que le critère économique résulte souvent d'une opinion occulte d'autres critères. Ainsi, à l'opposé, considérer que la variabilité climatique ou la lutte contre le réchauffement climatique comme unique objectif impliquerait de chercher le mix électrique avec moins de sources fluctuantes émettant moins de gaz à effet de serre, et ce peut importe son coût. Dès lors, afin d'être le plus exhaustif possible et pour permettre une réflexion plus globale, il est essentiel d'éclairer les questions non seulement économiques mais aussi techniques associées aux choix technologiques permettant d'objectiver le débat; plus spécifiquement d'examiner l'impact du **stockage, coût, complémentarités spatio-temporelles et changement climatique** sur l'intégration des énergies REs dans un mix électrique avec différents **scénarios de pénétration**. Ces paramètres ne sont pas encore suffisamment traités dans les différents exercices de prospectives sur les mix électriques, ce qui est l'objet de cette thèse (voir aussi page 201).

Nous prenons comme cas d'étude le **Maroc**, et considérons qu'il a pour objectif de **maximiser la production RE** à satisfaire la demande et de **réduire sa variabilité (i.e., risque d'adéquation production-demande)**¹ tout en **dépassant pas un budget consacré aux REs de 3.50 G€/yr**—correspondant au coût total des capacités actuellement (2018) installées.

Nous considérons également que le Maroc souhaiterait investir uniquement² dans **l'éolien terrestre avec une hauteur moyenne de mât; les centrales solaires à concentration (CSP) à miroirs cylindro-parabolique orientée nord-sud sans ou avec différentes capacités de stockage d'énergie thermique (TES) de 6 à 17 heures par jour en moyenne; et les centrales photovoltaïque (PV) en silicium multicristallin surdimensionnées à grande échelle avec une inclinaison fixe, égale à la latitude locale, orientée sud sans ou avec différentes capacités de stockage d'énergie par batterie lithium-ion (BES) de 5 à 13,5 heures par jour en moyenne**; en ignorant les contraintes du réseau et en considérant qu'aucune flexibilité n'est fournie au-delà de celle fournie par le CSP-TES et le PV-BES.

Cependant, le Maroc a besoin d'une ligne directrice pour atteindre les objectifs susmentionnés. Par exemple, sous différents **scénarios de pénétration** (i.e., fraction du REs dans la satisfaction de la demande), **configurations de stockage et combinaisons de technologies REs**, **(1) quelle technologie doit être installée et dans quelle région? faut-il privilégier les sources RE intermittentes et variables mais qui coûtent moins chères (comme le PV et l'éolien) ou plutôt les sources dispatchables (CSP-TES, PV-BES) qui peuvent produire en continu avec un bon dimensionnement mais qui ont des coûts d'investissement et d'opération plus élevés? qu'en est-il du CSP sans TES qui est variable et coûteux?** La question se pose également **entre les sources variables (éolien, PV et CSP sans stockage)** mais également **entre les sources dispatchables** surtout lorsque ces dernières sont intégrées dans le mix électrique avec différentes quantités de stockage. Par exemple, pour un même dimensionnement de stockage, est-ce que c'est le CSP-TES ou le PV-BES qui remplace mieux—i.e., à faible coût et avec un risque d'adéquation moindre—la production conventionnelle pendant les périodes de pointe de consommation et réduit mieux les contraintes qui émergent quand on augmente la pénétration du RE? En effet, tous les moyens de production RE ne contribuent pas de la même façon à l'équilibrage entre la consommation et la production et donc n'impliquent pas les mêmes coûts ni les mêmes besoins de flexibilité. Actuellement, on peut relever un certain déficit des recherches scientifiques qui se basent uniquement sur la technologie RE permettant, par exemple, d'avoir un coût de production moindre ou le rôle de l'hybridation de ces technologies dans l'intégration du RE dans le mix; mais aucune étude publiée ne fait une comparaison exhaustive de toutes ces technologies en tenant en compte leur sensibilité au climat (ex., température, nuages, vent), le rôle du tracking et/ou du stockage et les différences des coûts, tout en arbitrant entre différentes hypothèses de pénétration et de risque d'adéquation de mix, par exemple la distribution technologique et géographique des capacités REs dans les mix optimaux avec une part élevée de pénétration à faible coût (resp. risque d'adéquation) sans se soucier de la variabilité (resp. du budget économique), ou celle des mix avec une faible proportion du RE et nécessitant moins de flexibilité, etc. En outre, la manière dont chaque étude traite ces questions diverge selon les contextes des pays et les méthodes de modélisation et optimisation utilisées. Une autre problématique qui en ressort est la suivante: **(2) Ne ferait-on pas mieux de favoriser les technologies bon marché (PV, éolien) et bien gérer leur variabilité en les dispersant géographiquement et/ou en tenant en compte leur complémentarités temporelles au lieu de s'entêter d'investir dans des solutions (CSP-TES, PV-BES) qui sont à l'heure actuelle encore pas suffisamment déployées pour une utilisation à l'échelle du réseau?** Il y a un consensus sur le bien-fondé de tenir en compte les complémentarités spatio-temporelles pour réduire la variabilité pour le PV et l'éolien—en exploitant la diminution des corrélations des nuages et du vent avec la distance et/ou les corrélations négatives du cycle saisonnier solaire et éolien, ce qui a un impact sur les capacités d'équilibrage dans le marché d'électricité—mais aucune étude n'examine **comment l'intégration du CSP ou du stockage (TES, BES) influencerait ces complémentarités.** **(3)** Un autre point essentiel est que l'impact du changement climatique sur plusieurs segments de la chaîne de valeur du secteur d'énergie notamment la consommation électrique, les lignes de transmission, les ressources et/ou la production du PV et l'éolien domine la littérature mais aucune étude n'analyse l'impact du changement

¹De manière équivalente, de réduire le recours à la production fossile et donc implicitement réduire les coûts d'intégration et les émissions associées aux services d'équilibrage requis par la production conventionnelle.

²Le choix des technologies renouvelables étudié n'est pas exhaustif en cela qu'il comprend uniquement les technologies qui sont d'ores et déjà déployés et qui sont amenées à jouer un rôle important dans le futur étant donné qu'elles émettent peu de gaz à effet de serre tout au long de leur cycle de vie. L'éolien offshore, la biomasse, la géothermie ou les énergies marines, ou les autres technologies de stockage, bien que voués à jouer un rôle dans les prochaines décennies, ne sont pas considérées du fait des coûts ou d'horizons de déploiement trop incertains.

climatique sur un mix électrique optimal intégrant le CSP ou le stockage TES, principalement en raison de leur part dans le marché et les défis liés à la paramétrisation des nuages et des aérosols. En outre, les études sont difficiles à comparer car les conclusions sont souvent axées sur des régions spécifiques du monde et couvrent différents horizons temporels, différents scénarios d'émission et tiennent en compte différents paramètres climatiques. Et donc **quel est l'impact du changement climatique sur les mix optimaux marocains considérant le scénario pessimiste, RCP 8.5 «business as usual»³, dans lequel aucun effort de réduction des émissions de gaz à effet de serre n'est fait? quelle technologie est sensible ou résiliente au changement climatique? le stockage thermique rend le CSP résilient au changement climatique? quelles sont les conditions pour avoir des mix RE résilients au climat? quelles sont les principales sources d'incertitude dans les futurs mix REs? le RCP 8.5 a-t-il un impact sur la distribution géographique des capacités REs? les fluctuations intra-journalières ont-elles un impact substantiel sur les mix optimaux?** En outre, compte tenu de la baisse des coûts des technologies REs, leur déploiement va être davantage encouragé. En revanche, ces technologies bas-carbone sont elles même lourdement impactées par le changement climatique. Il paraît donc essentiel de voir **si les mix optimaux sont plus sensibles aux changements climatiques ou aux coûts?**

Le travail réalisé au travers de cette thèse cherche à explorer ces questions et à proposer un ensemble de réponses préliminaires et plausibles mais qui ne visent pas à être normatif, i.e., on ne cherche pas à dire ce qu'il faut faire, c'est pour cela qu'on considère plusieurs scénarios et pas qu'un seul.

Il résulte de l'analyse des trois travaux réalisés les conclusions suivantes.

- * Si de faibles pénétrations REs sont ciblées, une petite capacité sera nécessaire à installer, ce qui implique de faibles coûts d'investissement, d'exploitation et de maintenance à dépenser. Et donc la variabilité de la production de cette capacité RE à répondre à la demande reste prépondérante. Dans ce cas, la technologie avec le meilleur compromis entre un facteur de charge (CF) élevé et une faible variabilité doit être installée.

- (1) Technologies Dispatchables Vs. Variables: nous avons trouvé que le CSP-TES remplace complètement le PV sans stockage (quelle que soit la capacité TES), domine sur l'éolien (pour 6-11 heures/jour de TES), et remplace complètement l'éolien (pour 17 heures/jour de TES). PV-BES remplace complètement le CSP sans stockage, la part de l'éolien est supérieure à celle de PV-BES (5-9 heures/jour de BES) mais l'éolien est dominé par PV-BES (pour 9-13,5 heures/jour de BES). Entre les Technologies Variables: nous avons trouvé que l'éolien domine sur le PV et le CSP (en raison de sa production uniforme tout au long de la journée et de l'année); et le PV domine sur le CSP (en raison de sa faible sensibilité aux nuages). Le CSP sans stockage n'est pas une bonne option (une petite fraction peut être introduite dans le mix pour répondre à la pointe de consommation estivale en raison de ses performances lorsque la température augmente et en raison du tracking utilisé). Entre les Technologies Dispatchables: nous avons trouvé que si le CSP-TES et le PV-BES sont intégrés avec un dimensionnement similaire, CSP-TES remplace PV-BES (en raison de sa plus grande capacité de stockage résultant de l'utilisation du tracking). Cependant, lorsque ces technologies sont intégrées avec un dimensionnement différent, la technologie à installer dépend du niveau moyen de stockage souhaité. Si moins de 13,5 heures/jour est requis, PV-BES est installé; sinon CSP-TES est favorisé.

Dans quelle région l'éolien, le PV/PV-BES, et le CSP/CSP-TES doivent être installés? L'éolien dans le SUD (région venteuse avec une faible rugosité et une faible saisonnalité de la densité de l'air car elle est proche de l'océan Atlantique); PV/PV-BES dans le CENTRE (région qui bénéficie d'une température plus faible même si avec une faible irradiance); CSP/CSP-TES dans les régions désertiques avec une couverture nuageuse minimale et une température élevée, mais cela dépend de la capacité de stockage pour éviter la surproduction car une grande fraction du CSP-TES est installée dans ces scénarios de faibles pénétrations: EST (si sans stockage ou avec 6 heures/jour de TES est demandé); SUD (si 11-17 heures/jour de TES est demandé).

- (2) Avantages des Complémentarités Spatio-Temporelles: nous avons trouvé que la complémentarité temporelle n'est pertinente que dans le mix PV-éolien-CSP (en raison de la covariance positive entre PV et CSP), mais moins entre le PV et l'éolien ou entre PV-BES et CSP-TES (en raison de la faible covariance de leur production). Cependant, il est important de prendre en compte les corrélations négatives entre les technologies éoliennes et solaires, et les corrélations positives entre PV et CSP (ou entre PV-BES et CSP-TES), pour ne pas installer moins ou plus de capacité et ainsi réduire le risque d'adéquation. La complémentarité spatiale ou spatio-temporelle est également essentielle pour réduire le risque d'adéquation. Cependant, ces complémentarités sont moins bénéfiques au fur et à mesure que le surplus d'énergie disponible par TES et BES est augmenté (car la covariance entre CSP-TES et PV-BES avec d'autres technologies est réduite et les mix deviennent moins diversifiés). Pour résumer la répartition technologique dans ces scénarios de faibles pénétrations avec un faible budget alloué à l'installation des technologies REs et avec une grande résilience au climat, il existe deux options: soit installer un mix diversifié éolien+PV ou éolien+PV-BES (5-9 heures/jour en moyenne) ou éolien+CSP-TES (6-11 heures/jour en moyenne) tout en tenant compte les complémentarités spatio-temporelles et en favorisant l'intégration du tracking nord-sud (pour le PV et CSP); ou ne s'appuyer que sur le CSP ou le PV avec une grande capacité de stockage (17 heures/jour de TES; ou 13,5 heures/jour de BES) sans tenir en compte les complémentarités.
- (3) Nous constatons que les mix optimaux sont résilients au changement climatique RCP 8.5, mais avec une incertitude élevé du modèle climatique régional (RCM)—qui est plus importante que l'incertitude du modèle climatique global (GCM)—sur l'impact futur de ce scénario d'émission sur chaque technologie, ce qui ne permet pas de tirer des conclusions sur quelle technologie est résiliente ou sensible au changement climatique dans les futurs bouquets énergétiques avec de faibles proportions de REs; parce qu'il n'y a pas seulement une incertitude liée au modèle climatique (par exemple, la paramétrisation des aérosols et des nuages qui contribue aux erreurs dans les données de température, d'irradiance et de vitesse du vent), mais aussi une incertitude liée à la variabilité interne naturelle du système climatique et au scénario d'émission. Nous concluons cependant que pour l'éolien, les impacts du changement climatique seront positifs si l'augmentation de la vitesse du vent projetées dépasse la diminution de la densité de l'air résultant du réchauffement. En outre, le CSP et le PV auront un impact positif du changement climatique si l'augmentation prévue de l'irradiance solaire compense les effets négatifs induits par le réchauffement; ce qui suggère de re-localiser les futures centrales solaires en fonction des changements attendus de la couverture nuageuse, des aérosols et de la température; et explorer de nouvelles technologies rendant le PV et le CSP moins sensibles à la température, aux composants atmosphériques et à l'eau. Nous constatons également que le changement climatique n'a pas d'impact sur la répartition géographique pour aucune des cinq technologies étudiées dans ces scénarios de faibles pénétrations.

³Le choix du Representative Concentration Pathways (RCP) 8.5 est justifié par le fait qu'il est en accord avec les émissions historiques cumulées et les résultats attendus des politiques climatiques mondiales actuelles [472].

* Si des pénétrations élevées de REs sont ciblées, une grande capacité RE sera nécessaire à installer (avec une faible variation de sa production) et donc un budget économique élevé sera nécessaire. Dans ce cas, la technologie qui permet d'obtenir le meilleur compromis entre une CF élevée, un faible risque d'adéquation et un faible coût devrait être installée.

- (1) Technologies Dispatchables Vs. Variables: nous constatons que contrairement aux scénarios de faibles pénétrations, pour atteindre une pénétration élevée, il paraît optimal d'investir dans des technologies variables, mais qui coûtent moins cher, plutôt que dans des technologies dispatchables (pour éviter d'atteindre le coût maximal plus tôt).

Entre les Technologies Variables ou Entre les Technologies Dispatchables: nous constatons que l'éolien gagne une part plus importante que les technologies solaires.

Cependant, si CSP/CSP-TES est intégré uniquement avec le PV et l'éolien, ce dernier est suivi par le PV mais sa fraction diminue avec l'augmentation de la pénétration (en raison de son faible CF résultant de la sensibilité du silicium multicristallin PV au climat aride marocain). L'intégration du tracking peut augmenter la CF moyen, mais il peut aussi ajouter des coûts. Par conséquent, nous suggérons de privilégier les technologies PV avec un rendement de conversion élevé, dans des scénarios de pénétrations élevées où les coûts et la variabilité doivent être atténués, de sorte que moins de capacités REs et donc de budget seront nécessaires pour répondre aux besoins en électricité. Si BES est ajouté à ces scénarios de mix, et que CSP-TES et PV-BES sont intégrés avec un dimensionnement similaire, PV-BES est préféré (car une faible capacité de stockage, résultant de l'orientation fixe, implique un faible coût même si TES est plus compétitif que BES). Dans les scénarios où les technologies dispatchables sont intégrées avec un dimensionnement différent, la technologie à privilégier dépend encore une fois des exigences de stockage. Si moins de 13,5 heures/jour est nécessaire, les résultats recommandent d'installer CSP-TES ; sinon d'installer PV-BES. Dans quelle région l'éolien, le PV/PV-BES, et le CSP/CSP-TES doivent être installés? L'éolien est toujours dans le SUD (comme les scénarios de faibles pénétrations); et le PV dans le SUD (région avec une forte irradiance même si la température est élevée). L'ajout de BES au PV induit l'installation de PV dans l'EST au lieu du SUD (car la saisonnalité de la région orientale continentale est réduite avec l'intégration du stockage). CSP/CSP-TES dans le CENTRE (région avec une faible saisonnalité d'irradiance et de température). Dans l'ensemble, cette répartition optimale est conforme avec la distribution actuelle (2018) à 17% de pénétration (sans hydroélectricité ni biomasse), ce qui correspond au régime de pénétrations élevées.

- (2) Avantages des Complémentarités Spatio-Temporelles: la complémentarité temporelle ou spatiale, ou les deux, contribue à réduire le risque d'adéquation, mais moins au fur et à mesure que la capacité de stockage augmente.
- (3) Les mix optimaux sont également résilients au changement climatique, mais l'incertitude du RCM n'augmente que pour les trajectoires des capacités éoliennes et PV dans ces scénarios de fortes pénétrations (en raison de la non-robustesse de l'irradiance inclinée globale et de la vitesse du vent) par rapport aux trajectoires des capacités CSP qui sont robustes (en raison de la robustesse de l'augmentation de la température induite par l'augmentation des gaz à effet de serre dans l'atmosphère). Dans l'ensemble, tous les modèles ont tendance à projeter que l'éolien et le CSP (resp. PV) sont sensibles (resp. is résilient) au changement climatique. Nous constatons également que, contrairement à l'éolien, le changement climatique impacte la distribution géographique du PV et CSP/CSP-TES avec une incertitude élevée du RCM pour PV et une incertitude élevée du RCM et GCM pour CSP/CSP-TES.

* Si la pénétration maximale de REs (35% sans hydroélectricité ni biomasse) est ciblée, une très grande capacité sera nécessaire à installer et, par conséquent, un budget élevé alloué à l'investissement dans les technologies REs sera nécessaire. Dans ce cas, la technologie avec un CF élevé et un faible coût doit être installée.

- (1) Technologies Dispatchables Vs. Variables ou Entre Technologies Variables ou Entre Technologies Dispatchables: nous avons trouvé que l'éolien représente le meilleur compromis entre une production d'électricité plus importante par MW installé en moyenne et un faible coût total; mais contribue au curtailment—à une pénétration maximale où les technologies dispatchables sont éliminées du mix pour satisfaire la contrainte de coût—due au fait que la production éolienne est maximale en hiver lorsque la demande marocaine est faible (en raison de l'utilisation de la climatisation), engendrant une augmentation (resp. diminution) du risque d'adéquation (resp. de la pénétration du REs). Par conséquent, dans les scénarios avec une pénétration maximale mais avec un faible risque d'adéquation, le budget maximum doit être augmenté pour installer plus de CSP-TES et PV-BES (car leurs trajectoires de capacité ont une forme convexe avec une pénétration croissante).

Dans quelle région l'éolien, le PV/PV-BES, et le CSP/CSP-TES doivent être installés? L'éolien dans l'EST (région venteuse même si la rugosité est élevée avec une forte saisonnalité de la densité de l'air puisque la variabilité ne joue pas un rôle important à un tel scénario de pénétration maximale). La répartition géographique du PV/PV-BES/CSP/CSP-TES reste la même que celle des scénarios de fortes pénétrations.

- (2) Avantages des Complémentarités Spatio-Temporelles: la même remarque que les scénarios de fortes pénétrations.
- (3) Les mix optimaux sont moins résilients au changement climatique RCP 8.5, mais l'incertitude du RCM est très faible. Dans l'ensemble, l'éolien est resilient tandis que le PV et le CSP sont sensibles au changement climatique. L'impact du changement climatique sur la répartition géographique du PV/CSP/CSP-TES reste le même que celui des scénarios de fortes pénétrations. Cependant, nous constatons que l'éolien est sensible à la source de données climatiques et est installé dans le SUD au lieu de l'EST.

* Quelle que soit la pénétration, on note que:

- le mix marocain actuel (2018) est sous-optimal mais peut être optimal si le Maroc augmente la pénétration RE ou réduit la variabilité de sa production RE en augmentant la part du CSP-TES et de l'éolien et en éliminant complètement le PV (ou en remplaçant les capacités CSP-TES par le PV en cas de capacité et de coût de stockage thermique limités), et en tenant compte de les complémentarités spatio-temporelles.
- Nous concluons que dans le cas où le Maroc souhaiterait investir dans des systèmes solaires hybrides pour augmenter le CF, réduire la variabilité et le coût—quel que soit le scénario de pénétration—, combiner CSP+PV ou CSP+PV-BES ne sont pas une bonne option. Dans l'ensemble, les meilleures options sont de combiner PV+CSP-TES ou PV-BES+CSP-TES.

- Le stockage thermique rend le CSP résilient au changement climatique ? nous constatons que quel que soit le scénario de pénétration et le modèle climatique, une petite capacité de stockage (6 heures/jour de TES) n'est pas suffisante pour répondre à la demande qui devrait augmenter le soir (car la température du soir augmentera avec le changement climatique), ce qui rend le CSP-TES non résilient au changement climatique et le pénalise dans le futur mix électrique. Par conséquent, si le Maroc souhaite investir dans le CSP-TES dans son mix futur, nous avons trouvé qu'une grande capacité de stockage (plus de 17 heures/jour en moyenne) est nécessaire.
- Vulnérabilité des Technologies Bas-Carbone au Changement Climatique Vs. Réduction Éventuelle des Coûts:
nous constatons que le coût total, le stockage et les complémentarités spatio-temporelles ont un impact significatif sur les trajectoires des capacités optimales, tandis que le changement climatique RCP 8.5 n'est responsable que du signal de la fraction d'une technologie donnée (c'est-à-dire l'augmentation ou la diminution de cette fraction dans le mix futur). Par conséquent, l'effet du changement climatique est insignifiant par rapport aux éventuelles réductions des coûts.
- Nous avons également trouvé que les fluctuations intra-journalières de température, d'irradiance et de vitesse du vent doit être correctement pris en compte lors de la conception d'un mix PV-éolien-CSP.
- Est-ce que le CSP/CSP-TES est en compétition ou gagne sur le PV/PV-BES? Les résultats de cette thèse donnent une réponse à cette question en fonction du scénario de pénétration et des besoins de stockage. Cependant, les résultats dépendent fortement des technologies PV, CSP et de stockage; l'orientation ou l'utilisation du tracking; la relation entre les CF, le dimensionnement/modélisation du stockage et les coûts; les scénarios de données des coûts et de capacités installées; la prise en compte ou la négligence des complémentarités spatio-temporelles; et des conditions climatiques (climat actuel ou futur).

Key Messages of the Thesis

Considering that **Morocco** has an objective of **maximizing the Renewable Energy (RE) production** in satisfying the demand and **reducing its variability (i.e., adequacy risk)** while **not exceeding a maximum-cost budget of 3.50 G€/yr**—corresponding to the total cost of the actual (2018) installed capacities.

Considering also that Morocco would like to invest in only **onshore wind with medium hub height; North-South Tracked Parabolic Trough Concentrated Solar Power (CSP) without or with different Thermal Energy Storage (TES) capabilities of 6-17 hours per day on average; and large-scale Photovoltaic (PV) multicrystalline silicon with fixed-tilted toward south orientation, by an angle equal to the local latitude, without or with different Lithium-ion Battery Energy Storage (BES) capabilities of 5-13.5 hours per day on average;** ignoring the grid constraints and considering that no flexibility is provided beyond the one provided by CSP-TES and PV-BES.

However, Morocco needs additional guidelines to reach the above-mentioned objectives. For instance, under different penetration⁴ scenarios, storage configurations and combinations of RE technologies, **(1)** which technology must be installed and where? should Morocco install dispatchable but expensive technologies (CSP-TES, PV-BES) or low-cost but variable technologies (PV, wind)? what about variable and expensive CSP without TES? **(2)** Morocco has to take into account the correlations between technologies and regions (i.e., spatio-temporal complementarities)? or only correlations between technologies in the same region (i.e., temporal complementarities)? or only spatial complementarities? or ignore all the complementarities? how the integration of CSP and storage would influence the benefits from these complementarities? **(3)** what is the impact of climate change on the Moroccan optimal mixes, considering the severe “business-as-usual” RCP 8.5 scenario, in which no efforts to cut greenhouse gas emissions are made? optimal mixes are more sensitive to climate change or to cost (i.e., in the context of vulnerability of low-carbon technologies to climate change vs. eventual cost reductions)? intra-daily fluctuations have substantial impact on optimal mixes? which technology is sensitive or resilient to climate change? what are the conditions for climate-resilient RE mixes? what are the main sources of uncertainty in future RE mixes? thermal storage makes CSP resilient to climate change? does RCP 8.5 climate change impacts the geographical distribution of RE capacities?

* If low RE penetrations are targeted, small capacity will be needed to install which imply low investment and operation and maintenance costs to spend. In this case, the technology with the best compromise between high Capacity Factor (CF) and low variability should be installed.

- **(1) Dispatchable vs. Variable Technologies:** we find that CSP-TES replaces completely PV without storage (whatever the TES capacity), dominates over wind (for 6-11 hours/day of TES), and replaces completely wind (for 17 hours/day of TES). PV-BES replaces completely CSP without storage, the share of wind is higher than that of PV-BES (5-9 hours/day of BES) but wind is dominated by PV-BES (for 9-13.5 hours/day of BES). Between Variable Technologies: we find that wind dominates over PV and CSP (due to its uniform production throughout the day and the year); and PV over CSP (due to its low sensitivity to clouds). CSP without storage is not a good option (it can only help to meet the summer peak demand due to its performance when temperature increases and due to tracking use). Between Dispatchable Technologies: we find that if CSP-TES and PV-BES are integrated with similar sizing, CSP-TES replaces PV-BES (due to its larger storage capacity resulting from the tracking use). However, when they are integrated with different sizing, it depends on the average level of storage desired. If less than 13.5 hours/day is required, PV-BES is installed; otherwise CSP-TES is favored. Where wind, PV/PV-BES, and CSP/CSP-TES should be installed? Wind in SOUTH (windy region with low roughness and low seasonality of air density as it is near the Atlantic Ocean); PV/PV-BES in CENTER (region that benefit from cooler temperature even though low irradiance); CSP/CSP-TES in desertic regions with minimum cloud cover and high temperature, but it depends on the storage capacity to avoid over-production as high CSP-TES fraction is invested at such low penetrations: EAST (if no or with 6 hours/day of TES); SOUTH (if 11-17 hours/day of TES).
- **(2) Benefits from Spatio-Temporal Complementarity:** we find that the temporal complementarity is only relevant in PV-wind-CSP mix (due to the positive covariance between PV and CSP), but less between PV and wind or between PV-BES and CSP-TES (due to the low covariance of their production). However, it is important to take into account the negative correlations between wind and solar technologies, and the positive correlations between PV and CSP (or between PV-BES and CSP-TES), to not install less or more capacity and thus to reduce the adequacy risk. Spatial or spatio-temporal complementarity is also key to reduce the adequacy risk. However, these complementarities are less beneficial as the surplus of energy available for TES and BES is increased (because the covariance between CSP-TES and PV-BES with other technologies is reduced and mixes become less diversified). To sum up the technological distribution in these scenarios of low penetrations with low cost budget and high resilience to climate, there are two options: either install a mix diversified of wind+PV or wind+PV-BES (5-9 hours /day) or wind + CSP-TES (6-11 hours/day) while taking into account complementarities and favoring the integration of North-South tracking (for both PV and CSP); or rely only on CSP or PV with large storage capacity (17 hours/day of TES; or 13.5 hours/day of BES) without complementarities.
- **(3) We find that optimal mixes are resilient to RCP 8.5 climate change, but high Regional Climate Model (RCM) uncertainty—that is more important than Global Climate Model (GCM) uncertainty—on the future impact of this climate change scenario on each**

⁴Renewable Energy (RE) penetration refers to the percentage of electricity generated by a particular RE technology.

technology, which does not allow to draw conclusions on which technology is resilient or sensitive to climate change in future energy mixes with low proportions of REs; because there is not only uncertainty related to the climate model (eg., aerosols and clouds parametrization which contributes to errors in temperature, irradiance and wind speed), but also to the natural internal variability of the climate system and to the emission scenario. We, however, conclude that the wind climate change impacts will be positive if the wind speed increase overpasses the air density decrease resulting from warming. In addition, CSP and PV will have a positive climate change impacts if the projected increase in solar irradiance compensates the negative warming induced effects; which suggests to re-locate the future solar plants based on the expected changes in cloud cover, aerosols and temperature; and explore new technologies making PV and CSP less sensitive to temperature, atmospheric components and water. We also find that climate change does not impact the geographical distribution for any of the five technologies at such low penetration scenarios.

* If high RE penetrations are targeted, high capacity will be needed to install (with low variance of its output) and therefore high economic budget will be required. In this case, the technology that achieve the best trade-off between high CF, low adequacy risk and low cost should be installed.

- (1) Dispatchable vs. Variable Technologies: we find that contrary to low penetration scenarios, to achieve high penetration, it becomes optimal to invest in variable technologies, but low-cost, rather in dispatchable ones (to prevent reaching the maximum-cost sooner).

Between Variable or Between Dispatchable Technologies: we find that wind gains higher share than solar technologies.

However, if CSP/CSP-TES is integrated with only PV and wind, the latter is followed by PV but its fraction decreases with increasing penetration (due to its low CF resulting from the sensitivity of PV multicrystalline silicon to the Moroccan arid climate). The integration of tracking may increase the mean CF, however it may also add cost. Hence, we suggest to favor PV technologies with very high efficiency, at such high penetration scenarios where cost matters and variability needs to be mitigated, so that less capacity and thus budget will be required to accommodate the electricity needs. If BES is added to these scenario mixes, and CSP-TES and PV-BES are integrated with similar sizing, PV-BES is preferred (because low storage capacity, resulting from the fixed orientation, implies low cost even though TES is more competitive than BES). In scenarios where dispatchable technologies are integrated with different sizing, it depends once again on the storage requirements. If less than 13.5 hours/day is needed, the results recommend to install CSP-TES; otherwise to install PV-BES. Where wind, PV/PV-BES, and CSP/CSP-TES should be installed? Wind is always in SOUTH (as the low penetration scenarios); and PV in SOUTH (region with high irradiance even though high temperature). The addition of BES to PV induces the installation of PV in EAST instead of SOUTH (as seasonality of the continental eastern region is reduced with storage). CSP/CSP-TES in CENTER (region with low seasonality of irradiance and temperature). Overall, this optimal distribution is in line with the actual (2018) distribution at 17% penetration (without hydro and biomass), corresponding to high penetrations regime.

- (2) Benefits from Spatio-Temporal Complementarity: temporal or spatial complementarity or both helps to reduce the adequacy risk but less so as the storage capacity is increased.
- (3) Optimal mixes are also resilient to RCP 8.5 climate change, but the RCM uncertainty increases only for wind and PV capacity pathways at such high penetration scenarios (due to the non-robustness of the global tilted irradiance and wind speed) compared to CSP capacity pathways which are robust (due to the robustness in the temperature increase induced by the increasing greenhouse gases in the atmosphere). All in all, all models tend to agree that wind and CSP (resp. PV) are sensitive (resp. is resilient) to climate change. We also find that contrary to wind, climate change impacts the geographical distribution of PV and CSP/CSP-TES with high RCM uncertainty for PV and high RCM and GCM uncertainty for CSP/CSP-TES.

* If maximum RE penetration (35% without hydro and biomass) is targeted, very high capacity will be needed to install and therefore high budget allocated to RE investment will be required. In this case, the technology with high CF and low cost should be installed.

- (1) Dispatchable vs. Variable Technologies or Between Variable Technologies or Between Dispatchable Technologies:

We find that wind represents the best trade-off between more electricity production per MW installed on average with low rental cost; but lead to curtailment—at maximum penetration where dispatchable technologies are eliminated from the mix to satisfy the cost constraint—due to the occurrence of maximum wind production in winter when the Moroccan demand is low (due to air conditioning use), letting the adequacy risk (resp. RE penetration) increase (resp. decrease) in return. Therefore, in scenarios with maximum-penetration but with low adequacy risk, the maximum budget must be increased to install more CSP-TES and PV-BES (as their capacity pathways have convex shape with increasing penetration).

Where wind, PV/PV-BES, and CSP/CSP-TES should be installed? Wind in EAST (windy region even though high roughness and high seasonality of air density since the variability does not play a role at such maximum penetration scenario). The geographical distribution of PV/PV-BES/CSP/CSP-TES remains the same to that of the high penetration scenarios.

- (2) Benefits from Spatio-Temporal Complementarity: the same remark as the high penetration scenarios.
- (3) Optimal mixes are less resilient to RCP 8.5 climate change, but the RCM uncertainty is very small. Overall, wind is resilient while PV and CSP are sensitive to climate change. The impact of climate change on the geographical distribution of PV/CSP/CSP-TES remains the same to that of the high penetration scenarios. However, we find that wind is sensitive to the climate data source and is installed in SOUTH instead of EAST.

* Whatever the penetration, we note that:

- the actual (2018) Moroccan mix is sub-optimal but can be optimal if Morocco increases its RE penetration or reduce the variability of its RE production by increasing the share of CSP-TES and wind and removing completely PV (or replacing the CSP-TES capacities by PV in case of limited thermal storage capacity and cost), and by taking into account the spatio-temporal complementarity.
- We conclude that in case Morocco would like to invest in hybrid solar systems to increase the CF, reduce the variability and cost—whatever the penetration scenario—, combining CSP+PV or CSP+PV-BES are not a good options. Overall, the best options are to combine PV+CSP-TES or PV-BES+CSP-TES.

- Thermal storage makes CSP resilient to climate change? we find that whatever the penetration scenario and the climate model, small storage capacity (6 hours/day of TES) is not sufficient to meet the demand that is projected to increase in evening (as evening temperature will increase with climate change), making CSP-TES not resilient to climate change and penalize it in future energy mix. Therefore, if CSP-TES is targeted in future warming climate, we find that large storage capacity (more than 17 hours/day on average) is needed.
- Vulnerability of Low-carbon Technologies to Climate Change vs. Eventual Cost Reduction: we find that the rental cost, storage and spatio-temporal complementarity govern the optimal capacity pathways while RCP 8.5 climate change is only responsible for the technology fraction signal (i.e., either increase or decrease in the future mix). Therefore, RCP 8.5 climate change effect is trivial with projected cost reduction.
- We also find that intra-daily fluctuations of temperature, irradiance and wind speed must be correctly taken into account when designing a mix of PV-wind-CSP.
- Does CSP/CSP-TES competing or winning over PV/PV-BES? The results of this thesis give an answer to this question depending on the penetration scenario and storage requirements. However, the results are strongly dependent on the PV, CSP and storage technologies; the orientation or tracking; the relationship between CFs, storage sizing/modeling and costs; the scenarios of cost and installed capacity data; the consideration or negligence of time-space complementarity and the climate conditions (actual or future climate).

Contents

1	General Introduction	24
I	Research Motivation and Background	24
1	Climate Change Mitigation	24
2	Overview of Renewable Technologies and Flexibility Options	26
i	Renewable technologies vs. Fossil Fuels vs. Nuclear	26
ii	Energy Storage Technologies	27
iii	Other Flexibility Options	28
3	Concentrated Solar Power vs. Photovoltaic vs. Wind and Thermal vs. Battery Storage	29
i	Mean Production	30
ii	Variability or Adequacy Risk	38
iii	Total Cost	42
iv	Trade-Off Between Benefits and Costs	42
II	Knowledge Gap and Originality of this Thesis	43
III	Focus of the Thesis	44
1	Objectives and Tools	44
2	Case Study: Morocco	44
3	General Research Questions and Approach	46
IV	Thesis Outline	47
2	Energy System Modeling and Optimization	48
I	Introduction	48
II	E4CLIM 1.0 Model and Mean-Variance Optimization Problem	50
1	Brief Description of E4CLIM 1.0 Model	50
2	Objective Functions and Optimization Strategies	50
3	Optimization Solutions: Main Relevant Elements of the Pareto Front	51
III	Model Set-up and Main Contribution to E4CLIM	54
1	Domain and Calibration	54
i	Domain, Technologies and Grid Constraints	54
ii	Demand and Calendar Data	55
iii	Capacity Factor Data and Bias Correction Approach	55
2	Modules Added	56
i	CSP Production Modules	56
ii	PV Production Modules	57
iii	Storage Module	57
iv	Cost Modules	58
v	Optimization Post-Processing Module	59
vi	System Adequacy Diagnostics Module	59
IV	Climate Data Sources	59
1	MERRA-2 Reanalysis	60
2	CORDEX Simulations	60
i	Domain and Climate Models	60
ii	Experiments and Scenario	60
iii	Solar and Wind Intra-daily Parametrization	61
3	Period of Analysis	61
V	Storage Modeling	62
1	CSP Solar Multiple and PV Inverter Loading Ratio	62
2	Storage Model Approach	63
3	Typical Daily Operation of CSP-TES and PV-BES	63
VI	Predicted Demand and Bias-Corrected Capacity Factors	67
1	Thermo-Sensitivity Results	67
2	Bias-Corrected Capacity Factors	68
VII	Maximum-Cost Constraint	68
VIII	Rental Cost Modeling and Data	69

1	Case 1: Limited Storage Cost and Capacity	69
2	Case 2: Unlimited Storage Cost and Capacity	71
3	Case 3: Constant Thermal Storage Cost with Unlimited Capacity	72
IX	Optimization Post-Processing Ratios	72
1	At Maximum Penetration	72
2	At High Penetrations	73
3	At Low Penetrations	74
X	System Adequacy Diagnostics	74
XI	Conclusion	76
3	Adequacy of Renewable Energy Mixes with Concentrated Solar Power and Photovoltaic in Morocco: Impact of Thermal Storage, Cost and Spatio-Temporal Complementarity under Penetration Scenarios	77
I	Introduction	78
II	Optimization Experiments	80
III	Results	80
1	Impact of Thermal Storage and Cost: Technological and Geographical Distribution	80
i	Economic Carrying Capacity	81
ii	At maximum penetration	81
iii	At high penetrations	81
iv	At low penetrations	82
2	Impact of Spatio-Temporal Complementarity	84
i	Regional Complementarity	85
ii	Technological Complementarity	85
3	Role of CSP-TES vs. PV in Reducing the Adequacy Risk	85
i	System Variance-based Risk	85
ii	System Adequacy Diagnostics	86
IV	Discussion and Comparison with Existing Studies	91
1	Scenarios of Unlimited Thermal Storage Cost and Capacity	91
2	Scenarios of High Renewable Penetration with Low Investment, even though High Adequacy Risk	92
3	Scenarios of High Renewable Penetration with Low Adequacy Risk, but with High Investment	93
4	Scenarios of Low Adequacy Risk with Low Investment, but Low Renewable Penetration	95
V	Summary and Concluding remarks	95
4	Utility-Scale PV-Battery versus CSP-Thermal Storage in Morocco: Storage, Cost and Spatio-Temporal Complementarity Effect under Penetration Scenarios	97
I	Introduction	98
II	Optimization Experiments	99
III	Results	100
1	Impact of Thermal/Battery Storage and Cost: Technological and Geographical Distribution	100
i	Economic Carrying Capacity	101
ii	At Maximum Penetration	101
iii	At High Penetrations	101
iv	At Low Penetrations	102
2	Impact of Spatio-Temporal Complementarity	103
i	Regional Complementarity	104
ii	Technological Complementarity	104
3	Role of CSP-TES vs. PV-BES in Reducing the Adequacy Risk	104
i	System Variance-based Risk	105
ii	System Adequacy Diagnostics	105
IV	Discussion and Comparison with Existing Studies	114
1	Does CSP/CSP-TES Competing or Winning over PV/PV-BES ?	114
2	Scenarios of Unlimited Thermal and Battery Storage Cost and Capacity	117
3	Scenarios of High/Low Renewable Penetration-Adequacy Risk-Investment	117
4	Scenarios of Hybrid Solar Systems	117
V	Summary and Concluding remarks	119
5	RCP 8.5 Climate Change Versus Cost Effect on Optimal Scenario Mixes of Variable and Dispatchable Technologies in Morocco: Climate Model Inter-Comparison	120
I	Abstract	120
II	Introduction	121
III	Optimization Experiments	123
IV	Results	124
1	RCP 8.5 Climate Change vs. Cost Effect on Optimal Scenario Mixes	124
2	Climate Data Sensitivity and Importance of Intra-daily Fluctuations	126
3	Consistency of Climate Projections and Sources of Uncertainty	130
V	Discussion and Comparison with Existing Studies	140
1	Climate Change Scenarios vs. Cost Reduction	140
2	Uncertainties Associated with Future Energy Mixes	140
3	Options for Climate-Resilient Renewable Mixes	142

4	Regional Effects of Climate Change	143
VI	Summary and Concluding Remarks	144
6	General Conclusions	146
I	Synthesis	146
1	Research Motivation	146
2	Focus of the Thesis: Tool, Objectives and Methodology	147
3	Research Questions and Main Findings	147
i	<i>First Study: Adequacy of Renewable Energy Mixes with Concentrated Solar Power and Photovoltaic in Morocco: Impact of Thermal Storage, Cost and Spatio-Temporal Complementarity under Penetration Scenarios</i>	147
ii	<i>Second Study: Utility-Scale PV-Battery versus CSP-Thermal Storage in Morocco: Storage, Cost and Spatio-Temporal Complementarity Effect under Penetration Scenarios</i>	148
iii	<i>Third Study: RCP 8.5 Climate Change Versus Cost Effect on Optimal Scenario Mixes of Variable and Dispatchable Technologies in Morocco: Climate Model Inter-Comparison</i>	149
II	Contribution to Research and Implications	151
III	Thesis Limitations and Perspectives	151
1	Use Better Energy Data and Improve Bias Correction Approach	152
2	Additional Sensitivity Analysis	152
3	Compare the Flexibility of CSP-TES and PV-BES to Other Flexibility Options	153
4	Quantify the Avoided Costs and Emissions	153
5	Tackle Climate Change Uncertainty	154
A	Theoretical Modeling Framework	156
I	Electricity Demand Model	156
II	Wind Production Model and Parametrization	159
1	Wind Extrapolation at Hub Height	159
2	Wind Power Output	160
3	Wind Intra-daily Parametrization	160
III	Solar Angles and Tracking Modeling	161
IV	Solar Irradiance Decomposition and Parametrization	163
1	Solar Irradiance Decomposition	163
i	PV Global Tilted Irradiance	163
ii	CSP Direct Normal Irradiance	164
2	Solar Irradiance Intra-daily Parametrization	164
V	CSP Production Modules	164
1	Solar Field Modeling	164
2	Power Block Modeling	166
VI	PV Production Modules	167
1	Solar Panels Modeling	167
2	Inverter Modeling	167
VII	Storage Module	168
1	CSP Solar Multiple and PV Inverter Loading Ratio	168
2	Storage Model without Constraints	168
VIII	Capacity Factors, Covariances and Bias Correction	169
1	Observed CSP Solar Multiple and PV Inverter Loading Ratio	169
2	Bias Correction Approach	169
3	Inter-annual Variability of Predicted Mean CFs and Demand Obtained from Climate Reanalysis	169
4	Estimates of Correlations and Covariances	169
5	Critical Appraisal of the Obtained Profiles of Wind and Solar Capacity Factors	169
i	Wind Speed Extrapolation Approach	169
ii	PV Capacity Factors Profiles	172
iii	CSP Capacity Factors Profiles	172
IX	Rental Cost Modeling	174
X	Optimization Post-Processing Formulas	174
i	At Maximum Penetration	174
ii	At High Penetrations	175
iii	At Low Penetrations	175
B	Publication Overview	179
I	Oral Communications (Seminars/ Conferences)	179
II	Poster Presentations	180
III	Publications in Peer-Reviewed Journal as Main Author	180

List of Figures

- 1.1 Share of low-carbon technologies in the Total Final Energy Consumption (TFEC) for each Intergovernmental Panel on Climate Change (IPCC) emission scenario, RCP "Representative Concentration Pathways" [534, 366], for various time horizons (2030, 2050 and 2100). The four scenarios go from 2.6 to 8.5 W/m^2 of radiative forcing. The higher the value of the latter, the higher the projected increase of global temperature. **Right Corner:** The mitigating scenario allowing a 2°C global warming in 2100 above the pre-industrial temperatures (RCP 2.6 in light blue that falls in the 430-480 ppm CO_2eq). **Middle:** The intermediate scenarios (RCP 4.5 in dark blue; and RCP 6.0 in yellow). **Left Corner:** The most pessimistic scenario without additional efforts to constrain emissions (RCP 8.5 in red) lead to pathways where emissions continue to rise throughout the 21st century "baseline scenario". Source: The Fourth Assessment Report (AR4) of the IPCC (2014) [183]. 26
- 1.2 (a): Share of Renewable Energies (REs) in the Total Final Energy Consumption (TFEC), 2018. (b): Share of REs in the global electricity production, end 2019. Non-renewable electricity means fossil fuels and nuclear. (c): Share of REs in the TFEC, by final energy use, 2018. (d): Share of global energy storage installed capacity, by technology, 2019 and 2020. Source: Renewables 2020/2021 Global Status Report [446, 447]. 26
- 1.3 Balancing effect of different flexibility options on the Residual Load Duration Curve (RLDC), which displays the residual load (demand minus renewable production), in ordinate, of every single hour of the year, in abscissa (See section X, Chapter 2 for more details on the RLDC definition). Source: Müller et al. [370]. 29
- 1.4 **Top-left corner:** The basic working principle of Photovoltaic (PV) where an inverter converts the Direct Energy (DC) provided by the Solar Panels (SPs) or/and by the Battery Energy Storage system to Alternating Current (AC). **Bottom-left corner:** The basic working principle of Parabolic Trough Concentrated Solar Power (CSP) where a Power Block (PB), i.e., steam turbine connected to electrical generator, converts the thermal energy produced by the Solar Field or SF (concentrator and receiver) or/and by the Thermal Energy Storage (TES) system to electricity. **Right:** The basic working principle of wind turbine. Source: Own elaboration. 30
- 1.5 **Left:** Schematic of the atmospheric components, which absorb or scatter or reflect the sunlight on its way through the atmosphere, and of the solar irradiance components [178, 536, 232]. **Right:** Schematic of the vertical profile of the horizontal wind speed [363, 228]. 31
- 1.6 (a): Map of theoretical potential of Photovoltaic (PV), i.e., distribution of Global Horizontal Irradiance (GHI) referred as global (direct + diffuse) irradiance for horizontal surfaces [90]. To be compared with figure 1.6b. (b): Map of practical or technical potential simulating the conversion of the available GHI to electric power considering the factors affecting the PV performance as well as land use constraints [90]. (c): Map of theoretical potential of Concentrated Solar Power (CSP), i.e., distribution of Direct Normal Irradiance (DNI) [90] referred as the amount of solar irradiance received per unit area by a surface that is always held perpendicular (or normal) to the rays that come in a straight line from the direction of the sun. To be compared with figure 1.6d. (d): Map of suitable locations of solar CSP plants, where four zones can be distinguished depending on their potential for recording DNI [480]. (e): Global mean wind speed at 80 m (Map developed by 3TIER) [15]. The darker the color, the higher the solar irradiance or wind speed and consequently the energy output, and the more appropriate is the region for PV, CSP or wind. 32
- 1.7 **Top:** Solar Photovoltaic (PV) technologies: Monocrystalline (left); Polycrystalline (middle) and thin film (right) [17]. **Middle and Bottom:** Solar Concentrated Solar Power (CSP) technologies [75]: Parabolic Trough (PT) and Linear Fresnel (LF) reflector are line-focused technologies, focusing the sunlight to a line of receivers; Solar Tower (ST) or Central Receiver (CR) and Parabolic Dish Stirling (DS) are point-focused technologies, focusing the sunlight to a point where the receiver is located. . . . 35
- 1.8 Daily total solar irradiance variation throughout the year on south faced horizontal to vertical tilted surfaces (tilt = 0°-90°) on the northern hemisphere latitude 0° (left), 30° (middle) and 60° (right). Source: The Engineering ToolBox [36]. 35
- 1.9 Daily mean of irradiance, collected on a surface located at latitude 45° at the top of the atmosphere, as a function of the day in the year, when the surface is horizontal (tilt = 0°), tilted at 45° and vertical (tilt = 90°) facing south. Source: Wald et al. [537]. 36
- 1.10 **Left:** Irradiance on the surface over the day in different seasons (winter, equinox, summer) at North-South or N-S (continuous lines) and East-West or E-W (broken lines) oriented parabolic troughs [2]. Low seasonal irradiance variance is observed for E-W tracking than for N-S orientation. **Right:** Extraterrestrial solar irradiance, for latitude equal to 45°, on a surface slope equal to 45°, on North-South or N-S and on East-West or E-W single-axis tracking surfaces. The three dotted curves are for the winter solstice and the three solid curves are for the summer solstice [178]. During sunrise and sunset hours, N-S tracking tends to be more performant than E-W tracking which is more performant than fixed orientation, whatever the season. However, at noon, E-W tracking is more performant than N-S tracking and fixed orientation; but the performance between N-S tracking and fixed orientation depends on the season, i.e., N-S (resp. fixed orientation) is more performant than fixed orientation (resp. N-S) in summer (resp. winter). Overall, fixed-tilted orientation and E-W tracking are (resp. N-S tracking is) more performant in winter (resp. summer) than in summer (resp. winter). 37

1.11	Hourly solar height (left) and hourly incidence angle with tilt = 45° and oriented 0° (right), calculated at latitude 42° N and longitude 5.6° W, for the 15th day of each month: January to June (Top); July to December (bottom). Source: Diez et al. [163].	37
1.12	Variation of energy demand according to temperature variation. T_H (resp. T_C) is the threshold temperature below (resp. above) which the consumer switches the heating (resp. air-conditioning) system. Source: Own elaboration based on [397]	38
1.13	Illustration of Concentrated Solar Power (CSP) or Photovoltaic (PV) plants without (Top) or with different storage capacities (Bottom). When Solar Multiple-SM- (resp. Inverter Loading Ratio-ILR-) is equal to 1 (Top), the Solar Field-SF- (resp. Solar Panel-SP-) is sized exactly to the size of the Power Block-PB- (resp. Inverter-INV-), with no excess of thermal (resp. Direct Current-DC-) production to store in the Thermal-TES (resp. Battery-BES-) energy storage system, and nominal production is achieved only during hours of nominal irradiance. More the SM (resp. ILR) increases, more the SF (resp. SP) size increases in relation to the PB (resp. INV) size (Bottom), allowing to store the surplus thermal (resp. DC) production during the day and discharge it in the evening to expand production after sunset. $X = \{SF, SP\}$; $Y = \{PB, INV\}$; $\Theta = \{TES, BES\}$; $x = \{therm, DC\}$; $y = \{elec\}$; $P_{x,x,nom}$ is the thermal (resp. DC) production of SF (resp. SP) under nominal conditions; $P_{y,x,nom}$ is the thermal (resp. DC) production required by the PB (resp. INV) to operate at nominal capacity; and $P_{y,x,nom}^{ref}$ is the reference thermal (resp. DC) nominal capacity.	39
1.14	The illustration of the shape of electricity demand from camel shape to duck shape with the increase of solar Photovoltaic (PV)/(CSP) penetration without flexibility. Top: The electricity demand has manageable shape meaning that it never gets too high or too low (namely the camel curve). It rises in the morning to a little hump before noon, levels out over midday, and then rises to a higher hump in the evening, when everyone gets home from work and turns on their TVs and stoves. Bottom: As solar penetration increases, the load curves start looking like a duck curve. Demand is suppressed more during the day, when the sun is up; and the increase of demand become more and more pronounced in the evening and require faster response by other flexible generators. Source: Own elaboration based on [158].	40
1.15	Illustration of the differences between capacity factor and capacity credit. Capacity factor refers to ratio of the energy produced by a power system in a given period over the maximum energy that can be produced in the same period. Capacity credit is a measure of the amount of conventional power generating system that can be replaced with the addition of the renewable production and maintain the same reliability [55, 355].	41
1.16	(a): Relationship between mean Photovoltaic (PV) Capacity Factors (CFs) and Inverter Loading Ratio (ILR) with different hours of Battery Energy Storage (BES) [193]; (b): Relationship between mean Concentrated Solar Power (CSP) CFs and Solar Multiple (SM) with different hours of Thermal Energy Storage (TES) [193, 268]; (c): Annual CSP CFs as a function of SM and hours of TES [268]; (d): Levelized Cost Of Electricity (LCOE) as a function of Solar Field (SF) size and size of TES [268].	43
1.17	Organization of Morocco's electricity sector. Source: Energy Policies Beyond IEA Countries: Morocco 2019 [264].	45
1.18	The share of renewable energies and fossil fuel in the total Moroccan electricity generation in 2017 (left); and the electricity produced in TWh by each source from 1973 to 2017 (right). Other sources: heat from chemical processes (auto producers). Source: Energy Policies Beyond IEA Countries: Morocco 2019 [264].	45
1.19	Renewable Energy (only) in the electricity generation from 2005 to 2017 with the years in abscissa, and the total generation in TWh (resp. share in total generation in %) in the left (resp. right) ordinate axis. Source: Energy Policies Beyond IEA Countries: Morocco 2019 [264].	46
2.1	Flow chart of Energy for Climate Integrated Model (E4CLIM) components (dark blue) including the modules added (light blue) and the data sources (gray) illustrating the general framework of this thesis. The E4CLIM's flow is divided in three steps: (i) Capacity factors and demand time series are first estimated from climate grid points—assigned to electricity zones—and fitted to observations; (ii) The mix is then optimized using the Mean-Variance Portfolio approach; (iii) The mix properties (i.e., technological and geographical distribution) are analysed; (iv) The demand-production adequacy diagnostics are finally computed to give a more analysis of the reliability benefits provided by each renewable technology. Data Availability: The data used to support the findings of this thesis is included within this manuscript and is available upon reasonable request to ayataallahbouramdane@gmail.com. Code Availability: The E4CLIM open-source software is available online under GPL license at https://doi.org/10.14768/20191105001.1 and its full documentation at https://energy4climate.pages.in2p3.fr/public/e4clim/index.html . All components of E4CLIM model and some modules added can be found at https://gitlab.in2p3.fr/alexis.tantet/e4clim (branch "morocco_api" or "dev-aya" or "new_country_morocco", updated two years ago and accessed on 22 February 2021). Source: Own elaboration.	52
2.2	Example of optimal fronts of the mean-variance bi-objective optimization problem independently of the version of the variance that is minimized. It defines a set of fronts and mixes. Source: Own elaboration based on [167].	53
2.3	Left: Morocco's location—Undisputed territory (dark green) and Western Sahara (green), a territory claimed and occupied by Morocco. Middle: Morocco's administrative regions corresponding to the sub-division provided by the Global Administrative Areas (GADM) online database (https://gadm.org/); Right: Morocco's electrical zones according to the National Office of Electricity (ONE) [4]. Source: Own elaboration.	54
2.4	Based on [25, 21], at the end of 2018, the total wind, Photovoltaic (PV) and Concentrated Solar Power (CSP) without or with Thermal Energy Storage (TES) capacities are 1215 MW, 170 MW and 530 MW, respectively. Left: Localization of the operational solar and wind power plants in Morocco in 2018 (Table A.6, Appendix A). Right: Observed PV, wind and CSP/CSP-TES capacity distribution per electrical zones in Morocco in 2018 corresponding to the left panel of table 2.1. All CSP/CSP-TES (resp. PV) plants have similar Solar Multiple (SM) of 1.3-1.4 means 30-40% of thermal surplus (resp. Inverter Loading Ratio-ILR- of 1 means without storage) as shown in section 1 (Appendix A). All operational PV (resp. wind) plants are using tracking (resp. onshore without storage) [23]. The actual (2018) PV, wind, CSP-TES fraction of the most deployed system (PV-wind-CSP SM2 with 6 hours of TES) are displayed in brown, blue, and orange stars respectively in figure 3.1f (Chapter 3). The actual renewable penetration (without hydro and biomass capacities) is 17% with 9% comes from PV, 28% from CSP-TES and 63 % from wind. Source: Own elaboration based on data sources cited in table A.6 (Appendix A).	55

- 2.5 Schematic depiction of main components of Parabolic Trough Concentrated Solar Power plant illustrating the main calculated parameters (Section V, Appendix A and Section V of this chapter): **(a):** Thermal energy provided by the solar field ($P_{SF,therm}^{SM/ref}$); **(b):** Thermal energy stored ($P_{SF \rightarrow TES,therm}^{SM/ref}$); **(c):** Thermal energy discharged ($P_{TES \rightarrow PB,therm}^{SM/ref}$); **(d):** Thermal energy that goes directly to the power block ($P_{SF \rightarrow PB,therm}^{SM/ref}$); **(e):** Total thermal energy that enter to the power block ($P_{in} = P_{SF \rightarrow PB,therm}^{SM/ref} + P_{TES \rightarrow PB,therm}^{SM/ref}$); **(f):** The thermal power of the turbine ($P_{turb,therm}^{SM}$); and **(g):** The net electrical power output (P_{elec}^{SM}). $P_{PB,therm,nom}^{ref}$ is the thermal nominal capacity. We refer to "1" as the state of temperature and enthalpy after condensation; "2" after pump; "3" after steam generator (pre-heating, evaporation and superheating); and "4" after turbine (Figure A.4 (d), Appendix A). Adapted from Boukelia et al. [103]. 57
- 2.6 Flow chart of the general structure of the Concentrated Solar Power (CSP) model without and with Thermal Energy Storage (TES). DirNI is the Direct Normal Irradiation; T_{amb} is the ambient temperature; *store – capacity*SM (resp. *store – power*SM) is the CSP thermal storage capacity (resp. maximum-power of storage) given for each Solar Multiple (SM); η_{TES} is the TES efficiency; $P_{PB,therm,nom}^{ref}$ is the thermal nominal capacity of reference (Table A.2, Appendix A); $P_{SF \rightarrow TES,therm}^{SM}$ is the thermal energy stored; $P_{TES \rightarrow PB,therm}^{SM}$ is the thermal energy discharged; $P_{SF \rightarrow PB,therm}^{SM}$ is the thermal energy that goes directly to the power block; and $P_{in} = P_{SF \rightarrow PB,therm}^{SM} + P_{TES \rightarrow PB,therm}^{SM}$ is the total thermal energy that enter to the power block. Source: Own elaboration. 58
- 2.7 **Left:** Scheme of the three modules of Concentrated Solar Power-CSP- (resp. Photovoltaic-PV-) plant: Solar Field-SF- (resp. Solar Panel-SP-); Thermal-TES- (resp. Battery-BES-) Energy Storage; and Power Block-PB- (resp. Inverter-INV-). $X = \{SF, SP\}$; $Y = \{PB, INV\}$; and $\Theta = \{TES, BES\}$. The black arrows represent the energy flows: Thermal (resp. Direct Current-DC-) energy provided by SF (resp. SP) ($P_{X,x}^{SM/ILR}$); Energy from SF (resp. SP) to PB (resp. INV) ($P_{X \rightarrow Y,x}^{SM/ILR}$); Energy stored ($P_{X \rightarrow \Theta,x}^{SM/ILR}$); Energy discharged ($P_{\Theta \rightarrow Y,x}^{SM/ILR}$); Total thermal (resp. DC) available energy injected to the Power Block (resp. Inverter) ($P_{X \rightarrow Y,x}^{SM/ILR} + P_{\Theta \rightarrow Y,x}^{SM/ILR}$) and the State of charge ($SOC_{E,\Theta}^{SM/ILR}$). $x = \{therm, DC\}$ and $y = \{elec\}$. **Right:** Illustration of CSP (resp. PV) plant configuration with different Solar Multiple-SM- (resp. Inverter Loading Ratio-ILR-). ILR1 or SM1: without storage; ILR>1 or SM>1: with increasing levels of storage from PV or CSP. For more description of these parameters, see section 1 (Appendix A). Source: Own elaboration based on [2]. 63
- 2.8 Storage algorithm illustrating the dispatch conditions of Concentrated Solar Power-CSP- thermal (resp. Photovoltaic-PV- Direct Current-DC-) energy with constraints on the storage capacity and the maximum power of charging/discharging, for a given CSP Solar Multiple-SM- (resp. PV Inverter Loading Ratio-ILR-). See section 2 (Appendix A) for the storage model without constraints. $X = \{SF, SP\}$; $Y = \{PB, INV\}$; $\Theta = \{TES, BES\}$; $x = \{therm, DC\}$; and $y = \{elec\}$. Source: Own elaboration based on [432, 451]. 64
- 2.9 Illustration of the behavior of the Concentrated (CSP) Thermal Energy Storage (TES) model without constraints (Section 2, Appendix A) over two consecutive days in summer. **Top:** Time evolution of the thermal energies: Solar Field-SF- energy ($P_{SF,therm}^{SM}$), Energy from SF to Power Block-PB- ($P_{SF \rightarrow PB,therm}^{SM}$), Energy stored ($P_{SF \rightarrow TES,therm}^{SM}$), Energy discharged ($P_{TES \rightarrow PB,therm}^{SM}$), Total available energy injected to the PB ($P_{in}^{SM} = P_{SF \rightarrow PB,therm}^{SM} + P_{TES \rightarrow PB,therm}^{SM}$) and the State of charge ($SOC_{E,TES}^{SM}$) for a Solar Multiple (SM) of 2 (6 hours of TES). **Bottom:** CSP capacity factors for SM of 1, 2, 3 and 4; with $SM^{ref} = 1.87$ (87% of CSP thermal energy surplus). 65
- 2.10 Illustration of the behavior of the Photovoltaic (PV) Battery Energy Storage (BES) model without constraints (Section 2, Appendix A) over two consecutive days in summer. **Top:** Time evolution of the Direct Current (DC) outputs: Solar Panel-SP- energy ($P_{SP,DC}^{ILR}$), Energy from SP to Inverter-INV- ($P_{SP \rightarrow INV,DC}^{ILR}$), Energy stored ($P_{SP \rightarrow BES,DC}^{ILR}$), Energy discharged ($P_{BES \rightarrow INV,DC}^{ILR}$), Total available energy injected to the INV ($P_{in}^{ILR} = P_{SP \rightarrow INV,DC}^{ILR} + P_{BES \rightarrow INV,DC}^{ILR}$) and the State of charge ($SOC_{E,BES}^{ILR}$) for an Inverter Loading Ratio (ILR) of 2 (5 hours of BES). **Bottom:** PV capacity factors for ILRs of 2, 3 and 4; with $ILR^{ref} = 1$ (PV without BES). 66
- 2.11 Hourly predicted electricity demand versus the hourly surface temperature for each zone and day type, i.e., working days "work", Saturdays "sat" and off-days "off" corresponding to holidays and Sundays. The scatter plot represents the predicted demand and the lines represent the function $a_H^{work|sat|off} \Theta(T_H - T_{it}) g_t^{work|sat|off} + a_C^{work|sat|off} \Theta(T_{it} - T_C) g_t^{work|sat|off} + a_0^{work|sat|off} g_t^{work|sat|off}$ of the demand model (Section I, Appendix A). The two vertical dashed lines represent the heating (resp. cooling) temperature thresholds, $T_H = 14^\circ C$ (resp. $T_C = 24^\circ C$), below (resp. above) which the consumers, for all zones, switch the heating (resp. air-conditioning) system. 67
- 2.12 Relationship between Concentrated Solar Power-CSP- (resp. Photovoltaic-PV-) mean Capacity Factors (CFs) or η , variance, CSP Solar Multiple-SM- (resp. PV Inverter Loading Ratio-ILR-) and the amount of thermal (resp. battery) storage, i.e., TES (resp. BES). Different cases are represented to illustrate the effect of the bias correction. **(a)** Assuming the case **(i)** where the Solar Field-SF- (resp. Solar Panels-SPs-) size increases without increasing the amount of storage, the mean CFs for a given zone i will increase and the variance will increase even more (the CF variances tend to scale quadratically with CF means) which tend to reduce the ratio CF/variance with the increase of SM (resp. ILR). Assuming the case **(ii)** where the SF (resp. SP) increases with increasing the amount of storage, the mean CFs will increase and the variance will increase but will be reduced by ψ which tend to increase slightly the ratio CF/variance with the increase of SM (resp. ILR) compared to case (i). Since the bias correction **(b)** is bringing the mean of the CFs roughly equal to the CFs of the observed SM (resp. ILR) **(iii)**, the variance will decrease (i.e., the ratio CF/variance will increase) with the increase of SM (resp. ILR) due to the reduction in the variability associated with storage. $P_{SF,therm,nom}^{ref}$ (resp. $P_{INV,DC,nom}^{ref}$) is the thermal (resp. Direct Current-DC-) nominal capacity. \mathbb{E} and \mathbb{V} represent, respectively, the mathematical expectation and variance operators over time. The subscript "obs" denotes the observations. ILR>1 or SM>1: with increasing levels of storage from PV or CSP. Source: Own elaboration. 70
- 2.13 Technology-Region capacity (ordinate) versus the mean penetration (abscissa). Three penetration regimes are identified: **Right side:** at maximum-penetration (Section 1); **Middle side:** at high penetrations (Section2); and **Left side:** at low penetrations (Section 3). The Economic Carrying Capacity (ECC) denotes the level of penetration of Renewable Energy (RE) at which the costs outweigh the benefits and where some additional REs are no longer economically desirable [157]. Source: Own elaboration. 73

2.14	The Load Duration Curve (LDC) (b) is derived by sorting the predicted load (a) in descending order. The Residual Load Duration Curve (RLDC) (c) is derived by sorting the residual load (2.23) in descending order. It captures four main challenges of integration of Renewable Energies (REs): (1) The capacity credit or the peak load reduction; (2) the mid load reduction; (3) the base load reduction; (4) the capacity required from conventional dispatchable plants; and (5) the Renewable Energy (RE) curtailed. Source: Own elaboration computed from the predicted demand and RE production time series (for the RLDC) using hourly MERRA-2 climate data over the year 2018.	74
2.15	Load Duration Curve (LDC) (plain black), Residual Load Duration Curve (RLDC) (plain green), RLDC for Photovoltaic (PV) without storage only (dashed brown), RLDC for Concentrated Solar Power (CSP) with Thermal Energy Storage (TES) or CSP-TES with Solar Multiple (SM) equal to 2 only (dashed orange), and RLDC for wind only (dashed blue) for the optimal PV-Wind-CSP-TES SM2 mix for the global strategy (2.2) with the maximum-cost constraint (2.8) and at a mean penetration of 35 %. SM2: CSP with 6 hours of TES.	75
3.1	Left: Approximations of the optimal fronts obtained from hourly Modern-Era Retrospective Analysis for Research and Applications 2 (MERRA-2) climate data with the risk, $\sigma_{\text{global/technology/base}}$, in abscissa and the mean penetration (2.1), μ , in ordinate. Right: Shares of wind (blue line), Photovoltaic (PV) without storage (brown line) and Concentrated Solar Power (CSP) without or with Thermal Energy Storage (TES) (orange line) capacities versus the mean penetration for the global strategy (2.2) with maximum-cost constraint (2.8). (a, b): PV-Wind. (c, d): PV-Wind-CSP-SM1. (e, f): PV-Wind-CSP-TES SM2. (g, h): PV-Wind-CSP-TES SM3. (i, j): PV-Wind-CSP-TES SM4. Solar Multiple of 1 or SM1: CSP without storage; SM>1: with increasing levels of storage from CSP.	87
3.2	Heatmap of the national daily (ordinate) and seasonal (abscissa) variability of the predicted capacity factors and demand: Wind (a) , demand in MW (b) , Concentrated Solar Power (CSP) with Thermal Energy Storage (TES) with a Solar Multiple (SM) of 2 (c) , CSP-TES SM3 (d) , CSP-TES SM4 (e) ; obtained over the year 2018 from the hourly Modern-Era Retrospective Analysis for Research and Applications 2 (MERRA-2) climate data. The variation over time is shown in color by intensity in the colorbar. SM>1: with increasing levels of storage from CSP. Critical appraisal of the obtained wind profiles are discussed in section i (Appendix A) and that of the demand in section 1 (Chapter 2).	88
3.3	Heatmap of the national daily (ordinate) and seasonal (abscissa) variability of the solar irradiance components in (W/m^2): Global Horizontal Irradiance (GHI) (a) , Global Tilted Irradiance (GTI) (b) (to be compared with figure 3.3d), Direct Normal Irradiance (DNI) (c) (to be compared with figure 3.3e, 3.2c, 3.2d and 3.2c). The diurnal and seasonal patterns are also depicted for predicted Capacity Factors (CFs): Photovoltaic (PV) without storage (Inverter Loading Ratio of 1 or ILR1) (d) and Concentrated Solar Power (CSP) without storage (Solar Multiple of 1 or SM1) (e) . Solar Resources and CFs are obtained over the year 2018 from the hourly Modern-Era Retrospective Analysis for Research and Applications 2 (MERRA-2) climate data. The variation over time is shown in color by intensity in the colorbar. Critical appraisal of the obtained profiles are discussed in section ii and iii (Appendix A).	89
3.4	Capacity credit (top) , mid load reduction (Middle) , and base Load reduction (Bottom) by each technology—Wind (blue), Photovoltaic or PV (brown) and Concentrated Solar Power (CSP) with Thermal Energy Storage (TES) with a Solar Multiple (SM) of 2 (orange)—versus the mean penetration (2.1), μ , for the global strategy (2.2) with maximum-cost constraint (2.8) obtained from hourly Modern-Era Retrospective Analysis for Research and Applications 2 (MERRA-2) climate data over the year 2018. Left: PV-wind mix; Right: PV-wind-CSP-TES SM2 mix. SM2: CSP with 6 hours of TES.	90
3.5	Similar to the right panels of figure 3.1 for scenarios with unlimited thermal storage capacity and cost. Left: Case 2 (Section 2, Chapter 2). Right: Case 3 (Section 3, Chapter 2). Top: PV-Wind-CSP-TES SM2. Middle: PV-Wind-CSP-TES SM3. Bottom: PV-Wind-CSP-TES SM4. PV is Photovoltaic; TES is Thermal Energy storage and SM is Solar Multiple. SM>1: with increasing levels of storage from Concentrated Solar Power (CSP).	91
4.1	Left: Approximations of the optimal fronts obtained from hourly Modern-Era Retrospective Analysis for Research and Applications 2 (MERRA-2) climate data with the risk, σ , in abscissa and the mean penetration (2.1), μ , in ordinate. White (resp. gray) area to the right (resp. left) are not Pareto optimal (resp. not feasible). Particular mixes are depicted: the "2018 actual solar-wind mix" (gray cross); the "penetration-as-actual mix" (blue triangle) with lower risk; the "risk-as-actual mix" (blue diamond) with higher penetration; the "cost activation mix" (black dot) with the largest penetration for which the maximum-cost constraint (2.8) is not active; the "cost activated mix" (blue plus) with moderate penetration compared to the "maximum-penetration mix" (blue square) in which the cost constraint is activated; Right: Shares of wind (blue line), Photovoltaic (PV) with Battery Energy Storage (BES) (brown line) and Concentrated Solar Power (CSP) without or with Thermal Energy Storage (TES) (orange line) capacities versus the mean penetration for the global strategy (2.2) with maximum-cost constraint (2.8). The crosses represent the shares for the actual mix. (a, b): PV-ILR2-Wind-CSP-SM1 (c, d): PV-ILR3-Wind-CSP-SM1 (e, f): PV-ILR4-Wind-CSP-SM1 (g, h): PV-ILR2-Wind-CSP-TES SM2 (i, j): PV-ILR3-Wind-CSP-TES SM2. Solar Multiple of 1 or SM1: CSP without storage; Inverter Loading Ratio or ILR>1 or SM>1: with increasing levels of storage from PV or CSP.	107
4.2	Similar to figure 4.1. (a, b): PV-ILR4-Wind-CSP-TES SM2 (c, d): PV-ILR4-Wind-CSP-TES SM3 (e, f): PV-ILR2-Wind-CSP-TES SM4 (g, h): PV-ILR3-Wind-CSP-TES SM4 (i, j): PV-ILR4-Wind-CSP-TES SM4. Inverter Loading Ratio ILR>1 or Solar Multiple SM>1: with increasing levels of storage from Photovoltaic (PV) or Concentrated Solar Power (CSP).	108
4.3	Heatmap of the national daily (ordinate) and seasonal (abscissa) variability of the predicted capacity factors: Photovoltaic (PV) with Battery Energy Storage (BES) with an Inverter Loading Ratio of 2 or ILR2 (a) , PV-BES ILR3 (b) , PV-BES ILR4 (c) ; obtained over the year 2018 from the hourly Modern-Era Retrospective Analysis for Research and Applications 2 (MERRA-2) climate data. The variation over time is shown in color by intensity in the colorbar. ILR > 1: with increasing levels of storage from PV. Critical appraisal of the obtained profiles are discussed in section ii (Appendix A).	109
4.4	Capacity credit by each technology—Wind (blue), Photovoltaic (PV) with Battery Energy Storage (BES) (brown) and Concentrated Solar Power with Thermal Energy Storage (TES) with a Solar Multiple (SM) of 2 or SM2 (orange)—versus the mean penetration (2.1), μ , for the global strategy (2.2) with maximum-cost constraint (2.8) obtained from hourly Modern-Era Retrospective Analysis for Research and Applications 2 (MERRA-2) climate data over the year 2018. Left: PV-BES-wind mix; Right: PV-BES-wind-CSP-TES SM2 mix. Top: ILR2; Middle: ILR3; Bottom: ILR4. SM2: CSP with 6 hours of TES; ILR>1: with increasing levels of storage from PV.	110

4.5	Mid load reduction by each technology—Wind (blue), Photovoltaic (PV) with Battery Energy Storage (BES) (brown) and Concentrated Solar Power with Thermal Energy Storage (TES) with a Solar Multiple (SM) of 2 or SM2 (orange)—versus the mean penetration (2.1), μ , for the global strategy (2.2) with maximum-cost constraint (2.8) obtained from hourly Modern-Era Retrospective Analysis for Research and Applications 2 (MERRA-2) climate data over the year 2018. Left: PV-BES-wind mix; Right: PV-BES-wind-CSP-TES SM2 mix. Top: ILR2; Middle: ILR3; Bottom: ILR4. SM2: CSP with 6 hours of TES; ILR>1: with increasing levels of storage from PV.	111
4.6	Base load reduction by each technology—Wind (blue), Photovoltaic (PV) with Battery Energy Storage (BES) (brown) and Concentrated Solar Power with Thermal Energy Storage (TES) with a Solar Multiple (SM) of 2 or SM2 (orange)—versus the mean penetration (2.1), μ , for the global strategy (2.2) with maximum-cost constraint (2.8) obtained from hourly Modern-Era Retrospective Analysis for Research and Applications 2 (MERRA-2) climate data over the year 2018. Left: PV-BES-wind mix; Right: PV-BES-wind-CSP-TES SM2 mix. Top: ILR2; Middle: ILR3; Bottom: ILR4. SM2: CSP with 6 hours of TES; ILR>1: with increasing levels of storage from PV.	112
4.7	Left: Residual Load Duration Curve (RLDC) for different penetrations illustrating the variation of the RLDC parameters (peak, mid, and base load) with increasing penetration and the renewable share threshold at which curtailment occurs (negative residual load) for PV-wind-CSP-TES SM2 combination. Right: Load Duration Curve (LDC) and RLDC for different combinations, computed at 20% penetration (risk-as-actual mix) for the global strategy (2.2) with maximum-cost constraint (2.8), illustrating the system flexibility provided by CSP-TES. Solar Multiple of 2 or SM2: Concentrated Solar Power (CSP) with 6 hours of Thermal Energy Storage (TES). Photovoltaic (PV) is without storage.	113
4.8	Similar to figure 4.1 but for scenarios with unlimited thermal (TES) and battery (BES) storage capacity and cost. (a, b): PV-ILR2-Wind-CSP-SM1; (c, d): PV-ILR4-Wind-CSP-SM1; (e, f): PV-ILR3-Wind-CSP-SM2; (g, h): PV-ILR4-Wind-CSP-SM2; (i, j): PV-ILR4-Wind-CSP-SM3. Solar Multiple of 1 or SM1: Concentrated Solar Power (CSP) without storage; Inverter Loading Ratio or ILR>1 or SM>1: with increasing levels of storage from Photovoltaic (PV) or CSP.	118
5.1	Shares of wind (blue), Photovoltaic (PV) with an Inverter Loading Ratio of 1 or ILR1 (brown), Concentrated Solar Power (CSP) with Solar Multiple of 1 or SM1, and CSP with SM2 (orange) capacities versus the mean penetration (2.1), μ , for the global strategy (2.2) with maximum-cost constraint (2.8) obtained from hourly COordinated Regional climate Downscaling EXperiment-Coupled Model Intercomparison Project Phase 5 (CORDEX-CMIP5) climate data (with intra-daily parametrization) illustrating the optimal mixes changes projected to the end of this century, 2071-2100 (dotted line), versus historical period, 1976-2005 (solid line), obtained by one Regional Climate Model (RCM), the version 4 of the Rossby Centre regional Atmospheric model (RCA4), driven by two Global Climate Models (GCMs): Centre National de Recherches Météorologiques-Coupled Model (CNRM-CM5), Earth System Model (EC-EARTH). The name of each climate model is hereafter referred as GCM + RCM. Left: CNRM-CM5 + RCA4 model; Right: EC-EARTH + RCA4 model. Top: PV ILR1-Wind; Middle: PV ILR1-Wind-CSP SM1; Bottom: PV ILR1-Wind-CSP-TES SM2. ILR1 or SM1: without storage; SM2: with 6 hours of Thermal Energy Storage (TES). To be compared with figure 5.2.	125
5.2	Similar to figure 5.1 but for the two remaining COordinated Regional climate Downscaling EXperiment-Coupled Model Intercomparison Project Phase 5 (CORDEX-CMIP5) models: the version 4 of the Rossby Centre regional Atmospheric model (RCA4) is forced by the Geophysical Fluid Dynamics Laboratory's Earth System Model (GFDL-ESM2M); and the version 351 of the Weather Research and Forecasting model (WRF351) is forced by the Community Climate System Model (CCSM4). The name of each climate model is hereafter referred as Global Climate Model (GCM) + Regional Climate Model (RCM). Left: GFDL-ESM2M + RCA4 model; Right: CCSM4 + WRF351 model.	126
5.3	Relative change (%) of the regional bias-corrected Capacity Factors (CFs): Photovoltaic (PV) with an Inverter Loading Ratio of 1 or ILR1 (brown), Concentrated Solar Power (CSP) with Solar Multiple of 1 or SM1 (tan), CSP with Thermal Energy Storage (TES) with SM2 (orange), and Wind (blue), per zone and technology, obtained from COordinated Regional climate Downscaling EXperiment-Coupled Model Intercomparison Project Phase 5 (CORDEX-CMIP5) models: two Regional Climate Model (RCM) simulations—the version 4 of the Rossby Centre regional Atmospheric model (RCA4) and the version 351 of the Weather Research and Forecasting model (WRF351)—over the study region using boundary conditions from four different Global Climate Models (GCMs)—Centre National de Recherches Météorologiques-Coupled Model (CNRM-CM5), Earth System Model (EC-EARTH), Geophysical Fluid Dynamics Laboratory's Earth System Model (GFDL-ESM2M), Community Climate System Model (CCSM4). The name of each climate model is hereafter referred as GCM + RCM. (a): CNRM-CM5 + RCA4 model; (b): EC-EARTH + RCA4 model; (c): GFDL-ESM2M + RCA4 model; (d): CCSM4 + WRF351 model. ILR1 or SM1: without storage; SM2: with 6 hours of TES. To be compared with figure 5.9.	130
5.4	Similar to figure 5.3 but for the regional variance of the bias-corrected capacity factors.	130
5.5	Heatmap of the national daily (ordinate) and seasonal (abscissa) anomaly of the Capacity Factors (CFs) in %: Wind (a) , Photovoltaic (PV) with an Inverter Loading Ratio of 1 or ILR1 (b) , Concentrated Solar Power (CSP) with Solar Multiple of 1 or SM1 (c) , CSP with SM2 (d) ; and of the Demand (MW) (e) and Temperature (f) obtained from hourly COordinated Regional climate Downscaling EXperiment-Coupled Model Intercomparison Project Phase 5 (CORDEX-CMIP5) climate data (with intra-daily parametrization) using Centre National de Recherches Météorologiques-Coupled Model (CNRM-CM5) as Global Climate Model (GCM) + the version 4 of the Rossby Centre regional Atmospheric model (RCA4) as Regional Climate Model (RCM). The variation over time is shown in color by intensity in the colorbar. ILR1 or SM1: without storage; SM2: with 6 hours of Thermal Energy Storage (TES).	134
5.6	Similar to figure 5.5 but obtained from different COordinated Regional climate Downscaling EXperiment-Coupled Model Intercomparison Project Phase 5 (CORDEX-CMIP5) model: Earth System Model (EC-EARTH) as Global Climate Model (GCM) + the version 4 of the Rossby Centre regional Atmospheric model (RCA4) as Regional Climate Model (RCM).	135
5.7	Similar to figure 5.5 but obtained from different COordinated Regional climate Downscaling EXperiment-Coupled Model Intercomparison Project Phase 5 (CORDEX-CMIP5) model: the Geophysical Fluid Dynamics Laboratory's Earth System Model (GFDL-ESM2M) as Global Climate Model (GCM) + the version 4 of the Rossby Centre regional Atmospheric model (RCA4) as Regional Climate Model (RCM).	136

5.8	Similar to figure 5.5 but obtained from different COordinated Regional climate Downscaling EXperiment-Coupled Model Intercomparison Project Phase 5 (CORDEX-CMIP5) model: the Community Climate System Model (CCSM4) as Global Climate Model (GCM) + the version 351 of the Weather Research and Forecasting model (WRF351) as Regional Climate Model (RCM).	137
5.9	Anomaly of the regional wind speed ΔWS in (m/s) (blue); Temperature ΔT in (K) (light blue); and solar irradiance components in W/m^2 : Global Horizontal Irradiance (ΔGHI) (tan), Global Tilted Irradiance (ΔGTI) (brown), Direct Normal Irradiance (ΔDNI) (orange); obtained from COordinated Regional climate Downscaling EXperiment-Coupled Model Intercomparison Project Phase 5 (CORDEX-CMIP5) models: two Regional Climate Model (RCM) simulations—the version 4 of the Rossby Centre regional Atmospheric model (RCA4) and the version 351 of the Weather Research and Forecasting model (WRF351)—over the study region using boundary conditions from four different Global Climate Models (GCMs)—Centre National de Recherches Météorologiques-Coupled Model (CNRM-CM5), Earth System Model (EC-EARTH), Geophysical Fluid Dynamics Laboratory's Earth System Model (GFDL-ESM2M), Community Climate System Model (CCSM4). The name of each climate model is hereafter referred as GCM + RCM. (a): CNRM-CM5 + RCA4 model; (b): EC-EARTH + RCA4 model; (c): GFDL-ESM2M + RCA4; (d): CCSM4 + WRF351. To be compared with figure 5.3.	138
5.10	Similar to figure 5.1. Optimal mixes over the historical period 1976 -2005 (Left) and the future period 2071 - 2100 (Right) obtained from COordinated Regional climate Downscaling EXperiment-Coupled Model Intercomparison Project Phase 5 (CORDEX-CMIP5) models: two Regional Climate Model (RCM) simulations—the version 4 of the Rossby Centre regional Atmospheric model (RCA4) and the version 351 of the Weather Research and Forecasting model (WRF351)—over the study region using boundary conditions from four different Global Climate Models (GCMs)—Centre National de Recherches Météorologiques-Coupled Model (CNRM-CM5), Earth System Model (EC-EARTH), Geophysical Fluid Dynamics Laboratory's Earth System Model (GFDL-ESM2M), Community Climate System Model (CCSM4). The name of each climate model is hereafter referred as GCM + RCM. CNRM-CM5 + RCA4 model (octagon); EC-EARTH + RCA4 model (plus); GFDL-ESM2M + RCA4 model (square); CCSM4 + WRF351 model (diamond).	139
5.11	PV ILR1-wind-CSP SM1 mix, obtained from COordinated Regional climate Downscaling EXperiment-Coupled Model Intercomparison Project Phase 5 (CORDEX-CMIP5) climate data, using the Rossby Centre regional Atmospheric model (RCA4) as regional climate model, forced by the Centre National de Recherches Météorologiques-Coupled Model (CNRM-CM5) global climate model, without (left) and with (right) intra-daily parametrization over the historical period. Relatively similar optimal capacity pathways were found whatever the experiment and the CORDEX-CMIP5 climate model (Table 2.2, Chapter 2) and thus are not shown here. Inverter Loading Ratio (ILR) or Solar Multiple (SM) of 1 means without storage.	142
A.1	Left: Scheme of the vertical wind profile as a function of the altitude for the extrapolation of the surface wind U_s at a height h_s up to the height of the turbine h for a wind speed U_h . Right: A typical power curve indicating the relationship between wind speed (abscissa) and power output (ordinate). Source: Lassonde et al. [314]	159
A.2	Left: Incidence angle (θ_i), Zenith angle (θ_z), sun elevation (α_s), slope or tilt (β), surface azimuth (γ) and solar azimuth (γ_s) for Photovoltaic (PV) fixed-tilted arrays. Right: Same schematic depiction of solar angles for Concentrated Solar Power (CSP) parabolic trough tracked-horizontal collectors.	161
A.3	Mathematical formulation of the solar angles required to calculate the incidence angle (θ_i) for Photovoltaic (PV) fixed-tilted arrays (left panel of figure A.2) and for Concentrated Solar Power (CSP) tracked-horizontal collectors (right panel of figure A.2): Zenith angle (θ_z), sun elevation (α_s), slope or tilt (β), surface azimuth (γ) and solar azimuth (γ_s). δ is the solar declination; ω is the hour angle; LST is the Local Solar Time; LT is the Local Time; TC is the Time Correction factor; DST is the Daylight Saving Time; $LSTM$ is the Local Standard Time Meridian; ET is the equation of time; ϕ is the latitude; lon is the longitude; B is the day angle and n is the day number. Source: Own elaboration based on [178, 267, 497, 350].	162
A.4	(a) Shading effect; (b) End losses effect; (c) Thermal losses occurring on the receiver; (d) We refer to "1" as the state of temperature and enthalpy after condensation; "2" after pump; "3" after steam generator (pre-heating, evaporation and superheating); and "4" after turbine (Figure 2.5, Chapter 2). Source: Own elaboration based [403].	166
A.5	Relationship between Concentrated Solar Power-CSP- Solar Multiple-SM- (resp. Photovoltaic-PV- Inverter Loading Ratio-ILR-) and CSP Solar Field-SF- (resp. PV Solar Panels-SP-) area: Depending on the value of the CSP SM (resp. PV ILR), different amount of thermal (resp. Direct Current-DC-) energy is provided by the CSP SF (resp. PV SP) and thus stored in the thermal-TES- (resp. battery-BES-) storage system in order to be used by the Power Block-PB- (resp. Inverter-INV-) to produce electricity whenever it is needed. $X = \{SF, SP\}$; $Y = \{PB, INV\}$; $x = \{therm, DC\}$; and $y = \{elec\}$ (Section 1, Chapter 2). Source: Own elaboration based on [451].	168
A.6	Interannual variability of mean-variance optimization inputs over the whole period (1980 – 2019) available from the Modern-Era Retrospective Analysis for Research and Applications 2 (MERRA-2) reanalysis climate data. Photovoltaic (PV) and Concentrated Solar Power (CSP) Capacity Factors are without storage, i.e., PV Inverter Loading Ratio and CSP Solar Multiple of 1.	173

List of Tables

2.1	Reference or observed capacities, ω_k^{obs} , (Left); and Yearly-mean generation, $Prod_{y,k}^{obs}$, (Right) per zone i and technology j if no storage or j, j' if with storage, installed in Morocco in 2018 (Table A.6, Appendix A). Zone-technology pairs, $k = (i, j)$ or $k = (i, j, j')$, for which no capacity is installed are marked by an empty set \emptyset .	56
2.2	Climate models used to project the potential climate change impacts on optimal mixes (Chapter 5), with their modeling center (first column), host institution (second column), Global Climate Model (GCM) acronym (third column), as well as the Regional Climate Model (RCM) acronym (fourth column). We use two RCMs: version 4 of the Rossby Centre regional Atmospheric model (RCA4) and the version 351 of the Weather Research and Forecasting model (WRF351); driven by four GCMs: Centre National de Recherches Météorologiques-Coupled Model (CNRM-CM5); Earth System Model (EC-EARTH); Geophysical Fluid Dynamics Laboratory's Earth System Model (GFDL-ESM2M); Community Climate System Model (CCSM4) taken from the 5th Coupled Model Intercomparison Project (CMIP5) [506] of the Fifth Assessment Report (AR5) of the Intergovernmental Panel on Climate Change (IPCC) [499] in the COordinated Regional climate Downscaling EXperiment (CORDEX) framework for Middle East and North Africa (MENA) domain. Three models are provided by the Swedish Meteorological and Hydrological Institute (SMHI) and one is provided from the Cyprus Institute (CyI). The interested reader is referred to the sources mentioned for a more detailed description of the models.	61
2.3	Storage parameters: Storage capacity (MWh) (first column), Maximum power of charging / discharging (MW) (second column), Total energy discharged (TWh) (third column) and Storage duration (h/day) (fourth column) obtained from the thermal-TES- (battery-BES-) storage model without constraints (Section 2, Appendix A).	64
2.4	Regional predicted demand (MWh/yr) and bias-corrected wind and solar Capacity Factors-CFs- (%), for each Solar Multiple (SM) and Inverter Loading Ratio (ILR), obtained from hourly MERRA-2 climate reanalysis and averaged over the year 2018, per zone and technology. Thermal (TES) and Battery (BES) storage are with constraints. ILR1 or SM1: without storage; ILR>1 or SM>1: with increasing levels of storage from Photovoltaic (PV) or Concentrated Solar Power (CSP).	68
2.5	Capital investment (<i>CAPEX</i>), fixed and variable operation and maintenance costs (<i>FOM</i> and <i>VOM</i>), lifetime (<i>Lifetime</i>) of the production technologies j (Left) and thermal (TES) or Battery (BES) storage technologies j' (Right). This data is from the ETRI 2014 - Energy Technology Reference Indicator projections for 2010-2050 technical report, for the year 2013 [453, Table 7, Table 4 and Table 10 for PV, wind and CSP]; and [453, Table 66 and Table 61 for TES and Li-ion BES]. The discount rate (<i>DR</i>) is from the World Bank Report [344, page 27]. α_j is the yearly-mean CF in (hours) of the technology j (Eq. A.74) and the yearly rental cost per technology, c_j (€/kW/yr), is calculated using equation (2.15). Concentrated Solar Power (CSP) and Photovoltaic (PV), on the left panel, are without storage (i.e., for Solar Multiple-SM- and Inverter Loading Ratio-ILR-equal to 1).	71
2.6	The yearly rental cost c_k , Eq. (2.14), in (€/kW/yr) per production technology j or production technology with its storage technology j, j' calculated using equation (2.15) and (2.16); and using the storage parameters (Table 2.3). The index k is a multi-index representing a pair $k = (i, j)$ or $k = (i, j, j')$ with i are zones. ILR and SM denote, respectively, the Inverter Loading Ratio and Solar Multiple. ILR1 or SM1: without storage; ILR>1 or SM>1: with increasing levels of storage from Photovoltaic (PV) or Concentrated Solar Power (CSP).	71
2.7	Capital investment (<i>CAPEX</i>), fixed operation and maintenance costs (<i>OPEX</i>), lifetime (<i>Lifetime</i>) are from the European Commission Joint Research Center (JRC) technical report [266] for the year 2015 (see tables 12 and 10 for utility-scale Photovoltaic-PV- without tracking/storage, tables 2 and 5 for onshore wind with medium specific capacity and hub height; and tables 15 and 16 for Concentrated Solar Power-CSP- with 6-8 hours of thermal storage-TES-). The discount rate (<i>DR</i>) is from the World Bank Report [344, page 27]; and the yearly rental cost per technology calculated using equation (2.18). The cost of CSP is kept constant for all Solar Multiple-SMs- (1, 2, 3, 4) and also for the reference SM (SM^{ref}) for the calculation of (2.9).	72
3.1	Optimization Experiments. Integration of Concentrated Solar Power (CSP) without and with increasing Thermal Energy Storage (TES) capabilities—as measured by the Solar Multiple (SM)—with Photovoltaic (PV) without storage (Inverter Loading Ratio of 1 or ILR1) and wind.	80
3.2	Maximum-penetration ratios (yr/T€) given by (2.19) obtained from hourly Modern-Era Retrospective Analysis for Research and Applications 2 (MERRA-2) climate data over the year 2018. Inverter Loading Ratio of 1 (ILR1) or Solar Multiple of 1 (SM1): Photovoltaic (PV) or Concentrated Solar Power (CSP) without storage; SM>1: with increasing levels of storage from CSP.	82
3.3	Similar to table 3.2 but for the ratios (no units) given by (2.20).	82
3.4	Similar to table 3.2 but for the variance/cost ratio (yr/Ee MW) given by (2.21).	82
3.5	Similar to table 3.2 but for the minimum-variance ratios (10^3 MW) given by (2.22).	83

3.6	Mean-standard deviation ratios (2.5) of the global, technology and base fronts without the maximum-cost constraint (2.8) for different combinations (Table 3.1). Photovoltaic (PV) is without storage. Solar Multiple of 1 or SM1: Concentrated Solar Power (CSP) without storage; SM>1: with increasing levels of storage from CSP.	85
4.1	Optimization Experiments. Integration of Photovoltaic (PV) with increasing Battery Energy Storage (BES) capabilities—as measured by the Inverter Loading Ratio (ILR)—with Concentrated Solar Power (CSP) without and with increasing Thermal Energy Storage (TES) capabilities—as measured by the Solar Multiple (SM)—and wind.	100
4.2	Maximum-penetration ratios (yr/T€) given by (2.19) obtained from hourly Modern-Era Retrospective Analysis for Research and Applications 2 (MERRA-2) climate data over the year 2018. Solar Multiple of 1 or SM1: Concentrated Solar Power (CSP) without storage; Inverter Loading Ratio ILR>1 or SM>1: with increasing levels of storage from Photovoltaic (PV) or CSP.	101
4.3	Similar to table 4.2 but for the ratios (no units) given by (2.20).	102
4.4	Similar to table 4.2 but for the variance/cost (yr/E€ MW) given by (2.21).	102
4.5	Similar to table 4.2 but for the minimum-variance ratios (10^3 MW) given by (2.22).	103
4.6	Mean-standard deviation ratios (2.5) of the global, technology and base fronts without the maximum-cost constraint (2.8) for different combinations (Table 4.1). Solar Multiple of 1 or SM1: Concentrated Solar Power (CSP) without storage; Inverter Loading Ratio or ILR>1 or SM>1: with increasing levels of storage from Photovoltaic (PV) or CSP.	104
5.1	Minimum-variance ratios (10^3 MW) given by (2.22) obtained from COordinated Regional climate Downscaling EXperiment-Coupled Model Intercomparison Project Phase 5 (CORDEX-CMIP5) models: two Regional Climate Model (RCM) simulations—the version 4 of the Rossby Centre regional Atmospheric model (RCA4) and the version 351 of the Weather Research and Forecasting model (WRF351)—over the study region using boundary conditions from four different Global Climate Models (GCMs)—Centre National de Recherches Météorologiques-Coupled Model (CNRM-CM5), Earth System Model (EC-EARTH), Geophysical Fluid Dynamics Laboratory's Earth System Model (GFDL-ESM2M), Community Climate System Model (CCSM4). The name of each climate model is hereafter referred as GCM + RCM. The values correspond to the historical period (1976 -2005) - future period (2071-2100). Inverter Loading Ratio or Solar Multiple of 1 (ILR1 or SM1): without storage; SM2: with 6 hours of Thermal Energy Storage (TES).	127
5.2	Similar to table 5.1 but for the ratios (no units) given by (2.20).	128
5.3	Similar to table 5.1 but for the maximum-penetration ratios (yr/T€) given by (2.19).	129
A.1	Electricity demand model parameters (10^{-2})— $a_H^{work sat off}$ (resp. $a_C^{work sat off}$) which represents the degree of heating (resp. cooling) required with the change in temperature for each day type (week days "work", Saturdays "sat", and off-days "off" such as Sundays and holidays); $\alpha_0^{work sat off}$ is the coefficient of the interval within which the demand is insensitive to temperature—obtained from hourly (a): Modern-Era Retrospective Analysis for Research and Applications 2 (MERRA-2) climate reanalysis over the year 2018. (b), (c), (d), (e): COordinated Regional climate Downscaling EXperiment (CORDEX) climate data using different climate models (Table 2.2, Chapter 2) over the whole historical period (1951 -2005). The name of each climate model is hereafter referred as Global Climate Model (GCM) + Regional Climate Model (RCM): version 4 of the Rossby Centre regional Atmospheric model (RCA4); the version 351 of the Weather Research and Forecasting model (WRF351); Centre National de Recherches Météorologiques-Coupled Model (CNRM-CM5); Earth System Model (EC-EARTH); Geophysical Fluid Dynamics Laboratory's Earth System Model (GFDL-ESM2M); Community Climate System Model (CCSM4). We give the overall coefficient of determination R^2	158
A.2	Main characteristics of the 50 MW Concentrated Solar Power with Thermal Energy Storage Andasol 1 power plant, taken as reference for this thesis. Adapted from Silva et al. [483] (Appendix A).	165
A.3	Bias correction factor $\frac{\eta_{y,k}^{obs}}{\langle \eta_{h,k}^{clim} \rangle}$ by technology j or j' and region i , obtained from hourly (a): Modern-Era Retrospective Analysis for Research and Applications 2 (MERRA-2) climate reanalysis over the year 2018. (b), (c), (d), (e): COordinated Regional climate Downscaling EXperiment (CORDEX) climate data using different climate models (Table 2.2, Chapter 2) over the whole historical period (1951 -2005). The name of each climate model is hereafter referred as Global Climate Model (GCM) + Regional Climate Model (RCM): version 4 of the Rossby Centre regional Atmospheric model (RCA4); the version 351 of the Weather Research and Forecasting model (WRF351); Centre National de Recherches Météorologiques-Coupled Model (CNRM-CM5); Earth System Model (EC-EARTH); Geophysical Fluid Dynamics Laboratory's Earth System Model (GFDL-ESM2M); Community Climate System Model (CCSM4).	170
A.4	Estimates of the covariances (10^{-10}) between the predicted capacity factors and the inverse of the demand in the same region obtained from hourly MERRA2 climate data over the year 2018. ILR and SM denotes, respectively, the Inverter Loading Ratio and Solar Multiple. ILR1 or SM1: without storage; ILR>1 or SM>1: with increasing levels of storage from Photovoltaic (PV) or Concentrated Solar Power (CSP).	171
A.5	Estimates of the correlations between the predicted capacity factors and the inverse of the demand in the same region obtained from hourly MERRA2 climate data over the year 2018. ILR and SM denotes, respectively, the Inverter Loading Ratio and Solar Multiple. ILR1 or SM1: without storage; ILR>1 or SM>1: with increasing levels of storage from Photovoltaic (PV) or Concentrated Solar Power (CSP).	171
A.6	Characteristics of the onshore wind, Photovoltaic (PV) and Concentrated Solar Power (CSP) without or with Thermal Energy Storage (TES) operational plants in Morocco in 2018. PT: Parabolic Trough CSP. ST: Solar Tower CSP. h: expected hours of storage. We ignore the production from auto-producers, except for wind plants since their installed capacity is included in the total wind capacity. Data from: MEME [23], RES4MED [302], Energypedia [13], GEO [14], CSP FOCUS [10], SolarPACES [33] and MASEN [22]. The index k is a multi-index representing a pair $k = (i, j)$ or $k = (i, j, j')$ of region i and technology j or j' . $i = \{NORTH, CENTER, EAST, SOUTH\}$; $j = \{PV - ILR1, Wind, CSP - SM1\}$ and $j' = \{BES, TES\}$. ILR and SM denotes, respectively, the Inverter Loading Ratio and Solar Multiple. ILR1 or SM1: PV or CSP without storage.	177

General Introduction

Contents

I	Research Motivation and Background	24
1	Climate Change Mitigation	24
2	Overview of Renewable Technologies and Flexibility Options	26
3	Concentrated Solar Power vs. Photovoltaic vs. Wind and Thermal vs. Battery Storage	29
II	Knowledge Gap and Originality of this Thesis	43
III	Focus of the Thesis	44
1	Objectives and Tools	44
2	Case Study: Morocco	44
3	General Research Questions and Approach	46
IV	Thesis Outline	47

In this thesis introduction chapter, we review the main options to mitigate climate change, particularly the decarbonization of the electricity sector, by highlighting the actual share of Renewable Energy (RE) technologies in the Total Final Energy Consumption (TFEC) and in the global electricity production (Section 1). We give a comparison between RE technologies, storage technologies and other flexibility options in terms of technical, economic and environmental criteria (Section 2). We also provide an overview of the crucial elements of the integration of two distinct solar technologies, Concentrated Solar Power (CSP) and Photovoltaic (PV) without and with their associated thermal (TES) and battery (BES) storage, and wind in our current energy mixes or in the context of future warming climate (Section 3) by highlighting their differences in terms of mean production (sensitivity to clouds and temperature, the effect of tilt angle or tracking), variability or adequacy risk and total cost. A brief discussion of the knowledge gap on such integration and the originality of this thesis is presented in section II. The main objectives, tools and the general research questions that this thesis aims to answer are presented in section III. Finally, the thesis outline comes in the last section (Section IV).

I Research Motivation and Background

In this section, we present the elements that motivated the research for the present thesis.

1 Climate Change Mitigation

The impact of climate change was first identified by Fourier, Tyndale, and Arrhenius in 1827, 1859, and 1896, respectively, in France, Britain, and Sweden [30] due to the progress in science and technology, expansion in industry, transportation and agriculture, and rapid population growth; leading to fossil fuel consumption and consequently global greenhouse gases (GHGs). However, **scientific concerns about global warming grew during the 1980s**, and in 1988 (a year when North America faced an intense heat wave and drought) these spilled over into political concerns, and the **World Meteorological Organization (WMO)** and the **United Nations Environment Program (UNEP)** established the **International Panel on Climate Change (IPCC)** to investigate and report on scientific evidence on climate change and possible international responses to this phenomenon. These assessments present projections of future climate change based on different global emission scenarios (i.e., continued growth, rapid reduction. . .) and the corresponding risks for human and natural systems. **While they lay out response options and their implications, the reports do not tell policymakers what action to take.** Its first assessment report (in 1990) fed into the drafting of the **United Nations Framework Convention on Climate Change (UNFCCC)**, which was signed by several countries at the **Earth Summit in Rio de Janeiro** in 1992. The UNFCCC **did not contain any specific national or international targets to reduce GHG emissions, but it contained key points that have been foundational in subsequent international climate change debates.** These culminated in a **Conference of Parties (COP)** meeting in Kyoto, Japan, in 1997. This was the third COP meeting (COP 3) where delegates agreed what is known as the **Kyoto Protocol**. By 2007-2009, the existence and dangers of climate change were increasingly recognized with **growing scientific understanding of climate change and its impacts** (the publication of the IPCC Fourth Assessment Report-AR4- played a critical role in this), **public awareness about unusual weather patterns** (i.e., increasing temperatures, changing rain and snow patterns, warmer ocean, rising sea level, wilder weather, increased ocean acidity, shrinking sea ice), and **political change**.

The Paris Agreement, a historic agreement reached in Paris in 2015, has been a game-changer in international discussions on climate change. Nearly all major GHGs emitting countries have now ratified the Paris Agreement. Its aim is to (i) limiting global warming to well below

2°C, ideally to 1.5°C, relative to pre-industrial levels, (ii) deal with emission reductions considering **countries' different responsibilities** (i.e., historical contribution to the global GHG emissions) and **capacities** (i.e., ability to pay for mitigation), (iii) adaptation to impacts with particular concerns for **developing countries** and especially those **most vulnerable to damaging climate change impacts** such as Small Island Developing States and Least Developed Countries to avoid **major damage to food systems and economic development**, and (iv) mobilize finance to pay for these efforts [339].

There is widespread recognition that drastic emission reductions are needed. However, **deep divisions remain between countries with regards to the appropriate distribution of GHG emission limits and reductions**; and the Paris Agreement mentioned the remaining global carbon budget [339], but it is not clear which country should receive which share of such global emission budget. In fact, **governments do not want to bear the costs of such reductions** in terms of **increased energy costs, investments in new technologies and infrastructure, and lifestyle changes**. **Developed countries with high emissions per capita** face very large economic and social adjustment costs if they are to make substantial reductions in their emissions. **Developing countries have lower current emissions per capita**, but do not want either to be denied opportunities for economic growth and increased standards of living associated with increasing emissions, or to be forced down a more costly and slower development path constrained by keeping down GHG emissions. **Developing countries need large financial resources from developed countries**, primarily responsible for the GHGs, to enable them to adapt and cope with climate change.

The IPCC is currently in its Sixth Assessment Report (AR6) [227] in which it provides new estimates of the chances of crossing the global warming level of 1.5°C, in the next decades, and finds that **unless there are immediate, rapid and large-scale reduction in GHG emissions, limiting global warming to close to 1.5°C or even 2°C will be beyond reach**.

In addition, the combined national contributions announced, at the **26th United Nation climate change COP (COP 26)** held in Glasgow (United Kingdom-UK-), still **put the world on track for a temperature rise of 2.4°C**. The Glasgow Climate Pact signed at **COP 26 expresses the need for greater action now** and emphasizes that we are in a climate emergency, asserting that **climate change is impacting us today**. **World leaders have agreed to further improve their national targets at COP27 in Egypt in 2022**.

Moreover, the **Climate Action Tracker (CAT)** [7] evaluates progress towards this global goal by quantifying the aggregate effects of current mitigation plans and the pledges and targets put forward by countries, and compares these with the emission levels consistent over time with the 1.5°C limit. CAT finds that current policies presently in place around the world are projected to result in about 2.7°C warming. In case promised reductions are met, the pledges that governments have made under the Paris Agreement (known as Nationally Determined Contributions or NDCs) would limit the median warming estimate but it still lie well above emission pathways consistent with the Paris Agreement long-term temperature goal. Recently, world leaders also agreed to reach global peaking of GHG emissions as soon as possible to achieve a balance between sources and sinks of anthropogenic emissions during the second half of this century, so that the sum of all GHGs emitted by human activities is zero. However, this scenario is also expected to surpass 1.5°C above pre-industrial levels.

Therefore, there remains a substantial gap between the measures that have been put in place and the actions that must be undertaken by emerging economies and industrialized ones to fight climate change. In fact, **the urgency of these changes comes from the inertia of the climate system¹** but also from **the inertia of the Renewable Energy (RE) power plant infrastructure investment**.

To achieve the emission cuts required, **energy generation sector must reach net zero earlier to counterbalance harder-to-abate sectors** (e.g., transportation sector burning fossil fuels for our cars, trucks, ships, train, and planes; industrial processes; agriculture and waste management; deforestation associated with the burning of trees and thus the destruction of a carbon sink) [137]. For instance, **the mathematical Kaya formula**—developed by Japanese economist Yoichi Kaya in 1993 in his book [295]—sets out the possible solutions **to reduce the carbon dioxide (CO₂) emissions associated with the energy sector** by highlighting **the relationship between Gross Domestic Product (GDP), population and global energy consumption**. (1) One of the main strategies of reducing emissions and thereby the effects of climate change, is to **decarbonize the electrical grid to reduce the intensity of carbon in the global energy mix “CO₂/energy consumption”**. This can be realized through three major technology pathways: (i) **The implementation of Carbon Capture and Sequestration (CCS) technologies on existing electricity generators** so that electricity sector could continue to use fossil fuels without increasing emissions. However, current CCS technologies are expensive and reduce generator net efficiencies, which requires increasing the amount of fuel burned to produce a unit of electricity. On the other hand, fossil fuels are a finite resource, making CCS unsustainable. (ii) **The expansion of carbon-free resources (e.g., nuclear)**. However, due to some catastrophic events, there is a strong negative public opinion surrounding nuclear energy. And (iii) **the grid integration of RE resources** (e.g., wind, solar, hydro, geothermal, biomass, marine energy), which produce electricity without the use of fossil fuel, and their associated costs have significantly decreased in the last decade [447]. However, these technologies possess technological and economical challenges (see section i and section 3). (2) The second strategy is to **reduce the energy intensity of the economy “energy consumption/GDP” by increasing the energy efficiency** which involves using technology that requires less energy to perform the same function (e.g., isolate your buildings, use energy-saving light bulbs, make use of electric cars, a shift to a mode of transportation with a lower emission factor). (3) **Energy sobriety** is the third strategy to reduce emissions, which involves using less energy by adjusting our behaviors and habits (e.g., avoid using your car for short journeys and instead walk or cycle, use public transport or share a ride with other people, switch off lights and turn off electrical devices than leave them on standby, reduce the amount of animal products you eat, choose products that have little plastic packaging) to **increase the economic production per capita “GDP/population”**. **Political and economical responses** to date include forms of **carbon pricing or carbon taxes and carbon emission trading, reductions of fossil fuel subsidies, policy mechanisms to support RE development, and making simplified regulations for the integration of low-carbon energies**.

Currently, it seems that the “simplest” option to sustainably reduce CO₂ emissions in the energy sector is to decarbonize the electrical grid by shifting away from fossil fuels to an energy mix dominated by low-carbon sources over the next few years [182]. The figure 1.1 shows that to keep the global warming below 2°C (which corresponds to the stringent mitigation scenario, RCP 2.6, in light blue), the share of low-carbon technologies must grow very fast in the coming decades and reach more than 90% of the Total Final Energy Consumption (TFEC) in 2100 [183]. A few questions quickly come to one's attention: **what does our global energy mix look like today? Are we making progress in shifting towards a low-carbon energy system?** Currently, the share of REs in the TFEC has seen only moderate increase. As of 2018, RE accounted for a 11% of TFEC (Figure 1.2a). Overall, an installed RE capacity was enough to provide an estimated 27.3% of global electricity generation at the end of 2019 (Figure 1.2b). The highest share of RE use is in the power sector (Figure 1.2c). However, it accounted for only 17% of the TFEC. Energy use for transport represents 32% of TFEC but has the lowest share of RE. The remaining thermal energy sector accounted for more than half of the TFEC, where 10% was supplied by REs [446].

¹ Even if we could somehow immediately stop all carbon dioxide (CO₂) emissions being released into the atmosphere, the global temperature would stabilize but not decline because it takes centuries to millennia for the CO₂ already present in the atmosphere to be removed by natural processes. The sea level would continue to rise during this time as the entire ocean volume slowly expands in the response to past surface warming.

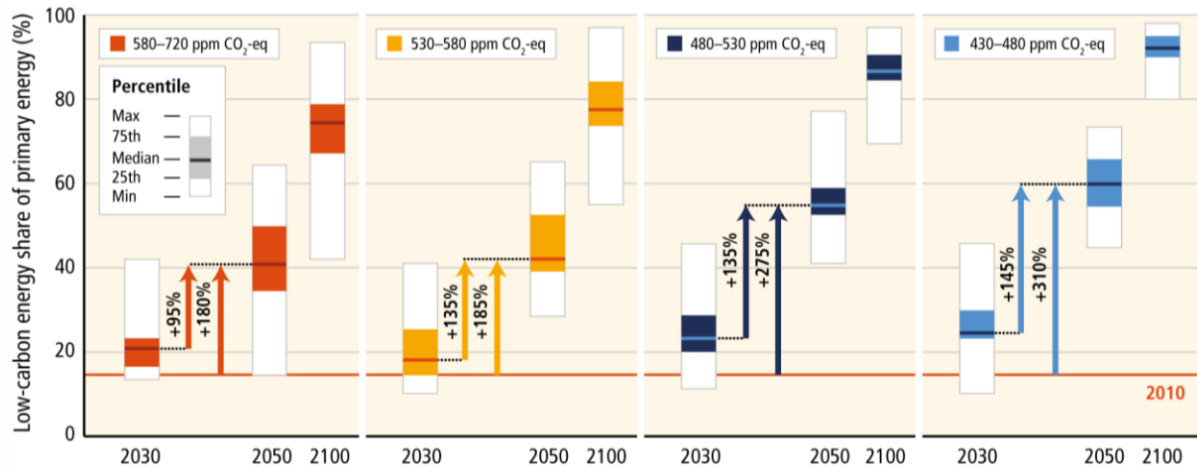


Figure 1.1: Share of low-carbon technologies in the Total Final Energy Consumption (TFEC) for each Intergovernmental Panel on Climate Change (IPCC) emission scenario, RCP "Representative Concentration Pathways" [534, 366], for various time horizons (2030, 2050 and 2100). The four scenarios go from 2.6 to 8.5 W/m^2 of radiative forcing. The higher the value of the latter, the higher the projected increase of global temperature. **Right Corner:** The mitigating scenario allowing a 2°C global warming in 2100 above the pre-industrial temperatures (RCP 2.6 in light blue that falls in the 430-480 ppm CO₂eq). **Middle:** The intermediate scenarios (RCP 4.5 in dark blue; and RCP 6.0 in yellow). **Left Corner:** The most pessimistic scenario without additional efforts to constrain emissions (RCP 8.5 in red) lead to pathways where emissions continue to rise throughout the 21st century "baseline scenario". Source: The Fourth Assessment Report (AR4) of the IPCC (2014) [183].

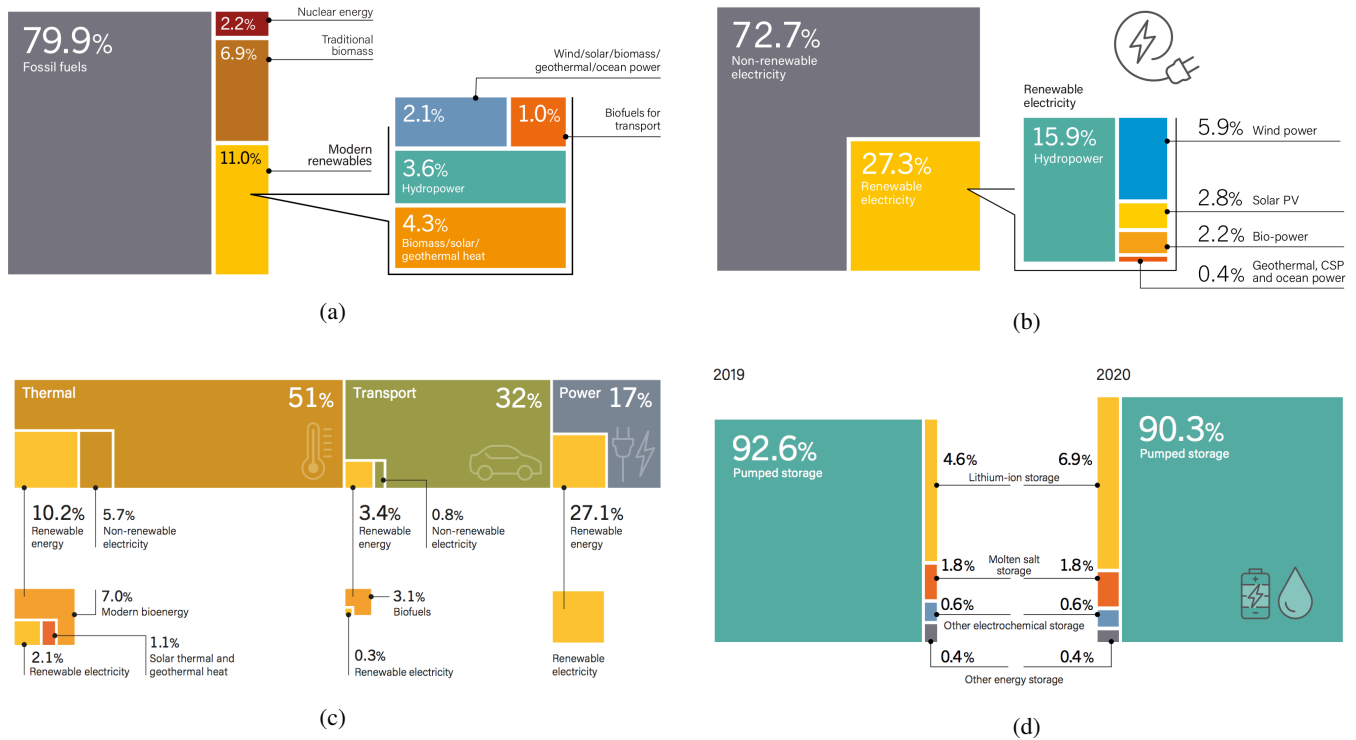


Figure 1.2: (a): Share of Renewable Energies (REs) in the Total Final Energy Consumption (TFEC), 2018. (b): Share of REs in the global electricity production, end 2019. Non-renewable electricity means fossil fuels and nuclear. (c): Share of REs in the TFEC, by final energy use, 2018. (d): Share of global energy storage installed capacity, by technology, 2019 and 2020. Source: Renewables 2020/2021 Global Status Report [446, 447].

2 Overview of Renewable Technologies and Flexibility Options

To increase the penetration of Renewable Energy (RE) technologies (i.e., the percentage of electricity generated by a particular RE resource), optimal mixes are expected to combine different RE technological options [66] with different energy storage systems [290] or other flexibility options because each RE technology, storage technology and flexibility option has its own advantages and disadvantages and play a different role.

i Renewable technologies vs. Fossil Fuels vs. Nuclear

On the basis of **total cost**, conventional fossil fuel generators tend to have lower upfront costs and high (if not dominant) fuel costs, which are highly sensitive to the price volatility of the fossil fuel markets. In contrast, RE technologies have, in general, high upfront investment

costs, moderate operation and maintenance costs and zero fuel costs, which are more sensitive to change in the cost of capital and financing conditions [391, 193]. When considering a transition from the dirtiest of fossil fuels, nuclear is also a possibility, and therefore, nuclear will be discussed along with RE technologies. However, the costs for nuclear are rising while RE technology costs are decreasing. In terms of electricity generation, RE technologies have, typically, low **Capacity Factor-CF**- (i.e., the ratio of the electrical energy produced over a given period of time to the energy it would have produced if it had operated at its rated power during the same period) and thus higher **cost of electricity production** than nuclear or fossil fuel production. It is, thus, necessary to install more RE capacity to produce the same amount of energy (high **power density** of electricity production, i.e., high amount of power of the physical system per surface unit) [530]. However, nuclear and fossil fuel plants have high **water requirements** for cooling. In addition, fossil fuels (resp. nuclear reactors) have a much higher **carbon footprint (resp. safety risks)** than RE technologies. The latter have, however, a hidden carbon footprint and safety risks as wind turbines, Photovoltaic (PV) panels and Concentrated Solar Power (CSP) plants—harnessing the energy generated from wind speed and sun—require industrial manufacturing processes that emit greenhouse gases (GHGs). For instance, the manufacture of PV cells involves the use of several toxic, carcinogenic, flammable and explosive chemicals. The environmental impacts of wind turbines are typically noise from the rotation of the blades and machinery noise from the gear-box and generator, visual intrusion and bird strike. Hydro (harnesses the power of water in motion), geothermal (heat that is generated within the earth) and biomass (energy that comes from organic material in plants and animals) have also environmental impacts (e.g., dam inundation, release of offensive chemical, food competition/wood for cooking and heating) [189]. CSP plants disturb the views of natural landscapes, and use materials, many of which are not recyclable and produce toxic substances that, when burnt at high temperatures, stay in the environment for many years and can be harmful to humans. Nuclear plants produce no GHG emissions during operation, and over the course of its life-cycle, nuclear produces about the same amount of carbon dioxide (CO_2)-equivalent emissions per unit of electricity as wind, and one-third of the emissions per unit of electricity when compared with solar [39].

It should also be noted that there are differences in the **efficiency** between nuclear, coal, oil compared to natural gas; and between hydro, biomass, geothermal compared to wind, PV, and CSP which are also different in terms of **availability, predictability** and **variability**. For instance, natural gas is the most efficient thermal technology. For RE, hydro has the highest efficiency. When located at a high-quality wind resources, wind power is the second most efficient RE technology, followed closely by biomass. Geothermal efficiencies vary due to the temperature of the geothermal sources (hotter geothermal sources give greater efficiencies). Hydro, biomass and geothermal are more available compared to wind (no power is generated at wind speed below 3-5 m/s and turbines must be stopped at high wind speeds above 20-25 m/s to avoid damage) or solar energy (which depends on the season, latitude, weather and time of the day) [189]. Marine energy—such as tidal energy (exploiting the oscillating movement of sea level due to the combined gravitational action of the moon and the sun); wave energy; energy of ocean currents (placing tidal turbines in the seabed and riverbeds which depends on the rotation of the earth and the cycle of the moon); offshore wind; osmotic energy (exploiting the difference in salinity between seawater and freshwater); and thermal energy of the sea (harnessing the temperature differences or thermal gradients between ocean surface waters and deep ocean waters)—has also several advantages. The production is more regular and predictable, which is of great interest compared to wind or solar energy (e.g., prediction of micro-scale circulations associated with wind turbulence or clouds are hard to predict). Moreover, the energy of ocean current can be advantageous as the water is much denser than the air which makes it possible to reduce the turbine size; or offshore wind where the wind is stronger and more regular than on the land. It also has the advantage of being in areas generally unusable for other activities, unlike other RE technologies. However, there are also issues related to marine energy, including the difficult conditions in which production equipment is installed, most of which does not yet have sufficient resistance to large-scale natural phenomena such as storms or tsunamis. Moreover, the process being relatively new, the cost of installation, operation and maintenance are still very high compared to other forms of energy, which makes the transition to industrial scale uncertain [372].

Data from the International Renewable Energy Agency (IRENA) [272] and from the Statistics Portal for Market Data, Market Research and Market Studies (Statista) [35] showed that at the end of 2019, **global RE generation capacity** amounted 2537 gigawatts (GW). Hydropower accounted for the largest share of the global capacity (1190 GW excluding Pumped Hydro Storage-PHS-), followed by wind (623 GW), solar (586 GW), biomass (124 GW), geothermal (14 GW), and marine (500 MW) energies. Fossil fuels remains the greatest source for electricity generation in the world (4213 GW). However, this was still far higher than the capacity of nuclear (369 GW).

Given the differences between these technologies, and particularly between REs and nuclear power, it is necessary to shed light on the technical, economic and environmental issues associated with the technological choices to fully ensure energy security and achieve carbon neutrality by 2050. For instance, France faces currently a crucial choice for its future electricity mix: **Should France build a new nuclear reactors, or it should gradually move towards a 100% RE mix?** Several studies have been published to inform the debate. The latest report of the Electricity Transmission System Operator (RTE) [151] looks at six scenarios based on REs (PV, wind, marine energy in addition to hydro and biomass) without and with nuclear (existing and new generation reactors); and finds that scenario mixes introducing the new generation of nuclear reactors are more competitive than scenario based on 100% RE. RTE also highlights the role of nuclear in providing heat and hydrogen to decarbonize hard-to-abate sectors. The latest report of Greenpeace France and the Rousseau Institute [188] contributes to this debate and finds that the cost of production of the new European Pressurized nuclear Reactor (EPR) is the highest due to its high investment and safety standards; while rooftop PV, onshore wind, ground-mounted PV systems are the cheapest solutions. However, existing nuclear reactors cost less than residential PV and offshore wind. While RTE and Greenpeace focus on the electric trajectory, the negaWatt scenario [386] and the scenarios of the Ecological Transition Agency (ADEME) [148] propose a vision of the transition over the entire energy system by studying the technical feasibility of 100% RE mix in France in 2050. They found that energy efficiency and energy sobriety are the keys to reduce energy consumption; and it is possible to cover France's energy needs with REs (biomass, wind, PV) without nuclear power. Imported fossil fuels could only be used for non-energy purposes.

ii Energy Storage Technologies

Energy supply from RE sources, particularly solar and wind energy, is often hit by fluctuations due to, for example, insufficient wind or sunshine. Energy storage is crucial means that mitigates such problems by (i) **providing power quality and regulation (for small-scale applications)**. For instance, **providing fast response to unpredictable variations** in demand and generation; or providing a **black start** (i.e., when large generators need an external source of electricity before they can begin generating electricity for the grid). (ii) Storage can also be used for **load following or ramping services (for medium-scale applications)** by varying its output energy to smooth the RE output fluctuations and balance generation and load at particular area of the power system network. (iii) Storage also **shifts electricity through several hours (i.e., arbitrage or load leveling for large-scale applications)**, which **reduces both the curtailment** (i.e., when the electricity generation from RE exceeds total demand) and **the shortage of energy** (i.e., when RE production cannot fulfill total demand) and **support the**

transmission congestion allowing to **maximize the energy value** (i.e., get benefits of price difference during on-peak and off-peak period). That is purchase of electricity during low demand at low price while storing the excess of production in the storage system; and deliver the energy stored, in wholesale network, during high demand periods with high prices. Thus, storage helps to **save additional grid investment cost and CO₂ emissions** by means of substitute or defer development of new power generation capacity [86, 68].

Based on the forms of energy stored, storage technologies can be categorized into five major types, i.e., (1) mechanical such as Pumped Hydro Storage (PHS), Compressed Air Energy Storage (CAES) and Flywheel Energy Storage (FES); (2) electrical consisting mainly of Super Capacitors Energy Storage (SCES) and Superconducting Magnetic Energy Storage (SMES); (3) electrochemical Battery Energy Storage (BES) systems include Lead-Acid (Pb-A), Nickel-Cadmium (Ni-Cd), Sodium-Sulfur (Na-S), Sodium Nickel Chloride (NaNiCl₂), Lithium-ion (Li-ion), and Flow Battery Energy Storage (FBES); (4) chemical such as hydrogen fuel cells; and (5) Thermal Energy Storage (TES) system.

With the increase of production from REs, it becomes much important to compare between storage technologies—from technical, economic and environmental criteria—to select the appropriate type of storage technology for RE integration applications in the electricity grid. The technical performance of energy storage technologies is determined by the following factors: **Energy and power density**, i.e., how much energy and power can be stored per unit mass. High power and energy density reflects lighter in weight and smaller in size. **The rated power (resp. energy) capacity** means the maximum power (resp. energy) that the storage system can achieve in MW (resp. MWh). **The discharge duration** means the amount of time a storage system can discharge at its rated power capacity, and it is defined as the ratio between the rated energy capacity and the rated power capacity. **The round-trip efficiency**, i.e., the ratio of the energy discharged to the energy charged, and it depends on the losses occurring during charge, discharge and storing process. Thus, low efficiency increases the cost since only a fraction of the stored energy can be used. **The response time** means the amount of time required to start deliver power, which is the time between no discharge to full discharge. **The lifetime**, i.e., the amount of time or cycles a storage system can provide regular charging and discharging before failure or significant degradation. One cycle corresponds to one charge and one discharge. A short lifespan increases long-term costs as the storage unit needs to be replaced more often. **The self-discharge** means the portion of energy that was initially stored and which has dissipated over a given amount of non-use time. **The technical maturity and the memory effect** (i.e., when a storage system repeatedly recharged after being only partially discharged).

Overall, **FES, SCES, SMES are the dominant storage technologies to be used for small-scale applications** as they have high power density, a low power range and a very short discharge time (seconds), a very high efficiency, a very fast response time, small power cost, and small environmental impact (i.e., no carbon emissions or toxic components, but stringent safety guards is necessary while in operation). However, the daily self-discharge of these technologies is very high and they are less mature, with medium lifetime and high energy cost.

BES are the dominant storage technologies to be used when very high energy density and medium power density, medium power range and long discharge time, high efficiency, fast response time, medium self-discharge, and medium energy and power cost are paramount, making them **mature and suitable for medium-scale applications**. However, they have small lifetime and require high operating temperature, they are affected by the memory effect and have high environmental impacts (i.e., batteries lead to prone toxic and corrosive due to usage of certain metals as electrodes and acid as electrolyte). Among batteries, Li-ion has the highest energy and power density, with medium power range but high storage duration (hours to days), highest efficiency, lowest self-discharge, with no memory effect and environmental impact, but has the lowest lifetime which increase the energy and power cost.

PHS and CAES are the dominant storage technologies to be used for large-scale applications as they belong to low energy and power density technologies, can store more energy for a long discharge duration (hours to days) and have a larger power rating, a very long lifetime, high maturity for PHS, and almost negligible rate of self-discharge, and low capital cost per unit of energy. However, these technologies have moderate efficiency, high response time, high power cost and non-negligible environmental impact (i.e., CAES needs large underground space with high pressure air storage and needs high fossil fuel combustion, and PHS technology needs specific geological formations with large land use, long development time and long payback periods).

Many studies have shown that **hydrogen** has real potential in the decarbonization of the energy, transport and industry sectors [42]. However, this technology represents some challenges such as high cost of production of hydrogen by electrolysis of water compared to steam reforming of methane, high cost of fuel cells and low efficiency compared to BES or TES. Besides, the reactions of hydrogen in the troposphere with other gases participate in the formation of ozone, water vapor and methane which increase the greenhouse effect.

TES has several advantages compared to other storage technologies, such as **low capital costs** and **high operating efficiency**. TES stores thermal energy either in the form of **sensible heat** (i.e., undergo no change in phase over the temperature range encountered in the storage process), **latent heat** (i.e., use materials known as Phase Change Materials or PCMs that undergo a phase change, for example, from solid to liquid, from liquid to gas or from solid to solid), or **a combination of both forms**, or **in the form of reversible chemical reactions** (i.e., energy is stored in the chemical bonds between the atoms that make up the molecules). To date, **sensible heat materials are the most widely used TES in commercial CSP systems**, while **latent heat or thermochemical materials are still in development**. **TES materials that can withstand high temperatures are costly and difficult to source**. Molten salt, for example, has a **limited operating range** because it **solidifies at low temperatures and decomposes at high temperatures**.

iii Other Flexibility Options

A range of flexibility options, other than storage technologies mentioned above, exist to provide the necessary compensation in situations of excess electricity generation from RE (i.e., negative residual load) as well as situations with RE deficit (i.e., positive residual load) [370].

Downward flexibility compensates the positive residual load with **load shedding** (i.e., switching off the power supply when the demand becomes greater than the supply to reduce consumption) and **thermal power plants** (in particular highly flexible gas turbine). Load shedding has a low response time but can only reduce demand for few peak hours (Figure 1.3). Thermal plants, however, need minutes to hours for response but have an almost unlimited duration time (steel blue in figure 1.3).

Shifting flexibility involves technologies which can be used for **spatial shifting** (i.e., shifting the surplus feed-in of RE to other regions which require **high capacity of the grid lines**), **temporal shifting** such as **Demand Side Management (DSM)** or **Load Shifting** (which consists in reducing the demand in times with high positive residual load and increase it when the residual load is low or negative), and **large or medium-scale energy storage system**, e.g., PHS, CAES, BES (that can be charged with excess electricity during times with negative residual load, and discharged in times with capacity deficits). Load shifting option is usually limited to avoid or minimize a loss of comfort for the consumer, and have lower duration of flexibility provision compared to energy storage and spatial shifting that can transfer larger amounts of

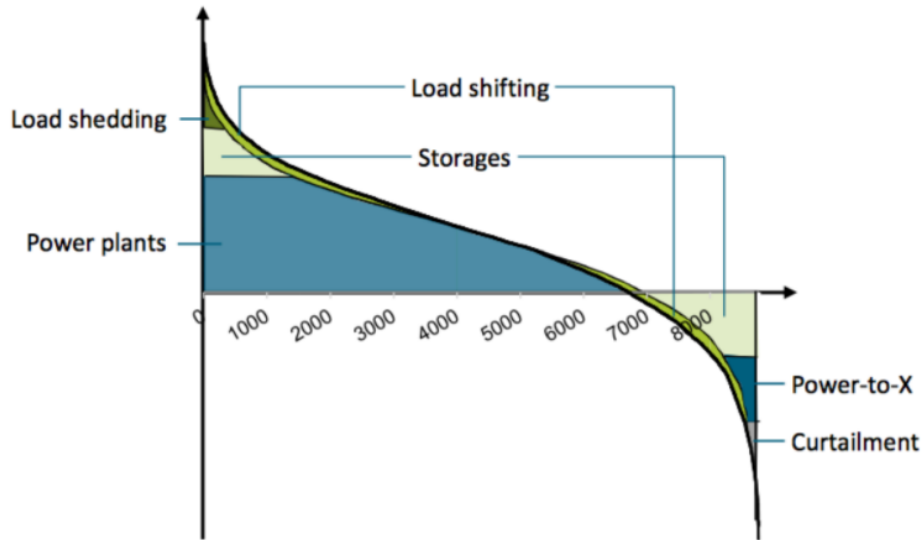


Figure 1.3: Balancing effect of different flexibility options on the Residual Load Duration Curve (RLDC), which displays the residual load (demand minus renewable production), in ordinate, of every single hour of the year, in abscissa (See section X, Chapter 2 for more details on the RLDC definition). Source: Müller et al. [370].

energy over hours or days depending on the storage size and transmission capacity, which helps to understand the small effect of load shifting on the residual load (i.e., it can only balance short-term fluctuations compared to storages) (Figure 1.3).

Upward flexibility reduces the surplus of RE feed-in from RE. To balance this negative residual load, PtX-technologies, curtailment of RE excess production, increasing demand are suitable as well as energy storage systems (Figure 1.3). **Power-to-X (PtX)** technologies can use this excess electricity for further purposes such as heating “**Power-to-Heat**” or gas production “**Power-to-gas**” for fuel cells in electrical mobility, thereby curtailment can be avoided. However, the use of PtX is only profitable if these excess situations occur frequently. Due to curtailment costs, RE curtailment is more costly than activating a PtX or storage systems.

In addition to these flexibility options, it is particularly noteworthy that wind and solar resources become less variable if aggregated across a broader region. The bigger the geographical area linked up by power lines, the more likely the sun is shining or the wind is blowing somewhere within that area. Thus, the variability may be partly smoothed out by aggregating the production from different units of a plant and from sites at different locations (**spatial complementarity**) or by exploiting the **temporal complementarity** between different energy sources in the same location or by exploiting both **the temporal and spatial complementarity**. The benefits of spatial complementarity is assessed for solar PV [336], wind output [298, 294] by for instance exploiting the quick decline in solar resources correlations [178] and wind speed correlations [273, 258] with distance. Some studies have assessed the benefits from the negatively correlated seasonal cycles of wind and solar resources over Europe [353, 223]; or the synergies of wind power in northern Europe and solar power in the MENA region [309, 524, 480]. Impact of complementarity on energy storage is examined for the European [252, 251] and Californian [490] power systems reporting a decrease in storage needs and balancing capacity requirements which increase the grid RE penetration. Instead of evaluating the benefits from complementarity, the majority of studies focus on assessing the spatial and temporal variability of solar resources [231, 91], PV output [146, 409], their implications on smart grid [487] and on the value of solar power in electricity markets [115]. Other focus on wind resources/power [560, 505, 538], or both wind and solar resources/power [119, 545, 496].

3 Concentrated Solar Power vs. Photovoltaic vs. Wind and Thermal vs. Battery Storage

Among the RE sources, wind and solar energy are the most promising source to replace fossil fuels in meeting the world’s future energy needs [324]. Currently, there are two main ways for converting solar energy into electricity: **Solar Photovoltaic (PV)** and **Concentrated Solar Power (CSP)**. However, CSP systems are not the same as PV systems.

The basic working principle of CSP (bottom-left corner of figure 1.4) is that solar irradiance is collected by an optical concentrator—that tracks the sun throughout the day so that the sun’s rays are perpendicular to the surface—and focused onto the receiver where the temperature of the working fluid is increased. The thermal energy produced (heat) by the Solar Field or SF (concentrator + receiver) is then used to operate a Power Block or PB (steam turbine connected to the electrical generator) to produce electricity; or the thermal energy is stored in a Thermal Energy Storage (TES) system for later use. Finally, CSP generates Alternating Current (AC) which can be distributed on the power network [2].

PV systems differ from CSP systems as they do not use the sun’s heat to generate power. Instead, solar PV panels use sunlight through the “photoelectric effect”² to generate Direct electric Current (DC). The DC is then converted to AC, usually with the use of an inverter (top-left corner of figure 1.4), in order to be distributed on the network³ [376]. Thus, unlike CSP, PV systems do not produce or store thermal energy

²PV systems uses the “Photoelectric effect” in which the photons of light are transformed into electrons (electricity) under the effect of light or by thermal agitation (by heating) using a semi-conductor material (i.e., they are not an insulators or conductors means they do not need a large or small energy to move the electrons). When the photons penetrate the semi-conductor, the electron moves which creates an electron-holes. To prevent the recombination so that the electron does not lose its energy by taking its place, a barrier called P-N junction or depletion zone is added by doping (i.e., adding impurities) and injecting an electric field to separate electrons from holes. Zone N “zone with excess of electrons” doped with phosphorus (i.e., the silicon is replaced with atoms that have more electrons), and zone P “zone with a lack of electrons” doped with boron (i.e., the silicon is replaced with atoms that have less electrons). Thus, by connecting each of the two faces of the junction with a conductive wire, the electrons move from N to P thus producing a Direct Current (DC) converted into Alternating Current (AC) by an inverter to be transported to the network.

³The transmission of electricity is done in Direct Current (DC) and Alternating Current (AC), but mainly in AC because the voltage can be easily varied in AC using a transformer, and the electricity is in general transported with high voltage over long distances (so that we use AC to reduce losses).

as they directly generate electricity and the latter cannot be easily stored (e.g., in batteries especially at large power levels). However, in some cases, the excess of DC energy is stored in Battery Energy Storage (BES) to provide electricity when solar irradiance is not available.

Solar PV and CSP with their associated battery and thermal storage system are hereafter referred as PV-BES and CSP-TES.

Wind turbines use the force of wind to turn blades which drives a rotor placed at the nacelle which activates an electrical generator (right panel of figure 1.4). The hub height must be high because the wind at altitude has a strong intensity (i.e., less disturbed by the roughness of the surface) and the temperature of the air decreases at altitude (i.e., the air becomes colder and thus denser). The wind turbines are, in general, installed on the continents (onshore) or along the coast (offshore).

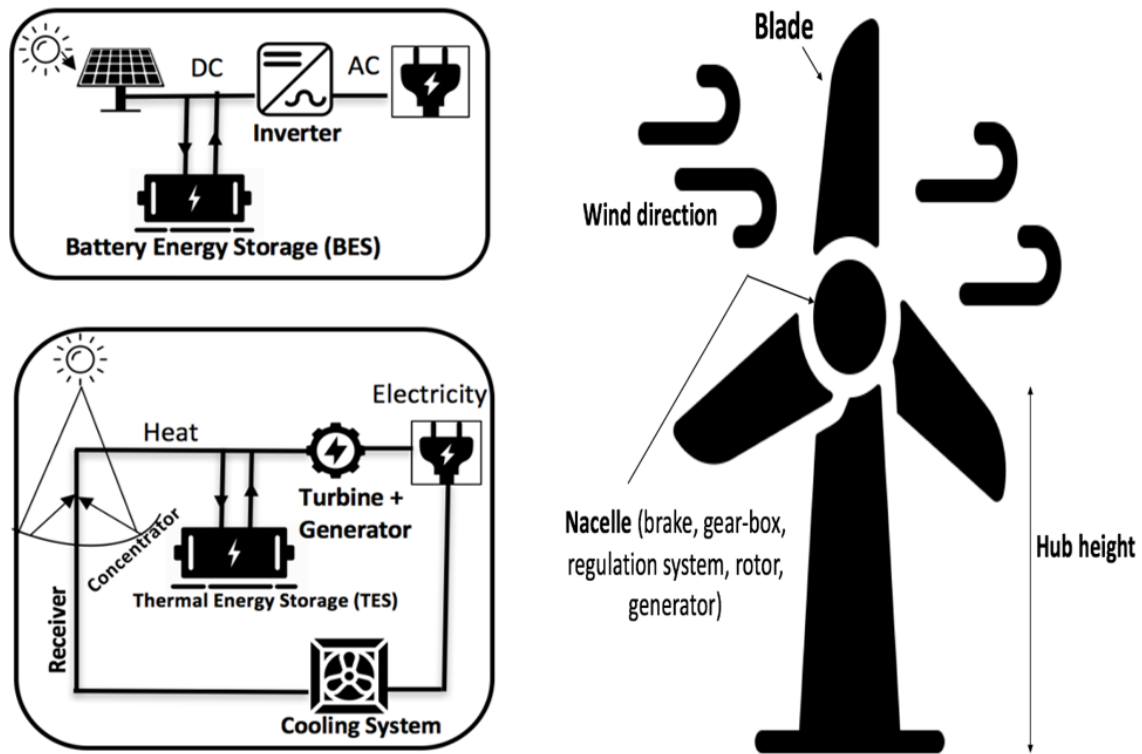


Figure 1.4: **Top-left corner:** The basic working principle of Photovoltaic (PV) where an inverter converts the Direct Energy (DC) provided by the Solar Panels (SPs) or/and by the Battery Energy Storage system to Alternating Current (AC). **Bottom-left corner:** The basic working principle of Parabolic Trough Concentrated Solar Power (CSP) where a Power Block (PB), i.e., steam turbine connected to electrical generator, converts the thermal energy produced by the Solar Field or SF (concentrator and receiver) or/and by the Thermal Energy Storage (TES) system to electricity. **Right:** The basic working principle of wind turbine. Source: Own elaboration.

Currently, CSP, PV and wind are reaching respectively 6.2 GW, 760 GW DC (on- and off-grid) and 743 GW (onshore and offshore) of installed power worldwide in 2020 mainly in Asia, United States (US), Middle East and North Africa (MENA) and Europe driven by policy mechanisms and availability of the resources [447]. Enough PV (resp. CSP) and wind capacities were in operation worldwide, by end 2019, to produce around 2.8% (resp. less than 0.4%) and 5.9% of global electricity generation (Figure 1.2b) [446].

Concerning storage technologies, the global operational energy storage capacity reached 191.1 GW in 2020, reflecting 3.4% growth year-on-year [447]. Pumped storage continued to represent the majority of the installed capacity (Figure 1.2d). Batteries (resp. thermal storage mainly in the form of molten salts) constituted the second (resp. third) largest energy storage technology by capacity, around 14.2 GW with 92% of this battery capacity was lithium-ion batteries (resp. 2.9 GW). Although the global TES capacity is smaller than that of BES, it is almost double that of utility-scale battery storage [446].

A key question moving forward is **how to compare interaction of PV/PV-BES and CSP/CSP-TES in particular prospective mix based on REs? Can Solar and Wind Power Coexist?** While these technologies collect solar irradiance, wind speed and produce electricity, they do so through different (i) mean production, (ii) variability (i.e., risk of not covering the load) and (iii) total cost; which create a challenges for direct comparison and have a great influence in the decision whether PV without/with BES or CSP without/with TES or wind should be employed.

i Mean Production

Solar and wind systems are exploiting different resources. However, although PV and CSP are two solar technologies, but they are collecting different solar resources and therefore have distinct sensitivity to clouds and temperature.

CSP Resource and Production

Because of the optics of concentration, CSP generates electricity by focusing the component of solar irradiance that travels directly from the sun (i.e., the beam irradiance). The diffuse irradiance which is scattered from the ground and the sky cannot be used, making it more sensitive to the presence of atmospheric components which absorb or reflect the sunlight on its way through the atmosphere (left panel of figure 1.5) [178, 536, 232]. The clouds have the strongest impact on the direct irradiance intensity, followed by aerosols (i.e., small solid or liquid particles suspended in the air), water vapour and other gases [132, 181]. The aerosol content of the atmosphere modifies the solar irradiance through different processes: their interaction through scattering and absorption (i.e., direct effect) and their capacity to modify the

micro-physical properties of clouds, acting as cloud condensation nuclei, known as indirect effect. These atmospheric components are low above high mountain ranges, where the atmosphere is both thinner and cooler. However, although in clear day, the influence of the atmospheric components on the attenuation of direct irradiance is stronger for higher zenith angle (i.e., morning, evening or winter) due to the increased air-mass. In fact, the bigger the air mass (i.e., the mass of the atmosphere through which the irradiance actually passes given a certain sun elevation over the mass to be passed if the sun would be at its zenith) to be travelled, the more particles causes scattering. The higher the scattering, the lower is the global irradiance (direct and diffused) received on the earth's surface. On cloudy days, for instance, there is more scattering and absorption due to a high number of particles in the air leading to more diffused and less beam irradiance compared to clear sky conditions. This makes CSP only suited for large capacities (high land requirements) and limits its installation in specific locations with minimum cloud cover, lack of atmospheric humidity and maximum direct irradiance and temperature to increase the CSP efficiency and reduce the cost of the MWh produced [74, 268]. These regions, however, tend to be far away from consumption sites making the transmission grid essential for CSP development, which may increase the grid-related costs. Particularly, suited sites for CSP are distributed along the descending branches of the Hadley cell in the subtropic arid regions [164]) (Figure 1.6c, 1.6d), from the Persian Gulf to the Atlantic Ocean, where air is cold, dry and dense leading to desert climate with little precipitations and clear sky conditions. But not all dry deserts are hot and thus suitable for CSP plants. For instance, Antarctica is under the descending branch of the polar cell and also classified as a desert but not suitable for CSP plants (Figure 1.6c, 1.6d). The resources for CSP in the MENA countries are considered the best—as shown by the studies of the German Aerospace Center [164, 165, 522]—as 45% of the world potential for direct solar energy is concentrated here [425, 435]. Therefore, building solar plants in this region is cheaper than those based on fossil fuels [164]. In addition, the high solar potential covering all MENA region is much larger than the whole electricity demand allowing for self-supply and for export of solar electricity to Europe [165, 523, 524]. Typical regions for CSP also includes South Western US, Australia, Southern Europe, Southern Africa, parts of Latin America, and parts of Asia (Figure 1.6d).

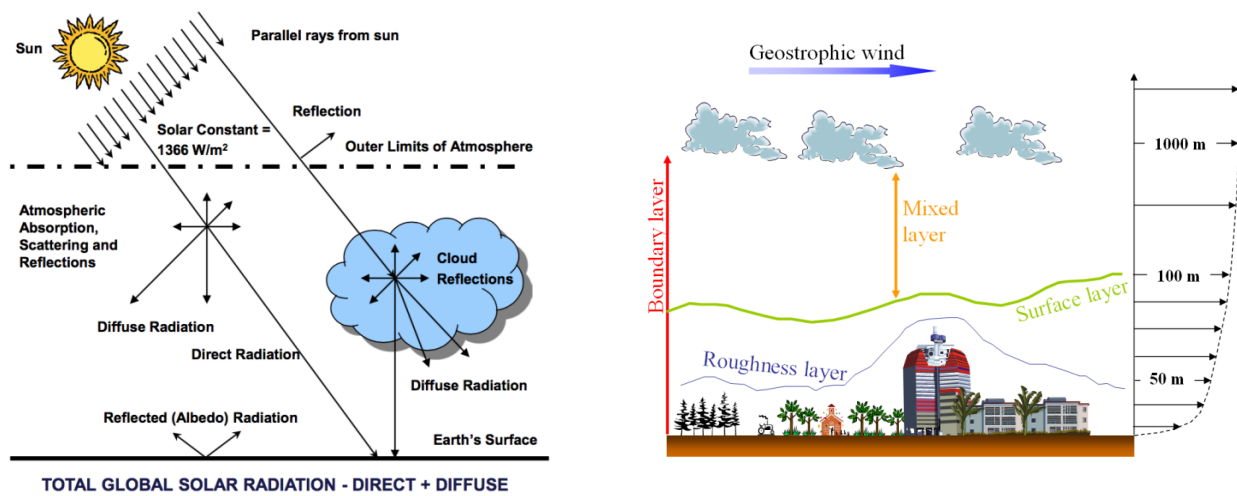


Figure 1.5: **Left:** Schematic of the atmospheric components, which absorb or scatter or reflect the sunlight on its way through the atmosphere, and of the solar irradiance components [178, 536, 232]. **Right:** Schematic of the vertical profile of the horizontal wind speed [363, 228].

PV Resource and Production

On the contrary, PV uses both direct and diffuse solar irradiance, namely the global solar irradiance (left panel of figure 1.5), so its average production tends to be less variable compared to CSP. In fact, beam irradiance can decrease close down to 0 W/m² due to clouds, in contrast to global irradiance that is always substantially greater than 0 W/m² due to its diffuse fraction. PV is less sensitive to clouds than CSP, but low irradiance intensity and high temperature—compared to standard levels, i.e., 1000 W/m² and 25°C—reduce the conversion of the PV panels [327, 438]. Changes in surface wind velocity also affect the mean PV production [276, 404, 405], but they can also cool down the modules, increasing efficiency and output [122]. For PV, regions with high global irradiance are mainly in the equatorial and tropical regions (from 0 to 35° latitude) (Figure 1.6a) where the meridional flow is dominated by the Hadley cell with warm and wet air rising around the equator which increase the probability of scattering the solar beams; and cold and dry air sinking about 35° latitude responsible for the air to be drier preventing the condensation, thus reducing the probability of scattering solar beams. This explain why the equatorial sky is obscured by clouds and strong nebulosity is occurring during most part of the year [417, 245]; to the contrary the sky is relatively clear above the high pressure tropical bands where major deserts are located. As consequence, the global irradiance is weak near the equator but with strong diffuse component; and it is stronger around the tropics dominated by the direct component. Overall, global irradiance remains generally high throughout the year over the entire African continent [417], in the Mediterranean and Middle East Regions [237] (Figure 1.6a). Some tropical regions near the mid-latitude regions receive on average less light but also have high solar resources (Figure 1.6a) due to their strong monsoon-related seasonality [439, 565]. Global irradiance is weak over mid-latitudes, sub-polar and polar regions, from 35° to 90° latitude (Figure 1.6a), where the temperature contrast between the tropics and the poles causes tropical cyclones (storms) to form, favoring the baroclinic instability. These weather disturbances increase the solar resource variability. The distribution of the global irradiance (Figure 1.6a) often counteracts the distribution of the temperature and the latter explains why some regions with the same irradiance differ in their PV production (compare figure 1.6a and figure 1.6b) which also impact the economical potential (i.e., cost of MWh produced). For instance, places with low irradiance may benefit from cooler temperature, and conversely, regions with high solar resources may hinder the PV power output due to the high temperature. As a result, global solar irradiance is available anywhere to greater or lesser extent (Figure 1.6a) and countries with lower solar resource availability, the PV production is not dramatically lower compared to countries boasting excellent conditions for PV or countries in favorable middle range (Figure 1.6b) [90]. Thus, unlike CSP, PV systems can be installed everywhere, from distributed or "decentralized" (i.e., off-grid applications such as for residential or pumping water for irrigation) to "centralized" plants (i.e., grid connected applications), and are therefore accessing a larger market than CSP [447] due also to its technological simplicity as PV revolves around solar cells while CSP plants

are a combination of many critical mechanical and chemical components.

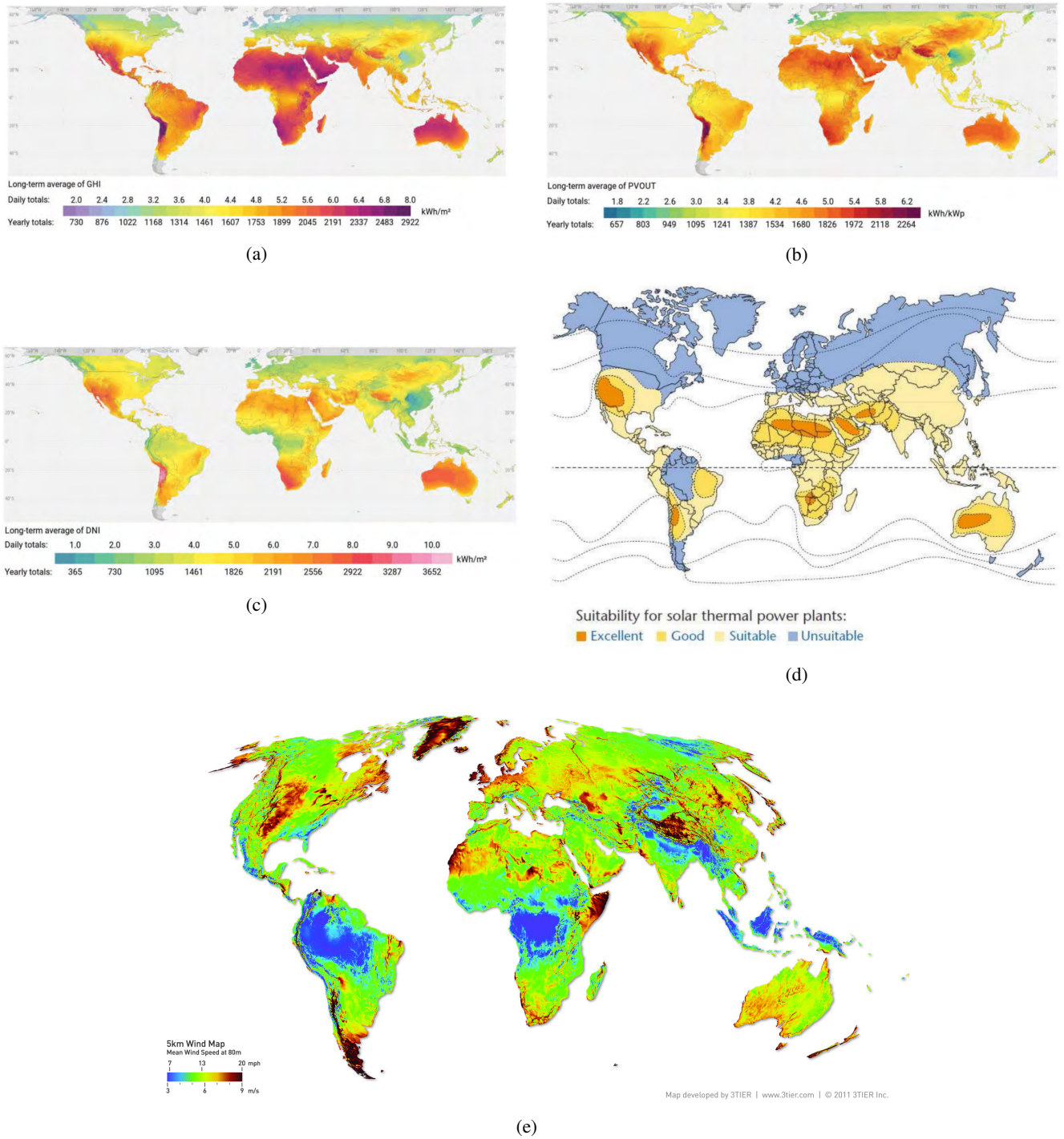


Figure 1.6: (a): Map of theoretical potential of Photovoltaic (PV), i.e., distribution of Global Horizontal Irradiance (GHI) referred as global (direct + diffuse) irradiance for horizontal surfaces [90]. To be compared with figure 1.6b. (b): Map of practical or technical potential simulating the conversion of the available GHI to electric power considering the factors affecting the PV performance as well as land use constraints [90]. (c): Map of theoretical potential of Concentrated Solar Power (CSP), i.e., distribution of Direct Normal Irradiance (DNI) [90] referred as the amount of solar irradiance received per unit area by a surface that is always held perpendicular (or normal) to the rays that come in a straight line from the direction of the sun. To be compared with figure 1.6d. (d): Map of suitable locations of solar CSP plants, where four zones can be distinguished depending on their potential for recording DNI [480]. (e): Global mean wind speed at 80 m (Map developed by 3TIER) [15]. The darker the color, the higher the solar irradiance or wind speed and consequently the energy output, and the more appropriate is the region for PV, CSP or wind.

CSP and PV Seasonality

The average annual of solar resource required by PV or CSP are not sufficient metric for comparing the performance of each technology. The seasonal variability of solar PV and CSP production is also important to maximize their operation [225, 567] as it characterizes the variability of the resource throughout the year and its correlation with the seasonal electricity demand. High solar potential countries tend to have low seasonality in solar output, meaning that the resource is relatively constant between different months of the year (i.e., seasonality index close to 1, a ratio between the highest and the lowest average monthly potential value in an average year). A moderate seasonal effect of solar

generation can be in natural synergy with seasonal demand. For instance, in generally dry and warm regions where cooling is the primary challenge, CSP has an advantage over PV as it can provide sufficient energy due to its performances at high temperature levels because, unlike PV, the efficiency of the CSP steam cycle's thermodynamic conversion to electricity increases with increasing temperature [141]. On the contrary, high seasonality challenges the countries in the higher latitudes, where the highest demand for energy is during cold winters, and where the angle of solar irradiance is smaller, causing energy to be spread over a larger area of the surface which reduces its intensity.

CSP and PV Climate Change Induced Impacts (Resource, Generation and Seasonality)

This strong dependence of PV and CSP on climate means that although these solar technologies play an important role in climate change mitigation and in accelerating the energy transition [169], they are themselves subject to positive or negative climate change impacts [141] through the changes in the temperature and the surface downwelling shortwave irradiance by changing the atmospheric water vapor content, cloudiness, aerosols and even cloud characteristics (i.e., increase or decrease of the volume of cloud condensation nuclei) that affect the atmospheric transmissivity [143] as known by the "dimming and brightening" phenomena (periods and regions with prevailing declines and inclines in surface solar irradiance) [369, 548, 549]. Other factors affect the amount of solar irradiance received by the earth before reaching the surface of the earth and being used by solar plants. In fact, these oscillations are related to the Milankowitch astronomical cycle and occur due to the earth-sun distance during the year resulting from the eccentricity of the earth's orbit around the sun, the precession of the earth's rotation axis, and the tilting of earth's rotation axis from the plane of its orbit [178]. These astronomical factors will significantly affect the earth's climatic patterns [88]. Due to uncertainty in projections related to future emissions (scenario uncertainty), internal climate variability and inter-model differences (e.g., atmospheric parametrization), a few studies so far used climate model projections to estimate multi-decadal changes in solar resources under climate change and its consequences on solar generation [206, 408]. We note different trends in incoming solar irradiance around the world. A negative impacts in Canada [143] and most of the African continent [261, 94, 551]; while an increase trend is reported over the Middle East [181], the United Kingdom (UK) [118]; Europe [78, 261], with higher values in the Mediterranean regions [415]. Overall, climate change projections tend to agree that except high latitude regions, cloud cover will decrease in low- to mid-latitude regions [520, 405] and are projected to become less cloudy and drier [341]. This is consistent with observed trends [521]. Some studies investigate the long term changes in the seasonality of the solar resource expecting variable changes (e.g., Western US [248, 231]), an increase (e.g., southern regions of UK [118]) or a decrease (e.g., US [399]) in seasonal variability. An increase in solar irradiance may be advantageous for CSP and PV but this rising solar irradiance will often be counterbalanced by decreasing PV efficiency due to rising temperatures [196, 433]. As such, existing studies tend to project changes in solar PV generation and only few in CSP output (Ref [550, 141] by the end of the century. For instance, Crook et al. [141] studied the global impact of climate changes on PV and CSP outputs—using model-derived climate projections through 2100—considering the air temperature and wind effects. It was found that solar PV output is generally declining in future scenarios worldwide (i.e., Western US, Saudi Arabia ...) except over a few areas in Europe (also in [551]), China and the Mediterranean region where the increase in solar irradiance—due to the decrease of cloud cover—is expected to overpass the temperature effect [217, 400]. Also, according to this study, Europe would be the biggest winner in terms of CSP with an increase of more than 10% in output. China, Algeria and Australia will also experience an increase in CSP output, whereas the western US and Saudi Arabia can expect a decline. Some studies found different results for Europe [516, 276] considering that, despite a positive trend in irradiance, expected changes in wind speed and temperature result in a decline in the PV generation. This result is also seen in another study [207], which projects a decline in PV production in Eastern Europe and Northern Africa, and an increase in Western Europe and the Eastern Mediterranean. The trend projected by Ref. [83] points to a decrease in PV output in Western Africa. In Western US, one study reports also a decrease in PV production [80] but only considers changes in air temperature, not irradiance. The results of Ref. [550] indicate a potential for future increase in CSP production in many parts of the globe, with a few exceptions such as the North of India and the polar areas. Overall, these studies are not easy to compare as the conclusions are often focused on specific areas of the world and cover different time frames, scenarios and climate parameters.

In addition to atmospheric components and temperature effects, other challenges still prevail and jeopardize the adoption of PV and CSP in current and future warming climate. For instance, typical regions with high solar resources and little rainfall are linked to lack of water and high dust deposition [122], which can seriously impact the performance of PV and CSP [327, 441, 145], especially in humid conditions [361]. In fact, thermal CSP plants are integrated with conventional steam Rankine cycle for power generation requiring an increased water use for cooling to condense exhaust steam from the turbines; the lower the efficiency, the higher the cooling needs. As water resources are often scarce in Sun Belt regions, in addition to the water scarcity due to climate change that will limit the potential water intakes (thus limiting their output [125, 563]), dry (air) cooling towers are often needed for CSP installations. In general, dry cooling towers are more expensive and less efficient than wet towers. The lower the condensation temperature is, the higher the conversion efficiency of the power block becomes. Wet cooling can provide higher conversion efficiency than dry cooling because the exhaust steam with wet cooling can be cooled faster to a lower temperature. So that a CSP plant with wet cooling can offer better thermal performance. On the other hand, dry cooling needs a bigger solar field than that for wet cooling with the same power output, and it results in higher investment costs. As a consequence, a trade-off between all the cooling options should be made for each specific site to know whether to use dry cooling or not. PV makes limited use of water as it does not use it for cooling but requires, as CSP, frequent cleaning to increase the efficiency [327].

PV and CSP Technologies

The sensitivity of PV and CSP to these elements (temperature, clouds, water use, dust deposition) depends on the PV and CSP technology used and on the orientation or the integration of tracking; which impact the mean Capacity Factor (CF), the prolongation of daily production after sunset or on cloudy days when there is little solar production but plenty of demand for power, the seasonal correlation with demand, and the capacity to install and thus the total cost.

In fact, just from 1970 to 2021, **the solar PV and CSP technology has been improved, the costs have been decreased and solar plants are now easier to finance**. The reference [38] highlights **the historical development of solar technology**, century by century, and year by year.

For several years, PV remained developed in the field of **space industry** (e.g., measuring devices that run on solar energy)—given the extremely high cost of solar cells in silicon—before the idea of **ground-mounted PV** or installing them on the **roof-top**. The cells were mainly based on **silicon**, then **a progress has been made** to achieve a **maximum solar-to-electricity efficiency** at **low cost** by developing new cells—manufactured in many different ways and from different materials [407, 269].

"Crystalline silicon (c-Si)" is the **most used semi-conducting material in PV panels**, occupying more than **90% of the global market**. The first commercially available solar cells were made from **"monocrystalline silicon"** which are **highly efficient**, but their **manufacturing**

process is slow and labor intensive, making them more expensive than their polycrystalline or thin film counterparts (top panel of figure 1.7). A "polycrystalline silicon" cells are cheaper but less efficient alternative.

Although crystalline PV cells dominate the PV market, cells can also be made from "thin film". One type of thin film PV cell is "amorphous silicon (a-Si)". The result is a very thin and flexible cell which uses less than 1% of the silicon needed for a crystalline cell. Due to this reduction in raw material and a less energy intensive manufacturing process, amorphous silicon cells are much cheaper to produce. Their efficiency, however, is greatly reduced because the silicon atoms are much less ordered than in their crystalline forms. These cells also suffer from a 20% drop in efficiency within the first few months of operation before stabilizing (i.e., Light-Induced Degradation or LID which is the initial degradation occurring due to defects that are activated on initial exposure to light) and are therefore sold with power ratings based on their degraded output. They are suitable for applications where low cost is more important than efficiency. Other types of thin film cells include "Copper Indium Gallium Selenide (CIGS)" and "Cadmium Telluride (CdTe)". These cell technologies offer higher efficiencies than amorphous silicon but contain rare and toxic elements including cadmium which requires extra precautions during manufacture and eventual recycling. The CIGS solar cells are turning out to be the more promising high efficiency and economic options for both residential and commercial installations.

"Gallium Arsenide (GaAs)" is an alternative semi-conductor which is highly suitable for PV applications. It has a similar crystal structure to that of monocrystalline silicon, but with alternating gallium and arsenic atoms. Due to its higher light absorption coefficient and wider band gap, GaAs cells are much more efficient than those made of silicon. Additionally, GaAs cells can operate at much higher temperatures without considerable performance degradation, making them suitable for Concentrating Photovoltaic (CPV). GaAs cells have higher material and manufacturing costs which currently prohibit widespread commercial use compared to silicon cells, making them useful only when high efficiency is needed, such as space applications.

Most PV cells, including those discussed above, contain only one p-n junction of semi-conductor material which converts energy from one discreet portion of the solar spectrum into useful electricity. "Multi-junction cells" have two or more junctions layered on top of each other, allowing energy to be collected from multiple portions of the spectrum. Light that is not absorbed by the first layer will travel through and interact with subsequent layers. Multi-junction cells are produced in the same way as GaAs cells, slowly depositing layers of material onto a single crystal base, making them very expensive to produce, and only commercially viable in CPV and space applications.

There is also an assortment of emerging PV cell technologies which include "Perovskite cells", named after their specific crystal structure. They can be produced from organic compounds of lead and elements such as chlorine, bromine or iodine. They are relatively cheap to produce, have an excellent light absorption property under low and diffuse light, and can boast efficiencies close to those of commercially available silicon cells but they are currently limited by a short lifespan. "Organic solar cells" consist of layers of polymers and can be produced cheaply at high volumes. These cells can be produced as a semi-transparent film but suffer from relatively low efficiencies. "Dye-sensitized solar cells" can be produced using semi-conducting titanium dioxide and a layer of "sensitizer" dye. These cells boast modest efficiencies but cannot withstand bright sunlight without degrading. "Quantum dots" which use nanotechnology to manipulate semi-conducting materials at extremely small scales. "Nanoparticles" consisting of small number of atoms can be tuned to different parts of the solar spectrum according to their size to absorb a wide range of energy. Although theoretical efficiencies are extremely high, laboratory test efficiencies are still very low.

In 2019, the top PV markets were China, the European Union, the United States and Honduras with the highest PV penetration level by far [265].

CSP has a long history going back to the late 1800s, when it was used to light the fires of the ancient olympic games and then of solar ovens. The first parabolic trough systems was installed in 1912, near Cairo, Egypt. The system was designed to generate steam for a pump of water for irrigation. Despite its origins in the MENA region, the US research budget for CSP tripled after the 1973 oil crisis and led to the construction of the first commercial parabolic trough CSP plant with no thermal storage in 1983 in California (US), the Solar Energy Generating Systems-SEGS- with 354 MW. But as oil prices decline in the 1980s, the sector stagnated until the 2000s. At this time, a second generation of commercial CSP plants was built, predominantly in the US and Spain, due to the series of incentives to mitigate CO₂ emissions and diversify the energy supply offered by policy makers [75]. Currently, Spain, US, MENA as well as India and China accounted for almost the majority of the world's CSP capacity. Among the larger CSP projects are the Ivanpah solar tower plant without TES (392 MW) in California (US), and the Ouarzazate (Morocco) solar plant which combines parabolic trough and solar tower technologies for a total of 510 MW with several hours of thermal storage.

Four commonly used types of CSP technologies are: Parabolic Trough (PT), Linear Fresnel (LF), Solar Tower (ST) and Dish Stirling (DS) (bottom panel of figure 1.7). PT and LF are line-focused technologies, focusing the sunlight to a line of receivers typically oriented in the North-South (N-S) or East-West (E-W) direction, and reach a maximum operating temperatures between 300 – 550°; whereas ST and DS are point-focused technologies, focusing the sunlight to a point where the receiver is located and can reach higher temperature because they have higher concentration factor (i.e., the ratio between the area of sunlight collected and area of the solar receiver onto which it is focused).

Currently, PT is the most mature and dominant CSP technology. It occupies more than 80% of the global CSP installations. However, most recent CSP installations are ST systems due to the potential enhancement in efficiency of converting heat into electricity and its suitability for achieving very high temperatures. The only disadvantage of ST is that the initial installation cost is high compared to other CSP technologies. LF and DS are less mature. The main advantage of DS systems includes modularity which is suitable for distributed generation. In addition, unlike other CSP options (PT, LF, ST), DS systems do not need cooling systems for the exhaust heat. This makes SDs suitable for use in water-constrained regions.

Heat Transfer Fluid (HTF) is an essential component of a CSP plant as it transfers heat concentrated by the receiver to steam generator. Currently, different types of HTFs are used in commercial CSP plants, including air, water or steam, thermal oils, organics and molten salts.

CSP plants are designed for electricity generation, but they also produce high temperature heat that can be used for industrial heating, water desalination, production of synthetic fuels (syngas), enhanced oil recovery (as the steam it produces can be used to concentrate heavy oil, so it is easier to pump) and refineries. There are also the Integrated Solar Combined Cycle (ISCC) which combines troughs and conventional fossil fuel heat systems.

Effect of Tilt Angle and Tracking

It is worthwhile mentioning that tracking systems are commonly used with CSP because it collects the direct solar irradiance; while PV panels are typically mounted at a fixed orientation [327].

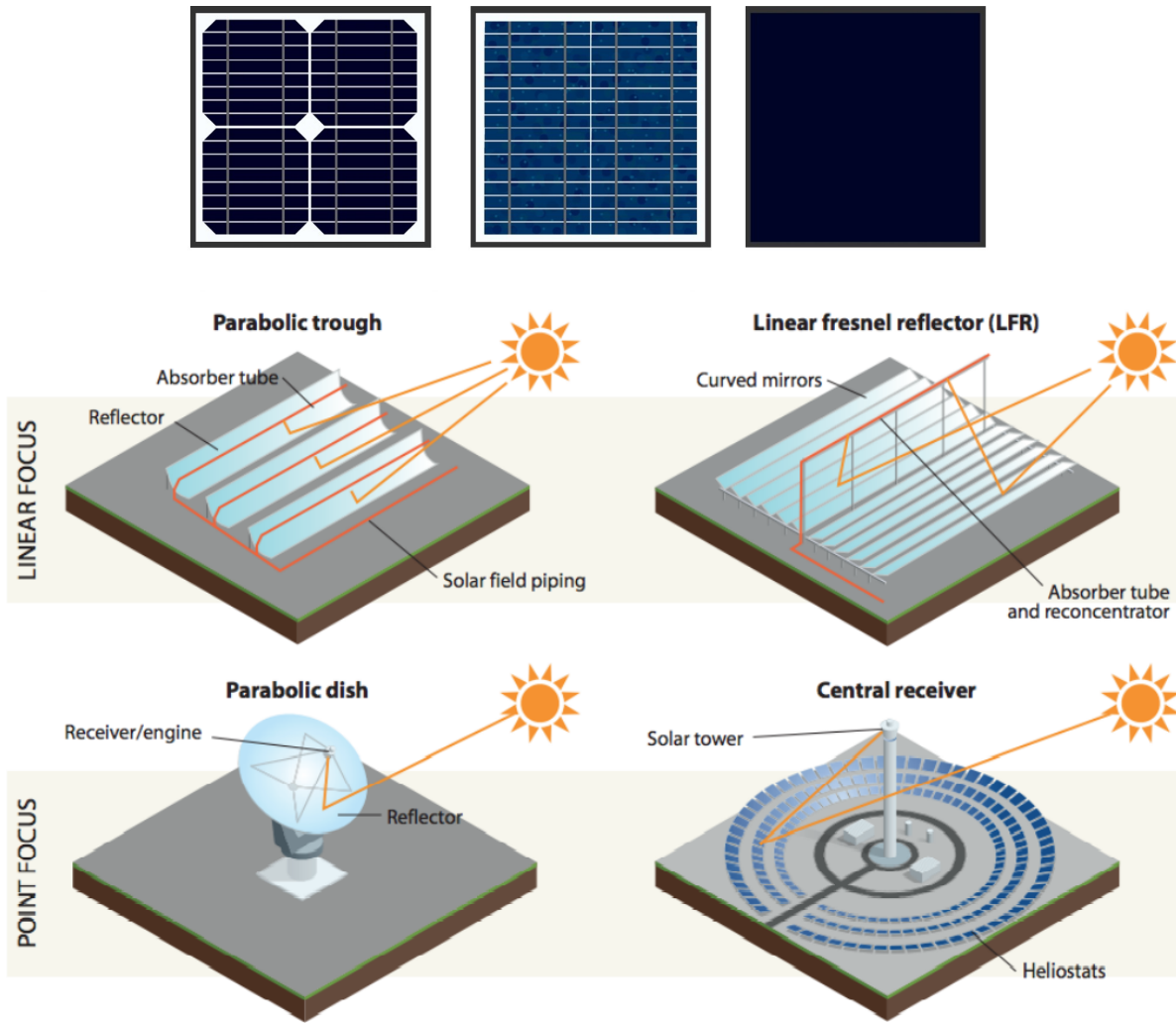


Figure 1.7: **Top:** Solar Photovoltaic (PV) technologies: Monocrystalline (left); Polycrystalline (middle) and thin film (right) [17]. **Middle and Bottom:** Solar Concentrated Solar Power (CSP) technologies [75]: Parabolic Trough (PT) and Linear Fresnel (LF) reflector are line-focused technologies, focusing the sunlight to a line of receivers; Solar Tower (ST) or Central Receiver (CR) and Parabolic Dish Stirling (DS) are point-focused technologies, focusing the sunlight to a point where the receiver is located.

For a fixed orientation, the maximum power over the course of a year is obtained when the **tilt angle is equal to the latitude of the location**. However, **the tilt and the orientation are in general optimized for each PV panel according to the location (i.e., latitude)**. The figure 1.8 shows—for latitude equal to 0° (left), 30° (middle) and 60° (right)—that **the tilt angle has a major impact on the seasonal solar irradiance incident on a surface**. As can be seen, for a module with a tilt angle of 0° (horizontal surface in blue), the irradiance increases in summer for high latitudes (30° and 60°) but less at the equator (latitude $=0^\circ$). However, more the tilt increases, more the irradiance decreases in the summer and winter solstices, and tends to have two maximum in the vernal and autumnal equinoxes (which also decrease with the increase of the tilt), whatever the latitude of the northern hemisphere. Overall, steeper tilt angles are preferred in the equinoxes, while lower tilt angles use a greater fraction of light in the summer [36].

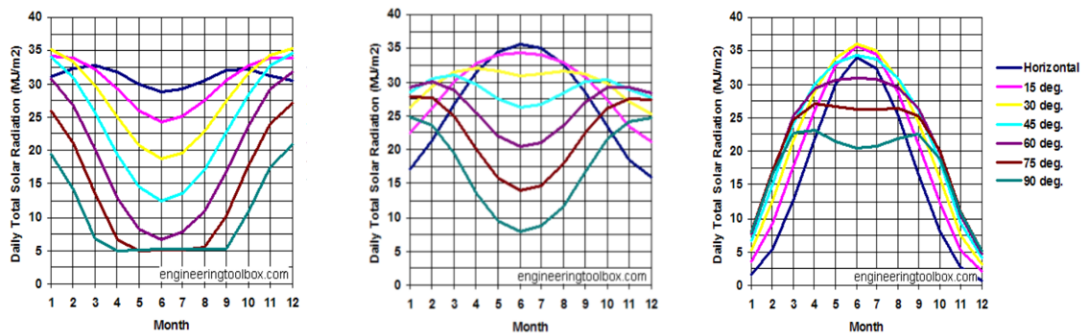


Figure 1.8: Daily total solar irradiance variation throughout the year on south faced horizontal to vertical surfaces (tilt = 0° - 90°) on the northern hemisphere latitude 0° (left), 30° (middle) and 60° (right). Source: The Engineering ToolBox [36].

Figure 1.9 presents the daily mean of the irradiance at the top of the atmosphere for a surface located at latitude 45° oriented towards the south and whose tilt is equal to 0° (horizontal), 45° and 90° (vertical). As can be seen, the daily mean irradiance received by a vertical surface

is the same than that received on a horizontal surface during winter, but is much lower during summertime. The same surface, but now inclined at 45° , receives more (resp. less) irradiance than the horizontal and vertical surfaces in winter (resp. summer).

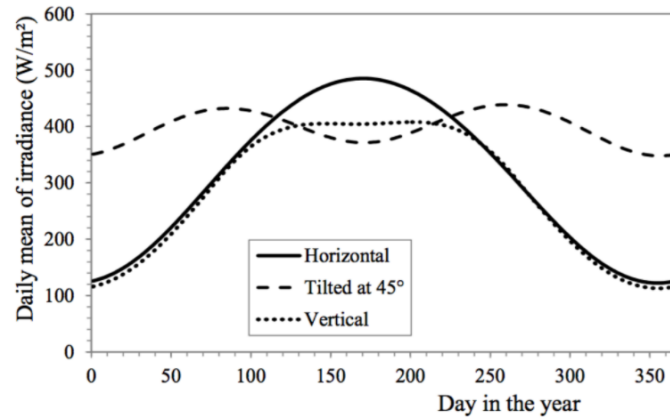


Figure 1.9: Daily mean of irradiance, collected on a surface located at latitude 45° at the top of the atmosphere, as a function of the day in the year, when the surface is horizontal (tilt = 0°), tilted at 45° and vertical (tilt = 90°) facing south. Source: Wald et al. [537].

Since low sun angles limit the solar irradiance incident on a surface due to the high zenith angle occurring during winter or during dawn or dusk, tracking system must be installed to reduce these losses and increase the average total annual irradiance (as the tracking system follows the sun as it moves across the sky). In fact, the maximum amount of irradiance is collected when a CSP collector or PV panel points directly toward the sun, and hence the angle of incidence (i.e., the angle between the beam irradiance on the surface and the normal of the surface) is zero. If the surface can be **tracked about two independent axes**, the angle of incidence can be maintained at zero throughout the day. However, **the horizontal single tracking axis is the most common configuration** that can be aligned on a **North-South (N-S) or East-West (E-W) orientation** depending on the electricity demand profile [498]. For instance, **E-W orientation is usually chosen if the demand is constant over the year because the seasonal irradiance variance is smaller for E-W tracking than for N-S orientation** (left panel of figure 1.10). However, N-S tracking may be an advantage for locations with higher summer peak demand than in the winter because **the day's solar irradiance received by a N-S single-axis tracking surface, in summer, is quite even over the day allowing to compensate the cosine losses occurring more at noon than in the morning and afternoon, whereas the amount of energy received by the surface oriented in the E-W direction is only high at noon, but less during sunrise and sunset hours. In winter, E-W tends to be more uniform throughout the day compared to N-S that is performant only during sunrise and sunset hours**. This can be seen in the right panel of figure 1.10 that shows the extraterrestrial irradiance on surfaces that track the sun about a horizontal N-S and E-W axis, and also on a fixed surface with slope equal to the latitude, 45° , at the summer (three solid curves) and winter (three dotted curves) solstices. Overall, it is clear that tracking can significantly change the time distribution of incident beam irradiance at noon and during sunrise and sunset (i.e., the production starts earlier in the day and ends later, particularly in summer). However, tracking does not always result in increased beam irradiance (compare the winter solstice irradiance on the N-S tracking surface with the irradiance on the fixed surface, at noon). In practice the differences will be less than indicated in the figure due to clouds and atmospheric transmission. **For fixed-tilted PV, the irradiance is higher towards the winter solstices and lower towards summer, at noon and during sunrise and sunset hours, because the incidence angle, at noon and during sunrise and sunset hours, is higher in the summer than in the winter** (right panels of figure 1.11) due to the wider sun path; although the solar height is higher in the summer than in the winter (left panels of figure 1.11); and although days become longer than nights, in summer, in northern hemisphere.

Wind Resource and Production

When it comes to wind systems, their production is affected by air temperature because colder air is more dense and therefore more effective at producing wind power [428, 429]. As a result, wind power is affected seasonally (more output in winter than summer) and by daily temperature variations [122, 124]. Wind output is also highly dependent on wind speed and a small change of the latter can have substantial impact on wind output (wind output is the cube of wind speed [335]); as turbines cannot operate in very low or extreme stormy winds [122, 41]. In fact, wind power production is a nonlinear function of hub-height wind speed, with no electricity generation below wind speeds of a few m/s, a saturation at nominal wind speed (typically 10-15 m/s). To protect wind turbines, production is usually cut beyond a threshold of about 25 m/s (the right panel of figure A.1, Appendix A). Wind speed is essentially affected in the lower part of the troposphere, particularly in the surface layer of the "Atmospheric Boundary Layer" (right panel of figure 1.5) [363, 228], where it displays rapid fluctuations strongly linked to the interaction of the flow with the surface friction or the "roughness" [180, 325]. The latter induces high vertical shear of the flow and thus generates micro-scale circulations (turbulence). As a result, winds over oceans are much stronger than over land due to the low roughness of the sea and due to the generation of regular sea-breezes [420] such as in the Red Sea, the Atlantic Ocean [164, 111] and over the Northwestern part of the Mediterranean Sea (the Gulf of Lions) [209, 392, 390]. Land surfaces are rougher as a result of their mountains, forests, and even buildings. All of these topographic features of the land slow down winds significantly over continent.

Overall, many parts of the world have high average wind speeds. However, this is usually not evenly distributed (Figure 1.6e), means some locations experience much stronger winds than others due to the unevenly heating of the earth's surface by the sun. For example, regions near the equator are characterized by low winds, while mid-latitudes experience much faster airflow. Due to the difference in temperature between polar and tropical regions, there are different atmospheric mechanisms that control synoptic scale variability of wind and impact the wind direction, its strength, and the energy density [226, 260]. For instance, in the mid-latitudes, the dominant patterns are driven by the storm track occurring as sequences of low pressure (cyclones) and high pressure (anticyclones) systems leading to higher average wind speeds in several areas [279].

In future decades, several studies using regional or global climate projections show that the wind speeds is likely to undergo a decrease in Southern Europe [518, 263]; and in the western Mediterranean region [263, 517] due to the poleward shift of the Hadley cell leading to

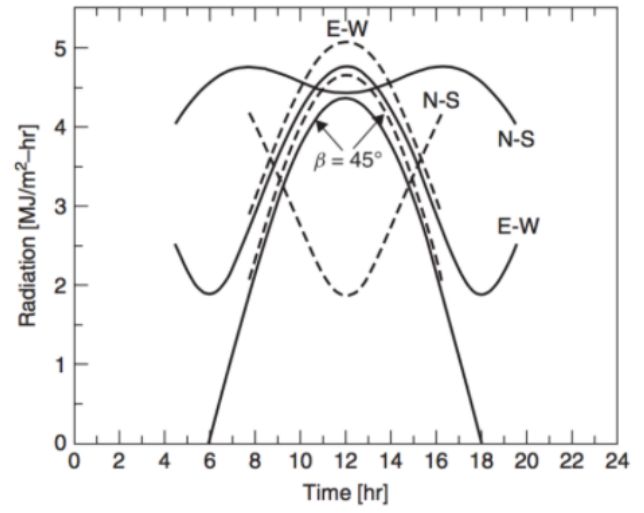
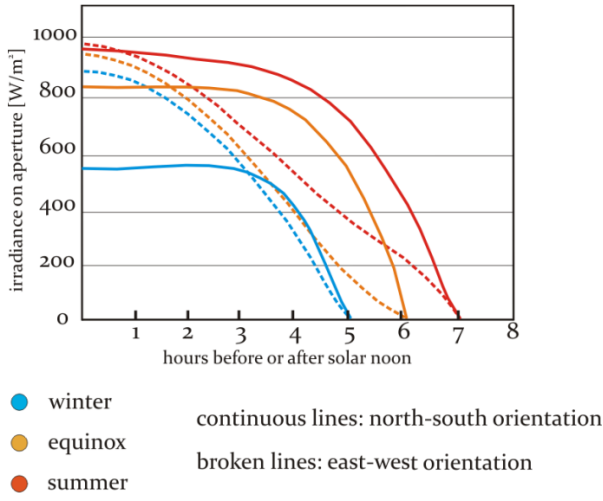


Figure 1.10: **Left:** Irradiance on the surface over the day in different seasons (winter, equinox, summer) at North-South or N-S (continuous lines) and East-West or E-W (broken lines) oriented parabolic troughs [2]. Low seasonal irradiance variance is observed for E-W tracking than for N-S orientation. **Right:** Extraterrestrial solar irradiance, for latitude equal to 45° , on a surface slope equal to 45° , on North-South or N-S and on East-West or E-W single-axis tracking surfaces. The three dotted curves are for the winter solstice and the three solid curves are for the summer solstice [178]. During sunrise and sunset hours, N-S tracking tends to be more performant than E-W tracking which is more performant than fixed orientation, whatever the season. However, at noon, E-W tracking is more performant than N-S tracking and fixed orientation; but the performance between N-S tracking and fixed orientation depends on the season, i.e., N-S (resp. fixed orientation) is more performant than fixed orientation (resp. N-S) in summer (resp. winter). Overall, fixed-tilted orientation and E-W tracking are (resp. N-S tracking is) more performant in winter (resp. summer) than in summer (resp. winter).

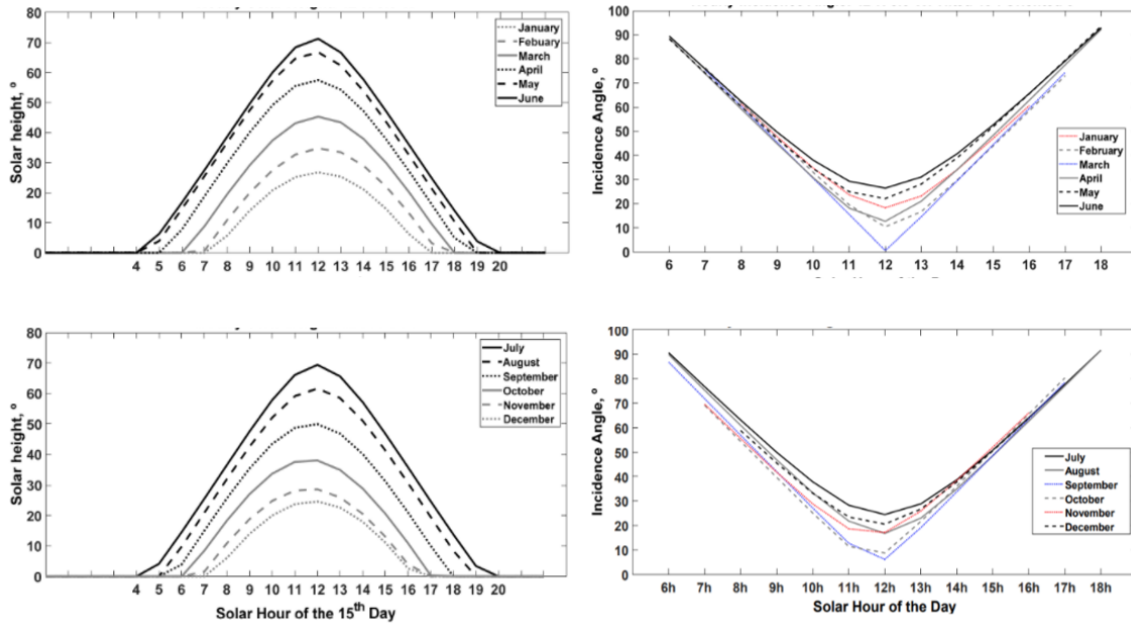


Figure 1.11: Hourly solar height (**left**) and hourly incidence angle with tilt = 45° and oriented 0° (**right**), calculated at latitude 42° N and longitude 5.6° W, for the 15th day of each month: January to June (**top**); July to December (**bottom**). Source: Diez et al. [163].

reduction in wind production [77, 207]. The surface wind speed declines remain, however, moderate in the Mediterranean region by the mid-century (generally of the order of a few percent). Overall, a 2°C warming does not systematically lead to higher change magnitudes in the wind resources than 1.5°C , while 3°C warming leads to stronger changes [516, 489]. Projections for Southern Africa point to almost no change in wind speed, with some seasonal variations [192]. By contrast, wind speeds are consistently projected to increase in Northern and Central Europe [517, 518, 539]. Projected seasonality, however, seems to change depending on the model and area.

Thermo-Sensitivity of Energy Demand

In future warming climate, the consequence of a change in the seasonal patterns of wind and solar PV and CSP would be judged in the context of any concurrent changes in demand patterns. For instance, an increase in output in winter would be advantageous if electric heating were to become more prevalent, whilst a decrease in summer output would be detrimental if air-conditioning were more used. The change in energy demand for heating and cooling in the 21st century associated with climate change depends on local climate via mainly the distribution of temperature, namely "the thermo-sensitivity of energy consumption" defined as the change in energy consumption associated with a unit

change in the temperature [397, 364, 254]. In fact, the relationship between demand and temperature is nonlinear (Figure 1.12): Electric heating system is only switched on for lower temperatures (high energy demand for heating), while air-conditioning system is only switched on for higher temperatures (high energy demand for cooling). Once an individual appliance is switched on, its electricity consumption is to a first approximation linear to temperature, which varies according to growth of population, income and level of technological development of the country (e.g., efficiency of appliances, thermal isolation in buildings, standard of living, etc). Thus, the demand-temperature has two branches marking the heating and cooling threshold temperatures (i.e., the temperature below and above which it is considered that a variation of the temperature causes a variation of the consumption). Intermediate temperatures correspond to lower energy demand. This U-shaped temperature dependence pattern may vary regionally and seasonally. However, it should be noted that the demand response is asymmetric,

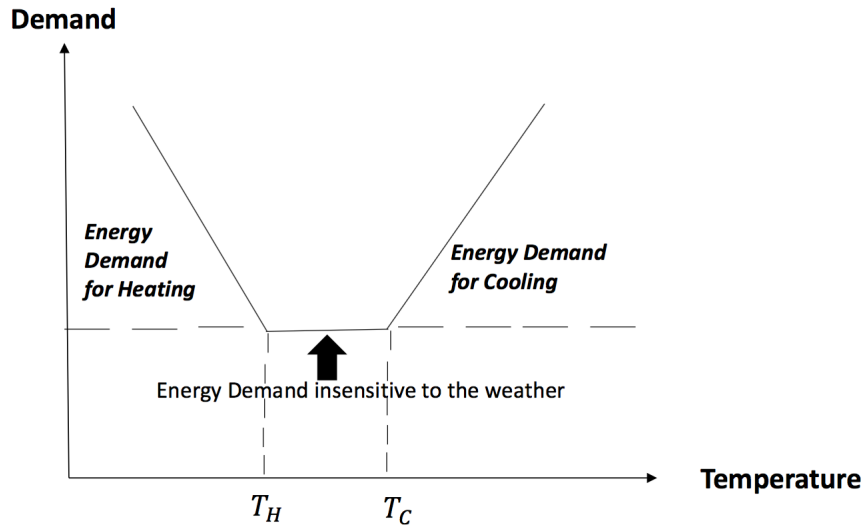


Figure 1.12: Variation of energy demand according to temperature variation. T_H (resp. T_C) is the threshold temperature below (resp. above) which the consumer switches the heating (resp. air-conditioning) system. Source: Own elaboration based on [397]

means $1^\circ C$ more when it is hot and $1^\circ C$ less when it is cold does not have the same impact on the load. The graphic representation of demand indicates that, on the ascending part, an increase in benefits and, on the descending part, a reduction in benefits and an increase in losses. This is owing to the fact that, in the ascending part of the curve, the increase in temperature induces a reduction in the use of heating that is higher than the increase in demand on air-conditioning, thus giving rise to a reduction of the costs for the country. In the descending part, this relation is reversed and induces an increase in costs [345]. For instance, due to heating, countries historically experiencing relatively low temperatures, such as in temperate regions, are expected to see a net decrease in energy demand [543] as opposed to countries which already or which will experience high temperatures, such as tropical regions and most Mediterranean countries [214, 187], are expected to see a net increase in the energy demand due to cooling, particularly in the summer season [60, 214]. This trend is most pronounced for a scenario of unabated climate change (RCP 8.5) but still holds for a scenario of mitigated climate change (RCP 4.5) [543]. According to the same logic as above, it is the countries with already the more moderate climate which will know the larger benefits.

Industrial energy demand is not particularly sensitive to climate change [547] because the temperature difference to bridge in industrial processes is often much larger than the outdoor temperature fluctuations. Therefore, part of the base-load electricity demand may be expected to be temperature independent [510]. Lastly, in the agriculture sector, warmer climate can increase the demand for irrigation, increasing the energy use for water pumping [547].

ii Variability or Adequacy Risk

This section compares the reliability and hence the economic and environmental challenges (resp. benefits) of Photovoltaic (PV), Concentrated Solar Power (CSP) and wind (resp. CSP and PV with Thermal-TES- and Battery-BES- energy storage).

In fact, when PV and CSP are integrated without storage (Top panel of figure 1.13), they can only produce electricity when irradiance is available and provide nominal turbine capacity only under nominal irradiance conditions (top-left corner of figure 1.13). Therefore, the size of the Solar Field (resp. Solar Panel) is sized exactly to the size of the Power Block-PB- (resp. Inverter-INV-) and no excess is produced to store in TES (top-right corner of figure 1.13). The ratio between the thermal (resp. Direct Current-DC-) production under nominal conditions and that required by the Power Block-PB- (resp. Inverter-INV-) to operate at nominal capacity is called the Solar Multiple-SM- for CSP (resp. Inverter Loading Ratio-ILR- for PV). Therefore, a solar plant without storage has a SM or ILR equal to 1.

More SM or ILR increases (>1) (bottom panel of figure 1.13), more the SF or SP size becomes large, which requires high storage capacities (bottom-right corner of figure 1.13) to store the surplus production during the day and discharge it in the evening to expand production after sunset (bottom-left corner of figure 1.13). The SM or ILR are therefore proportional to the production hours allowing an operation of a few hours to a continuous operation until the next day (Bottom panels of figures 2.9 and 2.10, chapter 2).

PV, CSP and Wind:

Electricity output from variable renewable energy (VRE), such as wind, PV and CSP without storage, has a variety of reliability, economic and environmental challenges of their integration in the power system, in particular with growing penetration rates. First, the power output is variable and fluctuates depending on the temporal availability of the resource (on hourly, daily and seasonal scales) [223]. For instance, in addition to the fluctuation of solar irradiance intensity (i.e., by clouds and shading of PV panels/CSP collectors due to low sun position), the intermittency of the production from solar PV and CSP technologies without storage can lead to an overproduction at midday (leading to curtailment or wasted energy) and a trough in the net load (i.e., total demand minus total RE production) in the evening; which impact the system's downward

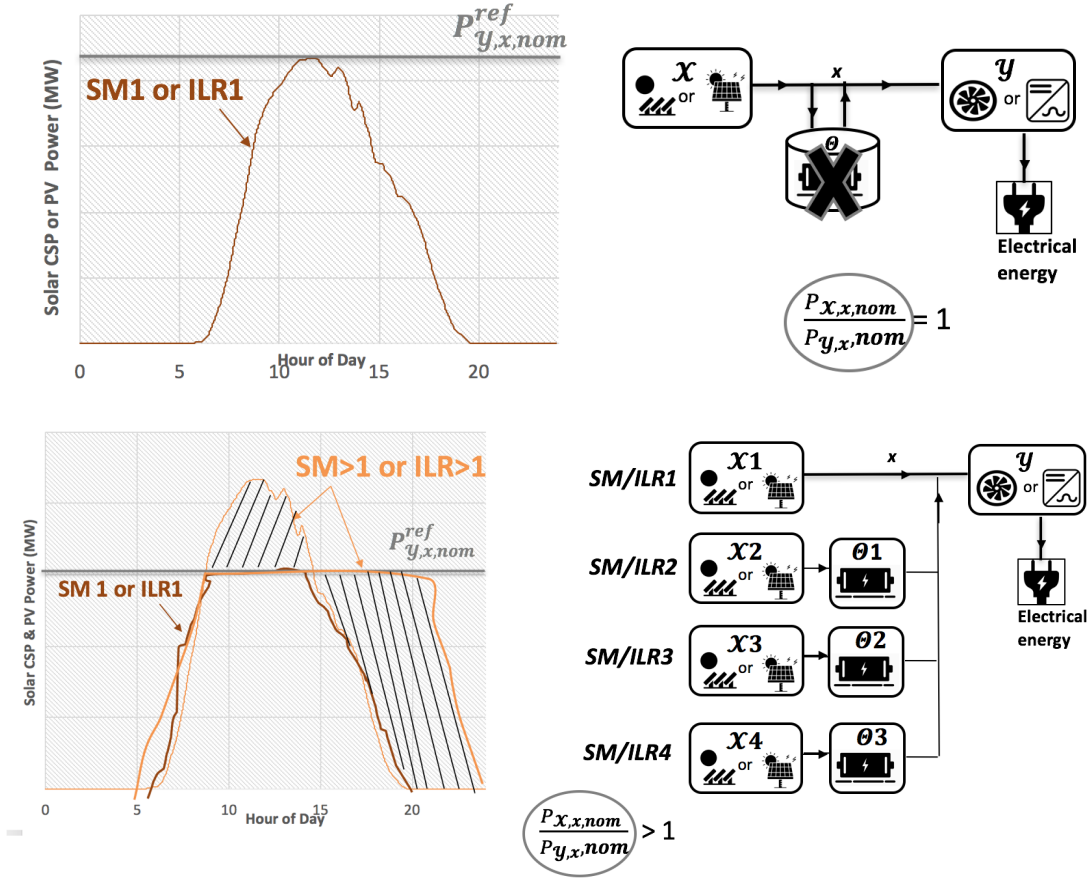


Figure 1.13: Illustration of Concentrated Solar Power (CSP) or Photovoltaic (PV) plants without (**Top**) or with different storage capacities (**Bottom**). When Solar Multiple-SM- (resp. Inverter Loading Ratio-ILR-) is equal to 1 (**Top**), the Solar Field-SF- (resp. Solar Panel-SP-) is sized exactly to the size of the Power Block-PB- (resp. Inverter-INV-), with no excess of thermal (resp. Direct Current-DC-) production to store in the Thermal-TES (resp. Battery-BES-) energy storage system, and nominal production is achieved only during hours of nominal irradiance. More the SM (resp. ILR) increases, more the SF (resp. SP) size increases in relation to the PB (resp. INV) size (**Bottom**), allowing to store the surplus thermal (resp. DC) production during the day and discharge it in the evening to expand production after sunset. $X = \{SF, SP\}$; $Y = \{PB, INV\}$; $\Theta = \{TES, BES\}$; $x = \{therm, DC\}$; $y = \{elec\}$; $P_{x,x,nom}$ is the thermal (resp. DC) production of SF (resp. SP) under nominal conditions; $P_{y,x,nom}$ is the thermal (resp. DC) production required by the PB (resp. INV) to operate at nominal capacity; and $P_{y,x,nom}^{ref}$ is the reference thermal (resp. DC) nominal capacity.

(resp. upward) ramping requirement at midday (resp. evening) (i.e., the camel curve turn into duck curve, figure 1.14) [47, 158]. Curtailment and shortage can be more challenged when solar plants are integrated in energy system with inflexible thermal generators which are enable to reduce output at midday and thus are shut down to maintain the solar production in the grid; which create challenge in the evening peak when solar plants cannot produce electricity long after the sunset and inflexible thermal generators cannot ramp up quickly. This effect is particularly striking in the dry regions with high solar resources. The daily variability of wind power, in some zones, is also large but more spread over the day since it is less tightly coupled to the diurnal cycle.

Second, due to deficiencies in forecasting weather conditions, output from VRE generation is less predictable and, hence, uncertain. The variability and uncertainty in VRE generation result, respectively, in “profile” and “balancing” costs arising from the need to use more system operating reserves (i.e., conventional “dispatchable” or non-VRE generation or other flexibility options such as imports/export, demand response mechanisms, etc) to smooth out the fluctuations and to maintain the system frequency within the allowable range [205, 262, 529].

Third, VRE resources are not evenly distributed geographically and may be located far from areas of high consumption. In addition, in contrast to conventional fossil fuels, wind and solar resources cannot be transported to other locations. This affect the transmission needs and result in “grid-related cost”. These VRE are also modular, i.e., the scale of VRE production unit is much smaller than of a conventional fossil fuel, nuclear or large hydro-generators. This affect the structure and the operation of the transmission and distribution network [482].

Finally, these VRE generators can produce electricity at very low short-run marginal costs, which increase the deployment of VRE and reduces the wholesale electricity prices “the wholesale price effect”. This affect the profitability of conventional generators “the utilization effect”. However, in the long run, the wholesale price effect is lower and hardly reduces the need for conventional capacity to safeguard system adequacy “the capacity credit effect”. This results in “adequacy costs”.

These costs result in “integration costs”. Balancing costs are generally the lowest component of total VRE system integration costs. The largest component consists of either grid-related costs or adequacy costs [482, 256].

With that being said, despite the high learning rates of VRE (i.e., potential for high cost reduction) [457], the possibilities for a future large-scale renewable penetration without flexibility are still controversial [492, 116, 243] and need subsidies to cover their fixed investment costs [467].

CSP-TES vs. PV or CSP without Storage:

On the other hand, CSP combined with TES is able of storing large midday spikes of PV generation that would otherwise be curtailed and using

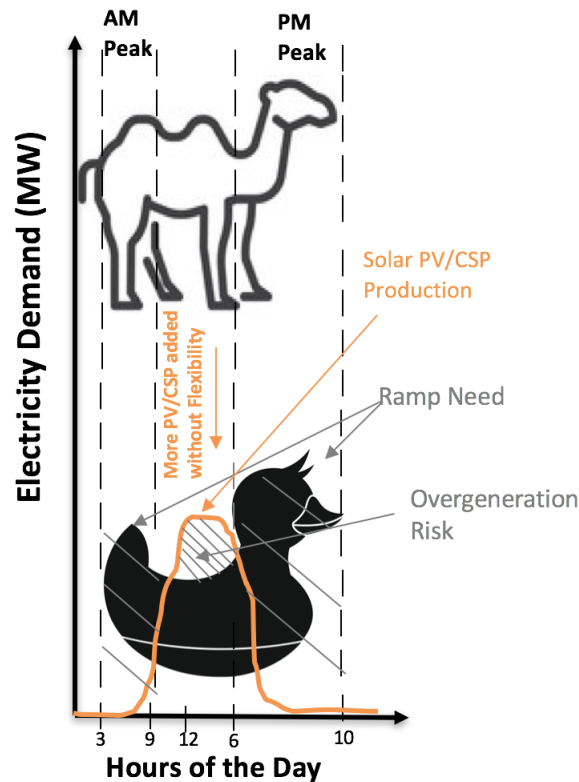


Figure 1.14: The illustration of the shape of electricity demand from camel shape to duck shape with the increase of solar Photovoltaic (PV)/(CSP) penetration without flexibility. **Top:** The electricity demand has manageable shape meaning that it never gets too high or too low (namely the camel curve). It rises in the morning to a little hump before noon, levels out over midday, and then rises to a higher hump in the evening, when everyone gets home from work and turns on their TVs and stoves. **Bottom:** As solar penetration increases, the load curves start looking like a duck curve. Demand is suppressed more during the day, when the sun is up; and the increase of demand become more and more pronounced in the evening and require faster response by other flexible generators. Source: Own elaboration based on [158].

it later on whenever it is needed throughout the day (e.g., reducing the effect of passing clouds), overnight (when the PV production drops), or from sunset to the next day in response to evolving needs [159]. Thus, the ability of CSP-TES to increase or decrease its power makes it an interesting solution to flatten the daily PV production profile and limit the morning and evening ramping concerns [201], enabling greater penetration of solar energy [161], reducing the needs of fossil-fuel generation to provide services at times of greatest need [330]. Therefore, depending on the number of hours of storage, a CSP plant should incur greatly reduced or even zero integration costs as it also helps reduce operator uncertainty due to solar forecast errors.

The fact that CSP-TES can continue to shift energy, away from the daylight hours, into the highest valued capacity hours (i.e., when electricity prices are high) increase the revenues [155]; and can provide higher marginal emission reductions than solar resources without storage [357]. This happens because PV and CSP without storage can only serve demand during the sunlight hours, and as long as demand growth increases capacity requirements within those hours, incremental solar PV and CSP without storage additions will continue to accrue capacity value; and there may be higher marginal emission reductions [357]. However, when additional demand growth creates capacity needs outside the sunlight hours, solar production without storage faces declining capacity value the more as PV (or CSP) penetration is increased [356].

Very often, the reliability and thus economic benefits of CSP-TES over PV are quantified using different indices such as the "Loss of Load probability (LOLP)" or the "Loss of Load Expectation (LOLE)" illustrating the number of hours in a given period during which the generating system cannot satisfy the overall system demand; means periods in which a loss of load occurs or hours in year the load is expected to be shed [55, 355]. Oukili et al. assess the impact of PV generation on the Moroccan grid adequacy with a non-sequential Monte-Carlo simulation and compare it with the impact of wind [394] and of CSP-TES [395] integration using the "Forced Outage Rate (FOR)" consisting in calculating the long-term probability of finding the energy system in healthy or risky state. It was found that adding PV reduces the risk of load non-recovery but cannot replace conventional generation; and for the same installed capacity, the probability of not satisfying the load when introducing PV is higher than the one calculated in the case of introducing wind or CSP-TES. Following Mills and Wiser et al. [356], we use the term "capacity credit" to represent the physical value (i.e., the actual fraction of the generators capacity that could reliably be used to offset conventional capacity during peak hours), which is typically measured as percentage of nameplate capacity, or in MW by computing the "Effective Load-Carrying Capacity (ELCC)" of a plant—the capacity credit multiplied by the nameplate capacity [284]. Previous studies indicate that high penetrations of PV adversely affect its capacity credit [356, 283]. Conventional gas generators are assumed to earn a full capacity credit of the same magnitude as that of some storage configurations of CSP-TES. The overall capacity credit of given technology can be translated into a "monetary capacity or energy value" to represent the energy value gained with shifting output over time, i.e., avoided costs of building new conventional thermal generators to meet the demand, which include fuel costs, start-up costs. Richts et al. [451] expresses the economic advantage of CSP-TES over PV in Morocco by the "difference cost"—the Levelized Cost Of Electricity (LCOE), expressed in average generation costs per unit produced, minus avoided costs of the conventional power system—and find that CSP-TES yields a lower difference cost than PV. Brand et al. [113] show that CSP-TES adds more value to Morocco's actual coal-based power system than to Algeria's gas-based system, since gas-fired plants ramp up and down more easily than coal-fired plants. The "capacity factor" approach compares actual energy output of a plant for a given period of time with the output of the plant if it operated at its 100% capacity over the same period (e.g.,

during peak load hours). However, the capacity credit is relevant for long-term system planning (system adequacy or security of supply), whereas the capacity factor derives from the instantaneous operation of the plant (Figure 1.15).

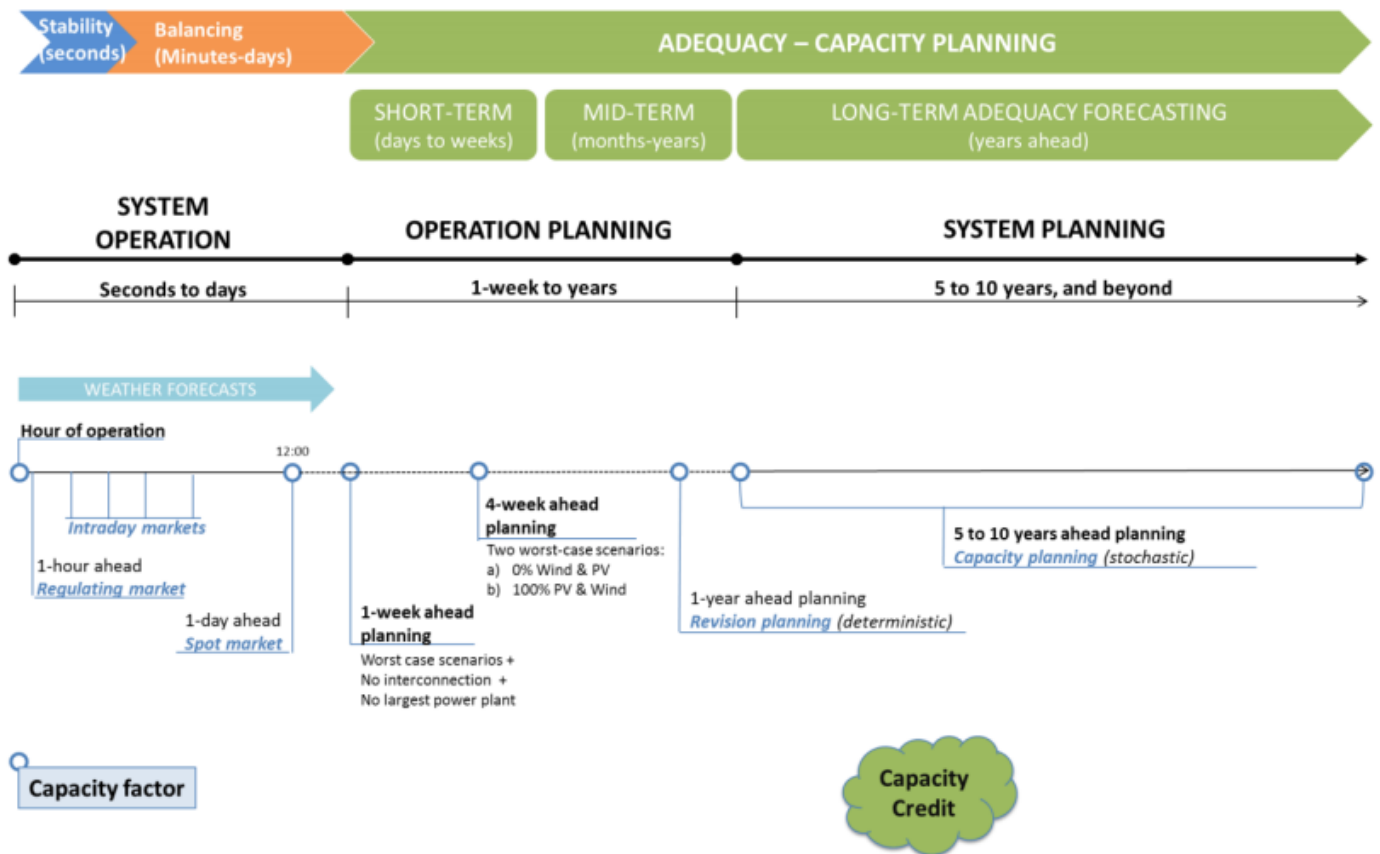


Figure 1.15: Illustration of the differences between capacity factor and capacity credit. Capacity factor refers to ratio of the energy produced by a power system in a given period over the maximum energy that can be produced in the same period. Capacity credit is a measure of the amount of conventional power generating system that can be replaced with the addition of the renewable production and maintain the same reliability [55, 355].

CSP-TES vs. PV-BES:

PV can also provide dispatchable and reliable capacity on demand, as CSP-TES does, when deployed with BES [484]. In general, literature pertaining to PV-BES systems suggests that utility-scale BES are also being considered to smooth power output during variations in solar resource [44], reduce integration costs due to their ability to store energy during periods of low electricity prices/demand and to displace this energy during periods of high prices/demand, which increase the grid stability and enable greater integration of REs [421, 354].

To date, several studies have investigated the interaction between PV-BES and CSP-TES by focusing on the technology that minimize the LCOE under different cost scenarios, amount of storage and services provided by each technology. Bogdanov et al. [96] analyze the role of solar energy towards a 100% RE power supply for Israel and found that under current (2020) cost, PV-BES capacities increase linearly till a 30% RE share due to low PV LCOE. After the 30% RE share threshold, PV stagnates due to expensive BES while CSP-TES is integrated due to cheap TES. The moderate wind conditions of Israel are the reason why wind has high LCOE and significant wind capacities are installed only after a 50% RE share. Under the future (2030) cost estimates, PV-BES capacities still increase linearly after the 30% RE share but small amount of CSP-TES is installed at high RE shares and no change for wind. Feldman et al. [194] examine the competitiveness of utility-scale PV-BES with CSP-TES through 2030 and found that at low solar penetrations and with low levels of storage needed (i.e., 3 hours), PV-BES tends to produce a lower projected LCOE. However, at high solar penetrations and with longer durations of storage needed, CSP-TES tends to have a lower projected LCOE. Papadopoulou et al. [401] show that, in scenarios with low storage requirements (i.e., low penetrations), PV coupled with storage constitute the predominant technological option presenting noticeably lower LCOE values, followed by offshore wind with storage, while CSP with storage land at the third place. However, when the storage requirements are double and for high penetrations, the LCOE of PV with storage is also the lowest but CSP with storage outperforms offshore wind coupled with storage. Chattopadhyay et al. [126] show that the policy targets on REs and the addition of PV-BES without or with spinning reserve capability (i.e., the ability to increase the power output of PV generators connected to the grid in case its production goes down or there is another disruption to the supply) may also impact the integration of CSP-TES. In fact, adding PV in a system driven by policy increases the system costs as the low-cost solar PV penetration is increased to meet the target, but small amount of CSP-TES is brought in to reduce the PV variability. In case grid-connected battery storage is added without spinning reserve capability, CSP-TES replace PV-BES at minimum solar target scenarios. However, at high solar target scenarios, battery does displace some CSP-TES capacities. On the other hand, the addition of spinning reserve capability to the battery storage eliminates the need for CSP-TES completely for all penetration scenarios.

Additional publications that concentrate on PV-BES and CSP-TES more frequently compare their operational value per unit of generation

and the avoided fuel costs associated with their addition. Sioshansi et al. [484] estimate the capacity value of energy storage systems and found that six hours of BES storage capacity is sufficient to earn full capacity credit. Jorgenson et al. [284] compare the "net cost" (calculated by summing up the present discounted value of all lifetime fixed and variable cost of a generation technology reduced by any benefits gained) of PV-BES to that of CSP-TES. The simulation results show that under current capital cost estimates, a combination of PV and conventional gas generators provides a lower net cost compared to CSP-TES and PV-BES—because CSP-TES and grid-scale battery storage are still relatively immature technologies compared to conventional gas—; and some configurations of CSP-TES (with low amount of storage) have a lower net cost than PV-BES for even the lowest battery cost estimate. Using projected capital cost target, however, some configurations of CSP-TES have a lower cost than PV with gas turbines and PV-BES even for the lowest battery cost estimate. Narimani et al. [375] found that CSP-TES and PV-BES plants would replace coal and gas generation and bring significant operational benefits to the network. However, the generation replacement by solar energy in CSP-TES case is more than PV-BES case. Their integration also increase the hydro generation by pumping hydro during off-peak hours using expensive PV-BES and dispatching it during peak periods using low cost energy of CSP-TES.

iii Total Cost

In terms of total cost, PV is approaching grid parity (e.g., in Morocco [451]), means it can generate power at a Levelized Cost Of Electricity (LCOE) less than or equal to the price of power from the electricity grid, as a result of declining costs during the last years [269, 447] and this trend is expected to continue due to the high learning rate of PV [447]. However, a system that combines PV with BES is more commonly used in smaller residential off-grid markets [542, 100] and still requires subsidies to be economically viable [246]. This limited deployment of PV-BES is because although PV costs are falling fast, the cost of BES has until now been prohibitively expensive for widespread use as a grid-scale storage [108]. The higher the installation power of the PV, the lower the investment and operating costs [453] (i.e., residential PV costs more than PV installed on roofs which are more expensive than PV on the ground [188]). Fixed tilt mounting systems are simpler, cheaper and have lower maintenance requirements than tracking systems. Almost all tracking system plants use crystalline silicon modules. This is because their higher efficiency reduces additional capital and operating costs required for the tracking system. However, relatively inexpensive single-axis tracking systems have recently been used with some thin film modules [327].

CSP, on the other hand, has high cost of capital [391], even though its LCOE tends to be lowered by its high Capacity Factor (CF) [418], and therefore requires a policy mechanisms to lower the investment risk [467, 468]. Although CSP has yet experience the same cost decline as PV, CSP combined with relatively cheap TES [242] has been deployed at scale with proven capability of providing a dispatchable and reliable generation. The Solar Field (SF) is the most important cost element in Parabolic Trough (PT) and Solar Tower (ST) plants. In the ST plants, the second cost element is the central receiver followed by TES and Power Block (PB); while in the PT plants, receivers are part of the SF and the second cost elements are the storage system and the PB.

The investment and operating costs of offshore wind are higher than that of onshore, and the high cost does not compensate for the larger offshore CF, resulting in higher production cost [188]. In addition, more the hub height is high and the specific capacity (i.e., the ratio of the nameplate capacity to the rotor swept area) decreases, more the investment cost increases, but the operation and maintenance cost remains the same [453].

The investment and operation costs (fixed and variable) are higher for CSP followed by wind and PV, but it has the largest lifetime followed by PV and wind. All costs are higher for lithium-ion BES than TES (except the energy cost) and TES has longer lifetime than BES [453].

iv Trade-Off Between Benefits and Costs

Since solar power connected to the electricity network is often contracted under a power purchase agreement, which is paid by the kilowatt hour generated, more hours of operation equals more money to amortize capital costs faster, so developers want to maximize the hours of operation each year. In order to increase the operating hours of both solar technologies, one may increase both TES (resp. BES) capacity and CSP solar field-SF- (resp. PV solar panels-SP-) compared to fixed electricity generating turbine (resp. inverter) capacity, as measured by the Solar Multiple-SM- (resp. Inverter Loading Ratio-ILR-) [194] (bottom panel of figure 1.13). .

With the integration of storage, not only the relative variance of CSP (resp. PV) Capacity Factors (CFs) is reduced, but the mean of the CFs is increased as well, even without storage (left side of figure 1.16 (a) for PV, and (b), (c) for CSP) because the system in this case rarely produces at nominal capacity. In addition, as can be seen in the right side of the same figures, increasing sizes of the SM (resp. ILR) of a CSP (resp. PV) plant while also increasing the storage capacity will generally achieve higher values of mean CFs; allowing to reach a more efficient operation of the electrical generation, which reduce the operation and maintenance costs [268, 269].

However, the adoption of high storage capacity of TES (resp. BES) in CSP (resp. PV) plants will generally lead to an increased capital costs because of the investment in storage systems, but also the cost of the additional CSP SF (resp. PV SP) that are required to produce electricity also in times when the sun does not shine. However, the greater electricity generation will generally result in a lower electricity generation cost [194, 268, 3]. Figure 1.16 (d) shows that at low SMs (left side), the minimum LCOE is achieved with zero or a few hours of storage; and as SM increases (right side), the resulting LCOE is significantly higher in systems with no storage, making the implementation of TES convenient from an economic point of view.

Given that, a trade-off between the incremental costs of the increased storage systems size and of the additional CSP SF (resp. PV SP) must be balanced against the decrease in the variability and the revenues that will accrue from the ability to dispatch generation at times of high demand and high electricity prices.

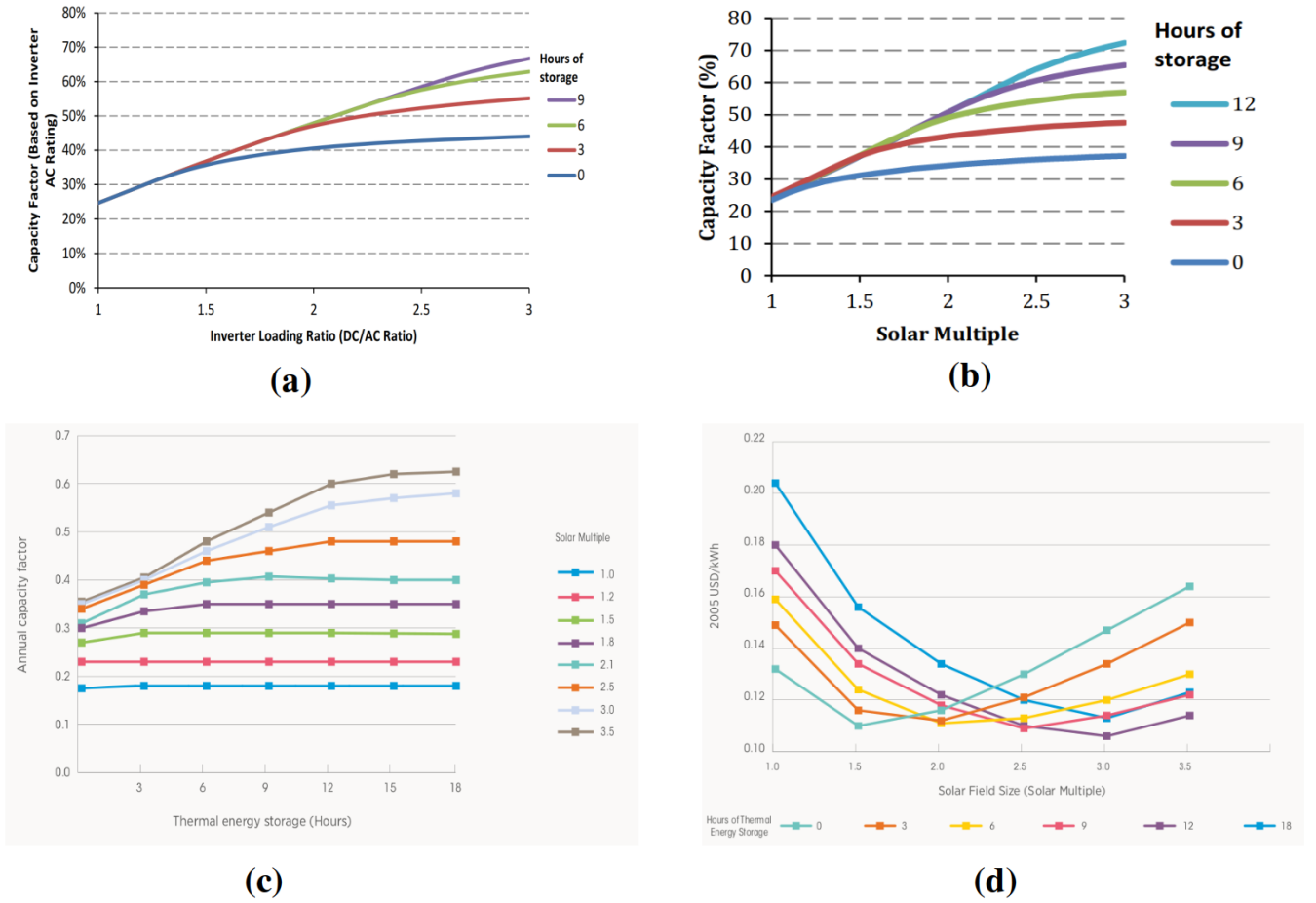


Figure 1.16: **(a)**: Relationship between mean Photovoltaic (PV) Capacity Factors (CFs) and Inverter Loading Ratio (ILR) with different hours of Battery Energy Storage (BES) [193]; **(b)**: Relationship between mean Concentrated Solar Power (CSP) CFs and Solar Multiple (SM) with different hours of Thermal Energy Storage (TES) [193, 268]; **(c)**: Annual CSP CFs as a function of SM and hours of TES [268] ; **(d)**: Levelized Cost Of Electricity (LCOE) as a function of Solar Field (SF) size and size of TES [268].

II Knowledge Gap and Originality of this Thesis

The interaction of solar technologies—Photovoltaic (PV) and Concentrated Solar Power (CSP) without or with their associated Battery Energy System (BES) and Thermal Energy System (TES)—with wind in optimal prospective mix taking into account the differences between these technologies—in terms of mean production (i.e., sensitivity to clouds and temperature, effect of tilt angle and tracking), variability and cost—under different penetration scenarios, storage configurations and combinations of Renewable Energy (RE) technologies—considering the impact of storage, cost, spatio-temporal complementarity and climate change—has rarely been addressed explicitly to our knowledge.

Optimization Objectives

In fact, so far, existing research works—focusing on optimal renewable-based mix—address questions related either to the minimization of variability only or to the minimization of cost of production only. For instance, Alhamwi et al. apply, for Morocco, the standard deviation of mismatch between demand and RE production and the so-called storage model approach adapted from previous contributions [251, 252] to quantify the optimal mix of a 100% solar-wind scenario [50], and of solar-wind-hydropower combination [51, 49]. Weitemeyer et al. [541] use the same approach for the European power supply. Moreover, the literature cited above (such as [113, 96, 194, 126, 401]) is limited to a mere comparison of the Levelized Cost Of Electricity (LCOE) or the total cost to assess the economic attractiveness of different generation technologies.

However, the differences between CSP/CSP-TES and PV/PV-BES based only on variability or only on total cost can be misleading because these objectives are likely to be conflicting to each other (i.e., we cannot reduce the total cost without increasing the risk of not covering the load and vice versa); and costs usually decrease with experience and cumulative installed capacity (i.e., for each doubling of installed capacity, investment costs decrease about a certain percentage; see the learning curve approach [378]). In this context, the Trans-Mediterranean Interconnection for Concentrating Solar Power (TRANS-CSP) study [165] reveals that the "best" RE mixes are not necessarily the cheapest, but a well-balanced mix of cheap but intermittent sources; and more expensive, but flexible sources.

Although some studies (e.g., [284, 375]) compare the economic but also the reliability benefits of solar technologies, they do not consider other factors (i.e., different penetration scenarios; PV versus CSP; PV-BES versus CSP-TES with similar or different storage sizing; PV versus CSP-TES; CSP versus PV-BES; interaction with wind; spatio-temporal synergies of PV, wind, CSP versus storage; climate change impacts and uncertainty in future energy mixes). This illustrates the still prevailing bias of many research papers conceptualizing the interaction of wind, CSP/CSP-TES and PV/PV-BES within an optimization framework.

Therefore, instead of choosing the technologies on the basis of cost alone or characterizing the variability of imbalances alone, energy system based on solar technologies (PV, CSP) without and with their associated storage (BES, TES) needs a multi-objective optimization

problem that considers the whole range of feasible solutions by determining a trade-offs between mean production (i.e., maximizing the RE penetration), variability (i.e., minimizing the adequacy risk) and cost (i.e., satisfying the maximum total cost constraint). Such trade-off can be satisfied by the "Pareto Optimal Front" of the bi-objective mean-variance optimization problem [337] used in this thesis (Section 1) allowing to arbitrate between different penetration scenarios.

In fact, in this thesis, we explore—**under different penetration scenario mixes, storage requirements and combinations of RE technologies**—the impact of different elements **(1) Storage and Cost; (2) Spatio-Temporal Complementarity; (3) Climate Change** that may either encourage or compromise the integration of RE technologies in optimal mixes by solving the following questions:

(1) Which technology must be installed and where? should Morocco install dispatchable but expensive technologies (CSP-TES, PV-BES) or low-cost but variable technologies (PV, wind)? what about variable and expensive CSP without TES?

To illustrate these points, and as stated in section 3, CSP is more expensive than PV, but not only the total cost that is relevant for identifying the optimal technology because they are also different in terms of sensitivity to clouds and temperature, and the use of tracking. **So, PV is competing with CSP? or PV is winning over CSP? what about wind as it collects different resource and it is different than PV and CSP in terms of investment and operation costs?**

In addition, although PV-BES and CSP-TES are both dispatchable technologies, but they are different in terms of cost of the production technology but also of the storage technology (i.e., PV is cheap but BES is expensive; CSP is expensive but TES is cheap) and may also provide different services [375, 126] (Section ii in this chapter and section I in chapter 4). In fact, in contrast to output from conventional dispatchable generators that can be turned on and off based on their economic attractiveness at every point in time to supply electricity and provide system services according to real-time power demand, the energy provided by CSP-TES and PV-BES depends also on the storage capacity which in turn depends on costs. Thus, they are also different in terms of variability and cannot be compared based only on economic criteria. **So, if PV-BES and CSP-TES are integrated with similar storage sizing, there is a winner or they may be integrated together? what about if they are integrated with different storage sizing?**

What about PV versus CSP-TES or CSP versus PV-BES? If the comparison criteria that is adopted is cost, the LCOE-based approach would overvalue intermittent generation technologies compared to dispatchable plants [286] because storage adds costs to the system. However, as already mentioned (Section 3), the addition of storage also reduces the variability and provides additional reliability and economic advantages that can outweigh the increase in costs.

(2) What about if we focus on installing cheap technologies (such as PV and wind) and properly manage their variability by dispersing them geographically and taking into account their temporal complementarities instead of investing in expensive technologies (CSP-TES, PV-BES) that are currently not yet sufficiently deployed at large-scale? There is currently a consensus that taking into account the spatio-temporal complementarities between PV and wind reduces the variability (e.g., [336, 298, 294]). However, no study analyze the benefits of complementarity on the mix integrating CSP/CSP-TES/PV-BES. So, Morocco has to take into account the correlations between technologies and regions (i.e., spatio-temporal complementarities)? or only correlations between technologies in the same region (i.e., temporal complementarities)? or only spatial complementarities? or ignore all the complementarities? how the integration of CSP and storage would influence the benefits from these complementarities?

(3) Because the costs of RE technologies keep going down, several countries are encouraging faster climate action by installing more carbon-free technologies. However, the latter are themselves altered by climate change as their production relies on climate. So, optimal mixes are more sensitive to climate change or to cost (i.e., in the context of vulnerability of low-carbon technologies to climate change vs. eventual cost reductions)? In addition, studies over the past decades have provided important information on the impact of climate change on PV and wind but not yet on CSP/CSP-TES (see existing research in section II, Chapter 5). So, what is the impact of climate change on the Moroccan optimal mixes, considering the severe "business-as-usual" RCP 8.5 scenario, in which no efforts to cut greenhouse gas emissions are made? optimal mixes are more sensitive to climate change or to cost (i.e., in the context of vulnerability of low-carbon technologies to climate change vs. eventual cost reductions)? intra-daily fluctuations have substantial impact on optimal mixes? which technology is sensitive or resilient to climate change? what are the conditions for climate-resilient RE mixes? what are the main sources of uncertainty in future RE mixes? thermal storage makes CSP resilient to climate change? does RCP 8.5 climate change impacts the geographical distribution of RE capacities?

III Focus of the Thesis

We take the existing generation portfolio and the recent cost data as a starting point for the analysis of possible electricity mix transformation trajectories with solar and wind energies.

On the one hand, this thesis aims to conduct a rigorous analysis of the sensitivity of optimal prospective mixes to the integration of solar technologies (CSP and PV) with wind by exploring the role of storage (TES and BES) and cost under various penetration scenarios and storage configurations, together with the role of technological and regional complementarity in reducing the production-demand adequacy risk of the Moroccan electricity mix. On the other hand, we integrate in our reflection some elements from the rich current debate on the energy transition and the long-term decarbonization by putting the issue of climate change impacts on the optimal mixes and the main sources of uncertainty in future RE mixes at the end of our analysis.

1 Objectives and Tools

Our objective is to maximize the RE production at a given cost and to lower the mismatch between the demand and the RE production (i.e., the variance-based adequacy risk for the electrical grid). Increasing the mean RE penetration towards 100% tends to reduce system costs and greenhouse gas emissions by decreasing the total conventional production.

This bi-objective mean-variance optimization problem is implemented in the open-source Python software "Energy for Climate Integrated Model (E4CLIM)" in which we implement additional modules as a special case for this thesis (Section III, Chapter 2).

2 Case Study: Morocco

We use Morocco as a case study as it is relevant country to analyze objectively various scenario mixes of PV/PV-BES/CSP/CSP-TES share and climate change scenarios. Morocco is indeed located in the best suited region of the world with favorable technical and economic conditions

for achieving large-scale implementation of solar energy [393, 104].

Morocco's electricity market has a **hybrid structure** with **two main markets**, as illustrated in figure 1.17. On the left side, the **regulated power market** with **Independent Power Producers (IPPs)**, **Public Private Partnerships (PPP)** of the Moroccan Agency for Sustainable Energy (MASEN) besides the **own generation of the National Office of Electricity (ONE)** and the **importations of electricity from Spain**; and on the right side, the **open market** for **private RE generators** and **self-generators**—with specific conditions regarding the capacity to install, the surplus limit to sell to ONE, the type of generation and the network access.

ONE supplies a major part of the electricity to the final customers of the **Very High Voltage (VHV)** and **High Voltage (HV)** and in rural areas (**Medium Voltage-MV-** and **Low Voltage-LV-**); followed by the **four private distribution utilities** in the **large urban areas (MV-LV)**, the so-called “**gestion déléguée**”. The remainder is supplied by the **seven public distribution companies** in the **remaining urban area**, the so-called “**régies autonomes**”.

While generation and distribution were opened to private investors, **ONE is the sole buyer of all the electricity produced and owns and manages the entire transmission network**. ONEE is also **in charge of the balancing and system services**, supported by ONE's **Pumped Hydro Storage (PHS)** and its role as **power importer/exporter**.

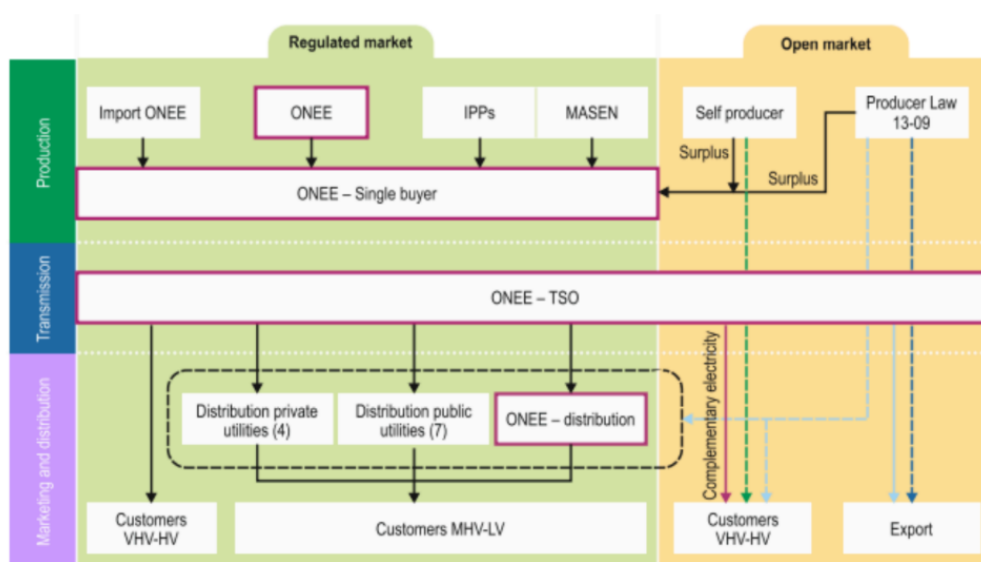


Figure 1.17: Organization of Morocco's electricity sector. Source: Energy Policies Beyond IEA Countries: Morocco 2019 [264].

In 2018, Morocco had 34% of its electricity covered by REs (510 MW CSP-TES, 20 MW CSP, 170 MW PV, 1215 MW wind and 1770 MW hydro) [23] and aims that 42% of the total electrical capacity should be covered by REs (solar, wind and hydro) by the end of 2021 with equal proportions of installed capacity, consisting of 14% (2GW) for each resource; and increase this share to 52% by 2030 [264, 7], with 20% should come from solar (PV or CSP or both); 20% from wind and 12% from hydro; and reach 100% RE supply between 2030 and 2050 [8].

In 2017, fossil fuels (coal, gas, oil) accounted for 82% of total electricity generation, and REs and waste heat made up the remainder (left panel of figure 1.18). Coal remains the most important fuel source for electricity generation in Morocco, accounting for 53% of total power generation in 2017. Natural gas power was introduced in 2004 (right panel of figure 1.18), when Morocco began importing gas from Algeria to fuel power plants. Since then, gas power has increased significantly and more than doubled in the last decade and accounted for 18% of total power generation in 2017 (left panel of figure 1.18). The role of oil in overall electricity generation has decreased in the last decade, with natural gas generation tending to displace oil (right panel of figure 1.18). In 2017, however, a large amount (11%) of power generated still comes from oil (left panel of figure 1.18), mainly in rural isolated areas.

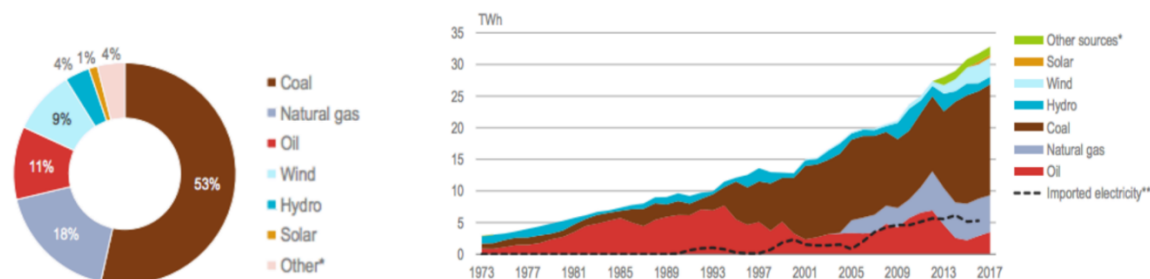


Figure 1.18: The share of renewable energies and fossil fuel in the total Moroccan electricity generation in 2017 (left); and the electricity produced in TWh by each source from 1973 to 2017 (right). Other sources: heat from chemical processes (auto producers). Source: Energy Policies Beyond IEA Countries: Morocco 2019 [264].

As can be seen in figure 1.19, the total power generation from REs was 4.6 TWh in 2017, three times higher than in 2007. Wind power generation increased rapidly from 0.3 TWh in 2007 to 3 TWh in 2017, making it the largest RE power source (it supports 9% of power production as shown in the left panel of figure 1.18) and it overtook oil in electricity generation in 2015 (right panel of figure 1.18). In recent years, solar power has grown rapidly (Figure 1.19) with the solar PV projects (Noor 4, Noor Laayoune 1 and Noor Boujdour 1) and CSP projects (Noor Ouarzazate 1, 2 and 3) (Table A.73, Appendix A); and solar has become another important power source with 0.4 TWh generated in 2017

(1% in the electricity generation mix as shown in the left panel of figure 1.18). Hydropower has shown a different trend. Despite stable installed capacity, the actual contribution of hydro in power generation has varied significantly during the decade (Figure 1.19), as water availability and precipitation levels have fluctuated due to climate change, raising concerns about the future of hydropower generation in the longer term.

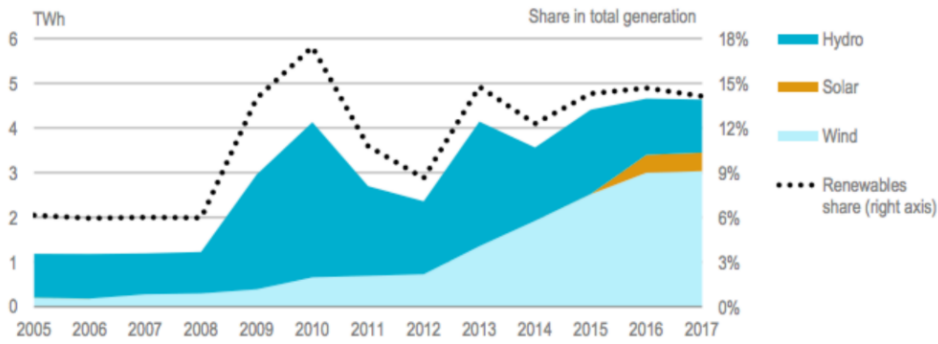


Figure 1.19: Renewable Energy (only) in the electricity generation from 2005 to 2017 with the years in abscissa, and the total generation in TWh (resp. share in total generation in %) in the left (resp. right) ordinate axis . Source: Energy Policies Beyond IEA Countries: Morocco 2019 [264].

In addition, under the Paris Agreement, in its National Determined Contribution (NDC), Morocco is committed to reduce 17% of its greenhouse gases (GHGs) below the business as usual level (current national policy projection), the so-called "unconditional reduction" and an additional 25% is conditional to the availability of an international technical and financial support from the international community (estimated at USD 50 billion in total funding between 2010 and 2030) [7, 26]. The GHG emission reductions include emissions in Agriculture, Forestry and Land Use (AFOLU) sectors.

However, this energy strategy does not explicitly set the share of PV and CSP but instead in global solar installed capacity. In addition, the plans are unclear about the amount of storage associated with CSP and about the integration of battery storage to PV. In fact, this strategy is not restricted to particular technology and only aims to reduce its energy dependency on externally sourced coal and heavy oil as well as electricity imports since 91.7% of its total primary energy supplies comes from outside [23] (Spain cover almost 9% of the total Moroccan electricity needs in 2018 [27]).

In addition, renewable expansion in Morocco is primarily perceived in terms of opportunities such as contribution to RE targets, reduction of carbon emissions and energy dependence [104, 129] while the issues related to cost and storage associated with solar technologies in the mix—considering the impact of time-space complementarity—one one hand; and their sensitivity to future warming climate on the other hand receive significantly less attention.

3 General Research Questions and Approach

In this thesis, we take the perspective that solar technologies and wind can very well form an integral part of the Moroccan electricity supply; and try to discuss a set of scenarios of large-scale solar integration with wind in Morocco. Providing a better understanding of the effects of such integration in terms of storage, cost, spatio-temporal complementarity and climate change is the overarching objective of this thesis.

First, we start by analyzing if the capability of cheap thermal storage combined with expensive CSP surpasses the benefits of low-cost but variable PV generation; and how an increased thermal storage duration together with time-space complementarity would influence the optimal mix and to what extent the variability can be reduced. In other words, **Q1: What is the response of the regional renewable energy scenario mix—including low-cost and variable solar PV and wind energy as well—to the integration of expensive CSP without or with increasing levels of cheap thermal storage; and how does it impacts the benefits of spatio-temporal complementarity ?** To properly address this question, answered in the first study of this thesis (Chapter 3), the model has to integrate the technical features inherent to parabolic trough plant—currently the most widespread type of CSP technology being built in Morocco—without and with different storage capabilities (i.e., Solar Multiple or SM); and take into account the different rental costs and adequacy services of each technology. We enabled the model to simulate competition among the following renewable technologies: wind, PV and CSP without storage, and CSP with increasing amount of TES. We carried out several model runs with different combinations and under different penetration scenario mixes using MERRA-2 climate reanalysis over one year.

Morocco may choose CSP for its energy storage to ensure better modulation of the demand because with all the PV that is added for days, Morocco needs electricity to meet the demand in the night. However, since CSP is expensive and the low-cost PV generation variability can be mitigated by BES, PV coupled with BES can also provide dispatchable energy and may eventually replace CSP-TES. However, the batteries are likely to make PV more expensive than CSP combined with competitive storage option (i.e., molten salt) [242, 564]; and the actual storage configurations and performance of these systems for dispatchable energy are still in the early research stages because large-scale PV-BES market is still nascent and thus not yet deployed in large-scale PV plants, if we exclude micro-grids [238]. Therefore, we take an approach similar to that of CSP-TES integration (Chapter 3) but the vision is more forward-looking aiming to expand the PV model to include BES with different storage duration (i.e., Inverter Loading Ratio) to explore the potential competitiveness of utility-scale PV-BES with CSP-TES in optimal mixes and to compare between them in terms of cost and storage, their impacts on benefits from spatio-temporal complementarity and system adequacy risk; considering different combinations of variably sizeable PV and CSP with wind under different penetration scenario mixes. So, the research question to be answered in the second study of this thesis (Chapter 4) is as follows: **Q2: If the low-cost PV system has expensive battery storage with different levels of storage as expensive CSP with cheap TES, how do the optimal mixes integrating these two solar technologies interact with wind under penetration scenarios; and which dispatchable solar technology displaces more conventional generators?**

In Morocco, where the RE expansion is still ongoing, it becomes apparent that electricity mix cannot be decided exclusively on the basis of economic costs and short-term variability, but must also consider low-frequency climate variability and climate change issues. In fact, PV

and CSP (resp. wind) output strongly depend on temperature and solar irradiance (resp. wind speed). Thus, the potential change in solar irradiance (resp. wind speed) in combination with the expected greenhouse warming may affect future output from PV and CSP (resp. wind) systems and hence will contribute less and less to meeting the grid's demand at peak times. The storage can maintain its value over the long term, even as demand profiles change, because it can alleviate intermittency problems. However, this depends on storage capacity, the related cost and the penetration scenario; and no study has been conducted on the impact of climate change on optimal mixes integrating storage to confirm this perception. The question that arises in this context is that **Q3: What is the response of scenario energy mixes integrating variable and low-cost technologies (PV, wind) with dispatchable and expensive technology (CSP-TES) to climate change compared to cost effect; and how robust results are to sensible changes in climate model?** This question has been answered in the third study of this thesis, Chapter 5, on the basis of the modeling framework implemented in chapter 3 but in future warming climate using four CORDEX-CMIP5 (COordinated Regional climate Downscaling EXperiment-5th Coupled Model Intercomparison Project) climate projections under one emission scenario (RCP 8.5) after the mid-21st century (compared to historical observed forcing).

IV Thesis Outline

The remainder of this thesis has been divided into six chapters.

After this thesis introduction chapter (chapter 1), chapter 2 elaborates the methodology adapted to address the research questions stated above (Section 3), from the data sources, demand profiles, output from CSP, PV and wind, and storage and cost modeling to the optimization solutions and post-processing diagnostics; including a brief description of the E4CLIM tool and the main contributions to it. More details on the theoretical energy and cost modeling and optimization framework are provided in Appendix A.

Chapter 3 and Chapter 4 address the scenarios of solar integration across a set of penetrations and under current climate and cost data. The main difference is that chapter 3 addresses the first research question of this thesis which analyzes the response of the Moroccan mix to the integration of CSP without and with increasing levels of TES with PV without storage and wind by examining the impact of thermal storage, cost, and spatio-temporal complementarity in reducing the adequacy risk; while chapter 4 addresses the second research question of this thesis which analyzes the effect of the addition of BES to PV and CSP/CSP-TES analyzed in chapter 3 under different scenarios of storage requirements.

Chapter 5 addresses the third research question of this thesis by reproducing some analysis of chapter 3 in future climate keeping the existing generation assets and current cost data. We evaluate the impact of climate change on the mix compared to cost effect, explore the role of flexibility provided by storage on this climate sensitivity, the sensitivity of the results to climate data sources together with the robustness of climate projections and sources of uncertainty in future RE mixes.

Synthesis of the methodology adapted and the main findings are presented in chapter 6. We give some research implications and limitations of this thesis to lay the groundwork for a more exhaustive analysis, and open questions that have not been addressed in this thesis but can be done in the future.

Energy System Modeling and Optimization

Contents

I	Introduction	48
II	E4CLIM 1.0 Model and Mean-Variance Optimization Problem	50
1	Brief Description of E4CLIM 1.0 Model	50
2	Objective Functions and Optimization Strategies	50
3	Optimization Solutions: Main Relevant Elements of the Pareto Front	51
III	Model Set-up and Main Contribution to E4CLIM	54
1	Domain and Calibration	54
2	Modules Added	56
IV	Climate Data Sources	59
1	MERRA-2 Reanalysis	60
2	CORDEX Simulations	60
3	Period of Analysis	61
V	Storage Modeling	62
1	CSP Solar Multiple and PV Inverter Loading Ratio	62
2	Storage Model Approach	63
3	Typical Daily Operation of CSP-TES and PV-BES	63
VI	Predicted Demand and Bias-Corrected Capacity Factors	67
1	Thermo-Sensitivity Results	67
2	Bias-Corrected Capacity Factors	68
VII	Maximum-Cost Constraint	68
VIII	Rental Cost Modeling and Data	69
1	Case 1: Limited Storage Cost and Capacity	69
2	Case 2: Unlimited Storage Cost and Capacity	71
3	Case 3: Constant Thermal Storage Cost with Unlimited Capacity	72
IX	Optimization Post-Processing Ratios	72
1	At Maximum Penetration	72
2	At High Penetrations	73
3	At Low Penetrations	74
X	System Adequacy Diagnostics	74
XI	Conclusion	76

I Introduction

Motivation

To answer the general research questions of this thesis (Section 3, Chapter 1) and therefore to (i) analyze the response of the Moroccan mix to the integration of solar technologies, Photovoltaic (PV) and Concentrated Solar Power (CSP), without and with increasing levels of battery (BES) and thermal (TES) storage in terms of cost and variability, (ii) examine the role of storage together with technological and regional complementarity in reducing the adequacy risk; and (iii) evaluate the impact of low-frequency climate variability and climate change on optimal mixes; we need an accurate system modeling with available climate data as well as energy observations; an appropriate method to assess the temporal and spatial characteristics of electricity demand and production of a given Renewable Energy (RE) technology; and an analytical approach to optimize the current and future energy mix scenarios achieving a trade-off between maximizing the mean penetration rate of REs and minimizing the variability of RE production while satisfying the economic constraints.

Existing Research

There is now an extensive research literature on energy system modeling and optimization. Benzohra et al. [87] predict the electricity demand and apply an algorithm of RE integration to analyze the role of storage in increasing the penetration of low-carbon technologies in the future Moroccan energy system. Azeroual et al. (2018) [359] forecast the electricity demand and estimate the capacity of wind and solar power in Morocco towards 2030, using the Load Duration Curve (LDC), and examine the effect of pumped hydro storage on wind capacity and the impact of interconnection on solar capacity. Kern et al. [299] overcome the limitations of conventional capacity planning tools based on the LDC and present the Moroccan RE Mix Capacity Expansion Model (MOREMix CEM)—an energy system modeling and optimization platform of thermal and RE assets—aiming to minimize the net present value of total system costs over the entire planning horizon; taking into account the impact of variable RE on the power system. Schinko et al. [467] assess the techno-economic feasibility of different electricity generation portfolios—comprising conventional fossil fuel-based technologies as well as RE technologies in varying shares—and the role of financing costs on the Moroccan energy system up to 2050; employing a downscaled version of the open source electricity market model "Renewable Energy Pathways Simulation System (RENPASS)". Rye et al. [461] use the flow-based market model, Power Grid and Market Analysis (PowerGAMA), to study the 2030 scenarios for the Moroccan power system with increased RE installed capacity and demand, and compare investments in storage capabilities for CSP and grid reinforcements using cost-benefit analysis. De Arce et al. [62] simulate the macro-economic effects of future RE scenarios in Morocco in the medium and long term using a dynamic input-output model. Brand et al. [112] use a linear optimization model to analyze the economic impact of RE integration on the electricity market of three North African countries, such as the cost savings due to avoided costs in the conventional plants. Trieb et al. [523] develop scenarios for RE expansion in North Africa including a Strengths, Weaknesses, Opportunities and Threats (SWOT) analysis of their energy strategies. Bonin et al. [99] use a MIXOPTIM model [98]—which is a monte carlo simulation tool for the evaluation and optimization of an electricity mix in Europe—to examine how different indicators, i.e., production cost, carbon dioxide (CO_2) emissions and security of supply, would evolve under an elementary change in the composition of the mix. Ref [97] use the same model to derive the maximum amount of mandatory stochastic sources that can be tolerated in the mix if frequent power cuts are to be avoided, and the role of interconnection, demand smoothing, storage in increasing the RE proportion in the mix. Després et al. [162] develop a short-term optimization model, European Unit Commitment And Dispatch (EUCAD), and couple it to long-term foresight energy models, Prospective Outlook on Long-term Energy Systems (POLES), to represent the RE variability challenges. Liu et al. [320] quantify the advantages of interconnecting contiguous Chinese regions based on two scenarios. The first is based on heuristic aiming to increase the heterogeneity by relocating solar and wind capacities in sites with better Capacity Factors (CFs) to minimize the total cost per MWh energy delivered without regards to the match between production and demand. The second approach optimizes the trade-off between low cost production and high utility value of the energy (i.e., low needs of backup from thermal units). Lund and Mathiesen et al. [328] discuss energy mix scenarios for a fully RE electricity supply in Denmark.

Knowledge Gap

As already pointed out, although the existing literature is rich in studies delving into the challenges and benefits related to future low-carbon electricity systems, they explore either the variability, by exploring the role of storage per se or the characteristics of the above mentioned flexibility options on the mix (e.g., [101, 304]), or focus on the flawed metric, the Levelized Cost of Electricity (LCOE), to assess the economic attractiveness of different RE technologies against dispatchable, conventional ones. However, an energy systems based on solar technologies (PV, CSP) without and with their associated storage (BES and TES) often require a multi-objectives functions of different nature (i.e., reducing variability, maximizing CFs, reducing the capital and operating costs) to be taken into account. Different criteria are thus important when selecting a suitable optimization approach: (i) ability to characterize the variability (i.e., risk of not covering the load), providing a better adequacy risk assessment of alternative technologies; and (ii) ability to evaluate the cost impact on the penetration of given technology. Therefore, instead of minimizing the economic costs alone [299, 113] or carbon costs [377] or balancing needs alone [51, 541, 252] or/and transmission needs [454, 84, 85] or applying a range of uncertainty to future cost of production generation and storage technologies [479] or minimizing the difference between the benefits and costs [284, 156, 451], approaches based on the Mean-Variance Portfolio (MVP) optimization rely on some measures of the variance of the RE production in addition to its expectation. The MVP do not reflect least-cost electricity systems in terms of investment and operational costs, but an optimized operational behavior taking into account all these elements, i.e., total costs, resource variability making use of regional and technological synergies, in order to leverage weaker correlations between production sites and sources, to minimize the variability of the production or production-demand mismatch once aggregated over regions, and to avoid the construction of RE power over-capacities and consequently to lower economic costs. The MVP, inspired by Markowitz's portfolio theory [337, 352], was initially used for the efficient selection of financial asset portfolios based on the investors' goal of maximizing future expected return for given level of risk they are willing to accept or minimizing the risk for a given level of return they wish to achieve. When faced with a choice between two investments with the same risk level they always choose the one with higher expected return. Therefore, the MVP approach highlights the advantages of investment diversification among several financial criteria. The MVP can also be used for the selection of RE electricity portfolios in the capacity planning context. Paz et al. [150] examine to what extent this approach can be implemented to define efficient sets of production technologies in Spain. Several authors have resorted to analyze the contribution of RE in terms of security of supply for a given energy mix considering international RE trade flows [202] by optimizing the portfolio production costs (based on external volatilities of fuel prices) or optimizing the expected power output or the CO_2 emissions—in Mexico [221], Europe [149, 72, 195], Brazil [322], Japan [93]—stating that lower risk portfolio can be obtained without increasing portfolio costs, typically by expanding the share of REs in Scotland [52], Italy [65]; taking advantage of a diversified mix [142, 274].

Objectives

Based on this, we take as objective to maximize the mean RE penetration at a given cost, and minimize the variance between the demand and the RE production. Thus, assuming that the share of the demand that is not satisfied by RE is supplied by the conventional production (e.g., thermal and hydroelectric plants or other flexibility options such as demand response management, interconnection, large-scale storage ...) normalized by demand, we expect that the mix minimizing economic costs from the conventional production and the mix minimizing greenhouse gas emissions simultaneously are close to one of the mixes on the optimal front. One can choose the desired compromise between the conflicting objectives, either maximizing the RE penetration or minimizing the risk. This approach based on heuristic limit the complexity of the optimization problem by reducing it to the optimization of RE capacities, independently from conventional systems.

Outline

The remainder of this chapter is structured as follows. Section II gives a brief description of the previous version of the Energy for Climate Integrated Model (E4CLIM) on which this thesis builds on (Section 1) before to develop the modules that we add to it, presents our objectives and the optimization strategies (Section 2) and gives an overview of the optimization solutions (Section 3) by highlighting the relevant elements

of the mean-variance optimization problem. Section III presents the stages of our research contribution to E4CLIM model. It comprises different sub-sections. We describe the adaptation of E4CLIM to Morocco in section I and the simulation modules added in section 2, including the storage module (Section V), the addition of a maximum-rental-cost constraint to the optimization problem (Section VII), the rental cost modeling framework and the cost data (Section VIII). The subsequent part provides the optimization post-processing ratios (Section IX) that define the technology, in a given region, that should be installed for each penetration regime. Finally, the system adequacy diagnostics are described in section X. The climate data sources used in this thesis are detailed in section IV. The thermo-sensitivity results and the bias correction results are summarized in section VI. An extensive supplementary material (Appendix A) is provided and specified in each section. A summary of the methodology made is presented in section XI.

II E4CLIM 1.0 Model and Mean-Variance Optimization Problem

In this section, we give a brief description of the Energy for Climate Integrated Model (E4CLIM) model and the mean-variance optimization framework, as an alternative to the more traditional least-cost approach or minimum balancing needs approach, before describing the methodology adapted in each of the modules that we add to it.

The flow chart, given in figure II, summarizes the components of E4CLIM (dark blue) including the modules added (light blue) and the data sources (gray) to illustrate briefly the general framework of this thesis.

1 Brief Description of E4CLIM 1.0 Model

To conduct energy mixes scenarios, we use the open-source Python software "Energy for Climate Integrated Model (E4CLIM)" that allows from geographical data for a specific area and from climate data to compute—using statistical learning or physical model—:

- **Onshore wind production without storage** at each climate grid cell from wind speed extrapolated at hub height and fed to a power curve (Section II, Appendix A for more information).
- **PV production for arrays without tracking and storage** at each climate grid point based on a parametric approach to model the sensitivity of PV efficiency to temperature (Section VI, Appendix A for more information).
- **Electricity demand** by taking into account the sensitivity of demand to temperature [367, 89] as well as to human economic activity (Section I, Appendix A for more information).

Once the wind and solar Capacity Factors (CFs) are obtained at each grid cell of the climate data—by dividing the computed production by its nominal value—they are spatially **averaged** over each zone and **bias-corrected** against observations (Section 2, Appendix A) to obtain the mean CFs for the whole region. It is thus assumed that the Renewable Energy (RE) capacities are uniformly spread over a zone—as discretized by the climate data grid point—rather than located at actual or most favorable locations within the zone.

After computing the regional electricity demand and bias correcting the regional CFs, these time series are used to generate an **electricity mix**—ignoring the actual mix—by optimizing the technological and geographical distribution of solar and wind capacities using the mean-variance analysis.

2 Objective Functions and Optimization Strategies

The mean-variance bi-objective optimization problem aims at maximizing **the mean penetration** (2.1) and minimizing **the aggregate RE supply risk squared**, $\sigma_{\text{global|technology|base}}^2$, of the mix with respect to optimization constraints. The mean RE penetration (μ) is defined as the expected value of the ratio of total predicted RE production over total predicted demand (refer to the share of solar and wind electricity generation in satisfying the demand) and can be calculated using the equation (2.1):

$$\mu(\hat{\mathbf{w}}) := \mathbb{E} \left[\sum_k \omega_k \frac{\eta_k(t)}{\sum_i D_i(t)} \right] = \sum_k \omega_k \mathbb{E} \left[\frac{\eta_k(t)}{\sum_i D_i(t)} \right]. \quad (2.1)$$

The definition of the aggregate RE supply risk depends on the optimization strategies considered as three versions of the variance:

- **A global strategy** (2.2) which considers the mean and the variance ($\mu, \sigma_{\text{global}}^2$) of the ratio between the total solar and wind production over the total demand. The global strategy considers the area of study (i.e., a country) as unique region, and try to optimize the national mix where production at each point is available to meet the overall demand regardless of any distance or transmission constraints by considering the covariance between regions and technologies:

$$\sigma_{\text{global}}^2(\hat{\mathbf{w}}) := \mathbb{V} \left[\sum_k \omega_k \frac{\eta_k(t)}{\sum_i D_i(t)} \right] := \sum_k \omega_k^2 \mathbb{V} \left[\frac{\eta_k(t)}{\sum_i D_i(t)} \right] + \sum_{k \neq l} \omega_k \omega_l \text{Cov} \left[\frac{\eta_k}{\sum_i D_i}, \frac{\eta_l}{\sum_i D_i} \right]^{\text{global}}; \quad (2.2)$$

- **A technology strategy** ($\mu, \sigma_{\text{technology}}^2$) for which the variance (2.3) is defined as the sum over zones of the variance of the total solar and wind production per technology over the total demand, thus setting covariances between different zones to zero and keeping only those between different technologies of the same zone:

$$\sigma_{\text{technology}}^2(\hat{\mathbf{w}}) := \sum_i \mathbb{V} \left[\sum_j \omega_j \frac{\eta_j(t)}{\sum_i D_i(t)} \right] = \sum_k \sum_l \omega_k \omega_l \text{Cov} \left[\frac{\eta_k}{\sum_i D_i}, \frac{\eta_l}{\sum_i D_i} \right]^{\text{technology}}; \quad (2.3)$$

- **A base strategy** ($\mu, \sigma_{\text{base}}^2$) for which the variance (2.4) is defined as the sum over zones and technologies of the variance of the production per zone and technology over the total demand, thus setting all covariances to zero:

$$\sigma_{\text{base}}^2(\hat{\mathbf{w}}) := \sum_k \mathbb{V} \left[\omega_k \frac{\eta_k(t)}{\sum_i D_i(t)} \right] = \sum_k \omega_k^2 \mathbb{V} \left[\frac{\eta_k}{\sum_i D_i} \right]^{\text{base}}, \quad (2.4)$$

where \mathbb{E} , \mathbb{V} and Cov represent respectively the mathematical expectation, variance and covariance operators over time. The symbol \sum denotes the sum over the index in subscript. The index k is a multi-index representing a pair $k = (i, j)$ of different production technologies j in different zones i . The quantity $\hat{\mathbf{w}}$ denotes the vector with components giving the optimal installed capacities, ω_k , for a zone-technology pair k ; $\eta_k(t)$ and $\eta_k(t) \cdot \omega_k$ represent respectively the time-dependent predicted CF and energy generation for k . Thus, for both objective functions, we normalize the CFs by the total predicted demand $\sum_i D_i(t)$.

Comparing mixes from these strategies allows us to assess the benefits from **technological and geographical complementarity**. For instance, having non-zero installed capacities, ω_k , in two negatively correlated region-technology pairs produces lower risk than in case in which they are positively correlated or even uncorrelated (right side of Equation (2.2)).

3 Optimization Solutions: Main Relevant Elements of the Pareto Front

For each strategy, an optimal mix is obtained by minimizing the variance for a given desired mean penetration or vice versa [504, Appendix B], allowing a re-powering of the whole electricity system.

Given that, the mean-variance approach does not provide a single optimal mix but several optimal choices, referred as the optimal front curve $(\mu(\hat{\mathbf{w}}), \sigma(\hat{\mathbf{w}}))$ visualized in **the mean-standard deviation graph** (Figure 2.2 independently of the version of the variance that is minimized). So, one can simply choose the point (μ, σ) appropriate to his particular circumstance and allocate the mix accordingly. This allows more space to arbitrate between different mixes with high share of REs (requiring higher investment and operating costs) and mixes requiring less flexibility (less integration costs and less carbon emissions).

When the optimization constraint is imposed, installed capacities of the optimal mixes are not proportional to the penetration and risk level. Points located along **the constrained front** (blue plain line) represent Pareto optimal energy mixes under the current or historical or future climate and across regions that achieve the best risk level at a certain penetration level, and vice versa.

The numerical results suggest that the front of the bi-objective problem without optimization constraint is an upward line (black) with a positive slope that we refer to as **the mean-standard deviation ratio** or mean-risk ratio (2.5). In this **unconstrained case**, increasing the mean penetration of the optimal mix necessarily comes at the detriment of an increased risk; and the solutions are of the form:

$$\alpha^{global|technology|base} := \frac{\mu(\hat{w})}{\sigma_{global|technology|base}(\hat{w})}. \quad (2.5)$$

Mixes that produce mean-standard deviation values to **the right and below the black line** (mixes in the white region) are sub-optimal. These solutions are not Pareto optimal, since an improvement of one objective could be achieved without compromising the other. The point B is an example of sub-optimal mix, i.e., a higher mean penetration is achievable for the same variance (point A) and a lower variance is achievable for the same mean penetration (point C).

The area to the left and up from the black line cannot be reached independently of the optimization constraints, i.e., a lower levels of risk cannot be attainable with the considered solar and wind technologies efficiencies and available climate resource.

The optimal front is bounded below by a "**minimum-risk optimal mix**" below which the risk may only increase. This mix has the lowest penetration but also the lowest variance.

The optimal front is bounded above by a "**maximum-penetration optimal mix**" above which higher penetration mixes are not feasible due to the constraints of the problem. It corresponds to limits beyond which it is not possible to further increase the mean total penetration while satisfying the optimization constraints.

If no preference is put on maximizing the mean penetration or on minimizing the variance, the point at which the constrained front and the unconstrained front intersect represents the optimal mix with the maximum mean-standard deviation ratio. We refer to this point as the "**maximum mean-risk optimal mix**".

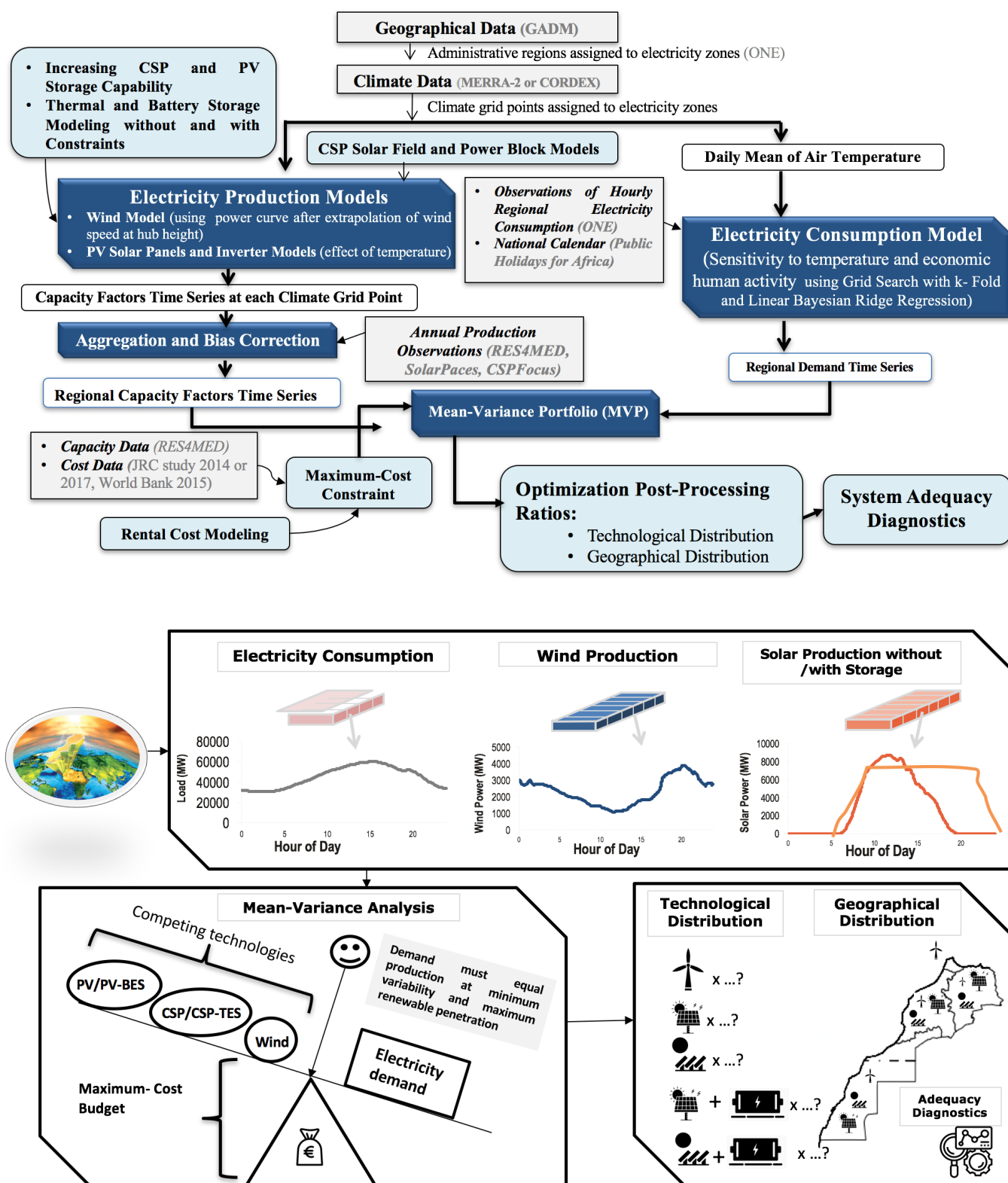


Figure 2.1: Flow chart of Energy for Climate Integrated Model (E4CLIM) components (dark blue) including the modules added (light blue) and the data sources (gray) illustrating the general framework of this thesis. The E4CLIM's flow is divided in three steps: (i) Capacity factors and demand time series are first estimated from climate grid points—assigned to electricity zones—and fitted to observations; (ii) The mix is then optimized using the Mean-Variance Portfolio approach; (iii) The mix properties (i.e., technological and geographical distribution) are analysed; (iv) The demand-production adequacy diagnostics are finally computed to give a more analysis of the reliability benefits provided by each renewable technology. **Data Availability:** The data used to support the findings of this thesis is included within this manuscript and is available upon reasonable request to ayataallahbouramdane@gmail.com. **Code Availability:** The E4CLIM open-source software is available online under GPL license at <https://doi.org/10.14768/20191105001.1> and its full documentation at <https://energy4climate.pages.in2p3.fr/public/e4clim/index.html>. All components of E4CLIM model and some modules added can be found at <https://gitlab.in2p3.fr/alexis.tantet/e4clim> (branch "morocco_api" or "dev-aya" or "new_country_morocco", updated two years ago and accessed on 22 February 2021). Source: Own elaboration.

III Model Set-up and Main Contribution to E4CLIM

In view of the controversial discussion of RE expansion that is going on in the Middle East and North African (MENA) region and specifically in Morocco, the E4CLIM model is implemented for Morocco and its electrical zones, as part of this thesis, by (i) calibrating it with the Moroccan geographical and energy data, (ii) integrating the specific production sources in Morocco (CSP with thermal storage) and other prospective sources (PV with batteries), (iii) adding a new modules enabling to analyze the sensitivity of the optimal mixes to solar technologies in terms of cost, storage and temporal system adequacy risk in historical, current and future climate conditions.

1 Domain and Calibration

To estimate the demand and Capacity Factors (CFs) time series needed for the mean-variance analysis (Section 2), regional boundaries to map climate grid points (Section ii) and energy data (Section ii and iii) are needed.

i Domain, Technologies and Grid Constraints

Morocco is located in the Maghreb region in North Africa. It is bordered to the North by the Strait of Gibraltar and the Mediterranean Sea, to the South by Mauritania, to the East by Algeria and to the West by the Atlantic Ocean (see the left graph of Figure 2.3). Morocco spans from the Mediterranean Sea and Atlantic Ocean on the north and the west respectively, into large mountains areas in the interior, to the Sahara desert in the far South.

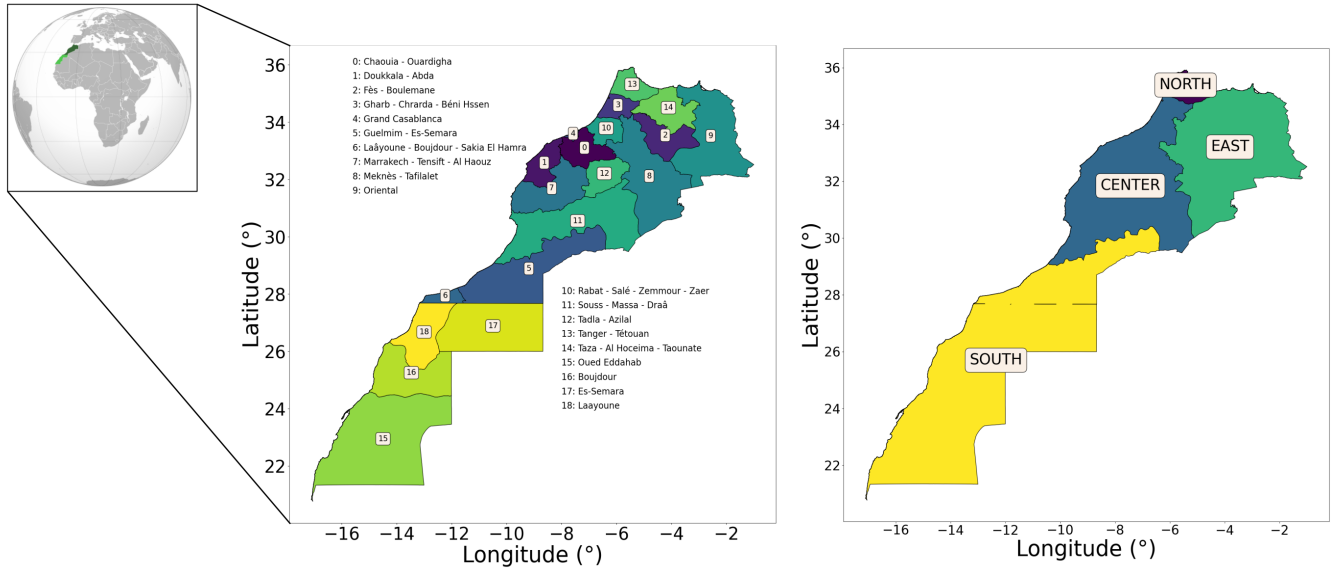


Figure 2.3: **Left:** Morocco's location—Undisputed territory (dark green) and Western Sahara (green), a territory claimed and occupied by Morocco. **Middle:** Morocco's administrative regions corresponding to the sub-division provided by the Global Administrative Areas (GADM) online database (<https://gadm.org/>); **Right:** Morocco's electrical zones according to the National Office of Electricity (ONE) [4]. Source: Own elaboration.

The geographical locations of the Moroccan administrative regions (the middle graph of figure 2.3) are downloaded from the Global Administrative Areas (GADM) online database (<https://gadm.org/>). GADM website provides maps and spatial locations of the world's administrative areas, at all levels of sub-division (countries, counties, departments, etc). The higher the level, the smaller is the polygon.

Morocco officially administers 12 administrative regions, including Dakhla-Oued Ed-Dahab, Laâyoune-Sakia El Hamra and Guelmim-Oued Noun that lies completely within the disputed territory of Western Sahara. However, at the time of this writing, the available data of GADM corresponds to the old division of the administrative regions where Morocco had 18 regions instead of the new territorial division into 12 regions announced in 2015 [24]. Moreover, GADM data considers the Moroccan territory to be just from the city of Tarfaya to the north, and the data do not include Western Sahara because this former Spanish is still considered a non-autonomous territory by the United Nations. Yet, the regional boundaries defined by the ONE [4] cover Western Sahara. We thus consider the region covered by Morocco and Western Sahara and concatenate the GADM data. **The 18 available administrative regions have been aggregated in the four electrical zones** (the right graph of figure 2.3) referred as NORTH, CENTER, EAST and SOUTH.

Morocco has seasonal droughts affecting its hydro resources [58] making the contribution of hydro power small in such country—where the largest percentage of its regions is characterized by semi-arid/arid climate—(currently 16% of the total electrical installed capacity in 2018 [23]). Although Morocco holds noteworthy hydro power stations, the technology in this country has reached its expansion limits, such that no major capacity additions are expected in the future if we exclude the pumped hydro storage technology (only 12% of the total electrical installed capacity is expected in 2030 [264, 7]). Therefore, operation of the existing hydro capacities has not been considered in the simulations; and due to the expected dominance of wind and solar power, we assume that, **a part from onshore wind, solar PV and CSP, both without or with storage, no other Renewable Energy (RE) technology takes part of the electricity generation**. Thus $j = \{PV, Wind, CSP\}$, and $j' = \{BES, TES\}$. The multi-index is thus either $k = (i, j)$ if no storage or $k = (i, j, j')$ if storage is integrated with solar technologies. This restriction is required to discern the influence of variable and flexible RE technologies with the least-cost and expensive RE technologies on the optimal mixes. We also consider that no new capacities are installed beyond **what is in service in 2018** (Table A.6, Appendix A).

In addition, Morocco is treated as “copper-plate” means that electricity power can flow unconstrained from any generation site to any demand site. In other words, we assume no network constraints and no exchanges with other countries. And, the mismatch between the demand and the RE production is taken into account in the mean (2.1) and risk, $\sigma_{\text{global}|\text{technology}|\text{base}}^2$ of the mean-variance optimization problem, used as proxies for the system adequacy services needed from the conventional plants or other flexibility options (e.g., imports, demand-response mechanisms, large-scale storage such as pumped hydro storage, etc).

ii Demand and Calendar Data

To fit the electricity demand model (Section I, Appendix A), the National Office of Electricity (ONE) provides us with a complete time series of hourly national electricity demand for Morocco in 2018 [4]. This time series data is broken down by electrical zone using scaling factors, provided by the ONE, based on the size, population density and economic activity of each zone. The electricity demand is higher for the most economically and populated CENTER zone (83 % of the national demand), followed by NORTH (10 %) and very low in EAST (5 %) and South (2 %) regions.

The national 2018 calendar used to separate the impact of working days, Saturdays and days-off (Sundays and holidays) on the electricity demand is collected from the web portal (<https://publicholidays.africa/>).

iii Capacity Factor Data and Bias Correction Approach

To get the time-mean observed CFs data for the four electrical zones, we first identify all the existing operational wind and solar power plants in Morocco in 2018 (Table A.6, Appendix A), and using their locations, we assigned these plants along with their installed capacities to the corresponding electrical zones, as shown in the left panel of figure 2.4. The actual (2018) geographical distribution of PV, onshore wind and CSP without or with thermal storage (TES), referred as CSP-TES, **capacities** is represented in the right panel of figure 2.4. As can be seen, there is a dominant contribution from wind energy in the SOUTH region. One also finds wind capacity in NORTH followed by CENTER. PV is installed in SOUTH followed by CENTER, while CSP-TES is installed in the CENTER and CSP in the EAST.

In addition to installed capacity, we need the **observations of production** to compute the observed CFs. Unfortunately, time series of observed solar and wind production from existing power plants, in Morocco,—allowing one to correct bias in the theoretical production models that stem from climate simulations—are not available in online databases at regional level and in appropriate intervals. All institutions involved in the energy sector, in Morocco, provide only figures and numbers with a monthly or annual resolution. Therefore, we collect the yearly electrical production and the associated installed capacity at the end of the year 2018 from various sources, such as the 2018 report on the Renewable Energy Solutions for the Mediterranean (RES4MED) [302], other websites emanating from public institutions involved in the energy sector in Morocco such as the Ministry of Energy, Mines and Environment (MEME) [23] and the Moroccan Agency for Sustainable Energy (MASEN) [25] [22]; or worldwide such as CSP focus website [10], Solar Power And Chemical Energy Systems (SolarPACES) website [33] and the Global Energy Observatory (GEO) website [14]. The table A.6 summarizes the installed capacity, $\omega_{k,p}^{obs}$, and the annual production, $Prod_{y,k,p}^{obs}$, and thus the observed capacity factors, $\eta_{y,k,p}^{obs}$, for each plant p , by specifying the region and the technology. Note that although the values of production and capacities appraised from these sources are compared, but this data is not consolidated since the different sources do not specify the year of the production estimation, but only the year of commissioning.

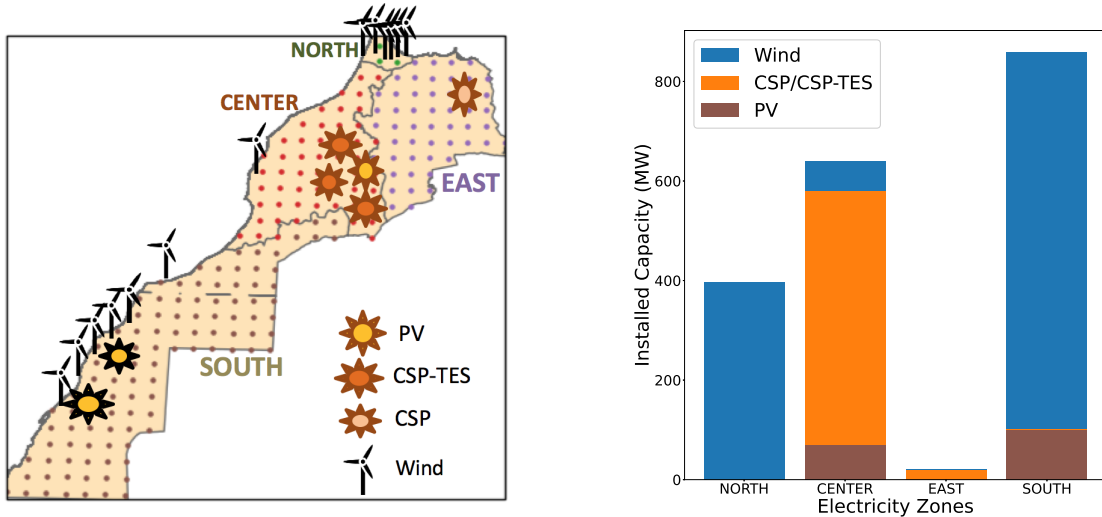


Figure 2.4: Based on [25, 21], at the end of 2018, the total wind, Photovoltaic (PV) and Concentrated Solar Power (CSP) without or with Thermal Energy Storage (TES) capacities are 1215 MW, 170 MW and 530 MW, respectively. **Left:** Localization of the operational solar and wind power plants in Morocco in 2018 (Table A.6, Appendix A). **Right:** Observed PV, wind and CSP/CSP-TES capacity distribution per electrical zones in Morocco in 2018 corresponding to the left panel of table 2.1. All CSP/CSP-TES (resp. PV) plants have similar Solar Multiple (SM) of 1.3-1.4 means 30-40% of thermal surplus (resp. Inverter Loading Ratio-ILR- of 1 means without storage) as shown in section 1 (Appendix A). All operational PV (resp. wind) plants are using tracking (resp. onshore without storage) [23]. The actual (2018) PV, wind, CSP-TES fraction of the most deployed system (PV-wind-CSP SM2 with 6 hours of TES) are displayed in brown, blue, and orange stars respectively in figure 3.1f (Chapter 3). The actual renewable penetration (without hydro and biomass capacities) is 17% with 9% comes from PV, 28% from CSP-TES and 63 % from wind. Source: Own elaboration based on data sources cited in table A.6 (Appendix A).

To this end, we compute the **regional bias-corrected CFs**, for each technology, from the 2018 wind, PV and CSP/CSP-TES installed

capacities, ω_k^{obs} for all k , and yearly-mean productions $Prod_{y,k}^{obs}$ given in the table 2.1. In fact, the computed CFs from climate data are rescaled so as their average over the climate data period, $\langle \eta_{h,k}^{clim} \rangle$, to coincide with the observations averages over 2018, $\eta_{y,k}^{obs}$ (Section 2, Appendix A). Since observed Renewable Energy (RE) production is not available in all the Moroccan regions, the bias correction approach is adapted so that instead of applying the mean bias correction factor, $\frac{\eta_{y,k}^{obs}}{\langle \eta_{h,k}^{clim} \rangle}$, to all regions indifferently, we get a bias correction factor by technology and region for each period of analysis depending on the climate data sources (Table A.3, Appendix A). And, for zones where no data is available for a given technology (marked by an empty set \emptyset in the table 2.1), a bias corrector averaged over all available zones for that technology is applied to the CFs computed from the climate data for that zone and technology. Let us insist that the present bias correction approach only corrects for differences in the yearly means of the CFs with the observed values but does not correct for the variances.

The subscript "obs" and "clim" denote, respectively, the observations and predictions from climate data. η_h and η_y correspond to hourly and yearly CFs. The brackets correspond to averages over all years available from the climate data (Section IV).

Zone	ω_k^{obs} (MW)			Zone	$Prod_{y,k}^{obs}$ (GWh)		
	Wind	PV	CSP/CSP-TES		Wind	PV	CSP/CSP-TES
NORTH	396.1	\emptyset	0	NORTH	1312	\emptyset	\emptyset
CENTER	60.0	70.0	510	CENTER	210	120	1734
EAST	\emptyset	\emptyset	20	EAST	\emptyset	\emptyset	55
SOUTH	759.6	100	\emptyset	SOUTH	3056	190	\emptyset

Table 2.1: Reference or observed capacities, ω_k^{obs} , (Left); and Yearly-mean generation, $Prod_{y,k}^{obs}$, (Right) per zone i and technology j if no storage or j, j' if with storage, installed in Morocco in 2018 (Table A.6, Appendix A). Zone-technology pairs, $k = (i, j)$ or $k = (i, j, j')$, for which no capacity is installed are marked by an empty set \emptyset .

In this thesis, all operational CSP and PV plants are considered (Table A.6, Appendix A) although PV and CSP technologies, tracking options and storage configurations are different from the ones considered in this thesis. For instance, the CSP technology of Noor 3 (solar tower) is different than CSP parabolic trough considered in our study (Section i). Moreover, the current (2018) PV plants integrate tracking system [23] which is not considered in our model (Section ii). And, no information is found if these plants uses our reference PV solar panel technology, the multi-crystalline silicon, or no [23]. This, however, together with the absence of consolidated hourly observations on time scales larger than a year **prevents validating CFs estimates against observations**. Due to the lack of better quality data, this annual production data is, at the moment, the best source of information.

2 Modules Added

With respect to the E4CLIM model described in section 1, it now includes additional modules, which will be described in the following sections, enabling us to conduct a sensitivity analysis of the optimal mixes to solar technologies (Section i, ii) in terms of storage (Section iii) and cost (Section iv), specifically the conditions under which each technology outpaces its counterpart across a set of penetration scenarios (Section v); together with the ability of each Renewable Energy (RE) technology to provide a reliability benefits (Section vi).

i CSP Production Modules

To investigate how solar PV and CSP technologies can be differentiated in optimized electricity mixes, **three CSP modules** (Figure 2.5) have been developed and added in the E4CLIM model: a generalized CSP module simulating the Solar Field (SF) which converts the solar irradiance into thermal energy (Section 1, Appendix A); a thermal energy storage module (TES) which stores the excess of thermal energy from SF (Section 2); and a Power Block (PB) module which converts into electricity the thermal energy from SF and/or from TES (Section 2, Appendix A).

In this thesis, **Parabolic trough (PT) has been selected among other CSP technologies** (i.e Linear Fresnel, Solar Tower, Dish Stirling) because it represents today's most widespread technology [268], in particular in Morocco [302, 33]. At the end of 2018, around 380 MW of CSP installed capacity connected to the grid used the PT technology in Morocco (Table A.6, Appendix A), mainly in the CENTER (the 160 MW Noor1 with 3 hours of TES; and the 200 MW Noor 2 with 7 hours of TES) and EAST (Ain Beni Mathar without TES). Autoproducers also generate electricity from PT plants such as the 3 MW Airlight Energy Ait Baha Pilot plant (with 5 hours of TES) in the SOUTH region [33, 10]. Fresnel technology is less commonly employed and if so, in much smaller plant size, mainly for auto-production or research purposes, such as the 1MW eCare Solar thermal project (with 2 hours of TES); or IRESEN 1MW CSP-ORC pilot project (with 20 min of TES) installed in the Green Energy Park (GEP) [18, 10]. There is still lack of commercial experience for solar tower due to its significant technical and financial risks, but could in the long-term provide cheaper electricity than PT and dish stirling system [11, 268]. Tower technology is recently being developed in CENTER region of Morocco (the 150 MW NOOR 3 with 7 hours of TES) [33].

At least for the coming decade, a large number of future CSP plants will most likely employ PT technology [37], and will have an increased number of minimum hours of thermal storage [12], particularly within the Moroccan Solar Plan (MSP) [451, 23]. Indeed, of the active worldwide CSP capacity by the end of 2018, around 53.6% of the CSP installed capacity is without storage, 12% has a TES capacity less than 6 hours, 29.2% have a TES capacity in the range of 6-10 hours and only 4.6% (resp. 0.5%) in the range of 10-<13 hours (>=13 hours). In contrast, 95.8% of the upcoming CSP capacity has storage (62.8% is with storage of 10-13 hours and 14% has over 13 hours storage); and only 4.2% is without TES [12]. This shows the increased interest to long hours of storage to provide reliable energy and reduce the cost of electricity generation from CSP by using a longer duration of TES [453].

In the following sections, CSP refers to PT CSP with **continuous north-south tracking** with the collectors facing the east in the morning and the west in the afternoon. In fact, north-south tracking allows the collectors to operate longer during the day and the energy generated to be more uniform. In addition, this orientation is relevant for locations with high summer peak and with relatively large seasonal irradiance variance [498] (i.e., Morocco, Figure 3.2b, 3.3c, Chapter 3).

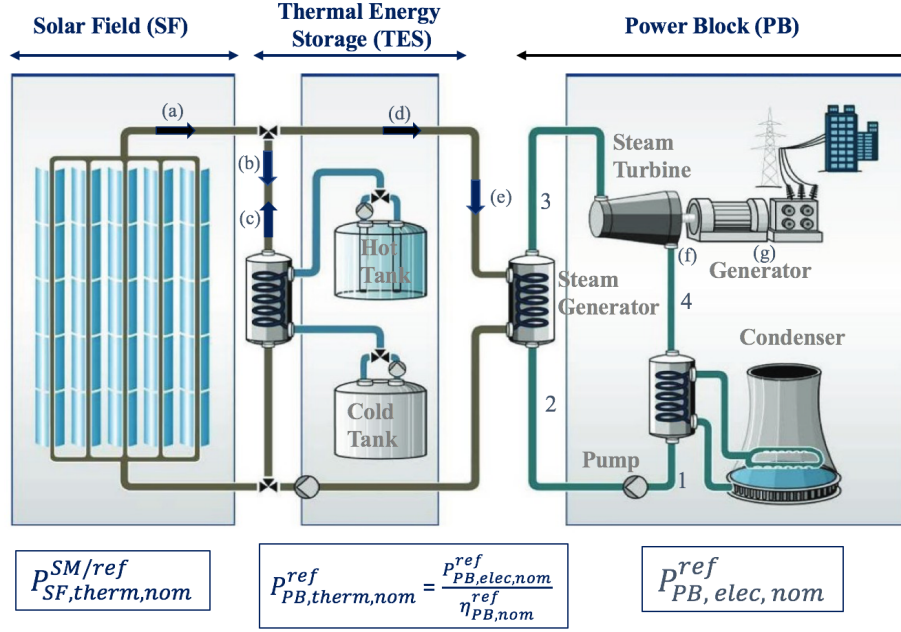


Figure 2.5: Schematic depiction of main components of Parabolic Trough Concentrated Solar Power plant illustrating the main calculated parameters (Section V, Appendix A and Section V of this chapter): **(a)**: Thermal energy provided by the solar field ($P_{SF,therm,nom}^{SM/ref}$); **(b)**: Thermal energy stored ($P_{SF \rightarrow TES,therm}^{SM/ref}$); **(c)**: Thermal energy discharged ($P_{TES \rightarrow PB,therm}^{SM/ref}$); **(d)**: Thermal energy that goes directly to the power block ($P_{SF \rightarrow PB,therm}^{SM/ref}$); **(e)**: Total thermal energy that enter to the power block ($P_{in} = P_{SF \rightarrow PB,therm}^{SM/ref} + P_{TES \rightarrow PB,therm}^{SM/ref}$); **(f)**: The thermal power of the turbine ($P_{turb,therm}^{SM}$); and **(g)**: The net electrical power output (P_{elec}^{SM}). $P_{PB,therm,nom}^{ref}$ is the thermal nominal capacity. We refer to "1" as the state of temperature and enthalpy after condensation; "2" after pump; "3" after steam generator (pre-heating, evaporation and superheating); and "4" after turbine (Figure A.4 (d), Appendix A). Adapted from Boukelia et al. [103].

The energy flow diagram (Figure 2.6) shows **the general structure of the CSP/CSP-TES model**. The complete set of equations needed to simulate the CSP (SF + PB) plant is described in section V (Appendix A). The modeling of a 50 MW reference CSP-TES plant Andasol 1 (Table A.2, Appendix A) is based on simplifying assumptions in order to keep the model as simple as possible and as detailed as necessary for this work. Firstly, the hourly Global Horizontal Irradiance (GHI) obtained from the climate data (Section IV) is partitioned into Direct Normal Irradiance (DNI) (Section 1, Appendix A) after calculating the solar angles required for the north-south CSP tracked surface (Section III, Appendix A). Then, the total thermal energy provided by the SF is modeled (Section 1, Appendix A), i.e., the geometrical, optical, thermal and field losses are calculated. The remaining energy per m^2 is then multiplied by the hourly DNI and the SF aperture area which depends on the thermal storage configuration, i.e., Solar Multiple (SM) of the CSP plant (Section 1). Secondly, the TES is modeled (Section 2). It is charged, if excess energy from the SF overpasses the maximum thermal capacity and discharged in case the SF cannot satisfy the load requirements of the PB for full load operation. The storage model is first simulated without constraints (Section 2, Appendix A) to calculate the storage parameters (i.e., energy storage capacity, maximum-power of charging/discharging). Then, these storage parameters (Table 2.3) are injected in the storage model with constraints (Figure 2.8). Thirdly, the PB model (Section 2, Appendix A) is set up by defining the steam turbine for dry cooling, used in this thesis, and generator efficiency; taking into account the parasitic losses.

ii PV Production Modules

For PV, a **multi-crystalline technology** is used due to its high market share [259]. Unlike CSP, the PV surface is not tracked-horizontal, it is **fixed-tilted up toward the South horizon by an angle equal to the local latitude**. This orientation is often selected since it averages the noontime irradiance peaks over the year [498, 327] to maximize the annual energy produced, particularly in Morocco [107].

The simulation of PV without or with Battery Energy Storage (BES) follow closely the methodology adapted in the CSP/CSP-TES model (Section i). The direct analog to CSP Solar Field (SF) is the PV Solar Panels (SP), and to thermal storage (TES) is the BES, and to CSP Power Block (PB) is the PV Inverter (INV), as illustrated in the left panel of figure 2.7.

The general structure of the PV/PV-BES model is as follows. First, the hourly GHI obtained from the climate data (Section IV) is decomposed into Global Tilted Irradiance (GTI) (Section 1, Appendix A) after calculating the solar angles required for the fixed latitude tilted PV surface (Section III, Appendix A). Then, the Direct Current (DC) energy provided by either the PV SP or the BES system is simulated (Section 1, Appendix A) for different battery storage durations, i.e., Inverter Loading Ratio or ILR (Section 1). Secondly, the BES is modeled (Section 2) following the maximal PV DC capacity. Finally, the electricity provided by the inverter is calculated (Section 2, Appendix A).

iii Storage Module

Due to weather and clouds, we rarely obtain the nominal conditions ratings from a solar CSP (resp. PV) plant. Moreover, a fraction of solar energy needs to be shifted due to the inherent coincidence of solar energy supply and energy demand patterns (i.e., duck curve phenomenon [47, 158], figure 1.14 in chapter 1). Therefore, an appropriate storage strategy is needed. A very common storage strategy is to save energy stored for time when the electricity prices and demand are high to achieve maximum revenues and only the remaining energy that the storage cannot admit goes to the turbine (resp. inverter) (e.g., for CSP [229, 1]). However, this operation strategy needs the ability to react

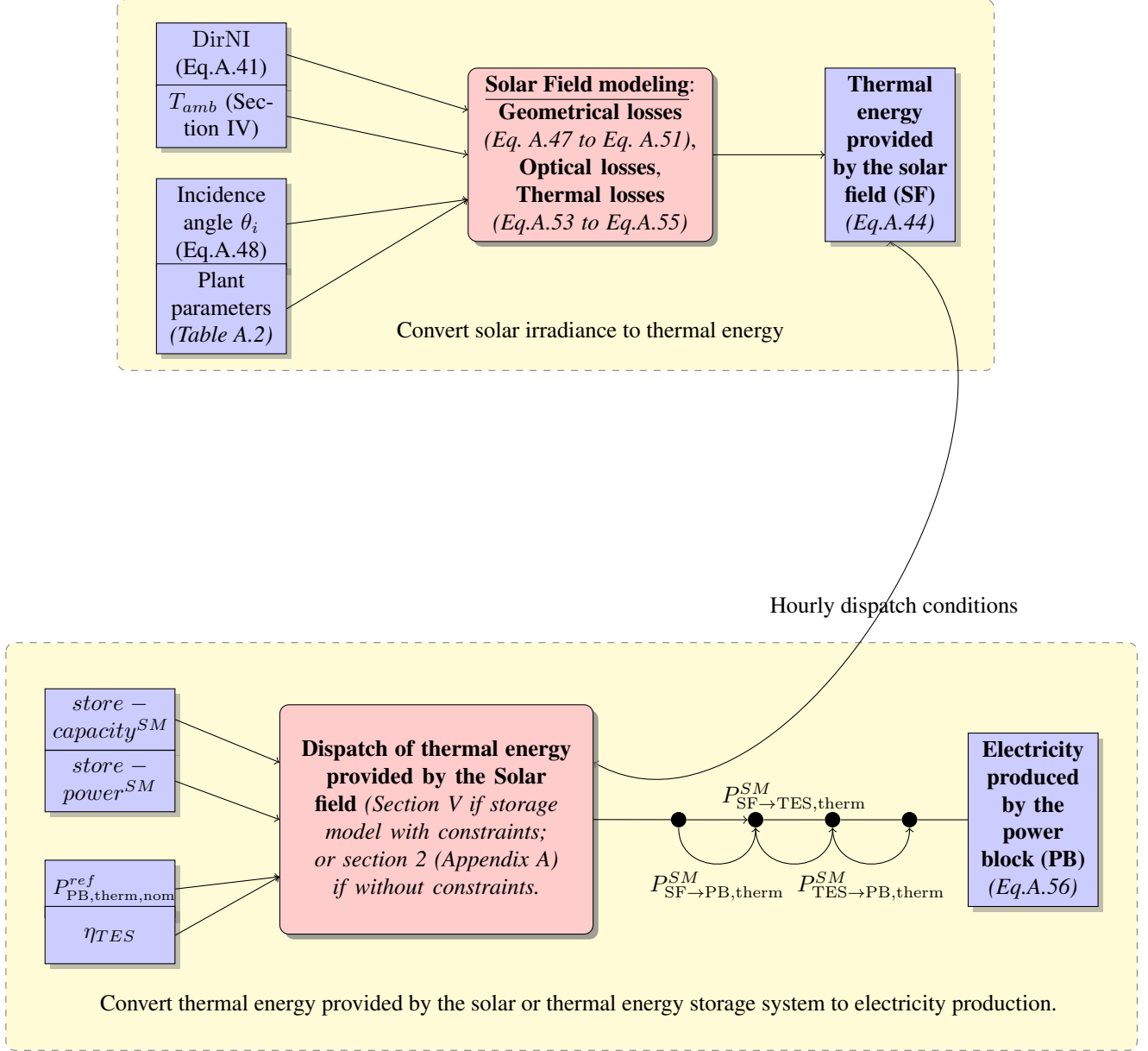


Figure 2.6: Flow chart of the general structure of the Concentrated Solar Power (CSP) model without and with Thermal Energy Storage (TES). DirNI is the Direct Normal Irradiation; T_{amb} is the ambient temperature; $store - capacity^{SM}$ (resp. $store - power^{SM}$) is the CSP thermal storage capacity (resp. maximum-power of storage) given for each Solar Multiple (SM); η_{TES} is the TES efficiency; $P_{PB,therm,nom}^{ref}$ is the thermal nominal capacity of reference (Table A.2, Appendix A); $P_{SF \rightarrow TES,therm}^{SM}$ is the thermal energy stored; $P_{TES \rightarrow PB,therm}^{SM}$ is the thermal energy discharged; $P_{SF \rightarrow PB,therm}^{SM}$ is the thermal energy that goes directly to the power block; and $P_{in} = P_{SF \rightarrow PB,therm}^{SM} + P_{TES \rightarrow PB,therm}^{SM}$ is the total thermal energy that enter to the power block. Source: Own elaboration.

very quickly to price fluctuations and only operate during peak load hours, so that low Capacity Factor (CF) is achieved. However, to maximize the RE penetration (2.1), one has to maximize the power output throughout the day and night (if possible).

In addition, by operating the CSP power block (resp. PV inverter) during more hours of the day its upfront costs can be distributed over more units of energy, which demonstrate the interest of increasing the hours of operation.

Since utility-scale PV-BES plant deployment has not yet reached the level of large-scale CSP-TES in providing dispatchable energy, the concepts and nomenclature of solar-plus-storage plant configurations are well established for CSP-TES than for PV-BES. For the sake of simplicity, we illustrate in section 1, **the general approach used to increase the full load operating hours** of CSP-TES and PV-BES by referring to related equivalent terms. In addition, section 2 presents the **storage model implemented to the thermal and battery storage systems** combined with CSP and PV, where for each storage configuration, we follow the nominal thermal (resp. DC) capacity in order to maximize the CSP (resp. PV) CFs.

iv Cost Modules

In the optimization problem, some constraints are necessary. First, the capacities, ω_k for all k , are constrained to be positive (i.e., $\omega_k \geq 0 \quad \forall k$, positivity bounds on capacities). Second, instead of using the total installed capacity as an upper bound in the optimization problem [504], so $\sum_k \omega_k = \omega_k^{pbs}$, in this thesis, a different strategy is followed.

To take into account the differences in rental cost between PV/PV-BES, wind, CSP/CSP-TES technologies in the optimization problem,

we add a **maximum-cost constraint** to allow the model to recommission PV/PV-BES, wind and CSP/CSP-TES capacities at a cost limited by the total cost of all capacities, ω_k^{obs} for all k , installed in Morocco in 2018 (Section VII).

Usually, the rental cost or the cost per installed capacity of CSP and PV plants utilizing storage with several hours will be much higher than those of plants without storage or with lower amount of storage. Therefore, evaluating a specific technology j or j, j' in the mix requires calculating the technology rental cost, c_j , but also the storage rental cost, $c_{j'}$. Adequate storage cost assessment is challenging due to the diversity of technologies possessing different characteristics [109]. A directly comparable metric to the Levelized Cost Of Electricity (LCOE) for generation technologies is the Levelized Cost Of Storage (LCOS) and represents an appropriate tool for cost comparison of electricity storage technologies [288, 311]. LCOS quantifies the discounted cost per unit of discharged electricity for a specific technology. The metric therefore accounts for all technical and economic parameters affecting the lifetime cost of discharging stored electricity. Despite an increasing number of LCOS calculations and analysis [316, 406, 81], there is not yet a common definition of this metric [185, 562, 387]. While some studies neglect cost parameters like replacement [562, 311, 387], others exclude relevant performance parameters, such as capacity degradation [46, 81, 316]. Schmidt et al. [470] present an approach for calculating the LCOS taking into account these parameters. However, available cost data is limited to investment, fixed and variable operation and maintenance costs.

For this reason, **different rental cost formulations** is implemented in this thesis (Section VIII), for production and storage technologies, based on the available cost parameters data. In case the increased cost related to increased storage size is considered, we have to apply constraints on the storage capacity and the maximum-power of charging/discharging in the storage model (Section 2). Otherwise, the storage constraints should be ignored (Section 2).

v Optimization Post-Processing Module

Different configurations of CSP solar multiple (resp. PV inverter loading ratio) change the properties of the plant's dispatchability (bottom panels of figures 2.9 and 2.10) and the plant's cost (Table 2.6). Although plants with high amount of storage should in principle cost more, they are able to achieve lower variability since they can generate power on demand although they depend on unstable solar irradiance conditions. Therefore, the trade-off between the increased cost and the lower variance must be examined under different penetration scenarios.

In addition, when looking for optimal mixes integrating both PV and CSP, both with different amount of storage, the relevant contributing factors towards determining what region a given capacity will be assigned to are; and the conditions under which the high cost of CSP—considering its benefits of dispatchable energy provided by cheap TES—can provide an advantage against the low-cost PV combined with costly BES so as to be part of the mix until a more advantageous condition prevents its integration need to be thoroughly investigated. Given the example of two solar plants, CSP and PV plants, with the same size, the one with less rental cost or high mean CF or less variance in the generation is undoubtedly preferred over the other according to the optimization objectives (i.e., maximizing the penetration or minimizing the variance). Therefore, some **optimization ratios** are computed to explain the behavior of the optimization problem in determining the technology that is installed in which zone in priority for each penetration regime (Section IX). A complementary tool to the mean-standard deviation diagram (Figure 2.2) to better visualize the technological distribution of installed capacities associated with particular mixes is **the technology-region fraction against the mean penetration** along a particular optimal front (Figure 2.13).

vi System Adequacy Diagnostics Module

In electricity grids, consumption and production of electricity need to be equal at all times and at every point to keep the operating grid frequency of 50 Hz (Kirchhoff law). If frequency drops below this value, more power is required to stabilize the grid (positive reserves is needed). In the case of a higher frequency, less power is required (negative reserves is needed) to reduce the curtailment. Grid services are thus required to deliver power in secure manner to maintain the system frequency within the predicted range.

The least-cost RE technologies (PV, wind) are variable with non synchronous production and thus are likely to affect the system adequacy (i.e., ability of the generator to supply a given demand in all the points and at any time [55]); while dispatchable plants (CSP-TES and PV-BES) provide grid flexibility (i.e., the ability to respond to uncertainty and variability) but they are expensive.

Given that, **the reliability benefits (resp.challenges) that each RE technology provides (resp. causes) need to be explored**. The definition of the risk (2.2) based on the variance of the RE production with respect to the demand is only an aggregate measure of the variability of the RE production which does not take into account the specific timing of the fluctuations (i.e., if the imbalances between RE production and demand occur during peak or mid or base load). For instance, the fuel cost of marginal generators operated during peak hours is much higher than that of base load plants operating during low-load periods. Thus, the RE production tend to be more valuable if it occurs during a peak load than during a low load since peak demand hours often place particular pressure on utilities both in terms of the availability of electrical energy and the associated cost to supply the energy demanded by consumers in such times. The timing of wind and solar power output has, thus, an important influence on the "physical" value of energy that is dispatched by PV-BES and CSP-TES or produced by PV/CSP or wind.

We implicitly illustrate this value by adding some system adequacy diagnostics (Section X) based on the Residual load Duration Curve (RLDC) such as the average capacity credit, the average mid and base load reduction and the average curtailed energy to compare the ability of different RE technologies in displacing conventional capacity in different load bands.

We use also the **heatmap tools** to illustrate the daily and seasonal correlation of CFs and demand.

IV Climate Data Sources

In order to conduct analysis of scenarios of Renewable Energy (RE) integration, historical and future changes in wind and solar Capacity Factors (CFs) and consumption—on which the mean-variance optimization problem (Section 2) relies—over Morocco at a high temporal resolution are required. As previously mentioned (Section ii and iii), observations of these time series are not available or often limited to a few years at best in only some regions of the world. This is not sufficient to take into account the effect of low and high frequency climate fluctuations on covariances between energy time series properly. In addition, relying on energy observation does not allow for analyzing future changes.

In this thesis, two climate data sources are used to compute these energy time series. First, the "MERRA-2 Reanalysis" (Section 1) presents the advantage to be hourly sampled and allows to conduct historical regional climate analysis for a broad range of weather and climate time scales. Another climate dataset, the "CORDEX Simulations" (Section 2), which is contrary to reanalysis products, is available on daily basis

but provides projections for the 21st century, which could be used to study scenarios of climate change to understand the variability and changes in regional climate phenomena, and their impacts on the energy mixes.

1 MERRA-2 Reanalysis

The Modern-Era Retrospective Analysis for Research and Applications 2 (MERRA-2) is the latest atmospheric reanalysis produced by the National Aeronautics and Space Administration (NASA) for the satellite era. As a **reanalysis**, it combines observation data from NASA's Global Modeling and Assimilation Office (GMAO) and NASA's Goddard Earth Observing System (GEOS) model. Observations are assimilated by the Atmospheric Data Assimilation System (ADAS) [210]. MERRA-2 products are **accessible online** through the NASA Goddard Earth Sciences Data Information Services Center (GES DISC) available at (<https://disc.gsfc.nasa.gov/datasets?project=MERRA-2>).

MERRA-2 reanalysis provides **hourly values of** surface density (RHOA), surface temperature (TLML), surface downward irradiance (SWGDN), zonal wind (U10M) and meridional wind (V10M), with a **horizontal resolution** of $0.4^\circ \times 0.62^\circ$ in latitude and longitude, respectively covering a **long period (from 1980 to present day)**. Note that the wind speed is provided for different heights. The height chosen is 10m, which is expected to be more impacted by surface friction than higher heights which are less turbulent and are closer to the hub height (101m) (See discussion in section 1, Appendix A).

2 CORDEX Simulations

The COordinated Regional climate Downscaling EXperiment (CORDEX) is a World Climate Research Program (WCRP) framework that enable to produce regional climate simulations through downscaling and through a set of experiments and emission scenarios. CORDEX simulations published on ESGF (<https://esgf-node.ipsl.upmc.fr/search/cordex-ipsl/>) can also be **accessed via the web portal** (www.climate4impact.eu).

i Domain and Climate Models

In this thesis, we consider the **MENA-CORDEX domain** covering the Middle East peninsula, North Africa, and Southern Europe; with a 0.44° (44 km) **horizontal resolution** "MNA-44".

The following **variables** are recorded on **daily basis**: surface temperature (tas), zonal wind (uas), meridional wind (vas), surface downward irradiance (rsds), surface specific humidity (huss), surface pressure (ps), and sea level pressure (psl).

The MENA-CORDEX simulations rely on global and regional climate models. In fact, **Global Climate Models (GCMs)** are able to simulate the largest scale features of atmospheric circulation and are capable of reproducing the three-dimensional structure of the ocean-atmosphere similar to that which is observed. However, they generally operate on a relatively coarse horizontal resolution of 100-300 Km. This implies that regional details of the mesoscale circulations such as the land-sea distribution and altitude of mountains and other processes are not well resolved [57]. As it is computationally expensive to run GCMs at high resolution, statistical and dynamical downscaling techniques are applied to increase the resolution and thereby improve the degree of detail. Statistical downscaling utilizes empirical relationships between large-scale features and local conditions assuming that these relations stay the same in a changing climate. Dynamical downscaling makes use of **Regional Climate Models (RCMs)** that are set up on a smaller domain at higher resolution compared to the GCM [460]. RCMs typically operate on a horizontal scale of 10-50 km.

As the climate in any region of the world is affected by global large-scale circulation features, the idea of RCM is that the GCM provides the large-scale weather systems as lateral boundary conditions for RCMs to obtain details of climatic patterns over a limited area. The difference between these models is that GCMs only need initial conditions (often from the reanalysis), while RCMs are driven by initial and lateral boundary conditions—updated every 6 h and provided by GCMs or reanalysis [57].

The dynamical downscaling cannot, albeit the higher resolution of the RCMs, resolve all problems inherited from the GCMs. Regional climate simulations thus reflect not only model-to-model differences among the driving GCMs but also added internal biases related to parameterization of physical processes (for example, cloud formation) and other factors. In addition to this **model uncertainty**, there are two other main sources of uncertainties in climate scenarios for the future such as the natural variability and emissions scenario uncertainty. The relative importance of these uncertainties varies with prediction length and resolution [249].

To assess the level of agreement between different models within an energy systems, we perform RCM simulations using two models over the area of study (Morocco) using a boundary conditions from four GCMs provided by two institutions. The two RCMs that have been considered to downscale the four coupled atmosphere-ocean GCM (AOGCMs)—taken from the 5th Coupled Model Intercomparison Project (CMIP5) [506] of the Fifth Assessment Report (AR5) of the Intergovernmental Panel on Climate Change (IPCC) [499]—, with their related modeling center as well as their host institution are represented in table 2.2.

ii Experiments and Scenario

Two experiments are performed. First, the historical simulations over the period (1951 – 2005) are used to study the evolution of the climate response to historical observed forcing. Second, a future simulations over the period (2006-2100) are used to analyze the future projections of climate conditions. The latter are based on the development of forward-looking scenarios.

Studies conducted before 2014 tend to use scenarios by the Special Report on Emissions Scenarios (SRES) [374] while later studies are usually based on those by the AR5 report of IPCC [499]. The former is sequential and is based on four families of emission scenarios (A1, A2, B1 and B2) depending on the focus of future development (economic -A- or environmental -B-) and on its homogeneity (globalized -1- or with regional focus -2-). The latter is based on a parallel approach and provides four trajectories of greenhouse concentrations in the long term, called Representative Concentration Pathways (RCP) [534, 366]. The four RCP scenarios have been translated in terms of radiative forcing, i.e., modification of the planet radiative balance which represents the difference between the solar irradiance received and the infrared irradiance re-emitted by the planet. The higher the concentration, the higher the value of the radiative forcing, the more the earth-atmosphere system gains in energy and heats up leading to high projected increase of global temperature. The four scenarios go from 2.6 to 8.5 W/m^2 of radiative forcing. The greenhouse gases, ozone and aerosol emissions as well as land use pathways were built with Integrated Assessment Models (IAMs) under several assumptions related to energy, demography and economy [135]. The climate scenarios emerging from these simulations are in turn used in impact models to assess the impacts and plan for adaptation and mitigation options.

Table 2.2: Climate models used to project the potential climate change impacts on optimal mixes (Chapter 5), with their modeling center (**first column**), host institution (**second column**), Global Climate Model (GCM) acronym (**third column**), as well as the Regional Climate Model (RCM) acronym (**fourth column**). We use two RCMs: version 4 of the Rossby Centre regional Atmospheric model (RCA4) and the version 351 of the Weather Research and Forecasting model (WRF351); driven by four GCMs: Centre National de Recherches Météorologiques-Coupled Model (CNRM-CM5); Earth System Model (EC-EARTH); Geophysical Fluid Dynamics Laboratory’s Earth System Model (GFDL-ESM2M); Community Climate System Model (CCSM4) taken from the 5th Coupled Model Intercomparison Project (CMIP5) [506] of the Fifth Assessment Report (AR5) of the Intergovernmental Panel on Climate Change (IPCC) [499] in the COordinated Regional climate Downscaling EXperiment (CORDEX) framework for Middle East and North Africa (MENA) domain. Three models are provided by the Swedish Meteorological and Hydrological Institute (SMHI) and one is provided from the Cyprus Institute (CyI). The interested reader is referred to the sources mentioned for a more detailed description of the models.

CORDEX-CMIP5 Climate Models			
Modelling Center	Host Institution	GCM Acronym	RCM Acronym
Centre National de Recherches Météorologiques - Centre Européen de Recherche et Formation Avancées en Calcul Scientifique (CNRM-CERFACS)	SMHI	CNRM-CM5 (Voldoire et al., 2012 [533])	RCA4 (Jones et al., 2011 [282])
EC-EARTH Consortium	SMHI	EC-EARTH (Hazeleger et al., 2010) [250]	RCA4 (Jones et al., 2011 [282])
Geophysical Fluid Dynamics Laboratory (GFDL) of the National Oceanic and Atmospheric Administration (NOAA)	SMHI	GFDL-ESM2M (Dunne et al., 2012 [179])	RCA4 (Jones et al., 2011 [282])
National Center for Atmospheric Research (NCAR)	CyI	CCSM4 (Gent et al., 2011 [211])	WRF351 (Powers et al., 2017 [422] and Skamarock et al., 2008 [486]).

In this thesis, the future simulations are performed with only **RCP 8.5 scenario** corresponding to the most emissive scenario with the highest projected global warming at the end of the 21st century [450, 472]. It, thus, relates to a radiative forcing of roughly 8.5 W/m^2 by 2100 relative to the pre-industrial period.

iii Solar and Wind Intra-daily Parametrization

A large fraction of the variance of the RE production and demand is contained in shorter periods than a day which significantly impact the mean-variance analysis and thus the technological and geographical distribution of capacities. For instance, solar production is more variable during the day than wind. Therefore, ignoring intraday fluctuations may results in distributing more solar capacities in the optimization problem. To overcome this problem, the solar and wind CF models include a parametrization of intraday fluctuations in case the daily mean climate data—which comes from the CORDEX simulations—is used.

To account for the intraday fluctuations of the solar production, the Global Horizontal Irradiance (GHI) data is parametrized by assuming that **the clearness index is constant within a day** and given by the CORDEX data. The hourly GHI is then computed by applying this clearness index to the hourly horizontal extraterrestrial irradiance that we calculate from solar position (Section 2, Appendix A).

To take into account the intra-daily fluctuations in wind output, wind speed data is parametrized by assuming that **the hourly wind speed realizations follow a multi-variate Weibull distribution**. The shape parameter and the correlation matrix of this distribution are assumed to vary in space only and are computed for each grid point using the MERRA-2 climate reanalysis. The scale parameter is computed for each day and each grid point (Section 3, Appendix A).

Hourly time series of the regional demand is predicted from the full length of the temperature record by randomly drawing samples from the posterior distribution of the model at each time step (Section I, Appendix A). That is to say that **the demand model do not include a parametrization of intraday fluctuations of surface temperature**. Indeed, using both climate data sources, we consider, for each day, the daily-mean temperature. In other words, we assume that the intraday fluctuations of the temperature is constant since the activation of the heating and air-conditioning systems do not vary throughout the day. This assumption may, however, amplify the amplitude of the daily demand and thus overestimate the variance of the predicted electricity consumption.

Intra-daily fluctuations of temperature are also not considered in wind and solar CF models.

3 Period of Analysis

To optimize the electricity mix, it is important to use a multiple years of climate data to account for low-frequency variations [208] in the electricity demand and CFs.

For the first study (Chapter 3) and second study (Chapter 4) of this thesis—where we aim to analyze the sensitivity of optimal mixes to thermal and battery storage and cost associated with solar CSP and PV technologies; together with the role of storage and spatio-temporal complementarity in reducing the adequacy risk—, **the MERRA-2 climate data is used**. We estimate the CFs and demand over the whole period (1980 – 2019) available from the MERRA-2 online database (Section 1). Since the inter-annual variability of the mean CFs and mean demand (inputs of the optimization problem) over the period (1980 – 2019) is found weak (Figure A.6, Appendix A); and since the length of the regional observed demand time series is limited to one year (2018) on hourly basis (Section ii) and only means of observed regional CFs over the same year are available (Section iii), we consider that the climate over the period (1980 – 2019) is represented by the year 2018 to correct bias in the RE production models and fit the demand model (Tables A.3a and A.1a, Appendix A). Thus, the **analysis of chapter 3 and 4 are carried out over one year** spanning the period from January of 2018 to December 2018 to improve the bias in the variance of the CFs since our objective is to analyze the sensitivity of the mix to storage and cost associated with solar technologies and not to find the long-term planning for system capacity (i.e., ensuring that sufficient RE production is available to meet the long-range consumption needs).

For the third study (Chapter 5) of this thesis, CORDEX regional simulations (Section 2) are used to assess the impact of climate variability and climate change on the optimal mixes. The CFs and demand energy time series are computed over the whole historical experiment period (1951-2005) to compute the bias correction factors and the demand model parameters (Tables A.3 and A.1, both (b)(c)(d)(e), Appendix A). These parameters are used for the calculations of the future hourly regional predicted demand and bias-corrected CFs computed using the whole RCP 8.5 experiment period (over 2006-2100). It should be noted that the year (2018), for which observations of CFs and demand are available, do not overlap with the end-year of the historical experiment (2005). Due to the lack of better data, we assume that the 2018 observed demand, the 2018 national calendar and the 2018 observed RE CFs (Table 2.1) are similar to that of 2005 (i.e., the yearly CFs and time series of the demand are stationary between 2005 – 2018 and without obvious trends) since the external (natural) forcing associated with the increase of solar irradiance change very little from year to another (i.e., no inter-annual variability of the daily and seasonal cycle). However, we assume that the internal forcing (e.g., chaos linked to the changes in the phases of the North Atlantic Oscillation (NAO) in the Mediterranean region [423]) is only considered as a noise that impacts the regression in the demand model and the bias correction of the CFs (Section I and 2, Appendix A). **For the analysis of chapter 5, we consider only 30 years for each experiment** (historical and future simulations) to estimate statistics resolving the climate variability and climate change on a sufficiently wide range of time scales, large enough to scale with the typical lifetime of wind, PV and CSP plants [453]. The historical experiment based on observed forcing is carried out over the period (1976 – 2005) which represent the available data that may represents the historical climate conditions. The last 30 years before the end 21st century (2071 – 2100) are chosen to analyze the future projections as compromise to keep the period sufficiently long for a reasonable signal-to-noise ratio.

V Storage Modeling

This section begins with a simplified method for the design of solar dispatchable plants (CSP-TES, PV-BES) allowing a full-load operation hours ranging from a few hours after sunset to continuous operation until the next day, thereby better adapting the profile of solar production to demand (Section 1). Then, we present an extensible approach of the developed storage model that can be used to represent a variety of storage operation strategies according to the context. In section 2, we present the general framework that can be implemented for the thermal and battery storage systems incorporated in CSP and PV plants by following the nominal thermal (resp. DC) capacity in order to obtain more energy output (i.e., greater penetration of REs).

The left panel of figure 2.7 represents a block diagram of a CSP-TES (resp. PV-BES) plant components. The left corner block is the CSP Solar Field -SF- (resp. PV Solar Panel -SP-) providing thermal (resp. Direct Current -DC-) output; the corner block on the right is the CSP Power Block -PB- (resp. PV Inverter -INV-) providing electrical output. To the bottom is the Thermal (resp. Battery) Energy Storage system (i.e., TES and BES). The black arrows represent thermal (resp. DC) / electrical flows to illustrate the meaning of each parameter calculated. To simplify, let us consider $X = \{SF, SP\}$; $Y = \{PB, INV\}$; $\Theta = \{TES, BES\}$; $x = \{therm, DC\}$; and $y = \{elec\}$.

1 CSP Solar Multiple and PV Inverter Loading Ratio

To extend the solar production for several hours, different sizing approaches exist depending on the desired type of plant (i.e., base, peak or intermediate plant ..) [327, 2]. In our study, we hold the CSP PB (resp. PV INV) fixed and size the CSP SF (resp. PV SP) and thermal (resp. battery) storage system in relation to the PB (resp. INV). In other words, **we install more thermal (resp. DC) power capacity on a PB (resp. INV) system than its power rating** (right panel of figure 2.7). The ratio between the thermal (resp. DC) power produced by the CSP SF (resp. PV SP) and the thermal (resp. DC) power required by the PB (resp. INV) at nominal conditions is called the Solar Multiple-SM- (resp. Inverter Loading Ratio-ILR-) [2, 194]. For more details on the definition of these parameters, see section 1 (Appendix A).

These parameters are proportional to the number of hours of production from the thermal (resp. DC) energy stored. There is, however, an indirect relationship between the SM (resp. ILR) and the storage size: **The higher the SM (resp. ILR), the higher is the aperture area of the SF (resp. SP) (2.6) (Figure A.5, Appendix A), which require larger storage capacity:**

$$A_X^{SM/ILR} := \frac{SM/ILR * P_{X,nom}^{ref}}{\eta_{X,nom}^{ref} * S} = A_X^{ref} * \frac{SM/ILR}{SM^{ref}/ILR^{ref}}, \quad (2.6)$$

with $S = \{DirNI_{DP}, GTI_{STC}\}$ is the Direct Normal Irradiance at the Design Point (DP); and the Global Tilted Irradiance at the Standard Test Conditions (STC) which are needed respectively by CSP and PV. The term, $P_{X,nom}^{ref}$ is the thermal (resp. DC) nominal capacity. The quantities A_X^{ref} , $\eta_{X,nom}^{ref}$ and SM^{ref}/ILR^{ref} are respectively the reference CSP SF (resp. PV SP) area, efficiency and CSP SM (resp. PV ILR) [451].

Unlike PV, almost all CSP plants, being developed in Morocco, are with storage (Table A.6, Appendix A). In our study, **the reference configuration of TES** is that of the 50 MW plant Andasol 1 (Table A.2, Appendix A) with SM^{ref} that we found equal to 1.87 (Figure A.5, Appendix A), means that the SF delivers a 87% greater thermal energy than is required to generate the nominal power. The 87% excess energy can be delivered to TES. We also consider a SMs of 2, 3 and 4 by increasing, A_{SF}^{SM} , proportionally from its reference value using equation (2.6). A case without storage is also considered in which the area, A_{SF}^{SM} , is set for SM equal to 1.

For PV, the case without storage, $ILR^{ref} = 1$, has been chosen as **reference configuration of BES**. For the sake of comparison between PV-BES and CSP-TES, ILR of 2,3,4 are considered. With CSP SM4 (resp. PV ILR4), the plants are able to run at nearly constant output

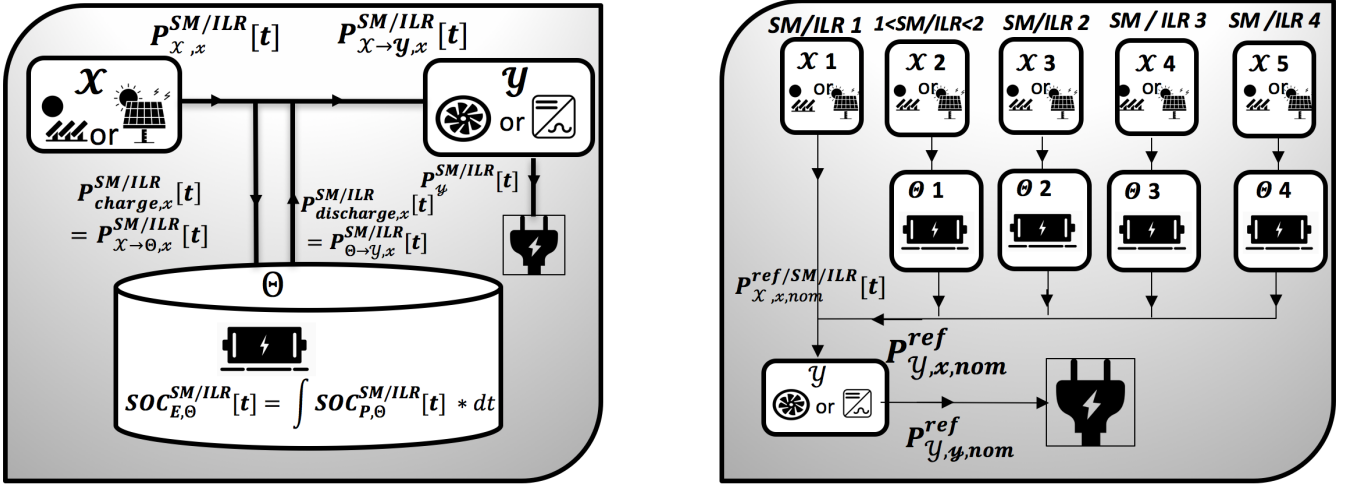


Figure 2.7: **Left:** Scheme of the three modules of Concentrated Solar Power-CSP- (resp. Photovoltaic-PV-) plant: Solar Field-SF- (resp. Solar Panel-SP-); Thermal-TES- (resp. Battery-BES-) Energy Storage; and Power Block-PB- (resp. Inverter-INV-). $X = \{SF, SP\}$; $Y = \{PB, INV\}$; and $\Theta = \{TES, BES\}$. The black arrows represent the energy flows: Thermal (resp. Direct Current-DC-) energy provided by SF (resp. SP) ($P_{X \rightarrow \Theta, x}^{SM/ILR}$); Energy from SF (resp. SP) to PB (resp. INV) ($P_{X \rightarrow Y, x}^{SM/ILR}$); Energy stored ($P_{X \rightarrow \Theta, x}^{SM/ILR}$); Energy discharged ($P_{\Theta \rightarrow Y, x}^{SM/ILR}$); Total thermal (resp. DC) available energy injected to the Power Block (resp. Inverter) ($P_{X \rightarrow Y, x}^{SM/ILR} + P_{\Theta \rightarrow Y, x}^{SM/ILR}$) and the State of charge ($SOC_{E, \Theta}^{SM/ILR}$). $x = \{therm, DC\}$ and $y = \{elec\}$. **Right:** Illustration of CSP (resp. PV) plant configuration with different Solar Multiple-SM- (resp. Inverter Loading Ratio-ILR-). ILR1 or SM1: without storage; ILR>1 or SM>1: with increasing levels of storage from PV or CSP. For more description of these parameters, see section 1 (Appendix A). Source: Own elaboration based on [2].

(Figure 3.2e and 4.3c in chapter 3 and 4). Therefore, further increasing CSP SM (resp. PV ILR) does not make sense, as during high irradiance periods they would increasingly unused surplus energy.

2 Storage Model Approach

In our study, the storage model is based on a **set of dispatch conditions** (Figure 2.8) that takes into account the frequency of charging and discharging instead of relying on heuristics or optimization problem [113] or applying a moving average filter [51] or Gaussian-based method [44] often used to smooth the hourly daily fluctuations.

CSP production tend to produce more in grid cell with the most favorable solar resource conditions, and often a minor portion of a grid points with high irradiance may host enough capacity installed. Given that, a higher percentile instead of the average could better illustrate **the storage parameters**, namely the storage capacity, $store - capacity^{SM/ILR}$, and the maximum-power of storage, $store - power^{SM/ILR}$. These parameters are respectively calculated as the 95th percentile of the state of charge, $SOC_{E, \Theta}^{SM/ILR}$, and the energy charged, $P_{X \rightarrow \Theta, x}^{SM/ILR}$, for all climate grid points over one year (2018) by running the storage model without constraints.

In fact, **the storage model without constraints** compared to the one with constraints (Figure 2.8) assumes that the storage system is never full, even after putting the CSP SF (resp. PV SP) excess, and thus always available (i.e. empty or half empty storage). That is to say, that the storage system is always over-dimensioned to explore the solar resource and maintain full output (Section 2, Appendix A).

The storage model with constraints assumes that the storage system can be already full if the state of charge, $SOC_{E, \Theta}^{SM/ILR}$, exceeds the storage capacity at some time spell $t - 1$, so that $P_{X \rightarrow \Theta, x}^{SM/ILR} = 0$. Thus, the storage system is no longer always available. In case the storage system will be full after adding the excess of SF (resp. SP), we store the maximum possible; otherwise we store all the excess while satisfying the storage constraints. The state of charge, $SOC_{E, \Theta}^{SM/ILR}$, is thus now limited by the storage capacity and the maximum power of charging/discharging that depend on the surface of the SF (resp. SP) $A_X^{SM/ILR}$ (2.6) and thus on the SM (resp. ILR).

All energy which goes at any point into the TES (resp. BES) is reduced by **the storage efficiency** which account for energy losses occurring. The TES (resp. Li-ion BES) can have an efficiency of about 95% [216] (resp. 90% [453, Table 61]). In this thesis, the efficiency of both is assumed to be 90 %.

An overview of the charging and discharging daily operation of the CSP-TES (resp. PV-BES) configuration with SM2 or 6 hours of TES (resp. ILR2 or 5 hours of BES), without applying the storage constraints, can be found in the top panel of figure 2.9 (resp. figure 2.10) in section 3.

The storage duration per day on average (2.7) is calculated by subtracting the mean Capacity Factor (CF) of the plant with storage, $\eta_{i, j, j'}$, from the one without storage, $\eta_{i, j}$:

$$h^{SM/ILR} = \frac{(\eta_{i, j, j'} - \eta_{i, j}) * 8760}{365}. \quad (2.7)$$

The resulted TES and BES parameters are given in table 2.3 and are used to compute the yearly rental cost of storage technologies (2.16).

3 Typical Daily Operation of CSP-TES and PV-BES

The top panel of figure 2.9 illustrates the CSP-TES operation over two consecutive days in summer, without storage constraints, of the CSP configuration with SM2 (6h of TES) to give an overview of **the storage model behavior**. We show, in ordinate, the time evolution of the thermal energies ($P_{SF, therm}^{SM}$, $P_{SF \rightarrow PB, therm}^{SM}$, $P_{SF \rightarrow TES, therm}^{SM}$, $P_{TES \rightarrow PB, therm}^{SM}$ and P_{in}^{SM}) on the left, and the state of charge ($SOC_{E, TES}^{SM}$) on

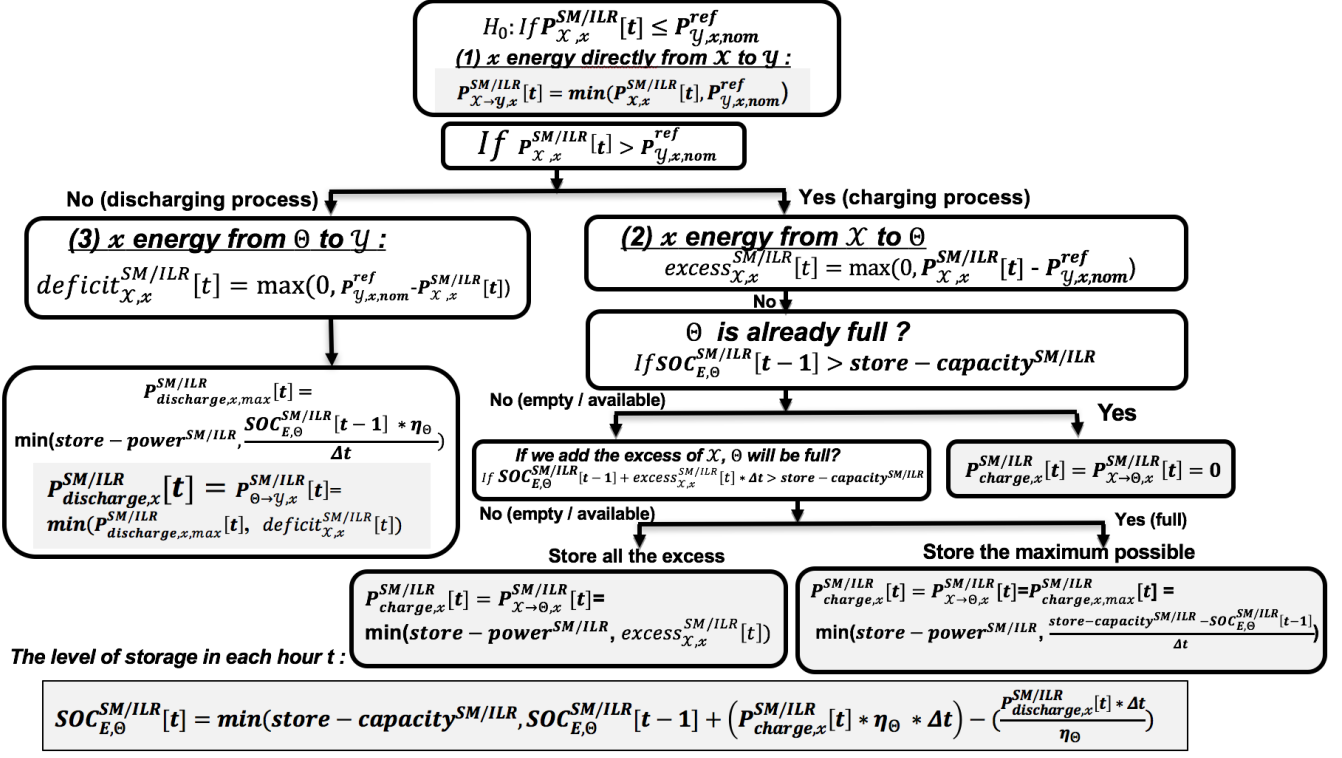


Figure 2.8: Storage algorithm illustrating the dispatch conditions of Concentrated Solar Power-CSP- thermal (resp. Photovoltaic-PV- Direct Current-DC-) energy with constraints on the storage capacity and the maximum power of charging/discharging, for a given CSP Solar Multiple-SM- (resp. PV Inverter Loading Ratio-ILR-). See section 2 (Appendix A) for the storage model without constraints. $X = \{SF, SP\}$; $Y = \{PB, INV\}$; $\Theta = \{TES, BES\}$; $x = \{therm, DC\}$; and $y = \{elec\}$. Source: Own elaboration based on [432, 451].

SM/ILR	TES/BES parameters			
	$\text{store} - \text{capacity}^{SM/ILR}$	$\text{store} - \text{power}^{SM/ILR}$	$\sum E_{discharged}^{SM/ILR}$	$h^{SM/ILR}$
SM^{ref}	649	149	36.5	5.48
SM2	754	169	42.7	6.13
SM3	1648	325	94.2	11.2
SM4	52793	480	148.3	17.2
ILR2	794×10^{-6}	183×10^{-6}	47.4×10^{-3}	4.73
ILR3	2038×10^{-6}	399×10^{-6}	122.7×10^{-3}	9.13
ILR4	4909×10^{-6}	616×10^{-6}	201.8×10^{-3}	13.4

Table 2.3: Storage parameters: Storage capacity (MWh) (**first column**), Maximum power of charging / discharging (MW) (**second column**), Total energy discharged (TWh) (**third column**) and Storage duration (h/day) (**fourth column**) obtained from the thermal-TES- (battery-BES-) storage model without constraints (Section 2, Appendix A).

the right, with hours of the day in abscissa. On day 1, at 7am, when the sun rises, the SF production, $P_{SF,therm}^{SM}$ (orange line), increases. Because during the first hours this energy is lower than the nominal thermal capacity, $P_{PB,therm,nom}^{ref}$ (horizontal gray line), it is directly supplied to the PB as, $P_{SF \rightarrow PB,therm}^{SM}$ (red line). At 9am, the SF production becomes larger than the nominal capacity so the excess, $P_{SF \rightarrow TES,therm}^{SM}$, is sent to the TES (brown line) and the PB produces at nominal capacity (red line). At 3pm, the SF production is smaller than the nominal capacity so the stored thermal energy, $P_{TES \rightarrow PB,therm}^{SM}$, is withdrawn from the TES (green line) to maintain the PB production at nominal capacity until 6pm (blue line). At 7pm, the state of charge (gray dashed line) does not allow the TES to fill the energy deficit up to $P_{PB,therm,nom}^{ref}$, and the residual thermal energy stored in the TES is discharged to the PB at once (blue line).

The bottom panel of figure 2.9 allows us to compare, for the same two days as in the top panel, the resulting **CSP CFs with respect to the SM**. We can see that with SM1 (gray line), the possibility to store is practically non-existent, so we produce only when solar irradiance is available. For SM^{ref} and SM2 (point-dashed line and plain line in purple), the generation is extended only few hours of stored energy to serve early evening loads. SM3 (green line), however, allows the collected energy to be spread over longer period of the day. The larger SF and TES capacity of SM4 (orange line) allow us to store and restore more energy to keep producing at nominal capacity from sunset to some point in the next operating day.

These results can be compared to figure 2.10 illustrating the process of storage charging and discharging over the course of a day for PV-BES plant, with the top panel is for ILR 2 (5 hours of BES). Overall, CSP with TES (resp. PV with BES) enables to shave the peak of SF (resp. SP) excess and shift energy over time which bridge the gap between supply and demand (i.e., reduce the variance).

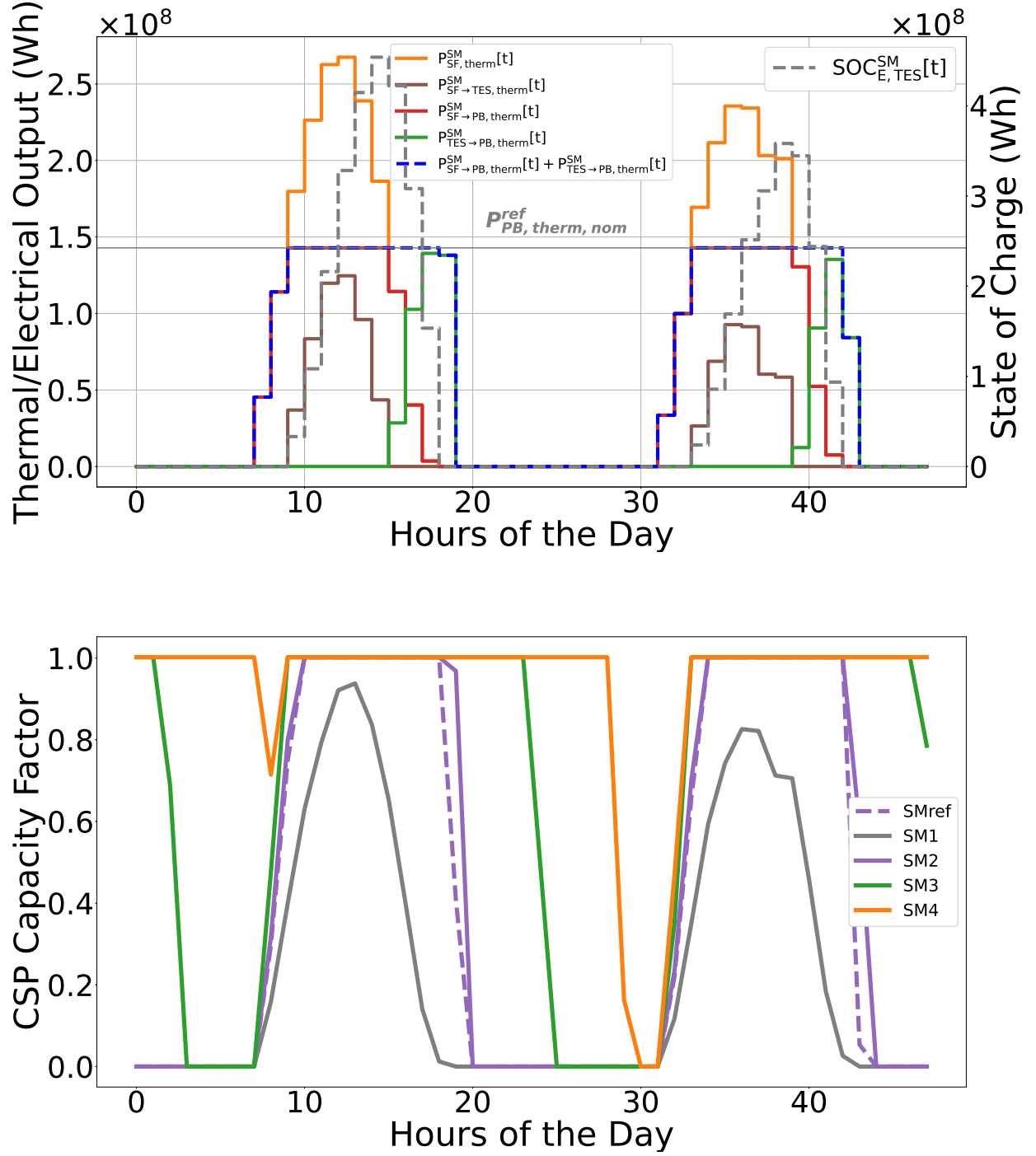


Figure 2.9: Illustration of the behavior of the Concentrated (CSP) Thermal Energy Storage (TES) model without constraints (Section 2, Appendix A) over two consecutive days in summer. **Top:** Time evolution of the thermal energies: Solar Field-SF- energy ($P_{SF, therm}^{SM}$), Energy from SF to Power Block-PB- ($P_{SF \rightarrow PB, therm}^{SM}$), Energy stored ($P_{SF \rightarrow TES, therm}^{SM}$), Energy discharged ($P_{TES \rightarrow PB, therm}^{SM}$), Total available energy injected to the PB ($P_{in}^{SM} = P_{SF \rightarrow PB, therm}^{SM} + P_{TES \rightarrow PB, therm}^{SM}$) and the State of charge ($SOC_{E, TES}^{SM}$) for a Solar Multiple (SM) of 2 (6 hours of TES). **Bottom:** CSP capacity factors for SM of 1, 2, 3 and 4; with $SM^{ref} = 1.87$ (87% of CSP thermal energy surplus).

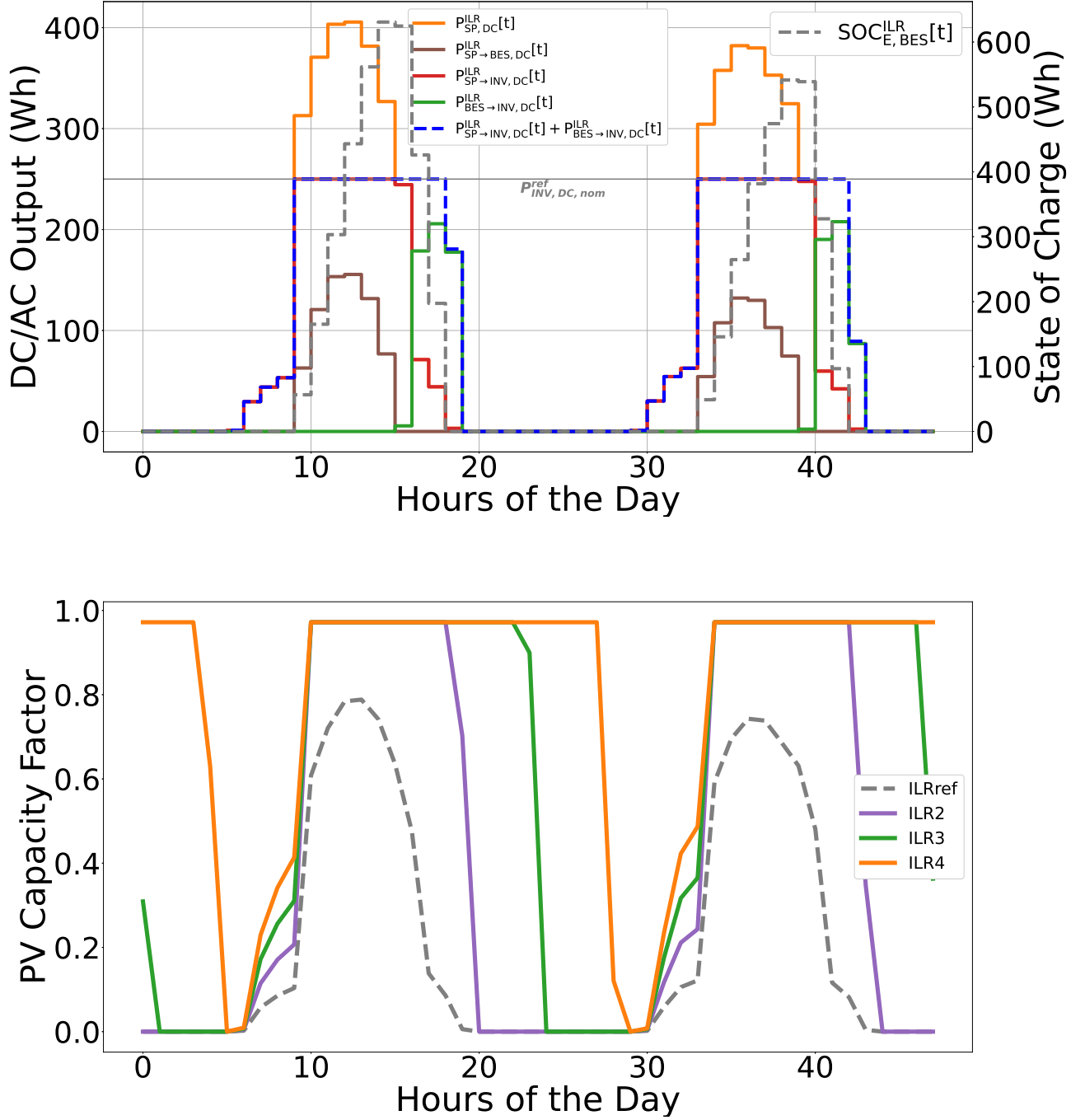


Figure 2.10: Illustration of the behavior of the Photovoltaic (PV) Battery Energy Storage (BES) model without constraints (Section 2, Appendix A) over two consecutive days in summer. **Top:** Time evolution of the Direct Current (DC) outputs: Solar Panel-SP- energy ($P_{SP,DC}^{ILR}$), Energy from SP to Inverter-INV- ($P_{SP \rightarrow INV,DC}^{ILR}$), Energy stored ($P_{SP \rightarrow BES,DC}^{ILR}$), Energy discharged ($P_{BES \rightarrow INV,DC}^{ILR}$), Total available energy injected to the INV ($P_{in}^{ILR} = P_{SP \rightarrow INV,DC}^{ILR} + P_{BES \rightarrow INV,DC}^{ILR}$) and the State of charge ($SOC_{E,BES}^{ILR}$) for an Inverter Loading Ratio (ILR) of 2 (5 hours of BES). **Bottom:** PV capacity factors for ILRs of 2, 3 and 4; with $ILR^{ref} = 1$ (PV without BES).

VI Predicted Demand and Bias-Corrected Capacity Factors

After computing the hourly regional demand time series (Section I, Appendix A) and aggregating the hourly wind, PV/PV-BES and CSP/CSP-TES Capacity Factors (CFs)—obtained at each climate grid cell— at regional level, we statistically adjust the CFs to observations (Section 2, Appendix A). In this section, we present the thermo-sensitivity results of the demand model and the bias-corrected CFs.

1 Thermo-Sensitivity Results

The hourly regional predicted electricity demand, obtained from hourly MERRA-2 climate data over the year 2018, is plotted against temperature to draw insight on **the responsiveness of the regional Moroccan demand to a change in the temperature** (Figure 2.11). Electricity consumption is disaggregated according to working days "work" (purple points), Saturdays "Sat" (green points) and off-days (Sundays and holidays) "off" (dark yellow points) **to capture the effect of human economic activity**. The thermo-sensitivity results reveal that there is an interval centered at $[14^\circ\text{C}, 24^\circ\text{C}]$ within which the demand is insensitive to temperature, marked by the two vertical dashed lines. This interval corresponds to the transient seasons of the year (spring and autumn) where the demand is fairly flat during the daytime and the overnight hours given the minimal need for heating or air-conditioning. One can see that the demand goes up when the temperature is above 24°C and grew significantly towards ends of high temperatures, while a very small sensitivity is found for heating degree days (low temperatures below 14°C). This can also be confirmed by the demand model coefficients (Table A.1a, Appendix A) that illustrate the thermo-sensitivity of the demand, means the change in the electricity consumption associated with a unit change in the temperature. As can be seen, the thermo-sensitivity is close to zero for low temperatures, a_H , due to the non-sensitivity of consumption to such low temperatures associated with no heating use; and positive with large values for high temperatures, a_C , due to increased consumption from cooling.

The thermo-sensitivity of the demand for working and non-working days is rather similar, with higher consumption occurring during working days, and higher for Saturdays than off-days linked to reduced residential, commercial and industrial activities.

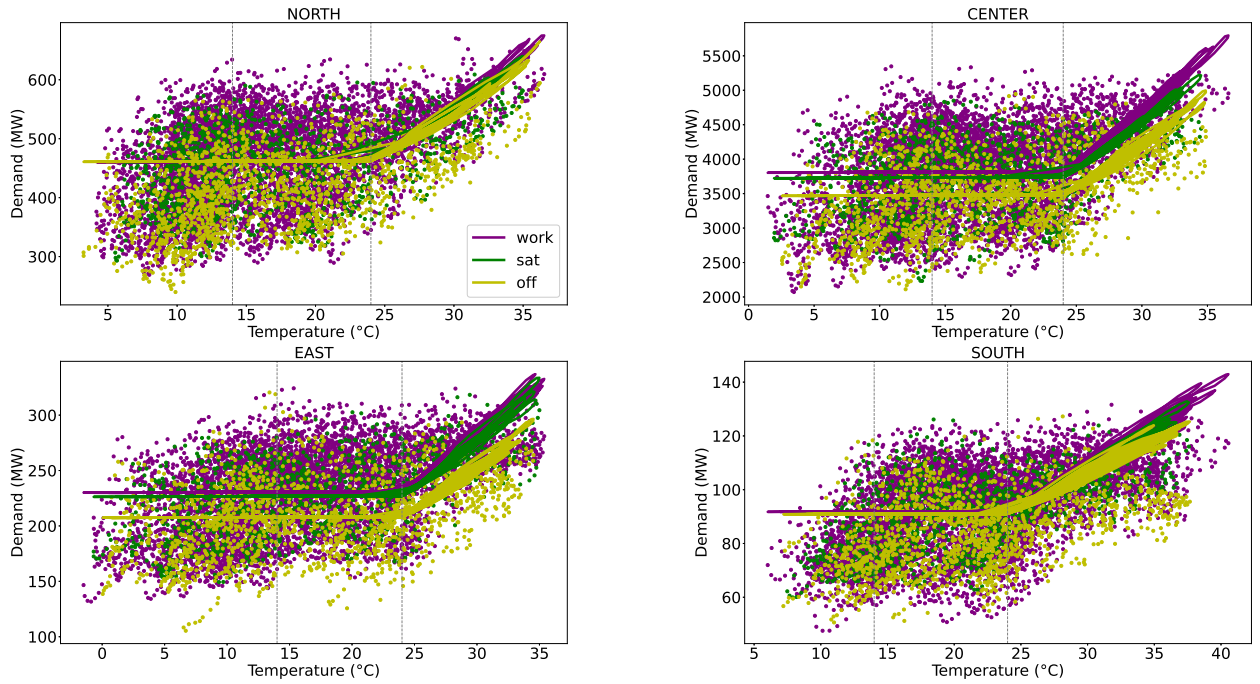


Figure 2.11: Hourly predicted electricity demand versus the hourly surface temperature for each zone and day type, i.e., working days "work", Saturdays "sat" and off-days "off" corresponding to holidays and Sundays. The scatter plot represents the predicted demand and the lines represent the function $a_H^{work|sat|off} \Theta(T_H - T_{it}) g_t^{work|sat|off} + a_C^{work|sat|off} \Theta(T_{it} - T_C) g_t^{work|sat|off} + a_0^{work|sat|off} g_t^{work|sat|off}$ of the demand model (Section I, Appendix A). The two vertical dashed lines represent the heating (resp. cooling) temperature thresholds, $T_H = 14^\circ\text{C}$ (resp. $T_C = 24^\circ\text{C}$), below (resp. above) which the consumers, for all zones, switch the heating (resp. air-conditioning) system.

It can also be observed that a slight differences exist among the regions. The temperature and day type dependence of the demand is more clear in the economically most dynamic region (CENTER) since the higher the population and urbanization, the higher the influence of weather conditions on electricity demand. The warmer regions are the EAST and SOUTH, with semi-arid/arid conditions, but the industrial activity and population are low in these regions, resulting in lower electricity demand (as stated in section ii). The cooling degree days are, however, lower in SOUTH (Table A.1a, Appendix A) because this region is placed at a more heterogeneous area capturing the desert climate with an oceanic influence, i.e., proximity to the Atlantic coast (Figure 2.3) compared to the continental eastern region.

We represent the **typical seasonal and daily cycle of the 2018 Moroccan predicted demand**, computed from MERRA-2 climate data, in figure 3.2b (Chapter 3). The figure shows the variation of the demand in color by intensity over time represented in the colorbar. A clear seasonality (in abscissa) is seen which peaks in summer and bottoms out in winter, while also showing a smaller peak each winter. This may corresponds to the coldest time of the year where the extra-electricity is being consumed for heating purposes, but of small order as discussed above. As can be seen, the summer peak prevails when air-conditioning causes the demand to peak in summer. When it comes to daily patterns (in ordinate), we can see an off-peak from midnight to early morning hours, when most people sleep; and two daily peaks. One relatively broad-spread at midday arising from an economic activity and a second more distinct peak later in the evening hours arising from high domestic consumption of electricity (lighting, appliances that depend on the lifestyle, etc). The same **daily pattern is noticed during**

Ramadan (not shown here) with very low consumption after dawn (after the morning meal "Suhur" before fasting), a peak consumption before each prayer, and a very strong consumption between the sunset and the evening prayers (after the evening meal "fudur" when muslims break their fast).

The yearly-means of the predicted regional demand obtained from the same data sources, MERRA-2 reanalysis over the year 2018, are reported in table 2.4.

2 Bias-Corrected Capacity Factors

The yearly-means of the bias-corrected CFs, obtained from MERRA-2 reanalysis over the year 2018, are reported in table 2.4. From this table, we can see that wind mean CFs are the largest, with CSP/CSP-TES CFs following before PV/PV-BES CFs. It thus appears that wind CFs are strong on average in Morocco; and the solar tracking by parabolic CSP more than compensates for the absence of conversion of diffuse irradiance compared to PV. Surprisingly, although higher amount of surplus production is obtained by increasing the CSP solar field (resp. PV solar panels) area, the bias correction is bringing the means of the CSP (resp. PV) CFs for different solar multiples-SMs-(resp. Inverter Loading Ratios-ILR-) to a similar value (Table 2.4). Closer inspection of table A.6 (Appendix A) shows that, for instance, for given region i =CENTER, the plants $p1$ =NOOR1 and $p2$ =NOOR2 have similar mean CFs even though the storage duration of $p1$ (3 hours) is smaller than $p2$ (7 hours). We verify that is indeed due to the fact that all the operational CSP (resp. PV) plants, used to correct bias in the solar CFs, have similar SM and ILR (Section 1, Appendix A).

Zones	Demand	Wind CFs	PV CFs				CSP CFs			
			ILR1	ILR2	ILR3	ILR4	SM1	SM2	SM3	SM4
NORTH	450.55	37.8	19.2	19.5	19.5	19.3	30.4	31.0	31.0	30.8
CENTER	3726.52	40.0	19.6	19.5	19.5	19.5	38.8	38.8	38.8	39.0
EAST	224.28	47.3	21.1	21.0	21.0	21.0	31.4	31.4	31.4	31.4
SOUTH	90.0	46.0	21.7	21.6	21.6	21.7	37.0	37.0	37.0	37.0

Table 2.4: Regional predicted demand (MWh/yr) and bias-corrected wind and solar Capacity Factors-CFs- (%), for each Solar Multiple (SM) and Inverter Loading Ratio (ILR), obtained from hourly MERRA-2 climate reanalysis and averaged over the year 2018, per zone and technology. Thermal (TES) and Battery (BES) storage are with constraints. ILR1 or SM1: without storage; ILR>1 or SM>1: with increasing levels of storage from Photovoltaic (PV) or Concentrated Solar Power (CSP).

Table A.3 (Appendix A) gives the **bias correction factors**, obtained for each climate data sources over the period specified in section 3. A relatively strong bias (up to 100%) is found between the yearly-averages of the computed regional CFs and the region's mean CF computed from the observed data, especially for wind (resp. PV) using MERRA-2 (resp. CORDEX) and CSP without storage (SM1) whatever the climate data source. It could be due to the climate data quality which may be not good in the region or the power curve and the assumptions done in the wind and solar production models do not reflect the observed production. A smaller bias are found, for wind CFs, using CORDEX but this may be due to the spurious effect of the time frame of simulation (only one year for MERRA-2).

VII Maximum-Cost Constraint

To take into account the cost of CSP that differs significantly from that of PV and wind, and account for the differences in the cost of storage configurations, we add a **new maximum-cost constraint** to the optimization problem in addition to the inequality constraint preventing Renewable Energy (RE) capacities to be negative, $\omega_k \geq 0 \quad \forall k$. We take a recommissioning approach¹ in which the total cost of a mix, $\sum_k \omega_k c_k$, is constrained to be lower than that of the actual 2018 Moroccan mix, C_{tot}^{obs} (2.9), as indicated in equation (2.8):

$$\sum_k \omega_k c_k \leq C_{tot}^{obs}. \quad (2.8)$$

Typically, the **total cost (€/yr)** of a power plant, in a given period, is made up of a fixed cost which is independent of the quantity of electricity produced, plus a variable cost that depends on how much electricity the plant produces in that period referred to as the "marginal cost" [139, 19]. Since only REs are considered, in this thesis, they generate electrical power at close to a zero marginal cost. Therefore, we assume that the total cost depends only on the fixed cost, which is calculated by multiplying the installed capacity, ω_k (MW), by the **yearly rental cost**, c_k (€/MW/yr) [139]. The later corresponds to the total discounted costs of installing and operating a given system over its lifetime, corresponding to the numerator of the Levelized Cost of Electricity (LCOE). The mathematical formulation of, c_k , under different cost and storage assumptions can be found in section VIII.

Given the above, the quantity, C_{tot}^{obs} indicated in equation (2.8) which denotes the **observed total cost** that is not to go beyond, is expressed as follows (2.9). We consider that it is equal to the rental cost of the most widely deployed RE system in Morocco in 2018—which is PV-wind-CSP-TES SM^{ref} with 5.5 hours of TES since, as already pointed out, all operational wind and PV (resp. CSP) plants are without storage (resp. with storage of 3-7 hours of TES on average) as shown in table A.6 (Appendix A)—multiplied by all capacities, ω_k^{obs} for all k , installed in Morocco in 2018 (left panel of table 2.1). We assume that the maximum total cost (2.9) remains constant, independently of the RE combination:

$$C_{tot}^{obs} := \sum_k \omega_k^{obs} c_k. \quad (2.9)$$

The mean-variance analysis, thus, consists in solving the below-mentioned **bi-objective optimization problem**. The mean penetration (2.10) and a given version of the variance (i.e., risk) (2.11) are the two objective functions. Moreover, equation (2.12) and equation (2.13)

¹A recommissioning approach is the re-powering of the renewable production, which consists in fully decommissioning the current capacities and re-allocating the capacities according to specific objectives (i.e., maximizing the penetration or minimizing the variability).

are respectively the inequality constraint fixing the total cost of RE capacities to some value, $C_{\text{tot}}^{\text{obs}}$, and an inequality constraint preventing RE capacity to be negative:

$$\text{maximize}_w \sum_k \mathbb{E} \left[\frac{\eta_k}{\sum_i D_i} \right] \omega_k \quad (2.10)$$

$$\text{minimize}_w \sum_{k,l} \omega_k \omega_l \text{Cov} \left[\frac{\eta_k}{\sum_i D_i}, \frac{\eta_l}{\sum_i D_i} \right] \quad (2.11)$$

$$\text{subject to } \sum_k \omega_k c_k \leq C_{\text{tot}}^{\text{obs}} \quad (2.12)$$

$$\omega_k \geq 0 \quad \forall k. \quad (2.13)$$

All parameters are described in section 2.

VIII Rental Cost Modeling and Data

In this section, we propose an approach—based on the Net Present Value method [139] (instead of the Annuity Factor method [451])—to calculate **the rental cost of the generation and storage technologies** based on the available cost parameters data. An essential point on which we build is that the rental cost of CSP-TES (resp. PV-BES) has to be defined relative to the Solar Multiple-SM- (resp. Inverter Loading Ratio -ILR-) to take into account the cost of the additional CSP Solar Field-SF- (resp. PV Solar Panel-SP-) and the amount of thermal-TES- (resp. battery-BES-) storage associated.

A few points are noted from section iv (Chapter 1) where we summarize the current scientific understanding about **the relationship between the annual CSP (resp. PV) Capacity Factors (CFs), the Levelized Cost Of Electricity (LCOE) and the SM (resp. ILR) for different storage duration**. First, we noted that the time averaged CFs can achieve higher values with increasing the SM (resp. ILR), even without storage, and even more when also the TES (resp. BES) size is increased (Figure 1.16 (a) for PV; and (b), (c) for CSP, Chapter 1). Second, medium LCOE is achieved with a few hours of storage and with small SM while increasing both the SM (resp. ILR) and the amount of storage decrease the LCOE (Figure 1.16 (d), Chapter 1). The most conclusion to emerge from these figures is that the relationship between CFs, costs, CSP SF (resp. PV SP) size and the amount of storage is very complex to define. In fact, it is commonly known that an increase in the SM (resp. ILR) does not give a proportionate increase in the hours of storage. For instance, the CSP SF (resp. PV SP) can be oversized without investing in the TES (resp. BES) and vice versa, which does not give a proportionate increase in the CFs and thus a proportionate reduction in the generation costs [194, 268, 3].

In this thesis, **the CSP SM (resp. PV ILR), the CSP SF (resp. PV SF) area, and the amount of storage are matched with one another**, i.e., an increase in the CSP SM (resp. PV ILR) results in an increase in the CSP SF (resp. PV SF) area which increase the storage capacity (Section 1, Table 2.3). Furthermore, **the mean solar CFs are kept constant for all SMs (resp. ILRs)** due to the bias correction (Section 2). In fact, having mean CFs that change very little with increasing SM (resp. ILR) avoid to increase the variance—associated with the increase of the CF means (quadratic term against linear term)—due to the increase of the surplus of energy available for storage with the increase of CSP SF (resp. PV SP) size (Figure 2.12a (i)), and this despite the reduction in the variability associated with the storage (Figure 2.12a (ii)). With fixed mean CFs, the mean of the CF time series of CSP SM2, for instance, will be similar to CSP SM1 but the difference in the amplitude is taken in the penetration (2.1) and they will be penalized differently. Thus, the model would not penalize CSP SM2 against CSP SM1 just for having larger average CF (i.e., larger variance). In this case, the model is only sensitive to the reduction in the variance associated with storage (Figure 2.12b (iii)) and to the cost associated with the change of SM and ILR, in addition to the differences between PV, wind and CSP in terms of cost and variability.

Fixed mean CF imply to keep the rental cost, c_j , of CSP (SF + PB) or PV (SP + INV) constant for all SMs and ILRs. However, as a matter of fact, ignoring the differential effect that storage (TES or BES) cost of each solar technology undermines the identification of truly optimal technology to install for each penetration level. Accordingly, we assume that **the cost of the CSP-TES and PV-BES rise almost in proportion with the size of the plant (i.e., SM and ILR), i.e storage parameters** (Table 2.3), and the cost of additional CSP SF and PV SP can scale without incurring much additional cost (in line with [6]) (the principal case of this thesis, section 1). This assumption reported here appear to support the assumption that the size CSP or PV plants utilizing storage with several hours will be much larger, which contributes implicitly to much higher cost per installed capacity, even though the mean CF is fixed. However, it is important to bear in mind that for CSP, the SF is by far the largest cost component of Parabolic Trough (PT) plants and accounts for 38.5% of the total installed costs (looking at the 50 MW PT Andasol plant with 7.5 h of TES, taken as reference plant in our study, Table A.2, Appendix A) while TES cost land at the third place after the PB and grid connections costs (see a detailed breakdown of the investment cost [268, Table 4.2]). The same for PV, the cost of PV module is higher than that of the inverter [269].

Given all these considerations, we run the mean-variance analysis considering **three cases of rental cost formulation**. Each case will be explained shortly in the following sub-sections.

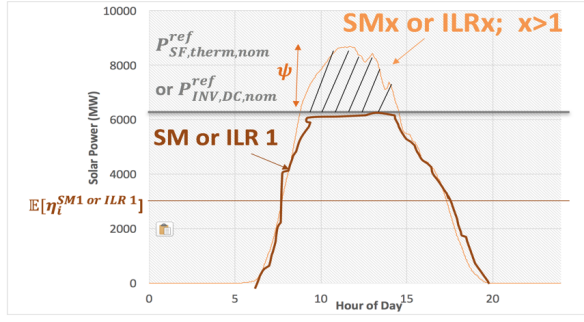
1 Case 1: Limited Storage Cost and Capacity

In this principal case of this thesis, explained above, we consider **the cost of CSP thermal (resp. PV battery) storage as function of the SM (resp. ILR) and thus as function of the storage constraints** (Table 2.3) applied to the storage model (Section 2) while the cost of CSP SF (resp. PV SP) is kept constant to remain coherent with the fact that the mean CSP (resp. PV) CF is constant, whatever the CSP SM (resp. PV ILR), due to the bias correction.

The yearly rental cost, c_k , is thus the sum of the yearly rental cost of the production technology, c_j , and the yearly rental cost of the storage technology, $c_{j'}$, as presented in equation (2.14):

$$c_k := c_j + c_{j'}. \quad (2.14)$$

(i): CSP SF (resp. PV SP) increases without increasing TES (resp. BES)



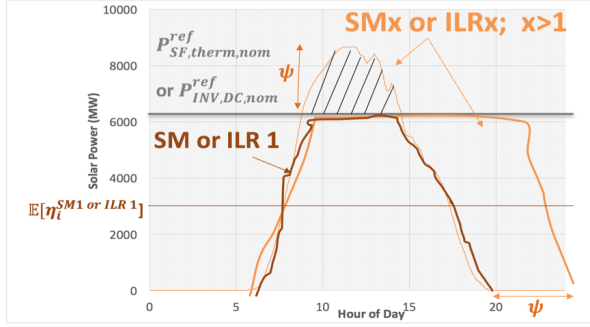
$$\mathbb{E}[\eta_i^{SMx \text{ or } ILRx}] = x \cdot \mathbb{E}[\eta_i^{SM1 \text{ or } ILR1}]$$

$$\mathbb{V}[\eta_i^{SM1 \text{ or } ILR1}] = \mathbb{E}[(\eta_i^{SM1 \text{ or } ILR1})^2] - \mathbb{E}[\eta_i^{SM1 \text{ or } ILR1}]^2$$

$$\mathbb{V}[\eta_i^{SMx \text{ or } ILRx}] = x^2 \cdot \mathbb{V}[\eta_i^{SM1 \text{ or } ILR1}]$$

$$\frac{\mathbb{E}[\eta_i^{SMx \text{ or } ILRx}]}{\mathbb{V}[\eta_i^{SMx \text{ or } ILRx}]} = \frac{1}{x} \cdot \frac{\mathbb{E}[\eta_i^{SM1 \text{ or } ILR1}]}{\mathbb{V}[\eta_i^{SM1 \text{ or } ILR1}]}$$

(ii): CSP SF (resp. PV SP) increases with increasing TES (resp. BES)



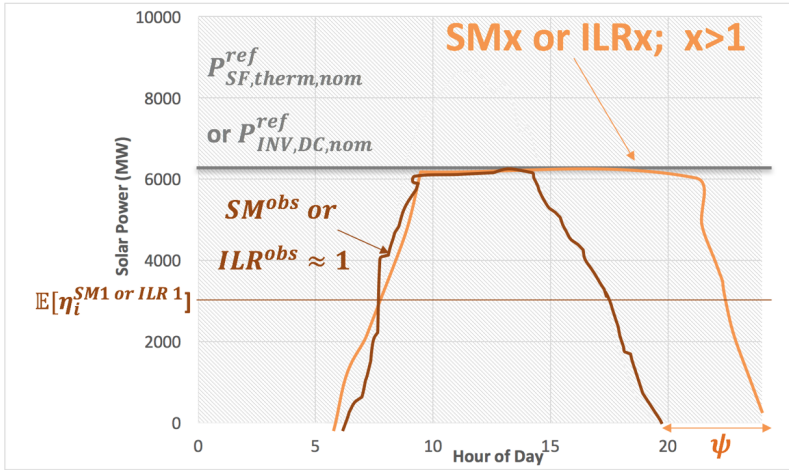
$$\mathbb{E}[\eta_i^{SMx \text{ or } ILRx}] = x \cdot \mathbb{E}[\eta_i^{SM1 \text{ or } ILR1}]$$

$$\mathbb{V}[\eta_i^{SMx \text{ or } ILRx}] = \frac{1}{\psi} x^2 \cdot \mathbb{V}[\eta_i^{SM1 \text{ or } ILR1}]$$

$$\frac{\mathbb{E}[\eta_i^{SMx \text{ or } ILRx}]}{\mathbb{V}[\eta_i^{SMx \text{ or } ILRx}]} = \psi \cdot \frac{1}{x} \cdot \frac{\mathbb{E}[\eta_i^{SM1 \text{ or } ILR1}]}{\mathbb{V}[\eta_i^{SM1 \text{ or } ILR1}]}$$

(a) Before Bias Correction

(iii): CSP SF (resp. PV SP) increases with increasing TES (resp. BES) but SM^{obs} or ILR^{obs} is constant



$$\mathbb{E}[\eta_i^{SMx \text{ or } ILRx}] = \mathbb{E}[\eta_i^{SM^{obs} \text{ or } ILR^{obs}}]$$

$$\mathbb{V}[\eta_i^{SMx \text{ or } ILRx}] = \frac{1}{\psi} \mathbb{V}[\eta_i^{SM^{obs} \text{ or } ILR^{obs}}]$$

$$\frac{\mathbb{E}[\eta_i^{SMx \text{ or } ILRx}]}{\mathbb{V}[\eta_i^{SMx \text{ or } ILRx}]} = \psi \cdot \frac{\mathbb{E}[\eta_i^{SM^{obs} \text{ or } ILR^{obs}}]}{\mathbb{V}[\eta_i^{SM^{obs} \text{ or } ILR^{obs}}]}$$

(b) After Bias Correction

Figure 2.12: Relationship between Concentrated Solar Power-CSP- (resp. Photovoltaic-PV-) mean Capacity Factors (CFs) or η , variance, CSP Solar Multiple-SM- (resp. PV Inverter Loading Ratio-ILR-) and the amount of thermal (resp. battery) storage, i.e., TES (resp. BES). Different cases are represented to illustrate the effect of the bias correction. (a) Assuming the case (i) where the Solar Field-SF- (resp. Solar Panels-SPs-) size increases without increasing the amount of storage, the mean CFs for a given zone i will increase and the variance will increase even more (the CF variances tend to scale quadratically with CF means) which tend to reduce the ratio CF/variance with the increase of SM (resp. ILR). Assuming the case (ii) where the SF (resp. SP) increases with increasing the amount of storage, the mean CFs will increase and the variance will increase but will be reduced by ψ which tend to increase slightly the ratio CF/variance with the increase of SM (resp. ILR) compared to case (i). Since the bias correction (b) is bringing the mean of the CFs roughly equal to the CFs of the observed SM (resp. ILR) (iii), the variance will decrease (i.e., the ratio CF/variance will increase) with the increase of SM (resp. ILR) due to the reduction in the variability associated with storage. $P_{SF,therm,nom}^{ref}$ (resp. $P_{INV,DC,nom}^{ref}$) is the thermal (resp. Direct Current-DC-) nominal capacity. \mathbb{E} and \mathbb{V} represent, respectively, the mathematical expectation and variance operators over time. The subscript "obs" denotes the observations. $ILR > 1$ or $SM > 1$: with increasing levels of storage from PV or CSP. Source: Own elaboration.

The yearly rental cost of the generation technology, c_j (2.15), is computed from the lifetime capital investment cost ($CAPEX_j$), the lifetime fixed and variable operation and maintenance costs (FOM_j and VOM_j respectively)—which are both annualized—the discount rate

(DR) and the lifetime ($Lifetime_j$):

$$c_j = \sum_{t=1}^{Lifetime_j} \frac{CAPEX_j + [FOM_j + \alpha_j VOM_j]}{(1 + DR)^t}. \quad (2.15)$$

The yearly rental cost of the storage technology, $c_{j'}$, is calculated using equation (2.16). In fact, the investment cost of the storage system is divided into power-related cost ($CAPEX_{P,j'}$) which is the cost of power of charging/discharging, and energy-related cost ($CAPEX_{E,j'}$) which is the cost of energy storage capacity or volume [479]. $FOM_{j'}$ and $VOM_{j'}$ are, respectively, the fixed and variable operation and maintenance costs, and $Lifetime_{j'}$ is the lifetime of the technology j' :

$$c_{j'} := \sum_{t'=1}^{Lifetime_{j'}} \frac{[\alpha_{j'} CAPEX_{E,j'} + \beta_{j'} CAPEX_{P,j'}] + [\beta_{j'} FOM_{j'}]}{(1 + DR)^{t'}} + \gamma_{j'} \sum_{t'=1}^{Lifetime_{j'}} \frac{VOM_{j'}}{(1 + DR)^{t'}}. \quad (2.16)$$

All the parameters are explained in Appendix IX.

Except for the discount rate, **the economic data** needed to compute the yearly rental cost (2.14) come from the 2014 Energy Technology Reference Indicator (ETRI) projections for 2010-2050 [266] of the European Commission Joint Research Center (JRC) for the year 2013. We have considered the following power production technologies j : solar thermal electricity power plants without thermal storage; commercial solar PV (more than 2MW) without tracking; and onshore wind. For storage technologies j' , we have considered: thermal energy storage for concentrating solar power applications; and Li-ion storage battery for power grid applications.

The total cost is critically dependent upon the choice of the discount rate (DR). Usually, low DRs are used when evaluating RE technologies [344]. A real DR of 4 %, in Morocco, for modeling purposes seems reasonable [344, page 27]. CSP would require a somewhat higher rate, a value of 5% [344] as also considered in [113], so a value of 4.5 % is used in this thesis for all production and storage technologies.

This cost data is summarized in table 2.5. **The resulted yearly rental cost** (2.14), calculated using equation (2.15) and equation (2.16), are summarized in table 2.6. It shows that the rental cost of wind is higher than that of PV but are relatively comparable, while they are more than three times lower than that of CSP. In addition, more the CSP SM (resp. PV ILR) increases, more the cost of CSP (resp. PV) increases. The rental cost range of CSP-TES is by far the largest, while PV-BES presents the lowest range. For instance, for the same design (SM2 vs. ILR2 or SM4 vs. IL4), rental cost estimates for CSP-TES extend to roughly double the rental costs of PV-BES.

Injecting the rental cost (Table 2.6) and capacity data (left panel of table 2.1), respectively, in equation (2.9) yields **a maximum total cost**, C_{tot}^{obs} , of **3.50 G€/yr**, corresponding to the PV-Wind-CSP SM^{ref} mix (with 5.5 hours of TES).

Chapter 3 (Section III) uses this case to analyze the response of the Moroccan mix to the integration of CSP/CSP-TES (SM1, 2, 3, 4) with wind and PV without storage (ILR^{ref} or ILR1). This case is also used in chapter 4 (Section III) to analyze the impact of the addition of PV-BES (ILR2, 3, 4) on the mix integrating CSP/CSP-TES (SM1, 2, 3, 4) and wind; and in chapter 5 to analyze the response of the optimal mixes to solar technologies in future warming climate.

Technology j	CSP	PV	Wind
$CAPEX_j$ (€/kW)	5600	980	1400
FOM_j (% $CAPEX_j$)	4	1.7	2.7
VOM_j (€/MWh)	8	0	0
Discount Rate DR (%)	4.50	4.50	4.50
$Lifetime_j$ (years)	30	25	20
α_j (h)	2240.91	1926.93	2147.73
Yearly Rental Cost c_j	3314.68	617.74	977.22

Technology j'	TES	BES
$CAPEX_{E,j'}$ (€/kWh)	24	752
$CAPEX_{P,j'}$ (€/kW)	1200	490
$FOM_{j'}$ (% $CAPEX_{P,j'}$)	0.2	1.4
$VOM_{j'}$ (€/MWh)	0	2.6
$Lifetime_{j'}$ (years)	20	10

Table 2.5: Capital investment ($CAPEX$), fixed and variable operation and maintenance costs (FOM and VOM), lifetime ($Lifetime$) of the production technologies j (**Left**) and thermal (TES) or Battery (BES) storage technologies j' (**Right**). This data is from the ETRI 2014 - Energy Technology Reference Indicator projections for 2010-2050 technical report, for the year 2013 [453, Table 7, Table 4 and Table 10 for PV, wind and CSP]; and [453, Table 66 and Table 61 for TES and Li-ion BES]. The discount rate (DR) is from the World Bank Report [344, page 27]. α_j is the yearly-mean CF in (hours) of the technology j (Eq. A.74) and the yearly rental cost per technology, c_j (€/kW/yr), is calculated using equation (2.15). Concentrated Solar Power (CSP) and Photovoltaic (PV), on the left panel, are without storage (i.e., for Solar Multiple-SM- and Inverter Loading Ratio-ILR- equal to 1).

Zones	Wind	PV				CSP				
		ILR1	ILR2	ILR3	ILR4	SM1	SM^{ref}	SM2	SM3	SM4
c_k	977.22	617.74	3379.8	7596.48	16008.52	3314.68	5966.48	6324.23	9164.94	28399.52

Table 2.6: The yearly rental cost c_k , Eq. (2.14), in (€/kW/yr) per production technology j or production technology with its storage technology j' calculated using equation (2.15) and (2.16); and using the storage parameters (Table 2.3). The index k is a multi-index representing a pair $k = (i, j)$ or $k = (i, j, j')$ with i are zones. ILR and SM denote, respectively, the Inverter Loading Ratio and Solar Multiple. ILR1 or SM1: without storage; ILR>1 or SM>1: with increasing levels of storage from Photovoltaic (PV) or Concentrated Solar Power (CSP).

2 Case 2: Unlimited Storage Cost and Capacity

At present, TES is cheap and CSP is expensive. Conversely, current Li-ions batteries costs are high and PV has low cost [453]. The question that arise in this context is that, **ignoring the storage cost and keeping the cost of CSP (resp. PV) constant for different SMs (resp. ILRs)**,

equal to that of SM1 (resp. ILR1) (2.17), will introduces a significant changes in the capacity mix? In other words, it will not penalize solar technologies, with high storage capability, at penetrations levels where the cost play a role?

$$c_k := c_j; c_{j'} := 0 \quad (2.17)$$

Ignoring the storage cost imply to **ignore the constraints on storage**. The resulted yearly rental cost, c_k , in this case, is given in the left panel of table 2.5. As can be seen, a higher values is experienced for CSP, followed by wind. The lowest cost estimated is attributed to PV.

This case is used in chapter 3 (Section 1) and chapter 4 (Section 2) to discuss the scenarios of solar PV/CSP/CSP-TES/PV-BES integration with unlimited storage cost and storage capacity; keeping the same maximum total cost, $C_{\text{tot}}^{\text{obs}}$ (2.9), of 3.50 G€/yr, corresponding to the PV-Wind-CSP SM^{ref} mix (with 5.5 hours of TES).

3 Case 3: Constant Thermal Storage Cost with Unlimited Capacity

For CSP, most of the available cost information refers to the Andasol parabolic trough CSP-TES plant with 6-8 hours of thermal storage on average [268]. Thus, instead of ignoring the TES cost completely as in case 2 (Section 2), we propose **an alternative definition of the rental cost** (2.18), **for only CSP-TES, that implicitly accounts for the TES cost, keeping it fixed for all SMs**, even though larger SF areas with larger thermal storage capacity should cost more.

$$c_k := c_{j,j'_{6-8h}} = \sum_{t=1}^{Lifetime_{j,j'_{6-8h}}} \frac{CAPEX_{j,j'_{6-8h}} + OPEX_{j,j'_{6-8h}}}{(1+DR_j)^t} \quad (2.18)$$

The terms CAPEX and OPEX are, respectively, the capital and operational expenditures over the lifetime of the plant, and DR is the discount rate.

Doing so, like case 2 (Section 2), the optimization problem is only sensitive to the change of the variance associated with the change of the SM and to the different rental costs of wind, PV and CSP while the cost of TES is considered but does not increase with the increase of SM. Given that, **the TES constraints are ignored** in the storage model (Section 2); and **only Noor 2 and Noor 3 with 7 hours of TES** (Table A.6, Appendix A) are selected to correct bias in the mean CSP CFs and to compute the maximum-cost constraint (2.8).

The cost data, in this case, come from the scenario-based cost trajectories to 2050 [266] of the European Commission Joint Research Center (JRC) for the year 2015. The following power production technologies are considered: onshore wind turbines with medium specific capacity and medium hub height, utility-scale PV without tracking/storage and parabolic trough with 6 to 8 hours storage. The data and **the resulted yearly rental costs** are summarized in table 2.7. As can be seen, even though using recent cost data, the CSP/CSP-TES rental cost remains higher than that of wind which is higher than that of PV.

Technology j, j'_{6-8h}	Wind	PV	CSP
$CAPEX_{j,j'_{6-8h}}$ (€/kW)	1350	1020	6000
$OPEX_{j,j'_{6-8h}}$ (% $CAPEX_{j,j'_{6-8h}}$)	3	1.7	1.7
DR_j (%)	4.50	4.50	4.50
$Lifetime_{j,j'_{6-8h}}$ (years)	25	25	30
Yearly Rental Cost (€/kW/yr)	861.85	642.96	3462.25

Table 2.7: Capital investment ($CAPEX$), fixed operation and maintenance costs ($OPEX$), lifetime ($Lifetime$) are from the European Commission Joint Research Center (JRC) technical report [266] for the year 2015 (see tables 12 and 10 for utility-scale Photovoltaic-PV-without tracking/storage, tables 2 and 5 for onshore wind with medium specific capacity and hub height; and tables 15 and 16 for Concentrated Solar Power-CSP- with 6-8 hours of thermal storage-TES-). The discount rate (DR) is from the World Bank Report [344, page 27]; and the yearly rental cost per technology calculated using equation (2.18). The cost of CSP is kept constant for all Solar Multiple-SMs- (1, 2, 3, 4) and also for the reference SM (SM^{ref}) for the calculation of (2.9).

Injecting the rental cost and capacity data from tables 2.7 and table A.6 (Appendix A) (for Noor2 and 3 only), respectively, in (2.9) yields **a maximum total cost, $C_{\text{tot}}^{\text{obs}}$, of 2.36 G€/yr**, corresponding to the total cost of PV-wind-CSP SM^{ref} (5.5 hours of TES).

The comparison of simulation results between case 2 and case 3, for the CSP/CSP-TES integration with PV and wind, can be found in section 1 (Chapter 3).

IX Optimization Post-Processing Ratios

After computing the rental costs and optimizing the bi-objective mean-variance problem, we obtain the efficient fronts for various levels of penetration and variance (e.g., Figure 2.2). For each level of penetration, we compute the technology-region share as illustrated in figure 2.13.

Due to the maximum-cost constraint (2.8), **we identify three penetration regimes along the optimal fronts** (left, middle and right side of figure 2.13). In the upcoming sub-sections, it will be examined the ratios identifying the technology, in given region, that should be installed in each regime.

1 At Maximum Penetration

As demonstrated in section i (Appendix X), the ratio determining which technology is installed in which zone in priority at the maximum penetration mix is called **"the maximum-penetration ratio"** (2.19). Therefore, at such maximum penetration point (right side of figure 2.13), only the mean Capacity Factor (CF) and the rental cost of each technology matter. This ratio can be considered as the reverse of what should be spent on average to meet the demand by the production of only one capacity, the one of the zone i and technology j or j' , for which the quantity (2.19) is maximized, taking numerical accuracy into account. If k^* maximizes (2.19), then $\omega_{k_0} = C_{\text{tot}}/c_k$ and $\omega_k = 0$ for all $k \neq k_0$. Thus, more the expectation of the CF over the total demand is large and the rental cost is small, more this ratio is high, and more we

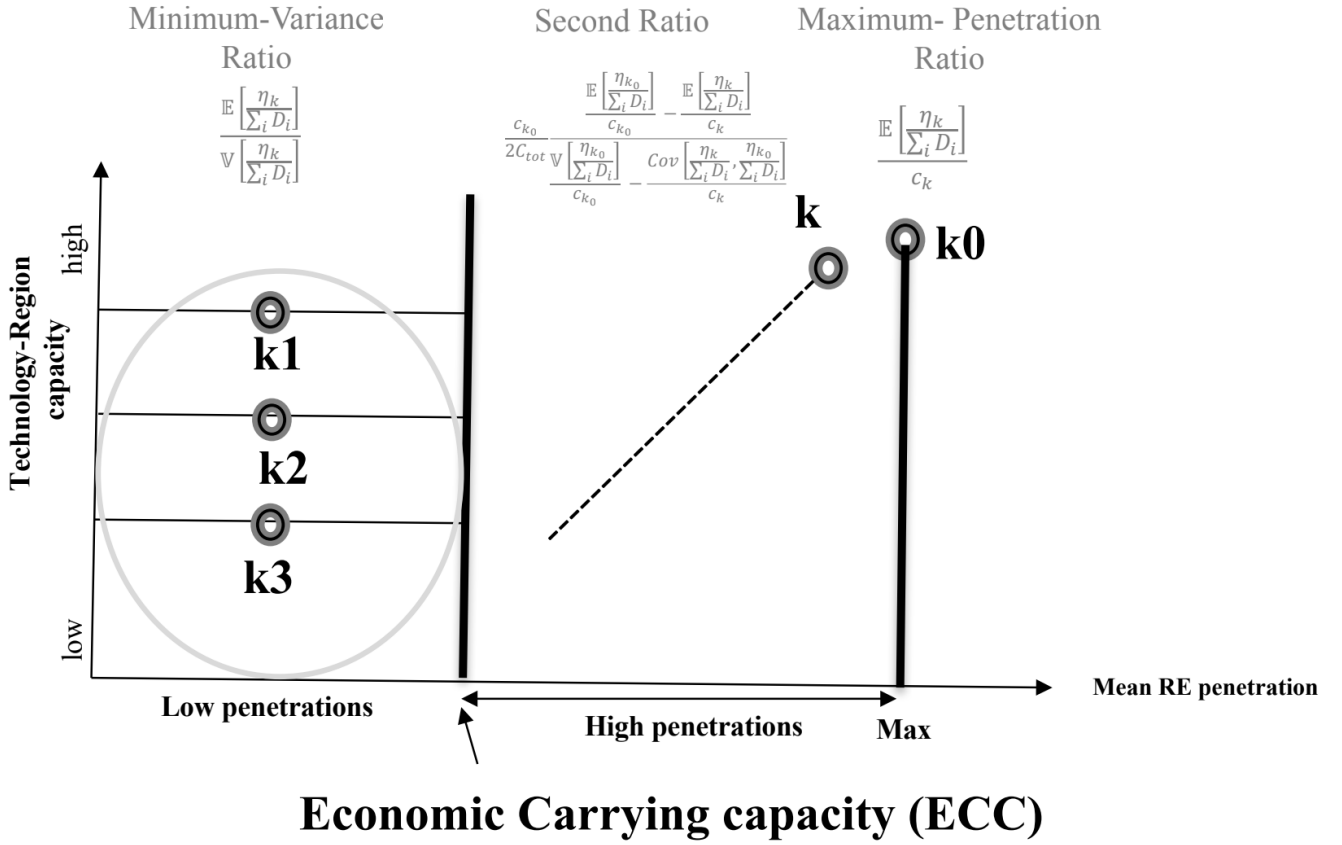


Figure 2.13: Technology-Region capacity (ordinate) versus the mean penetration (abscissa). Three penetration regimes are identified: **Right side**: at maximum-penetration (Section 1); **Middle side**: at high penetrations (Section 2); and **Left side**: at low penetrations (Section 3). The Economic Carrying Capacity (ECC) denotes the level of penetration of Renewable Energy (RE) at which the costs outweigh the benefits and where some additional REs are no longer economically desirable [157]. Source: Own elaboration.

spend less to install a very large capacity to achieve high penetration level. In fact, if the CFs are not normalized by the total demand, this ratio would be the inverse of the Levelized Cost Of Electricity (LCOE), for given technology in a particular zone.

$$\frac{\mathbb{E}\left[\frac{\eta_k}{\sum_i D_i}\right]}{c_k}, \quad (2.19)$$

with η_k is given in hours; D_i in MWh, and c_k in €/MW/yr.

2 At High Penetrations

To identify the second capacity to be installed as the penetration is decreased from its maximum (at high penetrations in the middle side of figure 2.13), it reveals the role of variances and covariances between CFs (normalized by the total demand) of different technologies and zones in addition to the mean CF and the rental cost. As shown in section ii (Appendix X), when the maximum-cost constraint is active and k_0 is the index of the capacity which is installed to maximize the mean penetration (Section 1), the first capacity, k , that is installed after k_0 for lower penetrations is the one that minimizes the quantity (2.20) that we call "**the second ratio**". This quantity is minimized when the correlation between k and k_0 is small and when the standard deviation of normalized CF of k divided by its cost—or the variance/cost ratio (2.21)—is small (resp. large) compared to that of k_0 if the correlation is positive (resp. negative).

$$\frac{c_{k_0}}{2C_{tot}} \frac{\frac{\mathbb{E}\left[\frac{\eta_{k_0}}{\sum_i D_i}\right]}{c_{k_0}} - \frac{\mathbb{E}\left[\frac{\eta_k}{\sum_i D_i}\right]}{c_k}}{\frac{\mathbb{E}\left[\frac{\eta_{k_0}}{\sum_i D_i}\right]}{c_{k_0}} - \frac{\text{Cov}\left[\frac{\eta_k}{\sum_i D_i}, \frac{\eta_{k_0}}{\sum_i D_i}\right]}{c_k}} = \frac{c_{k_0}}{2C_{tot}} \frac{\mathbb{E}\left[\frac{\eta_{k_0}}{\sum_i D_i}\right]}{\mathbb{E}\left[\frac{\eta_k}{\sum_i D_i}\right]} \frac{1 - \frac{\mathbb{E}\left[\frac{\eta_k}{\sum_i D_i}\right]/c_k}{\mathbb{E}\left[\frac{\eta_{k_0}}{\sum_i D_i}\right]/c_{k_0}}}{1 - \text{Corr}\left[\frac{\eta_k}{\sum_i D_i}, \frac{\eta_{k_0}}{\sum_i D_i}\right] \frac{\sqrt{\mathbb{V}\left[\frac{\eta_k}{\sum_i D_i}\right]}/c_k}{\sqrt{\mathbb{V}\left[\frac{\eta_{k_0}}{\sum_i D_i}\right]}/c_{k_0}}} \quad (2.20)$$

This equality is obtained by factorizing the numerator by $\frac{\mathbb{E}\left[\frac{\eta_{k_0}}{\sum_i D_i}\right]}{c_{k_0}}$ and factorizing the denominator by $\frac{\mathbb{V}\left[\frac{\eta_{k_0}}{\sum_i D_i}\right]}{c_{k_0}}$ and replacing the covariance term by $\text{Cov}\left[\frac{\eta_k}{\sum_i D_i}, \frac{\eta_{k_0}}{\sum_i D_i}\right] = \text{Corr}\left[\frac{\eta_k}{\sum_i D_i}, \frac{\eta_{k_0}}{\sum_i D_i}\right] \sqrt{\mathbb{V}\left[\frac{\eta_k}{\sum_i D_i}\right]} \sqrt{\mathbb{V}\left[\frac{\eta_{k_0}}{\sum_i D_i}\right]}$.

This ratio is without unit because c_{k_0} is in €/MW/yr; C_{tot} is in €/yr; $\frac{\mathbb{E}\left[\frac{\eta_{k_0}}{\sum_i D_i}\right]}{c_{k_0}}$ or $\frac{\mathbb{E}\left[\frac{\eta_k}{\sum_i D_i}\right]}{c_k}$ or $\frac{\text{Cov}\left[\frac{\eta_k}{\sum_i D_i}, \frac{\eta_{k_0}}{\sum_i D_i}\right]}{c_k}$ are in yr/€; and $\mathbb{V}\left[\frac{\eta_{k_0}}{\sum_i D_i}\right]$ or $\mathbb{V}\left[\frac{\eta_k}{\sum_i D_i}\right]$ are in 1/MW².

The **variance/cost ratio** (2.21) is an analogous to the benefit/cost ratio [156] which depend on the the annualized costs and the benefits associated with the reduction of the variability, i.e., illustrating implicitly the reliability and economic benefits/challenges:

$$\frac{V \left[\frac{\eta_k}{\sum_i D_i} \right]}{C_k}. \quad (2.21)$$

When we continue to decrease the penetration and the cost constraint remains active, a new capacities appear which each involve a new ratio which involves the means, variances and covariances between this new capacity and those already installed (middle side of figure 2.13); until we arrive at a penetration where the cost constraint is no longer active (the left side of figure 2.13) in which case it is the minimum variance ratio that takes over. This is only an approximation since we assume that the covariance matrix is diagonal to get this ratio (Section 3).

3 At Low Penetrations

At low variances and penetrations (the left side of figure 2.13), we show in section iii (Appendix X) that as long as the maximum-cost constraint is inactive and if we assume that all cross-correlations between the normalized CFs are zero (i.e., the covariance matrix is diagonal), all optimal capacities are positive and proportional to what we call "**the minimum-variance ratio**", and can be estimated by equation (2.22). Thus, in this regime, only the mean vector and variances of the CFs (normalized by the total demand) play a role. More this ratio is high, more we install less but in a proportional way.

$$\frac{\mathbb{E} \left[\frac{\eta_k}{\sum_i D_i} \right]}{V \left[\frac{\eta_k}{\sum_i D_i} \right]} \quad (2.22)$$

This minimum-variance ratio is given in MW because $\mathbb{E} \left[\frac{\eta_k}{\sum_i D_i} \right]$ is in 1/MW and $V \left[\frac{\eta_k}{\sum_i D_i} \right]$ is in $1/MW^2$.

X System Adequacy Diagnostics

In this section, we perform some additional load reduction diagnostics to assess the ability of each Renewable Energy (RE) technology to provide reliable energy to the system and thus to avoid investment in conventional generation capacity during peak, mid and base load hours. Our approach is based on the Load Duration Curve (LDC) and the Residual Load Duration Curve (RLDC), widely used for capacity planning [526, 204].

First, **the LDC** (middle panel of figure 2.14), which displays the electricity consumption of every single hour of the year, is derived by sorting the time series of the national predicted demand (the left panel of figure 2.14) for one year from the highest to the lowest value in descending order, thereby losing chronological information. Thus, the LDC gives an overall representation of the different load bands from the off-peak load (bottom right) to the base (light purple), mid (light green) and peak (yellow) load illustrating the probability of occurrence of each load band. We compute the hourly LDC for the year 2018 so that the number of samples is 8760. The 2018 Moroccan load curve (the middle panel of figure 2.14) shows that the peak load was 6272 MW (upper left) and the load never fell below 2500 MW (off-peak in the bottom right). The national demand amounted to some 4500 MW for almost 50% of the time (base load). Subtracting the electricity demanded in 500 hours from the base load, we get the mid load which was approximately 1042 MW. The LDC measures the capacity requirements to cover the total annual demand, which is reflected by the area below the curve. A part of this area can be satisfied by RE technologies and depend on the level of penetration and variability (green area of the right panel of figure 2.14), and the remainder cannot be covered by REs and needs to be met by conventional dispatchable production or flexibility options (gray area of the right panel of figure 2.14) such as fossil fuel plants, hydro plants, exchanges with neighboring countries, load shedding, demand response or storage units. There is, thus, a time index $h \mapsto t_h$ such that the demand, D , summed over all zones satisfies $LDC(h) := D(t_h) < D(t_{h-1}) =: LDC(h-1)$, where h is the time index, D is the national predicted demand and t_h is the peak/mid/base load time index.

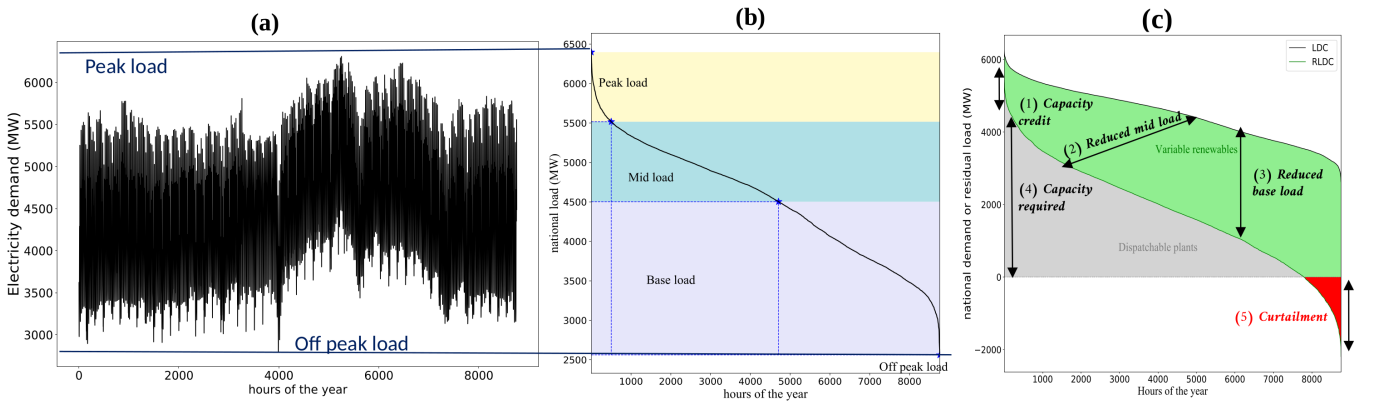


Figure 2.14: The Load Duration Curve (LDC) (b) is derived by sorting the predicted load (a) in descending order. The Residual Load Duration Curve (RLDC) (c) is derived by sorting the residual load (2.23) in descending order. It captures four main challenges of integration of Renewable Energies (REs): (1) The capacity credit or the peak load reduction; (2) the mid load reduction; (3) the base load reduction; (4) the capacity required from conventional dispatchable plants; and (5) the Renewable Energy (RE) curtailed. Source: Own elaboration computed from the predicted demand and RE production time series (for the RLDC) using hourly MERRA-2 climate data over the year 2018.

The capacity required from conventional dispatchable plants is illustrated by **the Residual Load (RL)** or the net load (2.23) defined as the total demand minus the total RE production for every point in time. When a new source is added to the system, the power generated from that source at each point in time can be subtracted from the load to arrive at a time series describing the RL that must be supplied by the rest of the system:

$$RL(t) = \sum_i D_i(t) - \sum_k \omega_k \eta_k(t). \quad (2.23)$$

The RLDC is derived by sorting the RL in descending order, just as it is done for the load. There is, thus, a time index $h \mapsto t'_h$ such that the RL satisfies $RLDC(h) := RL(t'_h) < RL(t'_{h-1}) =: RLDC(h-1)$ for $1 \leq h \leq 8759$, where t'_h is the residual peak/mid/base load time index.

With the RLDC (the right panel of figure 2.14), we can estimate the capacity supplied by RE during peak (1), mid (2) and base (3) load hours², the capacity required from flexible and inflexible conventional units (4) and the RE energy curtailed (5). Thus, the RLDC contains crucial information about the variability of wind and solar supply, as well as correlations with demand, thereby capturing the major integration challenges of integrating REs [525, 526, 527] (the right panel of figure 2.14), namely: (1) the capacity credit or the peak load reduction (LR) which is the fraction of RE capacity by which conventional power generation can be reduced, during peak load hours, without affecting the loss probability of the system (proxy of the probability of a plant to be available during periods of highest net load) [566]. In this sense, the capacity credit of conventional plants is always 100%, while its value for RE technologies is generally lower, but what about PV-BES vs. CSP-TES for the same design? (see section ii, chapter 4). (2) The reduction of the mid load and (3) the reduction of the base load.

To give a **graphical representation of these properties**, we show in figure 2.15, the LDC (black) and the RLDC (green) at a mean penetration of 35% for a particular optimal PV-wind-CSP-TES SM2 mix. We also represent the contribution of each technology to the RLDC: PV without storage (brown), wind (blue) and CSP-TES SM2 (orange).

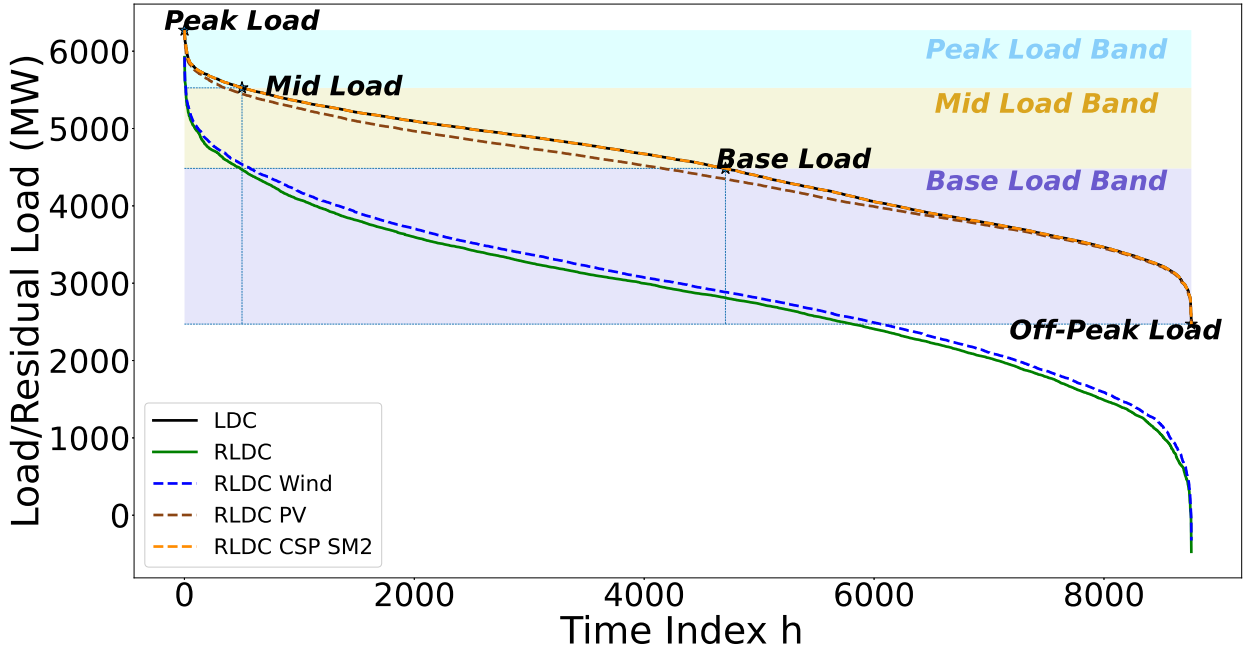


Figure 2.15: Load Duration Curve (LDC) (plain black), Residual Load Duration Curve (RLDC) (plain green), RLDC for Photovoltaic (PV) without storage only (dashed brown), RLDC for Concentrated Solar Power (CSP) with Thermal Energy Storage (TES) or CSP-TES with Solar Multiple (SM) equal to 2 only (dashed orange), and RLDC for wind only (dashed blue) for the optimal PV-Wind-CSP-TES SM2 mix for the global strategy (2.2) with the maximum-cost constraint (2.8) and at a mean penetration of 35 %. SM2: CSP with 6 hours of TES.

To calculate **the capacity credit, mid and base reduction**, we, first, divide the LDC and the RLDC into three intervals (vertical lines in figure 2.15 delimiting the peak, mid, and base time index). The peak load is associated with the highest 500 net load hours; the mid load associated with the 4706 largest values; and the base load associated with all values between the peak and the off-peak load. The horizontal bands corresponds to the load values of each load band. For each interval of the time index $1 \leq h \leq 8759$, we compute the LR by averaging the difference between the LDC and the RLDC over the band load time index and dividing the result by the total PV, wind, CSP installed capacity, of a given RE combination, as following (2.24):

$$LR(h_0, h_f) = \frac{\frac{1}{h_f - h_0} \sum_{h=h_0}^{h_f} LDC(h) - RLDC(h)}{\sum_k \omega_k} = \frac{\frac{1}{h_f - h_0} \sum_{h=h_0}^{h_f} D(t_h) - RL(t'_h)}{\sum_k \omega_k}, \quad (2.24)$$

where h_0 and h_f are the first and last time index of the load interval considered. For instance, for the capacity credit: $h_0 = 1$ and $h_f = 500$; for the mid LR: $h_0 = 1$ and $h_f = 4706$; and for the base LR: $h_0 = 1$ and $h_f = 8759$. This equation laid its formulation on the equation of the capacity credit stated in [241].

²Peak load plants operate only during times of peak demand while mid load plants usually run during the day and early evening; they either shut down or curtail output during the night and early morning. Base load plants operate all the time; they shut down or reduce power only to perform maintenance or repair.

At high RE mean penetration, there are hours in which combined wind and solar production exceeds the load, and thus the production must be curtailed if it cannot be stored or transmitted. Typically, the curtailment (5) occurs during the lowest net load hours of the year, represented by the lower tail of the figure (bottom right in red of the right panel of figure 2.14) and equals to the negative part of the RLDC. **The energy curtailed** can be calculated as follows (2.25):

$$E_{curt} = \frac{1}{h_f - h_0} \sum_{h=h_0}^{h_f} RL(t_h); RL(t_h) < 0. \quad (2.25)$$

XI Conclusion

To conduct a study of scenarios of solar integration, in Morocco, in which we aim to explore the impact of rental cost, storage, time-space complementarity and climate change on optimal mixes—considering the actual (2018) Renewable Energy (RE) Capacity Factors (CFs) and demand observations, distributed in four electrical zones, and recent cost data—we need to model and optimize the energy system.

The main model inputs are the geographical shapefiles, climate data, demand observations to fit the electricity demand, and the observed CFs to correct biases in the theoretical production of the different RE technologies—Wind, Photovoltaic (PV) without or with Battery Energy Storage (BES) and Concentrated Solar Power (CSP) without or with Thermal Energy Storage (TES)—investigated in this thesis. This chapter summarizes the data sources, the general approach adapted for the calculation of the electricity output for the different technologies without or with increasing levels of storage—as defined by the CSP Solar Multiple and PV Inverter Loading Ratio—, as well as for the calculation of electricity consumption, the optimization framework including the rental cost modeling, and the load reduction diagnostics.

The above-mentioned methodology is used to answer the sub-research questions of chapter 3, chapter 4 and chapter 5

Adequacy of Renewable Energy Mixes with Concentrated Solar Power and Photovoltaic in Morocco: Impact of Thermal Storage, Cost and Spatio-Temporal Complementarity under Penetration Scenarios

Contents

I	Introduction	78
II	Optimization Experiments	80
III	Results	80
1	Impact of Thermal Storage and Cost: Technological and Geographical Distribution	80
2	Impact of Spatio-Temporal Complementarity	84
3	Role of CSP-TES vs. PV in Reducing the Adequacy Risk	85
IV	Discussion and Comparison with Existing Studies	91
1	Scenarios of Unlimited Thermal Storage Cost and Capacity	91
2	Scenarios of High Renewable Penetration with Low Investment, even though High Adequacy Risk	92
3	Scenarios of High Renewable Penetration with Low Adequacy Risk, but with High Investment	93
4	Scenarios of Low Adequacy Risk with Low Investment, but Low Renewable Penetration	95
V	Summary and Concluding remarks	95

Abstract

Motivation

A key factor to differentiate the two solar technologies, Photovoltaic (PV) and Concentrated Solar Power (CSP), is their respective cost and the capability of Thermal Energy Storage (TES), combined with CSP, on reducing the variability of the Renewable Energy (RE) production.

Research Questions

The study's scope lies in investigating the impact of thermal storage duration and rental cost associated with these technologies on the Moroccan optimal mixes together with the time-space complementarity and TES in reducing the system variance-based risk (i.e., aggregate measure of the variation in the RE production). We also compare the contribution of PV and CSP-TES in reducing the system adequacy risk, e.g., increasing the capacity credit, taken as proxy of the operational value associated with the addition of PV and CSP-TES during peak load hours.

Objectives and Methodology

To do so, we model the optimal recommissioning of RE mixes including PV, wind and CSP without or with increasing levels of TES, as defined by the Solar Multiple (SM). We take as objective not only to maximize the RE production at a given cost, but also to limit the variance of the RE production stemming from meteorological fluctuations capturing the temporal and geographical smoothing effect. This mean-variance analysis is a bi-objective optimization problem that is implemented in the Energy for Climate Integrated Model (E4CLIM) which allows us to use climate reanalysis data provided by Modern-Era Retrospective Analysis for Research and Applications 2 (MERRA-2) to simulate hourly Capacity Factors (CFs) and demand profiles adjusted to observations for the four Moroccan electrical zones over the year 2018. To take into account for the different rental costs of wind, PV and CSP technologies, we add a maximum-cost constraint, in which the total cost of a mix is constrained to be lower than that of the actual 2018 Moroccan mix. We define the rental cost of production and storage technologies taking into consideration the storage size using recent (2013) cost data. We assess the contributing parameters under which PV can have a competitive advantage against comparable technology (CSP) or against dispatchable technology (CSP-TES) under various penetration scenarios. Finally, we compute the system adequacy diagnostics to compare the reliability benefits provided by each RE technology.

General Findings

We find that the optimal mixes are sensitive to rental cost at high penetrations, the more so as CSP with high solar field area and high storage capacity is installed. At such high penetrations, wind gains a higher share compared to solar technologies because wind has strong and regular CF on average, particularly in EAST and SOUTH, which involves less capacity to install. PV capacities are also installed in South at such penetrations due to its high mean CF compared to cost and its relatively low correlation with wind. At low penetrations, different RE combinations lead to differences in the sensitivity of the mix to minimum-variance ratios. The variance of normalized CFs are smaller for wind (in SOUTH) than for PV, and small for PV (in CENTER) than for CSP without storage. However, the addition of TES to CSP decreases the risk—the more as SM is increased keeping the mean CSP CFs fixed—which makes CSP-TES less variable than wind (particularly for $SM > 2$) and favors its installation (in EAST for SM2 and in SOUTH for SM3, SM4) compared to PV. To prevent reaching the maximum-cost sooner at high penetrations, the share of CSP decreases compared to PV and wind, letting the risk increase in return. Our results confirm that optimal mixes which not account for the thermal storage cost and with unlimited storage capacity affect the sensitivity of the mix to cost, but do not impact the technological and geographical distribution of capacities. This is, however, less true for the geographical distribution when the cost of CSP-TES is kept equal to the most widespread system (6–8 hours of TES). We also show that regional complementarity is key to reduce the risk because spreading RE deployment over a large area largely reduces the variability associated with the collective output of REs. The positive impact of technological complementarity, on the other hand, differs between combinations. It is weak between PV and wind, relevant only when installing both PV and CSP without storage, but less so as the surplus of energy available for TES is increased and the CSP profiles flatten. Finally, we find that the load reduction decline with increasing penetration and reach a saturation value. At high penetration, RE contributes primarily to base load, to smaller extent to mid load and only little to peak load. The larger the load, the less wind contributes to it. PV and CSP without storage contribute mainly to the mid load than the base load and little to peak load. Thanks to TES, CSP is more suited than PV and wind to meet peak loads and to reduce the curtailment of wind occurring at maximum-penetration point, driven by the elimination of CSP-TES.

I Introduction

Motivation

Solar Photovoltaic (PV) and Concentrated Solar Power (CSP) without or with Thermal Energy Storage (TES) integration in the electrical grid has been growing rapidly over the past decade to meet the increasing demand and reduce the negative impact of carbon emissions generated by conventional power sources [169, 290]. However, although both technologies use solar energy to generate electricity, they do so through different conversion processes; and are different in terms of mean production, variability and cost.

An approach to choosing a solar technology might be based simply on picking the option with the lowest Levelized Cost Of Electricity (LCOE). However, deployment based simply on cost ignores the relative benefits of each technology to the grid as a function of penetration and how they may actually interplay in an energy mix.

To begin with PV and CSP in terms of mean production, CSP systems can only benefit from the direct beam irradiance, rather than diffuse solar irradiance, and therefore are best suited to the regions with a high percentage of clear sky days. The locations that have significant cloudiness, smog, or dust are not favorable. PV, on the other hand, can use both direct and scattered sunlight and thus can be installed nearly anywhere. In addition to atmospheric components impacts, the operating temperature plays a key role in the PV and CSP conversion process. Solar panels performance decreases with increasing temperature; while the opposite is true for CSP collector performance [141]. Furthermore, the systems that specifically utilize the direct-beam sunlight benefit from tracking since these systems cannot produce energy unless pointed at the sun. This helps to minimize the angle of incidence and maximize the collected energy. As a result, the amount of energy produced per unit of installed capacity is increased. PV can also use tracking system, but the common orientation is fixed tilt where the orientation is the same at all times [327].

Whereas the capital costs of PV have dropped significantly in the last decade, resulting in large market adoption from near load centers to centralized locations, its intermittency, lack of affordable storage options, and a relatively low Capacity Factor (CF) during warm weather or at night mean that generation costs could be higher [269]. This is particularly true during periods of high generation at the middle of the day when demand is low, leading to over-production. When this happens, grid operators are forced to disconnect the plants, resulting in wasted energy at midday and shortage in the evening (the duck curve phenomenon [47, 158]).

Conversely, combining cheap TES with CSP can shift electricity over time even when the sun is not shining. Nevertheless, this advantage depends on the relative sizing of the CSP plant components (the solar field, storage tank and power block) which determines the CF of the plant. A smaller solar field results in reduced thermal energy delivered to the power block and a lower CF. An undersized power block relative to the solar field, in the absence of sufficient thermal storage capacity, can result in wasted energy during hours of high solar irradiance. A design parameter called the Solar Multiple (SM) normalizes the size of the solar field with respect to the power block. A system with a SM of 1 is sized for the solar field to provide the power block with enough energy to operate at its rated capacity under nominal conditions. A larger SM implies a larger solar collector area and a larger thermal storage capacity. However, the current capital cost of CSP without storage is relatively high for widespread deployment [268]. Moreover, increasing the SM and the storage capacity also increases the capital costs although its CF increases, which acts to reduce the LCOE [194, 268].

Drawing from the above, for any particular power system, Renewable Energy (RE) portfolio including these solar technologies with different thermal storage configurations are likely to result in different patterns of rental cost, mean penetration and variance or covariance, which have an influence on whether PV or CSP or CSP-TES should be installed.

Existing Research

Pragmatic approaches are carried out, relying for instance on the role of storage in accommodating a large-scale integration of RE [153, 461], the role of other flexibility options than CSP-TES such as pumped hydro storage and interconnection on the solar and wind capacity and their effect on the Moroccan load monotone [359], the technical and economic feasibility of systems with high RE penetration [116, 466], the impact of CSP-TES in such systems [147, 174, 176] and in enabling greater penetration of solar energy [161]. Du et al. [175] optimize operational decisions in a forecasting model for power systems with CSP at high RE penetrations. Richts et al. [451] perform technical and economical simulations of CSP/CSP-TES and PV in Morocco in which different scenarios of both technologies are modeled, highlighting the advantages and disadvantages of each one. A further study [164], likewise published by the German Aerospace Center, specifically explored scenarios of how RE plants—particularly CSP—could replace conventional generation in Southern Mediterranean countries by 2050. Alhamwi et al. use a mismatch energy modelling approach adopted with the objective to minimize the required storage capacities to find the optimal combination

between non-RE and RE power technologies integrating PV, wind, hydro and CSP-TES [49, 51], or to find the scenario mix of 100% solar-plus-wind [50]. Azouzoute et al. [74] give an overview of the integration of CSP as an alternative energy source in the Middle East and North African (MENA) region.

While the existing literature has mainly focused on assessing the impact of financing costs on the economic competitiveness of individual technologies [467], other studies focus on the sensitivity of the optimal mix to technology costs uncertainty [479], or the analysis of wind energy costs—compared to solar energy costs—in different sites of Morocco [515].

To these studies may be added a spate of other studies based on reliability and economic benefits of CSP-TES, like Madaeni et al. [330, 331] and Guedez et al. [229, 230] investigating the role of TES on the economic viability of CSP. Brand et al. [113] examine the effects of an increased integration of CSP-TES into the conventional electricity systems of Morocco and Algeria. Svendsen et al. [502] investigate the benefits of CSP-TES from a grid and market perspective in Morocco and Egypt. Oukili et al. evaluate the Moroccan power grid adequacy in presence of PV and wind generation [394] and with the introduction of CSP-TES [395] using a non-sequential Monte Carlo simulation. Alferidi et al. [48] highlight the reliability benefits of utilizing solar PV/CSP power in existing generation systems. Forrester et al. [201] analyze the role of CSP with TES in providing grid stability.

Studies combining different energy with CSP have been performed, including the combination with wind energy to reduce investment and electricity production prices for North African countries [309] or with PV plants to enhance energy production and profitability [414, 495] in Morocco [107].

Knowledge Gap

Yet to date, existing studies have not provided an analysis of the interplay between solar PV and CSP without or with different storage size in energy mixes under different penetration scenarios taking into account the cost and thermal storage duration effect. In fact, studies tend to focus on either reducing only the cost or reducing only the variability. In addition, our study covers Morocco as a whole allowing for weaker correlations between regions to be exploited whereas previous studies have focused on a limited specific sites or areas (e.g. Richts et al. [451] for PV and CSP/CSP-TES; and Tizgui et al. [515] for wind). In addition, even though there is a clear consensus that complementarity of wind [298, 294] and PV [336] leads to a smoothing effect that may reduce ramping requirements and transmission congestion, the magnitude of these benefits with the integration of CSP/CSP-TES has not been conducted by any study yet.

Implications and Originality of this Study

Particularly, the utilization of CSP with TES and PV is widely suggested within the Moroccan strategy that aims at deploying 2 GW (resp. 4 GW) of global solar installed capacity, which is equivalent to 14% (resp. 20%) of the electrical capacity by the end of 2021 (resp. 2030) [359]. However, the share between PV and CSP and the amount of thermal storage associated with CSP is still to be found. Currently, a number of CSP plants are being built or connected to the grid, or are planned [359], including hybrid PV-CSP-TES plants (such as the Noor Midelt project). However, an objective approach is missing to discuss possible scenarios for the PV/CSP/CSP-TES share in the actual Moroccan electricity mix.

Our study aims to bridge this gap and complements the above-mentioned research works as it is an analysis of the response of regional RE mix—including solar PV and wind energy as well—to large-scale integration of designed CSP with increasing TES capability and to the differences associated with solar technologies' rental costs. We also analyze the role of temporal and spatial correlations between CFs—for different zones and/or technologies—in reducing the system variance-based risk and the role of TES for electricity-systems adequacy.

Research Questions

This chapter addresses the first question of this thesis (**Q1**), raised in section 3 (Chapter 1), about the integration of CSP/CSP-TES with PV and wind in the Moroccan mix. We examine these issues by answering the following questions:

- **Q1-1:** How do the rental cost and thermal storage affect the ranges of penetration and risk where one of the solar technologies dominates over the others? What is the level of variance at which it becomes optimal to invest in CSP-TES rather in wind or PV or CSP without storage?
- **Q1-2:** Does technological or/and regional complementarity reduce the risk for the grid (i.e., variability of the aggregated RE production with respect to the electricity demand)? How the integration of CSP and CSP-TES impact the benefits of complementarity and to which extent this is affected?
- **Q1-3:** How does TES in a PV-wind-CSP mix help reduce the adequacy risk (i.e., the system variance-based risk and the system load reduction diagnostics)?

Objectives and Methodology

To find answers to the questions stated above, we use climate reanalysis data provided by MERRA-2 (Section 1, Chapter 2), for the four Moroccan electrical zones (Section i, Chapter 2) for the year 2018 (Section 3, Chapter 2), to simulate hourly CFs of wind (Section II, Appendix A); CFs of PV without storage referred as ILR^{ref} or Inverter Loading Ratio of 1 (ILR1) (Section ii, Chapter 2), CFs of CSP without or with increasing TES size (Section i, Chapter 2); and load curves (Section I, Appendix A) adjusted to observations (Section VI, Chapter 2). This study is adopted with the objective of maximizing the RE penetration and minimizing the imbalances between RE production and consumption—used as proxy for the system's adequacy risk. This mean-variance analysis is a bi-objective optimization problem that is implemented in the Energy for Climate Integrated Model (E4CLIM) (Section 1, Chapter 2). We optimize the electricity mix using a recommissioning approach in which the total cost of a mix is constrained to be lower than that of the actual 2018 Moroccan mix (Section VII, Chapter 2). We model the rental cost of each production technology considering the thermal storage cost and constraints related to energy and power capacity (Section VIII, Chapter 2). We analyze mixes along Pareto fronts — from low RE penetrations and low risks to high penetrations and high risks by examining the relevant parameters determining which RE technology stand at a leading position (Section IX, Chapter 2). Finally, we use the system adequacy diagnostics (Section X, Chapter 2) to explore the contribution of each technology to peak/mid/base load hours and analyze the variation of these diagnostics with increasing penetrations.

Outline

The remainder of this chapter is organized as follows. The data sources and the mathematical formulation of the modules needed for this study are specified in the previous paragraph and can be found in chapter 2. Section II summarizes the RE combinations adopted for this study. In section III, we present the results under different penetration scenarios highlighting the sensitivity of the technological and geographical distribution of capacities to rental cost and thermal storage (Section 1); followed by an analysis of the system adequacy benefits gained by taking into account the technological and regional complementarity (Section 2) and by adding TES (Section 3). Section IV discusses the actual mix and propose optimal alternatives to the current installed capacity distribution under different objectives and thermal storage assumptions

by highlighting the role of CSP-TES for electricity-systems adequacy. The last section, Section V, summarizes the methodology adapted and concludes the findings before presenting the extensions of our work.

This chapter has been submitted in peer-reviewed article published in the journal, *Energies*, and has been accepted for publication under the following reference [105] (Appendix B):

Bouramdane, A.-a.; Tantet, A.; Drobinski, P. Adequacy of Renewable Energy Mixes with Concentrated Solar Power and Photovoltaic in Morocco: Impact of Thermal Storage and Cost. Energies 2020, 13, 5087.

This chapter is the updated version of this first publication—in which the mean-variance analysis is applied using only the case 3 (Section 3, Chapter 2). Here, we represent in section III, the results obtained for case 1 (Section 1, Chapter 2) and compare between the three cases (Section 1, 2 and 3, Chapter 2) in section 1.

II Optimization Experiments

To investigate the response of the Moroccan mix to large-scale integration of Concentrated Solar Power (CSP) without Thermal Energy Storage (TES) or with increasing storage capabilities, as measured by the Solar Multiple (SM), and examine the sensitivity of optimal mixes to the different rental cost of Photovoltaic (PV) without storage (ILR^{ref} or Inverter Loading Ratio of 1 or ILR1), wind and CSP/CSP-TES, we carry out six optimization experiments summarized in table 3.1. Thus, all combinations with CSP but PV-Wind and PV-Wind-CSP-SM1 include storage.

All combinations are optimized using the same value, C_{tot}^{obs} , i.e. 3.5 G€/yr corresponding to the PV-Wind-CSP-TES combination (with 5.5 hours of TES or $SM^{ref} = 1.87$) (Section 1, Chapter 2).

Table 3.1: Optimization Experiments. Integration of Concentrated Solar Power (CSP) without and with increasing Thermal Energy Storage (TES) capabilities—as measured by the Solar Multiple (SM)—with Photovoltaic (PV) without storage (Inverter Loading Ratio of 1 or ILR1) and wind.

Combination	Wind	PV (ILR1)	CSP	
			TES	SM
PV-Wind	Yes	Yes	∅	∅
PV-Wind-CSP-SM1	Yes	Yes	No	1
PV-Wind-CSP-SM2	Yes	Yes	Yes	2
PV-Wind-CSP-SM3	Yes	Yes	Yes	3
PV-Wind-CSP-SM4	Yes	Yes	Yes	4

III Results

In this section, we examine the impact that Concentrated Solar Power (CSP) without or with Thermal Energy storage (TES) has on the optimal mixes by drawing insight on the sensitivity to the different rental cost of wind, Photovoltaic (PV) without storage (Inverter Loading Ratio or ILR of 1), and CSP without and with an increased TES cost and the variance associated with the change of the CSP Solar Multiple (SM); and how this might further increase the share of solar and wind energy and decrease the adequacy risk.

The simulation results of this section are obtained from hourly Modern-Era Retrospective Analysis for Research and Applications 2 (MERRA-2) climate data by running the mean-variance analysis using case 1 (Section 1, Chapter 2).

1 Impact of Thermal Storage and Cost: Technological and Geographical Distribution

Approximations of the optimal fronts of the mean-variance problem are represented in the left panels of figure 3.1 for the PV-Wind (a, b), PV-Wind-CSP SM1 (c, d), PV-Wind-CSP-SM2 (e, f), PV-Wind-CSP-SM3 (g, h) and PV-Wind-CSP-SM4 (i, j) combinations. The risk, $\sigma_{global/technology/base}$, is in abscissa and the mean penetration $(2.1), \mu$, in ordinate. In each panel, different fronts are represented. Each point of the front represented by the plain blue curve is associated with a Pareto-optimal mix—means there exists no other feasible solutions with a better or equal value for each of the objective functions—taking into account correlations between technologies and zones (global strategy (2.2)) while satisfying the maximum-cost constraint (2.8). In this case, nonlinear trade-offs of penetration and risk emerge. The straight black line passing through the origin represents the front for the global strategy as well, but without the maximum-cost constraint (i.e., in the context of unlimited cost of available capacity to install). Points to the right of this front (white) are not Pareto optimal or sub-optimal. Points to the left of this front (in gray) cannot be reached. The 2018 mix, or actual mix, is represented by the gray cross. In addition, particular optimal mixes from the global front with the total-cost constraint are depicted, ranging from maximizing the total renewable energy (RE) penetration to minimizing the variance, and so, flexibility requirements to meet the demand. The blue triangle represents the optimal mix with the same penetration as the actual mix, namely the penetration-as-actual mix. The blue diamond represents the optimal mix with the same risk as the actual mix, namely the risk-as-actual mix. The blue square represents the optimal mix with the largest penetration, namely the maximum-penetration mix. The blue plus represents the optimal mix for which the maximum-constraint is activated but with moderate penetration, namely the cost-activated mix. The black dot is the point with the largest penetration to be on both the constrained (plain blue line) and unconstrained (plain black line) global fronts, namely the cost-activation mix. In other words, it represents the optimal mix with the highest penetration for which the maximum-cost constraint is not active.

The right panels of figure 3.1 represents, as a function of the mean penetration and for the constrained global front and for different combinations, the shares of wind (blue line), PV without storage (brown line) and CSP/CSP-TES (orange line) capacities summed over all

zones. The blue, brown and orange crosses represent respectively the shares of wind, PV and CSP/CSP-TES capacities for the actual mix. The dashed vertical line is the penetration level to the right of which the maximum-cost constraint is active and corresponds to the black dot in the left panels. The dominant contribution from PV, wind, CSP/CSP-TES technologies in each region and penetration regime is associated with the three ratios presented in section IX (Chapter 2). We represent in bold, for each technology, the maximum of the maximum penetration ratio (Table 3.2), the minimum of the second ratio (Table 3.3) and the maximum of the minimum-variance ratio (Table 3.5) to illustrate the sensitivity of geographical distribution of capacities to solar technologies.

i Economic Carrying Capacity

For all combinations, as long as the constrained global front (plain blue) coincides with the unconstrained one (straight black) at low penetrations, the shares of the different technologies in the mix are nearly independent of the penetration and remain fairly constant (see the side of the right panels of figure 3.1 to the left of dashed line). At such low penetrations, little capacity needs to be invested in to achieve low penetrations so that both fronts overlap and the maximum-cost constraint is satisfied without activation. In this case, the optimal mixes are not sensitive to rental costs. At high penetrations, a higher Renewable Energy (RE) penetration involves more investments and operation costs which will ultimately increase the overall cost. As expected, the global constrained front bends away considerably from the unconstrained one to the right (left panels of figure 3.1) as the inequality constraint (2.8) to not exceed the total cost of actual RE capacities installed in Morocco in 2018 prevents the investment in additional capacities that would be needed to increase the penetration while limiting the increase in the variance. Moving beyond the point at which the total cost constraint is activated, the fractions of each technology are no longer constant function of the mean penetration.

The mean penetration of the tipping point at which the global constrained front deviates from the unconstrained one (i.e., cost-activation mix in black dot of the left panels of figure 3.1 corresponding to the black dashed line in the right panels of figure 3.1) is different from combination to another. In other words, the penetration at which the system becomes sensitive to cost varies between combinations, and the more we introduce CSP with large solar field and storage capacity, the more the system becomes sensitive to rental cost at low penetrations; pushing back—along the efficient pathways—its ability to compete with fluctuating technologies at high penetrations, letting the risk of load non-recovery increase (a proxy for the system's reliability or integration costs) as shown in the left panels of figure 3.1 where the constrained front shows a larger risk than the unconstrained one as the penetration is increased. Consequently, at penetrations beyond which the maximum-cost constraint is active, the wind share increases at the expense of solar technologies whatever the combination. In fact, wind has higher Capacity Factor (CF) with low cost (Tables 2.4 and 2.6, Chapter 2). Even though PV has lower rental cost than wind, it runs less often throughout the year, thus carry increased total cost compared to wind which help understand the downward trend of its fraction with an increasing share of REs. When looking at CSP/CSP-TES capital costs compared to its mean CF, we understand why it is penalized at high penetrations—although for increasing SMs—given that the solar field size is increased to feed the thermal storage system making the plant more expensive while providing the same mean CFs whatever the SM (Section 2, Chapter 2). Thus, installing more CSP at a higher cost than PV and wind means reaching the maximum budget sooner.

With that being said, this tipping point illustrates the level of penetration and variance at which it becomes more economically competitive to invest in intermittent and low-cost technologies (wind, PV) rather than the more capital intensive CSP-TES despite its high dispatchability. Therefore, it represents the economic carrying capacity [157], at which the benefit of low-cost PV and wind generating technologies exceed the benefits of CSP-TES (ability to provide firm capacity and the ability to shift energy from noon to sunset or nighttime).

It is clear that wind capacities are preferably installed and built with large capacity whatever the level penetration but not for all combinations; and the results are qualitatively and quantitatively different between solar PV/CSP/CSP-TES technologies, particularly at low penetrations. In the following subsections, we will examine the potential factors identifying the optimal technology that show an advantage by achieving relatively lower variance or higher penetration.

ii At maximum penetration

At maximum penetration, i.e., at the point approaching 100% wind share (the value of 100 % is not reached because of the limited resolution of the mean target) (on the right side of the right panels of figure 3.1), wind is dominating the mix, for all combinations, because it represents the best trade-off between more electricity production per megawatts (MW) installed on average (i.e., high mean CF) and low rental cost resulting in lower total cost for all combinations. This is reflected by the maximum-penetration ratio (2.19), which is given in table 3.2 for each technology and zone. As can be seen, the maximum-penetration ratios are larger for wind than for PV, and larger for PV than for CSP/CSP-TES. This helps to understand why, whatever the combination including CSP, CSP/CSP-TES is first replaced by PV which is then replaced by wind as the penetration is increased and the maximum-cost constraint becomes more and more active. In fact, because wind CFs are higher than solar ones on average compared to its cost (Table 2.4 and 2.6, Chapter 2), the PV and CSP/CSP-TES fractions are decreasing function of the mean penetration as more installed capacity is required and thus investment to reach the high penetration level; and CSP/CSP-TES fraction is zero at such maximum-penetration, compared to PV, due to its higher capital cost (in addition to lower CF compared to wind).

It is apparent from table 3.2, that the maximum penetration mix (i.e., blue square in the left panels of figure 3.1) is located in EAST whatever the combination, being the region with the strongest CF on average (Table 2.4, Chapter 2) which imply less capacity to install, leading to almost exclusive use of wind in the eastern region although highly variable wind in part due to the presence of the eastern Atlas mountain ridge where the interaction of the ambient atmospheric flow with the underlying orography results in regions of enhanced variance, but the variance is less important at such maximum penetration (see discussion in section 1, Chapter 2), .

iii At high penetrations

Optimal mixes for values of the penetration smaller than the maximum where the variances and covariances start to play a role in addition to rental cost and mean CFs, the second capacity that should be installed is the one that minimize the second ratio (2.20). This ratio for each technology and zone is displayed in table 3.3. We can see that, the smallest value of this ratio is for wind in SOUTH where the coastal climate effect of the southern Atlantic coast on wind speed can be more intense and reliable. We verify that this is indeed the second capacity to be installed by the numerical model (on the middle side of the right panels of figure 3.1). This could be attributed to the large maximum-penetration ratio of wind in SOUTH compared to that of wind in EAST already installed (Table 3.2), since the CF of wind in this region is also strong on average (Table 2.4, Chapter 2), and by the smaller variance/cost ratio of wind in the SOUTH compared to that of wind in EAST (Table 3.4)

Table 3.2: Maximum-penetration ratios (yr/T€) given by (2.19) obtained from hourly Modern-Era Retrospective Analysis for Research and Applications 2 (MERRA-2) climate data over the year 2018. Inverter Loading Ratio of 1 (ILR1) or Solar Multiple of 1 (SM1): Photovoltaic (PV) or Concentrated Solar Power (CSP) without storage; SM>1: with increasing levels of storage from CSP.

Zones	Wind	PV (ILR1)	CSP				
			SM1	SM^{ref}	SM2	SM3	SM4
NORTH	86.1	69.2	20.4	11.5	10.8	7.52	2.41
CENTER	91.0	70.5	26.0	14.4	13.6	9.43	3.05
EAST	107	76.0	21.0	11.7	11.05	7.62	2.46
SOUTH	104	78.1	24.8	13.8	13.03	9.0	2.90

as discussed in section 2 (Chapter 2), confirmed also by the largest minimum-variance ratio of wind in SOUTH compared to that of wind in EAST (Table 3.5).

PV without storage in SOUTH with its high mean CF compared to cost (Table 2.4 and 2.6, Chapter 2) is quickly introduced in these intermediate levels of penetration with a positive share, whatever the combination (on the middle side of the right panels of figure 3.1). This is mainly accounted to its low second ratio (Table 3.3) as a result of the relatively low correlations between PV ILR1 and wind CFs and the inverse of the demand (Table A.5, Appendix A) and of the small variance/cost ratio of PV in SOUTH (Table 3.4) compared to wind in EAST, already installed (see discussion in section 2, Chapter 2).

When it comes to CSP/CSP-TES, more the CSP solar field produces thermal energy greater than the capacity of the power block, more the correlation between normalized CFs of CSP-TES and other technologies is small (Table A.5, Appendix A). However, CSP/CSP-TES in CENTER at such penetrations is installed with very small share (on the middle side of the right panels of figure 3.1) due to its maximum-penetration ratios (resp. second ratio) that decrease (resp. increase) with increased SM (Table 3.2 and 3.3). One reason for low share of CSP-TES (compared to maximum-penetration point in section ii), despite its high cost (Table 2.6, Chapter 2), is the fact that the CSP thermal energy produced during the sunniest hours should be sufficient to enable maximum utilization of steam produced during summer peak. Reaching higher penetration of CSP would be feasible, at such high penetrations, if higher budget is allowed for allocating RE capacities to ensure the electricity system's adequacy whilst increasing the overall RE penetration.

The predominance of CSP-TES in CENTER, wind in SOUTH and PV in SOUTH at such high penetrations levels goes in line with the actual distribution (right panel of figure 2.4, Chapter 2).

Table 3.3: Similar to table 3.2 but for the ratios (no units) given by (2.20).

Zones	Wind	PV (ILR1)	CSP				
			SM1	SM^{ref}	SM2	SM3	SM4
NORTH	0.205	0.194	0.389	0.420	0.422	0.432	0.454
CENTER	0.112	0.198	0.376	0.412	0.414	0.426	0.452
EAST	\emptyset	0.170	0.393	0.422	0.424	0.434	0.454
SOUTH	1.47×10^{-2}	0.169	0.387	0.416	0.418	0.429	0.453

Table 3.4: Similar to table 3.2 but for the variance/cost ratio (yr/Ee MW) given by (2.21).

Zones	Wind	PV (ILR1)	CSP				
			SM1	SM^{ref}	SM2	SM3	SM4
NORTH	26020	6041	3455	1057	907	295	36.7
CENTER	7690	5700	4529	1207	1017	259	10.3
EAST	12767	6696	3083	834	705	188	10.3
SOUTH	2930	7208	4021	1076	900	221	5.0

iv At low penetrations

At low penetrations, different RE combinations lead to differences in the sensitivity to solar technologies (left side of right panels of figure 3.1) and thus to differences in the minimum-variance ratios (Table 3.5).

To illustrate this behavior at such low penetrations where the variance and time averaged CFs play a role (Section 3, Chapter 2), we represent the typical yearly cycle in abscissa (days of the year) and the daily cycle in ordinate (hours of the day) of the national CFs obtained using MERRA-2 climate data over the year 2018: Wind (Figure 3.2a), demand (Figure 3.2b), CSP SM2 (Figure 3.2c), CSP SM3 (Figure 3.2d), CSP SM4 (Figure 3.2e), PV without storage (Figure 3.3d), and CSP SM1 (Figure 3.3e).

Wind vs. PV

As shown on the left side of figure 3.1b, wind gains higher share than PV without storage because it has strong and regular mean CF compared to PV (Table 2.4, Chapter 2) which is installed, whatever the combination, in SOUTH (Table 3.5) due to the favorable circular air movement of the nearby Atlantic ocean enabling to achieve a significant and uniform energy production; compared to EAST where wind capacity is installed at maximum-penetration point, and where mountain ranges make the wind output more variable. In fact, both the mean and the variance of

the wind production tend to be larger than those of the PV production (Table 2.4, Figure 3.2a and 3.3d), but the variability of wind is more spread during the course of the day and the year since it is less tightly coupled to the diurnal cycle (ordinate of figure 3.2a) and although wind production peak yield in winter (which corresponds to low demand periods as shown in abscissa of figure 3.2b)—because low temperatures lead to higher air density—, it is uniformly distributed over the whole year (seasonal cycle in abscissa of figure 3.2a). Conversely, PV without storage is affected by day/night alternations and by fast-moving clouds (daily cycle in ordinate of figure 3.3d); and characterized by a stronger seasonal variability due to the sensitivity of fixed latitude-tilted multi-crystalline PV efficiency to high temperature occurring in the summer peak load which causes the solar production to be unevenly distributed throughout the year (seasonal cycle in abscissa of figure 3.3d). Due to the seasonal cycles of PV and wind energy production which are phase shifted and thus negatively correlated which reduces the covariances as shown in tables A.5 and A.4 (Appendix A), both technologies are kept in the mix to yield lower adequacy risk. Thus, this negative temporal correlation between irradiance and wind speed—as the irradiance values tend to increase the wind speed values reduce and vice versa—is important to take into account to not install less capacity which would turn to higher risk (See, however, the magnitude of this correlation impact on the variability in section ii).

Table 3.5: Similar to table 3.2 but for the minimum-variance ratios (10^3 MW) given by (2.22).

Zones	Wind	PV (ILR1)	CSP				
			SM1	SM^{ref}	SM2	SM3	SM4
NORTH	3.40	11.35	5.86	10.82	11.9	25.3	65.2
CENTER	11.73	12.26	5.71	11.90	13.3	36.1	291.5
EAST	8.36	11.25	6.78	14.0	15.5	40.2	235.9
SOUTH	35.4	10.74	6.12	12.7	14.3	40.3	578.3

PV vs. CSP SM1

We also observe, by comparing left side of figure 3.1b with left side of figure 3.1d, that at low penetrations, the introduction of CSP without storage (SM1) does not significantly affect the optimal technology shares compared to PV-wind combination. However, the mixes are more diversified as both PV and CSP capacities are represented. Little CSP is indeed introduced at the expense of PV, but PV remains largely dominant over CSP since there is a strong correlation between CSP and PV outputs which is assumed to have high covariances (Table A.5 and A.4, Appendix A) as both exhibit greater variability. Thus, adding new intermittent capacity will be subject to more significant variation, which make it more difficult for the grid to reduce the adequacy risk.

Indeed, in the absence of storage, one would expect that the model to be insensitive towards PV and CSP, both without storage, as the cost constraint is inactive at such low penetrations and both are linked to temporal availability of the solar resource and both are affected by the atmospheric conditions. This can be shown in figures 3.3d and 3.3e (ordinate) where the CSP SM1 or PV ILR1 plants operate mainly during midday load and their production drops after sunset because the solar production hours of CSP SM1 and PV ILR1 occur only when the sun is shining. However, the higher mean CF of CSP compared to that of PV (Table 2.4, Chapter 2) associated with the use of tracking and the positive CSP efficiency response to high temperature occurring in summer peak (abscissa of figure 3.3e and 3.2b) do not compensate the sensitivity of CSP to clouds since CSP is not exploiting the diffuse light while all components of solar irradiance are useful for PV production. It thus appear that the diffuse irradiance contribution limits the variance of PV compared to CSP by compensating for losses in direct irradiance associated with the atmosphere's variance of the clearness index (i.e. clouds passing over the solar field and reducing the direct normal irradiance). As a consequence, the minimum-variance ratio of PV tends to be larger than that of CSP (Table 3.5) and PV is installed more than CSP (left side of figure 3.1d).

The reason to install small fraction of CSP SM1 with PV ILR1 despite the variability of CSP SM1 is mainly related to the performance of CSP SM1 in summer peak as it performs better with increasing temperature compared to PV. This is also, indeed, due to the differences between the fixed-tilted PV surface and tracked-horizontal CSP surface since different orientations of the PV and CSP will intercept different amounts of solar energy (due to the motion of the sun) and thus show different patterns over the year and the day. To illustrate this point, the Global Horizontal Irradiance (GHI) (abscissa of figure 3.3a) and the Direct Normal Irradiance (DNI) (abscissa of figure 3.3c)—needed for CSP production—tend to increase in summer period while Global Tilted Irradiance (GTI)—needed for PV production—decreases in summer (abscissa of figure 3.3b). In fact, as the sun rises and sets, the cosine effect significantly reduces the rate of energy incident upon the PV fixed tilted surface, especially during summer days when the cos-losses are higher causing a stronger widening of the sunbeams. Tracked CSP, on the other hand, tend to reduce these angular losses occurring usually when sun elevation is low and sun rays are coming from east and west (morning and evening hours) and allow higher concentration ratios to be achieved (i.e., higher intercept factor measuring the percentage of rays that intersect the absorber tube against the total of all the reflected rays). For example, during dawn or dusk, shading losses between CSP collectors and PV panels account for 100%. In the early morning, all of the collectors face the east. Due to the low solar altitude angle of the sun in the morning, the eastern-most row of collectors will receive full sun, but this row will shade all subsequent rows to the west (Figure A.4(a), Appendix A). As the sun rises and the CSP collectors track the sun, this mutual row shading effect decreases, until a critical zenith angle is reached at which no row shading occurs. Collectors rows remain unshaded through the middle of the day, from late morning through early afternoon. Mutual row shading then re-appears in the late afternoon and evening, when the solar altitude angle is again very low. However, as distance between CSP collector rows in this model is large (Table A.2, Appendix A) shading only occurs in few hours. Therefore, over the entire day, the amount of solar energy entering the PV surface is lower than that could have been collected if the cosine effect had been reduced all the day using tracking as CSP. Given that, the north-south oriented tracking horizontal CSP surface receives more aperture solar energy over the day than does a latitude-tilted PV south-facing surface in the summertime (Figure 3.3d and 3.3e), when the Moroccan electricity demand is high (abscissa of figure 3.2b). The only time the PV solar panels points towards the sun, in summer, is noon (Figure 3.3d) since low irradiance levels, at sunrise and sunset, also decreases the power output (it does so following logarithmic relationship, Eq. (A.64)). However, in the winter when demand for cooling decreases, the CSP horizontal surface receives relatively less daily energy that a latitude-tilted surface PV does (consonant with [498, Chapter 4]). As can be seen in figure 3.3e, during a typical winter day, CSP production starts later in the day and ends earlier than the CSP production in summer, while for PV the situation is different (Figure 3.3d) since the incidence angle is much larger at noon in December than it is during morning or afternoon hours. Taken over the entire year, the north-south oriented single-axis

tracking CSP aperture receives slightly more energy than does the PV surface. However, the variation of the daily irradiance over the year is much greater for the CSP north-south axis orientation than for the PV fixed orientation (see discussion on the effect of the tilt angle and tracking in section i, Chapter 1).

The low variance optimal mixes locates PV capacities in the CENTER (Table 3.5) with relatively low value of average CF compared to the southern regions and the Saharan side of the Atlas in the EAST (Table 2.4, Chapter 2). This suggests that the higher generation regions and clear-sky irradiance (desert), EAST and SOUTH, are being penalized for their higher variability caused by the larger daily cycle amplitude of the irradiance resource. This allocation may not be surprising since region with significant cloud cover is preferred due to the diminishing effect of the cloud cover on the variance which can be more efficient for PV than southern and eastern regions as it also benefit from cooler temperatures. However, the region with cloud coverage is only favored at such low penetrations, but losing its predominant position at very high penetration levels when installing all the capacities in this region could not satisfy the penetration required, and the model would favor southern regions (Table 3.2 and 3.3) despite having larger average daily irradiance oscillations to install less capacities (and thus reducing the total cost) while reaching higher penetrations. The installation of PV in CENTER can also be explained by the relatively small correlations between the PV generation and wind generation in the CENTER and between PV generation and wind generation in the windy region (EAST), as shown in table A.5 (Appendix A).

Wind vs. CSP SM1

The share of wind is larger than CSP without storage (left side of figure 3.1d). This can be explained by the absence of sunlight during night (involving no CSP generation) and thus a lower annual energy coming from CSP when the integration is made over one year (Figure 3.2a and 3.3e). In case CSP dominates over wind, this will lead to increase the risk during this period of time even if its normally an off-peak period.

CSP-TES vs. PV

More the SM is increased, more the electricity needed to quickly ramp up energy production when the sun sets and the contribution from PV falls is reduced (ordinate of figure 3.2c, 3.2d and, 3.2e). Therefore, CSP-TES is installed while PV is phased out from the mix (left side of figures 3.1f, 3.1h and 3.1j). In fact, this might be explained in this way: PV correlates only with the midday peak (ordinate of figure 3.3d) but a large capacity is required after the sunset period. CSP-TES, on the other hand, can produce partially electricity during the day—which replaces PV instead of adding a new capacity although having low covariance with CSP-TES as shown in table A.4 (Appendix A)—, stores the excess during the day and reconstitute the energy later at the moment when solar irradiance no longer correlates with peak electricity demand which helps to reduce the diurnal and seasonal power fluctuations such as curtailment or lack of energy, enabling greater penetration of solar energy in the mix (left side of figures 3.1f, 3.1h and 3.1j) compared to the case without storage (left side of figure 3.1b and 3.1d). This is also confirmed by the CSP-TES minimum variance ratio that increases with the SM to become larger than that of PV (Table 3.5). This finding is consistent with [161] showing that a solar portfolio which includes CSP-TES and PV would support less curtailment of aggregate solar production, which increase the proportion of solar power in the mix (see also discussion in section ii, Chapter 4).

As can be seen in table 3.5, the distribution of CSP-TES capacities along the constrained front is mainly on two regions located on the eastern or southern regions depending on the ability of the thermal storage system to retain solar heat generated during the sunny period to convert it to electricity when needed. CSP-TES capacities with medium storage duration (SM2 or 6 hours) are installed in EAST; and high storage duration (SM3,4 or 11-17 hours) are installed in SOUTH. Therefore, more the SM is increased, more regions with higher generation (Table 2.4, Chapter 2) are preferred against lower amplitude oscillating solar resources because the variance is reduced by the introduction of thermal storage. We note that the mean CF in CENTER is higher than that of the SOUTH (Table 2.4, Chapter 2). However, the CSP generation deficit attributable to cloudiness, as has been commented on previously (PV vs. CSP; Section iv), makes this region variable. This region may be favored with higher storage capacity ($SM > 4$ or > 17 hours).

CSP-TES vs. Wind

From the left side of the right panels of figure 3.1, we can see that once CSP-TES with medium storage duration (SM2) is brought into the mix (left side of figure 3.1f), it can contribute to reaching the necessary risk with wind in the convenient regions but wind dominates over CSP-TES SM2. The wind predominance is explained by the largest minimum-variance ratio of wind in SOUTH (Table 3.5). However, the larger the SM — i.e. the larger the surplus of energy available for storage—, the higher the share of CSP-TES compared to wind, particularly for combinations with SM3 (left side of figure 3.1h) and CSP-TES tends to replace completely wind for SM4 (left side of figure 3.1j). This is also confirmed by the CSP minimum-variance ratios that increases with the SM and becomes larger than that of wind in SOUTH (Table 3.5).

2 Impact of Spatio-Temporal Complementarity

To investigate the role played by aggregating the production of a given technology at different locations (taking into account correlations between CFs of a given technology for different zones, namely "the regional complementarity"); and/or by exploiting the complementarity between energy sources located in close proximity (taking into account correlations between CFs of different technologies in the same zone, namely "the technological complementarity"), we compare the global (black line), technology (dashed black line) and base (point-dashed black line) fronts without the maximum-cost constraint (left panels of figure 3.1). These unconstrained fronts agree with the corresponding fronts with the maximum-cost constraint (the global one being represented in blue) only at low penetrations, when this constraint is inactive. They thus help understand the role of correlations at low penetrations only. In the global strategy (2.2), all correlations between different zones and technologies are considered. In the technology strategy (2.3), all correlations between different zones are ignored, while, in the base strategy (2.4), correlations between different technologies of the same zone are also ignored. Thus, moving from the base (resp. technology) front to technology (resp. global) front allow us to evaluate the benefits of temporal (resp. regional) complementarities; and comparing the base front with the global front allows us to examine the role of spatio-temporal complementarities on reducing the adequacy risk.

These fronts are straight lines with a slope given by the mean-standard deviation ratio (2.5). At any point on the front, this ratio quantifies the increase in percentage point in the mean penetration achieved by letting the standard deviation rise by one point. Its values for the three strategies and six combinations are reported in Table 3.6. We can see that the ratios decrease from the global to the base front so that the technology front is flatter than the global front and the base front flatter than the technology front. This shows that ignoring correlations between different zones and between different technologies of the same zone prevents reducing the risk as much as possible.

Table 3.6: Mean-standard deviation ratios (2.5) of the global, technology and base fronts without the maximum-cost constraint (2.8) for different combinations (Table 3.1). Photovoltaic (PV) is without storage. Solar Multiple of 1 or SM1: Concentrated Solar Power (CSP) without storage; SM>1: with increasing levels of storage from CSP.

Combination/ Strategy	PV-Wind	PV-Wind CSP-SM1	PV-Wind CSP- SM^{ref}	PV-Wind CSP-SM2	PV-Wind CSP-SM3	PV-Wind CSP-SM4
Global	1.95	1.95	2.06	2.11	2.56	5.29
Technology	1.64	1.63	1.74	1.79	2.33	4.95
Base	1.57	1.36	1.50	1.55	2.12	4.88

i Regional Complementarity

For all combinations, the reduction of the mean-standard deviation ratio from the global to the technology strategy (Table 3.6) and the difference between these fronts (left panels of figure 3.1) is significant. Therefore, because variations in Moroccan climatic conditions from one zone to the other are relatively small on average, it is thus essential to take correlations between CFs of different zones into account in order to reduce the risk, whatever the technological combination. In fact, the major variability of the solar and wind resource is associated with the diurnal and the seasonal cycle and is thus highly correlated in space; although a fraction of the solar (resp. wind) resource variability is associated with clouds (resp. wind speed) and decorrelates quickly with distance [178, 273, 258], but it seems to be negligible on an annual scale.

However, as CSP solar field produces more energy than the power block can transform (i.e., increase of the SM), more the differences between the global and the technology fronts are reduced. This finding may partly be attributable to the fact that mixes become less diversified as CSP in SOUTH (for SM3, SM4) becomes dominant (Table 3.5 and the left side of the right panels of figures 3.1h, 3.1j).

ii Technological Complementarity

The effect of correlations on the optimization, however, varies between combinations. Table A.5 (Appendix A) displays the correlations between the CFs and the inverse of the demand in the same region over the year 2018.

For PV-Wind, the reduction of the mean-standard deviation ratio from the technology to the base strategy (Table 3.6) is small. And, the front for the technology strategy and the front for the base strategy for the PV-wind mix are relatively close to each other (Figure 3.1a); a sign that the technological complementarity between PV and wind production is weak in this case (Table A.5, Appendix A). This can be understood from the fact that correlations between irradiance and wind speed are weaker, different resources being harvested by these two technologies so that taking them into account is not as critical. In fact, due to local effects such as the mountain/valley breezes, on average, the highest wind power generation levels occur during nighttime, showing no correlation with the PV production.

With the introduction of CSP without storage, however, the difference between the technology and the base fronts is much larger (Figure 3.1c). In addition, the reduction of the mean-standard deviation ratio from the technology to the base strategy (Table 3.6) for the PV-wind-CSP-SM1 mix is large. In this case, correlations between PV and CSP CFs are large (Table A.5, Appendix A) since the production of PV or CSP is directly linked to the temporal availability of the solar resource, although the latter is not exploiting the diffuse irradiance and the former is sensitive to high temperatures, as stated previously. Therefore, ignoring these high covariances between PV and CSP lead to install much of PV and CSP which results in an increased risk (as discussed in section iv).

Taking correlations between technologies into account has a stronger impact in the case of the PV-wind-CSP and PV-wind-CSP-TES combinations, although less so for the latter. As the SM is increased (Figures 3.1e, 3.1g, 3.1i), however, the difference between the technology and the base front weaken (confirmed also by table 3.6) because the increased available storage results in weaker correlations between PV/wind and CSP-TES CFs (Table A.5, Appendix A).

Overall, comparing the base front with the global front (left panels of figure 3.1), the results clearly show that the temporal and spatial dispersion of wind and solar resources smooth their power output. This show that sudden drop in power generated in one source in one region can be replaced by a simultaneous increase in power provided by another source in another region. It should be noted, however, that according to our results, complementarity can be effective on reducing the risk if the different technologies and/or regions are negatively correlated (e.g., technological complementarity between PV and wind); but still often of minor importance compared to case where they are positively correlated (e.g., regional complementarity or time complementarity between PV and CSP).

3 Role of CSP-TES vs. PV in Reducing the Adequacy Risk

This section is divided into two subsections, starting with a general analysis of the potential of CSP-TES to provide grid flexibility and enable increased RE penetration in given RE system by comparing the mean-standard deviation ratio (2.5) between combinations at low penetrations (where the CSP/CSP-TES is integrated due to the maximum-cost constraint) (Section i). Section ii is dedicated to explore its role in reducing the main integration challenges of RE in the grid (Section X, Chapter 2), specifically its ability to displace fossil-fired generation during peak, mid and base load hours; and implicitly their associated costs and emissions.

i System Variance-based Risk

Since the RE generation from wind and PV are weather-driven and have different ramping patterns, table 3.6 reflects the increasing balancing needs when these technologies are integrated without storage, i.e low mean-standard deviation ratio. Adding CSP to PV-wind mix slightly reduces the mean-standard deviation ratio, giving the rise to greater flexibility necessity, which affect notably the costs induced into the system.

The reduction of the CSP CF's variability due to storage, for PV-wind-CSP-TES combinations, results in a decline of the optimal-mix risk for a given low penetrations. For instance, changing the SM parameter from SM3 to SM4 increases the share of CSP-TES (left side of figures 3.1h and 3.1j), which results in bridging the gap between supply and load (i.e., increasing the mean-standard deviation ratio as shown in table 3.6). Thus, RE systems including CSP capacities, especially those with high SMs, can allow generation to be shifted to periods without

resources and to provide backup energy during periods with reduced sunlight that can be caused by clouds cover; which will generally reduce the need for other capacity to be built.

Having more CSP-TES at low penetrations does not imply that significantly more CSP-TES is installed at higher penetrations unless the maximum total cost is increased. At such high penetrations, the mean-standard deviation ratio is deteriorated for the global strategy (left panel of figure i) since only PV and wind take part of the mix as explained in section i. Therefore, if small level of risk and higher penetrations are targeted, investment must be increased to install more CSP with storage to alleviate the inherent variability with more RE installed capacity.

ii System Adequacy Diagnostics

For a more detailed description of the effect of CSP-TES on the reliability of the grid compared to fluctuating PV and wind, we now look at properties of specific RE system in reducing the peak, mid and base load. We analyze how these load reductions are affected by RE shares, and the contribution of each technology to each load band. Figure 3.4 presents the peak (top) load reduction (i.e., capacity credit), mid (middle) and base load reduction (bottom) for PV-wind mix (left) and PV-wind-CSP-TES SM2 (right). Whatever the combination, we select optimal mixes on the constrained global front at different levels of penetration from 5 % to 35 %.

For PV-wind and PV-wind-CSP-TES SM2 combinations, we can see that, the Load Reductions (LR) tend to decline and reach a saturation value with the increase of mean penetration. This is true for the peak load reduction, the mid load reduction but less true for the base load reduction that decreases slightly as RE shares continues to increase. Intuitively, it seems possible that the decrease of LR with increasing penetrations are due to the decrease of CSP-TES fraction since adding relatively large share of CSP-TES with 6 hours of thermal storage to PV-wind mix (left side of figure 3.1f) allows to increase the capacity credit from 45% to 53% at 5% RE share (compare the left and right top panels of figure 3.4). From the middle and bottom panels of figure 3.4, we can observe that CSP-TES also contributes to increase the mid (resp. base) load reduction from 53% (resp. 48%) in PV-wind mix to 60% (resp. 50%) in PV-wind-CSP SM2 mix, consistent with [176]. The slightly decrease of base LR, with increasing penetrations, compared to mid and peak LR is due to the occurrence of wind curtailment at such high penetrations—due to the strong wind CF in winter (abscissa of figure 3.2a) when the demand is low (abscissa of figure 3.2b)—and where the fraction of CSP-TES is reduced. In addition, with increasing penetrations, the base LR is higher than the mid LR which is higher than the peak LR (compare the right side of the top, middle and bottom panels of figure 3.4). The section ii (Chapter 4) looks into these aspects in a far more detailed way.

Whatever the combination, the LR are mostly due to wind. However, it is associated to the high wind shares and does not necessarily mean that solar technologies do not contribute to reduce the load efficiently in relative terms (as discussed in section 1). For wind, the base load reduction is larger than the mid-load reduction, which is larger than the capacity credit. This is also confirmed in figure 2.15 (Chapter 2). The strong contribution of wind to base load reduction could be attributed to the evenly daily and seasonal profile of wind CFs (Figure 3.2a) compared to that of solar technologies (Figure 3.3d, 3.2c, 3.2d and 3.2e). For PV without storage, the mid LR is larger than the base LR, which is larger than the peak LR. This is also visible in figure 2.15 (Chapter 2). Its weak contribution to the base load, compared to wind, can be understood from the fact that it does not generate at night when the load is small in addition to its profile during summer peak demand (Figure 3.3d). For CSP with storage, the mid LR is larger than the capacity credit, which is larger than the base LR. Thus, while the addition of TES to CSP does not change the fact that CSP (i.e., PV) mainly contributes to the mid load, it helps improves the capacity credit significantly, in agreement with the previous paragraph. Moreover, the decomposition of the capacity credit, mid and base LR by technology shows that the increase in the capacity credit for combinations with storage is mainly due to CSP-TES rather than to PV because CSP-TES represents the best compromise between high mean CF and low variance (i.e., the minimum variance ratios of CSP-TES tend to be larger than that of CSP or PV, Table 3.5). Thus, in addition to reducing the variance-based risk, the introduction of CSP with storage helps satisfy peak, mid and base loads more than PV at almost equivalent shares (left side of figures 3.1b and 3.1f before the activation of the total cost constraint) because CSP-TES could change the temporal distribution of the net load by charging and discharging frequently and influence the correlation with the demand.

However, while further increasing the SM may help increase the LR, this also depends on the share of CSP-TES in the mix, since the load reductions are based on CSP-TES but also on PV and wind.

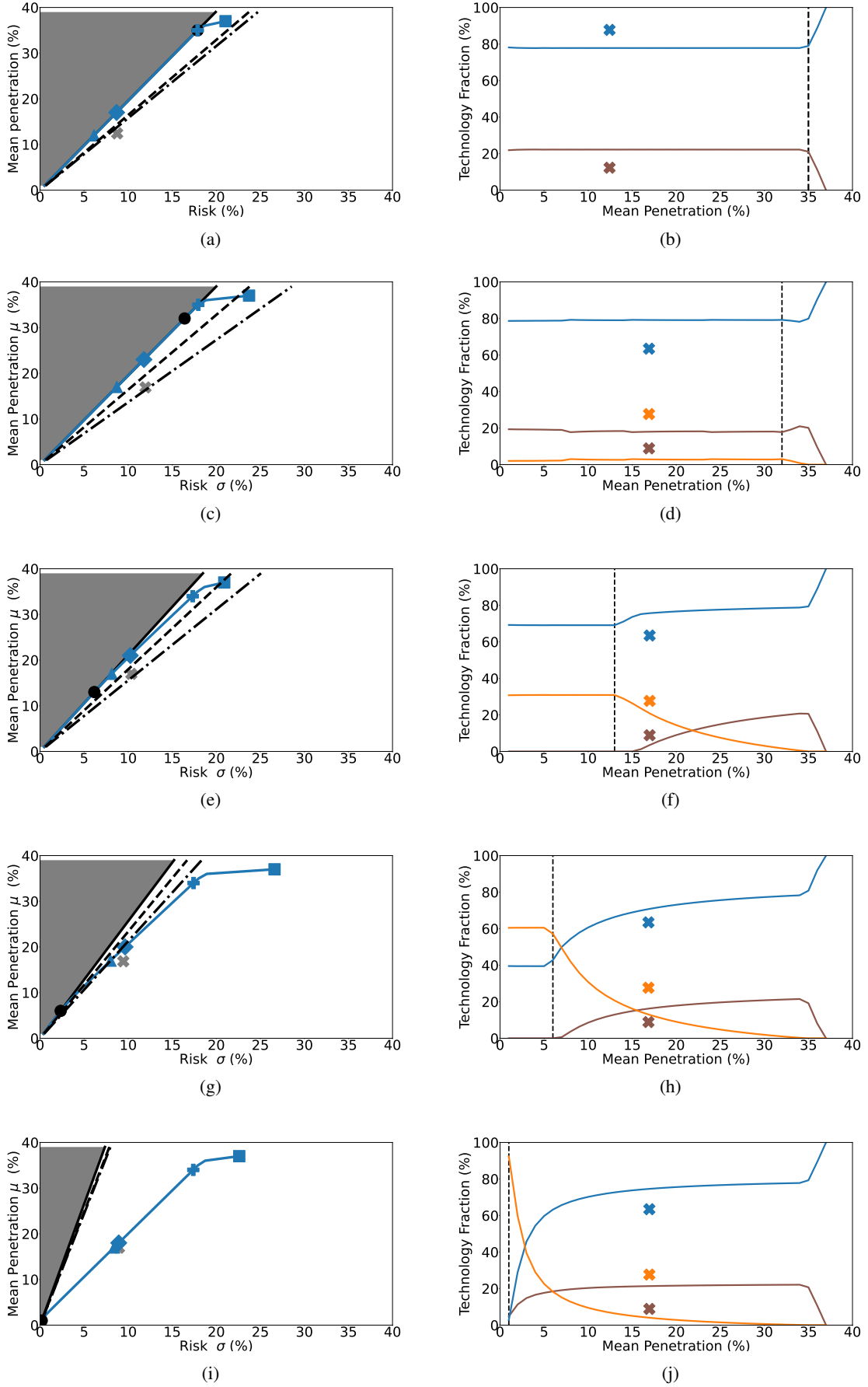


Figure 3.1: **Left:** Approximations of the optimal fronts obtained from hourly Modern-Era Retrospective Analysis for Research and Applications 2 (MERRA-2) climate data with the risk, $\sigma_{\text{global/technology/base}}$, in abscissa and the mean penetration (2.1), μ , in ordinate. **Right:** Shares of wind (blue line), Photovoltaic (PV) without storage (brown line) and Concentrated Solar Power (CSP) without or with Thermal Energy Storage (TES) (orange line) capacities versus the mean penetration for the global strategy (2.2) with maximum-cost constraint (2.8). (a, b): PV-Wind. (c, d): PV-Wind-CSP-SM1. (e, f): PV-Wind-CSP-TES SM2. (g, h): PV-Wind-CSP-TES SM3. (i, j): PV-Wind-CSP-TES SM4. Solar Multiple of 1 or SM1: CSP without storage; SM>1: with increasing levels of storage from CSP.

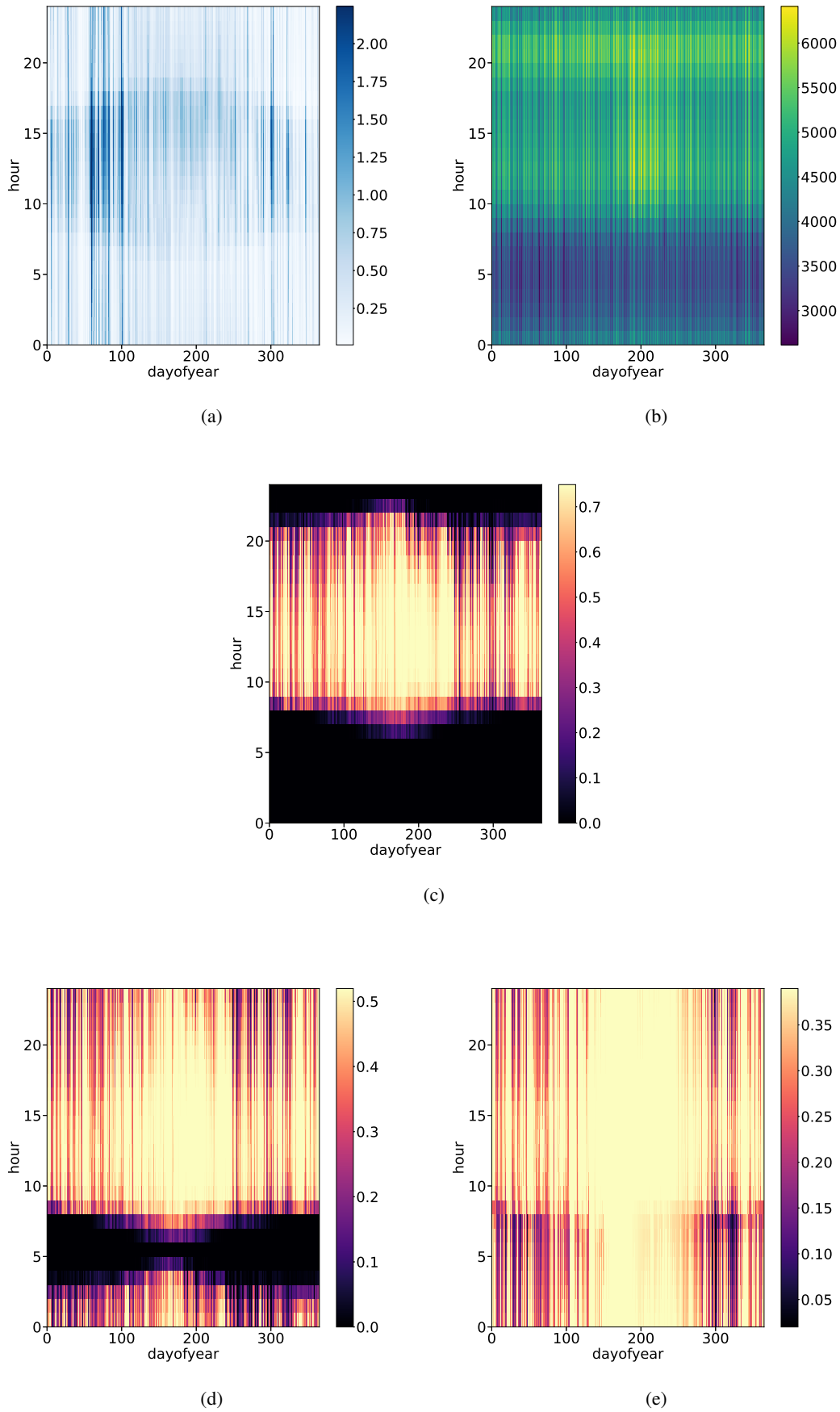


Figure 3.2: Heatmap of the national daily (ordinate) and seasonal (abscissa) variability of the predicted capacity factors and demand: Wind **(a)**, demand in MW **(b)**, Concentrated Solar Power (CSP) with Thermal Energy Storage (TES) with a Solar Multiple (SM) of 2 **(c)**, CSP-TES SM3 **(d)**, CSP-TES SM4 **(e)**; obtained over the year 2018 from the hourly Modern-Era Retrospective Analysis for Research and Applications 2 (MERRA-2) climate data. The variation over time is shown in color by intensity in the colorbar. $SM > 1$: with increasing levels of storage from CSP. Critical appraisal of the obtained wind profiles are discussed in section i (Appendix A) and that of the demand in section 1 (Chapter 2).

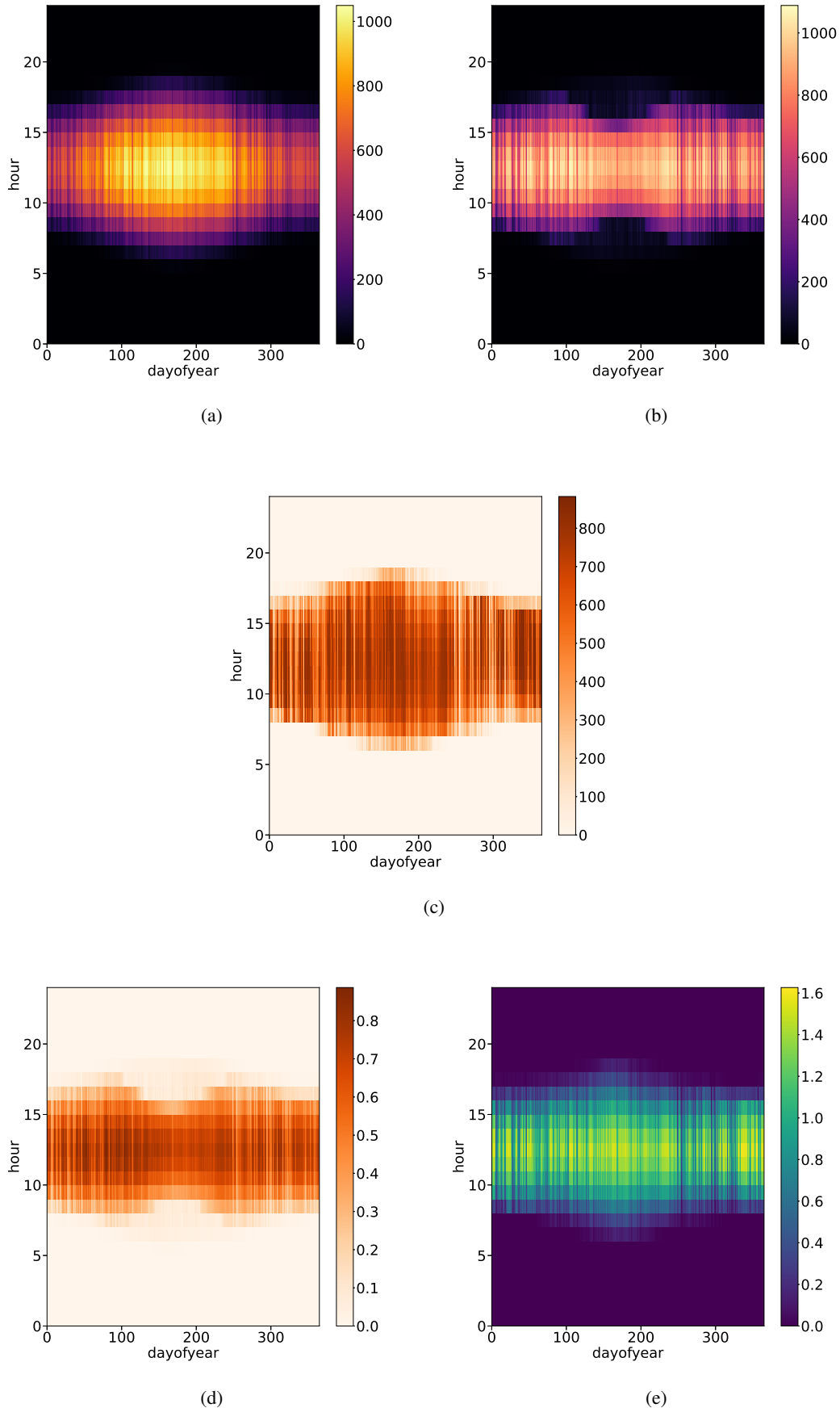
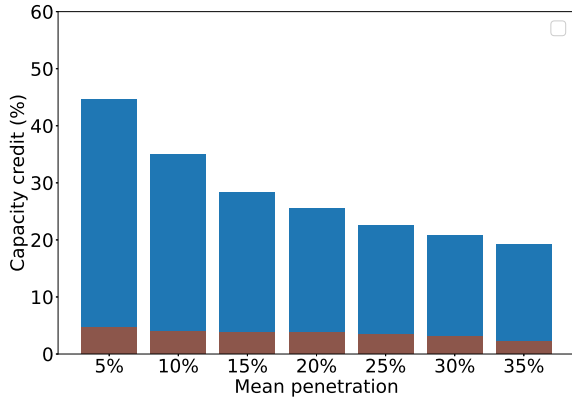
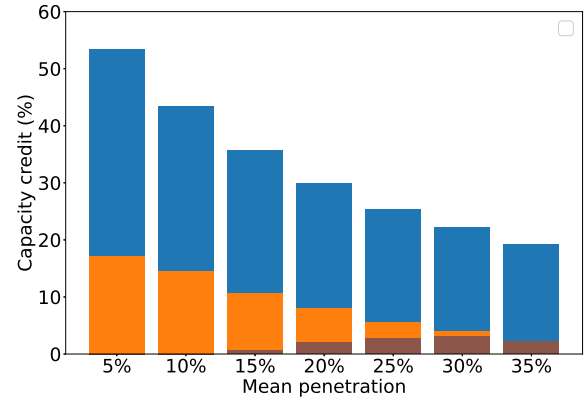


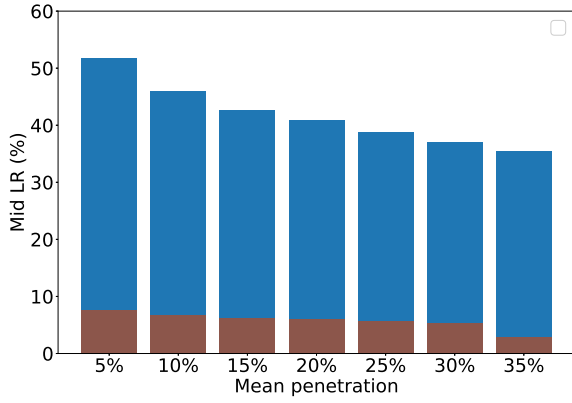
Figure 3.3: Heatmap of the national daily (ordinate) and seasonal (abscissa) variability of the solar irradiance components in (W/m^2): Global Horizontal Irradiance (GHI) **(a)**, Global Tilted Irradiance (GTI) **(b)** (to be compared with figure 3.3d), Direct Normal Irradiance (DNI) **(c)** (to be compared with figure 3.3e, 3.2c, 3.2d and 3.2c). The diurnal and seasonal patterns are also depicted for predicted Capacity Factors (CFs): Photovoltaic (PV) without storage (Inverter Loading Ratio of 1 or ILR1) **(d)** and Concentrated Solar Power (CSP) without storage (Solar Multiple of 1 or SM1) **(e)**. Solar Resources and CFs are obtained over the year 2018 from the hourly Modern-Era Retrospective Analysis for Research and Applications 2 (MERRA-2) climate data. The variation over time is shown in color by intensity in the colorbar. Critical appraisal of the obtained profiles are discussed in section ii and iii (Appendix A).



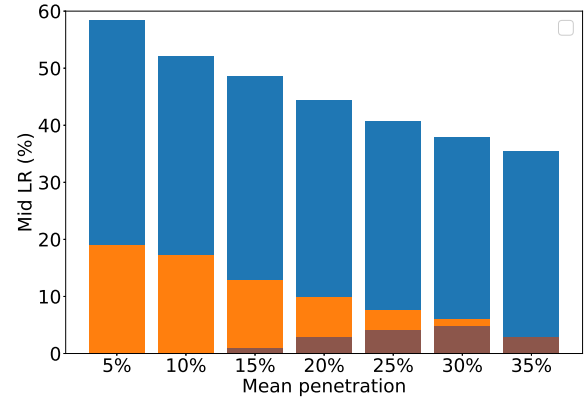
(a)



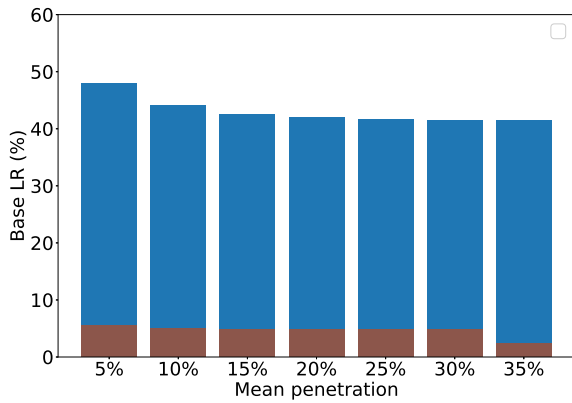
(b)



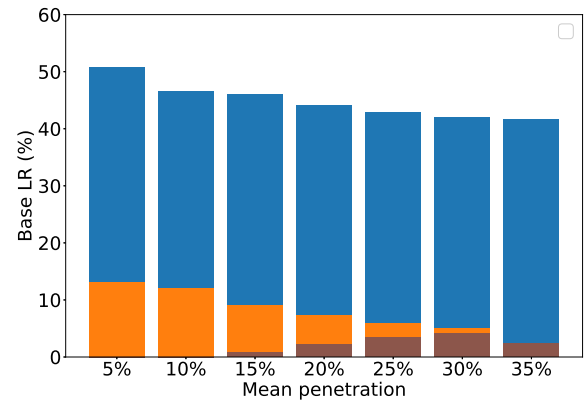
(c)



(d)



(e)



(f)

Figure 3.4: Capacity credit (**top**), mid load reduction (**Middle**), and base Load reduction (**Bottom**) by each technology—Wind (blue), Photovoltaic or PV (brown) and Concentrated Solar Power (CSP) with Thermal Energy Storage (TES) with a Solar Multiple (SM) of 2 (orange)—versus the mean penetration (2.1), μ , for the global strategy (2.2) with maximum-cost constraint (2.8) obtained from hourly Modern-Era Retrospective Analysis for Research and Applications 2 (MERRA-2) climate data over the year 2018. **Left:** PV-wind mix; **Right:** PV-wind-CSP-TES SM2 mix. SM2: CSP with 6 hours of TES.

IV Discussion and Comparison with Existing Studies

The results obtained so far allow us to discuss scenarios of solar Photovoltaic (PV) without storage, Concentrated Solar Power (CSP) without or with Thermal Energy Storage (TES) integration, for instance scenarios of unlimited thermal storage cost and capacity (Section 1). We highlight promising options of energy mixes within the context of low adequacy risk and/or high Renewable Energy (RE) penetration and cost budget (Section 2;3 and 4). We also discuss the role of CSP-TES compared to PV and wind in reducing the adequacy risk and provide a new insights regarding the distribution of solar-wind capacities in Morocco (Section 3).

1 Scenarios of Unlimited Thermal Storage Cost and Capacity

In section III, we present the results of the sensitivity of optimal mixes to cost and storage duration associated with PV, CSP/CSP-TES and wind (Case 1, Section 1, Chapter 2). Considering now the cases where the optimization problem is only sensitive to the different rental costs of wind, PV, and CSP; and the variance associated with the change of the CSP Solar Multiple (SM); while the cost of storage is ignored (Case 2, Section 2, Chapter 2) or kept constant—taken into account implicitly in the cost of the whole parabolic trough CSP-TES system with 6-8 hours of storage (Case 3, Section 3, Chapter 2)—and thus the constraints on storage model are not applied. In other words, we consider the scenarios of unlimited/fixed thermal storage cost and capacity. The obtained optimal technological distribution is represented in figure 3.5 for PV-wind-CSP-TES SM2 (top); PV-wind-CSP-TES SM3 (middle) and PV-wind-CSP-TES SM4 (bottom). The left (resp. right) panels corresponds to case 2 (resp. case 3).

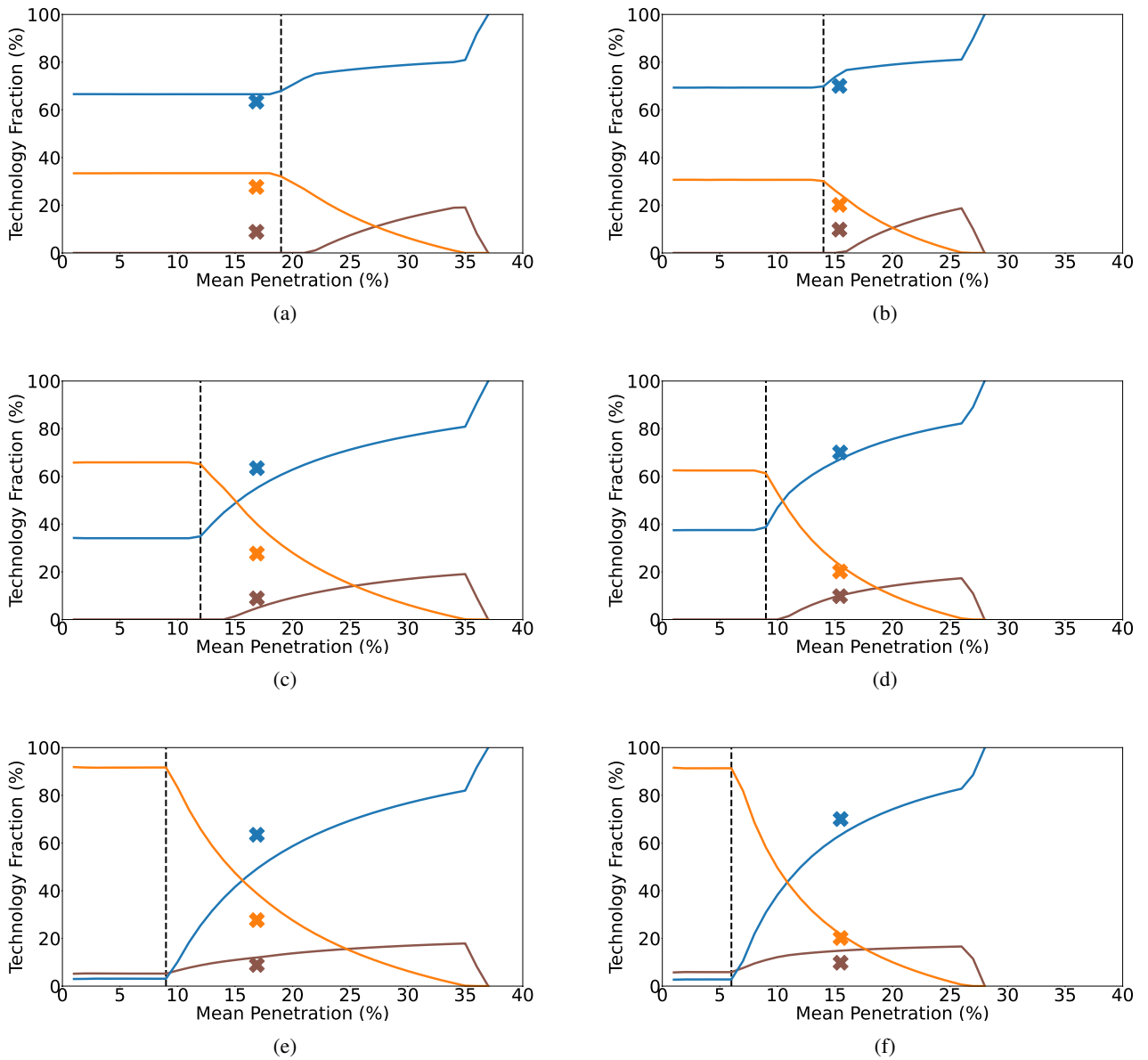


Figure 3.5: Similar to the right panels of figure 3.1 for scenarios with unlimited thermal storage capacity and cost. **Left:** Case 2 (Section 2, Chapter 2). **Right:** Case 3 (Section 3, Chapter 2). **Top:** PV-Wind-CSP-TES SM2. **Middle:** PV-Wind-CSP-TES SM3. **Bottom:** PV-Wind-CSP-TES SM4. PV is Photovoltaic; TES is Thermal Energy storage and SM is Solar Multiple. $SM > 1$: with increasing levels of storage from Concentrated Solar Power (CSP).

→ Capacity Pathways Remain Unchanged

As can be seen by comparing figure 3.5 (case 2 and 3) with the right panels of figure 3.1 (case 1) for the above-mentioned combinations, even

though unlimited storage cost and capacity induces a change in the CSP-TES mean Capacity Factors (CFs), variance and covariance (not shown here) which in turn alter the optimization ratios; but, the interplay between technologies do not seem to be impacted. Thus, we do not compute the maximum-penetration ratios, the second ratios and the minimum-variance ratios for these cases but an examination of equations (2.19), (2.20) and (2.22) will convince the reader of the following findings. In fact, keeping the CSP cost constant for all SMs while keeping the mean CSP CFs fixed (as discussed in section VIII, Chapter 2), implies that the CSP maximum-penetration ratios (2.19) for different SMs have similar values in case 2 and 3; while these ratios decrease with increasing the CSP solar field area (Case 1, Table 3.2). In addition, CSP second ratio (2.20) decreases for higher SMs in case 2 and case 3 (because correlations between normalized CFs, variance and cost are reduced); where these ratios increase for higher SMs in case 1 (Table 3.3). At low penetrations, ignoring the constraints on thermal storage, in case 2 and 3, further reduce the variance of mean CSP CFs which increases the values of the CSP minimum-variance ratios (2.22) of case 2 and 3 compared to case 1 (Table 3.5).

Given the above, even though the variance of CSP-TES CFs is further reduced and are likely to provide more flexibility to meet the demand and even though the storage cost of CSP is ignored, CSP-TES integration remains hindered in high penetration scenarios of REs due to the high initial investment of CSP and the low correlations between CSP-TES CFs and wind CFs (Table A.5, Appendix A). This show that the high capital cost of CSP more than surpass the benefits of low-cost TES with large storage capacity. At low penetrations, the decrease of the CSP-TES variance further favors its installation to overcome the PV and wind variability.

→ **Optimal Mixes Become Less Sensitive To Cost**

Even though the optimal capacity pathways and the geographical distribution remain relatively unchanged, a few insights can be drawn from the comparison of left panels of figure 3.5 (case 2) with right panels of figure 3.1 (case 1). Looking at the maximum-penetration level, one can see that optimal mixes achieve the same maximum-penetration value because the mixes obtained by running the mean-variance using both cases are optimized with the same maximum-cost budget (2.9). However, the area in which optimal mixes are not impacted by cost is no longer narrow. For instance, for PV-wind-CSP-TES SM4 mix, CSP-TES fraction shows an abrupt fall at low penetrations in case 1 (left side of figure 3.1j) while the CSP-TES fraction remains constant in these levels of penetration before decreasing with increasing penetration and the cost constraint becomes more and more active (Figure 3.5e).

When it comes to case 3 versus case 2, it should be noted that in case 3 (right panels of figure 3.5), the cost data source (Table 2.7, Chapter 2) is different from that of case 2 (the left panel of table 2.5, Chapter 2). Therefore, the maximum-total cost, the maximum-penetration ratios and the second ratios are different between the two cases. The minimum-variance ratios are also not the same since only Noor 2 and Noor 3 with 6-8h of storage are used to correct CSP-TES CFs (Table A.6, Appendix A). However, no significant differences are found in the optimal capacity allocation, but less true for the optimal geographical distribution (See our first publication [105] in which the response of the optimal mixes are analyzed using case 3). The mixes are, however, more sensitive to cost (right panels of figure 3.5) than case 2 (left panels of figure 3.5) since the cost of TES, in case 3, is not ignored (as case 2) but it is taken equal to the most deployed CSP-TES system, as mentioned above. This show that with the rapid growth in installed capacity of RE technologies and the rapid decline in the cost of production and storage systems, even cost data few years old can significantly overestimate or underestimate the rental cost of RE technologies, but has minor effect on the optimal mixes since the cost of CSP/CSP-TES remains always higher than that of wind and PV.

It seems possible, however, that the changes in the CSP/CSP-TES optimization ratios, in all cases, result in change in the composition of the mix across penetration regimes.

2 Scenarios of High Renewable Penetration with Low Investment, even though High Adequacy Risk

Regarding the competitiveness of the investigated technologies at high penetration scenarios, the results show that wind prevails as the major source of energy at the maximum penetration mix, reflected by the much higher energy production per installed capacity of wind, with low rental cost, compared to solar generation (Table 2.4 and 2.6, Chapter 2), leading to curtailment when the fraction of CSP-TES is zero (not shown here, see discussion in section ii of Chapter 4), letting the risk increase in return.

→ **Investing in Wind with Low-Cost and High Mean Capacity Factor**

Therefore, from an economic standpoint, under scenarios aiming to increase the RE penetration—setting aside the risk related to system adequacy (i.e., curtailment or shortage situations) or in case Morocco rely on its current flexibility options such as managing the consumption through the peak/off-peak pricing; strengthening interconnection with neighboring countries notably with Spain and Portugal to offer a simultaneous stabilization of the grid; and developing pumped hydro storage [104] to alleviate these issues—Morocco has to invest more in wind in its renewable goals due to its strong and regular CF which could reduce the costs that an investor would face every year compared to currently expensive CSP-TES plants. This finding goes in line with the analysis done by Brand et al. [113] stating that the 2 GW wind target by end 2021 appears relatively small compared to the country's overall wind potential of 25 GW. In fact, Morocco is investing more than USD 20 billion in developing its renewable energy sector with an investment of USD 9 billion for only solar technologies and approximately USD 3.5 billion for wind. However, the wind program aims at installing 2 GW with an annual wind production of 6600 GWh by end 2021; while an annual production of solar will be just 4500 GWh for the same expected installed capacity [9].

Thus, investors should be encouraged to continue investment in wind plants as they are more economically appropriate for producing energy and, according to our results, the strong reliance on wind is evident not only at high penetrations where the cost of investing in a given technology matters more than the costs of balancing, but also at low penetrations where the main objective is to lower the balancing capacity needs. This show that investments in wind capacity may be more resilient to different levels of penetrations.

→ **Where Wind Should Be Installed?**

The results suggest to install wind along the Atlas mountain ridge in eastern regions at maximum-penetration mix (Table 3.2), where the variance is trivial. In fact, the mean CF of this region is strong but it captures the continental climate which increases the inter-seasonal variability of the wind production, and eventually this variability causes a decrease of production when the temperature is high (i.e., low air density) and when the demand for air-conditioning increases as well. For this reason, at penetrations lower than the maximum and where the variance start to play a role in determining the technology that should be installed, the model favors the southern region (Table 3.3) where the temperate coastal climate effect of the Atlantic ocean results in more intense and reliable wind speed leading to relatively uniform fluctuations of wind production with small inter-seasonal variability.

This corroborate the finding of El Khchine et al. [303] that revealed a good consistency of wind behavior in two Moroccan cities, in particular Taza (EAST) and Dakhla (SOUTH), showing that the highest value of wind potential occurs in SOUTH during the summer peak

demand in contrast to EAST where the maximum production is during the winter months with high wind direction variability compared to SOUTH.

When it comes to cost, Tizgui et al. [515] show that a good result of wind leveled cost can be attained in NORTH, CENTER and SOUTH of Morocco, which explain why most operational plants are installed in these regions (right panel of figure 2.4, Chapter 2). Indeed, the northern regions are also promising for wind installation due to the proximity to the Mediterranean region with strong regional wind regimes [209, 318]. CENTER region is also favored due to nearby Atlantic ocean.

→ **What About Low-Cost PV at High Penetrations Where Costs Matter?**

Overall, PV was found to be less variable in CENTER (Table 3.5) and more economic in SOUTH (Table 3.2, 3.3). However, the low fixed-tilted multi-crystalline PV mean CF (Table 2.4, Chapter 2) resulting from the moderate PV conditions of Morocco—mainly due to its sensitivity to temperature which limits the PV efficiency [196]—is the reason why despite its rather lowest rental cost (Table 2.6, Chapter 2), only small amounts of PV capacities are installed at high penetrations (middle and right side of the right panels of figure 3.1).

To favor the PV installation at such high penetrations and to take advantages of its low cost, PV mean CF and PV capacity credit can be improved by using north-south tracking, as CSP, to increase the correlation of the summer PV production with that of the demand. Although the addition of tracking or/and storage increase the cost of installing a PV plant [266], it will reduce the variance and thus the cost of power generated by the plant.

→ **What About CSP-TES at High Penetrations Where Flexibility is Needed?**

Generally, achieving higher RE penetrated systems require considerable operational flexibility to hedge the variability but also high investment to install RE capacity. However, in this study, to find a trade-off between maximizing the RE penetration (2.1) in the overall electricity mix and minimizing the aggregate RE supply risk (i.e. required balancing services from conventional) (2.2) while satisfying the total cost constraint (2.8), CSP-TES capacity is only invested at low RE penetrations (left side of right panels of figure 3.1) due to the fixed maximum-cost budget because the cost of achieving high RE penetration will be significantly increased given the relative cost of CSP-TES (Table 2.6, Chapter 2). As such, CSP-TES is penalized at high penetrations and we allow ourselves to deteriorate the mean-standard deviation ratio (2.5) by installing more intermittent and fluctuating technologies (wind, PV) but that are cheaper than CSP-TES to not reach the limit budget soon. An indicator of the increase of the adequacy risk with the introduction of wind and PV and the elimination of CSP-TES for larger values of the mean penetration is the convex (resp. concave) shape of CSP-TES (resp. PV and wind) fraction curve (right side of the right panels of figure 3.1). As a result, the penetration level at which the optimal mixes start to be sensitive to cost represent the threshold at which intermittent technologies (PV, wind) with their potentially lower costs challenge the dispatchable but expensive technologies (CSP-TES) to the detriment of the adequacy risk and thus its the threshold at which CSP becomes uncompetitive with alternative resources (i.e., the economic carrying capacity [157]). Thus, the following remark can be made: under scenario mixes where high RE share is targeted with low investment, CSP with storage is not competitive at high penetrations due to the disadvantages of CSP's higher yearly rental cost and it will likely be more cost-effective to deploy low-cost generation technologies (wind, PV).

Taking that into consideration, CSP-TES advantages are only analyzed at low penetrations where, in reality, the stochastic character of wind and PV is small and would not increase the risk (i.e., destabilizing the electricity grid) compared to high proportion of REs. However, since CSP is combined with storage, its generation behavior has less variance as it helps to bridge the lack of PV during night and the variability of wind feed-in (curtailment) which could need less required energy to balance the load when the share of REs rises. Therefore, if a high penetration is to be reached while preventing the risk to go past a given reliability threshold, more investment in RE is necessary (Section 3). The smaller this threshold, the more unlikely is a high share of CSP-TES with a large SM (large solar field size and storage capacity) to be optimal compared to PV.

3 Scenarios of High Renewable Penetration with Low Adequacy Risk, but with High Investment

→ **Actual vs. Optimal Mix: PV and CSP/CSP-TES Proportions**

To compare the optimal mixes discussed so far with the actual 2018 Moroccan mix, we represent the latter by gray cross in the left panels of figure 3.1. The actual (2018) PV, wind, CSP/CSP-TES fraction are displayed in brown, blue, and orange stars respectively in the right panels of figure 3.1.

We can see that the actual mix (gray cross) in the left panels of figure 3.1 is to the right of the constrained global front (blue line), whatever the combination. Therefore, it does not belong to the set of the Pareto optimal mixes. This shows that the current geographical and technological distribution of PV, wind and CSP/CSP-TES in the four Moroccan regions is sub-optimal; means that there are better solutions depending on the objectives. The mean penetration level of the actual mix is approximately the same as the penetration-as-actual mix (blue triangle) which could imply the same investment cost for REs; but the risk is reduced in the penetration-as-actual mix and consequently fewer costs could be incurred for the system balancing needs. Moreover, the actual mix has smaller penetration than the risk-as-actual mix (blue diamond) but the risk is the same.

Considering the present day situation, the actual mix could be Pareto optimal (on the blue line) and thus be modified by yielding a greater RE production for the same level of variability (risk as actual mix), or lower the level of output variability while keeping the current level of penetration (penetration as actual mix), or by taking into account the correlations between regions and technologies (moving from the base front to technology or global fronts).

To go further, we compare the technological composition of the optimal mixes and the actual technology fraction that can be derived from the right panels of figure 3.1 and the panels of figure 3.5. For instance, according to the model, if all the CSP plants in Morocco have a SM of 2 and the cost of storage is taken equal to that of the most widely deployed system with 6-8h storage (case 3), the actual risk could be reduced (or the actual penetration could be increased) by increasing the wind and CSP shares and removing PV completely (compare the optimal mix with the actual mix in figure 3.5b). Increasing the share of CSP would also lower the risk for higher SMs (Figure 3.5d, 3.5f). The main reason for the differences between the actual and the optimal mix is that the renewable production in the actual mix was tuned to low fraction of solar PV and CSP-TES while to decrease the variance, the model suggests no PV and more CSP-TES, demonstrating the role of storage to reduce the fluctuation between day and night and thus the risk of not covering the load. The figure 3.5b reveals a quite similar results to case 2 for the PV-wind-CSP-TES SM2 mix (Figure 3.5a) where the storage cost is ignored, but this is less true where the cost of storage is proportional to storage size of SM2 and storage constraints are considered (case 1) (Figure 3.1f). In this case, the model suggests to slightly reduce the share of CSP-TES due to storage cost at the expense of solar PV share but the fraction of PV remains lower in the optimal mix compared to the actual mix and lower than CSP-TES share.

This outcome corroborates the findings of Brand et al. [113] that show that for a RE integration scenario, where CSP has to compete with other RE technologies, like PV or wind, the investment in CSP-TES is only justified when a high RE quota is targeted. It was also found that at high RE penetrations, CSP-TES may prove more optimal than PV, due to increased reserve requirements [55], while PV tends to suffice for low penetrations [451]. In this regard, the value of storage is clear, however, it is difficult to make firm conclusions regarding optimal storage capacity.

Drawing from the above, CSP-TES could very well constitute an appropriate technology in scenarios with very high RE shares and low risk. However, Morocco has to increase the RE budget. In fact, although CSP-TES allow to achieve low variance and high generation, its high cost of capital is sometimes expressed as high Weighted Averaged Capital cost (WACC) [468, 391] which lead to a strong increase in the levelized cost of electricity from CSP and therefore tend to discourage CSP investments at scale [308, 307, 56]. To illustrate this point, an investor cannot take the risk of investing in a huge solar project for 30 years of operation in the form of a solar collector field if he is unsure of the stability of a project's revenue streams. Projects with costs that are fixed but revenues that are not will have a difficult time attracting the desired financing at the required cost [71, 473]. One method that can be used to overcome this barrier is a long-term power purchase agreement (PPA) in which the off-taker guarantee the electricity will be off taken independently of the actual need on the grid. This allow for a reasonable return for investors which de-risk CSP plants' investment through accessing lower debt interest rate [559, 467, 340] leading to levelized cost reductions.

→ **Where CSP-TES should be installed?**

Overall, we found that CSP tends to be economic in CENTER for all SMs (Table 3.2, 3.3) while the minimum-variance ratio is sensitive to the amount of storage (Table 3.5), with much more preference for EAST and SOUTH regions. For CSP without or with medium storage duration (SM2), CSP-TES is preferred in EAST, while for high storage duration (SM3, SM4), the model suggest to install it in the SOUTH. The explanation is a more fairly homogeneous distribution of irradiance around the year in these sub-Saharan/ Saharan regions [451], with much more average production in CENTER followed by SOUTH (Table 2.4, Chapter 2). EAST has lower energy yields for CSP [451], reason why it is favored when only medium storage capacity is integrated.

Ref. [347, 393] also show that Midelt city (East), Ouarzazate city (CENTER) and SOUTH region have a high suitability to host CSP plants and could support CSP with wet and dry cooling. Whereas both the northern Mediterranean and Atlantic coasts have a quite important solar potential, which limits the large use of all solar technologies.

→ **Benefits of CSP-TES in Mitigating the RE Integration challenges**

In section ii, we show that CSP-TES reduces the adequacy risk in several ways. In fact, we find that the capacity credit (i.e., the fraction of the rated capacity able to meet the peak demand) of CSP-TES is higher than that of PV since CSP-TES can reduce the net load in the day and again in the evening. Thus, at very high share of CSP-TES, the diurnal double peak of the load (Figure 3.2b and as illustrated in figure 1.14 in chapter 1) may be depressed, given its capabilities to absorb and discharge energy, which could be one of the best solutions to flatten the "duck curve" [47, 158] to procure enough ramping capability in the system by not only reducing the shortage situations or power cut from neighboring countries but also the occurrence of saturation situations, enabling greater penetration of solar energy [87], in agreement with section iv (CSP-TES vs. PV) and sectioniii (Chapter 4).

PV capacity credit, on the other hand, is affected due the more irregular PV profile and its variability, particularly at high RE share. This is, indeed, the reason why the PV fraction is limited to 20% whatever the combination (left side of right panels of figure 3.1). In fact, PV helps the load during a significant number of hours during the day and reach its maximum at midday. In the evening, however, the load increases while PV output decreases during many hours, with zero production during nighttime hours. Thus, once the demand at midday is covered, further PV production with no storage mostly lead to over-production. To maintain the PV production in the mix, this effect will force to shut down baseload generation during midday and when the demand increases in the evening we will need backup to meet the load because baseload generation are not fast response to start again to maintain the system flexibility. The so called "duck chart" [47, 158]. Higher PV penetration is, thus, particularly disadvantageous in the Morocco's electricity mix which is composed largely of fossil fuels (mainly inflexible coal power plants) [23] because PV, contrary to CSP-TES, is not able to shift generation to other periods of the day and coal power plants have to be ramped down more frequently to manage this variability. In this case, the value of CSP's dispatchability will be higher than in flexible gas-based power systems such as Algeria [113]. This finding broadly supports the work of other studies [283, 154] in this area linking curtailment, solar penetration with economic costs and the challenges of PV impacts on the reliability of the grid [395, 394].

Several studies [201, 55] have pointed to the prospects that fixed-tilt PV obtains the lowest capacity credit because the maximum output is only in a few midday hours; PV with tracking or CSP without storage gets a higher capacity credit because their production can better fit the hours with high capacity requirements (e.g., early evening). CSP-TES has the highest capacity credit as it can provide energy in evening peak.

With that being said, with CSP-TES integration, the "profile cost" and "grid-related cost" associated with the temporal and geographical availability of the resource and the short-term balancing cost from conventional associated with the uncertainty of production will be reduced, including the energy bill associated with the foreign energy dependence. This show that thermal storage has made CSP a very interesting options for delivering RE and operational flexibility without adding carbon emissions, that would be satisfied by fossil-fuel generation needed for reliability, leading to an increase in its economic value [201, 160]. In particular, the gap between conventional generation and solar energy costs becomes smaller in later years due to the increase of production costs of conventional (which are also subject to strong fluctuations) and the decrease of the CSP investment over time [451]. Overall, CSP-TES yields lower economic costs than PV although LCOE are higher, because fossil fuel generation is avoided during high-priced time periods. In future cost reductions, PV may also achieve higher avoided costs due to the high learning rate; however, we cannot draw conclusions because the CSP market is uncertain and not very well explored (we do not know if costs will explode, go down or stay constant).

All in all, while the low cost of PV compared to CSP may motivate producers and planners to install more PV than CSP today when the RE penetration worldwide is not as large as what is aimed for, planning an efficient energy transition towards a high penetration may require steering the energy market to favor CSP-TES over PV. In fact, if the variability of the production is not ignored (resp. ignored), the largest minimum-variance ratio (resp. maximum-penetration ratio) of CSP-TES (resp. PV) can lead to favor CSP-TES (resp. PV) over PV (resp. CSP-TES). One has to find a trade-off between sparing costs and limiting the variability of the production via the storage capabilities of CSP-TES (e.g., the higher the peak demand, the more CSP-TES should be used; the lower the peak, the more PV can be employed).

4 Scenarios of Low Adequacy Risk with Low Investment, but Low Renewable Penetration

For a hypothetical scenario in which Morocco aims only to reduce the risk of not covering the load (i.e., the fluctuations in the residual load), and consequently the costs of balancing, with relatively low proportion of renewable and with no need for further investment in building more RE capacity, we found that different options would be sufficient.

→ Diversified Mix of Wind and PV without Storage or CSP-TES with Small/Medium Storage Capacity

The mix minimizing the risk is heavily leaning toward solar PV and wind power (left side of figures 3.1b, 3.1d). A mix of solar CSP-TES with small storage capacity (SM2 or SM3, 6-11 hours) and wind is also found to give small adequacy risk (left side of figures 3.1f, 3.1h). In fact, at such low penetrations, unlike the maximum penetration point (Section 2), even though wind achieve higher minimum-variance ratio than PV or CSP-TES SM2 (Table 3.5), it is not dominating the mix, but the proportion of wind is higher than that of solar technologies because of the large imbalances of solar power caused by daily and seasonal generation; which are reduced in CSP-TES SM3 case where CSP-TES dominates over wind.

→ Regional Complementarity

In addition, we found that spatial complementarity carries significant benefit to the power grid due to its smoothing effect on variable RE resource output. However, as capacity increases and with an increased potential for surplus of CSP-TES, the capability of complementarity to increase grid penetration approaches its limit due to the reduced matching of global, technology and base fronts resulting from the pursuant increase in the total cost.

→ Stand-alone CSP-TES System With Large Storage Capacity

Stand-alone CSP-TES with large storage capacity (SM4, 17 hours) would also be efficient to achieve a very low grid variability (left side of figure 3.1j).

→ What about CSP Without Storage at Low Penetrations Where Cost Does Not Matter? Is It Important To Take Into Account Its Temporal Synergy With PV?

The analysis to this point assumes that CSP-TES and PV are complementary in their ability to serve different parts of the demand pattern; and the technology that should be installed—at such low penetrations where the cost does not matter—depends on if the thermal storage is assumed to be in place or not.

Between PV and CSP on the other hand, the optimal mix is shifted in favor of solar PV (left side of figure 3.1d) because CSP cannot compete economically and reliably with PV. In fact, although the cost-effectiveness criteria is neglected at such low proportion of RE, installing CSP with high capital cost will lead to reach the maximum cost budget sooner, especially that it requires larger capacity than PV because cloudy weather limit its CF since CSP system only works with direct irradiance while PV systems could even use the diffuse irradiance. Eventually, CSP might rather reveal interesting to enhance the grid penetration (without caring about the variability) in future warming climate (Chapter 5)—given the fact that the rising air-conditioning system use causes the demand to peak in summer—to replace fixed-tilted PV since although both technologies produces similar output daily profiles—contributing only to midday load and anti-correlated with evening peak demand—, CSP has an advantage over PV, in Moroccan climate that is generally hot and dry for most of the year. Indeed, CSP production has a positive correlation with the summer peak demand for cooling, not only due to tracking system that increase the amount of energy produced per unit of installed power generating capacity, but also because the efficiency of the steam cycle's thermodynamic conversion to electricity increases with increasing temperature, while for PV cells, higher temperatures reduce their efficiency, and because of the medium latitudes, the seasonal variation in solar PV output is more pronounced (abscissa of figure 3.3d and figure 3.3e). This show that the benefits of PV (no sensitivity to clouds) outperforms that of CSP (positive seasonal correlation with summer peak) because even though the variability of production is strongly dominated by seasonal fluctuations, it cannot be reflected in the solar generation at this rather low penetrations. The importance of this measure with respect to renewable generation capacities will, however, increase with an increase in penetration, but in this case and according to our results, the low-cost PV overpasses the high mean CF of CSP and PV stand at a leading position whatever the penetration level. This explains why investors and policy makers have gotten interested in PV rather than CSP because the former can be installed in any location covering the residential and power plant sector; while CSP do not scale down well because the suitable areas for CSP are much more limited as it requires large desert areas with high direct irradiance and where the air is dry and cloudless.

It is worth noting that the relative similarity between CSP and PV generation regarding the fluctuating patterns during the day is important to take into account (as done in our simulations), which could be one reason for the model choice of installing the least variable technology than both to counter the variability (i.e., adding another intermittent and variable technology will only increase the variance) (Section ii).

To sum up, our results illustrate the advantages of complementarity of RE generation between wind and PV/CSP-TES to reduce the variability along with regional complementarity (since mean climatic conditions vary little within Morocco); or only maximizing the contribution of CSP-TES to take advantage of its high storage capability. These options achieve a trade-off between maximizing the mean CFs and decreasing the variability in SOUTH for wind; CENTER for PV and EAST or SOUTH for CSP-TES according to table 3.5; and table 3.6 for regional complementarity.

V Summary and Concluding remarks

Motivation

Photovoltaic (PV) and Concentrated Solar Power (CSP) without or with Thermal Energy Storage (TES) present remarkable differences in terms of cost and variability. The existing literature either delves into these technologies partially or investigates the features of one of them within an optimization framework based on cost only or on variability only.

Research Questions

Our study is an analysis of the sensitivity of the Moroccan optimal Renewable Energy (RE) mixes—based on combination of three competing technologies, namely PV, wind and CSP without or with different amount of storage as defined by the Solar Multiple (SM)—to cost and thermal storage duration, making use of regional and technological synergies in the optimization of the proportion of these technologies in the electricity mix. This study also evaluates the impact of these synergies together with TES on the risk of not covering the load imposed by variable RE technologies on the Moroccan electricity system.

Objectives and Methodology

Our objectives is to maximize the RE penetration and minimize the variability of RE production which is considered to be a measure of cost in additional generation capacities from conventional. We use Modern-Era Retrospective Analysis for Research and Applications 2 (MERRA-2) climate reanalysis to simulate hourly demand, solar and wind Capacity Factors (CFs) adjusted to observations for the four Moroccan electrical zones over the year 2018. We account for the different rental costs of the three RE technologies by using the maximum total cost constraint in which the rental cost of each technology is modeled taking into consideration the storage size. We perform some optimization ratios to characterize the circumstances, under which each intermittent technology outperforms its counterparts (PV, wind, CSP) and the condition under which CSP-TES could have a niche against these low-cost technologies across a set of penetration scenarios and considering recent (2013) cost data. Finally, we use the load reduction diagnostics to compare between the reliability services provided by each RE technology during peak/mid/base load hours.

General Findings

At low penetrations, the share of each technology remains constant because optimal mixes are more sensitive to the reduction of the variance than to cost. Wind dominates over PV and CSP without storage because wind mean CFs are stronger and more regular in the SOUTH zone. However, the model suggests that an appropriate mix of wind and PV would be more efficient to achieve a small risk than only investing in wind power.

Due to the differences between PV and CSP without storage associated with the diffuse irradiance harvesting in addition to the use of solar tracking by CSP and its positive efficiency response to temperature changes, the means of CSP CFs tend to be larger than that of PV. Therefore, the variance of the high production series of CSP is significantly larger than that of the PV production series (i.e., the variance of CF tend to scale quadratically with CF mean) and optimal mixes seem to be favoring PV installation in CENTER.

While the addition of CSP without storage does not impact the technology share of PV-wind mix considering the complementarity traits of PV and CSP without storage, the addition of TES to CSP—keeping the mean CSP CF fixed—worth as TES favors the installation of CSP at such low penetrations where the satisfaction of the cost constraint is feasible and eliminates the need for PV completely, having larger amounts of solar share in the mix. Moreover, more the SM increases (11 - 17 hours or SM3-SM4), more CSP-TES tends to be more regular than wind and the model relies almost exclusively on generation from CSP-TES to cover the demand continuously (in EAST for SM2 and in SOUTH for SM3, SM4).

At high penetrations, the maximum recommissioning budget allowed becomes a limiting factor, making optimal mixes sensitive to cost—the more so as CSP with high solar field size and storage capacity is installed—and the technology shares are no longer constant relatively to the mean penetration. Consequently, in addition to the variances and correlations, the cost of each technology compared to the CF mean (in our case, an analog of the Levelized Cost of Electricity, LCOE) contributes to determining which technology is installed in which zone in priority. The rental costs of wind and PV being comparable and being much smaller than that of CSP; and the mean wind CFs being higher than the mean CSP/CSP-TES/PV CFs, wind capacities are preferably installed in EAST followed by PV in SOUTH while the share of CSP/CSP-TES is zero because the maximum-cost constraint prevents the increase of the RE penetration without reducing the share of CSP compared to PV and wind, letting the mean-standard deviation ratio decrease in return.

Ignoring the storage cost and considering unlimited thermal storage capacity makes the mix less sensitive to cost. However, it does not seem to affect the technology share and the geographical distribution of capacities. This is less true for the latter when the cost of storage is considered constant whatever the SM, equal to that of 6-8 hours of TES on average.

Yet, the model favors CSP with TES mostly at low penetrations due to the fixed total cost constraint. However, the results show that introducing CSP-TES, in particular with large SMs, may reduce the adequacy risk of the actual (2018) Moroccan mix, in scenarios of high RE penetrations, if Morocco increase the maximum-budget allocated for RE technologies.

We also show that a strong RE variability reduction is achieved through spatial complementarity. This can be understood from the fact that correlations between CFs in different zones are large and must be taken into account. The correlations between technologies in the same zone has also the potential to smooth the energy generation but depends on the combination. The efficient role played by the temporal smoothing between the PV and wind CFs is relatively small. It is, however, essential to take the strong correlations between the CSP without storage CFs and the PV CFs into account (even if CSP harvests the direct irradiance only which is compensated by solar tracking and by its positive efficiency to high temperatures). However, the role played by correlations between CSP CFs and CFs from other technologies in the same zone or for different zones is less important for high SMs because mixes become less diversified.

Finally, we find that, RE tend to serve the peak load less per unit of capacity than previously installed RE plants do. This is also true for the mid-load reduction but less true for the base-load reduction that decreases slightly as RE share continues to increase. At high penetrations, the fraction or the capacity reduced in base load is higher than the mid load which is also higher than the peak load. Wind contributes mainly to base load than mid and peak load. While CSP contributes to reducing the mid load similarly to PV, adding TES to CSP significantly increases the overall peak load reduction of the optimal mixes. This can be measured by the capacity credit, but not by the variance-based risk, suggesting that the latter is only a crude representation of the adequacy risk. At maximum-penetration point, and without measures to enhance grid flexibility (i.e. CSP-TES fraction is zero), not all of the electricity generated by wind can serve demand. As a result, some wind electricity must be curtailed (i.e. the strong wind feed-in occurring during the winter period with low demand).

A step in this direction while preserving the tractability of the optimization problem is to examine the effect of the addition of designed utility-scale PV deployed with battery storage on the optimal mixes and compare the role of CSP-TES and PV-BES, both with increasing storage duration, on the adequacy risk (Chapter 4). This modeling framework could also be implemented in future warming climate to assess the impact of climate change on optimal mixes compared to cost effect and the role of CSP-TES flexibility in reducing the Moroccan climate sensitivity (Chapter 5).

Utility-Scale PV-Battery versus CSP-Thermal Storage in Morocco: Storage, Cost and Spatio-Temporal Complementarity Effect under Penetration Scenarios

Contents

I	Introduction	98
II	Optimization Experiments	99
III	Results	100
1	Impact of Thermal/Battery Storage and Cost: Technological and Geographical Distribution	100
2	Impact of Spatio-Temporal Complementarity	103
3	Role of CSP-TES vs. PV-BES in Reducing the Adequacy Risk	104
IV	Discussion and Comparison with Existing Studies	114
1	Does CSP/CSP-TES Competing or Winning over PV/PV-BES ?	114
2	Scenarios of Unlimited Thermal and Battery Storage Cost and Capacity	117
3	Scenarios of High/Low Renewable Penetration-Adequacy Risk-Investment	117
4	Scenarios of Hybrid Solar Systems	117
V	Summary and Concluding remarks	119

Abstract

Motivation

Concentrated Solar Power (CSP) can shift electricity over time using cheap Thermal Energy Storage (TES). However, the cost of CSP is still high. Conversely, the cost of Photovoltaic (PV) systems have fallen. However, the Battery Energy Storage (BES) used to mitigate the generation variability has drawn less much attention for grid-scale storage due to its scalability and cost.

Research Questions

In this study, we examine how BES and TES combined with PV and CSP technologies with an increased storage duration and rental cost together with complementarity would influence the Moroccan mix and to what extent the variability (i.e., adequacy risk) can be reduced; using recent (2013) cost data and under various penetration scenarios.

Objectives and Methodology

To do that, we use Modern-Era Retrospective Analysis for Research and Applications 2 (MERRA-2) climate reanalysis to simulate hourly demand and Capacity Factors (CFs) of wind, solar PV and CSP without and with increasing storage capabilities—as defined by the CSP Solar Multiple (SM) and PV Inverter Loading Ratio (ILR). We adjust these time series to observations for the four Moroccan electrical zones over the year 2018. Our objective is to maximize the Renewable Energy (RE) penetration and minimize the imbalances between RE production and consumption considering three optimization strategies. We analyze mixes along Pareto fronts using the Mean-Variance Portfolio approach—implemented in the Energy for Climate Integrated Model (E4CLIM)—in which we add a maximum-cost constraint to take into account the different rental costs of wind, PV, and CSP. We propose a method to calculate the rental cost of storage and production technologies taking into account the constraints on storage associated with the increase of SM and ILR in the added PV-BES and CSP-TES modules, keeping the mean solar CFs fixed. We compute some optimization ratios to examine the circumstances under which the added value of PV-BES can really provide a competitive advantage against comparable technologies (CSP-TES). Finally, we perform some load reduction diagnostics to assess the reliability benefits provided by each RE technology.

General Findings

We find that, at low penetrations, the maximum-cost budget is not reached because a little capacity is needed. The higher the ILR for PV, the larger the share of PV in the mix compared to wind and CSP without storage is removed completely. Between PV-BES and CSP-TES, the latter is preferred as it has larger storage capacity and thus stronger impact in reducing the adequacy risk. As additional BES are installed, more than TES, PV-BES is favored. At high penetrations, optimal mixes are impacted by cost, the more so as CSP (resp. PV) with high SM (resp. ILR) are installed. Wind is preferably installed due to its high mean CF compared to cost, followed by either PV-BES or CSP/CSP-TES.

Scenarios without or with medium storage capacity favor CSP/CSP-TES, while high storage duration scenarios are dominated by low-cost PV-BES. However, scenarios ignoring the storage cost and constraints provide more weight to PV-BES whatever the penetration level. The addition of limited cost and capacity of BES to PV only impact the geographical distribution of PV at high penetrations. We also show that significant reduction of RE variability can only be achieved through geographical complementarity. Technological complementarity may only help to reduce the variance when PV and CSP are both installed without or with small amount of storage. However, the complementarity effect is slightly less when the SM and ILR are increased and mixes become less diversified.

I Introduction

Motivation

Solar technologies such as Photovoltaic (PV) and Concentrated Solar Power (CSP) are foreseen in future climate [169, 133] with energy storage systems [66, 290]. Nonetheless, these technologies are different in several ways.

On one hand, CSP can shift electricity over time using cheap Thermal Energy Storage (TES) [242] and is able to provide energy at times of greatest need [330, 343]. However, although CSP-TES is less variable in output than PV [159], it has struggled to compete with PV because of the low cost of the latter which has further steeply declined recently [269].

On the other hand, PV and indeed other variable generation technologies such as wind relies on the availability of the resource and thus are unable to produce constant and smooth power overtime. Moreover, when the sun falls, electricity demand increases but PV output decreases, resulting in the famous duck curve phenomenon [47, 158]. This fluctuating generation imposes a significant reliability and economic challenges [205, 482, 256] for the electrical generation and transmission system [152] and for the distribution system [398]. To mitigate the intermittency of PV production and the system's ramping requirements, PV must be combined with Battery Energy System (BES) that can produce stable output as CSP with TES does [283, 284]. The batteries have until now been uneconomical to utilize as a grid-scale storage [108]. Currently, a system that combines PV with BES is more commonly used in smaller residential markets [542, 509] (i.e., for household [471, 432], or for university campus [296] or for electric vehicle [255]) to reduce the grid electricity use [503, 465] and particularly to increase the rural electrification rate (e.g., in Morocco [385]) because it still requires subsidies to be economically viable [246, 40]. PV-BES can also include hybrid options with wind [100] or with diesel generators to reduce fuel consumption [67, 474]. However, the declining costs of both PV and batteries due to the recent development has raised interest in the optimization of BES capacity for a grid-connected PV system [220, 452, 383] and has created high expectations that PV-BES can be dispatched in the market [478, 384, 338] or lead to an autonomous micro-grids [300] to provide dispatchable and reliable capacity [191] and achieve high PV penetration [45].

This issue of falling PV and BES prices increasingly questions the competitiveness of CSP-TES in the electricity mix, which for a long time has been considered to be the first choice technology for solar power expansion, particularly in the Middle East and North Africa (MENA) region [524, 365]. The rationale behind this is not only related to cost but also to the fact that both can achieve high operation hours, if both are designed to provide dispatchable energy, by increasing the CSP Solar Multiple or SM (resp. PV Inverter Loading Ratio or ILR). This parameter normalizes the size of the CSP solar field (resp. PV solar panels) in terms of the power block size (resp. amount of inverter capacity). A SM (resp. ILR) of 1 is of sufficient size to provide energy during daylight hours and to operate the power block (resp. inverter) at its rated capacity under nominal conditions. A SM (resp. ILR) of 2 or greater is delivering more energy than what can actually be used by the power block (resp. inverter) under nominal conditions. Increasing the SM of a CSP (ILR of a PV) plant will increase its Capacity Factor (CF) and will generally decrease the Levelized Cost Of Electricity (LCOE) due to increased utilization of the power block (resp. inverter) resulting from the increased capability of CSP solar field (resp. PV solar panels) to collect greater amount of energy that is either sent to the grid or to the storage system. However, more the SM (resp. ILR) increases, more the investment cost on additional CSP solar field (resp. PV solar panels) and on increased storage capacity is increased even though the variance tends to be lowered.

Given these differences in terms of variability and cost between these technologies and given that, as opposed to CSP-TES, there have been no large-scale deployment of PV-BES systems designed to provide dispatchable energy, the performance of utility-scale PV-BES systems is unclear and may represent an integration barrier for CSP-TES. Does one technology will be dominated or they will co-exit? Within this context, further analysis is required towards the determination of the optimal technology for given penetration scenario and storage requirement under current or future cost scenarios and climate conditions.

Existing Research

Over time, the cost and storage effect that solar technologies PV and CSP with their associated storage (BES and TES) have on an energy mix has been addressed in the literature. Bogdanov et al. [96] analyze the role of these technologies towards 100% Renewable Energy (RE) mix. Feldman et al. [194] use a range of cost projections to compare the competitiveness of PV-BES and CSP-TES through 2030. Chattopadhyay et al. [126] perform capacity planning model to evaluate the impact of the addition of PV-BES without or with spinning reserve capability on the integration of CSP-TES. Lovegrove et al. [323] examine different dispatchable generation technology combinations in regard to their development status, performance characteristics, storage capability and costs. Kumar et al. [528] present a comparative economic analysis of supplying solar PV-BES and CSP-TES power to a particular load in India. Zurita et al. [567] evaluate different dispatching strategies of a hybrid CSP-PV-TES-BES in Chile considering different seasons and locations. Papadopoulou et al. [401] assess the techno-economic performance of combination of these technologies with offshore wind with storage. Overall, these publications [96, 194, 401, 126, 528, 567, 323] tend to analyze the competitiveness of PV-BES with CSP-TES over a range of storage requirements and under several projected cost declines for PV, batteries and CSP, focusing only on generation costs. However, the inherent differences between these technologies cannot be examined using a single metric as both provide different grid services and thus lead to different economic values. For instance, depending on the amount of storage associated, a PV-BES system may provide additional services [126, 421, 271] such as responding very quickly to changing system needs compared to CSP-TES which requires time to start up and ramp [194]. Alternatively, CSP-TES may allow a greater capture of solar energy, reducing the curtailment in very high solar penetration scenarios [161]. In addition, the value of dispatchable solar energy operating during peak hours—when the fuel cost of conventional generators is high—is much important than that of solar base load plants operating only during low-load periods.

So, while these analysis evaluate only cost per unit of generation, additional studies focus also on the variability by considering the incremental avoided capacity and fuel costs associated with the incremental addition of PV-BES and CSP-TES. For instance, Narimani et al. [375] compare this operational value in the Australian electricity market. Existing research tend to compare the capacity credit (i.e., the amount of energy that can reliably be expected to produce at the times when demand for electricity is highest [55]), or the effective load-carrying capacity of a plant (i.e., the capacity credit multiplied by the nameplate capacity) between PV and CSP-TES or conventional gas

generators [356, 283] and PV-BES [284]. Similar contributions have been made to compare the net cost or the benefits-costs ratio [284] (resp. benefits/costs) [156] determined by subtracting (resp. dividing) the annualized capital and fixed operation and maintenance costs of a generator from (resp. by) the system cost savings.

Knowledge Gap

However, an analysis of the conditions under which each technology outperforms its counterpart within an optimization framework under different scenarios of penetration and storage configurations considering both the cost and the storage impact on the mean penetration, variance and covariance between different RE technologies and climate regions remain not explored.

Implications and Originality of this Study

Particularly, the Moroccan strategy plan aims at deploying 20% of its electrical capacity from solar energy by 2030 [104] and foresees to mix between CSP and PV power plants, probably both with storage. However, the share between PV and CSP and the amount of storage associated is not clearly known yet in the electricity mix planned as part of this energy strategy.

This study addresses these issue by discussing scenarios of solar PV-BES/CSP/CSP-TES integration in Morocco.

Research Questions

This study is follow-on work to a previous study presented in chapter 3 exploring the response of the Moroccan mix to the integration of CSP/CSP-TES with different storage capabilities with wind and PV without storage and examine the role of thermal storage and complementarity in reducing the variability. In this study, the optimization problem is not only sensitive to the change of the variance associated with the change of the CSP SM and to the different rental costs of wind, PV and CSP but also to (i) the variance associated with the change of the PV ILR and to (ii) the different rental cost of PV and CSP storage configurations. As in this previous study, we optimize the electricity mix using a recommissioning approach in which the total cost of a mix is constrained to be lower than that of the actual (2018) Moroccan mix with the following analysis. We try to see what role the addition of battery to PV can play in reducing the variability and whether or not it becomes part of the mix examining its integration with CSP/CSP-TES and wind across a set of penetration regimes and under the recent (2013) cost data. Concerning the competitiveness between PV-BES and CSP-TES, this study does not aim to identify the best technology or analyze the sensitivity of the mix to cost uncertainty, but rather to investigate the circumstances, under which PV-BES could have an advantage against comparable technologies (i.e., CSP-TES) along with a range of other points of comparison in terms of rental cost and variability (i.e., load bands reduction such as the average capacity credit). Therefore, this chapter addresses the second research question of this thesis (Q2) (Section 3, Chapter 1) by solving the following three questions:

- **Q2-1:** Does the cost and storage capability of CSP-TES and PV-BES that increase with the SM and ILR introduce a significant change in the scenario mixes? At what RE share, the fluctuating but least-cost generation technologies (i.e., wind, solar without/with low storage capacity) can balance the extra-cost of dispatchable but expensive technologies (CSP-TES, PV-BES with large capacities)?
- **Q2-2:** How PV-BES impacts the benefits of complementarity compared to PV/CSP/CSP-TES ?
- **Q2-3:** Does PV-BES displaces conventional generators more than CSP-TES? (i.e., system variance-based risk and system load bands reduction diagnostics)? How are major integration challenges affected by the share of REs ?

Methodology

In order to find answers to the questions stated above, we use the Energy for Climate Integrated Model (E4CLIM) that allows from climate data provided by Modern-Era Retrospective Analysis for Research and Applications 2 (MERRA-2) reanalysis (Section 1, Chapter 2) for the four Moroccan electrical zones (Section i, Chapter 2) for the year 2018 (Section 3, Chapter 2), to simulate hourly wind (Section II, Appendix A), PV with BES (Section ii, Chapter 2), CSP without and with TES (Section i, Chapter 2), and demand curves (Section I, Appendix A) adjusted to observations (Section VI, Chapter 2). We address different combinations of variably sizable PV and CSP with wind (Section II). We choose similar sizing to make the technologies as comparable as possible to ensure if two different solar technologies with similar amount of energy available for storage will have similar ability to displace conventional plants (Section X, Chapter 2). We develop a method of rental cost modeling in which the cost related to energy and power capacity of both storage technologies is considered keeping the cost of the additional CSP solar field (resp. PV solar panel) constant (Section VIII, Chapter 2) to remain coherent with the fact that the mean solar CFs of different storage sizes are roughly equal due to bias correction (Section 2, Chapter 2). Therefore, an increase in the CSP SM (resp. PV ILR) gives an increase in the storage capacity and the maximum power of charging/discharging which increase the rental cost. So far, most studies are based on an uniform distribution of RE capacities. In our study, the distribution of RE capacities is optimized technologically or geographically or both in order to evaluate the impact of complementarity in reducing the standard deviation of the RE production.

Outline

In this chapter, we proceed as follows. The data sources and the theoretical framework needed for this study has been mentioned in the previous paragraph and can be found in chapter 2 including the storage model, the cost model and the system adequacy diagnostics. Section II presents the optimization experiments considered in this study. Section III presents the resulted optimal scenario mixes by analyzing the impact of thermal and battery storage on the technological and geographical distribution of RE capacities (Section 1), the impact of complementarity (Section 2) and the role of CSP-TES compared to PV-BES in reducing the adequacy risk (Section 3). Points of discussion regarding the scenarios of solar integration in Morocco will be further considered and analyzed in section IV. Section V summarizes the methodology adapted and the results gained for all scenarios.

This chapter has been submitted in peer-reviewed article published in the journal, *Energies*, and has been accepted for publication under the following citation [106] (Appendix B):

Bouramdane, A.-a.; Tantet, A.; Drobinski, P. Utility-Scale PV-Battery versus CSP-Thermal Storage in Morocco: Storage and Cost Effect under Penetration Scenarios. Energies 2021, 14, 4675.

Here, we represent the updated version of this second publication.

II Optimization Experiments

To investigate the response of the Moroccan mix to the addition of utility-scale Photovoltaic (PV) combined with Battery Energy Storage (BES) to the designed Concentrated Solar Power (CSP) with Thermal Energy Storage (TES)—both with different storage capabilities as defined by

the PV Inverter Loading Ratio (ILR) and CSP Solar Multiple (SM)— and to the different rental cost of PV-BES, wind and CSP/CSP-TES, the optimization problem has been applied to different technological combinations (Table 4.1). These combinations are chosen to represent the general trend of the competitiveness of various PV and CSP storage configurations along the efficient capacity pathways.

Table 4.1: Optimization Experiments. Integration of Photovoltaic (PV) with increasing Battery Energy Storage (BES) capabilities—as measured by the Inverter Loading Ratio (ILR)—with Concentrated Solar Power (CSP) without and with increasing Thermal Energy Storage (TES) capabilities—as measured by the Solar Multiple (SM)—and wind.

Combination	Wind	CSP		PV	
		TES	SM	BES	ILR
PV-ILR2-wind-CSP-SM1	Yes	No	1	Yes	2
PV-ILR3-wind-CSP-SM1	Yes	No	1	Yes	3
PV-ILR4-wind-CSP-SM1	Yes	No	1	Yes	4
PV-ILR2-wind-CSP-SM2	Yes	Yes	2	Yes	2
PV-ILR3-wind-CSP-SM2	Yes	Yes	2	Yes	3
PV-ILR4-wind-CSP-SM2	Yes	Yes	2	Yes	4
PV-ILR4-wind-CSP-SM3	Yes	Yes	3	Yes	4
PV-ILR2-wind-CSP-SM4	Yes	Yes	4	Yes	2
PV-ILR3-wind-CSP-SM4	Yes	Yes	4	Yes	3
PV-ILR4-wind-CSP-SM4	Yes	Yes	4	Yes	4

All combinations are optimized using the same value, C_{tot}^{obs} , i.e. 3.5 G€/yr corresponding to the PV-Wind-CSP-TES combination (with 5.5 hours of TES or $SM^{ref} = 1.87$) (Section 1, Chapter 2).

III Results

In this section, we analyze the effect that the Battery Energy Storage (BES) added to Photovoltaic (PV) has on the optimal mixes studied in section III (Chapter 3) considering the differences in the variance and rental cost between not only PV, wind, and Concentrated Solar Power (CSP) but also between different CSP Thermal Energy Storage (TES) and BES design, i.e., different Solar Multiples (SMs) and Inverter Loading Ratio (ILRs).

The simulation results of this section are also obtained from hourly Modern-Era Retrospective Analysis for Research and Applications 2 (MERRA-2) climate data by running the mean-variance analysis using case 1 (Section 1, Chapter 2).

1 Impact of Thermal/Battery Storage and Cost: Technological and Geographical Distribution

Approximations of the optimal fronts of the mean-variance bi-objective optimization problem are represented in the left panels of figures 4.1 and 4.2, with the standard deviation or risk, $\sigma_{global/technology/base}$, in abscissa and the mean penetration, μ , in ordinate for each combination (Table 4.1). The thick plain blue curve represents the Pareto-optimal distribution of solar and wind capacities—for the global strategy with the maximum total-cost constraint (2.8)—, means there is no other mixes better in all objectives. When the maximum-cost constraint is not imposed, and for the global strategy as well, installed capacities of the optimal mixes are proportional to the penetration and risk (upward plain black line).

The fraction of PV-BES (plain brown line), wind (blue plain line), CSP/CSP-TES (orange plain line) capacities summed over all four regions along the global constrained front are shown in the right panels of figures 4.1 and 4.2. The dashed vertical black line corresponds to the optimal mix with the highest penetration that can be achieved before the total-cost constraint becomes active (black dot in the left panel).

The sensitivity of geographical distribution of optimal mixes to solar technologies is analyzed by representing in bold, for each technology, the maximum of the maximum-penetration ratio (Table 4.2); the minimum of the second ratio (Table 4.3) and the maximum of the minimum-variance ratio (Table 4.5), determining what region a given capacity will be assigned to at maximum, high and low penetrations respectively. We note that the addition of BES to PV do not seem to impact the geographical distribution of capacities examined in section III (Chapter 3), except at high penetrations (Section iii).

i Economic Carrying Capacity

For all combinations, for low values of the variance reached by the optimal mixes, the unconstrained and constrained global fronts are close to each other (left panels of figures 4.1 and 4.2). Thus, the total cost constraint is satisfied without the need to force it and optimal mixes are not impacted by cost (i.e., the share of each technology is constant function of the mean Renewable Energy (RE) penetration as shown on the left side of the right panels of figures 4.1 and 4.2). However, a higher RE penetration involves a higher RE capacity to install (and thus additional investment) to satisfy the demand due to the low Capacity Factors (CFs) of REs. As expected, the constrained front diverges from the unconstrained one, due to the maximum-cost constraint (2.8), and the fractions of each technology are no longer constant function of the mean penetration (the right side of the left and right panels of figures 4.1 and 4.2).

For all combinations, the level of penetration at which cost becomes a constraint (i.e., black dot or dashed vertical line) decreases with the increase of PV ILR and CSP SM, which show the strong sensitivity of the mix towards storage (TES and BES) and CSP cost; pushing the evolution of solar capacities even further back along the efficient fronts at high penetrations (see the dashed vertical line in the right panels of figures 4.1 and 4.2).

Shifting away from the dashed vertical black line shows a relatively strong penalization of CSP-TES and PV-BES while wind share has a clear upward trend (the right side of the right panels of figures 4.1 and 4.2). At first sight, it might be surprising because one may first observe that flexibility is required at high penetrations. However, this relatively greater penetration of wind is partly a result of the lower mean CF of PV-BES and CSP/CSP-TES compared to wind (Table 2.4, Chapter 2), which basically means that more installed capacity is required to provide a given amount of energy and, thus, more investment is needed to reach higher penetrations. With the costs of CSP-TES and PV-BES still comparatively higher than wind (Table 2.6, Chapter 2), the model omit CSP-TES and PV-BES capacity additions in its optimization process, preferring an investment pathway in the least-cost solutions although intermittent and fluctuating to not reach the maximum budget limit sooner. This helps to understand why the constrained front shows a larger risk than the unconstrained one (the left panels of figures 4.1 and 4.2) at high penetrations. Thus, this transition point indicates the level of penetration at which the cost of variable but least-cost technologies (i.e., wind or solar with small storage capacity) outweigh the benefits of dispatchable but expensive technologies (CSP-TES, PV-BES with large storage capacity), namely "the economic carrying capacity" [157].

In section 1 (Chapter 3), different renewable combinations affect only the low penetrations regimes. However, with the integration of PV-BES, optimal mixes are sensitives to solar technologies—specifically to storage—at low and high penetrations (Section iv and iii).

ii At Maximum Penetration

As can be seen on the right side of the right panels of figures 4.1 and 4.2, wind penetration approaches 100% at the point on the constrained front with the maximum-penetration point (blue square in the left panels). This can be strengthened by the large maximum-penetration ratio (Table 4.2). This show that wind represents the best technology to satisfy the demand accounted for at the highest penetration point, and remains the same in the mean-standard deviation plane for all combinations. Eastern regions concentrate all installed capacities, with negligible capacities installed in other regions, being the region with more electricity produced per megawatts (MW) installed on average resulting in lower total cost as rental cost of wind is low compared to solar technologies (Table 2.4 and 2.6, Chapter 2).

At such maximum penetration, PV-BES or CSP/CSP-TES capacities disappear almost entirely from the optimal mix. In fact, keeping the CSP (resp. PV) mean CFs for different SMs (resp. ILR) fixed (Table 2.4, Chapter 2) while increasing the storage cost (Table 2.6, Chapter 2) imply that the CSP (resp. PV) maximum-penetration ratios decrease with the increase of SM (resp. ILR) (Table 4.2), in agreement with section i.

Table 4.2: Maximum-penetration ratios (yr/T€) given by (2.19) obtained from hourly Modern-Era Retrospective Analysis for Research and Applications 2 (MERRA-2) climate data over the year 2018. Solar Multiple of 1 or SM1: Concentrated Solar Power (CSP) without storage; Inverter Loading Ratio ILR>1 or SM>1: with increasing levels of storage from Photovoltaic (PV) or CSP.

Zones	Wind	PV			CSP				
		ILR2	ILR3	ILR4	SM1	SM^{ref}	SM2	SM3	SM4
NORTH	85.3	12.75	5.684	2.67	20.2	11.4	10.78	7.45	2.39
CENTER	90.1	12.76	5.680	2.70	25.8	14.3	13.5	9.34	3.02
EAST	106	13.7	6.08	2.90	20.8	11.6	11.0	7.55	2.44
SOUTH	103	14.1	6.29	2.98	24.5	13.7	12.9	8.91	2.87

iii At High Penetrations

While decreasing the penetration from the maximum and keeping the cost constraint active, optimal mixes appear to favour a higher wind energy contribution than solar (the middle side of the right panels of figures 4.1 and 4.2) due to its low cost (Table 2.6, Chapter 2) in addition to its ability to generate electricity at night and its less defined diurnal output profile (ordinate of figure 3.2a, Chapter 3) as confirmed by the small second ratio of wind in SOUTH (Table 4.3). Indeed, this could be attributed to its large maximum-penetration ratio (Table 4.2), large minimum variance ratio (Table 4.5) or small variance/cost ratio (Table 4.4) compared to wind in EAST already installed (see discussion on the second ratio in section 2, Chapter 2).

After wind in SOUTH, mixes show optimal solar installation either PV-BES in EAST (whatever the ILR) or CSP/CSP-TES in CENTER (whatever the SM). This is mainly due to the sensitivity of optimal mixes to storage options since CSP can store the heat in thermal storage—less expensive than the battery coupled with PV [564]. The dependence on storage sizing is thus strong at such high penetrations and the solar technology with storage configuration that can provide energy for lower rental cost and with high CF would likely be preferred.

For the same design, for instance PV-ILR2-wind-CSP-TES SM2 mix (the middle side of figure 4.1h) or PV-ILR4-wind-CSP-TES SM4 mix (the middle side of figure 4.2j), PV-BES is preferably installed and built with a large capacity compared to CSP/CSP-TES. In fact, the higher mean CF of CSP-TES compared to PV-BES (Table 2.4, Chapter 2) is not able to compensate for the considerable higher cost of CSP-TES

(Table 2.6, Chapter 2) because the storage capacity of CSP is higher than that of PV (Table 2.3, Chapter 2) due to the large CSP nominal thermal capacity compared to the PV nominal DC (direct current) capacity (Section i and ii, Chapter 2).

For different design, for instance between PV-BES and CSP SM1, the lower variance of PV-BES for all ILRs compared to CSP SM1 is not able to compensate for the much higher cost of PV-BES compared to CSP SM1 (the variance/cost of PV-BES is smaller than that of CSP SM1, Table 4.4) which favors the installation of CSP SM1 for all ILRs (the middle side of figures 4.1b, 4.1d, and 4.1f). The same remark can be made for PV-ILR3-wind-CSP-SM2 mix (the middle side of figure 4.1j), PV-ILR4-wind-CSP-SM2 mix (the middle side of figure 4.2b), PV-ILR4-wind-CSP-SM3 mix (the middle side of figure 4.2d). The investment in CSP SM4 is higher than that of PV-BES whatever the ILR (Table 2.6, Chapter 2) which will ultimately increase the total cost of the mix. Thus, PV-BES is installed and the model compensates by installing more PV-BES to achieve the high penetration in the mix (the middle side of figures 4.2f, 4.2h and 4.2j).

There is therefore an imperfect substitution of CSP-TES by PV-BES. In others words, although PV-BES and CSP-TES are similarly sized, they are differently penalized as both have different storage capacity and thus different mean CFs and costs leading to almost exclusive installation of the technology representing the best trade-off between increasing penetration while satisfying the maximum-cost constraint. What stands out from the middle side of the right panels of figures 4.1, 4.2 and table 2.3 (Chapter 2) is that for low or medium storage requirements (5 to 13.5 hours or SM<4 and all ILRs), CSP electricity coupled with cheap TES provides a relative advantage in this high penetration regime because compared to PV, higher level of storage and mean CFs can be achieved (i.e., high variance/cost ratio and large maximum-penetration ratio) which involves less capacity to install and thus less cost. However, if longer storage duration (>13.5 hours or SM4) is the desired level, PV-BES is installed with larger fraction to fulfill the high-penetration requirements.

The predominance of CSP-TES in CENTER and wind in SOUTH at such high penetrations levels goes in line with the actual distribution (right panel of figure 2.4, Chapter 2). However, the addition of BES to PV (and the non-use of tracking) induces the installation of PV in EAST (Table 4.3) instead of SOUTH (Table 3.3, Chapter 3) because the correlations between PV-BES and wind in EAST (already installed) is higher than the correlation between PV-BES and wind in SOUTH (Table A.5, Appendix A); and the variance/cost of PV-BES in EAST is smaller than in SOUTH (Table 4.4).

Table 4.3: Similar to table 4.2 but for the ratios (no units) given by (2.20).

Zones	Wind	PV			CSP				
		ILR2	ILR3	ILR4	SM1	SM^{ref}	SM2	SM3	SM4
NORTH	1.74	1.072	1.121	1.147	1.00	1.069	1.072	1.093	1.147
CENTER	4.21	1.079	1.123	1.148	0.98	1.05	1.058	1.080	1.142
EAST	\emptyset	1.071	1.1201	1.1461	1.022	1.08	1.082	1.098	1.149
SOUTH	3.98×10^{-2}	1.074	1.1204	1.1466	1.026	1.068	1.071	1.088	1.145

Table 4.4: Similar to table 4.2 but for the variance/cost (yr/Ee MW) given by (2.21).

Zones	Wind	PV			CSP				
		ILR2	ILR3	ILR4	SM1	SM^{ref}	SM2	SM3	SM4
NORTH	25755	668	158	29.8	3420	1046	898	292	36.3
CENTER	7611	570	123	15.0	4482	1195	1006	256	10.2
EAST	12637	670	147	19.0	3051	825	698	186	10.2
SOUTH	2900	729	162	23.3	3980	1065	891	219	4.92

iv At Low Penetrations

As can be seen by comparing the left side of the right panels of figures 4.1 and 4.2, the fractions of each technology are qualitatively and quantitatively different between combinations at low penetrations where only the variance and the mean CFs play a role. To illustrate this behavior, we represent the daily (ordinate) and seasonal (abscissa) variability of the national demand, solar and wind CFs obtained using MERRA-2 climate data over the year 2018 in figure 3.2 (Chapter 3) and figure 4.3.

PV-BES vs. Wind

As can be seen on the left side of figure 4.1b, the technology share between PV ILR2 and wind remain similar to that of PV without storage (ILR1) and wind (Section iv, Chapter 3). Thus, the potential to produce electricity from wind is significantly greater and more spread over time than adding BES to PV with small amount of storage, 5 hours (Table 2.3, Chapter 2), as can be seen in figure 3.2a (Chapter 3) and figure 4.3a.

However, the addition of BES to PV with high ILR, ILR3 or 4, makes PV less variable than wind, i.e., larger minimum-variance ratio (Table 4.5) and favors its installation in CENTER over wind, the more as the ILR is increased (the left side of the right panels of figures 4.1 and 4.2).

PV-BES vs. CSP SM1

Due to the use of solar tracking by CSP, the mean CF of CSP tend to be larger compared to PV without storage (Table 2.4, Chapter 2). Therefore, the variance of larger amounts of electricity produced by CSP is higher than that of PV. In addition, CSP technologies cannot harness diffuse part of solar irradiance which result from scattering of direct sun light making it more sensitive to the presence of clouds and aerosols in the air as it cannot be concentrated; compared to PV that exploit all components of solar irradiance (i.e., can work on direct as well as diffused irradiance). As a consequence, the minimum-variance ratio of PV tends to be larger than that of CSP (Table 3.5, Chapter 3). Without

BES, the PV-wind-CSP SM1 mix is however diversified (left side of figure 3.1d, Chapter 3). The reason to install CSP SM1 with limited full load hours of PV ILR1 despite the high variability of CSP SM1 is the difference between CSP SM1 and PV ILR1 seasonal profiles (abscissa of figures 3.3e, 3.3d, Chapter 3). CSP SM1 full load hours are maximal during the summer months (i.e., peak load) while multi-crystalline PV efficiency is reduced in summer. It thus appear that tracked CSP tend to reduce the angular losses especially in summer when the cos-losses are higher due to the wider sun path. To illustrate this point, the global horizontal irradiance or GHI and the direct normal irradiance or DNI—needed for CSP production—(abscissa of figure 3.3a and 3.3c, Chapter 3) tend to increase in summer period while the global tilted irradiance or GTI—needed for PV production—decreases in summer (abscissa of figure 3.3b, Chapter 3). However, CSP SM1 is only kept in the mix at small fraction (left side of figure 3.1d, Chapter 3) since CSP generation is highly correlated with PV generation which is assumed to have high covariances (Table A.5 and A.4, Appendix A) as both have large variance. Thus, adding a new intermittent source will only increase the risk (2.2).

Obviously, adding storage to PV will not affect the large minimum-variance of PV compared to CSP SM1 (Table 4.5). However, the mixes are not diversified and CSP capacities can no longer take part in the optimal mix. This can be explained by the fact that CSP SM1 operate mainly during midday and can achieve full load operation only during summer when irradiance reaches the design point level (Figure 3.3e, Chapter 3) while PV-BES with high ILR can be used to provide continuous output at any time (Figure 4.3). Therefore, the optimal mixes with BES favors the installation of PV-BES over CSP SM1 at low penetrations where the cost constraint is weak (left side of figures 4.1a, 4.1c and 4.1e). The installation of PV-BES in CENTER can also be explained by the relatively small correlations between the PV-BES and wind in the CENTER and between PV-BES and wind in highly wind productive region (EAST) (Table A.5, Appendix A).

PV-BES vs. CSP-TES

As can be observed in figure 4.3, and figures 3.2c, 3.2d and 3.2e (Chapter 3), more CSP SM (resp. PV ILR) is increased, more the variance of CSP (resp. PV) is reduced since larger CSP solar field (resp. PV solar panel) allow the collected energy to be spread over longer period of the day and the year for continuous production. The SM and ILR are thus decisive to achieve high full load hours of solar plant operation. With SM2 or IL2, only few operating hours in evening are achieved. With higher SM and ILR (3,4), the TES and BES are used to run even at times when solar irradiance no longer correlates with peak electricity demand.

The results obtained from mixes with PV-BES and CSP-TES (the left side of the right panels of figures 4.1 and 4.2) suggest that there is always a dominant solar technology either PV-BES or CSP-TES depending on the SM and the ILR. When one technology is installed, the other one is phased out from the mix and vice versa. Thus, the optimal mixes are less diversified since both technologies can shift output over time without the need of other source to cover the demand yielding a mix with less total output variability. Moreover, the fact that CSP-TES and PV-BES are able to reduce the diurnal and seasonal solar power fluctuations such as curtailment or lack of energy, by adjusting their power output, allow to achieve higher share of solar generation, as can be observed on the left side of the right panels of figures 4.1 and 4.2 where the proportion of solar power in the optimal mixes, at such low penetrations, increase the more so as CSP SM or PV ILR is increased.

For the same design (i.e., SM2 vs. ILR2 or SM4 vs. ILR4), although PV-BES tends to have large minimum-variance ratio than CSP-TES, except the SM4 case (Table 4.5), the model install CSP-TES instead of PV-BES (left side of figures 4.1h, 4.2j). This rather contradictory result between technology fraction curves and the minimum-variance ratio could be attributed to the assumption done in section 3 (Chapter 2) where we assume that the covariance matrix is diagonal in the calculation of the minimum-variance ratios. The latter, thus, rule out the influence of covariances which are important, especially when the mix contains technologies with distinct proportions of solar irradiance (high variance) versus cloud cover (low variance), particularly between CSP and PV, as explained above (Section iv or Section iv in Chapter 3). CSP-TES mean CFs have a low standard deviation compared to their mean than PV-BES because as stated previously, CSP-TES has larger storage capacity (Table 2.3, Chapter 2). This can also be shown by comparing figures 3.2d and 3.2e (Chapter 3) with figures 4.3b, 4.3c where the operation at full load of CSP SM3 or SM4 is substantially higher than PV ILR3 or ILR4. In addition, the covariance between CSP-TES and wind are smaller than covariances between PV-BES and wind (Table A.4). Thus, installing CSP-TES over PV-BES produces lower risk.

However, for different amount of storage (i.e., SM2 vs. ILR3,4 or SM3 vs. ILR4 or SM4 vs. ILR2,3), the technology with the higher storage duration (h^{SM} and h^{ILR} in table 2.3, Chapter 2) that is installed. For instance PV-BES with ILR3 or ILR4 dominates over CSP-TES SM2 (left side of figures 4.1j, 4.2b); PV ILR4 also dominates over CSP SM3 (left side of figure 4.2d); and CSP SM4 dominates over PV ILR2 or ILR3 (left side of figures 4.2f, 4.2h).

Table 4.5: Similar to table 4.2 but for the minimum-variance ratios (10^3 MW) given by (2.22).

Zones	Wind	PV			CSP				
		ILR2	ILR3	ILR4	SM1	SM^{ref}	SM2	SM3	SM4
NORTH	3.31	19.0	35.8	89.6	5.92	11.0	12.0	25.5	65.8
CENTER	11.8	22.3	46.0	179	5.76	12.0	13.4	36.5	294
EAST	8.44	20.4	41.3	152	6.85	14.0	15.7	40.6	238
SOUTH	35.7	19.4	38.7	127	6.18	12.8	14.5	40.7	584

2 Impact of Spatio-Temporal Complementarity

The role played by complementarity on reducing the adequacy risk can be only investigated at low penetrations where the three unconstrained fronts—for the global (2.2) (thick black line), technology (2.3) (dashed black line) and base (2.4) (point-dashed black line) strategies—converge with the global constrained front (blue line) in the left panels of figures 4.1, and 4.2. In fact, due to the maximum-cost constraint, the global constrained front achieve smaller mean penetration while shifting towards a larger values of risk than the global unconstrained front (with unlimited total cost). This show that the economic constraints can limit the benefits of complementarity because the matching of the production and demand, at high penetrations, is mainly satisfied by fluctuating and low-cost technologies (i.e., wind and small contribution from solar) which could not fully smooth the variability of RE production (as discussed in section i), thus requiring a higher maximum budget to install more RE capacity—exhibiting larger periods of production availability which are complementary in the time and/or space domain—to improve the supply/demand fit.

By comparing, at such low penetrations, the technology strategy with the global strategy, we can see the importance of taking correlations between CFs, of a given technology, from different regions into account (regional complementarity), while comparing the base strategy to the technology strategy allows us to evaluate the impact of correlations between different technologies in the same region (technological complementarity). Thus, comparing the base front with the global front allows us to examine the role of spatio-temporal complementarities.

The slope of these fronts, the mean-standard deviation ratio (2.5), is given in table 4.6. This ratio quantifies the increase in mean penetration (%) achieved by letting the standard deviation rise by 1%.

Combination/ Strategy	ILR2- Wind	ILR3- Wind	ILR4- Wind	ILR2- Wind- SM1	ILR3- Wind- SM1	ILR4- Wind- SM1	ILR2- Wind- SM^{ref}	ILR3- Wind- SM^{ref}	ILR4- Wind- SM^{ref}
Global	2.06	2.36	3.41	2.09	2.39	3.41	2.06	2.40	3.42
Technology	1.71	2.02	3.22	1.74	2.05	3.22	1.74	2.05	3.22
Base	1.66	1.99	3.20	1.49	1.81	3.02	1.51	1.78	2.98

Combination/ Strategy	ILR2- Wind- SM2	ILR3- Wind- SM2	ILR4- Wind- SM2	ILR2- Wind- SM3	ILR3- Wind- SM3	ILR4- Wind- SM3	ILR2- Wind- SM4	ILR3- Wind- SM4	ILR4- Wind- SM4
Global	2.13	2.36	3.39	2.61	2.58	3.39	5.48	6.11	5.82
Technology	1.80	2.03	3.19	2.37	2.32	3.18	5.10	5.58	5.43
Base	1.56	1.77	2.96	2.11	2.17	3.01	4.97	5.39	5.26

Table 4.6: Mean-standard deviation ratios (2.5) of the global, technology and base fronts without the maximum-cost constraint (2.8) for different combinations (Table 4.1). Solar Multiple of 1 or SM1: Concentrated Solar Power (CSP) without storage; Inverter Loading Ratio or ILR>1 or SM>1: with increasing levels of storage from Photovoltaic (PV) or CSP.

i Regional Complementarity

For all combinations, the technology front (dashed black line) lies to the right of the global front (plain black line) and the difference between these fronts is large (left panels of figures 4.1 and 4.2). This is also confirmed by table 4.6 where this ratio increase from the technology to the global strategy. Thus, for a given level of mean penetration, because the CFs vary little within Morocco on average (Table 2.4, Chapter 2), taking correlations between regions into account allows for the reduction of the variance.

However, more the SM and ILR increase, more the difference between the global and the technology front is reduced because mixes become less diversified as CSP in EAST (for SM1 and SM2) or in SOUTH (for SM3 and SM4) and PV-BES (for all ILRs) in CENTER become dominant (Table 4.5, left side of the right panels of figures 4.1, 4.2); see discussion in section iv.

ii Technological Complementarity

Correlations between CFs of different technologies for the same region also appear to play a role, as can be seen in left panels of figures 4.1, and 4.2 by comparing the optimal front for the base strategy (point-dashed black line) and the technology front (dashed black line), which corresponds to the lower values of the mean-standard deviation ratio for the base strategy, reported in table 4.6.

As found in section ii (Chapter 3), this effect of temporal complementarity on the optimization varies between combinations. The technological complementarity is weak between PV and wind, relevant in case PV and CSP are both installed without storage or with small amount of storage (Table A.5, Appendix A). Therefore, ignoring the high (resp. low) covariance between technologies in the same region (or for different regions as shown in the preceding section i) lead to install much (resp. less) of capacities which results in an increased risk (right side of Equation (2.2), Chapter 2).

However, as the surplus of energy available for TES and BES is increased, the difference between the base and technology fronts is small (table 4.6 and left panels of figures 4.1, and 4.2). Therefore, taking into account correlations between CSP-TES or PV-BES CFs and CFs of other technologies do not seem to impact the variance because the storage induces a change in the CSP and PV CFs that reduces their correlation with the other technologies which also reduces the covariances (Table A.5 and A.4, Appendix A). Note that although the correlations between PV-BES and CSP-TES increases with the increase of storage, the covariances is small since the variance of CSP-TES and PV-BES is decreased as well. This is the reason why the differences in the technology and the base front at such high SMs and ILRs is weak.

The foregoing discussion shows that complementarity brings significant advantages to the grid due to its smoothing effect on variable RE resource output, which reduce the times of power unavailability and thus reduce ramping needs while contributing to improved system adequacy. However, this effect is reduced when dispatchable technologies are integrated as they are already able to reduce the number of times over which energy is not generated. In the upcoming section, it will be examined the role of storage combined with CSP and PV on the system adequacy risk.

3 Role of CSP-TES vs. PV-BES in Reducing the Adequacy Risk

In order to compare the effect of the introduction of PV-BES and CSP-TES on the ability of given RE system to cover the load, we compute, for different combinations, the mean-standard deviation ratio (2.5), i.e., an aggregate measure of the variability of the RE production with respect to the demand (Section i); and the load reduction diagnostics (described in section X, Chapter 2). These additional diagnostics allow us to examine which dispatchable solar technology is more efficient in reducing the imbalances between RE production and demand occurring during peak or mid or base load (Section ii).

i System Variance-based Risk

We observe from table 4.6 that the mean-standard deviation ratio for the global strategy is significantly larger for combinations with high ILRs and SMs than for the others. This shows that, for a given level of penetration and without the total-cost constraint, lower risk may be reached when TES and BES are introduced in the mix which reflects the decreasing balancing needs and costs. This is expected from the lower variance of the CSP-TES and PV-BES CFs explained by the ability of TES and BES to smooth the CSP and PV generation by shaving midday peaks and shifting energy over time (Section 3, Chapter 2).

CSP generation without storage clearly meet the seasonal demand but the variability is high (Figures 3.3e, 3.2b, Table 3.6 for PV-wind-CSP SM1 mix, Chapter 3) since it mainly operates during midday load but its production drops after sunset. Similarly, PV-wind uncurs the risk of depending on the availability of the resource, thus increasing the probability of not adequately satisfying the load (Table 3.6 for PV-wind mix, Chapter 3).

By increasing the SM (resp. ILR) and depending on its value, the seasonal and daily variability gradually disappear (Figure 3.2c, 3.2d, 3.2e for CSP-TES in Chapter 3 and figure 4.3 for PV-BES), which effectively reduces the variance (Table 4.6). This result demonstrates the interest of increasing the original size of the CSP solar field (resp. PV solar panel) by increasing the SM (resp. ILR) in order to operate flexibly and for longer hours; achieving an efficient way to meet any increase of the load.

We note, however, that the mean-standard deviation ratio in the case of introducing BES to PV-wind mix are lower than the ones encountered in the case of the introduction of CSP-TES generation (i.e., since CSP-TES has larger storage capacity than PV-BES, as shown in table 2.3, Chapter 2). Thus, we deduce that for the same installed capacity, the annual produced energy by CSP-TES is less variable than the one produced by the PV-BES demonstrating that PV-BES generation cannot alone replace CSP-TES generation. This is, however, only valid at low penetrations (as discussed in Section iv) but less true at high penetrations where both, the variance and cost, have a role in identifying the optimal technology (Section iii).

ii System Adequacy Diagnostics

The peak load reduction (i.e., capacity credit), mid and base load reduction are presented respectively in figures 4.4, 4.5 and 4.6 as a function of the mean penetration (2.1) from 5 % to 35 % for the global strategy (2.2) with total cost constraint (2.8), for PV-BES-wind mix (left) and PV-BES-wind-CSP-TES SM2 (right); with ILR2 (top), ILR3 (middle) and ILR4 (bottom). We analyze how these load reduction are affected by the RE shares, and the contribution of each technology to each load band. For instance, the effect of CSP-TES on the reliability of the grid compared to PV-BES and to fluctuating wind.

Figure 4.4 shows, for both mixes (PV-BES-wind mix or PV-BES-wind-CSP-TES SM2 mix), that with the increase of the installed capacity, the fraction of RE that displaces conventional capacity in peak load hours tend to decline. However, this does not mean that less conventional capacity can be replaced by RE in absolute terms, but rather that a new renewable plant added to a system with high RE penetration levels will substitute less than the first RE plants in the system. Therefore, high shares of CSP-TES or PV-BES in the mix (at low penetrations) increases the capacity credit while small shares of these technologies (due to the maximum-cost constraint) reduces the capacity credit (the right panels of figures 4.1 and 4.2). Thus, in addition to reducing the system variance-based risk, the introduction of CSP or PV with storage helps satisfy peak loads because CSP-TES or PV-BES could change the temporal distribution of the net load by charging and discharging frequently which influence the correlation with the demand. To illustrate the effect of storage to mitigate the decline in the capacity credit, we show the Load Duration Curve or LDC (black line) and compare the Residual Load Duration Curve or RLDC of three combinations (PV-wind in blue; PV-wind-CSP SM1 in yellow, PV-wind-CSP-TES SM2 in green), in the right panel of figure 4.7, assuming combined wind and solar energy share of the risk-as-actual mix (20%) with relatively high share of CSP-TES (blue diamond) (Figure 3.1f, Chapter 3). We found the same behavior of storage for all combinations with CSP-TES (with $SM > 1$) or PV-BES (with $ILR > 1$), not shown here. We can see that PV-wind and PV-wind-CSP-SM1 shift down the LDC but both move in the same direction (similar net load shape), however, the combination with storage (PV-wind-CSP-TES SM2 mix) reduces the peak load (upper left of RLDC) and increases the time of off-peak load (bottom right of the RLDC). This can be explained by the fact that when the demand is low, the excess of the thermal energy provided by the solar field is stored which then can be recovered and used to provide generation at times of high consumption. This effect of CSP-TES on the Moroccan load (Figure 4.7, in the right) is similar to the effect of pumped hydro storage and interconnection on the Moroccan LDC analyzed by Azeroual et al. [359], demonstrating the ability of CSP-TES to replace other flexibility solutions.

As can be seen in the left panels of figure 4.4, the increase of the ILR in PV-BES-wind mix do not seem to impact the capacity credit. For instance at 5% RE share (with high shares of PV-BES), the value of the capacity credit remains constant and equal to 45% in PV-ILR2-wind mix (Figure 4.4a), PV-ILR3-wind mix (Figure 4.4c), and PV-ILR4-wind mix (Figure 4.4e). This can be explained by the fact that we analyze the average capacity credit on an annual basis (2.24) which keeps the differences between mean capacity credit of PV-ILR2 and PV-ILR3 or PV-ILR4 the same due to the moderate effect of the nights and the days where clouds are not present. The marginal capacity credit of additional BES capacities (i.e., proxy of the incremental avoided capacity and costs associated with the incremental generation of PV-BES) may increase at a greater rate (not shown here).

Comparing the evolution of the mid and base Load Reduction (LR) with an increasing contribution from renewables in PV-BES-wind mix (left panels of figure 4.5 and 4.6), one can see that the mid (resp. base) LR decreases (resp. increases) with the increase of mean penetration since high shares of PV-BES are introduced only at low penetrations and are compensated by wind capacities at high penetrations (on the right side of the right panels of figures 4.1 and 4.2). This is attributed to the fact that PV-BES capacities contributes mainly to midday load and due to their small storage capacity (Table 2.3, Chapter 2) cannot generate electricity for longer operation (for instance at night) and thus are not able to provide base load generation compared to wind that is evenly distributed over the day and the year (Figure 4.3 and figure 3.2a in chapter 3). Because more the ILR increases more the PV-BES fraction decreases rapidly when the share of renewable increases (due to sensitivity of optimal mixes to BES cost), the total mid (resp. base) LR tends to decline when moving from ILR2 to ILR3 or ILR4. For instance, at 5% RE shares, the total mid (resp. base) LR drops from 49% (resp. 43%) in PV-ILR2-wind mix (Figure 4.5a, 4.6a) to 45% (resp. 38%) in PV-ILR3-wind mix (Figure 4.5c, 4.6c).

Comparing the left and right panels of figures 4.4, 4.5 and 4.6, we observe that the addition of CSP-TES SM2 tend to reduce the peak, mid and base load more than the addition of BES only in PV-wind mix. Since the optimal mixes are sensitive to these solar technologies at low and high penetrations (Section 1), the LR trend is thus quite revealing at low and high penetrations.

At high penetrations, only PV-BES is installed in PV-ILR2-wind-CSP-TES SM2 mix (middle side of figure 4.1h), the LR tend to decrease with increasing penetration except the base LR that increases where PV-BES capacities are replaced by wind, at 30-35% RE shares (Figure 4.4b,

4.5b and 4.6b). However, only CSP-TES is installed in PV-ILR3-wind-CSP-TES SM2 mix (middle side of figure 4.1j) and PV-ILR4-wind-CSP-TES SM2 mix (middle side of figure 4.2b) and thus the RE capacity contribution to the guaranteed generation capacity at mid and base load increases with the increase of energy penetration (Figure 4.5d, 4.6d and 4.5f, 4.6f).

At low penetrations, for instance, at 5% share (low penetrations with significant share of either CSP-TES or PV-BES), in PV-ILR2-wind-CSP-TES SM2 mix (left side of figure 4.1h) the fraction of CSP-TES is high and that of PV-BES is zero, we can see that the capacity credit is 55% (Figure 4.4b), the mid LR is 60% (Figure 4.5b) and the base LR is 50% (Figure 4.6b). In PV-ILR3-wind-CSP-TES SM2 mix (left side of figure 4.1j) where at low penetrations, the fraction of PV-BES is high and that of CSP-TES is zero, we can see that the capacity credit is decreased to 45% (Figure 4.4d), the mid LR is decreased to 45% (Figure 4.5d) and the base LR is decreased to 38% (Figure 4.6d). In PV-ILR4-wind-CSP-TES SM2 mix (left side of figure 4.2b) where at low penetrations, both are installed but the fraction of CSP-TES is higher than that of PV-BES; we can see that the capacity credit is increased again to 48% (Figure 4.4f), the mid LR is increased to 49% (Figure 4.5f) and the base LR is increased to 43% (Figure 4.6f).

This ability of CSP-TES to displace more high cost conventional generators than PV-BES during peak, mid and base load hours can be attributed to the inherent advantage of CSP-TES that it can store a larger fraction of solar energy than PV-BES because of the larger power capacity of the storage system (Table 2.3, Chapter 2), consistent with [194, 375], in addition to the use of tracking and the non-sensitivity to high temperatures occurring during summer periods. On the other hand, PV-BES generation with smaller storage system (Table 2.3Chapter 2) only shave the peak load but would not be able to satisfy the whole peak load over the time which illustrates the increasing imbalances variability in meeting the load and thus fluctuate following the weather. As a result, CSP-TES remains the ideal choice to supply capacity reserve.

An interesting point is that when the installed capacity gets higher and wind share continue to increase at the expense of the solar technologies, the relative base LR tails off towards value and the marginal increasing effect is decreased (Figure. 4.6). This saturation effect shows that additional wind capacities (without storage in the mix) are not efficient at meeting the base load at higher penetrations. We verify that is indeed due to the wind curtailment that occur as more RE capacities are added to the system (due to its high mean CF, table 2.4, Chapter 2). In fact, the left panel of figure 4.7 shows the RLDC of for different penetrations illustrating the variation of the RLDC parameters (peak, mid and base load) with increasing penetration and the threshold at which curtailment occurs for PV-wind-CSP SM2 combination. We found the same result for all combinations (not shown here). As can be seen, the RLDC never intersect the x-axis at low and medium penetration, means that the RE production never exceeds the demand, so that the demand is never entirely satisfied by RE and no production is lost. However, beyond the identified 30% RE share threshold, we have negative residual off peak load that occur during period of low demand (bottom right side of the left panel of figure 4.7) due to the feed-in of wind power that occur more at times of low demand in winter when the wind CFs are strong (abscissa of figure 3.2b and 3.2a, Chapter 3). This suggest that once the demand of winter days is covered, further wind deployment mostly leads to overproduction at such high penetrations where the storage is not integrated in the mix (i.e., the CSP-TES or PV-BES fractions are reduced due to the cost constraint).

In addition, the increase of the capacity credit (Figure 4.4) is lower than the mid LR (Figure 4.5) which is lower than the base load reduction (Figure 4.6). This is confirmed by the left panel of figure 4.7 where the upper left of the RLDC converges with the LDC while the mid and base load bands shift away from the LDC. Therefore, there is only a small fraction of RE output that can be relied upon in peak load hours, because RE system with small fraction of flexible PV-BES and CSP-TES technologies is not able to provide energy during time of high load. However, it can reliably contribute some fraction of its capacity during these hours to meet the residual load. This suggest that increased RE deployment introduces more supply intermittency and fluctuations, requiring more flexibility during peak load periods; but less mid and base load capacities will be needed at such high penetrations due to the high share of wind. However, it is clear from the left panel of figure 4.7 that for all penetrations, RLDC cross the abscissa at same point of the LDC, meaning that the number of hours of operation for capacity usually designed as base load is not decreased too much. In other words, there is a significant fraction of the base load which is not varying and could therefore be balanced by plants that provide constant output throughout the year. The ability of CSP with TES to shift the timing of RE generation to better match the peak load could have played role in limiting the amount of energy curtailed or needed by flattening the daily production. For instance, the CSP storage provides a power sink at times of negative residual demand (bottom right side of left panel of figure 4.7) and enables the recovery of some of the excess during the period of high consumption (top left side of left panel of figure 4.7).

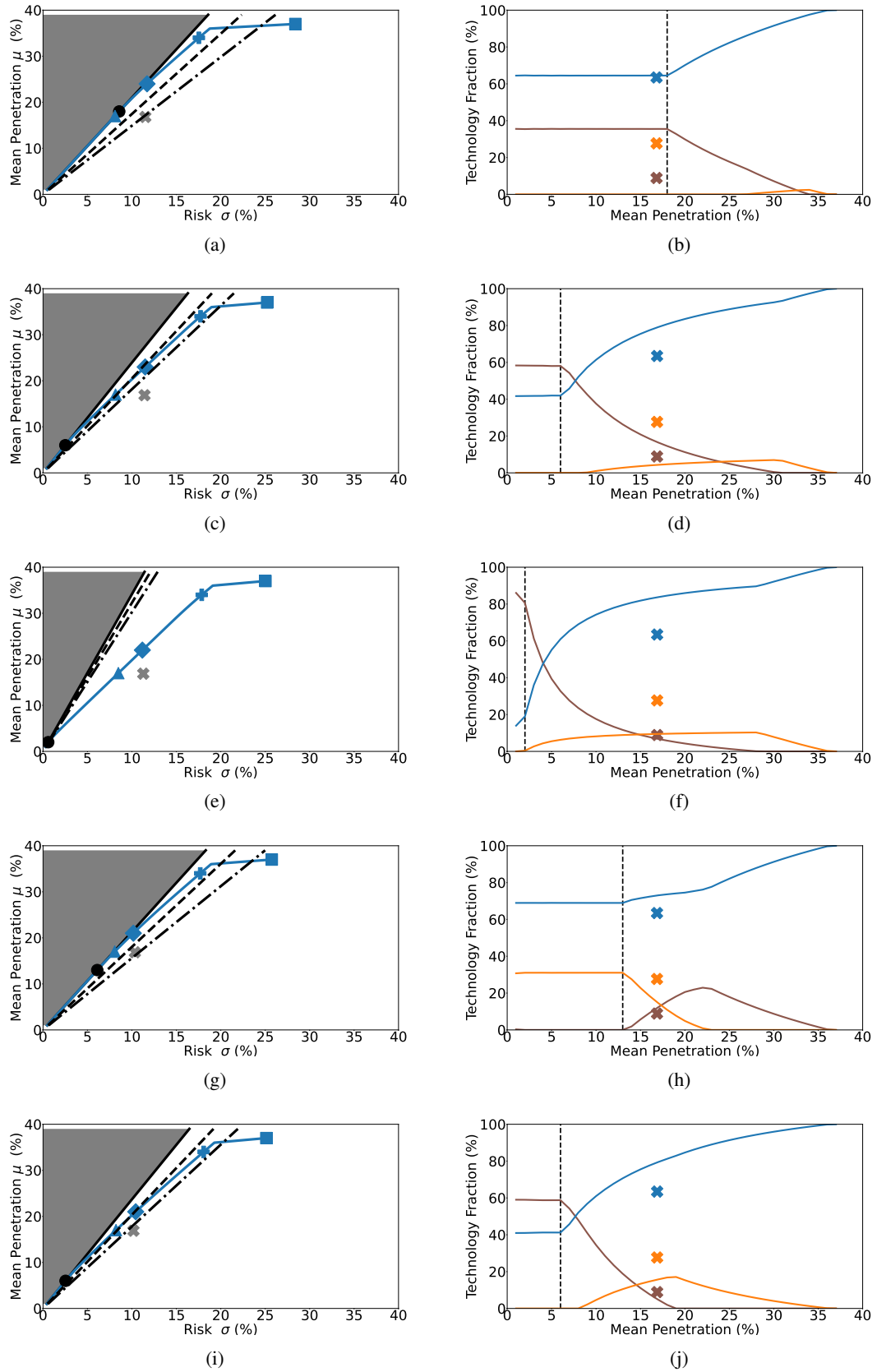


Figure 4.1: **Left:** Approximations of the optimal fronts obtained from hourly Modern-Era Retrospective Analysis for Research and Applications 2 (MERRA-2) climate data with the risk, σ , in abscissa and the mean penetration (2.1), μ , in ordinate. White (resp. gray) area to the right (resp. left) are not Pareto optimal (resp. not feasible). Particular mixes are depicted: the "2018 actual solar-wind mix" (gray cross); the "penetration-as-actual mix" (blue triangle) with lower risk; the "risk-as-actual mix" (blue diamond) with higher penetration; the "cost activation mix" (black dot) with the largest penetration for which the maximum-cost constraint (2.8) is not active; the "cost activated mix" (blue plus) with moderate penetration compared to the "maximum-penetration mix" (blue square) in which the cost constraint is activated; **Right:** Shares of wind (blue line), Photovoltaic (PV) with Battery Energy Storage (BES) (brown line) and Concentrated Solar Power (CSP) without or with Thermal Energy Storage (TES) (orange line) capacities versus the mean penetration for the global strategy (2.2) with maximum-cost constraint (2.8). The crosses represent the shares for the actual mix. **(a, b):** PV-ILR2-Wind-CSP-SM1 **(c, d):** PV-ILR3-Wind-CSP-SM1 **(e, f):** PV-ILR4-Wind-CSP-SM1 **(g, h):** PV-ILR2-Wind-CSP-TES SM2 **(i, j):** PV-ILR3-Wind-CSP-TES SM2. Solar Multiple of 1 or SM1: CSP without storage; Inverter Loading Ratio or ILR>1 or SM>1: with increasing levels of storage from PV or CSP.

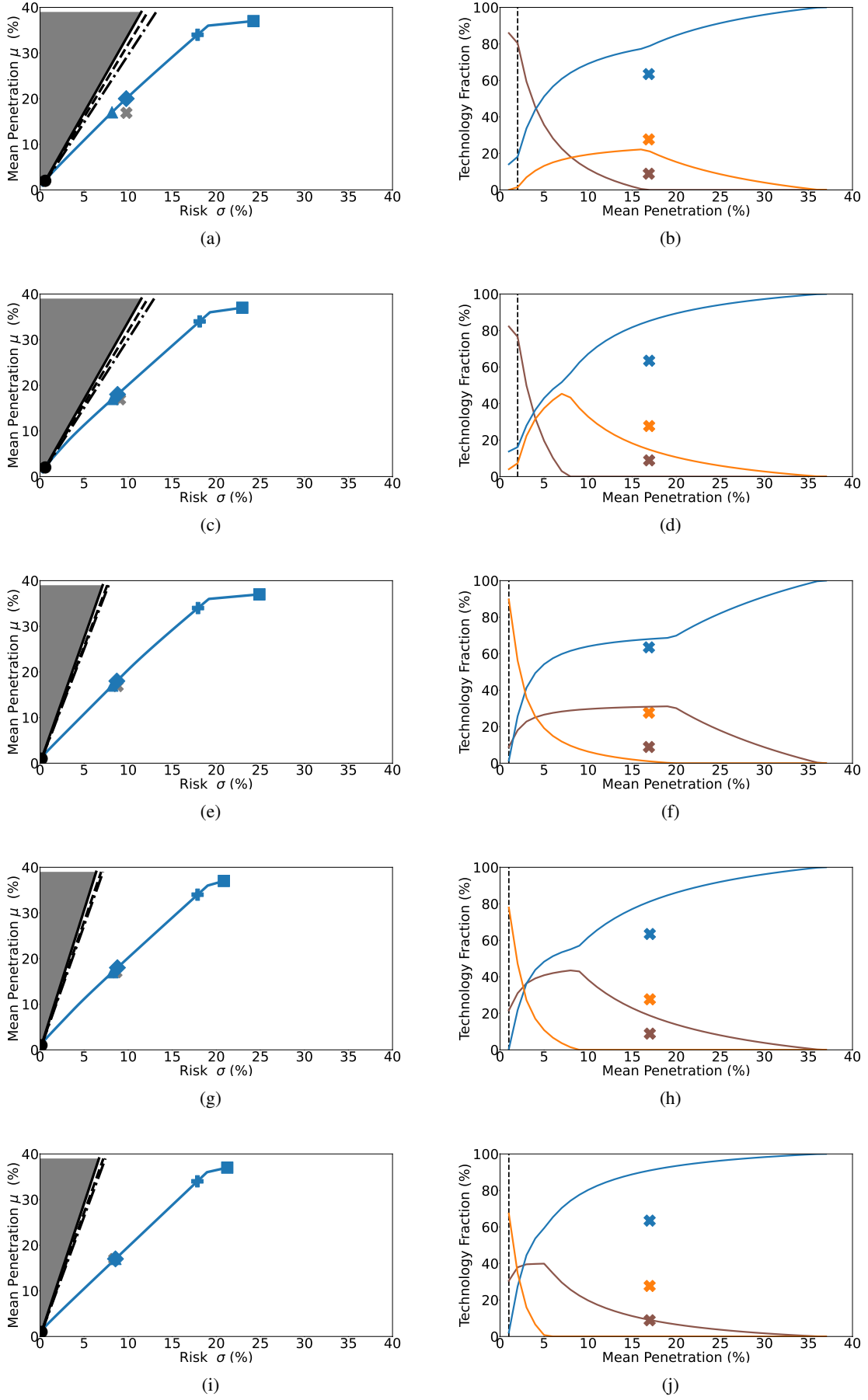


Figure 4.2: Similar to figure 4.1. **(a, b)**: PV-ILR4-Wind-CSP-TES SM2 **(c, d)**: PV-ILR4-Wind-CSP-TES SM3 **(e, f)**: PV-ILR2-Wind-CSP-TES SM4 **(g, h)**: PV-ILR3-Wind-CSP-TES SM4 **(i, j)**: PV-ILR4-Wind-CSP-TES SM4. Inverter Loading Ratio ILR>1 or Solar Multiple SM>1: with increasing levels of storage from Photovoltaic (PV) or Concentrated Solar Power (CSP).

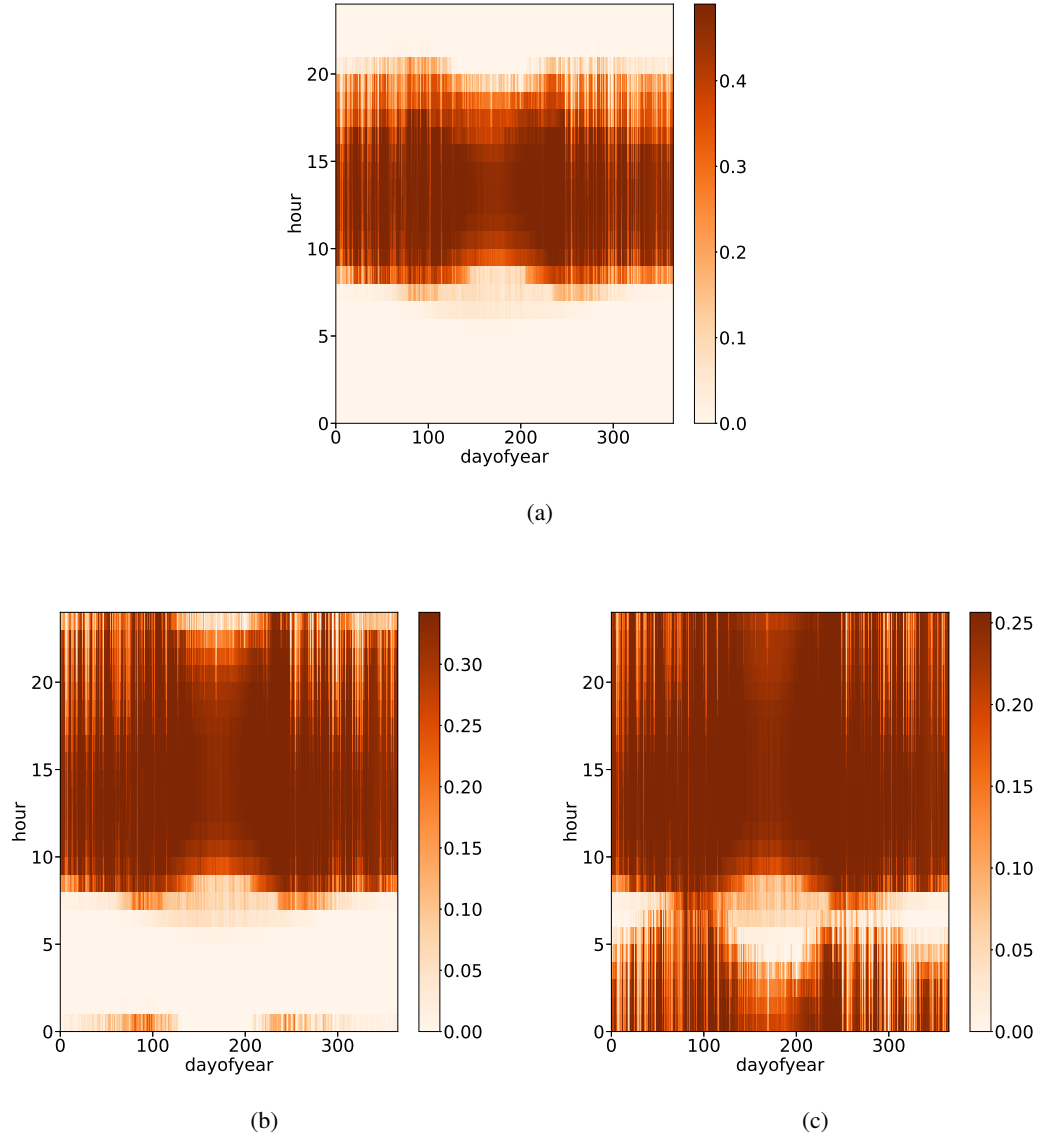
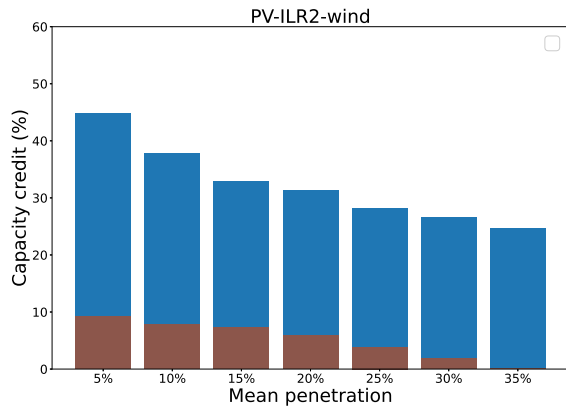
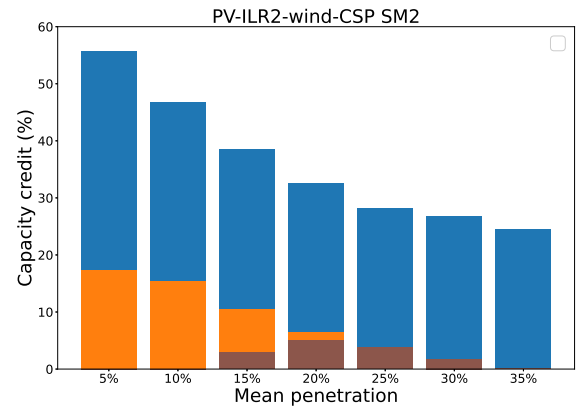


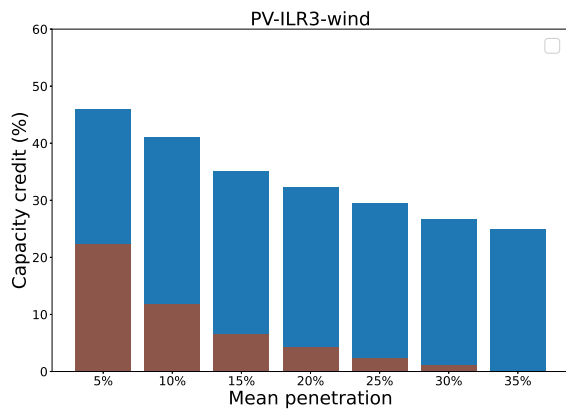
Figure 4.3: Heatmap of the national daily (ordinate) and seasonal (abscissa) variability of the predicted capacity factors: Photovoltaic (PV) with Battery Energy Storage (BES) with an Inverter Loading Ratio of 2 or ILR2 (a), PV-BES ILR3 (b), PV-BES ILR4 (c); obtained over the year 2018 from the hourly Modern-Era Retrospective Analysis for Research and Applications 2 (MERRA-2) climate data. The variation over time is shown in color by intensity in the colorbar. ILR > 1: with increasing levels of storage from PV. Critical appraisal of the obtained profiles are discussed in section ii (Appendix A).



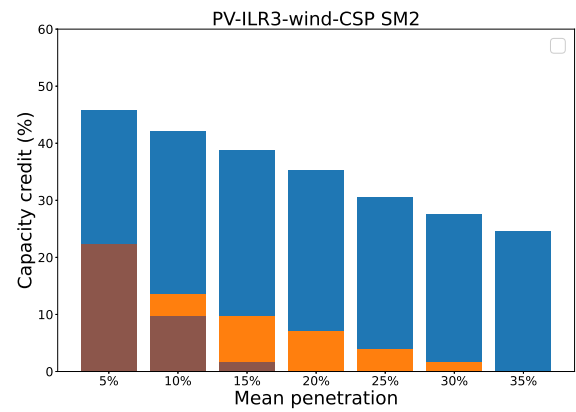
(a)



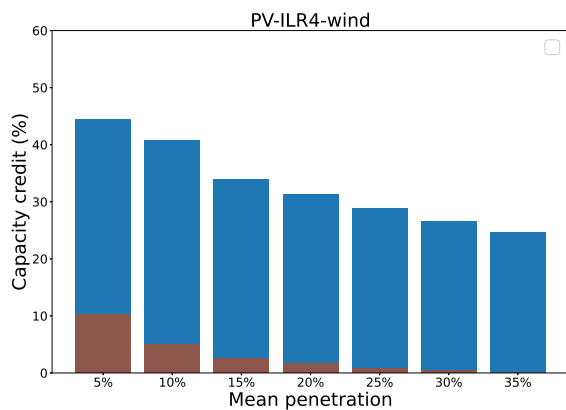
(b)



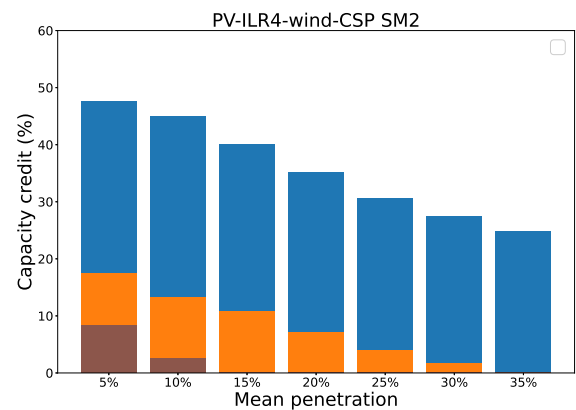
(c)



(d)

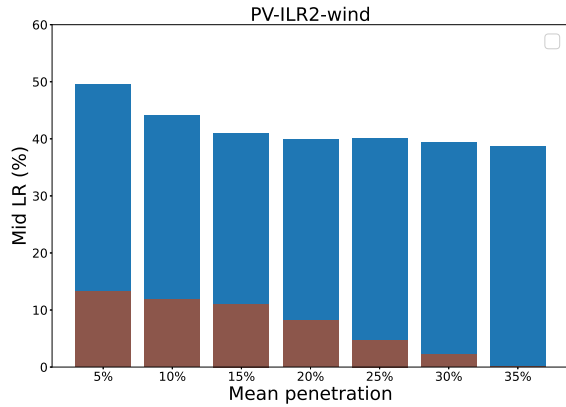


(e)

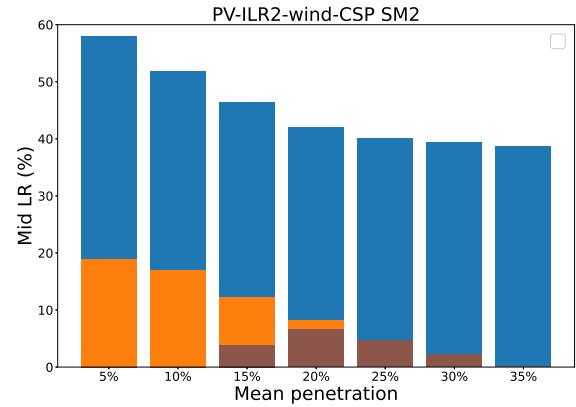


(f)

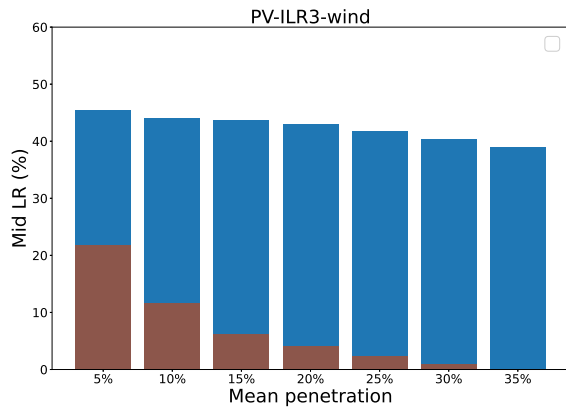
Figure 4.4: Capacity credit by each technology—Wind (blue), Photovoltaic (PV) with Battery Energy Storage (BES) (brown) and Concentrated Solar Power with Thermal Energy Storage (TES) with a Solar Multiple (SM) of 2 or SM2 (orange)—versus the mean penetration (2.1), μ , for the global strategy (2.2) with maximum-cost constraint (2.8) obtained from hourly Modern-Era Retrospective Analysis for Research and Applications 2 (MERRA-2) climate data over the year 2018. **Left:** PV-BES-wind mix; **Right:** PV-BES-wind-CSP-TES SM2 mix. **Top:** ILR2; **Middle:** ILR3; **Bottom:** ILR4. SM2: CSP with 6 hours of TES; ILR>1: with increasing levels of storage from PV.



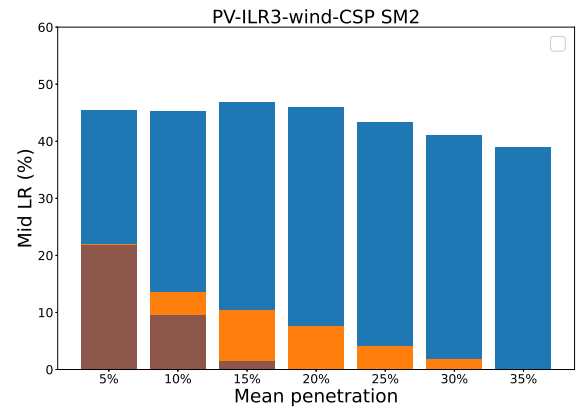
(a)



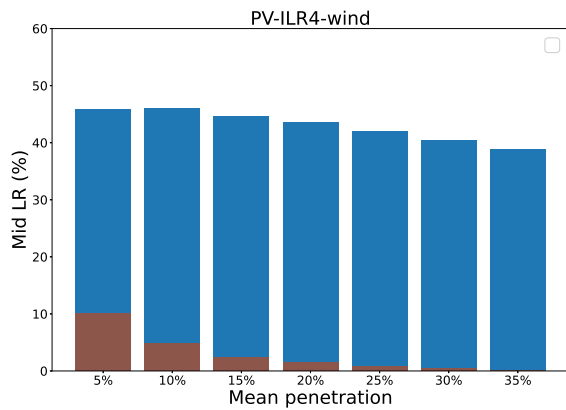
(b)



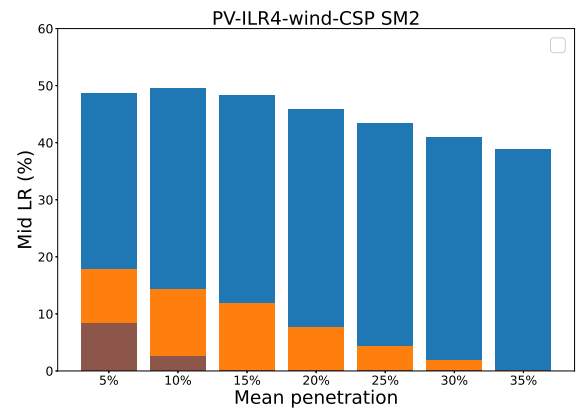
(c)



(d)

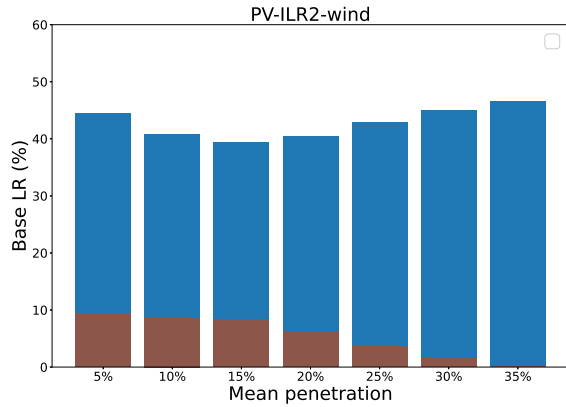


(e)

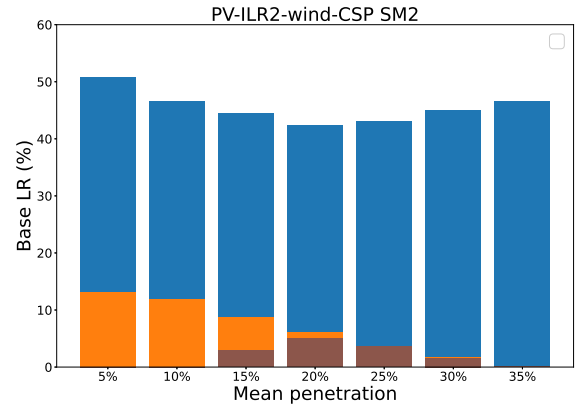


(f)

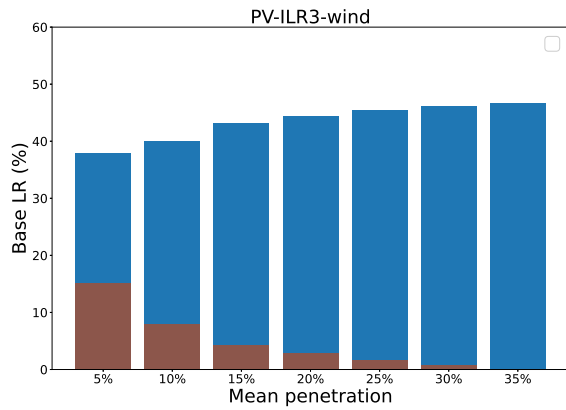
Figure 4.5: Mid load reduction by each technology—Wind (blue), Photovoltaic (PV) with Battery Energy Storage (BES) (brown) and Concentrated Solar Power with Thermal Energy Storage (TES) with a Solar Multiple (SM) of 2 or SM2 (orange)—versus the mean penetration (2.1), μ , for the global strategy (2.2) with maximum-cost constraint (2.8) obtained from hourly Modern-Era Retrospective Analysis for Research and Applications 2 (MERRA-2) climate data over the year 2018. **Left:** PV-BES-wind mix; **Right:** PV-BES-wind-CSP-TES SM2 mix. **Top:** ILR2; **Middle:** ILR3; **Bottom:** ILR4. SM2: CSP with 6 hours of TES; ILR>1: with increasing levels of storage from PV.



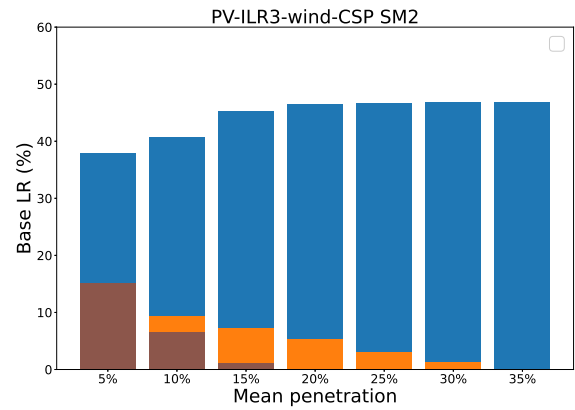
(a)



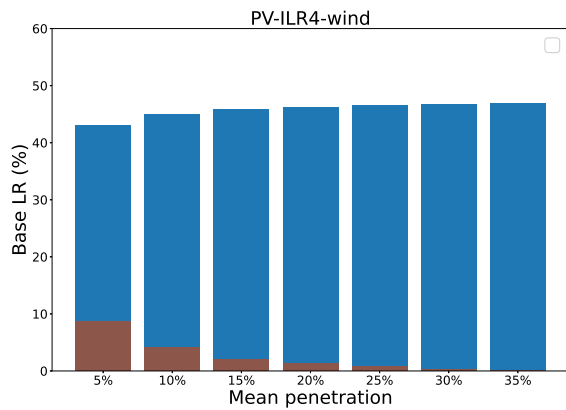
(b)



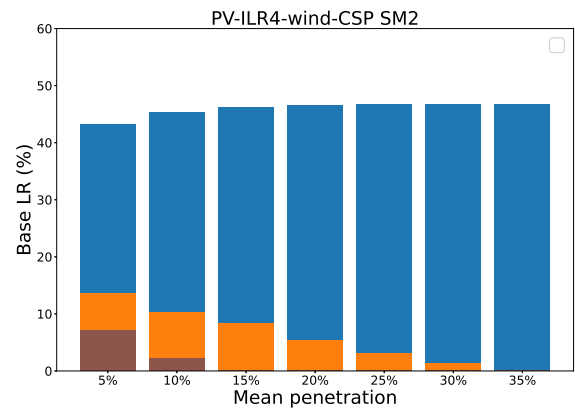
(c)



(d)



(e)



(f)

Figure 4.6: Base load reduction by each technology—Wind (blue), Photovoltaic (PV) with Battery Energy Storage (BES) (brown) and Concentrated Solar Power with Thermal Energy Storage (TES) with a Solar Multiple (SM) of 2 or SM2 (orange)—versus the mean penetration (2.1), μ , for the global strategy (2.2) with maximum-cost constraint (2.8) obtained from hourly Modern-Era Retrospective Analysis for Research and Applications 2 (MERRA-2) climate data over the year 2018. **Left:** PV-BES-wind mix; **Right:** PV-BES-wind-CSP-TES SM2 mix. **Top:** ILR2; **Middle:** ILR3; **Bottom:** ILR4. SM2: CSP with 6 hours of TES; ILR>1: with increasing levels of storage from PV.

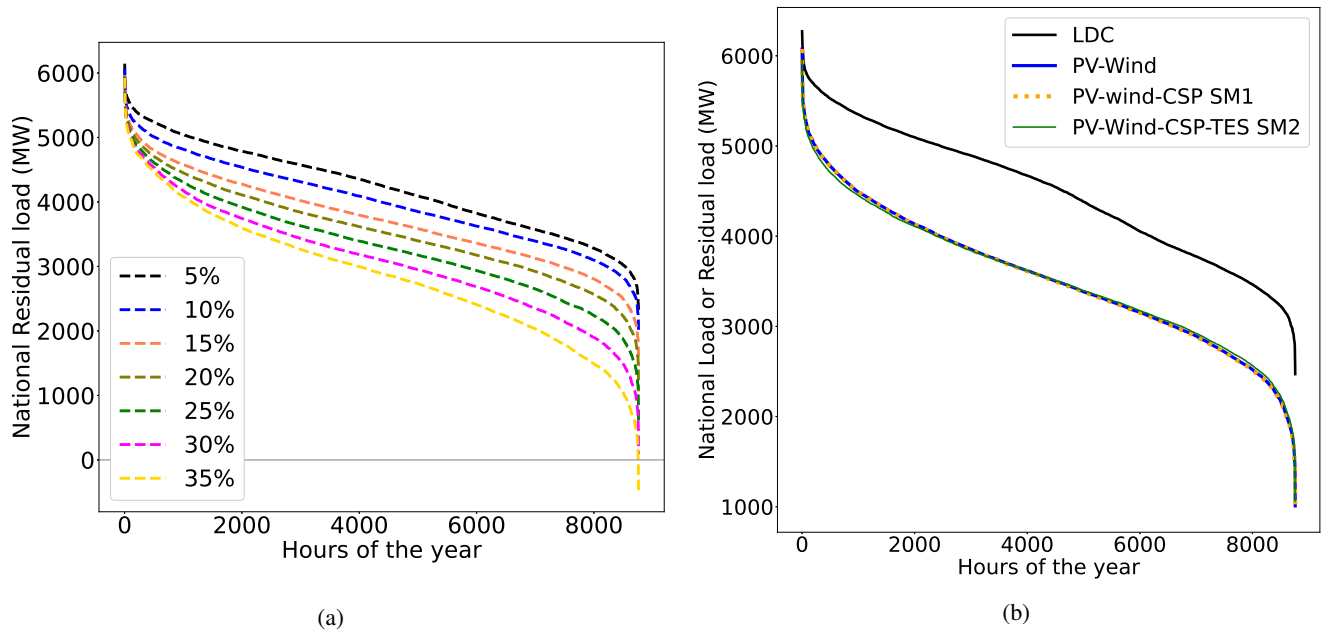


Figure 4.7: **Left:** Residual Load Duration Curve (RLDC) for different penetrations illustrating the variation of the RLDC parameters (peak, mid, and base load) with increasing penetration and the renewable share threshold at which curtailment occurs (negative residual load) for PV-wind-CSP-TES SM2 combination. **Right:** Load Duration Curve (LDC) and RLDC for different combinations, computed at 20% penetration (risk-as-actual mix) for the global strategy (2.2) with maximum-cost constraint (2.8), illustrating the system flexibility provided by CSP-TES. Solar Multiple of 2 or SM2: Concentrated Solar Power (CSP) with 6 hours of Thermal Energy Storage (TES). Photovoltaic (PV) is without storage.

IV Discussion and Comparison with Existing Studies

The two dominant technologies for generating electricity from the sun are Photovoltaic (PV) and Concentrated Solar Power (CSP), both without or with different Battery (BES) and Thermal (TES) Energy Storage duration, as defined by the Inverter Loading Ratio (ILR) and Solar Multiple (SM). Many investors see significant opportunities for large-scale deployment of these technologies [524]. The results obtained in this study and in chapter 3 allow us to discuss scenarios of integration of solar CSP/CSP-TES and PV/PV-BES in Morocco and to show if these technologies are competing against each other or there is a technology that is winning over the other (Section 1). We also discuss scenarios of unlimited thermal and battery storage cost and capacity (Section 2), scenarios under different circumstances of penetration, adequacy risk and investment budget (Section 3) and scenarios of hybrid solar systems (Section 4).

1 Does CSP/CSP-TES Competing or Winning over PV/PV-BES ?

Looking at the optimal mixes obtained for each Renewable Energy (RE) combination (Figure 4.1, 4.2), one can see how outfitting PV and CSP plants with storage systems have a perceptible impact on optimal mixes. The degree of this impact depends on the intended penetration, on the storage requirement as well as rental cost. Indeed, the optimal mixes reveal high sensitivity to solar technologies not only at low penetrations due to the reduced variance of storage (TES, BES) but also at high penetrations due to the differences in the storage capacity and rental cost. Along the optimal fronts, we identified a highly non-linear relationship between CSP/CSP-TES and PV/PV-BES. It is noticed that when one technology is introduced in the mix, the other one is phased out and vice versa.

At low penetrations, only the time averaged Capacity Factors (CFs), variance and covariance play a role.

→ **CSP vs. PV:** PV dominates over CSP (Section iv, Chapter 3) because the diffuse component cannot be optically focused by CSP, making it more variable, although the tracking system of CSP improves the mean CFs and allows to satisfy the demand for energy in the summer compared to fixed-tilted PV that gets affected by high solar panel temperature.

→ **CSP-TES vs. PV and PV-BES vs. CSP:** PV-BES dominates over CSP (left side of figures 4.1b, 4.1d, and 4.1f) and CSP-TES also dominates over PV (left side of figures 3.1f, 3.1h, and 3.1j, Chapter 3). In fact, CSP-TES (resp. PV-BES) has the dual role of contributing to solar generation requirement and providing energy even when the sun is not available because it is able to directly store energy during daylight hours and to convert it into electricity later on for several hours; eliminating the need for PV (resp. CSP) completely at low penetrations, having larger amounts of solar energy deployed instead (Section iv; and section iv, Chapter 3). Therefore, CSP-TES (resp. PV-BES) is a complementary energy source to PV (resp. CSP SM1) generation. An indicator for this complementarity is the convex shape of the CSP-TES and PV-BES fractions and the concave shape of CSP SM1 and PV at high RE share; meaning that dispatchable technologies can achieve high mean penetration while reducing the adequacy risk compared to intermittent technologies which cannot adequately cover the load, particularly when the rate of RE penetration increases.

This suggest that PV-BES and CSP-TES with high storage capacity allow the generation of power on demand which contribute to stable grid conditions allowing to meet the increased summer peak load due to sustained economic growth and increased use of air-conditioning system, to bridge the intermittent cloudiness, and to equilibrate the day/night patterns; resulting in lower curtailment (at noon, when the sun is at its highest point and PV/CSP production reaches its maximum) and shortage (in the evening when the PV/CSP production drops off and electricity demand peaks); which reduce the need for support from fossil fuels; and lead to increase the reliability (more adequacy services are provided) and economic benefits (integration costs are reduced) while reducing the emissions of carbon dioxide (CO_2) in the atmosphere, i.e., a solution to the duck curve phenomenon and climate change issues.

Particularly, given that it is more likely that Morocco would not be able to achieve the solar target of installing 2 GW by the end of 2021, since until now only 700 MW is installed (20 MW CSP; 510 MW CSP-TES and 170 PV), these dispatchable technologies allow to increase the solar fraction more quickly at minimum variance.

→ **CSP-TES vs. PV-BES:** While integrating the storage may help decrease the variance and achieve high mean penetration (i.e., high mean-standard deviation ratio), this also depends on the storage capacity. CSP-TES has the inherent advantage over PV-BES of having large storage capacity. Thus, CSP-TES generally substitutes PV-BES as it achieves higher mean-standard deviation ratio and higher capacity credit compared to PV-BES (i.e., lower system adequacy risk). As a result, the total required installed capacity for minimal variance is higher for PV-BES. Consequently, fewer costs could be incurred for the system balancing needs when integrating CSP-TES instead of PV-BES. This can be seen as an indicator that CSP-TES has a higher economic value than PV-BES.

It should be noted that the analysis of this study shed light on the cost and storage effect on optimal mixes (Section 1) and compare between CSP-TES and PV-BES in terms of aggregate variability (Section i) and which technology is more suited to displace conventional during peak/mid/base load hours and to reduce the curtailment and which one is more correlated with the summer and evening peak (Section ii). However, it did not quantify the avoided costs and emissions. These aspects are left for future work (Section 4, Chapter 6).

→ **Complementarity:** Solar technologies integration without or with storage also induces a change in the correlations (Table A.5, Appendix A) which affect significantly the benefits provided by complementarity. Specifically, we show that the temporal complementarity between solar PV and CSP, both without storage, provides a good prospects for reducing the variability (Section ii, Chapter 3), which is possible to reduce the capacity requirements and thus decrease the system cost. However, since the dispatchable technologies (PV-BES, CSP-TES) with large storage size make the optimal mixes less diversified (Section iv), the benefits from time-space complementarity are reduced (Section ii).

At high penetrations, only the cost and CF matter.

→ **CSP vs. PV:** PV dominates over CSP because the high mean CSP CF—compared to PV—does not compensate its high capital cost (Table 2.4 and left panel of table 2.5, Chapter 2). Thus, PV is the preferred option simply because of its affordable rental cost (Section iii, Chapter 3).

→ **CSP-TES vs. PV and PV-BES vs. CSP:** Although energy storage is, in general, needed at high RE penetrations, we can observe that PV-BES and CSP-TES shares stagnate before the point at which the cost constraint is not active, but after this penetration threshold their share decrease (right side of figures 4.1, 4.2). In fact, although large storage systems reduce the variance, CSP (resp. BES) constitutes a capital-intensive technological options and thus the storage (resp. production) component is expected to incur additional costs; which influence their competitiveness and as a result the model favors the installation of intermittent or fluctuating technologies (with low amount of storage) but low-cost generation technologies over expensive and more dispatchable technologies to not reach the maximum cost budget sooner. Thus, this

tipping point represents the penetration level at which the reliability and economic benefits of dispatchable technologies outweigh the reliability and economic challenges of intermittent technologies (Section i). This calls for higher investment to install more CSP-TES and PV-BES with storage.

→ **CSP-TES vs. PV-BES:** In case of integration of CSP-TES with PV-BES, the optimal mixes are sensitive to the storage cost estimates associated with the storage capacity of each dispatchable solar technology. For the same design, PV-BES is by far the cheapest option for large-scale plants (Table 2.6, Chapter 2). However, we need to look at the level of operation hours provided by each technology.

Overall, for low and medium storage duration (5 to 13.5 hours or $SM < 4$ and all ILRs), adding battery storage to PV tends to make PV less economical than CSP combined with TES; and it is also apparent that it more than outweighs the difference in cost between CSP and PV plants (Table 2.6, Chapter 2). As a result, CSP electricity coupled with cheap TES is more competitive source of electricity for higher shares of RE than the PV-BES alternative (Section iii) due to the longer lifespan of TES than BES (consistent with [528]), despite its higher upfront capital cost. Taking the particular case of 5-5.5 hours, the actual most widespread storage configuration in Morocco (Table A.73, Appendix A), the cost of CSP parabolic trough with 5.5 h of molten salt storage (or $SM_{ref}=1.87$) is currently cheaper than a solar PV farm with almost equivalent design (ILR2) with 5 hours of lithium-ion batteries (Table 2.3, Table 2.6, Chapter 2). Thus, Morocco can opt for CSP technology as it has the most competitive storage option for providing energy production for longer period for the time being.

However, in cases of storage requirements exceeding 13.5 hours (or SM_4), expensive CSP with storage is not competitive and hence large fraction of PV-BES capacities are installed.

Thus, we notice that the exact value of the storage capacity threshold beyond which PV-BES presents a lead, at such high penetrations, over competing technologies is 13.5 hours.

This outcome—obtained between CSP-TES and PV-BES at such high penetrations—is deemed not tenable according to the existing literature [96] under current scenario costs stating that PV-BES (resp. CSP-TES) can provide lower cost for supplying the load in scenarios with low (resp. high) storage requirements or penetration levels. In addition, Ref. [401] found that PV-BES is more competitive than CSP-TES whatever the storage requirement. However, these studies focus only on cost of energy produced. Jorgenson et al. [284] that focus on the cost and the benefits show that all configurations of CSP-TES are able to provide more energy than PV-BES at lowest cost.

Before all these analysis between CSP/CSP-TES and PV/PV-BES one would get the idea that these technologies are competing against each other. At first glance, it actually makes a lot of sense to make this inference because after all, these technologies are absorbing the sunlight and generating electricity. However, when we look closely to the results obtained under different penetration scenarios, we realize that the rental cost and variability (sensitivity to clouds/temperature, storage capacity, the use of tracking)—namely the economic and reliability benefits/challenges—play a crucial role; and we can say that in reality, PV (resp. PV-BES) is actually not comparable to CSP (resp. CSP-TES) and they are not competing against each other. Instead, they are complementary energy sources and the winning technology depends on the objectives (i.e., minimizing the risk with low penetration and cost, or maximizing the penetration with low cost at the detriment of the adequacy risk).

It is worth to shed light on the complexity of the decision-making process in an issue related to the choice of the solar technology because it has many crucial factors (capacity factor, variance, temporal and spatial patterns) that affect which technology should be installed under different penetration scenarios, storage requirements and cost scenarios. Even more complex, these parameters are strongly interlinked to each other.

Overall, there is insufficient convergence in the results because each study uses different approaches and assumptions. This study reflects only the general trends related to specific solar PV and CSP technology, PV orientation and CSP tracking option, storage configuration and cost scenario. However, alterations of these parameters can entail significant changes in the optimization results. Therefore, the elicited conclusions should be treated as a revealing qualitative trend. It is outside the scope of this chapter to conduct a sensitivity analysis of these parameters. However, a short discussion is worthwhile.

Variability

→ Alternative Solar PV and CSP Technology, Tracking Options and Optimization Strategies

First, is important to bear in mind that in this study, PV multi-crystalline and CSP Parabolic Trough (PT) have been used as reference solar technologies in the PV/PV-BES and CSP/CSP-TES models, each with its specific characteristics. Moreover, the output is for CSP north-south tracking and fixed latitude-tilted PV (Section i and section ii, Chapter 2). However, care should be taken to test different PV and CSP technologies and orientation types since each option has its own characteristics in terms of sensitivity to climate (temperature and clouds) which affect the energy output and costs. For instance, the multi-crystalline PV efficiency decreases as the PV cells get hotter [433]. However, Amorphous silicon solar cells are less sensitive to high temperature (0.19% vs. 0.50% degradation per degree over $25^{\circ}C$) [28]. In addition, it is possible that technology innovations in the CSP sector will lead to future market preference for other CSP technologies instead of the PT, like Solar Tower (ST). The latter has lower cost of storage and power block [268] due to the higher operating temperature which creates higher temperature differential and higher performance. Therefore, ST has the potential to reduce costs for providing mid and peak load in hot and arid climate, further improving their competitiveness at high penetrations scenarios in Morocco. Moreover, the wind production variability may also be sensitive to the choice of the power curve.

Moreover, we find (not shown here) that the orientation of PV and CSP (e.g., fixed/vertical tilted orientation, tracked about two independent axes or aligned on a north-south/east-west tracking) has a strong impact on which technology stands at a leading position (see discussion on the effect of tilt angle and tracking in section i, Chapter 1). Thus, further sensitivity analysis on this matter could produce interesting findings.

It is also important to note that the resulted capacity pathways (Section III) are for the global strategy (2.2) with maximum total cost constraint (2.8). Further research should be undertaken to explore the optimal mixes, under different penetration scenarios, using the technology strategy (2.3) or base strategy (2.4) with/without maximum total cost constraint (2.8) or also the global strategy but without the cost constraint as they lead to different conclusions (not shown here).

→ Storage Configurations

One of the most obvious finding to emerge from this study is that the capacity of storage desired at each scenario mix is a key design parameter for PV and CSP, and it has a significant impact on which technology is likely to have lower rental cost at high penetrations, and which technology is likely to have minimum variance at low penetrations, while keeping the mean CFs fixed. It also impacts the covariances and thus the benefits of complementarity.

The CSP and PV sizing—measured by the CSP solar multiple (SM) and PV inverter loading ratio (ILR)—considered in this study ranges from 1 to 4 leading to an average storage duration per day of 5.5 to 17h for CSP and to 5 to 13.5 h for PV (Table 2.3, Chapter 2). Other configurations may lead to different results.

In addition, in our study, the CSP solar field (resp. PV solar panel) and the amount of storage are increased in the same way, i.e., an increase in the CSP SM (resp. PV ILR) gives an increase in the CSP solar field (resp. PV solar panel) area which increase the storage capacity. The integration of inappropriately sized CSP and PV plants in related to storage systems leads to sub-optimal solutions. For instance, dumping and increase of costs becomes detrimental when the TES (resp. BES) capacity is significantly undersized in relation to the CSP solar field (resp. PV solar panel). In this case, the plant ability to shift the strong CSP and/or PV feed-in during the daylight hours to other periods of the day (e.g., peak hours) is reduced. Thus, it either forces CSP and PV production curtailment or requires the conventional plants to reduce their output. This is particularly disadvantageous in the Moroccan case, as coal plants have to be ramped down. Algeria or California, alternatively, have fewer problems with large amounts of solar power because flexible gas plants can more easily (and comparatively more cost-efficiently) follow the variation of electricity production. As a result, the cost disadvantages are smaller than in the Moroccan case. On the other hand, over-sizing the storage system compared to CSP solar field (resp. PV solar panel) also lead to sub-optimal solutions. A sensitivity analysis in this area could further challenge the competitiveness of CSP and PV plants in electricity systems and left for future work (Section 2, Chapter 6).

Cost and Penetration Scenarios

In addition, drawing final conclusions about the general competitiveness of each technology is still premature since the analysis relied on only one cost data and capacity data (reflecting the status quo in Morocco) stemming from studies published in the recent years. However, the costs of PV, wind, CSP and batteries are expected to come down due to large-scale deployment and technology improvements (i.e., solar and wind technologies are getting better at extracting RE resources) [445].

→ Optimal Dispatchable Solar Technology Under Future Cost Reduction

Bogdanov et al. [96] found that CSP-TES is more competitive for high shares of RE under current (2020) cost scenarios. However, PV-BES is more likely to produce energy at lower costs than CSP-TES in the future (2030) scenarios costs. Jorgenson et al. [284] that focus on the cost and the benefits show that CSP-TES is better than PV-BES under current and future scenarios. Papadopoulou et al. [401] found that the Levelized Cost of Electricity (LCOE) achieved in the case of PV plus storage are by far the lowest ones compared to offshore wind-storage and CSP-storage. Feldman et al. [194] show that, under future (2030) cost scenarios, if three hours of storage is the desired level, PV tends to produce a lower projected LCOE; if nine hours of storage is the desired level, CSP tends to have a lower projected LCOE.

Therefore, the competitiveness of each solar technology depends on how successfully they reach cost reduction targets [193]. The future reduction in the levelized cost is critically dependent upon the change of the economic parameters. Several studies report the economic factors that influence the energy cost of wind [515], of solar PV and CSP/CSP-TES [451, 528, 268] and of PV-storage and offshore wind-storage and CSP-storage [401].

For instance, lower discount rate will lead to lower the levelized cost [344] and thus the sensitivity of optimal mixes to rental cost will be reduced. The levelized cost may also drops with the increase of energy output. We also note that an extend in a project lifetime decreases the cost of energy production. However, the latter is relatively insensitive towards the variation on operation and maintenance costs.

For CSP with storage, the impact of the investment cost of CSP on the LCOE is predominant, followed by the discount rate and the variable operation and maintenance costs. The influence of the fixed operation and maintenance costs is noticeably weaker [401].

For PV with storage, the CF and the storage investment cost constitute the two most important parameters, followed by the discount rate and the PV investment cost. The parameters that affected the PV-storage LCOE the least are the fixed operation and maintenance costs for the PV and the storage components [401].

For offshore wind coupled with storage, the strongest impact on the LCOE is presented by the CF, while the second most pivotal parameters are the wind investment cost and the discount rate. The impact of the storage investment cost and the offshore wind operation and maintenance costs (both fixed and variable) are deemed weak, whereas the storage operation and maintenance costs is negligible [401].

→ Uncertainty in Future PV/PV-BES and CSP/CSP-TES Cost Projections

The prospects for continued future cost reduction of storage and production technologies is clear but the rate at which each technology will decline is still perceived as highly uncertain. The uncertainty could be in part attributed to different methods used to assess future cost reduction (e.g., “learning curves” indicating the cost reduction of the technology by a constant factor “learning rate” or “progress ratio” with every doubling of cumulative installed capacity “experience indicator”). For instance, a progress ratio of 90% means that the specific investment cost is reduced by 10% for each time the worldwide installed capacity doubles [524].

Further uncertainties in the cost projections—for both technologies—might likewise emerge from the hardly predictable PV market which is currently seeing dramatic price drops on a worldwide level due to the high module learning rate. CSP cost reduction potential is lower than PV although higher growth rates for installed capacity have been assumed [451]. The future trend of these technologies will also depend on the storage systems. For now, the development of large PV capacities is restrained by battery storage costs. Li-ions batteries costs is high, as they cannot simply be scaled up and need enhanced safety and reliability, although high learning rates and large research efforts promise a rapid costs reduction [453]. However, CSP thermal storage is already competitive, but the research effort into cost reduction for electrical energy storage is growing at a much faster rate than for TES, so it is logical to expect battery costs to fall more quickly. However, even with declining battery storage prices, CSP thermal storage is likely to remain cheaper due to its long duration while battery degradation is still a severe problem at the moment [453]. Overall, small differences in cost scenarios for PV/PV-BES and CSP/CSP-TES can have a big impact on the projected growth and vice versa.

Given the above, it is possible to envisage one of at least these scenarios playing out in the CSP/CSP-TES and PV/PV-BES market. In the likely cost scenario that PV costs decrease more quickly than in our assumptions, CSP deployment—being expensive—would be pushed even further into the future; or will only be used to cover the peak load reliably at any time by way of cheap thermal storage. However, this scenario is still unlikely, particularly if TES and CSP have gone down in price. On the other hand, if PV and battery storage costs fall rapidly and batteries begin to be used in grid scale plants. CSP with TES may lose its competitive advantage.

However, it is difficult to say at present that these solar systems combining mature and immature production and storage technologies are substitutable, based only on the future trend of cost, since our results have shown that even though for the same design they lead to different patterns of variability and cost due the storage capacity resulting from the fact that CSP-TES is more suited for large-scale plants than PV-BES. Both systems will need to demonstrate high performance in all attributes, sensitivity to clouds/temperature, dispatchability, etc in order to remain attractive and competitive. In case PV-BES and CSP-TES achieve the same performance, they can be perfectly substitutable; and although CSP (resp. BES) may present a higher rental cost it does not necessary mean that the overall cost of the mix becomes more expensive. For instance, the inclusion of CSP-TES or PV-BES technology with high performance in the mix is a way to reduce the total cost and the adequacy risk, although in a stand-alone basis the rental cost of this technology might be higher.

2 Scenarios of Unlimited Thermal and Battery Storage Cost and Capacity

The results obtained in this study are significantly determined by the assumptions regarding the storage capacity and the related costs. In section 1, we present the results of case 1 (Section 1, Chapter 2) where the mean-variance analysis is sensitive to the variance and the storage cost associated with the increase of CSP Solar Multiple (SM) and PV Inverter Loading Ratio (ILR). To examine if the cost and storage capacity of BES and TES make sense in optimal mixes, we run the mean-variance results applying case 2 (Section 2, Chapter 2) in which we remove the substantial part of storage cost and ignore the storage constraints (i.e., the constraints on the volume of storage in MWh and the capacity of storage in MW are not applied in the storage model). Doing so, the optimization problem will only be sensitive to the reduction of the CSP (resp. PV) variance that decreases with the increase of SM (resp. ILR) and to the different rental cost of PV, wind and CSP.

A can be inferred from the comparison of optimal mixes of case 1 (right side of figures 4.1, 4.2) with optimal mixes of case 2 (right side of figure 4.8), the penetration value at the maximum-penetration mix remains unchanged for both cases as all combinations are optimized with the same maximum-budget (2.9). However, the penetration level of the cost-activation mix (i.e., the penetration at which mixes become impacted by cost corresponding to the black dashed vertical line) in case 2 is higher than the one of case 1. Thus, it can be stated that ignoring the cost of TES and BES makes the optimal mixes less sensitive to rental costs and the area of moderate additional costs (before the activation of the total cost constraint) are larger than in case 1. As regards PV, this result is expected, given the wider impact of battery storage cost and low investment cost of PV. In addition, although the cheap CSP thermal storage may have a relatively weaker impact on optimal mixes, but it adds cost to the higher investment cost characterizing the CSP technology.

When it comes to technological distribution, the results show that in scenarios of solar integration with unlimited PV and CSP storage capacity and ignoring the storage cost, PV-BES is preferred at all levels of penetrations (Figure 4.8) and no more CSP-TES capacity would be required. This finding corroborates the finding of Chattopadhyay et al. [126] stating that PV-BES with spinning reserves replaces CSP-TES whatever the level of penetration (if we consider here that unlimited storage capacity is equivalent to ability to provide spinning reserves).

At high penetrations, with the increase of BES capacity, the CSP-TES capacity substitution by PV-BES increases. The obvious reason for this outcome is that the rental cost of PV is lower than that of CSP and larger TES investment costs are higher than those of BES systems (Table 2.6, Chapter 2) due to the larger storage capacity of CSP-TES compared to PV-BES (Table 2.3, Chapter 3).

At low penetrations, adding BES and TES to PV and CSP with unlimited capacity, the systems will be able to store the excess of energy during the day and satisfy the load during night. However, the potential to provide continuous and stable energy production by PV-BES—while also not reaching the maximum budget sooner even the cost constraint is weak here—is higher than CSP-TES because the former is less sensitive to clouds while the diffuse solar irradiance is useless to CSP as it cannot be reflected onto the receiver tube by the concentrator. Thus, the fact that the storage constraints are ignored makes the comparison of CSP-TES and PV-BES equivalent to the comparison of CSP and PV, both without storage (Section iv, Chapter 3), which explain why PV-BES replaces CSP-TES at such low penetrations.

This triggers PV-BES capacity additions when the storage cost and constraints are ignored; or only small amount of TES with CSP (SM2) is targeted at low penetrations. Nevertheless, this finding begins to change with a noticeable integration of CSP-TES with large storage capacities of SM3 (PV-ILR4-wind-CSP-TES SM3 mix, on the left side of figure 4.8j) at low penetrations. In fact, in this case, PV-BES ILR4 and CSP-TES SM3 both have high energy surplus and that both take part in solar generation at low penetrations, although PV-BES remains dominant over CSP-TES. The integration of only small fraction of CSP SM3 compared to PV ILR4 can be explained by the fact that large-scale BES of ILR4 coupled with PV can reach 13.5 hours of storage capacity; while the size of CSP SM3 tank has fewer hours of storage capacity (11 hours), as shown in table 2.3, Chapter 2 (obtained by running the model without storage constraints). Since PV-BES poorer the adequacy risk compared to CSP-TES (Section 3), small CSP-TES is introduced to reduce the PV-BES variability. This confirms our previous conjecture that storage-based CSP plants provide a comparatively better match than PV-BES.

3 Scenarios of High/Low Renewable Penetration-Adequacy Risk-Investment

To achieve large penetration of REs with small investment (in addition to what we found in section 2, Chapter 3), low-cost wind is always preferred instead of expensive PV-BES and CSP/CSP-TES (right side of figures 4.1 and 4.2) due its high mean CF, leading however to curtailment (high adequacy risk) at maximum penetration mix (Section ii) where the fraction of dispatchable solar technologies is zero.

To reduce the adequacy risk and increase the mean penetration (in addition to what we found in section 3, Chapter 3), the results between CSP-TES and PV-BES confirm the interest of increasing the investment budget for CSP-TES plants on basis of their great thermal storage properties than PV-BES (Section iv and ii). PV-BES can be a good option for short-term generation to balance out impacts of clouds and the like; and respond to the demand very quickly. However, if additional BES are installed more than that of TES, PV-BES is preferred. Thus, investment must also be increased to use battery with large storage or/and tracking system to achieve high average capacity credit and high mean CF [201].

In case Morocco is not able to increase the RE budget, and aims to achieve only small penetration level with low variability and low budget allocated to REs, the results at low penetrations (in addition to what we found in section 4, Chapter 3) show that a diversified mix of PV with low storage duration (5 - 9 hours or ILR2, ILR3) with regional complementarity; or relying only on PV-BES are other options for these scenarios (Section iv and 2).

4 Scenarios of Hybrid Solar Systems

These results also allow us to discuss the scenarios of hybrid solar systems. In fact, the costs of generating electricity and the electricity demand are not uniform throughout the day. Thus, the choice of the hybrid system is based on the technologies that requires a moderate cost and produces a higher amount of energy.

→ **CSP-TES with PV:** One operation strategy to reduce the cost and the variability and thus to take advantage of the energy produced by both technologies is to couple the PV with the CSP-TES plant and dispatch the energy by the two systems. For instance, in the morning, when the PV system starts to produce electricity and its energy is large enough to cover the load, the exceed thermal CSP production can be stored or only used to provide the daytime transient needs. In this case, the demand will be satisfied by low cost PV. In the evening, when the PV system cannot deliver the electricity demanded, the CSP uses the energy stored during the day to cover the load throughout the night until the sun rises again. The key of this hybridization is the storage capacity required. If only few hours of storage are needed after sunset (6 hours), CSP-TES with SM2 can meet the demand. If, however, high storage capacity is required (> 6 hours), CSP-TES with SM2 or SM3 allow to dispatch the electricity at any time (Table 2.3 and section 3, Chapter 2).

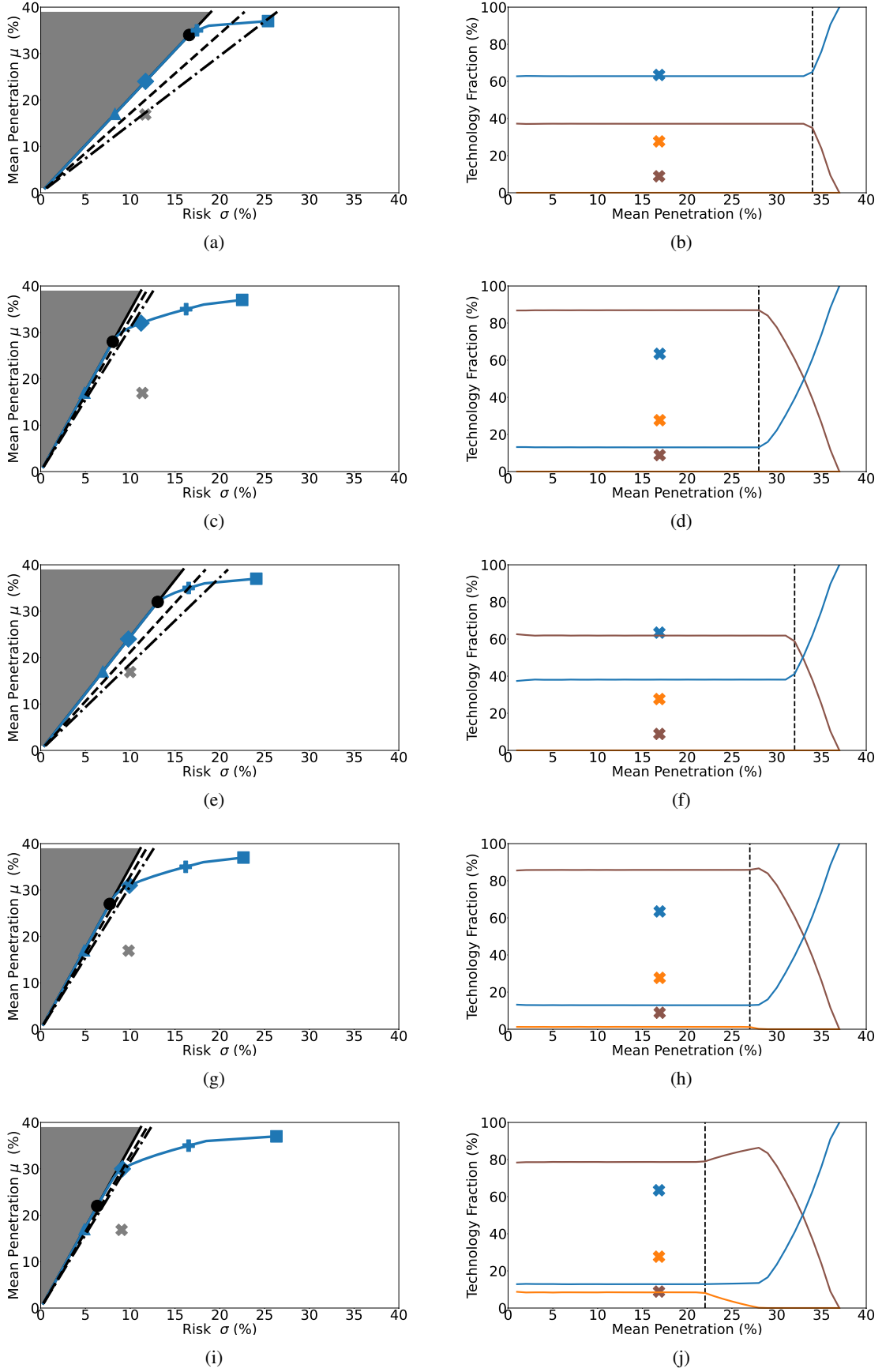


Figure 4.8: Similar to figure 4.1 but for scenarios with unlimited thermal (TES) and battery (BES) storage capacity and cost. (a, b): PV-ILR2-Wind-CSP-SM1; (c, d): PV-ILR4-Wind-CSP-SM1; (e, f): PV-ILR3-Wind-CSP-SM2; (g, h): PV-ILR4-Wind-CSP-SM2; (i, j): PV-ILR4-Wind-CSP-SM3. Solar Multiple of 1 or SM1: Concentrated Solar Power (CSP) without storage; Inverter Loading Ratio or ILR>1 or SM>1: with increasing levels of storage from Photovoltaic (PV) or CSP.

→ **CSP-TES with PV-BES:** Hybrid PV-BES with CSP-TES system may also be a good option in case the demand has irregular profile to arbitrage between the two technologies depending on the storage requirements to provide energy at low cost. For instance, the costs to provide

electricity are usually lower during the daytime hours and thus cost does not matter. Thus, CSP-TES can be turned on to produce electricity with low adequacy risk. In the afternoon and early evening (peak hours), when the electricity demand and costs start to increase, if low/medium (resp. high) amount of storage is needed, CSP-TES (resp. PV-BES) should be turned on. Overall, for more energy and slightly higher cost, we would opt for CSP-TES; for a lower cost and slightly lower amount of energy, we would encourage the choice of PV-BES. This may be particularly advantageous in regions with high solar resources. For instance, if the storage of one solar system is full or empty, the other system can store the surplus or cover the missing load.

→ **PV-CSP:** Hybrid PV-CSP system is not a good option because PV is less variable and less expensive; and thus, PV is preferred whatever the penetration level. Adding CSP will only increase the risk (Section iv, Chapter 3) and the cost.

→ **PV-BES with CSP:** Hybrid PV-BES with CSP system is also not a good option because PV-BES is less variable than CSP although CSP tends to replace some PV-BES capacities at high penetrations due to its lower cost and higher CF but the flexibility would be needed at such high penetrations.

V Summary and Concluding remarks

Motivation

Photovoltaic (PV) coupled with Battery Energy Storage (BES) and Concentrated Solar Power (CSP) combined with Thermal Energy Storage (TES) are both two dispatchable solar technologies that bear many different advantages and disadvantages. Current literature delves into either storage per se or the integration of storage solutions in single Renewable Energy (RE) technology. However, the comparative analysis of each technology within an energy mix based not only on cost but also on the temporal and spatial variability; under different scenarios of penetration and storage requirements remain under-explored.

Research Questions

This study aims to deal with this gap, by means of assessing how two solar technologies, PV and CSP, with different storage duration and rental costs interact with wind in an optimal capacity mix using recent (2013) cost data and under several scenario mixes. We analyze the role of temporal and spatial meteorological patterns as well as the impact of TES and BES associated with these solar technologies in reducing the system variance-based risk. We compare the value that CSP-TES and PV-BES bring to the grid as defined by the capacity credit, mid/base load reduction and curtailment.

Objectives and Methodology

To do, we use hourly climate data provided by Modern-Era Retrospective Analysis for Research and Applications 2 (MERRA-2) climate reanalysis to compute time series of demand, Capacity Factors (CFs) of wind, solar CSP (resp. PV) without and with increasing size of CSP solar field (resp. PV solar panel) relative to a fixed capacity of CSP power block (resp. PV inverter), as measured by the Solar Multiple or SM (resp. Inverter Loading Ratio or ILR). These predictions are then adjusted to energy observations for the four Moroccan electrical zones over the year 2018. For the optimal mix analysis, a Mean-Variance Portfolio approach is adopted with the objective of maximizing the RE production and minimizing its variability while not exceeding the total cost of the actual PV-Wind-CSP-TES mix (with 5.5 hours of TES). We define the rental cost of storage and generation technologies taking their dependence on the storage size into account. We examine the accent conditions required for PV-BES deployment to become more favorable than CSP-TES. By diagnosing the contribution of different RE technologies to the reduction of different load bands, we give an analysis of the services provided by each technology.

General Findings

To summarize, we find that at low penetrations, the optimal mixes satisfy the maximum-cost budget without being constrained by it. More the battery storage combined with PV is large, more PV-BES in CENTER is able to meet the daily and seasonal peak demand and is winning over the low-variance wind of southern regions while CSP capacities without storage are null. When co-locating PV-BES and CSP-TES with the same design, the latter leads to lower variability due to its larger storage capacity. If substantial BES capacity is deployed, more than that of TES, PV-BES is more likely to produce energy at minimum variance which replaces CSP-TES capacities installed in eastern or southern regions.

At high penetrations, mixes are sensitive to cost, the more so as CSP and PV with high amount of energy available for storage are introduced. Therefore, capacities are no longer linearly dependent on the mean penetration. Wind in EAST (resp. SOUTH) constitutes the predominant technology at maximum penetration mix (resp. at penetrations smaller than the maximum) presenting strong mean CF and noticeably lower rental cost while PV-BES has low mean CF and CSP/CSP-TES has high capital cost leading to a downward trend of their fraction with increasing penetration letting the variability increase (i.e., wind curtailment). Since costs matter at such high penetrations, the sizing of BES and TES is critical. That is, for scenarios with low-medium storage duration, ranging from 5 to 13.5 hours, CSP-TES (in CENTER) is preferred while scenarios with longer plant operation favor PV-BES (in EAST/SOUTH) which allows more PV-BES to be added instead to satisfy the high penetration level.

However, in the case of unlimited PV and CSP storage capacity and ignoring storage cost, PV-BES is preferred at low and high penetrations due to its low sensitivity to clouds and low rental cost compared to CSP.

The amount of storage and the associated rental cost are thus a determinant for the technology that should be installed at low and high penetrations. It also impacts the extent to which leveraging weaker correlations between electricity zones and technologies allows for the reduction of the variability of the aggregate RE production with respect to the demand. If regional complementarity and covariances between solar technologies are essential to take into account in the absence or with small amount of storage, the role they play in the optimization is reduced with an increase in the storage sizing since mixes become less diversified.

Drawing from the above, solar technologies seem to beat each other but no technology is winning over the other because for each circumstance, there are various aspects making one of the technology more suitable for a given region. We discuss several crucial elements that should be considering when choosing a solar technology in given RE integration scenario, i.e., PV/CSP technology type, orientation/tracking option, scenarios of storage requirements, penetration and cost.

RCP 8.5 Climate Change Versus Cost Effect on Optimal Scenario Mixes of Variable and Dispatchable Technologies in Morocco: Climate Model Inter-Comparison

Contents

I	Abstract	120
II	Introduction	121
III	Optimization Experiments	123
IV	Results	124
1	RCP 8.5 Climate Change vs. Cost Effect on Optimal Scenario Mixes	124
2	Climate Data Sensitivity and Importance of Intra-daily Fluctuations	126
3	Consistency of Climate Projections and Sources of Uncertainty	130
V	Discussion and Comparison with Existing Studies	140
1	Climate Change Scenarios vs. Cost Reduction	140
2	Uncertainties Associated with Future Energy Mixes	140
3	Options for Climate-Resilient Renewable Mixes	142
4	Regional Effects of Climate Change	143
VI	Summary and Concluding Remarks	144

I Abstract

Motivation

Climate change mitigation plans call for an increase in the use of Renewable Energy (RE) technologies. However, the later are in turn dependent on climate, which could affect the reliability and feasibility of future low-carbon supply systems.

Research Questions

This chapter particularly addresses the impacts that projected climate change will have on the Moroccan mix by the end-21st century (2071-2100) relative to the historical period (1976 - 2005) compared to cost effect by analyzing the interaction between solar technologies—Photovoltaic (PV) and Concentrated Solar Power (CSP) without and with Thermal Energy Storage (TES) of 6 hours (Solar Multiple of 2 or SM2)—with wind, taking into account the strength of both technologies in terms of sensitivity to temperature and solar irradiance taken from the Coupled Model Intercomparison Project Phase 5 (CMIP5).

Objectives and Methodology

To do, we take as objective not only to minimize the variance, but also to maximize the RE penetration at a given cost. Climate data obtained by COordinated Regional climate Downscaling EXperiment (CORDEX) in the Middle East and North Africa (MENA) region "MENA-CORDEX" are used. We perform two Regional Climate Model (RCM) simulations—the version 4 of the Rossby Centre regional Atmospheric model (RCA4) and the version 351 of the Weather Research and Forecasting model (WRF351)—over the study region using boundary conditions from four different Global Climate Models (GCMs)—Centre National de Recherches Météorologiques-Coupled Model (CNRM-CM5), Earth System Model (EC-EARTH), Geophysical Fluid Dynamics Laboratory's Earth System Model (GFDL-ESM2M), Community Climate System Model (CCSM4)—assuming one emission scenario, Representative Concentration Pathways (RCP) 8.5, referred as a very high baseline emission scenario in the absence of policies to combat climate change. The impact of the latter on the mean wind and solar resources and Capacity Factors (CFs) along on the seasonal variability of CFs and demand are assessed, the sensitivity of optimal mixes (technological and geographical distribution of RE capacities) to climate change is analyzed under several scenarios of RE penetration, and the level of consistency in the climate projections and the main sources of uncertainty are examined; keeping the existing capacities and rental costs data.

General Findings

We find that RCP 8.5 climate change is relatively responsible for the variation of optimal mixes at high penetrations, but less so at low penetrations where this unlikely high-risk warming future induces a small changes in the mean and variance of CFs. Overall, the rental cost, storage and spatio-temporal complementarity govern the optimal capacity pathways while RCP 8.5 climate change is only responsible for the technology fraction signal. At maximum penetration, the capacity pathways are more sensitive to rental cost effect than to climate change-related risks, and thus all climate models agree on the technology fraction evolution between the historical and future simulations although non-robust at some specific penetration points due to changes in the mean CFs, but involves non-significant differences. Wind is (resp. PV and CSP are) resilient (resp. sensitive) to RCP 8.5 climate change. At low and high penetrations, the RCM uncertainty prevails more than GCM uncertainty. If high penetrations are targeted, this RCM uncertainty increases more for PV and wind fraction—due to uncertainty in projected global tilted irradiance and wind speed changes—compared to CSP fraction—as all CMIP5 models tends to agree in the projection of temperature increase. At such high penetration scenarios, wind and CSP are (resp. PV is) sensitive (resp. resilient) to RCP 8.5 climate change. If low penetrations are targeted, optimal mixes are not impacted by cost and the RCM uncertainty increases for all technologies. RCA4 simulations driven by different GCMs (CNRM-CM5, EC-EARTH, GFDL-ESM2M) are largely consistent in the projected changes in optimal mixes expecting a moderate increase in wind and CSP share, and a decrease in PV share. However, these projections are still fairly inconsistent with WRF351 regional model forced by another GCM (CCSM4), expecting an increase in PV and a decline in wind and CSP shares. We also show that the surface temperature, solar irradiance and wind speed impact the solar and wind mean CFs and the regional patterns, but that is the seasonal correlation of CFs with the summer peak demand that governs the technological distribution in the mix. Overall, there is a low confidence in projected changes of resources between CMIP5 models, used in this study, which limit the ability to draw conclusions about what will happen in future optimal mixes with low proportions of REs since results are not only associated with model uncertainty but also uncertainty related to forcing conditions and to the natural internal variability of the climate system. We discuss, however, the conditions for climate-resilient RE mixes. We also show that the clearness index and wind speed parametrization—included in the CF models to take into account the intra-daily fluctuations of PV, CSP and wind CFs not resolved by daily CORDEX climate data, keeping a daily record of the temperature—may also be responsible for the largest uncertainties in the mean-variance results, whatever the penetration scenario, compared to hourly simulations from the Modern-Era Retrospective Analysis for Research and Applications 2 (MERRA-2) climate reanalysis. The fraction of CSP with small amount of thermal storage decreases whatever the model and the penetration scenario and thus large storage (more than 17 hours per day on average or $SM > 4$) is needed if CSP-TES is considered in future optimal mixes. At high penetrations, the geographical distribution of PV and CSP/CSP-TES is sensitive to changes in climate with high climate-sensitivity models while that of wind is only sensitive to climate data sources at maximum-penetration mix. At low penetrations, the geographical distribution of wind and solar technologies are neither altered by climate change nor by climate data sources.

II Introduction

Motivation

In light of recent cost reductions, Renewable Energies (REs) have a large part to play in the decarbonization of the energy system [183, 339]. However, components of the energy system such as energy demand, solar and wind supply systems are themselves subject to climate change impacts via long-term increase or decrease in the mean and variability of a range of climatic parameters, which erate significant variations in the amount of solar and wind energy produced in a certain area to satisfy the future demand [140].

Scientific literature indicates that ongoing climate change, particularly when reaching levels beyond 2°C , will have severe consequences [198, 257]. Particularly, the effect of climate change is more and more present in Morocco as it is affected by the increasing average temperatures and changing rainfall patterns, widening the gap between demand and supply [199]. Ait Brahim et al. [110] and Driouech et al. [170] show that the humid climate in Morocco disappears gradually and the arid climate is gaining ground even in the North of the country by the late 21st century.

Therefore, in order to be prepared for future warming climate beyond 2°C , long-term system planning based on energy scenario mixes from numerical optimization models should account for climate change induced alterations on resources and their implications on Capacity Factors (CFs) and demand.

Existing Research

Initial studies on climate change topic addressed its effects from demand perspective [166, 187] (in Europe [543] particularly in Mediterranean climate [561, 410], Australia [510], California [82], Ontario [92], Algeria [213]), but there are growing number of studies analyzing impacts on transmission lines [131, 449] as well as other areas along the value chain of the energy sector [181, 171]. For instance, on RE-based electricity system [310, 95] or on electricity market [351, 125] by highlighting some options for climate risk management and adaptation [212, 122] including the economic impacts [70] (i.e., on levelized cost of electricity [138]) to build a resilient power sector [346, 516, 519]. Patt et al. [404, 405] review the potential vulnerability of solar energy systems to future extreme events risks. Nahmmacher et al. [373] analyze how different power design strategies are able to deal with shocks on the European power system, such as heat waves or periods of low wind production. Grant et al. [224] analyze the role of government and donors to address climate related issues.

Various studies [207, 488] examine the RE resource or/and generation changes projected by climate models in different regions of the world (i.e., Europe [136, 535], Mediterranean islands [531] and adjacent regions [234, 402], United States-US- [248, 59], Southern Africa [192]). We note that the impacts of gradual changes of warming and precipitation trends have been studied [60, 491] more than changes in extreme weather events [134, 301, 342]—as existing tools have limited ability to capture extreme events [140]—to identify vulnerable areas of heatwaves and droughts over the Mediterranean [173] and assess their impacts on economic growth in Africa [388].

Some studies provide a specific estimate for the impact of climate change particularly on the RE technologies currently in use such as wind [226, 429] mainly in Europe [448, 358, 124] (i.e., Spain [489]), China [127], UK [513], California [437], US [114, 476] and Brazil [325] by highlighting the limitations of climate projections when reproducing wind speeds distribution and directional wind changes [428].

Other focus on solar Photovoltaic (PV) based on the Coupled ocean–atmosphere Model Intercomparison Project Phase 5 (CMIP5) projections [551] or other models in Europe [276, 197], Mediterranean countries [408, 400] and Africa [94, 83]; assessing the related uncertainty in projections [511].

To date, with the noticeable exception of Ref [550], no study has been conducted to examine the impact on Concentrated Solar Power (CSP) generation. Crook et al. [141] examine how projected changes in temperature and solar irradiance over the 21st century will affect PV and CSP using projections from the coupled ocean-atmosphere, Hadley Centre Global Environment Model (HadGEM1 and HadGEM3), under

the Intergovernmental Panel on Climate Change (IPCC) Special Report on Emissions Scenarios (SRES) A1B scenario which describes a future world of rapid economic growth with a balanced use of renewable and fossil fuel generation. François et al. [203] analyze the impact of climate change on combined solar and run-of-river in Northern Italy.

This research gap on climate change on CSP had been filled by examining the vulnerability of the solar resources [79, 555, 444] in the tropical regions [546] (i.e., Nigeria [389], Burundi [315] or Iberian peninsula [217]), United Kingdom-UK- [118], United States-US- [231, 143] and Europe [78, 463]. Research studies tend to focus on the sensitivity of solar irradiance to clouds and aerosols [493, 278] in the Euro-Mediterranean area [275, 233], Europe [416] and in Asian countries [54]. Other variables that can affect solar generation such as dust are usually mentioned but seldom quantified, which may lead to an underestimation of their importance [514, 334, 145]. Water is a key variable, as its availability not only affects the hydroelectric plants, but also any generation plant that depends on water for cooling including thermal generation [306] such as CSP cooling [563] or carbon capture and storage [120].

To simulate the response of the global climate system to increasing greenhouse gas concentrations, numerical models (Global Climate Models or GCMs) representing physical processes in the atmosphere, ocean, cryosphere and land surface are the most advanced tools currently available. The low resolution of GCMs, however, limits a precise assessment at a regional scale. A better assessment requires the use of Regional Climate Models (RCMs), which provide a higher spatial and temporal resolution, and thus a better representation of the topography, coastline, and small scale processes through the use of parametrization schemes [219, 236]. Projections for impacts on the resources and production technologies using climate models are more varied. Key uncertainties between climate projections remain due to the modeling limitations and the variation between RCMs or GCMs used as boundary conditions for RCMs or uncertainties related to the emission scenario or to the natural internal variations [249]. Cronin et al. [140] address which areas does the literature largely agree on, the direction and magnitude of the impacts and which elements and regions are not well covered in the literature. To assess the uncertainties of the models, researchers have developed projects to compare the outputs of different models, namely the CMIP5 [506] which provides GCM outputs to drive different RCMs in the context of the COordinated Regional climate Downscaling EXperiment (CORDEX) project. Currently, the CMIP is in its sixth phase (CMIP6) [235]. Woldemeskel et al. [558] indicate a visible reduction in the uncertainty of CMIP5 precipitation relative to its predecessor (CMIP3) but no significant change for temperature. Scenarios for the future in CMIP3 and CMIP5 are remarkably similar [305], confirming that even though more and more complex models are used we can have some confidence with the results.

Besides the climate models, climate change scenarios rely on emission scenarios which estimate the amount of carbon dioxide (CO_2) and other greenhouse gases launched to the atmosphere at each of the GCM cells. In the Fourth Assessment Report (AR4), the IPCC considered the SRES with a sequential approach [374] while the 2013 IPCC report (AR5) [499] rely on new emission scenarios, Representative Concentration Pathways (RCP), ranging from 2.6 to 8.5 W/m^2 of radiative forcing with a parallel approach [534, 366] (Section ii, Chapter 2). Strandberg et al. [500] perform CORDEX scenarios for Europe from the Rossby Centre regional Atmospheric model (RCA4) under RCP 4.5 and RCP 8.5 to assess the impact on climate variables relevant for PV, CSP and wind. Other studies use these scenarios to assess the impacts on air quality [285] or on wave energy resource in the Mediterranean coast of Morocco [481]. Recent studies conducting assessments of future climate change impacts have focused on RCP 8.5 warming scenario as it is in close agreement with both historical total cumulative CO_2 emissions and anticipated outcomes of current global climate policies [472]. Schlott et al. [469] apply a detailed greenfield power system (i.e., the capacity mix in each year is built without consideration of existing capacities from preceding years) using an investment model to derive the cost-optimal European wind, solar and hydro capacities and transmission lines. Wohland et al. [557] and Weber et al. [539] focus on back-up energy requirements in the European electricity system associated with wind induced climate change impacts. Peter et al. [411] assess the impacts of this drastic climate change on the European electricity systems—considering changes in wind and solar resources, hydro power, cooling water availability for thermo-electric generation and electricity demand—and assess the welfare gained by applying a system design strategy with climate change anticipation.

The focus of the great majority of studies is on the future climate change impacts. However, some studies focus also on climate variability [494]. Nabat et al. [371] evaluate the direct and indirect effect of aerosols on solar irradiance variability in the Mediterranean. Tantet et al. [504] use the mean-variance analysis to derive regional mixes based on PV and wind accounting explicitly for climate variability in Italy.

Knowledge Gap

As can be inferred from the above-mentioned publications is that climate change impact studies on solar PV and wind dominate the literature mainly due to their rapid growth [446]. However, the existing literature includes a relatively little discussion of the impacts on technologies which may become important in the future (e.g. bio-energy or CSP). Particularly, to our knowledge, only Ref [550] and [141] that assess the climate change impacts on CSP, likely due to their low market share [446] and to the challenges involved in modeling aerosols and cloud cover changes at the necessary spatial scales.

Particularly, in Morocco, most of the existing literature on the climate change topic focus on the past and future changes of temperature and precipitation to assess the impacts on water resources as well as threats to agricultural production and biodiversity [61, 43, 396]. Studies such as [436, 128] analyze the environmental impacts of RE following the actual and projected Moroccan strategies (up to 2030) and investigate how different actions could affect the energy demand, the electricity generation and emissions within the system. Suphachalasai et al. [501] show that Morocco has made significant progress on the implementation of its energy strategy. The effort has so far resulted in electricity demand saving, more RE generation and significant emissions reductions.

However, yet to date there are no studies that have examined the interplay between variable (PV, CSP, wind) and dispatchable solar technologies such as CSP with thermal energy storage (TES) in prospective energy mixes under climate change scenarios, let alone the impact on PV-wind mix in the Mediterranean region but the analysis of storage impact is lacking and analysis at large spatial scale are less effective for system planning [200].

Originality of this Study and Implications

Our contribution with respect to the existing literature is to compare the impact of cost and climate change on optimal mixes; and to understand the factors that are responsible for the changes in the technological and geographical distribution of capacities of different RE combinations under different penetration scenarios, including the main sources of uncertainty in the climate model projections. We also highlight features that characterize the climate variables of relevance for CSP and PV across different zones in Morocco; and discuss options for climate-resilient RE mixes, particularly the potential ability of tracked CSP with small storage capacity to strengthen the resilience of the energy mix.

In fact, current and future large-scale plants represent a considerable investment, so understanding likely impacts from climate change will guide the choice of the technology that should be installed for given circumstance (i.e., either reducing the variability, or increasing the penetration while satisfying the economic constraints), especially that the energy strategy [104] does not specify the optimal proportions between PV and CSP/CSP-TES in the future mix (Section 2, Chapter 1).

Research Questions

This chapter addresses the third research question of this thesis (**Q3**) (Section 3, Chapter 1), in which we aim to examine, under different penetration scenarios, the following research questions:

- **Q3-1:** What is the impact of climate change on the Moroccan optimal mixes, considering the severe “business-as-usual” RCP 8.5 scenario, in which no efforts to cut greenhouse gas emissions are made? Optimal mixes (i.e., technology fraction and capacity pathways) are more sensitive to climate change or to cost (i.e., in the context of vulnerability of low-carbon technologies to climate change vs. eventual cost reductions)?
- **Q3-2:** Intra-daily fluctuations have substantial impact on optimal mixes (i.e., capacity allocation or pathways)?
- **Q3-3:** Which technology is sensitive or resilient to climate change? What are the conditions for climate-resilient RE mixes? What are the main sources of uncertainty in future RE mixes? Thermal storage makes CSP resilient to climate change? Does RCP 8.5 climate change impacts the geographical distribution of RE capacities?

Objectives and Methodology

We take as objectives both to maximize the mean of the total RE production and to minimize the variance of the latter while not exceeding the maximum-cost budget (2.8). In this chapter, we expand the study done in chapter 3 in future warming climate—using 21st century regional projections and keeping the existing generation assets (Table 2.1, Chapter 2) and current rental costs (Table 2.5, Chapter 2)—, now focusing on the impact of climate change on optimal mixes considering the difference between PV and CSP/CSP-TES in terms of sensitivity to temperature and solar irradiance (i.e., clouds and aerosols) rather than the sensitivity of the optimal mixes to rental cost and storage. To compute the effect of low-frequency variability and climate change on optimal mixes, we have to estimate historical/future changes in demand, solar PV, CSP and wind CFs and related climate quantities. To do, we can obviously no longer use actual climate observations provided by the Modern-Era Retrospective Analysis for Research and Applications 2 (MERRA-2) reanalysis, but have to rely on projections from climate models together with historical simulations to reproduce the characteristics of CFs and demand based on long time series typically of the range of 30 years, which corresponds to the climatological scale and to the technical lifetime of solar and wind plants. Projected climate data was obtained from the CMIP5 climate models under one forcing scenario—the IPCC RCP 8.5 scenario. The selection of CORDEX data was in a way to cover the whole Morocco which is provided by CORDEX in the Middle East and North Africa (MENA) domain. The data consists of daily series of climate parameters. We parametrize the solar and wind intraday fluctuations not resolved by CORDEX keeping a daily record of the temperature. The model derives the long-term evolution of optimal capacity mixes from 2071 until the year 2100 (future climate projections) and compare it with the power system optimized based on historical period (1976 – 2005). We also analyze the seasonal variability of CFs and demand, the change of the mean resources and their implications on the mean CFs. To assess the consistency of the projections amongst the various model predictions, two RCMs are used to downscale four GCMs.

Outline

The climate data, the scenario framework and the assumptions made are described in section 2 and section 3 (Chapter 2). The RE combinations considered in this study are described in section III;

The general analysis of the optimal mixes, under different RE penetration scenarios, based on historical climate conditions and the projected future changes towards the end of century are presented in section IV. Section 1 highlights the common features between CORDEX-CMIP5 models. We examine the sensitivity of optimal mixes to RCP 8.5 climate change and if this worst carbon emissions pathway is altering optimal mixes (i.e., technology fraction and capacity pathways) more than rental cost. Section 2 analyzes the properties of the mixes in terms of weight given to each technology compared to hourly simulations from MERRA-2 climate reanalysis and highlights the importance of taking into account intra-daily fluctuations on optimal mixes (i.e., capacity allocation or pathways). A brief analysis of the robustness of the numerical results on the response to climate change along with the sources of uncertainty is presented in section 3. We examine the seasonal response of CFs and demand to climate change; the change in the mean resources and mean CFs and their implications on the technological and spatial distribution of capacities. Section V discusses the results, i.e., the vulnerability of low-carbon technologies to climate change scenarios versus the eventual cost reduction of these technologies; the uncertainty associated with future RE mixes together with the influence of different options in reducing the climate sensitivity and the regional effects of climate change. Section VI concludes the study.

At the time of this writing, this chapter has not been submitted or published (Appendix B).

III Optimization Experiments

All Renewable Energies (REs) are vulnerable to climate change [326] but they are impacted differently. Therefore, the scale of future climate change and its impacts will depend on the combination of technological solutions.

It is very likely that Photovoltaic (PV) and wind power will be of major importance for the future electricity supply [66]. Therefore, as reference, we consider that only PV without storage (Inverter Loading Ratio of 1 or ILR1) and wind are integrated into the electrical grid to meet the demand ("**PV ILR1-wind mix**").

Concentrated Solar Power (CSP) technologies will also earn great growth in the future [169, 133]. However, PV and CSP may have different response to climate change. In fact, CSP output has an approximately linear response to ambient temperature with a positive dependency, namely an increase with increasing ambient temperatures, and an approximately proportional response to direct irradiance (Section 1, Appendix A). PV output has a linear response to solar panel temperature with a negative gradient, and an approximately proportional response to total irradiance except under low levels (Equation A.64, Appendix A). Therefore, the future change in temperature and solar irradiance (i.e., clouds and aerosols) are crucial for estimating the expected changes in PV and CSP Capacity Factors (CFs) [141], and thus may affect the optimal mixes in different ways. As previously mentioned, the strong sensitivity of surface solar irradiance to aerosol–cloud interactions [275], which also impact the surface temperature [416], have been studied more than changes in CSP output. Thus, in this study, PV and CSP without storage (Solar Multiple of 1 or SM1) are integrated with wind ("**PV ILR1-wind-CSP SM1 mix**") to examine their interaction in optimal mixes.

Results obtained in section iv (Chapter 3) have shown that the storage reduces the adequacy risk with stronger impact from CSP with Thermal Energy Storage (TES) than PV with Battery Energy Storage (BES) (Section iv and ii, Chapter 4). Thus, thermal storage combined with CSP may enhance the resilience of the mix to climate change and it is expected in energy transition from fossil fuels to REs [290], particularly as climate change brings more extreme weather events and greater potential for loss of power. Thus, to illustrate the role of storage

in future warming climate, we also consider "PV ILR1-wind-CSP-TES SM2 mix" with the most widely storage configuration (6 hours of TES).

All combinations are optimized using the same value, C_{tot}^{obs} , i.e. 3.5 G€/yr corresponding to the PV ILR1-Wind-CSP-TES combination (with 5.5 hours of TES or $SM^{ref} = 1.87$) (Section 1, Chapter 2).

IV Results

In this section, based on the introduced modeling framework, we assess the robustness of four COordinated Regional climate Downscaling EXperiment-Coupled Model Intercomparison Project Phase 5 (CORDEX-CMIP5) climate model projections on the climate variables of relevance for demand patterns, solar Photovoltaic (PV), Concentrated Solar Power (CSP) and wind production; to examine how Representative Concentration Pathways (RCP) 8.5 climate change is likely to alter the Moroccan optimal mix (i.e., technological and geographical distribution of capacities) by the late 21st century compared to cost effect; and explore which technology is sensitive or resilient to climate change and the main sources of uncertainty in future energy mixes, under different penetration scenarios. Similar features generated from the CORDEX-CMIP5 climate models, such as the impact of the choice of the climate data (i.e., CORDEX vs. the Modern-Era Retrospective Analysis for Research and Applications 2 or MERRA-2) on the optimization problem, is highlighted together with the importance of correctly estimating the intra-daily fluctuations of demand and Capacity Factors (CFs).

It should be noted that the simulation results of this study are obtained by running the mean-variance analysis using case 1 (Section 1, Chapter 2) in which the thermal storage cost depends on the constraints of storage.

1 RCP 8.5 Climate Change vs. Cost Effect on Optimal Scenario Mixes

The share of Photovoltaic (PV) without storage (brown)—means with an Inverter Loading Ratio of 1 or ILR1—, wind (blue), Concentrated Solar Power (CSP) without storage (orange)—means with Solar Multiple of 1 or SM1—, and CSP with 6 hours per day on average of Thermal Energy Storage (TES) or SM2 (orange), obtained from hourly CORDEX-CMIP5 data with intra-daily parametrization, versus the mean penetration (2.1) for the global strategy (2.2) with total cost constraint (2.8) of the PV ILR1-wind mix (top), PV ILR1-wind-CSP SM1 mix (middle) and PV ILR1-wind-CSP-TES SM2 mix (bottom) are represented in figures 5.1 and 5.2. These simulations are obtained using four coupled atmosphere-ocean Global Climate Models (GCMs)—Centre National de Recherches Météorologiques-Coupled Model (CNRM-CM5), Earth System Model (EC-EARTH), Geophysical Fluid Dynamics Laboratory's Earth System Model (GFDL-ESM2M), Community Climate System Model (CCSM4)—to provide boundary conditions to two Regional Climate Models (RCMs)—the version 4 of the Rossby Centre regional Atmospheric model (RCA4) and the version 351 of the Weather Research and Forecasting model (WRF351)—assuming RCP 8.5 scenario. The name of each climate model is hereafter referred as GCM + RCM: CNRM-CM5 + RCA4 (left panels of figure 5.1); EC-EARTH + RCA4 (right panels of figure 5.1); GFDL-ESM2M + RCA4 (left panels of figure 5.2); and CCSM4 + WRF351 (right panels of figure 5.2). The climate change impact on optimal mixes can be examined by comparing the two experiments: the solid lines corresponding to the historical period (1976 – 2005) and the dotted lines corresponding to the future period (2071 – 2100).

The optimization ratios (Section IX, Chapter 2) are also computed for each technology to examine the impact of climate change on the technological and geographical distribution. The minimum-variance ratio determines the technology that should be installed at low penetrations (Table 5.1); while the second ratio at high penetrations (Table 5.2) ; and the maximum-penetration ratio at maximum-penetration mix (Table 5.3). Changes of these ratios projected to the end of this century compared to the historical period, by each CORDEX-CMIP5 climate model, is represented as "historical - future period".

To illustrate the technology trend obtained by each CORDEX-CMIP5 model, we compute the relative change of mean Capacity Factors (CFs) (Figure 5.3) and of their variance (Figure 5.4) depicted as bar plots of wind (blue), CSP SM1 (tan), CSP-TES SM2 (orange) and PV ILR1 (brown). The relative change of mean (resp. variance) CFs—expressed in % and expected by the end of the century—is computed as the difference between the mean (resp. variance) of the time series over the future period (2071-2100) and the mean (resp. variance) value in the historical period (1976 – 2005) divided by the climatological average (resp. variance) of this historical period considered as reference.

Sensitivity to Cost

For all combinations, climate models and experiments, as the global constrained and unconstrained fronts diverge from each other (not shown here), as a result of the increasingly strong total cost constraint for larger penetrations, the technology fractions are no longer constant function of the mean penetration (right side of the panels of figures 5.1 and 5.2). However, at relatively low penetrations, the mixes minimizing the variance are not constrained by the maximum-cost constraint and the fraction of the different technologies in the mix is nearly independent of the penetration (left side of the panels of figures 5.1 and 5.2). The point at which the technology fractions start to diverge corresponds to the optimal mix for which the total cost constraint becomes active (i.e., the largest penetration at which the constrained and unconstrained fronts join) and beyond which the optimal fronts are shifted towards higher risk values. The sensitivity of optimal mixes to rental cost is only briefly reported, here, as it is already discussed in section 1 (Chapter 3) or section 1 (Chapter 4).

What is the impact of RCP 8.5 climate change on the Moroccan optimal mixes?

With reference to figures 5.1 and 5.2, it is clearly noticeable that more the penetration is increased, more the difference between historical (solid) and future (dotted) curves is large whatever the combination and the climate model. It is, thus, clear that the RCP 8.5 climate change has a large impact on the optimal mixes at high penetrations where the climate change induces a change in the mean CFs (a reduction or an increase as shown in figure 5.3 or at the maximum penetration point represented on the right side of figures 5.1 and 5.2) and to some extent a changes in the correlations between technologies and regions (not shown here). This is reflected by the relatively greater change in the maximum-penetration ratio (Table 5.3) and in the second ratio (Table 5.2) between the value obtained over the historical period (left) and the one obtained over the future period (right).

At low penetrations, where the mean CF and variance matter (Section 3, Chapter 2), the technology fractions are relatively close between the two experiments for all combinations and climate models (solid and dotted lines on the left side of figures 5.1 and 5.2). Therefore, the change unveil negligible variations and thus mixes are less sensitive to climate change at such penetrations. This suggest that the CFs and the variances may increase in some regions and decrease in others (Figure 5.3, 5.4), but the minimum-variance ratios generally increase or remain constant between the two experiments (Table 5.1). Thus, the aggregated changes do not seem to endanger the variability and the variance tend to scale with the mean at low penetrations.

→ These findings suggest that in general the future optimal Renewable Energy (RE) mixes are resilient to RCP 8.5 climate change if low penetrations are targeted, but less true for high penetration scenarios.

Optimal mixes (i.e., technology fraction and capacity pathways) are more sensitive to climate change or to cost (i.e., in the context of vulnerability of low-carbon technologies to climate change vs. eventual cost reductions)?

As inferred from projections of the four CMIP5 models, the severe “business-as-usual” RCP 8.5 scenario, in which no efforts to cut greenhouse gas emissions are made, energy systems based on wind, PV, and CSP SM1 or CSP-TES SM2 with greater penetration of RE seem to be more subject to climate-induced alterations (compare the solid and dotted lines on the right side of figures 5.1 and 5.2) and optimal mixes are highly sensitive to rental cost (Section 1 and 2, Chapter 2); while at low penetrations, all the systems are resilient to the effect of climate warming (compare the solid and dotted lines on the left side of figures 5.1 and 5.2) and not impacted by costs (Section 3, Chapter 2).

→ All in all, the influence of the cost on optimal mixes prevails more than climate change as the latter affects only the signal of technology fraction (either increase or decrease, in the future mix, according to the climate model, as discussed in section 3); while the former changes completely the capacity pathways (see discussion on climate change scenarios vs. cost reduction in section 1).

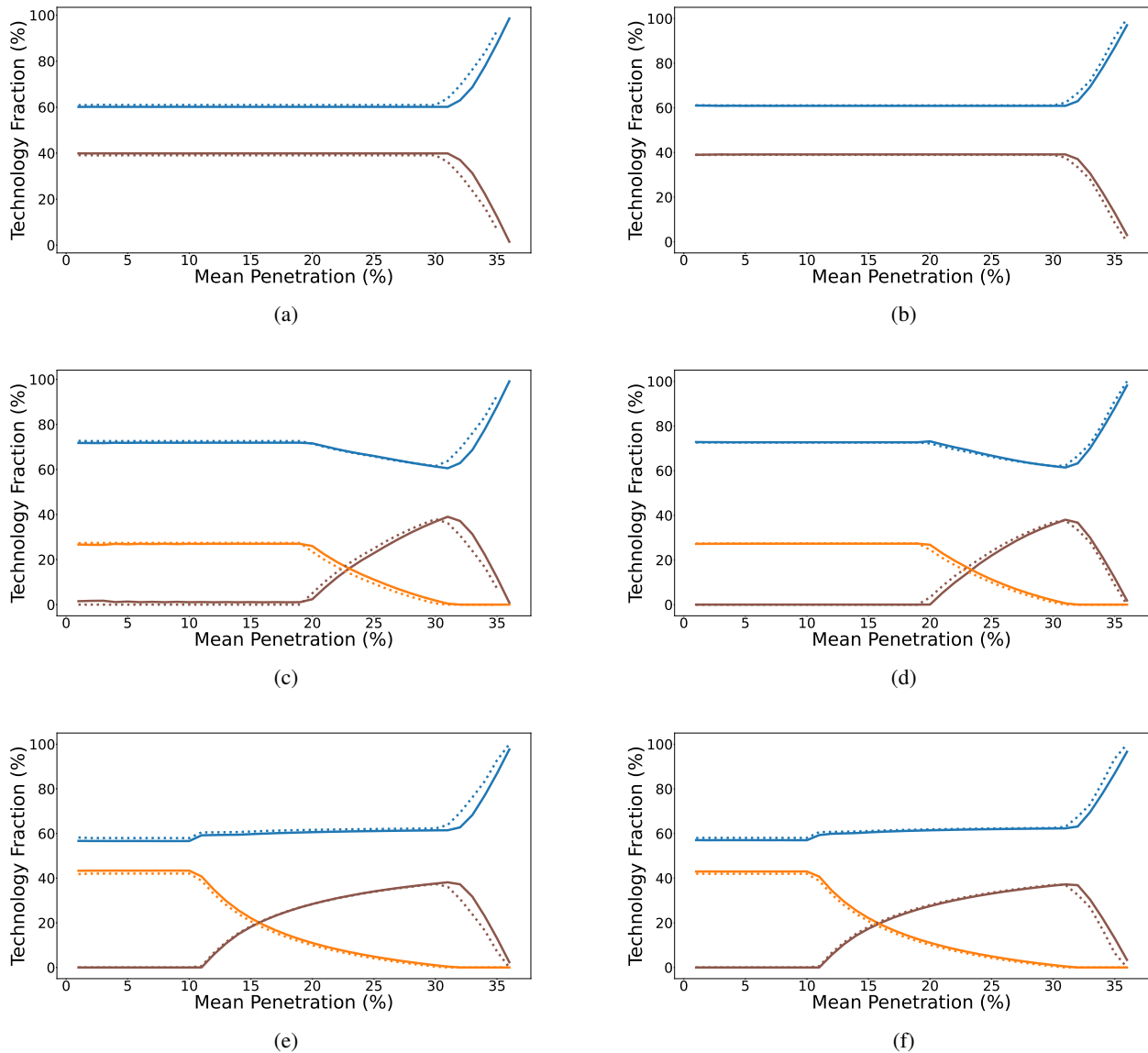


Figure 5.1: Shares of wind (blue), Photovoltaic (PV) with an Inverter Loading Ratio of 1 or ILR1 (brown), Concentrated Solar Power (CSP) with Solar Multiple of 1 or SM1, and CSP with SM2 (orange) capacities versus the mean penetration (2.1), μ , for the global strategy (2.2) with maximum-cost constraint (2.8) obtained from hourly COordinated Regional climate Downscaling EXperiment-Coupled Model Intercomparison Project Phase 5 (CORDEX-CMIP5) climate data (with intra-daily parametrization) illustrating the optimal mixes changes projected to the end of this century, 2071-2100 (dotted line), versus historical period, 1976-2005 (solid line), obtained by one Regional Climate Model (RCM), the version 4 of the Rossby Centre regional Atmospheric model (RCA4), driven by two Global Climate Models (GCMs): Centre National de Recherches Météorologiques-Coupled Model (CNRM-CM5), Earth System Model (EC-EARTH). The name of each climate model is hereafter referred as GCM + RCM. **Left:** CNRM-CM5 + RCA4 model; **Right:** EC-EARTH + RCA4 model. **Top:** PV ILR1-Wind; **Middle:** PV ILR1-Wind-CSP SM1; **Bottom:** PV ILR1-Wind-CSP-TES SM2. ILR1 or SM1: without storage; SM2: with 6 hours of Thermal Energy Storage (TES). To be compared with figure 5.2.

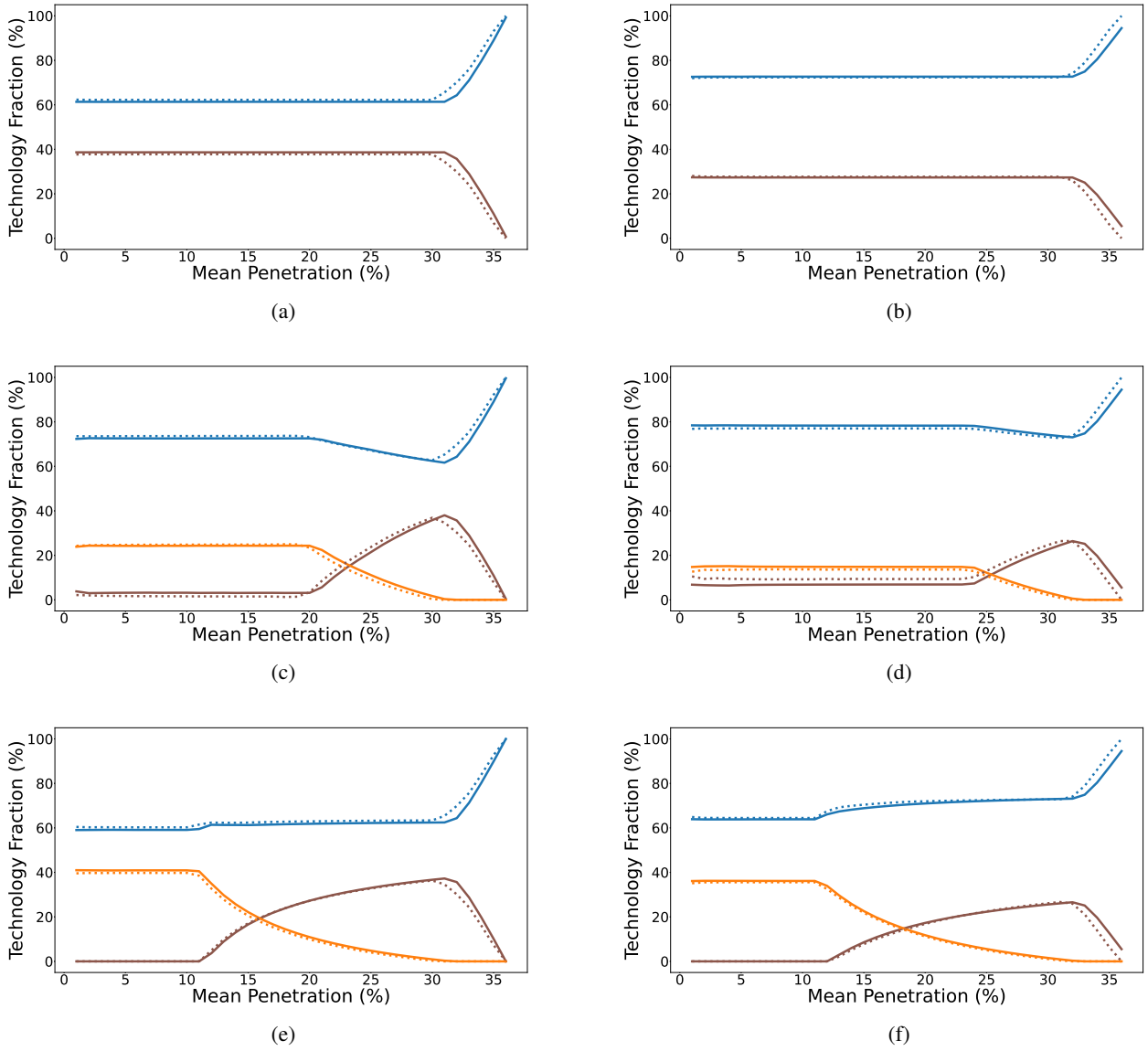


Figure 5.2: Similar to figure 5.1 but for the two remaining COordinated Regional climate Downscaling EXperiment-Coupled Model Inter-comparison Project Phase 5 (CORDEX-CMIP5) models: the version 4 of the Rossby Centre regional Atmospheric model (RCA4) is forced by the Geophysical Fluid Dynamics Laboratory’s Earth System Model (GFDL-ESM2M); and the version 351 of the Weather Research and Forecasting model (WRF351) is forced by the Community Climate System Model (CCSM4). The name of each climate model is hereafter referred as Global Climate Model (GCM) + Regional Climate Model (RCM). **Left:** GFDL-ESM2M + RCA4 model; **Right:** CCSM4 + WRF351 model.

2 Climate Data Sensitivity and Importance of Intra-daily Fluctuations

In this section, we focus on analyzing the capacity pathways, under penetration scenarios, by drawing insight on the climate data sensitivity.

For all CMIP5 climate models and focusing on the low values of the penetration (left side of figures 5.1 and 5.2), the composition of the mixes over 30 years of the historical (solid line) and future (dotted line) time period obtained by hourly CORDEX data with intra-daily wind and solar parametrization remain similar to that obtained from hourly MERRA-2 climate reanalysis over one year, 2018, (Figure 3.1b for PV-wind mix; figure 3.1d for PV-wind-CSP SM1 mix; and figure 3.1f for PV-wind-CSP-TES SM2 mix, Chapter 3) with the only exception of PV ILR1-wind-CSP SM1 mix (Figure 3.1d, Chapter 3) at such **low penetrations**, as will be explained in the following paragraphs.

Wind vs. PV ILR1 or CSP SM1/CSP-TES SM2

As can be seen, at low penetrations (left side of top, middle and bottom panels of figures 5.1 and 5.2), wind dominates over PV ILR1 and over CSP without or with small amount of storage. This can be explained by the fact that wind minimum-variance ratio is larger than that of PV ILR1 and CSP SM1/CSP-TES SM2, whatever the climate model and experiment (Table 5.1).

CSP-TES SM2 vs. PV ILR1

When CSP-TES is introduced instead of CSP alone (left side of bottom panels of figures 5.1 and 5.2), the share of CSP-TES is nearly identical to that of wind, while PV ILR1 capacities are zero. This can be understood from the fact that the CSP-TES minimum-variance ratio is larger than that of PV ILR1 whatever the model and experiment (Table 5.1), thanks to the reduction of variance of the CSP CFs associated with the introduction of thermal storage.

CSP SM1 vs. PV ILR1: Uncertainty related to Solar Parametrization

In this study, CSP without storage also dominates over PV without storage (left side of middle panels of figures 5.1 and 5.2) although the

Table 5.1: Minimum-variance ratios (10^3 MW) given by (2.22) obtained from COordinated Regional climate Downscaling EXperiment-Coupled Model Intercomparison Project Phase 5 (CORDEX-CMIP5) models: two Regional Climate Model (RCM) simulations—the version 4 of the Rossby Centre regional Atmospheric model (RCA4) and the version 351 of the Weather Research and Forecasting model (WRF351)—over the study region using boundary conditions from four different Global Climate Models (GCMs)—Centre National de Recherches Météorologiques-Coupled Model (CNRM-CM5), Earth System Model (EC-EARTH), Geophysical Fluid Dynamics Laboratory’s Earth System Model (GFDL-ESM2M), Community Climate System Model (CCSM4). The name of each climate model is hereafter referred as GCM + RCM. The values correspond to the historical period (1976 -2005) - future period (2071-2100). Inverter Loading Ratio or Solar Multiple of 1 (ILR1 or SM1): without storage; SM2: with 6 hours of Thermal Energy Storage (TES).

Zones	Wind	PV (ILR1)	CSP	
			SM1	SM2
NORTH	9.47 - 9.88	12.17 - 12.6	6.70-7.10	11.50-12.10
CENTER	12.36 - 14.07	12.29- 12.75	6.38-6.59	13.88 - 14.10
EAST	10.49 - 11.18	11.81 - 12.24	7.75-7.97	16.91-17.07
SOUTH	18.9 - 19.57	10.80 - 11.36	6.61-6.93	15.11 - 15.26

(a) CNRM-CM5 + RCA4 model

Zones	Wind	PV (ILR1)	CSP	
			SM1	SM2
NORTH	9.06 - 9.37	12.07 - 12.59	6.89 - 7.26	12.02 - 12.6
CENTER	11.34 - 12.84	12.25 - 12.87	6.41 - 6.68	13.94 - 14.3
EAST	10.39 - 11.18	11.71 - 12.27	7.78 - 8.06	16.99 - 17.34
SOUTH	18.12 - 19.36	10.79 - 11.47	6.77 - 7.17	15.23 - 15.46

(b) EC-EARTH + RCA4 model

Zones	Wind	PV (ILR1)	CSP	
			SM1	SM2
NORTH	10.15 - 10.72	12.18 - 12.77	6.70 - 7.14	11.07 - 11.74
CENTER	12.81 - 15.08	12.19 - 12.82	6.27 - 6.54	13.23 - 13.69
EAST	11.68 - 13.11	11.75 - 12.29	7.63 - 7.87	16.13 - 16.48
SOUTH	17.85 - 19.24	10.83 - 11.6	6.53 - 6.92	14.29 - 14.7

(c) GFDL-ESM2M + RCA4 model

Zones	Wind	PV (ILR1)	CSP	
			SM1	SM2
NORTH	14.60 - 14.8	11.60 - 12.02	7.30 - 7.52	16.18 - 16.22
CENTER	21.44 - 23.12	12.47 - 13.17	6.60 - 6.97	15.84 - 15.81
EAST	20.68 - 22.05	11.46 - 12.06	8.10 - 8.48	19.31 - 19.35
SOUTH	31.15 - 32.06	10.86 - 11.76	7.19 - 7.82	17.78 - 17.47

(d) CCSM4 + WRF351 model

minimum-variance ratio of PV ILR1 is higher than that of CSP SM1 whatever the model and experiment (Table 5.1). However, as previously mentioned (Section 3, Chapter 2), the calculation of the minimum-variance ratios assumes that the covariance matrix is diagonal while taking covariances between technologies into account is critical to limiting the adequacy risk.

The interaction of PV and CSP in optimal mixes, at such low penetrations, is different between hourly CORDEX-CMIP5 (left side of middle panels of figures 5.1 and 5.2) and MERRA-2 simulations (left side of figure 3.1d, Chapter 3), but less true between the two experiments of CORDEX (solid and dotted lines in figures 5.1 and 5.2). In fact, solving the optimization problem using MERRA-2 climate data over one year yields more PV than CSP; while using CORDEX data—whatever the experiment and the climate model over 30 years—the share of CSP is higher than that of PV. It must be premised that simulations are generally subject to high sensitivities with regards to the input assumptions, such as the climate data sources, the length of the record and the intra-daily parametrization more than the impact of climate variability/change.

To illustrate this point, the 2018 year being shorter than the CORDEX historical record covering several decades, the mean-variance analysis using MERRA-2 over one year may be insufficient to resolve the long-term climate variability. As a result, PV is installed more than CSP due to its low variance associated with the exploitation of the diffuse light and only small fraction of CSP is introduced due to its positive correlation with the summer peak demand (Section iv, Chapter 3). Given that, one may first expect that the installation of CSP over PV, using CORDEX, may be due to the increased demand over a long time horizon provided by CORDEX data compared to energy consumed over only one year provided by MERRA-2 dataset; and that CSP with north-south tracking is favored over fixed-tilted PV due to its positive correlation with the summer peak demand as found with MERRA-2 simulations (Figure 3.3e, 3.3d, Chapter 3). We indeed

Table 5.2: Similar to table 5.1 but for the ratios (no units) given by (2.20).

Zones	Wind	PV (ILR1)	CSP	
			SM1	SM2
NORTH	0.195 - 0.337	0.399 - 0.339	0.866 - 0.779	0.953 - 0.874
CENTER	0.168 - 0.338	0.346 - 0.325	0.791 - 0.727	0.915 - 0.849
EAST	0.318 - 0.992	0.300 - 0.285	0.839 - 0.778	0.941 - 0.877
SOUTH	0 - 0	0.267 - 0.279	0.774 - 0.730	0.907 - 0.852

(a) CNRM-CM5 + RCA4 model

Zones	Wind	PV (ILR1)	CSP	
			SM1	SM2
NORTH	0.207 - 0.337	0.360 - 0.376	0.822 - 0.870	0.909 - 0.977
CENTER	0.163 - 0.500	0.327 - 0.373	0.756 - 0.816	0.876 - 0.951
EAST	0.389 - 1.307	0.281 - 0.326	0.803 - 0.871	0.901 - 0.981
SOUTH	0 - 0	0.254 - 0.319	0.747 - 0.826	0.872 - 0.957

(b) EC-EARTH + RCA4 model

Zones	Wind	PV (ILR1)	CSP	
			SM1	SM2
NORTH	0.181 - 0.434	0.373 - 0.446	0.819 - 0.987	0.900 - 1.102
CENTER	0.170 - 0.550	0.319 - 0.417	0.744 - 0.915	0.863 - 1.067
EAST	0.326 - 1.382	0.276 - 0.370	0.791 - 0.979	0.887 - 1.101
SOUTH	0 - 0	0.246 - 0.366	0.792 - 0.921	0.855 - 1.072

(c) GFDL-ESM2M + RCA4 model

Zones	Wind	PV (ILR1)	CSP	
			SM1	SM2
NORTH	0.336 - 0.428	0.488 - 0.471	1.36 - 1.264	1.53 - 1.428
CENTER	0.307 - 0.422	0.566 - 0.570	1.30 - 1.22	1.51 - 1.410
EAST	0.463 - 1.05	0.442 - 0.454	1.39 - 1.29	1.55 - 1.445
SOUTH	0 - 0	0.432 - 0.479	1.32 - 1.266	1.52 - 1.429

(d) CCSM4 + WRF351 model

verify that these seasonal patterns obtained from MERRA-2 simulations are similar to the ones obtained using CORDEX-CMIP5 models by plotting the difference between time series over future and historical period to illustrate the anomaly occurring over the day (in ordinate) and the year (in abscissa) of demand and CFs (Figures 5.5, 5.6, 5.7, and 5.8)¹. As can be seen, differences between RCM simulations exist in the seasonal intensity of the response to climate change (See discussion in section 3) but overall CSP CFs (c) are positively correlated with the summer peak (e), whatever the CORDEX-CMIP5 climate model. This is driven by the fact that the CSP tracking system helps to minimize the angle of incidence, in summer, between the incoming sunlight and CSP collectors which decrease the air mass effect (i.e., reduction in the power of light as it passes through the atmosphere and is absorbed by air and dust) that is, in turn, a consequence of the increase in the amount of energy produced (as explained in section i in chapter 1 and section iv, Chapter 3). The fixed-tilted PV surface, on the other hand, is sensitive to high temperature, which explains the decline of PV CFs (b) in summer peak demand. Nevertheless, by computing the technological distribution of the PV ILR1-wind-CSP SM1 mix over the year 2018 using CORDEX-CMIP5 models (not shown here), we found indeed that CSP is always favored over PV. This give a confirmation that the errors stemming from these two independent climate data sources are not attributable to the time frame of the simulation (or seasonal correlation with summer peak demand), but rather to biases in the solar intra-daily parametrization included in the CF models when running the model with daily mean CORDEX climate data because the latter is not available at an hourly sampling. In fact, to compute the hourly PV and CSP CFs, the Global Horizontal Irradiance (GHI)—referred as irradiance for horizontal surfaces—given by CORDEX data is parametrized to resolve the intra-daily fluctuations and decomposed to get the Global Tilted Irradiance (GTI) and the Direct Normal Irradiance (DNI) required by PV and CSP, respectively (Section iii, Chapter 2, Section 1, Appendix A). The solar parametrization suggests that the clearness index is constant over the day which tends to underestimate the solar irradiance variance contained in the intraday time scales which translates into an overestimation of the solar CFs compared to the MERRA-2 estimates that provide climate variables on hourly basis. As a result, because CSP production is more variable during the day than PV due to its sensitivity to clouds, underestimating intraday fluctuations—using CORDEX—has further contributed to install more CSP capacities than PV. This show that the intra-daily fluctuations impact the correlations more than CFs and variances (according to the logic above on the minimum variance calculations

¹Similar patterns are found for wind speed (compared to wind CFs); solar irradiance such as Global Tilted Irradiance-GTI- (compared to PV CFs), and Direct Normal Irradiance-DNI- (compared to CSP CFs) and are thus not shown here

Table 5.3: Similar to table 5.1 but for the maximum-penetration ratios (yr/T€) given by (2.19).

Zones		Wind	PV (ILR1)	CSP	
				SM1	SM2
NORTH		86.34 - 81.32	64.9 - 65.37	18.24 - 19.10	9.79 - 10.26
CENTER		91.72 - 83.9	70.12 - 68.27	25.90 - 25.73	13.58 - 13.55
EAST		77.07 - 64.77	74.6 - 72.63	20.97 - 20.85	10.99 - 10.98
SOUTH		104 - 102	77.83 - 74.26	27.76 - 26.58	14.52 - 14.0

(a) CNRM-CM5 + RCA4 model

Zones		Wind	PV (ILR1)	CSP	
				SM1	SM2
NORTH		83.84 - 83.94	67.3 - 66.31	19.22 - 19.58	10.3 - 10.49
CENTER		91.35 - 79.47	70.5 - 67.70	26.14 - 25.56	13.7 - 13.45
EAST		68.77 - 58.37	75.3 - 72.26	21.16 - 20.78	11.08 - 10.93
SOUTH		104 - 103	78.0 - 73.90	27.21 - 25.84	14.27 - 13.63

(b) EC-EARTH + RCA4 model

Zones		Wind	PV (ILR1)	CSP	
				SM1	SM2
NORTH		85.71 - 81.0	65.3 - 64.5	18.3 - 18.9	9.78 - 10.2
CENTER		90.32 - 79.4	70.7 - 68.1	26.27 - 26.0	13.78 - 13.6
EAST		74.13 - 61.1	75.2 - 72.2	21.2 - 21.0	11.10 - 11.01
SOUTH		104 - 103	78.1 - 73.3	28.0 - 26.4	14.62 - 13.88

(c) GFDL-ESM2M + RCA4 model

Zones		Wind	PV (ILR1)	CSP	
				SM1	SM2
NORTH		85.7 - 84.47	75.5 - 72.77	22.7 - 21.8	12.11 - 11.6
CENTER		90.38 - 87.71	70.6 - 66.73	26.16 - 24.6	13.71 - 13.0
EAST		80.17 - 78.57	78.1 - 74.0	21.16 - 21.1	11.09 - 10.6
SOUTH		104 - 103	78.3 - 72.8	24.83 - 22.5	13.0 - 12.04

(d) CCSM4 + WRF351 model

vs. capacity pathways). Besides, these results may also be sensitive to temperature estimations as only daytime temperature that is considered.

In mixes favoring a high mean penetration and for all combinations, CORDEX-CMIP5 models and experiments (solid and dotted lines) on the right side of panels of figures 5.1, 5.2, there is a clear upward trend in wind fraction with an increasing penetration while the fraction of PV and CSP/CSP-TES have a downward trend. This can be explained by the lowest second ratio of wind followed by PV which is followed by CSP/CSP-TES (Table 5.2). At maximum penetration, CSP/CSP-TES fraction is quasi null due to its high rental cost compared to wind and PV (Table 2.6, Chapter 2); and wind is always solely installed at such maximum-penetration mix due to its largest maximum-penetration ratio (Table 5.3) while PV continues to decrease due to its low CF. Thus, the results seem not to be impacted by the climate data source as the same finding was found with MERRA-2 simulations (Section ii and section iii, Chapter 3).

This large contribution of variable technologies (PV, wind) compared to dispatchable technology (CSP-TES) in these high RE penetration scenarios prevents reaching the budget limit sooner but alters the adequacy risk (Section i, Chapter 3). In fact, the convexity of both CSP/CSP-TES and wind fraction curves (right side of panels of figures 5.1, 5.2) show that, in future warming, both wind and CSP/CSP-TES can achieve a higher mean total penetration without deteriorating the risk (although less true for wind when the storage is integrated in the bottom panels); while the concave shape of PV fraction show that the square root of the global variance increases for both smaller and higher values of the mean penetration. Worth to note, once again, that the solar and wind intraday parametrization may underestimate the variance of CSP and wind resulting in small increase of the risk with the mean penetration, as confirmed also by the relatively concave shape of CSP and wind fraction curve using hourly MERRA-2 climate data at such high penetrations for the PV-wind-CSP SM1 mix (right side of figure 3.1d, Chapter 3).

→ Overall, this section strengthens the idea that ignoring intraday fluctuations of cloud cover (i.e., constant clearness index throughout the day) and temperature results in installing more CSP than PV at low penetrations; and underestimate the variance of CSP also at high penetrations (i.e., convex shape). Therefore, the daily cycle of PV and CSP CFs is important to take into account for optimal capacity allocation whatever the penetration scenario (See discussion at the end of section 2).

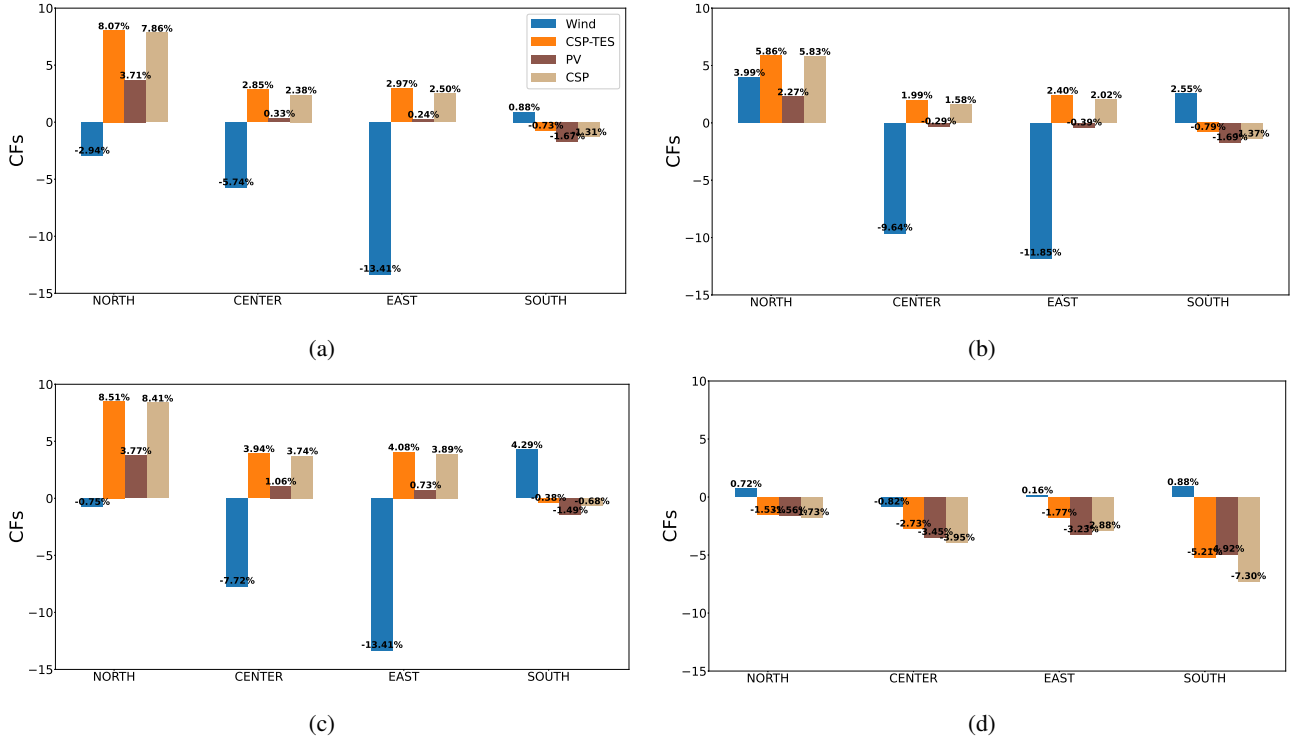


Figure 5.3: Relative change (%) of the regional bias-corrected Capacity Factors (CFs): Photovoltaic (PV) with an Inverter Loading Ratio of 1 or ILR1 (brown), Concentrated Solar Power (CSP) with Solar Multiple of 1 or SM1 (tan), CSP with Thermal Energy Storage (TES) with SM2 (orange), and Wind (blue), per zone and technology, obtained from COordinated Regional climate Downscaling EXperiment-Coupled Model Intercomparison Project Phase 5 (CORDEX-CMIP5) models: two Regional Climate Model (RCM) simulations—the version 4 of the Rossby Centre regional Atmospheric model (RCA4) and the version 351 of the Weather Research and Forecasting model (WRF351)—over the study region using boundary conditions from four different Global Climate Models (GCMs)—Centre National de Recherches Météorologiques-Coupled Model (CNRM-CM5), Earth System Model (EC-EARTH), Geophysical Fluid Dynamics Laboratory’s Earth System Model (GFDL-ESM2M), Community Climate System Model (CCSM4). The name of each climate model is hereafter referred as GCM + RCM. (a): CNRM-CM5 + RCA4 model; (b): EC-EARTH + RCA4 model; (c): GFDL-ESM2M + RCA4 model; (d): CCSM4 + WRF351 model. ILR1 or SM1: without storage; SM2: with 6 hours of TES. To be compared with figure 5.9.

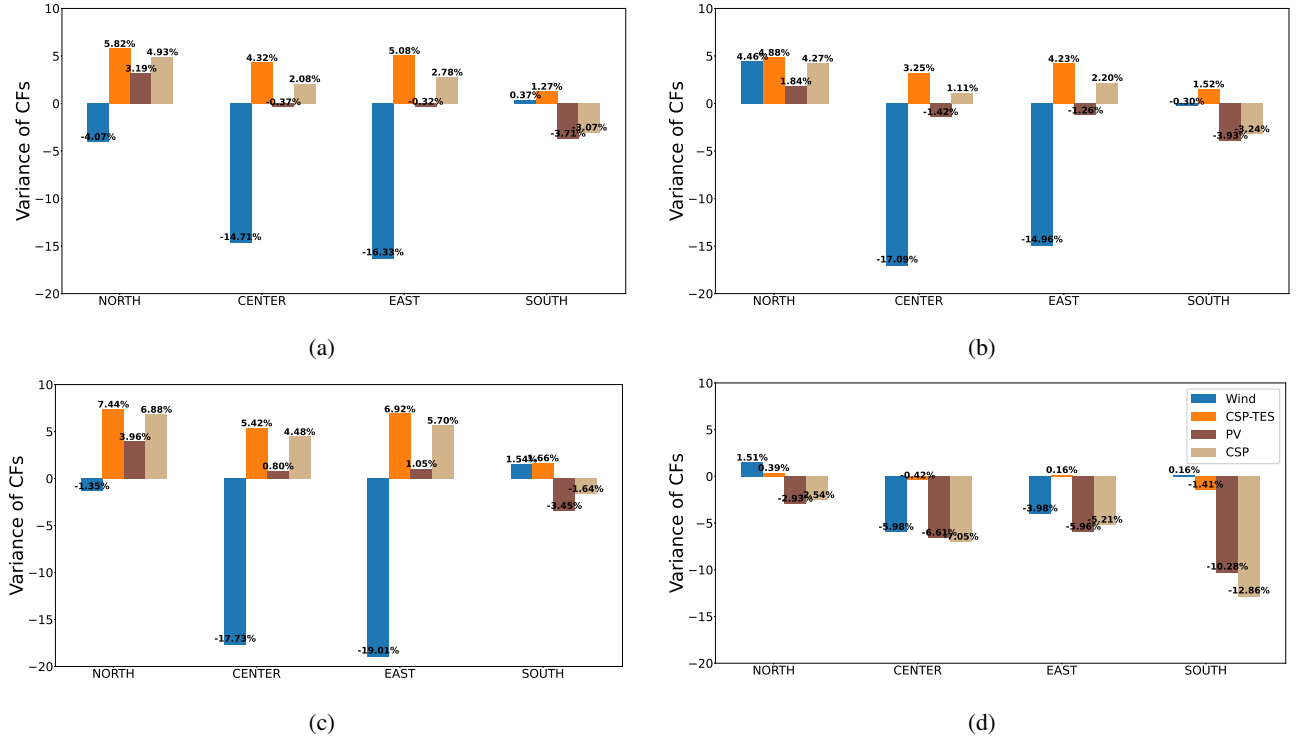


Figure 5.4: Similar to figure 5.3 but for the regional variance of the bias-corrected capacity factors.

3 Consistency of Climate Projections and Sources of Uncertainty

Which technology is sensitive or resilient to climate change? What are the conditions for climate-resilient RE mixes? What are the main sources of uncertainty in future RE mixes?

To assess the consistency of climate projections on the response of optimal mixes to RCP 8.5 climate change (i.e., technological fraction signal) and the main sources of uncertainty under different penetration scenarios, we compare the optimal mixes obtained over the historical period (Left) and future period (Right) between the climate models in figure 5.10. In addition, to examine, under different penetration scenarios, which technology is sensitive or resilient to climate change, we compare for each technology the fraction curves between the two experiments (solid and dotted lines) in figures 5.1, and 5.2.

At maximum penetration mix, the capacity pathways are rental cost induced (Section 1, Chapter 2). Thus, the climate change effect is broadly similar across all the CORDEX-CMIP5 models (right side of figure 5.10). In fact, the robustness of the response of optimal mixes to climate change at such maximum penetration is attributed to the fact that warming climate induces a changes in the mean CFs and in the overall complementarity of the generation portfolio but of small order compared to the effect of cost (as already discussed in section 1), which involves no-significant differences although non-robust at some specific penetration points. Overall, we report an evident trend towards increasing wind fraction. Contrariwise, PV and CSP fractions tend to decrease in future mixes (compare, on the right side of top and middle panels of figures 5.1 and 5.2, the future mix in dotted curves to historical mix in solid curves).

Comparing the differences between future optimal mixes (dotted lines) and ones obtained with historical forcing (solid lines), at **low penetrations** (left side of top and middle panels of figures 5.1 and 5.2) and **high penetrations** (middle side of top and middle panels of figures 5.1 and 5.2), we observe that the qualitative picture is fairly robust in the rate of the response to climate change, but important quantitative differences exist from one model to another (as can also be clearly seen on the left and middle side of figure 5.10). Disparities stem from differences in the means, variances and covariances of the estimated demand and CFs required to compute the mean-variance results. The quality of the latter depends on the quality of the RCM simulations which is, in turn, dependent on the quality of the GCM outputs that provide the initial and lateral boundary conditions for the RCM runs. However, we notice a consistency between almost all models having the same RCM forced by different GCMs but a divergence across models when the RCM and GCM are both changed. Indeed, we can see that the technology fractions in CCSM4-driven WRF351 simulations (diamond) become considerably larger or smaller in the mix compared to simulations from the remaining three downscaled GCMs using RCA4, at low and high penetration where the variance play a role (left and middle side of figure 5.10). Therefore, biases between models can be more attributed to the dynamical downscaling than to the driving GCM.

Difference between RCMs in the PV, CSP and wind trend between historical (solid line) and future period (dotted line) at low and high penetrations (left and middle side of top and middle panels of figures 5.1, 5.2 and left and middle side of figure 5.10) can be explained by the uncertainty in the daily and seasonal response of the CFs to climate change (i.e., correlation with the evening and summer demand) (Figure 5.5, 5.6, 5.7 and 5.8); and the relative change of mean CFs (Figure 5.3), which in turn, depend on anomalies in mean resources (Figure 5.9). In fact, for each CORDEX-CMIP5 model, the changes in wind mean CFs is driven by the change of wind speed and temperature (i.e., air density) (Section II, Appendix A); while that of PV or CSP mean CFs are basically linked to an increase or decrease of solar irradiance and temperature (Section V for CSP and Section VI for PV, Appendix A). It is, thus, informative to attribute changes in wind, PV and CSP output to changes in the associated resources that would be induced by the end of the century. Each pair of bars in figure 5.9 show the difference between the mean of the time series over the future period and the mean value over the historical period of temperature (light blue), wind speed (blue), Direct Normal Irradiance or DNI (orange), Global Tilted Irradiance or GTI (brown) and Global Horizontal Irradiance or GHI (tan). As can be seen, the seasonal and daily response of the CFs to climate change (Figure 5.5, 5.6, 5.7) and the regional anomalies in mean resources (Figure 5.9 (a), (b), (c)) and thereby in mean CFs (Figure 5.3 (a), (b), (c)) obtained from the three downscaled GCMs using RCA4 appeared to be close to each other although a slight influence of driving model uncertainties was observed by comparing each of the GCM driven simulations. However, these GCMs-driven RCA4 simulations provide a consistently different picture from that of CCSM4-driven WRF351 simulations in the seasonal and daily patterns (Figure 5.8) and the anomalies in the mean resources and mean CFs (Figure 5.9 (d), and Figure 5.3 (d)); which helps understand the relatively dispersion in the projected optimal mixes between the two RCM simulations at low and high penetrations (left and middle side of top and middle panels of figures 5.1, 5.2 and left and middle side of figure 5.10).

At high penetrations, we note from figure 5.10 that the difference between RCMs is more significant for PV and wind capacity pathways while the fraction curve of CSP/CSP-TES is robust. This can be explained by the fact that to increase the mean CFs of CSP, the temperature (dry air) plays an important role than DNI while to increase the PV (resp. wind) CFs, the GTI (resp. wind speed) matter more than temperature. And, since the climate change signal for temperature is robust as all CMIP5 models tend to agree broadly in the projection of temperature change expecting that the average temperature will increase in RCP 8.5 climate change (Figure 5.9), induced by the increasing concentration of greenhouse gases in the atmosphere; while solar irradiance and wind speed reflect lower robustness in the sign of the change (Figure 5.9), the CSP/CSP-TES capacity pathways are relatively robust compared to PV and wind capacity pathways. Indeed, uncertainty in projected irradiance changes suggests a strongest confidence in the results for southern regions and least confidence in results for the remaining regions (NORTH, CENTER and EAST) where discrepancies persist between RCA4 simulated climate and WRF351 simulations. The latter show a negative signal of the average solar irradiance for all regions (Figure 5.9 (d)) compared to RCA4 simulations (Figure 5.9 (a),(b),(c)) where the solar irradiance is projected to increase in the above-remaining regions. For mean wind speed, there is a poor agreement among different simulations on the sign of the change (Figure 5.9). There are tendencies for a decline in wind speed in almost all regions. Nevertheless, an increase in wind speed is seen over southern regions whatever the model, which favor wind installation in this region (the last paragraph of this section 3). For all models, we note at such high penetrations, an overall trend toward a decrease in wind and CSP share with an opposite trend for PV (compare, in the middle side of top and middle panels of figures 5.1 and 5.2, the future mix in dotted curves to historical mix in solid curves).

For mixes favoring a lower level of risk, the RCM uncertainty increases for all technologies (left side of figure 5.10) and an opposite response to climate change across RCM models is noted (compare, on the left side of top and middle panels of figures 5.1 and 5.2, the future mix in dotted curves to historical mix in solid curves) although the variations is smaller than high penetrations levels (as discussed in section 1). This can be explained by the fact that, at such low penetrations, the mean and variance of CFs play a role, and the variance of CSP and PV strongly depend on clouds and aerosols. The quality of estimation of these atmospheric components depends mostly on the parametrization scheme of each regional model. Difference may exist between RCMs in this process and to some extent between GCMs which explain the dispersion between climate projections (See discussion in section 2). According to the projections of CNRM-CM5 + RCA4 model (compare, on the left side of left panels of figure 5.1, the future mix in dotted curves to historical mix in solid curves) and GFDL-ESM2M+RCA4 model (compare, on the left side of left panels of figure 5.2, the future mix in dotted curves to historical mix in solid curves), we identify a trend towards an increase in wind and CSP share in the future mix whereas PV share is expected to decrease or quasi null (depending on the RE combination). For future projections from EC-EARTH + RCA4 model (compare, on the left side of right panels of figure 5.1, the future mix

in dotted curves to historical mix in solid curves), the technology fraction evolution shows the same evolution as CNRM-CM5 + RCA4 model (left side of left panels of figure 5.1) and GFDL-ESM2M+RCA4 model (left side of left panels of figure 5.2), but the difference between the historical and future curve is very weak and non-significant, at such low penetrations. For CCSM4 + WRF351 model (compare, on the left side of right panels of figure 5.2, the future mix in dotted curves to historical mix in solid curves), the distribution of RE capacities over the future period differs from that obtained over the historical period as less wind and CSP capacities are installed in future mix while a clear tendency towards an increase in the PV fraction.

In fact, the magnitude of the response of temperature to RCP 8.5 climate change in the model simulations varies widely although in runs with similar RCA4. Particularly, the three different downscaled GCMs using RCA4 simulations, project the weakest warming (Figure 5.9 (a),(b),(c)) compared to WRF351 simulations (Figure 5.9 (d)). In addition, all CORDEX-CMIP5 models project small seasonality of the temperature (Figure 5.5f, 5.6f, 5.7f and 5.8f) projecting an uniform increase of temperature throughout the day (abscissa) and the year (ordinate). This suggest that, the seasonal patterns of PV and CSP CFs (resp. wind CFs) are more related to solar irradiance (resp. wind speed) than to temperature. The same applies to the daily patterns since the variation of temperature throughout the day is time average in this study (Section iii, Chapter 2). Looking at the seasonal amplitude of the response of solar irradiance to climate change (not shown here) and thereby of PV CFs (Figure 5.5b, 5.6b, 5.7b and 5.8b) and CSP CFs (Figure 5.5c, 5.6c, 5.7c and 5.8c), dynamical downscaling using RCA4 model project similar seasonal changes, with a trend towards more irradiance in the winter and less in the summer (consistent with [192] for Southern Africa) and thus intense PV CFs (Figure 5.5b, 5.6b, 5.7b) and CSP CFs (Figure 5.5c, 5.6c, 5.7c) in winter and less in summer. Future simulations from WRF351 model, on the other hand, indicate an intense increase of PV CFs (Figure 5.8b) and CSP CFs (Figure 5.8c) in summer and small amplitude in winter.

For RCA4 simulations, the projected increase in the mean irradiance and average temperature causes the CSP CFs to increase (Figure 5.3 (a), (b), (c)). As can be seen, the spatial patterns of CSP CFs resembles to the ones of the DNI (Figure 5.9 (a), (b), (c)) and regions that show increasing DNI show even more positive trends for CSP CFs; and the contribution from changes in irradiance is always dominant than temperature (consistent with [141]). This explains why the CSP fraction tends to increase in GCMs-driven RCA4 simulations (left side of figures 5.1c, 5.1d, and 5.2c). In addition, CSP is installed more than PV due to the underestimation of the variance of the clearness index in the solar parametrization approach but also because CSP with tracking is already positively correlated with the summer peak demand (Figure 5.5c, 5.6c, 5.7c), as discussed in section 2, despite its negative response to climate change in summer peak. Comparing the GTI in figure 5.9 ((a), (b), (c)) and its implication on mean PV CFs (Figure 5.3 (a), (b), (c)) for GCMs-driven RCA4 simulations projecting the highest temperature and positive irradiance trends in almost all regions, we can see that anomalies relative to a 1976-2005 climatology of temperature—varying from 3.5 to 4.5 K—, exert the largest influence on PV and causes PV CFs to be reduced despite relatively significant trends in solar irradiance as small errors arise from the non-linear terms of irradiance (A.64). As can be seen, regions with larger increase in temperature (EAST, CENTER) (Figure 5.9 (a),(b),(c)) show a distinct decline in PV mean CFs (Figure 5.3 particularly for EC EARTH + RCA4 model (b)). Therefore, the increase in average temperature cannot outweigh the increase in solar irradiance (Figure 5.3 (a), (b), (c)), resulting in a decrease of PV fraction (left side of figures 5.1c, 5.1d, and 5.2c) due to its negative dependency on temperature (A.64). In addition, fixed tilted-latitude PV is already negatively correlated with the summer peak (Section 2) and the increase in temperature attenuates the response of PV output to climate change in summer peak load (Figure 5.5b, 5.6b, and 5.7b) which further penalize PV compared to CSP (left side of figure 5.1c, 5.1d, and 5.2c).

For CCSM4-driven WRF351 simulations, small rise of temperature cannot compensate for decreasing trends in solar irradiance, being negative in all regions (Figure 5.9 (d)), resulting in an overall large decrease in the PV and CSP mean CFs (Figure 5.3 (d)). Since CSP (resp. PV) is impacted by temperature and irradiance with a dominant contribution from changes in solar irradiance (resp. temperature), the fraction of CSP decreases (left side of figures 5.1c, 5.1d, and 5.2c) while the small increase of mean temperature in WRF351 implies a positive response of PV to climate change in summer (Figure 5.8b) which results in an increase of PV fraction (left side of figures 5.1c, 5.1d, and 5.2c). However, CSP remains dominant over PV since it is correlated with the summer peak demand in addition to its response to warming climate with a positive gradient (Figure 5.8c) and due to the underestimation of intradaily CSP variance (Section 2).

We can see that regions where an increase in mean wind speed is expected—mainly in SOUTH for all models and NORTH for EC-EARTH+RCA4 and CCSM4+WRF351 models (Figure 5.9 (b), (d))—also show a relatively significant increase in wind mean CFs (i.e., wind output is proportional to the cube of the wind speed, which means that alterations in the latter can have significant impacts on the former [335]). The small increase in average wind speed in the remaining regions (EAST, CENTER) does not compensate for the increase of average temperature (i.e., decrease of average air density) (Figure 5.9) leading to larger decrease of wind CFs (Figure 5.3). This is to be expected due the fact that a rise in temperature will lead to slight decline in air density and thus wind output [428, 429]. Rising temperature in RCA4 simulations would imply declining wind CFs as both higher temperature or humidity make air less heavy (due to an increase in moisture content). However, the wind fraction increases in RCA4 simulations (left side of left and right panels of figure 5.1 and left panel of figure 5.2) because the wind speed increase in RCA4 simulations (Figure 5.9 (a), (b), (c)) in SOUTH, where wind is installed (see the last paragraph of this section 3), overpasses the air density decrease (i.e., rising temperature) compared to WRF351 simulations (Figure 5.9 (d)). However, the fraction is smaller than in WRF351 simulations (Figure 5.10), where the average temperature increase is smaller (Figure 5.9 (d)). In addition, wind dominates over solar technologies since it is uniformly distributed over the day and the year compared to PV and CSP (Figure 5.5, 5.6, 5.7 and 5.8) which have a positive impact on wind minimum-variance ratios.

We can conclude that the compensation between temperature, irradiance and wind speed changes and the dominant dependence on these parameters accounts for the greater sensitivity of optimal mixes—with high and low penetrations—integrating PV, CSP and wind to climate change. Similar mean resources, seasonal variability of CFs, and mean CFs changes preclude significant differences between the corresponding capacity distributions.

→ The following conclusions can be drawn from the present section. If maximum penetration is targeted in future energy mixes, low RCM or GCM uncertainty in RE mixes is noted. Wind is (resp. PV and CSP are) resilient (resp. sensitive) to climate change. The RCM uncertainty prevails more than GCM uncertainty at high and low penetrations. If high penetrations are targeted, the RCM uncertainty increases more for PV and wind capacity pathways (due to non-robustness of GTI and wind speed) but not for CSP fraction curve (as all CMIP5 models tend to agree in the projection of temperature increase). At such high penetrations, wind and CSP are (resp. PV is) sensitive (resp. resilient) to climate change. If low proportions of REs are targeted, high RCM uncertainty is identified for all technologies (due to the difficulties associated with the parametrization of clouds and aerosols which contributes to errors in temperature and irradiance). For RCA4 simulations, wind is resilient (i.e., the wind speed increase overpasses the air density decrease compared to WRF simulations), CSP is resilient (i.e., positive response to climate change in winter, when demand is low, but already positively correlated with the summer peak demand due to tracking use). PV is sensitive (i.e., the increase of temperature in summer does not compensate the increase in GTI). For WRF351 simulations, wind is sensitive (small increase in wind speed even though high air density), CSP is sensitive (i.e., strong decrease of DNI) and PV is resilient (i.e., the increase

of temperature in winter compensates the decrease of GTI). Therefore, wind climate change induced impacts are positive if the wind speed increase overpasses the air density decrease resulting from warming. In addition, CSP and PV will have a positive climate change impact if the projected increase in solar irradiance (i.e., cloud cover and aerosols decrease) compensates the negative warming induced effect (see discussion on options for climate-resilient RE mixes in section 3).

Thermal Storage makes CSP resilient to Climate Change?

Resulted optimal mixes provide consistent model projections of the CSP-TES response to climate change, expecting that CSP-TES fraction will show a moderate decrease in future warming climate, whatever the penetration scenario (compare, in the bottom panels of figures 5.1, and 5.2, the future mix in dotted curves to historical mix in solid curves). This shows that the combined period of darkness and prolonged cloudiness projected by the climate models exceeds the thermal capacity of CSP-TES SM2 (6 hours, Table 2.3, Chapter 2). Therefore, in future RCP 8.5 climate change, CSP-TES with small storage capacity will not be able to satisfy the increasing evening peak demand in nighttime resulting from the high temperature which is also result of the high outgoing long-wave irradiance since the fraction of opaque clouds peak in the early afternoon [130], which are not able to trap the infrared irradiance, preventing the CSP with thermal storage to perform better at night [405].

The difference between the models is that the large increase of temperature in GCMs-driven RCA4 simulations (Figure 5.9 (a),(b)(c)) compared to WRF351 simulations (Figure 5.9 (d)) is translated into relatively less significant trend of demand in summer in WRF351 model where the demand tends to increase throughout the year and particularly in winter (Figure 5.8e) compared to RCA4 simulations (Figure 5.5e, 5.6e, 5.7e) which peaks more in summer. This increase in temperature (i.e., humidity) in summer (resp. winter) in RCA4 simulations (resp. WRF351 simulations) is translated into a decrease of CSP-TES SM2 CF in summer (resp. winter) in RCA4 simulations (resp. WRF351 simulations) (Figures 5.5d, 5.6d, 5.7d for RCA4 and 5.8d for WRF351).

→ Whatever the penetration scenario and the climate model, the combined period of darkness, the prolonged cloudiness and the temperature/demand increase in evening exceeds the thermal storage capacity of CSP-TES (SM2, 6 hours of TES). Therefore, large storage capacity (we find more than 17 hours of TES or SM>4, not shown here) is needed if CSP-TES is considered in future energy mixes (see discussion at the end of section 3).

Does RCP 8.5 climate change impacts the geographical distribution of RE capacities?

At low penetrations, from table 5.1 and table 3.5 (Chapter 3) (see the maximum of minimum-variance ratio, in bold), we can see that the climate change and uncertainty related to climate data sources do not seem to impact the geographical distribution of wind and solar technologies at low penetrations. Overall, to achieve a lower variance, more frequent and persistent winds are expected in Southern region due to the nearby presence of the Atlantic ocean (i.e., with denser air and low roughness). PV is installed in CENTER due to relatively low mean temperature in CENTER although this region is characterized by low solar resource compared to NORTH or EAST (Figure 5.9). However, this is to be expected to reduce the variance since the variance-based risk (2.2) favors all factors reducing the variability associated with high CF (as discussed in section iv, Chapter 3). The minimum risk scenarios distribute CSP/CSP-TES capacities in EAST with relatively high solar irradiance (i.e., no clouds)—although less than NORTH but the models favors EAST to remain coherent with the risk definition—and it is the most affected region by warming confirming the continental character of this region which would imply increasing power output for CSP.

At high penetrations, wind remains non-sensitive to climate change and the production is always intense and recurrent in SOUTH (not shown here) which favors its installation in this region (see the minimum of second ratio, in bold, in table 5.2). However, it seems that the geographical distribution of wind is sensitive to climate data source at maximum penetration mix. In fact, from simulations of hourly CORDEX data with parametrization of intraday variations over 30 years, wind is installed in SOUTH even at the point approaching 100% RE share (see the maximum of maximum-penetration ratio, in bold, table 5.3) instead of EAST that we found when using hourly MERRA-2 climate reanalysis over the year 2018 (Table 3.2, Chapter 3). This is owing to the fact that wind mean CFs are projected to decrease in the EAST region and increase in SOUTH whatever the model (Figure 5.9, 5.3) due to the decrease (resp. increase) of wind speed in EAST (resp. SOUTH) and due to the weak signal of temperature in SOUTH compared to EAST (Figure 5.9) as the relatively slow warming of the Atlantic ocean dampens the temperature increase. Once again, results may be prone to bias due to the wind parametrization (Section iii, Chapter 2) as discussed in section 2.

Despite the projected reduction in solar irradiance over the southern region (Figure 5.9), this region remains, paradoxically, favored by the model for PV installation at high penetrations (see the minimum of second ratio for PV, in bold, in table 5.2) since the reduction of solar resources is of small order (whatever the model), insufficient to alter the PV output and thus omitted by the model. In addition, the decrease of solar irradiance in this region implies that this region may benefit from cooler temperature. Thus, the climate change and the use of different climate data source (Table 3.3, Chapter 3) does not impact the geographical distribution of PV; but less true when running the mean-variance with WRF351 model as the RCP 8.5 induces the installation of PV in EAST (Table 5.2d) due to the fact the the highest reduction of global tilted irradiance (GTI) and PV mean CFs is recorded in SOUTH more than in EAST (Figure 5.9(d) and 5.3(d)).

Achieving higher levels of mean penetration requires the installation of CSP/CSP-TES in SOUTH or CENTER depending on the experiment and the climate model. Thus, CSP/CSP-TES seems to be substantially more sensitive to climate change and the differences between climate models are attributed not only to RCM but also to the driving GCMs (see the minimum of second ratio for CSP/CSP-TES, in bold, in table 5.2).

→ The climate change does not impact the geographical distribution of RE capacities at low penetrations. If high penetration scenarios are however targeted, high RCM uncertainty for PV, and high GCM and RCM uncertainty for CSP/CSP-TES, while wind is only sensitive to climate data sources at maximum-penetration mix (see discussion on the regional effects of climate change in section 4).

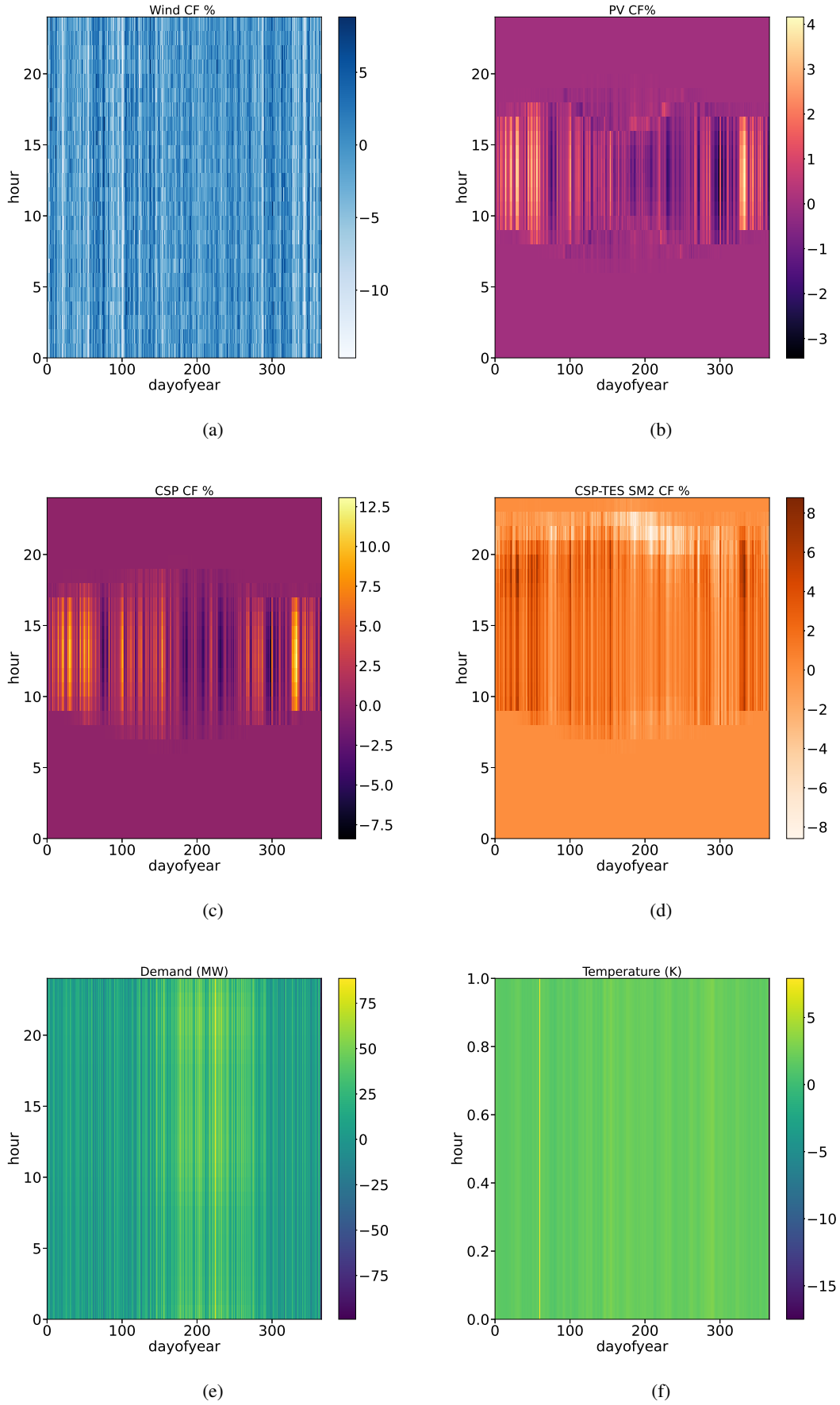


Figure 5.5: Heatmap of the national daily (ordinate) and seasonal (abscissa) anomaly of the Capacity Factors (CFs) in %: Wind **(a)**, Photovoltaic (PV) with an Inverter Loading Ratio of 1 or ILR1 **(b)**, Concentrated Solar Power (CSP) with Solar Multiple of 1 or SM1 **(c)**, CSP with SM2 **(d)**; and of the Demand (MW) **(e)** and Temperature **(f)** obtained from hourly COordinated Regional climate Downscaling EXperiment-Coupled Model Intercomparison Project Phase 5 (CORDEX-CMIP5) climate data (with intra-daily parametrization) using Centre National de Recherches Météorologiques-Coupled Model (CNRM-CM5) as Global Climate Model (GCM) + the version 4 of the Rossby Centre regional Atmospheric model (RCA4) as Regional Climate Model (RCM). The variation over time is shown in color by intensity in the colorbar. ILR1 or SM1: without storage; SM2: with 6 hours of Thermal Energy Storage (TES).

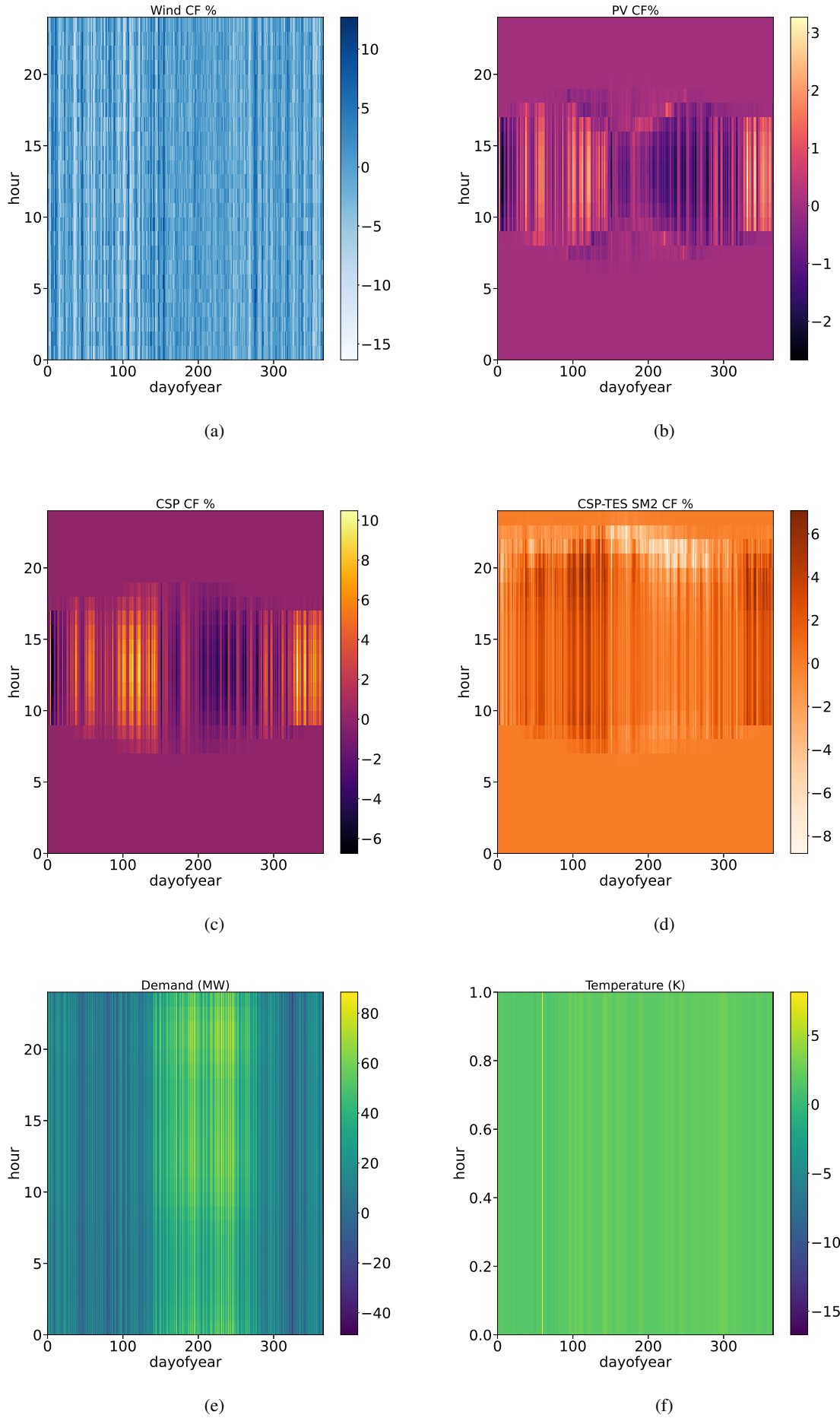


Figure 5.6: Similar to figure 5.5 but obtained from different COordinated Regional climate Downscaling EXperiment-Coupled Model Inter-comparison Project Phase 5 (CORDEX-CMIP5) model: Earth System Model (EC-EARTH) as Global Climate Model (GCM) + the version 4 of the Rossby Centre regional Atmospheric model (RCA4) as Regional Climate Model (RCM).

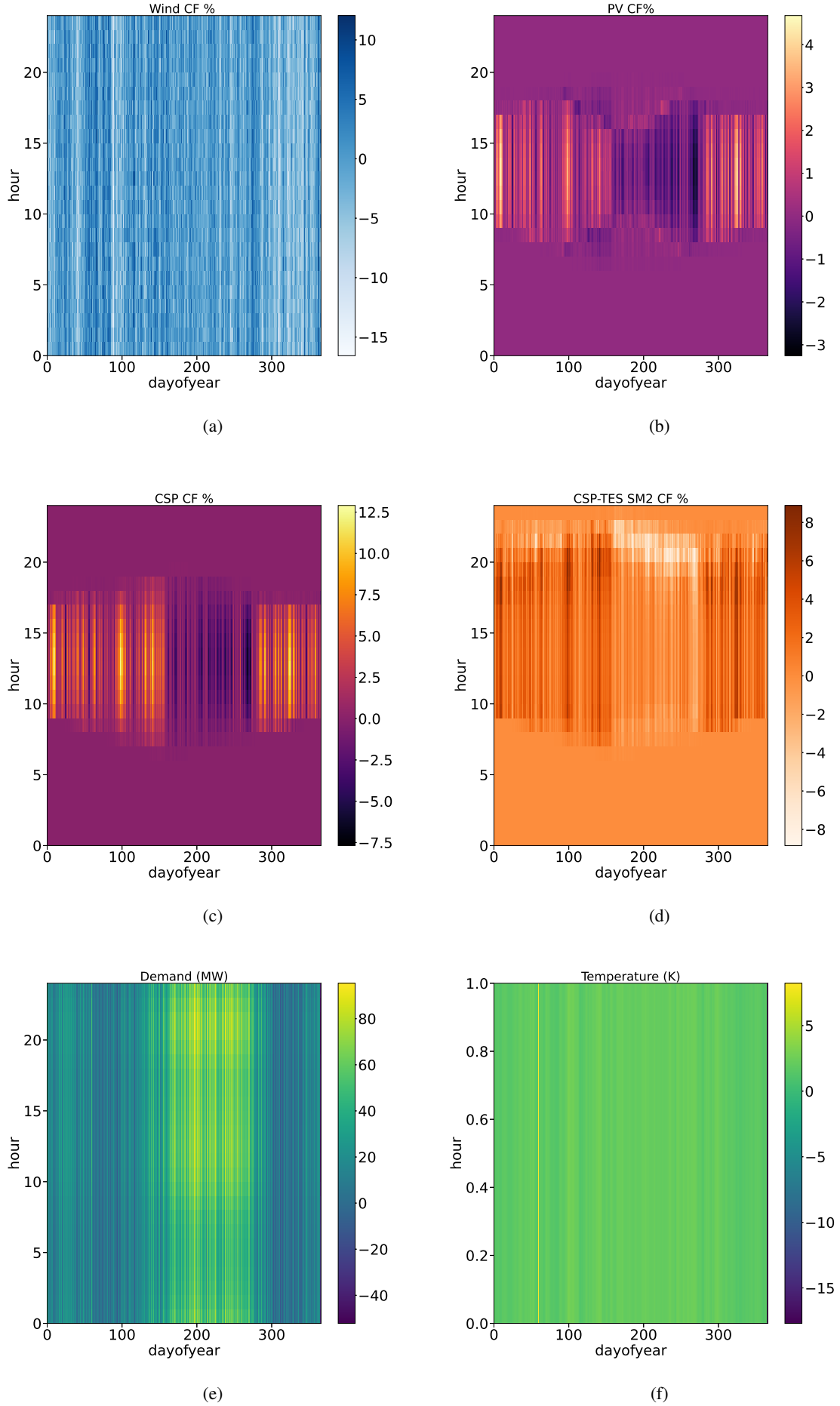


Figure 5.7: Similar to figure 5.5 but obtained from different COordinated Regional climate Downscaling EXperiment-Coupled Model Inter-comparison Project Phase 5 (CORDEX-CMIP5) model: the Geophysical Fluid Dynamics Laboratory's Earth System Model (GFDL-ESM2M) as Global Climate Model (GCM) + the version 4 of the Rossby Centre regional Atmospheric model (RCA4) as Regional Climate Model (RCM).

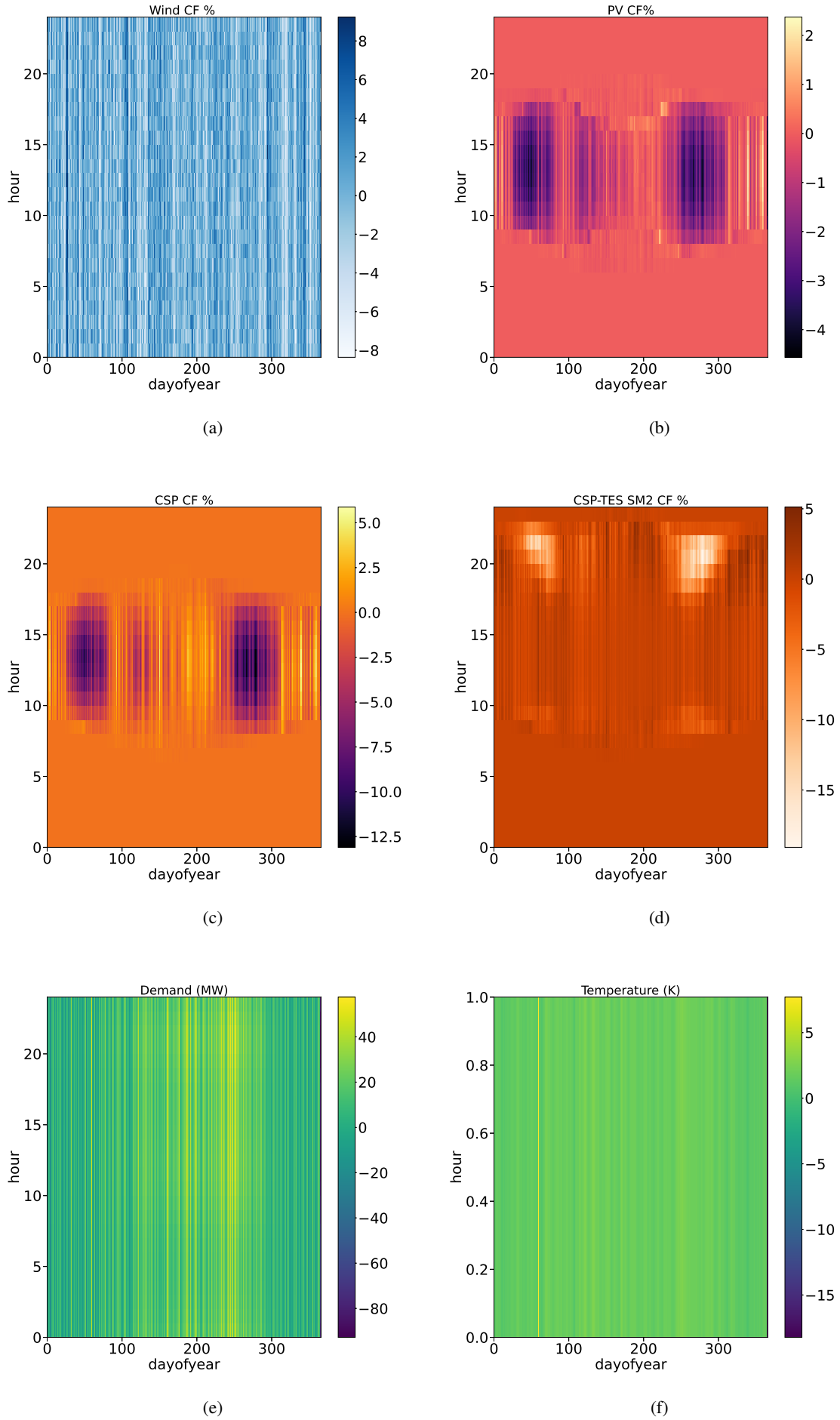


Figure 5.8: Similar to figure 5.5 but obtained from different COordinated Regional climate Downscaling EXperiment-Coupled Model Inter-comparison Project Phase 5 (CORDEX-CMIP5) model: the Community Climate System Model (CCSM4) as Global Climate Model (GCM) + the version 351 of the Weather Research and Forecasting model (WRF351) as Regional Climate Model (RCM).

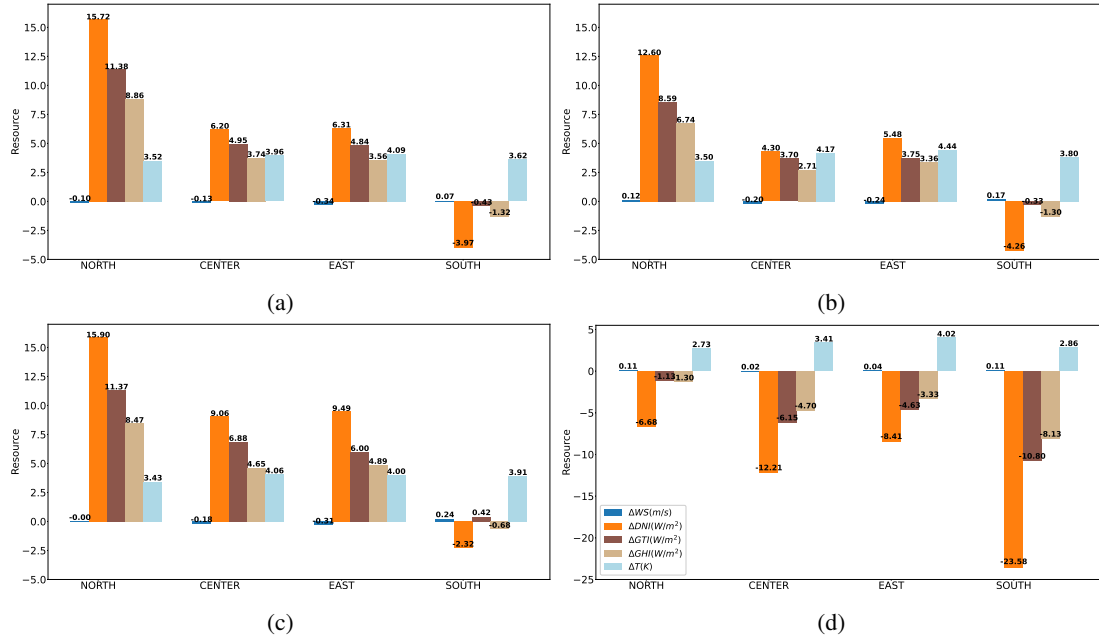


Figure 5.9: Anomaly of the regional wind speed ΔWS in (m/s) (blue); Temperature ΔT in (K) (light blue); and solar irradiance components in W/m^2 : Global Horizontal Irradiance (ΔGHI) (tan), Global Tilted Irradiance (ΔGTI) (brown), Direct Normal Irradiance (ΔDNI) (orange); obtained from COordinated Regional climate Downscaling EXperiment-Coupled Model Intercomparison Project Phase 5 (CORDEX-CMIP5) models: two Regional Climate Model (RCM) simulations—the version 4 of the Rossby Centre regional Atmospheric model (RCA4) and the version 351 of the Weather Research and Forecasting model (WRF351)—over the study region using boundary conditions from four different Global Climate Models (GCMs)—Centre National de Recherches Météorologiques-Coupled Model (CNRM-CM5), Earth System Model (EC-EARTH), Geophysical Fluid Dynamics Laboratory's Earth System Model (GFDL-ESM2M), Community Climate System Model (CCSM4). The name of each climate model is hereafter referred as GCM + RCM. (a): CNRM-CM5 + RCA4 model; (b): EC-EARTH + RCA4 model; (c): GFDL-ESM2M + RCA4; (d): CCSM4 + WRF351. To be compared with figure 5.3.

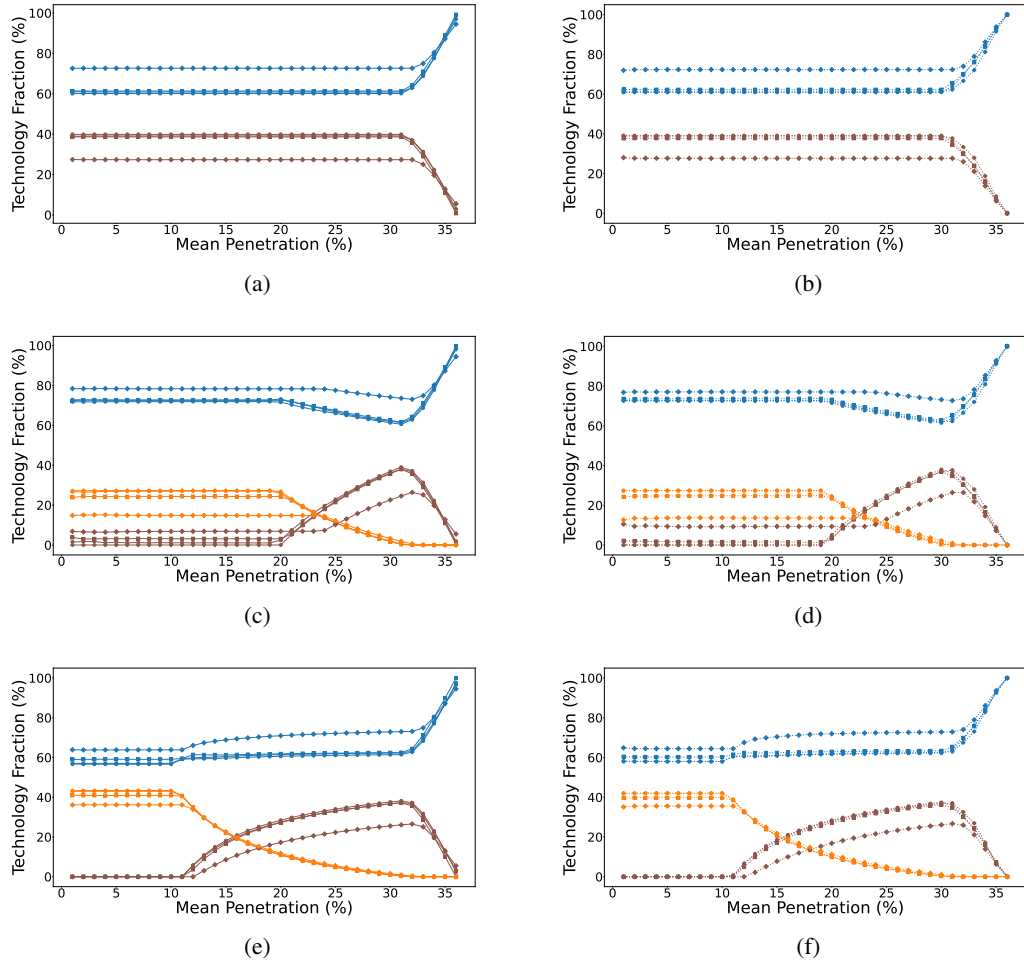


Figure 5.10: Similar to figure 5.1. Optimal mixes over the historical period 1976 -2005 (**Left**) and the future period 2071 - 2100 (**Right**) obtained from COordinated Regional climate Downscaling EXperiment-Coupled Model Intercomparison Project Phase 5 (CORDEX-CMIP5) models: two Regional Climate Model (RCM) simulations—the version 4 of the Rossby Centre regional Atmospheric model (RCA4) and the version 351 of the Weather Research and Forecasting model (WRF351)—over the study region using boundary conditions from four different Global Climate Models (GCMs)—Centre National de Recherches Météorologiques-Coupled Model (CNRM-CM5), Earth System Model (EC-EARTH), Geophysical Fluid Dynamics Laboratory’s Earth System Model (GFDL-ESM2M), Community Climate System Model (CCSM4). The name of each climate model is hereafter referred as GCM + RCM. CNRM-CM5 + RCA4 model (octagon); EC-EARTH + RCA4 model (plus); GFDL-ESM2M + RCA4 model (square); CCSM4 + WRF351 model (diamond).

V Discussion and Comparison with Existing Studies

1 Climate Change Scenarios vs. Cost Reduction

The results obtained show that climate change is impacting the optimal mixes through changes in mean conditions and in climate variability. We show that the variations are relatively very small at low penetrations but less true for higher ones. However, the degree to which optimal mixes are affected by climate change is much more less significant than the cost effect (Section 1). In fact, we find that the rental cost governs the capacity pathways at high penetrations while the mean and variance of Capacity Factors (CFs) and particularly the daily and seasonal correlation of CFs with evening and summer peak demand—which depend on the climate model estimations—play a role in optimal capacity allocation at low penetrations (Section 2 and section 3).

In addition, none of the climate simulations analyzed so far, here, project strong changes in the solar and wind mean CFs. In fact, the relative change (reduction) of all technologies are projected to vary by no more than a few percentages, about -1% down to -13.5% for wind; and about -1% down to -5% for Photovoltaic (PV) as shown in figure 5.3, which are trivial with projected cost reductions which have declined by 9% for wind and by 13% for PV in 2019 [445]. An exception states Concentrated Solar Power (CSP) which the future changes (loss), about -5% max, exceed its cost decline (1%) in 2019. This is consistent with studies (e.g., [516]) that find that the impacts of climate change remains limited for solar and wind technologies compared to hydro or thermal production. It is also important to bear in mind that our projections result solely from the future changes imposed in the forcing under the Representative Concentration Pathways (RCP) 8.5 scenario. The choice of the later gives a distinct climate change signal, which facilitates the detection of significant changes. Other scenarios (RCP 2.6, RCP 4.5) would give smaller changes and the technologies will be penalized differently. However, Wild et al. [551] show that before 2050, the differences between scenarios are still fairly small and thus the exact choice of the scenario is not critical and the deviations between the different RCP scenarios start to strongly diverge only after 2050. In this study, the time horizon considered is after 2050 (2071-2100). This shows that, whatever the penetration scenario mix or emission scenario, the projected future RE mix is resilient to RCP 8.5 climate-related changes.

2 Uncertainties Associated with Future Energy Mixes

We show that climate change may either increase or conversely decrease the share of given technology depending on the COordinated Regional climate Downscaling EXperiment-Coupled Model Intercomparison Project Phase 5 (CORDEX-CMIP5) model and the penetration scenario. Moreover, we find that the contribution from Regional Climate Model (RCM) uncertainty is higher than that from Global Climate Model (GCM), particularly at low penetrations where the variance play a role. Thus, the trend of change is not certain, except for CSP with small storage capacity (Solar Multiple of 2 or SM2, 6 hours of Thermal Energy Storage-TES-) where it clearly decreases by a few percent in all the CORDEX-CMIP5 models, whatever the penetration scenario (Section 3).

Regardless of the uncertainty related to the choice of GCM or RCM, the resulted optimal mixes with low proportions of Renewable Energies (REs) on 30 years timescales are not purely random, but provide an overall reasonably consistent response pattern to the imposed forcing assuming RCP 8.5 scenario showing the RE technology that may be more affected by climate change. The overall assessment is that at the end of the century and for the scenario corresponding to a greater content of greenhouse gases (RCP 8.5), Community Climate System Model (CCSM4) driven Weather Research and Forecasting model (WRF351) simulations project that CSP and wind are more sensitive to climate change than PV (Crook et al. [141] could confirm this result between CSP and PV), while the reverse is true for the Centre National de Recherches Météorologiques-Coupled Model (CNRM-CM5) or Earth System Model (EC-EARTH) or Geophysical Fluid Dynamics Laboratory's Earth System Model (GFDL-ESM2M) driven the Rossby Centre regional Atmospheric model (RCA4) simulations (in agreement with Jerez et al. [276] between PV and CSP for Spain and Perez et al. [408] for the Canary Islands). EC-EARTH-driven RCA4-simulations project little change in optimal mixes.

These uncertainty in optimal mixes comes from uncertainty in the estimated solar and wind CFs which in turn depends on the quality of the resources projected by the GCMs and RCMs.

Differences between RCMs

The temperature and irradiance changes indicate a potential future increase for RCA4 simulations; while solar irradiance decreases in WRF351 model and the temperature increase is smaller in the latter. It is not clear why the projection of these variables does show such pattern. This may be at least partly caused by the difficulties associated with the parameterization of cloud and aerosols in the climate models (which is a common problem in GCM [434, 544, 556] and RCM [276, 458] but more in RCMs than GCMs [79]) since errors in these atmospheric particles contribute to errors in temperature and surface downward short-wave [462].

In fact, Dong et al. [168] explain that the decline in aerosols lead to an increase in the summertime extreme temperatures. Thus, the missing aerosol effects in a given RCM means that projections of future temperature rise will be larger than if the model did include the aerosol effects [211].

Furthermore, the underestimation of the accumulation of aerosols in the atmosphere would affect the estimation of mean solar irradiance in a significant manner [555, 54] especially the clear sky irradiance (required by CSP) whose variations depend mostly on atmospheric composition [553]. First, aerosols have a direct effect on the irradiance balance. They can diffuse and absorb irradiance. Scattering of solar irradiance increases the albedo and induces cooling, while absorption of irradiance induces a warming. This aerosol direct effect is usually represented via monthly climatology of the aerosol optical properties. Such representation is not sufficient to capture the high spatial-temporal variability of aerosols [292]. Second, an increase (resp. decrease) of the aerosols can in turn increase (resp. decrease) cloud cover by providing greater (resp. smaller) number of cloud condensation nuclei. This aerosols indirect effect induces a negative radiative forcing. The indirect effects of, for instance, natural aerosols (e.g. Saharan dust) and anthropogenic aerosols (e.g. pollution) are currently poorly represented or totally ignored in RCMs [206]. This effect has been traditionally only implemented in atmospheric chemistry models, which are significantly expensive computationally than numerical weather prediction models that do not include detailed chemistry [292].

→ RCA4 vs. WRF351

The last version of RCA model (RCA4), used in this study, includes atmospheric parametrization. However, the model assumes clouds to be homogeneously distributed throughout a given grid box, the so-called plane-parallel approximation (i.e., cloud albedo are always higher than real clouds) [282]. Ayugi et al. [73] assess the performance of RCA4 in the simulation of mean seasonal precipitation over East of Africa. Results show an underestimation or overestimation depending on the season and regions with weak correspondence of the model with

observations. Strandberg et al. [500] demonstrate that RCA4 performs generally well when simulating the recent past climate taking boundary conditions from GCMs, as done in our simulations, than from ERA-interim.

WRF model has significant biases mostly in the representation of the aerosol-cloud-irradiance [422, 486]. WRF Solar—a configuration of WRF developed for solar energy applications—has improved representations of these interactions accounting for the aerosols direct effects [459] and indirect effect [512]; which has been found to yield more accurate shortwave irradiance [281].

Although the parametrization scheme of clouds and aerosols may explain the divergence between RCMs [312, 426], these differences between RCA4 and WRF351 models stated above are not sufficient to explain the potential contributors to the larger trend of solar irradiance and temperature of RCA4 simulations compared to WRF351 simulations.

Differences between GCMs

We also found a large spread in estimated amplitudes of solar irradiance and temperature between GCMs (Figure 5.9) which may be partly caused by the substantial differences in how GCMs project changes in sea-ice concentration and sea-surface temperature [500] or due again to the shortcomings in the representation of clouds and aerosols which tend to underestimate the low-frequency variations in surface solar irradiance [54, 555, 546], or precipitation [554, 53], soil moisture [317] and diurnal temperature range [552, 239].

→ CNRM-CM5.1 vs. EC-EARTH vs. GFDL-ESM2M vs. CCSM4

The version CNRM-CM5.1, used in this study, introduces a new irradiance scheme to improve the treatment of the tropospheric and stratospheric aerosols properties associated to volcanoes eruptions; and to better simulate the indirect effect of aerosols. However, major errors in the precipitation and cloud radiative forcing still persist [533].

The interaction of the EC-EARTH with slow components of the climate system and the parametrization of fast processes can still lead to severe biases impacting the climate sensitivity [250].

For the GFDL-ESM2M, biases in the representation of the shortwave irradiance budget and the shortwave albedo at the top of the atmosphere reveal large scale patterns (high albedo in some areas or low albedos in others with excessive low cloud resulting in overly high shortwave irradiance reaching the surface) [179].

The CCSM4 does not include a representation of the indirect effects of aerosols which tend to overestimate the globally averaged surface temperature over observations in addition to the poor representation of the direct effect of aerosols and the biases in the precipitation and clouds distribution [211].

No model is superior

Given the above, there is a clear indication that all models have certain limitations. However, due to our incomplete knowledge of the climate system, it is difficult to give a precise answer that one model is superior to the other in its aerosol and clouds representation because each model has a different description of physical phenomena and different numerical solutions, which produce different results and thereby high uncertainty of the projections of future optimal mixes [192, 511]. The question now relates to how different would the results be if different GCMs and RCMs are used? An in-depth investigation is required to explain the model-to-model differences obtained in our results and to “realistically” capture the changes of solar and wind CFs, which is left for future works (Section 5, Chapter 6).

Other Sources of Uncertainty

→ Natural Variability and Emission Scenario

In addition, as Tebaldi et al. [507] point out, inter-model comparison do not cover all ranges of uncertainty. Indeed, the climate projections are associated with different other sources of uncertainty than model uncertainty [57], namely the natural internal variations of the complex, nonlinear and dynamical climate system. If this variability is large, climate change signals can be difficult to detect. For instance, climate models indicate increasing frequency of extreme El Niño events in a future warmer climate [121], a change that would have an impact on the interannual variability of global mean temperature and on regional precipitation patterns. The uncertainty from natural variability can be reduced by better initialization of climate model runs when the forced climate change signal is still relatively small [249].

Another source of uncertainty comes from the emission scenario which is related to the several forcing components influencing future climate (i.e., greenhouse gases, aerosols and changes in the land surface). For instance, the climate scenarios used in CORDEX-Africa have been shown to strongly underestimate the present and future anthropogenic emissions of aerosols in Africa [319].

Hawkins et al. [249] conclude that the relative contribution from internal variability is largest in the near future (it does not affect the climatology but rather influence the daily synoptic condition [218]), while forcing conditions and climate system response dominates on longer time perspective.

→ Intra-daily Parametrization

At last, it is important to recall that an additional source of uncertainty in the projected optimal mixes may also results from the quality of the estimation of the intraday fluctuations of wind and solar PV and CSP CFs. Indeed, because CORDEX in the Middle East and North Africa (MENA) domain is only available at the daily time step, we apply the instantaneous output to daily means of wind speed and global horizontal irradiance. This parametrization approach is fairly simplistic and seems to not correctly resolve the intraday fluctuations which have a large impact on optimal mixes [215, 338], especially for CSP capacities, as shown in section 2, because it is highly dependent on the intraday variability of direct irradiance [313].

Indeed, as solar PV and CSP production are more variable during the day than wind production, ignoring intra-day fluctuations (left panel of figure 5.11) results in the distribution of more solar capacity than wind (with more CSP than PV) at low penetrations and to not reach the maximum budget sooner, PV is favored over CSP at high penetrations. When running the mean-variance analysis of PV-wind-CSP mix over the historical period with parametrization (right panel of figure 5.11), the problem is relatively solved between PV and wind (the share of wind is higher than that of PV and CSP as it leads to lower adequacy risk due to its uniform production, as shown in figure 3.2a in chapter 3) but not between PV and CSP. This demonstrates the importance of taking into account correctly the intra-day fluctuations not only when analyzing the interaction between solar (PV, CSP) and wind in optimal mixes but also between PV and CSP.

We recall here that the temperature estimations are computed from daily means. In fact, with the current climate conditions, this may cause a slight difference between hourly values due to the covariability between temperature and irradiance (low temperature and no irradiance at night; high temperature and high irradiance during daytime). However, under future global warming conditions, this covariability may be reduced due to anthropogenic gas emissions (implying high temperature and no irradiance at night, large temperature and irradiance during daytime) and thus intra-day estimations should be taken into account. Particularly, this matters more in summer when temperature errors in the diurnal cycle are largest and irradiance errors likely maximize [462].

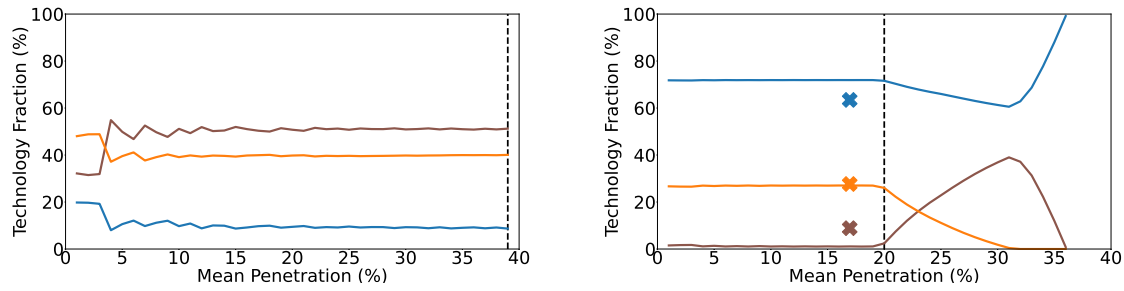


Figure 5.11: PV ILR1-wind-CSP SM1 mix, obtained from COordinated Regional climate Downscaling EXperiment-Coupled Model Intercomparison Project Phase 5 (CORDEX-CMIP5) climate data, using the Rossby Centre regional Atmospheric model (RCA4) as regional climate model, forced by the Centre National de Recherches Météorologiques-Coupled Model (CNRM-CM5) global climate model, without (left) and with (right) intra-daily parametrization over the historical period. Relatively similar optimal capacity pathways were found whatever the experiment and the CORDEX-CMIP5 climate model (Table 2.2, Chapter 2) and thus are not shown here. Inverter Loading Ratio (ILR) or Solar Multiple (SM) of 1 means without storage.

3 Options for Climate-Resilient Renewable Mixes

The expected changes in solar irradiance and temperature are important to take into account as they can modulate changes in PV and CSP output and may have an impact on the reported signals of CSP and PV CFs.

Conditions for Positive CSP, PV and Wind Climate Change Induced Impacts

CSP power plants may profit more from projected temperature than PV plants since greater CSP efficiency is achieved for high operating temperature (i.e., small differences between the fluid and ambient temperatures). However, the increase in the saturation water vapor pressure associated with warming—according to Clausius-Clapeyron law describing the changes in humidity with temperature—and increasing aerosol and clouds may limit the CSP penetration. The increase of temperature also affects the CSP efficiency plant as the water supply for cooling purposes is constrained.

Rising average temperatures will improve the performance of solar PV modules in cold regions, but will have a somewhat negative impact on the efficiency of PV panels, especially crystalline silicon used in this study. PV also perform less in the event of prolonged cloudiness which may impact the penetration rate of PV in the grid [278, 186], but less so for PV than CSP since the total amount of solar irradiance reaching the panel is relevant (i.e. the sum of the direct and diffuse irradiance) for PV, while CSP only depends on energy obtained through the direct radiative beam and does not use diffuse irradiance [141, 550].

Therefore, CSP and PV will have a positive climate change impacts if the projected increase in solar irradiance (i.e., cloud cover and aerosols decrease) compensates the negative warming-induced effect (i.e., increase of humidity, decrease of cooling CSP efficiency and decrease of PV solar panel efficiency). In this context, Ebinger et al. [181] suggest the re-location of solar plants based on expected changes in cloud cover and temperature.

For wind, regions with low temperature and high wind speed would have a relative advantage for wind development. However, extremes of low temperature present also a potential risk to wind turbine blades, causing icing [428]. Therefore, wind climate change induced impacts are positive if the wind speed increase overpasses the air density decrease (resp. increase) resulting from warming (resp. cooling).

Solution for Negative Temperature-induced Effect: Temperature-dependent PV and Water-dependent CSP

This paradoxical effect of temperature calls for exploring new options for making PV less temperature-sensitive [405] and to reduce the dependency of CSP plants on water for cooling by using dry cooling systems [563] to resist to drought (especially with upcoming water resources scarcity [144]) even though the efficiency of the plant will decrease [348, 451] which would, *ceteris paribus*, increase the levelized cost of electricity. Water desalination may also be good option in such arid regions [522].

In general, increased temperature has a negative effect on crystalline silicon solar panels [433, 362] making them relatively sensitive to climate change in regions expecting a large temperature rise indicating that these technologies will also perform poorly in regions with high solar irradiance. As crystalline silicon is a mature technology, efficiency improvements have been relatively small in the last decade. However, the efficiencies of other technologies have been improved during the last years [419] and may perform better in warming climate [333, 123, 222]. For instance, in section i (Chapter 1), we report some PV technologies that have large and positive temperature and irradiance coefficients, indicating that they are notably robust to climate change in regions where irradiance and temperature are expected to increase.

An increase in wind speed may reduce the solar panel temperature (A.66) because forced air convection removes heat from the solar panel [408, 456] and therefore increase the PV output. However, wind speed can negatively affect the solar mean CFs via their impacts on the synoptic circulation and the displacement of dust from the source regions (e.g., African Sahel) which emit greater quantities during dry years to the different regions; favoring the dust deposition on PV arrays and CSP collectors which decrease the efficiency of PV and CSP plants and increase the costs and water use [427, 280]. The use of tracking systems to turn them out of the wind, are possible responses to this problem [244].

Solution for Negative Clouds-induced Effect: Tracking or Mounting Angles

We also observe from RCA4 simulations (Figure 5.9 (a),(b)(c)) that, the Direct Normal Irradiance (DNI) increase is the largest with Global Tilted Irradiance (GTI) following before Global Horizontal Irradiance (GHI); which further increases CSP mean CFs compared to PV mean CFs (Figure 5.3). Thus, changes (e.g. increase) in solar irradiance on tracked or tilted planes, investigated here for CSP and PV, can be higher compared to the respective changes on horizontal plane (consistent with [368]). The mounting angle [64] and tracking system [297] can increase the solar production under diffuse light conditions by reducing the zenith angle and thus the air mass (Section 2). However, this also depend on the amount of clouds projected since the opposite trend is projected by WRF351 simulations (Figure 5.9 (d)), namely DNI is more altered by climate change than GTI or GHI.

For PV where the diffuse light is useful, it would be beneficial to use rougher surface as they capture light from multiple angles [376].

Solution for Negative Temperature and Clouds Induced Effects: Large Storage Capacity or Diversified Mix

One would expect that the warming and clouds induced effect on PV and CSP CFs can be reduced by using storage. Our results show, however, a robustness in the trend of CSP-TES projecting a decrease of the fraction of this technology, whatever the penetration scenario (Section 3). We explain that by the fact that the combined period of cloudiness and darkness exceeds the low thermal storage capacity of CSP-TES SM2 (6 hours), and the system operators have to rely on other options to cover the demand in nighttime where the increase in temperature (and hence the demand for air-conditioning) is expected to be higher than in daytime, partly because the greenhouse effect hinders nighttime cooling, and partly because of changes in cloud [321]. Unlike PV which operate primarily in the daytime, CSP with thermal storage generates throughout the night and thus is negatively impacted in hottest conditions [405]. This encourages the installation of CSP-TES in deserts that are cold at night because of the lack of water in the soil and little water vapor in the air.

From our results, CSP-TES with small amount of storage (SM2) is not a good option to reduce the climate sensitivity. However, in spite of being more expensive than PV and wind (Table 2.6, Chapter 2), CSP-TES with higher storage capacity (we find more than 17 hours per day on average of TES or SM>4, not shown here) may help maintain the production during night or during sand storms [63, 405] or cloudy weather. In fact, the ability of CSP with large solar multiple (i.e., CSP solar field size and storage capacity) to meet the demand whenever it is needed provides a potential to more easily follow the variations of other RE production. For instance, when the increase of temperature pose a problem for PV solar panel efficiency or wind output. This means that fewer inflexible base-load generators will be needed to operate at part load during periods of high or low solar output due to its high capacity credit (as shown in section ii, Chapter 3 and section ii, Chapter 4). In this context, the deployment of CSP-TES plant with high amount of storage could allow the de-commitment of the Moroccan coal plants and can avert future investments into conventional plants; making Morocco powered by 100% RE which helps to full-fill present and upcoming greenhouse gas mitigation targets. This may also reduce the Morocco's dependence on externally sourced coal and heavy oil as well as electricity imports. In consequence, the investments in 2100 must be increased to install more CSP with storage (as discussed previously in section 3, Chapter 3).

However, if Morocco is not ready to increase its investment in REs, a mix that rely on wind and PV or CSP without storage or CSP-TES with small storage capacity will be particularly important to reduce the variance (left side of top, middle and bottom panels of figures 5.1 and 5.2) in order to be able to cope with the growing future peak demand to substitute the consumption of fossil fuels as stated previously in section 4 (Chapter 3), but confirmed here with different climate data sources and the period of analysis is longer and covers also the future projections. Having alternative means to produce energy instead of relying on a single source can reduce the vulnerability of the system to climate change [455].

4 Regional Effects of Climate Change

The change of mean solar irradiance and mean temperature over 2071-2100 versus 1976-2005 climatology under the RCP 8.5 climate change (Figure 5.9) show that there are considerable regional differences giving an indication about the future warming in Morocco exhibiting the regions the most affected along with uncertainty in the projection of solar and wind resources.

Regional Projection of Temperature

As can be seen, it is evident that all regions are very likely to warm during the 21st century with high confidence (Figure 5.9). However, the warming is still limited along the coasts (NORTH) than in land surfaces (EAST, CENTER). This is consistent with the multi-model ensemble used by Ref. [341] suggesting that the greatest warming is projected over more arid areas; and Ref [540] show that seasonal warm anomalies over land are more pronounced during summer than during winter. Enhanced warming of continental regions relative to oceans occurs simply because continental air masses are drier than maritime ones suggesting a trend towards drought. The strong land-sea contrast in the Mediterranean basin (In the NORTH) is caused by the significantly larger heat capacity of the oceans, which attenuate the warming compared to land areas (because of moisture advection from the seas). Along the Atlantic coast, the climate is semi-arid/arid but with oceanic influence (CENTER and SOUTH) resulting in smaller increase of temperature.

According to temperature projections, the increase in the number of summer days will reach high values in the continental regions and thus more frequent drought period are expected by the late 21st century than in regions along the coast.

Regional Projection of Irradiance

Negative signals of solar irradiance prevail everywhere in CCSM4 driven WRF351 simulations (Figure 5.9 (d)), with higher magnitude albeit rarely over-passing the limit of $20W/m^2$; while GCMs-driven RCA4 simulations are generally consistent with a pattern of increasing solar irradiance over the northernmost regions (NORTH, CENTER and EAST) and decrease over only southern regions (Figure 5.9 (a),(b),(c)). A likely explanation of the non-robustness in the sign of change in the northernmost regions is the highly complex orography of these regions, which has a strong impact on the simulated regional climates.

The southern regions—featuring a desert climate (clear sky conditions) with a moderate temperature along the coast—display a decrease in solar mean CFs (Figure 5.3) as a result of the limited solar irradiance in this region and all models agree with this negative signal of solar irradiance (compare Figure 5.9(a)(b)(c) with Figure 5.9(d)) probably due to the poleward shift of the Hadley cell. An interpretation of this could be that the clouds and aerosols—the first and second climate variable contributing to solar power output changes [181]—will experience a slight increase or the climate model overestimates the cloud cover and / or overestimate the radiative impact of the simulated clouds in this region and thus strong enough to offset the increase in DNI and GTI and produce a decline in CSP and PV mean CFs.

RCA4 model project a positive signal in the northernmost areas with an intermediate strip in CENTER and EAST. In fact, this response is typical of that of the North Atlantic Oscillation during its negative phase which induces less windy and cloudy conditions in northern areas and windier and cloudier conditions in South, compared with what prevails during its positive phases [424, 277]. In fact, the northerly regions along the Mediterranean coast are benefiting from increased solar irradiance (Figure 5.9(a)(b)(c)) due to the penetration of slightly hot and dry air from the Mediterranean Sea by coastal circulation. In addition, over the Mediterranean areas there is agreement among studies that irradiance will increase [415] and this will lead to an increase in solar PV output despite the temperature increase, which explain the high PV mean CFs in northerly region (Figure 5.3 (a)(b)(c)). This projection seems also to agree that cloud cover will decrease in low- to mid-latitude regions [520, 405, 341] (i.e., Morocco).

With that being said and according to GCM-driven RCA4 simulations, the northerly regions may profit from climate change in terms of CSP since the formation of clouds is blocked by high mountains; but also of PV energy production since the substantial increase in solar irradiance trends can compensate for rising surface temperatures, whereas continental regions (EAST and CENTER) are likely to face declining PV energy outputs but does not compromise the development of CSP.

However, our model (the last paragraph of section 3) is given less weight to the northern regions at low penetrations (Table 5.1) since higher amplitude oscillating energy sources implies high variance^{2.2} as the region also faces a lot of variability between the Atlas Mountains and the coasts. The regions along the Atlantic coast (CENTER) and continental region (EAST) where the deficit of solar irradiance (Figure 5.9(a)(b)(c)) may be attributable to cloudiness are favored to reduce the variance of PV and CSP/CSP-TES (Table 5.1). In fact, optimal mixes strongly depend on the level of variance that is tolerated. As a consequence, capacities are not necessarily distributed where they would be expected based on the mean.

VI Summary and Concluding Remarks

Motivation

Climate change will have a notable impact on solar and wind plant output and energy demand.

Research Questions

In the first and second part of this study, we focus on the common features obtained from COordinated Regional climate Downscaling EXperiment-Coupled Model Intercomparison Project Phase 5 (CORDEX-CMIP5) models by comparing the climate change and cost effect on Moroccan optimal allocation of variable and dispatchable Renewable Energy (RE) technologies—after the mid-21st century compared to historical climate trend across a set of penetration scenarios keeping the current capacities and rental costs data—and by shedding light onto differences in capacity pathways with hourly simulations from the Modern-Era Retrospective Analysis for Research and Applications 2 (MERRA-2) climate reanalysis; while in the third part we examine the robustness of the sensitivity of technological and geographical distribution of capacities to climate change through analysis of solar and wind mean resources and mean Capacity Factors (CFs) along with the seasonal variability of these CFs and demand.

Objectives and Methodology

To do, our objective is to minimize the variance for a given level of expected penetration or, equivalently, to maximize the expected penetration for a given constraint on variance; while not outpacing the maximum-cost budget. Hourly time series of demand and production of wind, Photovoltaic (PV) and Concentrated Solar Power (CSP) without and with 6 hours of Thermal Energy Storage (TES), Solar Multiple of 2 or SM2, over Morocco are computed using two Regional Climate Models (RCMs), the version 4 of the Rossby Centre regional Atmospheric model (RCA4) and the version 351 of the Weather Research and Forecasting model (WRF351), obtained by CORDEX in the Middle East and North Africa (MENA) region "MENA-CORDEX". Different Global Climate Models (GCMs)—Centre National de Recherches Météorologiques-Coupled Model (CNRM-CM5), Earth System Model (EC-EARTH), Geophysical Fluid Dynamics Laboratory's Earth System Model (GFDL-ESM2M), Community Climate System Model (CCSM4)—have been used to provide initial and lateral boundary conditions. Simulations are done under one emission scenario, Representative Concentration Pathways (RCP) 8.5 (business as usual). To take into account the intraday fluctuations not resolved by CORDEX data in the solar and wind production, a rough estimation of the order of magnitude of the intraday variability of the clearness index and wind speed are included in the CFs models keeping a daily record of the temperature.

General Findings

In summary, the analysis of the future climate change projections (2071-2100) on the distribution of capacities with respect to the historical climate conditions (1976-2005) could identify that optimal mixes under RCP 8.5 scenario undergo relatively significant changes at high penetrations, albeit one that is minor in the context of anticipated cost reductions. However, the impacts of changes on the mean climate conditions do not appear to be substantial for any of the four technologies at low penetrations.

The results confirm the robustness of the optimal mixes at maximum penetration where the maximum-cost constraint is strong and thus optimal capacity distributions are more sensitive to cost of the technological combinations than to climate change-related risks. Wind is (resp. PV and CSP are) resilient (resp. sensitive) to RCP 8.5 climate change.

If high penetrations are targeted, the RCM uncertainty increases for PV and wind, but not for CSP. It is noted that these uncertainties are associated with large uncertainties in the projections of the resources. In conclusion, we find that the results are robust in projected temperature change, while projections for solar irradiance and wind speed are largely uncertain. At such high penetration scenarios, wind and CSP are (resp. PV is) sensitive (resp. resilient) to RCP 8.5 climate change.

At low penetrations, where the cost effect is negligible and the variance play a role, the RCM uncertainty increases for all technologies. For all the three downscaled GCMs using RCA4, given that change in CSP output is dominated by change in irradiance rather than temperature, it is not surprising that the CSP CFs range due to temperature change is very small and an increase in solar irradiance implies an increase in CSP CFs. However, the increase in temperature induces a significant reduction in the PV CFs compared to CSP CFs which imply negative response to climate change in summer peak load and thus strong penalization of fixed tilted PV in optimal PV-wind-CSP mix compared to tracked horizontal CSP surface. In this case, optimal mixes react to RCP 8.5 climate change impacts with increased wind and CSP electricity generation to compensate for the reduced PV CFs and increased summer peak demand. However, the projected changes diverge as a result of increasing both RCM and GCM uncertainty. For CCSM4 driven WRF351 simulations, the large decrease in solar irradiance coincides with comparatively small increase in surface temperature and wind speed. Thus, optimal mixes computed from WRF351 simulations with future RCP 8.5 climate change result in an increase in PV capacity due to its positive response to climate change in summer peak load, and a reduction of wind and CSP capacity.

Yet, it is not possible to tell, from the results obtained in this study, whether the discrepancies between models, particularly at low penetrations, are due to the uncertainty related to the formulation of the climate models we use to produce scenarios for the future; or to the imposed changes in aerosols (and thus their impacts on the atmospheric properties and/or cloud cover patterns); or the variability in projections is due to the chaotic and nonlinear nature of the climate system, which complicate drawing conclusions. In particular, we suggest that the different parametrization used in each RCM, and more specifically the ones for cloud cover and aerosols, play an important role explaining this large RCM dispersion. In fact, aerosols can fully modulate irradiance via their direct impacts on the incoming solar irradiance and their indirect impacts on cloud cover. Aerosol-cloud-irradiance interaction are, thus, among the characteristics that should be taken into account when dealing with climate modeling.

Our results also show that the uncertainty in climate data sources and associated assumptions can be large and impact the mean-variance results. At low penetrations, we find that optimal mixes are prone to biases in the resolution of the intraday variance of the solar production resulting in installing more CSP than PV. At high penetrations, we find that the underestimation of CSP CF variance makes CSP able to achieve high penetration range while reducing the global variance.

All climate models agree that CSP with small storage capacity (6 hours per day on average) is insufficient to serve the demand and it is expected to decrease in future energy mixes, whatever the level of penetration.

Lastly, we discuss that the technologies making PV less temperature-sensitive and CSP less water-dependent, tracking system, CSP with high storage capacity (more than 17 hours per day on average or $SM > 4$) and a diversified mix of wind and PV/CSP or CSP-TES with small storage capacity in an energy system may have a profound influence on its resilience to climate impacts.

At low penetrations, the geographical distribution of capacities by the end of this century compared with the estimations made under historical climate conditions is not altered by climate change nor by climate data sources, with the largest minimum variance ratio in SOUTH for wind, CENTER for PV and EAST for CSP/CSP-TES. At high penetrations, the geographical distribution of CSP/CSP-TES seems to be substantially more sensitive to climate change than PV due to the model projections of direct solar irradiation whose variation depends on the clouds and aerosols; while the geographical distribution of wind is only sensitive to climate data source at maximum-penetration mix where the climate change induces the installation of wind capacities in SOUTH due to the reduction of the mean CFs in eastern region.

Qualitatively, CSP CFs are expected to increase in large parts of Morocco, mainly in the northernmost regions (NORTH, CENTER, EAST) as a result of climate warming and increasing direct solar irradiance over the coming decades according to RCA4 simulations. However, the results in these regions are non-robust with WRF351 simulations. All models agree that negative trends are only projected to be reached in region where cloud cover may increase substantially (i.e., direct irradiance decreases) most notably in the southern region. In contrast to CSP, PV output decreases with increasing temperatures and given that all CMIP5 models project an increase in temperature, PV solar panel temperature effect prevails everywhere resulting in a decreasing PV CFs over different regions, with few exceptions in northernmost regions (NORTH, CENTER and EAST) where RCA4 simulations project that all components of solar irradiance retains high values, while southern regions or other regions (according to WRF351 simulations) project negative trend in irradiance which is also combined with the temperature effect leading to a little relevance for PV.

General Conclusions

Contents

I	Synthesis	146
1	Research Motivation	146
2	Focus of the Thesis: Tool, Objectives and Methodology	147
3	Research Questions and Main Findings	147
II	Contribution to Research and Implications	151
III	Thesis Limitations and Perspectives	151
1	Use Better Energy Data and Improve Bias Correction Approach	152
2	Additional Sensitivity Analysis	152
3	Compare the Flexibility of CSP-TES and PV-BES to Other Flexibility Options	153
4	Quantify the Avoided Costs and Emissions	153
5	Tackle Climate Change Uncertainty	154

I Synthesis

1 Research Motivation

Recognizing the potential for further cost reductions [270], projections of renewable energies (REs) in climate change mitigation plans have risen. Specifically, the growth in deployment of solar technologies such as Photovoltaic (PV) and Concentrated Solar Power (CSP) with their Battery (BES) and Thermal (TES) energy storage systems will be needed in the next three decades to achieve the Paris climate goals [133]; and could together provide a relevant proportion in the energy mix for a country with high solar resources such as Morocco [393].

However, although both technologies generate electricity from the sun, there are three crucial elements for their integration. Firstly, PV and CSP collect different resources which affect their mean production and market deployment. Secondly, the technology to be installed should feature low cost. Thirdly, it should contribute to satisfy the consumption during peak times occurring in the evening or when hot weather begets ever more demand for air-conditioning; and thus enhance the energy system resilience to climate change.

In terms of mean production and market deployment, multi-crystalline PV has a negative response to high temperature and a positive response to global irradiance (direct and diffuse); while CSP has a positive dependence on both temperature and direct irradiance but more sensitive to clouds and aerosols [141]. As a result, PV can be installed anywhere that the sun is shining; and the higher scalability of PV systems makes them suitable to cover both power plant and residential sectors and are able to perform well also at high latitudes [412]; whereas CSP is heavily location specific (viable only within the sunbelt [90]) and hence transmission grid is essential for CSP [165].

Considering these dependence on climate, one can expect that although these technologies could help lessen the worst possible impacts of climate change, the changing climate also impact their resources and generation. Another barrier in adoption of CSP and PV in the context of climate change is the dust deposition on these plants and the limited water availability in typical locations with high irradiance [563, 122]. In fact, water is primarily used as a cooling agent for CSP steam turbine condensers. PV makes limited use of this resource as it is only needed for cleaning purposes.

When it comes to cost and variability, the capital cost of CSP seems to be much higher than PV [266]; while the generation of both is constrained by the temporal availability of the resource in a particular location. In addition, the overproduction of both at midday lead system operators to either curtail their generation (resulting in wasted energy) or turn off the base-load generation and once they are shut down they cannot ramp up quickly to deliver energy into peak evening demand period when the sun sets and the contribution from solar falls and electricity prices increases as well (i.e., the famous duck curve phenomenon [47, 158]). Our results have demonstrated that the variability of both can be alleviated by tracking or /and storage systems. For instance, if north-south tracking is used, the production can be distributed evenly during the day and can be positively correlated with the Moroccan summer peak. It also meets heating demand due to being available during winter seasons. However, tracking is commonly used for CSP while PV mounting systems are fixed. On the other hand, if both integrate storage, they can store energy during daylight hours and transform it into electricity at a later time (e.g., during night, cloudy periods) making them competitive with fossil fuel generators. However, Lithium-ion batteries deployed with PV could not compete economically with the thermal storage option combined with CSP [266]. Besides, most batteries only provide backup for transient daytime needs and thus are not commonly employed in large-scale grid-connected PV plants [108]. In addition, to increase the hours of operation of both technologies, the size of the

plants and that of the storage system must be increased to be able to capture more solar irradiance and control the production over time by shifting the production of electricity from off-peak periods to peak periods while simultaneously arbitrating inter-temporal electricity price differences; which affect both the production costs (i.e., revenues) and carbon emissions [284]. Yet, current investment costs are too high for large-scale solar plants with large storage capacity [194, 268].

These differences between solar technologies influence their competitiveness in optimal mixes with different penetration scenarios. **The solar integration paradigm, thus conceals some important questions:** Does PV/PV-BES competing with or winning over CSP/CSP-TES? For instance, PV is better than CSP? If the comparison criteria is money, the answer is probably yes, but if we want to meet the demand in the most economic way (low cost) but also in the most reliable way (low variability), which solar technology will prevail? where should be installed and how much of it? How should these solar systems co-locate with wind in current and future optimal capacity mix taking into account the temporal and spatial complementarity of production between Moroccan regions with diverse climate? Which technology lead to curtailment? Does the addition of TES to CSP and BES to PV worth in reducing the integration challenges (i.e., reducing curtailment, increasing capacity credit)? What are the benefits gained by using tracking? Do these options (storage and tracking) enable greater penetration of solar energy and thus bring evening and seasonal needs to a minimum? If yes, this mean that flexibility (i.e., imports of electricity; or conventional generation systems, etc) are eliminated and thus energy dependence, integration costs and greenhouse gas emissions are reduced? What about the actual mix? How far could the Moroccan RE penetration increase without assuming higher risks?

Overall, what is the impact of storage, cost, spatio-temporal complementarity and climate change on optimal capacity allocation under different scenarios of penetration and storage requirements?

In review of the latest developments in RE, the answer to these questions is rather controversial.

2 Focus of the Thesis: Tool, Objectives and Methodology

This thesis is divided into three studies to give an answer to above-stated questions by discussing a set of penetration scenarios of large-scale solar and wind capacities in prospective optimal mix; considering current and future climate conditions and addressing different combinations of onshore wind without storage and variably sizable fixed latitude-tilted multi-crystalline PV and north-south tracked horizontal parabolic trough CSP; keeping recent (2013) cost data and existing (2018) generation assets.

To elaborate energy mix scenarios, we use the E4CLIM tool that allows from geographical data for specific area and from climate data to compute hourly Capacity Factors (CFs) and energy demand profiles adjusted to observations and to optimize the RE electricity mix; taking into account the time-space variability of both the generation and the demand [504]. The adaptation of E4CLIM to the four Moroccan electrical zones, including the data sources and the calibration process, and the main contribution to it are presented in chapter 2.

We take as objective not only to maximize the mean RE penetration at a given cost, but to provide adequacy services to the electricity system by reducing the variance of the RE production; which corresponds to minimizing costs or emissions of conventional production (proxy of risk). This bi-objective optimization problem is inspired by the Markowitz Mean-Variance Portfolio theory in which the distribution of RE capacities is optimized technologically or geographically or both in order to evaluate the impact of spatio-temporal complementarity. To explore the sensitivity of mixes to storage, we propose a methodology for increasing the storage capabilities—in the added CSP-TES and PV-BES modules—in which the size of the CSP solar field (resp. PV Solar Panel) determines both the thermal power capacity and the volume of storage — as defined by the CSP Solar Multiple or SM (resp. PV Inverter Loading Ratio or ILR). We take into account the differences in terms of cost by adding a maximum total cost constraint to the optimization problem that is not to go beyond; and propose a method to define the rental cost of production and storage technologies accounting for the increasing storage size compared to the CSP Solar Field (resp. PV Solar Panel) while keeping the cost of the latter fixed to be coherent with the fact that the mean solar CFs of different amount of storage change a little bit due to bias correction. We present some optimization post-processing ratios to identify the relevant contributing factors in determining the region where a given capacity will be allocated to, as it makes more sense when compared to another technology in another region; and thus determine the conditions under which each technology presents an advantage over the others for each penetration regime. Finally, to examine the ability of each technology to replace conventional production during the peak/mid/base load hours (which is not measured by the variance-based risk), we perform some load reduction diagnostics to assess the average “physical” value of electricity. To analyze the seasonal and daily correlation of production with consumption (which is also not measured by the variance-based risk), we use the heatmap tools. Finally, an inter-model comparison has been carried out for climate change induced impacts on optimal capacity pathways.

3 Research Questions and Main Findings

The design of scenarios of solar integration with wind, and particularly the best split between solar technologies under specific objectives (either increasing the penetration while not reaching the maximum budget sooner or minimizing the risk) is discussed by solving many questions. The research questions to be answered in this thesis are summarized as follows with a brief discussion.

i *First Study: Adequacy of Renewable Energy Mixes with Concentrated Solar Power and Photovoltaic in Morocco: Impact of Thermal Storage, Cost and Spatio-Temporal Complementarity under Penetration Scenarios*

The first study of this thesis addresses the first research question: **Q1: What is the response of the regional renewable energy scenario mix—including low-cost and variable solar PV and wind energy as well—to the integration of expensive CSP without or with increasing levels of cheap thermal storage; and how does it impacts the benefits of spatio-temporal complementarity ?** This question is answered in chapter 3 in three steps after modeling the optimal recommissioning of RE mixes including PV, wind, and CSP without and with different storage size (SM 1 to 4) using the Modern-Era Retrospective Analysis for Research and Applications 2 (MERRA-2) climate reanalysis over the year 2018 (Chapter 2).

First, we analyzed the impact of cost and thermal storage associated with these technologies on the Moroccan optimal mixes. We examine their interaction under penetration scenarios, particularly the level of variance/penetration at which the benefits of CSP-TES are outperformed by that of PV and wind (i.e., the economic carrying capacity). Second, we examined the role of temporal, spatial and spatio-temporal complementarity in smoothing power output over the year. Third, we compare the role of PV, wind and CSP-TES in replacing peak/mid/base conventional generators.

→ **Sensitivity to Cost and Thermal Storage—Technological and Geographical Distribution:** At high penetrations, the optimal mixes are highly impacted by cost the more so as CSP with large solar field size are installed. Thus, to prevent reaching the maximum-cost sooner,

wind has higher share than solar technologies due to its largest mean Capacity Factor (CF) compared to rental cost implying less capacity to install to fulfill the high-penetration requirements. PV has the lowest rental cost but its limited CF leads to a downward trend of its fraction with the increase of installed capacity. CSP is by far the largest expensive technology and its CFs, although for high SMs, are roughly equal (due to the bias correction) which unfairly penalize CSP/CSP-TES at such high penetrations.

At low penetration levels, the optimal mixes are sensitive to thermal storage rather than cost. **Wind vs. PV/CSP:** Wind dominates over PV and CSP without storage because it provides a regular source of energy over the day and the year. **PV vs. CSP:** PV replaces CSP because despite their similar daily profile, the solar tracking of CSP compensates for the absence of conversion of diffuse irradiance which increase its CF compared to PV implying larger variance. **PV vs. CSP-TES:** CSP with storage, however, can generate enough power during daylight and release stored energy at night or during a period of cloudy weather and thus tend to have larger minimum-variance ratio and replace completely PV. **CSP-TES vs. Wind:** CSP-TES with small amount of storage (<6 hours or < SM2) is still have smaller minimum-variance ratio than wind. However, the more the storage duration is increased (>6 hours), the more CSP-TES becomes less variable in output than wind and dominates over the latter.

To increase the mean CFs, PV is installed in SOUTH while CSP/CSP-TES tend to be economic in CENTER. In mixes favoring a low variance, PV is favored in CENTER; CSP without / with small amount of storage (SM1, SM2) is installed in EAST but if large storage capacity (SM3, SM4) is assumed to be in place, southern regions are preferable. Wind, on the other hand, is installed in SOUTH with high wind speed and low roughness (due to nearby coast) at low/intermediate penetrations. However, at the point approaching 100% wind share, wind is favored in eastern mountain ridge although highly variable wind, but the variance does not play a role at such maximum penetration.

→ **The Temporal Complementarity** between PV and wind in the same region is weak (different resources are exploited) and thus are both installed to reduce the risk of not covering the load. The technological complementarity between PV and CSP without storage is relevant and must be taken into account to reduce the variance. The mix, in this case, is less diversified although little north-south tracked CSP is introduced at the expense of fixed tilted PV to satisfy the summer peak demand.

→ **The Regional Complementarity** has large effect in reducing the standard deviation of RE production such as PV/CSP and wind whose energy production trends exhibit decreasing coefficient of correlation with an increasing distance between sites (micro-scale circulations such clouds and turbulence of wind speed decorrelate quickly with distance). Thus, the deficit of RE production in region x is complemented by its availability in region y.

However, this effect of technological and regional complementarity is less relevant when the surplus of energy available for thermal storage increases because mixes become less diversified.

→ **Role of CSP-TES in Displacing Peak/Mid/Base Conventional Generators Compared to PV and Wind:** PV or CSP without storage can only contribute to some midday load hours while wind CF is uniformly distributed over the day and the year and is strong on average allowing to reduce the base load but leads to curtailment at very high penetrations. CSP-TES is able to increase the capacity credit and reduce the mid/base load reduction better than PV/wind enabling higher solar penetration in the mix which avoid wind curtailment.

Several scenarios are further discussed below.

→ **Scenarios of Unlimited Thermal Storage Cost and Capacity:** We found that ignoring the thermal storage cost and considering unlimited storage capacity do not impact the technological and geographical distribution of capacities because thermal storage can be affordable to store the energy at large-scale in the form of heat; and unlimited storage capacity does not make sense since the maximum thermal power of CSP is already large enough to capture the surplus of production although in case where the constraints on the volume of storage are applied. However, we note that optimal mixes are less sensitive to cost as the CSP-TES fraction curve does not show an abrupt fall, in very low penetration levels, after the activation of the cost constraint.

→ **Scenarios in which High Penetration is targeted but with Low Investment without caring about the Adequacy Risk (or minimized by existing flexibility options):** The results have proved that investors should be encouraged to continue investment in wind plants to increase the penetration because the needed investment is lower and wind has strong CF on average in Morocco; and despite the output tend to be higher during windier periods of the year, it also increases through the remainder of the year (i.e., summer peak demand). In this case, the adequacy risk may be minimized by existing flexibility options such as imports or demand response mechanisms, etc.

→ **Scenarios in which High Penetration and Low Adequacy Risk are targeted and with High Investment Budget:** Due to the maximum cost constraint, the model installs CSP-TES only at low penetrations. We discuss that although the upfront capital cost of CSP is still high, if CSP incorporates cheap TES with sufficiently large solar field size and storage capacity (17 hours for SM4), it may be an appropriate technology for high penetration scenarios because the operators may dispatch electricity generated at any time which helps address grid integration challenges related to the variability of solar PV and wind energy, i.e., solving the problem of the duck curve phenomenon by exploiting the surplus of production during the midday and increasing the capacity credit by restituting the energy when the output correlates poorly with energy consumed, which will ultimately lower the cost of energy (increase the economic revenues) and reduce renewable-related reserve costs and emissions, which translate into low system cost. However, the investment in this technology would need to increase by implementing a de-risking approach to reduce the investors' risk perceptions and to push forward the installation of large-scale CSP-TES plants in Morocco.

→ **Scenarios in which Low Penetration and Low Adequacy Risk are targeted and with Low Investment:** The results show that to reliably meet the electricity demand without further investment in RE capacities, the solution has to come from a diversified mix of wind and PV or CSP-TES (SM2, SM3) with regional complementarity as it can help reduce the temporal fluctuations of RE production and the location-constraints (as resource availability tends to be far away from consumption centers).

CSP without storage is not economically advantageous and despite its positive correlation with the summer peak, a rainy/cloudy climate and no CSP generation at night respectively, limit its high penetration.

The low or high temporal co-variability between energy sources in the same region should also be taken into account to not install less or too much capacities, avoiding the increase of the adequacy risk (since deficit of production or adding more generation from new intermittent source increase the risk).

ii **Second Study: Utility-Scale PV-Battery versus CSP-Thermal Storage in Morocco: Storage, Cost and Spatio-Temporal Complementarity Effect under Penetration Scenarios**

The second study of this thesis addresses the second research question: **Q2: If the low-cost PV system has expensive battery storage with different levels of storage as expensive CSP with cheap TES, how do the optimal mixes integrating these two solar technologies interact with wind under penetration scenarios; and which dispatchable solar technology displaces more conventional generators?** This question

is answered in chapter 4 in three steps following closely the methodology adapted in chapter 3 but the PV model integrates now the battery with different storage size, ILR2,3 and 4 (Chapter 2).

First, we analyzed the conditions under which the advantages of CSP-TES overpass the advantages of PV-BES by examining how they interact with wind under various penetration scenarios. Particularly, the total optimal capacity level at which the fluctuating but least-cost generation technologies (i.e., wind or solar with small storage capacity) should have a priority on dispatchable but expensive technologies (CSP-TES or PV-BES with large storage capacity). Second, we compare their influence on spatio-temporal complementarity. Third, we explore how major integration challenges that represent the impact of the variability are affected by the share of RE; and which technology has stronger impact on reducing the adequacy risk (i.e., typically reducing the need for peaking capacity due to its coincidence with demand patterns).

→ **Sensitivity to Cost and Storage—Technological and Geographical Distribution:** We deduced that, the more we introduce CSP with larger solar field (resp. PV with larger solar panels) area, the more the optimal mixes become sensitive to rental cost demonstrating the highly sensitivity of the mix to storage (TES and BES) and CSP cost.

At high penetrations, wind remains a preferable option as it generates enough electricity to reduce the total cost followed by either PV-BES or CSP/CSP-TES. **Scenarios with High Penetrations—High vs. Low Storage Requirement:** While installed CSP-TES capacities vastly outpace PV-BES in scenarios without or with medium storage capacity (5 to 13.5 hours or SM<4 and all ILRs), PV-BES with lower storage cost configurations would be preferable for scenarios with longer storage duration (>13.5 hours or SM4).

At low penetrations, **PV-BES vs. wind:** PV-BES with low storage capacity (5 hours or ILR2) delivers more fluctuating power than wind. However, as the stored electricity needed to be available increases over peak hours, PV-BES is favored. **PV-BES vs. CSP:** Obviously, adding storage to PV will not affect the large minimum-variance ratio of PV-BES compared to CSP without storage. **PV-BES vs. CSP-TES:** CSP-TES is far favored than the equivalent storage design of PV-BES because the former has larger storage capacity and thus stronger impact on reducing the adequacy risk and replacing the expensive peak load plants while PV-BES is found to perform worst due to its low storage capacity which involve the need for balancing whenever the sun does not shine, that is, every night or when clouds blocks solar irradiance. As the surplus of electricity provided by PV-BES outstrips available storage capacity of CSP-TES for a given storage design, PV-BES gains greater penetration than CSP-TES. We note that both can reduce the wind curtailment since the solar fraction is increased in the mix when one of the solar technologies is installed with large fraction.

The introduction of BES to PV induces the installation of PV in EAST at intermediate penetrations instead of SOUTH. However, the optimal geographical distribution of other technologies does not seem to be impacted whatever the level of penetration.

→ **Impact of Spatio-Temporal Complementarity:** We also find that more PV and CSP systems contribute to making energy available on demand, more mixes become less diversified and hence taking into account the technological and spatial complementarity does not significantly reduce the variance.

→ **Does CSP/CSP-TES Competing with or Winning over PV/PV-BES?** Although there is not a clear winner due to the imperfect substitution of CSP-TES by PV-BES and due to the differences between PV and CSP in terms of cost and variability, this study has identified various aspects that could make one of these generation technologies more suitable for a specific location and penetration level. However, we would like to stress that the results presented can significantly depend on the assumptions such as the cost data, i.e., current or future cost reduction scenarios and the uncertainty associated to the method of cost projections. In addition, using different solar PV and CSP technologies with different tracking options and storage sizing may also affect the results.

Overall, this study corroborates the earlier investigation (Chapter 3) in which we find that the key factors in improving grid flexibility include increasing the rate of all solar generation sources with storage to better match the supply of RE resources with demand or increase spatial diversity. For the strategy forwards, a high penetration of REs into the Moroccan power supply system would appear to be possible if Morocco increases the investment budget in CSP-TES more than PV-BES since, for the same design, the probability of not covering the load when introducing PV/CSP/PV-BES is higher than the one of CSP-TES. However, **scenarios with unlimited storage cost and capacity** favor PV-BES whatever the penetration (as it is similar to PV versus CSP).

Currently, to reduce the costs and the variability, actual developers of the CSP technology in Morocco paid attention to the PV-CSP hybrid systems with small storage capacity of TES, aiming to combine the advantages of both technologies. For instance, exploiting the daily production of low-cost PV while storing the energy produced by CSP during the day and reconstitute it later when the PV production drops to provide electricity some hours after dark (i.e., Midelt hybrid solar project). In this study, we discussed other **scenarios of hybrid solar systems** (e.g., CSP-TES-PV-BES; CSP-PV; PV-BES-CSP).

iii Third Study: RCP 8.5 Climate Change Versus Cost Effect on Optimal Scenario Mixes of Variable and Dispatchable Technologies in Morocco: Climate Model Inter-Comparison

The third study (Chapter 5) rises the issue of solar integration with wind in future warming climate. **Q3: What is the response of scenario energy mixes integrating variable and low-cost technologies (PV, wind) with dispatchable and expensive technology (CSP-TES) to climate change compared to cost effect; and how robust results are to sensible changes in climate model?**

To assess the climate variability/change induced impacts on optimal mixes, numerical modeling and downscaling are needed to simulate the time series of demand and Capacity Factors (CFs) representative of a region on a broad range of time scales, i.e., the climatological scale which is large enough to scale with the technical lifetime of solar and wind plants. The study is based on climate data provided by COordinated Regional climate Downscaling EXperiment (CORDEX) in the Middle East and North Africa (MENA) domain covering all the territory of Morocco to have more observations over the Sahara. The robustness of the results is impacted by climate model biases; so that we use climate change projections from Coupled Model Inter-comparison Project 5 (CMIP5) of the Fifth Assessment Report (AR5) of the Intergovernmental Panel on Climate Change (IPCC). We perform two Regional Climate Model (RCMs) simulations—the version 4 of the Rossby Centre regional Atmospheric model (RCA4) and the version 351 of the Weather Research and Forecasting model (WRF351)—using boundary conditions from four different Global Climate Models (GCMs)—Centre National de Recherches Météorologiques-Coupled Model (CNRM-CM5), Earth System Model (EC-EARTH), Geophysical Fluid Dynamics Laboratory's Earth System Model (GFDL-ESM2M), Community Climate System Model (CCSM4)—and assuming the worst-case climate change forcing scenario, Representative Concentration Pathways (RCP) 8.5, rather than the multitude of more likely pathways in between. We repeat the mean-variance analysis using two blocks of 30 complete years, one for each experiment (historical and future period).

In the first part of this study, we focused on the common features obtained from all climate models. We analyzed how resilient is optimal RE mix, across a set of penetration scenarios, by the end 21st century (2071-2100) relative to the historical period (1976-2005); for three

different technological combinations: PV-wind, PV-wind-CSP without storage and PV-wind-CSP with 6 hours of TES (Solar Multiple of 2 or SM2). We also examined if the “extreme” climate change scenario is altering optimal capacity pathways more than cost. In the second part, the sensitivity of capacity allocation to biases stemming from the estimation of demand, wind and solar profiles in each climate data sources—hourly simulations from MERRA-2 climate reanalysis and hourly CORDEX with solar and wind intraday parametrization—has been examined. In the third part, the climate model agreement on the technological and geographical distribution in terms of response to climate change together with the main sources of uncertainty has been analyzed. Confidence in projections of potential future changes in climate variable of relevance for demand, solar and wind production—namely temperature, solar irradiance and wind speed—and their implications on the mean CFs and demand patterns along with the seasonal variability have been also examined.

What is the impact of climate change on the Moroccan optimal mixes? The results show that the optimal mixes are not impacted by climate change at low penetrations where the minimum variance ratios increase (i.e., the variance of CFs decreases and tends to scale with the mean of CFs) while RCP 8.5 climate change has a notable impact as RE capacity is increased—where the maximum-cost constraint is strong—and induces a change in the CFs which alters the correlations between technologies and regions.

Optimal mixes (i.e., technology fraction and capacity pathways) are more sensitive to climate change or to cost (i.e., in the context of vulnerability of low-carbon technologies to climate change vs. eventual cost reductions)? At qualitative levels, it appears that the optimal mixes are relatively resilient to climate change whatever the climate model, the penetration scenario and also the emission scenario—as the analysis are carried out for the extreme RCP 8.5 scenario after 2050—; and the changes are negligible compared to projected cost reductions. In fact, we find that the cost governs the capacity pathways at high penetrations while the seasonal response of CFs and demand to climate change, computed from climate models, plays a role in capacity allocation at low penetrations.

Which technology is sensitive or resilient to climate change? What are the main sources of uncertainty in future RE mixes?

At maximum penetration—where the optimal fronts are shifted towards higher risk values—the optimal mixes are more sensitive to the budget limit than to climate change. Thus, there is a relatively high confidence in the projected changes of the capacity pathways. Wind is (resp. PV and CSP are) resilient (resp. sensitive) to climate change.

At high and low penetrations, results unveil that the choice of the GCM exerts a small role in explaining the robustness of the results compared with the GCM+RCM-induced spread. In fact, the results are prone to RCM uncertainties as large spread in the mean and variance of CFs, across the four CORDEX-CMIP5, are more evident when the RCM is changed, which is likely the result of the wide spread in solar irradiance, wind speed and temperature projections. Accordingly, this applies also for the estimated impacts on the seasonal variability of CFs and demand which translates in differences in the technological and geographical distribution of capacities.

If high penetrations are targeted, the RCM uncertainty increases more for PV and wind—due to the non-robustness of Global Tilted Irradianceor GTI and wind speed—but not for CSP—as all CMIP5 models tend to agree in the projection of temperature increase. At such high penetrations, wind and CSP are (resp. PV is) sensitive (resp. resilient) to climate change.

Making quantitative analysis of the projections of climate change induced impacts on the optimal mixes with low proportions of REs, using different models, give a reasonably consistent picture of the changes to be expected showing that there is more or less considerable variation in contribution of PV, wind and CSP/CSP-TES. However, the signal is uncertain. For instance, climate projections from the three downscaled GCMs (CNRM-CM5, EC-EARTH, GFDL-ESM2M) using RCA4 as RCM, projecting the weakest warming, consistently indicate that wind and CSP fraction may increase and PV decreases. On the other hand, the CCSM4-driven WRF351 simulations indicate an increasing trend for PV technology while wind and CSP may decrease in future RE mixes.

The response of PV and CSP (resp. wind) systems to climate change would be induced by the changes in either temperature or solar irradiance (resp. wind speed) or both. Thus, the uncertainty in the projected optimal mixes comes from the uncertainty in the projected resources. Results are robust in the projected temperature change; while projections for all components of solar irradiance and wind speed are largely uncertain. We highlighted the most affected regions by climate change; and the main differences between RCMs and GCMs, used in this study, to explain the dispersion between models. However, we conclude that no model is superior and the confidence in climate model simulations cannot be adequately inferred solely from its degree of agreement with other climate models. In other words, in addition to the uncertainty related to GCM or RCM (such as the clouds and aerosols parametrization), there are other sources of uncertainty related to emission scenario and to the chaotic natural internal variability, which prevents conclusions on the future mixes, particularly with low RE penetrations.

Intra-daily fluctuations have substantial impact on optimal mixes (i.e., capacity allocation or pathways)? The uncertainty in the results comes also from the solar and wind intra-daily parametrization approach adapted to solve the intra-daily fluctuations not resolved by CORDEX climate data. In fact, the solar (resp. wind) parametrization approach, keeping daily record of the temperature, underestimates (i.e., overestimates) the variance of solar (resp. wind) CFs. Thus, the variance in optimal mixes, obtained over the historical or future period of CORDEX climate data, are probably being underestimated/overestimated compared to those obtained using hourly simulations from MERRA-2 climate reanalysis. For instance, we found that the underestimation of the intraday variance of the clearness index favors the installation of CSP—whose variation strongly depends on the atmospheric components—over PV at low penetrations.

At high penetrations, the underestimation of the variance makes CSP/CSP-TES and wind favored in future warming climate with greater penetrations and with low global variance.

Thermal storage makes CSP resilient to climate change? The combined period of darkness and prolonged cloudiness in addition to the greenhouse effect that hinders the nighttime temperature, resulting in an increased electricity consumption, prevents CSP-TES with small amount of storage (6 hours or SM2) to sufficiently satisfy the demand. As a result, the variance is increased and all climate models project that the CSP-TES fraction is expected to decrease in future RE mix, whatever the penetration scenario.

What are the Conditions for Positive Climate Change Impacts on PV, CSP and wind? We also show that the choice of the solar technology to be installed in future warming climate depends on the trade-off between the expected change in temperature and in solar irradiance. In fact, CSP may profit more from projected climate change than PV plants because the warming could benefit CSP production but it is not favorable for CSP cooling efficiency, CSP-TES and PV performance. In addition, if the clouds patterns are expected to increase (i.e., for instance in polar regions [520, 405]), it would decrease the solar irradiance and diminish the warming (negative feedback). Thus, the resulting cloud changes will lead to negative response of CSP output to climate change but the efficiency of CSP cooling will increase. The opposite is true if the clouds patterns are expected to decrease. Moreover, as clouds block the sun, the relative fraction of diffuse light increases. This means that PV technology, that deals better with diffuse light, would have a relative advantage under frequently cloudy conditions over CSP. However, if the warming is enhanced more than the positive induced impact on solar irradiance, PV will be affected. Overall, both solar technologies may benefit from climate change if the increase in solar irradiance (i.e., decrease of clouds) overpasses the negative effect of temperature (i.e., CSP cooling efficiency and PV solar panel efficiency). Moreover, wind climate change induced impacts are positive if the wind speed increase overpasses the air density decrease resulting from warming.

What are the Options for Climate-Resilient Renewable Mixes? We discuss that temperature-dependent PV technologies and water-dependent CSP technologies (dry cooling or use of water desalination) are solutions for negative temperature-induced effect. In addition, we discuss that large storage capacity (more than 17 hours per day on average or $SM > 4$), integration of tracking to CSP and/or PV to reduce the zenith angle (i.e., decrease the air mass) and a diversified mix—combining wind with PV or CSP with small storage capacity—will be an interesting options to strengthen the resilience to climate-sensitive energy mixes and for the deployment of variable energies, in Morocco, since the energy output will be more evenly spread over time (in agreement with chapter 3 and chapter 4 using current climate conditions). Particularly, the ability of large capacity of CSP-TES to supply dispatchable generation also allows to bridge the gap created by the phase-out of fossil fuels contributing to the solution of environmental climate change and pollution; and to alleviate the technical and economical challenges associated with the incorporation of intermittent sources (i.e., PV, wind).

Does RCP 8.5 climate change impacts the geographical distribution of RE capacities? The geographical distribution of PV and CSP/CSP-TES, at high penetrations, is highly sensitive to climate model while that of wind is only sensitive to climate data sources at maximum-penetration point. At low penetrations, the geographical distribution of capacities is neither altered by climate change nor by climate data sources for any of the four technologies.

II Contribution to Research and Implications

As already mentioned, instead of relying on both cost and variability, existing research tend to focus either on only the reduction of the total cost [113]; or on only the impact of financing costs on the economic competitiveness of RE technologies [467]; or on the sensitivity of optimal mixes integrating PV and wind to future technology cost uncertainty [479]. Other focus on only reducing the variability [49] by analyzing the role of storage [461] or CSP-TES [174, 147, 176] or other sources of flexibility such as interconnection or Pumped Hydro Storage (PHS) [359] for large-scale integration of REs by highlighting their reliability and economic benefits (i.e., avoided costs and emissions) [55, 284].

However, the interaction between solar technologies with wind in optimal mixes considering current and future climate conditions, different storage configurations of PV and CSP, under ranges of penetration and variability, and different RE combinations has not been thoroughly explored. The conditions at which it becomes more optimal to invest in one technology rather than another has not yet been addressed deeply enough by any study. In addition, some studies perform technical and economical simulations on PV and CSP [451, 107] or wind [515] on limited area of Morocco but no study covers whole Morocco allowing to exploit the benefits from spatio-temporal complementarity, especially for CSP/CSP-TES/PV-BES. Chapter 3 and chapter 4 of this thesis address these issues.

Moreover, we already indicated that, in the fast-moving field of climate change impacts, studies largely focus on the impact of climate change on the areas of the energy sector, i.e., demand [410], energy mixes based on technologies currently in use such as PV [276] and wind [431]—by focusing on either resources (i.e., temperature-humidity-precipitations [110, 173], aerosols-clouds [94]) or generation [171]—, and to smaller extent on transmission lines [449] and electricity market [351] including the economic impacts [70] and climate risk management and adaptation [212]; making use of various sets of Global Climate Models (GCMs) and Regional Climate Models (RCMs). We also note that most of studies perform scenarios under the RCP 4.5 and RCP 8.5 [500] with much more focus on the extreme RCP 8.5 scenario [411]. Other focus not only on climate change impacts but also on climate variability [494].

However, the future changes in CSP output have been discussed to a much lesser degree (only Ref. [550, 141]) compared to wind and PV which dominate the literature of global warming induced effects on optimal mixes. There is no doubt that market share and the uncertainty in the modeling processes of the effects of aerosols on deep convective clouds are strongly related. In addition, the impact of climate change on optimal mixes integrating not only variable but also dispatchable energies such as CSP-TES is still lacking. Chapter 5 of this thesis addresses these issues.

→ Implications for Energy Strategy

The energy demand in Morocco is expected to increase in the next few years [264]. Without high amounts of fossil fuel reserves, the country is highly dependent on energy imports. Hence, Morocco will face in future possibly huge energy costs if fuel prices continue to increase [23]. Recognizing this challenge, Morocco aims that, by 2030, 52% of its total installed electricity capacity should come from REs; and 42% of its greenhouse gases should be reduced compared to the business as usual level [7]. This 2030 RE target serves as guidance for a rough distribution of wind and solar capacities showing an interest in installing PV and CSP/CSP-TES. However, this strategy does not specify the optimal proportions between solar technologies and the amount of storage associated. Morocco is currently investing in solar plants but it stands at the very beginning of solar energy expansion, with only few solar plants having been realized so far (170 MW PV, 20 MW CSP and 530 MW CSP-TES) [23]. In addition, to date, the current PV-BES systems are commonly used to achieve the country's rural electrification objectives but are not yet connected to the grid as large-scale CSP-TES plants [302].

Since investors' risk perceptions are particularly high for RE which are characterized by high capital expenditures (CSP/CSP-TES, large-scale PV-BES), the negligence of the benefits of storage, spatio-temporal complementarity and climate change effect may discourage capital intensive RE investments at scale. The general outcomes of this thesis may be of interest to many other geographical settings and to all those who have to make decisions concerning the planning and implementation of solar projects. This is to support the choice of the appropriate RE technology/system arbitrating between different scenarios that would ensure either maximum penetration or mixes with low risks levels or scenarios with low or high storage requirements; taking into account the correlations of RE output across different regions within a RE portfolio in current and future climate conditions.

Our analysis allows to stress the role of CSP-TES/PV-BES in providing adequacy services and explore the impact of storage, cost, spatio-temporal complementarity and climate changes on optimal mixes, but the current set up is too crude to make operational recommendations for the Moroccan energy transition as some refinements are needed to be taken into consideration (Section III). In particular regarding a quantitative estimate of the optimal shares of CSP/CSP-TES and PV/PV-BES, let alone the optimal distribution of Solar Multiple (SM) for CSP plants and Inverter Loading Ratio (ILR) for PV plants; which helps to raise the question of whether there are other possibilities for improvement in the qualitative national RE electricity targets of Morocco.

III Thesis Limitations and Perspectives

This thesis relates both the meteorology, climate, modeling, optimization and economics of energy systems and provide exploratory and plausible scenarios for a prospective purpose that could be beneficial for countries that benefit from the same climate conditions. However,

these scenarios are not intended to be prescriptive (this is why we consider several scenarios and not only one).

In order to facilitate further improvements of this thesis, let us finish by mentioning some of the limitations or open questions that have not been answered.

1 Use Better Energy Data and Improve Bias Correction Approach

The accuracy of the mean-variance analysis depends on the inputs of this optimization problem, namely, the vector of mean Capacity Factors (CFs) and demand entering the definition of the mean penetration (2.1). To correct bias in the CFs that stem from climate simulations and to fit the demand model, real hourly Renewable Energy (RE) production time series per zone and technology and hourly demand time series per region are required. As indicated in section ii (Chapter 2), we were able to collect hourly demand time series per region but only for the year 2018. However, the RE production data is difficult to acquire at regional level and in appropriate intervals, in Morocco. RE production and capacity data, used in this thesis, was provided by recent literature on yearly basis for each technology and region (Table 2.1, Chapter 2). In fact, while knowing an averaged value over the region is useful, this may not be representative enough for regions with strong variability since short-term yearly average of CFs does not tell the full story in the temporal domain, as it hides various profiles of not only intraday and seasonal fluctuations but also it is not sufficient to correct the low-frequency climate variability of electricity production. The latter, however, has a substantial impact on the design of optimal mixes [208]. For instance, running the mean-variance analysis with MERRA-2 climate reanalysis over only one year can be misleading. The simulations are independent of the chronicles of past years. The shorter the time horizon, the larger variation in average, because there is an averaging effect when considering large time horizon. Another source of uncertainty of the bias-corrected CFs stems from the fact that the observed production, for a given operational plant capacity installed in 2018, is estimated for typical meteorological year (Table A.6, Appendix A). As previously indicated (Section 3, Chapter 2), due to lack of high-quality hourly data for several years and due to weak inter-annual variability of the simulated optimization inputs (Figure A.6, Appendix A), this annual observed production data per region and technology and this hourly demand time series per region were used to correct bias in the theoretical production and to fit the demand model; and we carried out the analysis of chapter 3 and chapter 4 over only the year of observations (2018) to allow a better estimation of CFs and demand because our objective is to examine the sensitivity of optimal mixes (i.e., technological and geographical distribution of RE capacities) to storage and cost associated with solar technologies in addition to the spatio-temporal complementarity of wind and solar production; and not to find the long-term capacity planning (i.e., how much capacity is needed in order to meet greater demand). For the analysis done in chapter 5—where the main objective is to assess the climate variability/change impacts on optimal mixes compared to cost effect and explore the source of uncertainty in future energy mixes—, given that the year of available observations (2018) does not take a part of the climate simulations over the whole historical period (1951-2005), we consider that the 2018 observed demand, the 2018 calendar and the 2018 observed RE CFs are similar to those of the year 2005; and thus biases in the mean CFs (resp. the demand time series) over the historical period are corrected (resp. fitted) using the 2018 observed mean CFs (resp. demand time series). Finally, the obtained bias correction factors and demand model parameters over the historical forcing are used to compute the future estimations of CFs and demand over the RCP 8.5 period (2071-2100). We have found that this data is inconsistent with the simulated yearly means provided by climate data as discussed in section 2 (Chapter 2) for the CFs and table A.1 (Appendix A)—which displays relatively low coefficient of determination—for the demand model parameters.

Moreover, an important point to note is that CFs of solar Photovoltaic (PV) without or with Battery Energy Storage (BES) and Concentrated Solar Power (CSP) without or with Thermal Energy Storage (TES) have been corrected by all operational technologies independently of the technology used, orientation or tracking type and storage configuration (Section iii, Chapter 2). In other words, we consider that all the operational solar technologies are PV multi-crystalline fixed-tilted up toward South horizon by an angle equal to the latitude (resp. North-South or N-S tracked-horizontal CSP) without storage, i.e., Inverter Loading Ratio-ILR- (resp. Solar Multiple-SM-) of 1, and with increasing levels of battery (resp. thermal) storage corresponding to 5-13 (resp. 6-17) hours per day on average, i.e., ILR (resp. SM) of 2-4. This implies that the simulated CFs are constant with the increase of the production surplus from PV and CSP (Section 2, Chapter 2), which is an advantage as it avoids to artificially increase the variance (Figure 2.12, Chapter 2), but it is also a constraint as it, in turn, implies to keep the cost of the additional PV Solar Panels-SP- (resp. CSP Solar Field-SF-) constant although it is the most expensive part of PV (resp. CSP) plant [268, 269] and increase only the cost of storage systems to remain coherent with the fact that PV (resp. CSP) plants with high storage capabilities are higher in cost than plants with smaller storage size range or without storage (Section VIII, Chapter 2). In this case, the storage sizing approach (Section 1, Chapter 2) does not matter since increasing the PV SP (resp. CSP SF) or PV Inverter-INV- (resp. CSP Power Block-PB-) in relation to BES (resp. TES) will lead to the same results according to the fact that CFs remain constant due to the bias correction. However, the figure 1.16 (Chapter 1) shows the strong influence of the PV ILR (resp. CSP SM) or the SP (resp. SF) size and the storage capacity on the mean CFs and thus on the costs. For instance, if the observed PV (resp. CSP) production was available for each SM and ILR, keeping the fact that the required battery (resp. thermal) storage capacity increases with increasing the PV ILR (resp. CSP SM), the mean CFs will increase with the increase of the amount of storage, and the sizing approach will matter, which will make a big difference on the total costs and thus on the resulted optimal capacity pathways and thus different conclusions would have been drawn (see key messages of this thesis).

While the bias correction approach used—to correct solar and wind CFs against available energy observations—removes discrepancies in the zonal mean CFs, it does not correct errors in the variance (Section iii, chapter 2). For instance, it may not be appropriate to resolve the nonlinear response of the production to intra-daily, seasonal and low-frequency changes in climate variables if production data was available for shorter time scales than a year and for several years. In addition, we want to point that, for zone-technology pairs for which no capacity is installed and thus without observed production data (marked by an empty set \emptyset in the table 2.1, chapter 2), the national bias correction factor is applied indifferently to the regional CFs calculated from climate data (Section iii, Chapter 2). Affecting the bias correction factor of nearby region with good wind or sun conditions could improve the estimation of the CFs.

A better energy data and bias correction approach that take into account the high- and low-frequency climate variability for each solar PV and CSP technology, tracking option and storage configuration would help us to establish a greater degree of accuracy on the estimation of the simulated CFs and demand time series and would allow us to conduct further sensitivity analysis on the relationship between storage, CFs and costs and its impacts on the optimal mixes.

2 Additional Sensitivity Analysis

Overall, this thesis provides technical and an analytical framework that could be reproduced by other authors using alternative assumptions. In fact, our results are based on fixed tilted-latitude multi-crystalline PV and N-S tracked horizontal parabolic trough CSP (Section i and section ii,

Chapter 2). In addition, our results reflect the efficient capacity pathways of the global strategy (2.2) with total cost constraint (2.8) obtained using recent (2013) cost data (Section 1, Chapter 2) and actual (2018) capacity data (Table 2.1, chapter 2) and for a set of storage capacity ranging from 5.5 to 17 hours for TES and 5 to 13 hours for BES (Table 2.3, Chapter 2). **Efforts must be devoted to simulate different cost and capacity data scenarios, different optimization strategy, various solar technologies (e.g., PV amorphous, CSP solar tower) with different PV mounting angles or PV/CSP tracking options and storage configurations as they exhibit different response to temperature and clouds (mean production) and are characterized by different variability and rental costs** which imply an imperfect substitution between CSP/CSP-TES and PV/PV-BES (as discussed in section 1, chapter 4); in addition to the fact that costs could increase or decrease (due to the large scale deployment and technology improvement).

The same applies to wind as different wind turbines can be used with various hub heights and power curves.

For future work, it could also be interesting to **assess the robustness of the mean-variance results to different energy CFs, demand and cost modeling approach**. For instance, using the electrical model instead of EVANS model to simulate PV CFs allow to perform fault detection and diagnosis method for PV systems. In addition, it is worth to mention that, we proposed a method of rental cost of generation and storage technologies based on available cost parameters (Section VIII, Chapter 2). However, conventions on how to calculate the total cost and the yearly rental cost may influence the total cost and thus the findings. Particularly, to take into account the replacement or storage degradation in the variable operating cost of the storage system, we assumed a fixed number of full equivalent cycles equal to 365 per year (one cycle of charge and discharge per day). This is a convenient hypothesis, since it makes it easy to calculate the yearly rental cost of TES and BES. However, the number of full equivalent cycles is usually less than one per day, and is highly dependent on the storage capacity. For instance, a small storage system tends to have almost one full cycle every day, while a large storage system has much more limited average charge/discharge cycles.

These features are beyond the scope of this thesis, but are highlighted as a topic that would benefit from future investigation because they are likely to cause significant differences in the results; which put forward the importance of interpreting the results in alignment with the assumptions considered.

3 Compare the Flexibility of CSP-TES and PV-BES to Other Flexibility Options

The results have demonstrated that wind is favored in optimal mixes whatever the level of penetration but its variability could compromise its integration, particularly in scenario mixes with high penetrations (Sections III, IV in chapter 3 and sections III, IV in chapter 4). It could, thus, be interesting to expand the modeling framework of this thesis by **adding the Pumped Hydro Storage (PHS) or Compressed Air Energy Storage (CAES) to wind**—to compare the flexibility of Wind-PHS or Wind-CAES to that of CSP-TES and PV-BES under different storage configurations—by adjusting the developed storage model (Section V, Chapter 2) in which the wind electrical capacity can be considered as the threshold that should not be exceeded. In fact, for PHS, when this threshold is overpassed, the excess of wind production can be used to pump the water from the lower reservoir to the upper reservoir; and at peak hours, the water flows out of the upper reservoir and activates the turbines to generate electricity. For CAES, the surplus of electricity can be used to compress the air during off-peak hours, and then to produce electricity during peak hours.

A greater focus on other storage technologies or flexibility options (mentioned in section ii and iii, chapter 1) **with other services** is important to explore and could produce interesting findings as only peak shaving and load shifting services, provided by CSP-TES and PV-BES, that were analyzed in this thesis. In addition, the E4CLIM model, used in this thesis, is not flow-based meaning that the power flow in the electrical grid is not determined by physical power flow constraints (recall from section i, Chapter 2), making the analysis of the benefits brought by spatial and technological complementarity only partial. To better evaluate the benefits from complementarity, **the transmission network would have to be modeled as well; and expand the model to other regions to exploit the benefits from imports/exports**. For example, it could be important to evaluate the benefits—in terms of CO_2 emission reduction, cost saving, energy supply security—of the transmission of CSP production from Sun Belt regions (e.g., Middle East and North Africa or MENA region)—with high solar irradiance and thus low cost of production—to Europe

In addition, Morocco has invested in solar and wind energies which are less expensive than **marine energy** which requires advanced technologies. In fact, it has been observed [372] that Morocco is one of the countries with high potential for marine energies on the Atlantic coast of Morocco and will ensure decentralized energy at a competitive price and allow carbon neutrality of facilities exposed to the sea (e.g., port). Research in this field of RE technologies **together with the impact of biomass, geothermal energy and Carbon Capture and Sequestration (CCS) on the reliability, economic and environmental value may be necessary in the future** (see discussion in section i, chapter 1).

With global warming, there will be more evaporation, and thus more risk of droughts. **The integration of sea water desalination processes [522], particularly for CSP cooling or PV cleaning, and understand its implications on the plant's efficiency, compared to dry cooling technologies, could be interesting to examine** (see discussion in section i, chapter 1). Currently, the desalination coupling with CSP plant technology is still in an early stage. The most popular desalination technologies are Reverse Osmosis (RO) using electrical power as the driving force, Multi-Effect Desalination (MED) and Multi-Stage Flash (MSF) using thermal power as the driving force. RO and MED are the two most promising desalination technologies for utility-scale CSP desalination cogeneration plants. MSF is excluded due to high investment, high power and cooling water requirements. CSP-MED technology is more competitive and cheaper compared to CSP-RO at large capacity. It is also more thermodynamically efficient. Besides, RO is highly dependent on the effectiveness of water pre-treatment, MED nevertheless can treat very saline water.

More broadly, research is also needed to determine **the effect of energy efficiency, electrical mobility and energy sobriety on the energy consumption in the most energy intensive sectors such as industry, residential and transport** and not only energy sector (see discussion in section 1, chapter 1).

4 Quantify the Avoided Costs and Emissions

While evaluating the impact of storage, cost, spatio-temporal complementarity, and climate change—including the main sources of uncertainty—on the integration of RE capacities, and particularly of solar PV and CSP, in the optimal mixes under different hypothesis of penetrations is a first step, the findings of this thesis may be enhanced if other technical and economical aspects were to be brought into account.

In section V (Chapter 2), we present an extensible approach of the storage model that can be used to represent a variety of operation strategies depending on the optimization objectives. In fact, since we take as objective to maximize the RE production while minimizing its

variability (Section 2, Chapter 2), the storage model has been developed by following the CSP thermal (resp. PV Direct Current-DC-) maximal capacity—to increase the mean Capacity Factor (CF)—instead of following the fluctuations of electricity prices and electricity consumption—that would otherwise reach low CF as it will be operated at maximum capacity only during peak hours of demand. Doing so, the mean-variance optimization problem will be sensitive to increasing storage capabilities; and the results suggest maximizing the contribution of dispatchable generation, CSP-TES and PV-BES, in the Moroccan mix with large CSP solar field and PV solar panels, both with large storage capacity, to reduce the adequacy risk. Our results also show that, for the same design, CSP-TES has a stronger impact on reducing the adequacy risk due to its larger storage capacity associated with the tracking use. In addition, the variance-based risk is only an aggregate measure of the variability as it does not specify if the timing of fluctuation is occurring in summer or winter, or at midday or in the evening, or during peak or mid or base load hours; and thus, it does not take into account the ability of CSP or PV with storage to meet different load bands and to reduce curtailment. To compare this physical value of CSP-TES and PV-BES with that of PV or CSP or wind, we added some adequacy diagnostics (Section vi, Chapter 2) and heatmap tool. However, we have not examined the broader question of the reliability and economic benefits together with emission reductions—which are equivalent to the avoided capacity costs or carbon emissions—that CSP-TES and PV-BES might provide compared to other intermittent RE technologies (i.e., PV, wind, CSP)—such as maximizing the energy revenues by shifting output to high energy price hours or during period of high peak demand and by providing services that would otherwise be satisfied by conventional fossil fuel plants, which may allow for improved emission reductions. These elements are still not explicitly quantified in this thesis as an accurate analysis of these aspects require data on price of energy and energy sold in each time step [283, 284, 184]. In the short-term future, these elements can be quantified in a simple way by calculating the avoided costs (resp. emissions) as the yearly rental cost (resp. emission factor multiplied by the hours of operation) multiplied by the avoided capacity; and the latter represents the Effective Load Carrying Capacity (ELCC) which is the load reduction (in %) multiplied by the total installed capacity. In future work, **investigating if these avoided costs and emissions will compensate the increase in costs resulting from the increase of SM or ILR, and how these indicators evolve under an elementary change in the composition of the mix might prove important.**

Given that the technologies studied are different in terms of mean production, variability and cost (Section 3, Chapter 1), they can not be compared on the basis of economic criteria only or of variability criteria only. The advantage of the Mean-Variance Portfolio (MVP) optimization approach, used in this thesis, is that it considers these elements at the same time. To illustrate this point, the risk definition (2.2) as implemented in the mean-variance optimization problem is based on heuristic that the more the RE production is variable, the more adequacy services and integration costs will be required to satisfy the demand at all times, leading to penalization of this variable production at low penetrations (where the variance plays an important role) and favoring this fluctuating but low-cost production at high penetrations (where the cost matters). Thus, we assess the regional capacity allocation by choosing the Renewable Energy (RE) mean penetration and the variance as a proxy for costs and emissions arising from the variability of the RE production (i.e., the mismatch between the demand and the RE production that should be counterbalanced by conventional plants or other means such as imports or demand response mechanisms); and we add a maximum-cost constraint to examine the ability of each technology to achieve high mean penetration while not achieving the maximum-cost budget sooner. In addition, the MVP reflects several choices (instead of a single mix) allowing to arbitrate between different scenario mixes (mixes with a high share of RE with low investment and operating costs without caring about the variability or it will be reduced by other options than REs; mixes with high penetration and low risk but high budget; and mixes with low proportions of REs, low variability and low budget). This choice facilitates performing sensitivity analysis akin to the one conducted here—i.e., sensitivity to the variability (storage, time-space complementarity) and cost instead of relying on one of them—while avoiding having to model the whole energy system. Yet, this is at the cost of providing only an imperfect measure of the system cost (total cost + integration costs). Further research should be devoted to study different operation strategy of the developed storage model and optimization problem which are based on the questions that we wish to answer. For example, instead of seeking to minimize the variability or the total cost (sum of the annualized fixed and variable costs multiplied by the installed capacity)—which takes into account all costs over the lifetime of the system but ignores the timing of fluctuations between RE production and demand—, **an optimization approach based on minimizing the total cost of the system—calculated as the total cost plus integration costs accounting for the nonlinear costs—under a constraint on carbon dioxide (CO_2) emissions (using Kaya equation) or a constraint on the carbon budget or climate sensitivity (using emissions allocation approaches for Morocco) could prove quite beneficial.** And in this case, for the storage model, either we keep the current approach in which we follow the nominal CSP thermal (resp. PV DC power) to maximize the CF; or we use the most common strategy by following the fluctuations of energy demand and electricity prices. **The minimization of the system total cost could continue to explore the differences between technologies in terms of integration costs.** For instance, between PV, CSP and wind or between CSP-TES and PV-BES in terms of profile and balancing costs, grid-related costs—given the fact that PV can be installed everywhere while the transport network is essential for CSP—and adequacy costs (by examining the utilization effect and the capacity credit effect). It should be noted that it is necessary to optimize the electrical mix for each time step because if we consider the expectation of the system cost, this will not allow us to see if the system costs increase more during the hours of surplus or rather during the hours of energy deficit.

5 Tackle Climate Change Uncertainty

To analyze the impact of climate change on optimal mixes (Chapter 5), we used the RCP 8.5 scenario (Section ii, Chapter 2). A study similar to that done in chapter 5 may be carried out **using different scenarios as the technologies may be penalized differently (depending on the compensation between temperature, irradiance and wind speed which impacts the mean CFs, variability and cost).**

To explore the consistency of climate projections on the impacts that expected climate change will have on future optimal mixes (Chapter 5), we used two Regional Climate Models (RCMs) simulations forced by four different Global Climate Models (GCMs) (Section i, Chapter 2). We found conflicting signals, particularly when comparing the results of the version 4 of the Rossby Centre regional Atmospheric model (RCA4) and the results of the version 351 of the Weather Research and Forecasting Model (WRF351) regarding the projections of the resources and their implications on CFs and demand and thus optimal mixes with low and high proportions of RE (where the variance play a role) but the results are relatively robust at maximum penetration. We noted that the RCM uncertainty increases for all technologies (PV, wind, CSP) at low penetrations (with an opposite trend between RCMs) and for only PV and wind at high penetrations (but with similar projections between RCMs) which limit the ability to draw conclusions on future energy mixes with low proportions of REs. We concluded that **in-depth examination of these models, and other RCMs and GCMs which would give other results, to simulate aerosols dynamics and clouds physics and in turn their effect on solar irradiance and temperature and thereby solar PV and CSP CFs needs further investigation in future works to better understand the obtained trends and get a higher confidence in the results.**

In addition, the results of chapter 5 (Section 2), over the historical period, have demonstrated the sensitivity of the mean-variance results

to climate data sources, at low and high penetrations where the variance play a role. We explained that this is not related to the period of the simulations (or the seasonal correlation of solar CFs with the summer peak demand) but to **solar and wind intraday parametrization—****included in the CF models** when using daily CORDEX climate data—which tends to underestimate (resp. overestimate) the standard deviation of the solar (resp. wind) CFs (Section iii, Chapter 2). The problem is resolved between PV and wind but not between PV and CSP (Section 2, Chapter 5). A possible direction to improve the bias in the variance of the solar CFs is either to compute the solar production from hourly climate data, or to design a better parametrization of the intraday variability of the clearness index.

The parametrization of the intradaily fluctuations of temperature should also be designed and added to the CFs and demand models to explore how it impacts the RE integration in the scenario mixes, particularly PV and CSP integration.

A

Theoretical Modeling Framework

Contents

I	Electricity Demand Model	156
II	Wind Production Model and Parametrization	159
1	Wind Extrapolation at Hub Height	159
2	Wind Power Output	160
3	Wind Intra-daily Parametrization	160
III	Solar Angles and Tracking Modeling	161
IV	Solar Irradiance Decomposition and Parametrization	163
1	Solar Irradiance Decomposition	163
2	Solar Irradiance Intra-daily Parametrization	164
V	CSP Production Modules	164
1	Solar Field Modeling	164
2	Power Block Modeling	166
VI	PV Production Modules	167
1	Solar Panels Modeling	167
2	Inverter Modeling	167
VII	Storage Module	168
1	CSP Solar Multiple and PV Inverter Loading Ratio	168
2	Storage Model without Constraints	168
VIII	Capacity Factors, Covariances and Bias Correction	169
1	Observed CSP Solar Multiple and PV Inverter Loading Ratio	169
2	Bias Correction Approach	169
3	Inter-annual Variability of Predicted Mean CFs and Demand Obtained from Climate Reanalysis	169
4	Estimates of Correlations and Covariances	169
5	Critical Appraisal of the Obtained Profiles of Wind and Solar Capacity Factors	169
IX	Rental Cost Modeling	174
X	Optimization Post-Processing Formulas	174

In this appendix, we present the details of the theoretical energy and cost modeling and optimization. In each section, we present the steps of calculations describing the physical meaning of the formulas and their respective graphical representation.

I Electricity Demand Model

To compute the regional electricity demand taking into account the effect of Cooling Degree Days (CDD) and Heating Degree Days (HDD) on the demand as well as the human economic activity¹, the model requires as **inputs** the daily mean surface air temperature averaged over each zone, the calendar separating the working days from Saturdays and off-days (Sundays and holidays), and the hourly regional demand observations (Section IV and section ii, Chapter 2).

Let the **electricity demand**, $D_{it}(T_{it})$ (A.1), for the zone, i , at the time step, t (day or hour), and for particular day type, g_t , marked "work", "Sat", and "off":

$$\begin{aligned}
 D_{it}(T_i) = & a_H^{work|sat|off} \Theta(T_H - T_{it}) g_t^{work|sat|off} \\
 & + a_C^{work|sat|off} \Theta(T_{it} - T_C) g_t^{work|sat|off} \\
 & + a_0^{work|sat|off} g_t^{work|sat|off} + \epsilon_{it},
 \end{aligned} \tag{A.1}$$

¹The behaviour of the consumers differs significantly between the week days "work", Saturdays "sat", and off-days "off" such as Sundays and holidays, i.e., the demand decreases (resp. increases) due to the low (resp. high) economical activity.

where Θ is the Heaviside step function; T_{it} is the regionally daily-mean temperature; $g_t^{work|sat|off}$ are given by the average—over all days of the same day type and all hours of the same hour of the day—of the observed demand on which the model is trained. The resulting model is fitted assuming that the thresholds temperature at which the consumer switches the heating (resp. air-conditioning) system, T_H (resp. T_C), are constant over all zones and day types. The parameter, $a_H^{work|sat|off}$ (resp. $a_C^{work|sat|off}$), represents the degree of heating (resp. cooling) required with the change in temperature for each day type. High values of these parameters indicate high sensitivity of the electricity demand to the change in low (resp. high) temperatures. They are adjusted for each zone and day type (Table A.1, for the different climate data sources). The residual, ϵ_{it} , accounts for the other factors impacting the demand such as the changes in the population, the economy, the tourism, the demand management mechanisms (i.e., the part curtailed due to the pricing policy developed by utilities to reduce consumption), energy efficient technology, etc. Here, our objective is to model the part of the demand depending on climate variables while preserving the statistics associated with the other factors.

First, the model uses the **Grid Search with K-fold cross validation** [247] to find the hyper parameters such as **the heating and cooling thresholds** and **the regularization parameter of the Bayesian Ridge Regression** that gives the lowest prediction error. The dataset is divided into two samples, one of the sample is selected as learning set and the other sample constitutes the validation set. Once the performance score is calculated, the operation is reversed by selecting the validation sample that has not yet used for model validation. Then, the regional demand is fitted to electricity demand observations using **the Linear Bayesian Ridge Regression method** [329]. We adopt a Bayesian approach allowing not only for the prediction of the mean of the demand conditioned on the temperature, but also of the conditional distribution around this mean by adding, to the posterior distribution of the model, random perturbations drawn from a normal distribution whose variance depends both on the noise in the demand and the uncertainty in the parameters of the model. The model is fitted using this method both to avoid over-fitting and to take into account the variance arising from factors that are not fully resolved by the deterministic part of the model. The implementation from Scikit-learn [117] of the Bayesian ridge regression is used.

Table A.1: Electricity demand model parameters (10^{-2})— $a_H^{work|sat|off}$ (resp. $a_C^{work|sat|off}$) which represents the degree of heating (resp. cooling) required with the change in temperature for each day type (week days "work", Saturdays "sat", and off-days "off" such as Sundays and holidays); $a_0^{work|sat|off}$ is the coefficient of the interval within which the demand is insensitive to temperature—obtained from hourly (a): Modern-Era Retrospective Analysis for Research and Applications 2 (MERRA-2) climate reanalysis over the year 2018. (b), (c), (d), (e): COordinated Regional climate Downscaling EXperiment (CORDEX) climate data using different climate models (Table 2.2, Chapter 2) over the whole historical period (1951 -2005). The name of each climate model is hereafter referred as Global Climate Model (GCM) + Regional Climate Model (RCM): version 4 of the Rossby Centre regional Atmospheric model (RCA4); the version 351 of the Weather Research and Forecasting model (WRF351); Centre National de Recherches Météorologiques-Coupled Model (CNRM-CM5); Earth System Model (EC-EARTH); Geophysical Fluid Dynamics Laboratory's Earth System Model (GFDL-ESM2M); Community Climate System Model (CCSM4). We give the overall coefficient of determination R^2 .

Zones	a_0			a_H			a_C		
	work	sat	off	work	sat	off	work	sat	off
NORTH	0.477	0.477	0.477	-0.410	-0.410	-0.410	33.5	33.5	33.5
CENTER	0.527	0.527	0.527	-0.305	-0.305	-0.305	33.3	33.3	33.3
EAST	0.399	0.399	0.399	-0.260	-0.260	-0.260	33.4	33.4	33.4
SOUTH	0.334	0.334	0.334	-0.444	-0.444	-0.444	32.8	32.8	32.8

(a) MERRA-2 Reanalysis. $R^2 = 0.58$.

Zones	a_0			a_H			a_C		
	work	sat	off	work	sat	off	work	sat	off
NORTH	0.538	0.538	0.538	-0.212	-0.212	-0.212	32.8	32.8	32.8
CENTER	0.516	0.516	0.516	-0.169	-0.169	-0.169	32.9	32.9	32.9
EAST	0.664	0.664	0.664	-0.148	-0.148	-0.148	33.1	33.1	33.1
SOUTH	0.413	0.413	0.413	-0.065	-0.065	-0.065	31.8	31.8	31.8

(b) CORDEX—CNRM-CM5 + RCA4 model. $R^2 = 0.56$.

Zones	a_0			a_H			a_C		
	work	sat	off	work	sat	off	work	sat	off
NORTH	0.663	0.663	0.663	-0.312	-0.312	-0.312	32.7	32.7	32.7
CENTER	0.662	0.662	0.662	-0.34	-0.34	-0.34	32.8	32.8	32.8
EAST	0.630	0.630	0.630	-0.222	-0.222	-0.222	33.0	33.0	33.0
SOUTH	0.51	0.51	0.51	0	0	0	32.0	32.0	32.0

(c) CORDEX—EC-EARTH + RCA4 model. $R^2 = 0.57$.

Zones	a_0			a_H			a_C		
	work	sat	off	work	sat	off	work	sat	off
NORTH	0.78	0.78	0.78	-0.520	-0.520	-0.520	32.7	32.7	32.7
CENTER	0.807	0.807	0.807	-0.444	-0.444	-0.444	32.5	32.5	32.5
EAST	0.868	0.868	0.868	-0.281	-0.281	-0.281	33	33	33
SOUTH	0.44	0.44	0.44	0	0	0	31.7	31.7	31.7

(d) CORDEX—GFDL-ESM2M + RCA4 model. $R^2 = 0.61$.

Zones	a_0			a_H			a_C		
	work	sat	off	work	sat	off	work	sat	off
NORTH	0.32	0.32	0.32	-0.243	-0.243	-0.243	33.0	33.0	33.0
CENTER	0.365	0.365	0.365	-0.104	-0.104	-0.104	32.6	32.6	32.6
EAST	0.382	0.382	0.382	-0.100	-0.100	-0.100	32.6	32.6	32.6
SOUTH	0.306	0.306	0.306	0.455	0.455	0.455	31.7	31.7	31.7

(e) CORDEX—CCSM4 + WRF351 model. $R^2 = 0.48$.

II Wind Production Model and Parametrization

To calculate the onshore wind production without storage at each climate grid cell, we choose as **inputs** the Siemens wind turbine with an electrical capacity of $P_{elec,nom}^{ref} = 2.3MW$, hub height of 101 m, rotor area of 8000 m² and a specific capacity of 0.29 kW/m² corresponding to medium specific capacity and medium hub height according to [266]. This specification is important for the calculation of wind rental cost (Table 2.7, Chapter 2).

1 Wind Extrapolation at Hub Height

We first calculate **the wind magnitude** from climate data (Section IV, Chapter 2), $U = \sqrt{u^2 + v^2}$ with u and v are the zonal and meridional wind speed, respectively. Then, the wind speed has to be extrapolated to the hub height. The logarithmic law and the power law are the two most used approaches for the extrapolation of vertical profile of wind speed [314] (left panel of figure A.1).

Gualtieri et Secci et al. [228] explain, based on boundary layer similarity theory (Monin-Obukhov theory) [363], that in the surface layer (right panel of figure 1.5, chapter 1), the vertical profile of wind speed displays a **logarithmic profile** and depends on the surface roughness, z_0 , and on the friction velocity, u^* , which describe the turbulence of the flow that diminish the velocity of the wind. The wind speed, U_h , at height h (left panel of figure A.1) is calculated as follows (A.2) [253]:

$$U_h = \frac{u^*}{k} \left[\ln\left(\frac{h}{z_0}\right) - \psi\left(\frac{h}{L}\right) \right], \quad (A.2)$$

where $k = 0.4$ is the Von karman constant; $\psi(\frac{h}{L})$ is the thermal stability of the atmosphere as a function of the height, h , relative to the similarity scale L (Monin-Obukhov length) which influences the structure of the turbulence. Considering the neutral conditions of stability, i.e. $\psi = 0$, the expression of wind speed, U_h , at the height of the turbine, h (A.3), is calculated by replacing the term, $\frac{u^*}{k}$, in equation (A.2), considering the surface wind speed, U_s , at the surface wind altitude, h_s (left panel of figure A.1):

$$U_h = U_s \cdot \frac{\ln(\frac{h}{z_0})}{\ln(\frac{h_s}{z_0})}. \quad (A.3)$$

The equation (A.3) shows that the wind speed increases rapidly with the height in the surface layer (right panel of figure 1.5, chapter 1) because the vertical shear is generally reduced above the surface layer. However, equation (A.3) is valid only in a neutral stratified atmosphere (i.e., the density does not vary with the height) [172] with horizontal homogeneity and stationarity [508] and for shorter period wind speed data (<1 hours) [76]. Corrections must be applied to account for thermal stratification. Jourdiier et al [287] explain that we very often deviate significantly from the case of neutral stability, and that the current hub heights sometimes lead to having to estimate the wind speed beyond the surface layer. However, the complexity is to determine precisely the surface roughness, z_0 .

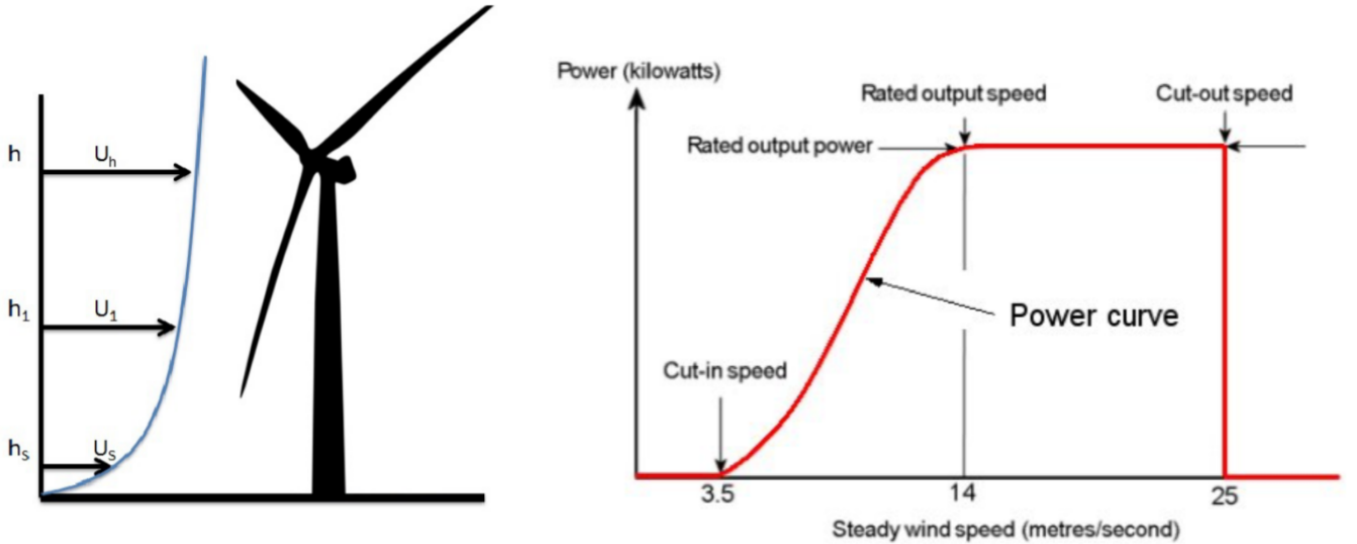


Figure A.1: **Left:** Scheme of the vertical wind profile as a function of the altitude for the extrapolation of the surface wind U_s at a height h_s up to the height of the turbine h for a wind speed U_h . **Right:** A typical power curve indicating the relationship between wind speed (abscissa) and power output (ordinate). Source: Lassonde et al. [314]

The **power law** wind profile is often used to substitute for the logarithmic wind profile when the information on surface roughness or stability is not available [413, 475]. The power law (A.4) is expressed to a power, α , which is the "Hellmann exponent" or "friction exponent" or "wind shear" representing the influence of surface roughness and atmospheric stratification [440, 485]:

$$U_h = U_s \left(\frac{h}{h_s} \right)^\alpha. \quad (A.4)$$

Von karman et al. [293] show that the value, $\alpha = 1/7$, is valid under certain conditions of neutrality and smooth terrain to extrapolate the vertical profile of the wind. For instance, as the surface temperature increases (unstable conditions), the value of the Hellman exponent decreases. In contrast, during periods of cooling of the earth (stable conditions), the exponent increases. Therefore, when a constant exponent

is used, it does not account for the roughness of the surface, or the stability of the atmosphere, which may impact the wind power potential and wind production [430, 263, 485]. Some studies seek to refine the expression of the Hellman exponent [335, 379, 477]. Another approach frequently used for the vertical extrapolation of the wind profile is given by **Justus and Mikhail et al.** [289], where the power law depends on the surface wind speed (A.5) (left panel of figure A.1):

$$\alpha = \frac{0.37 - 0.0881 \ln(U_s)}{1 - 0.0881 \ln(\frac{h_s}{10})}. \quad (\text{A.5})$$

In the case where $h_s = 10m$, a standard height of the wind in the outputs of climate models and reanalysis, we find the equation of Tobin et al. [518]: $\alpha = 0.37 - 0.0881 \ln(U_s)$.

Tobin et al. [518] evaluated these two power laws with observations of winds at 10, 60 and 100 m on a hub height in south of Paris (Saclay). They observe significant differences between the two approaches but cannot conclude that one power law is better than the other. Among the power laws, we have chosen to restrict the laws tested to the most used law, namely that of **von karman** (A.4) with $\alpha = 1/7$.

2 Wind Power Output

To obtain wind energy production, the power curve of wind turbine taken as reference in this thesis is applied to the wind speed distribution. An example of typical power curve indicating the relationship between wind speed and power output is presented in the right panel of figure A.1.

Before doing so, the real power obtained from a wind turbine, indeed, differs from the one expected from the manufacturer's power curve, for instance due to the variations of the air density or the varying intensity of turbulence. We, thus, multiply the extrapolated wind speed (A.4) by a factor, $(\rho/\rho_0)^{1/3}$, **accounting for deviations of the daily mean air density from the standard density**, $\rho_0 = 1.225kg/m^3$, for which the power curve has been obtained. The air density, ρ , is computed using the ideal gas law for moist air (A.6):

$$\rho = \frac{press_h M_w}{R * T_{amb}}, \quad (\text{A.6})$$

where $M_w = \frac{M_d M_v}{(1-huss)M_v + hussM_d}$ is the molar mass of wet air; $M_d = 0.028964Kg/mol$ is the molar mass of dry air; $M_v = 0.018016Kg/mol$ is the molar mass of vapor air; and $huss$ is the surface humidity. The pressure at height, h , is calculated as follows (A.7):

$$press_h = press_{h_s} * [\frac{T_h}{T_h - L(h - h_s)}]^x, \quad (\text{A.7})$$

with $press_{h_s}$ is the surface pressure; $x = exp$ for $z \geq z_0$; $x = -exp$ for $z < z_0$; and $exp = \frac{g_0 * M_w}{R * L}$. The quantity, $g_0 = 9.80665m/s^2$, is the gravitational acceleration; $R = 8.3144598J/K/mol$ is the universal gas constant and $L = 0.0065K/m$ is the temperature lapse rate. The temperature at height, h , is calculated as (A.8):

$$T_h = T_{h_s} - L(h - h_s), \quad (\text{A.8})$$

with $temp_{h_s}$ is the surface temperature.

This corrected wind speed is then fed to a power curve using a transfer function to compute the wind CFs at each grid point.

3 Wind Intra-daily Parametrization

To parametrize intraday fluctuations of the wind CFs at all grid points from the daily means obtained from COordinated Regional climate Downscaling EXperiment (CORDEX) climate data (Section 2, Chapter 2), one approach could be to randomly draw independent and identically distributed realizations of hourly wind speed, at each grid point, using the Weibull distribution which is commonly used to represent wind speed distribution. It can be described by the probability density function (PDF)(A.9):

$$f(U_h, \lambda, k) = \frac{k}{\lambda} * (\frac{U_h}{\lambda})^{k-1} * exp(-(\frac{U_h}{\lambda})^k). \quad (\text{A.9})$$

A very variable wind locations with very strong winds would have a value of dimensionless shape parameter, k , of below 2, whereas locations with very steady wind speeds around the median would have a shape value of 3. In most other locations around the world the value of k is approximately 2 making this distribution a Rayleigh distribution. λ is the scale parameter with the same wind speed unit (m/s). It describes the abscissa scale on a plot of the wind distribution. Higher λ means windy sites.

Using univariate Weibull distribution, we would not, however, account for correlations between intraday wind fluctuations at nearby grid points. When averaging the wind production computed from these hourly estimates of the wind speed over a zone, the part of the variance explained by intraday fluctuations would thus be underestimated or overestimated. To take these correlations into account, we instead assume that **intraday wind speed fluctuations follow a multivariate Weibull distribution**. Villanueva et al. [532] show how to derive the multivariate Weibull PDF from the multivariate standard normal one with a mean vector given by the daily mean wind-speed at hub height. Such a distribution is defined by three parameters: **the scale parameter, the shape parameter and the matrix of correlation between grid points**.

To calculate the shape parameter, we first divide the standard deviation of the wind distribution by the mean of the distribution of hourly wind speed data (A.10):

$$ratio = \frac{\sigma(U_h)}{\mu(U_h)} = \frac{\lambda * [\Gamma(1 + \frac{2}{k}) - \Gamma(1 + \frac{2}{k})^2]^{1/2}}{\lambda * \Gamma(1 + \frac{1}{k})}. \quad (\text{A.10})$$

The ratio can be calculated numerically using a linear regression between the average wind speed, $\mu(U_h)$, and the standard deviation of the wind speed data, $\sigma(U_h)$, [291], with Γ is the gamma function.

The scale parameter, λ (A.11), is obtained by considering the mean of the distribution, $\mu(U_h)$, to coincide with the daily mean wind speed provided by CORDEX data, to allow the daily variance to adapt to changes in the daily mean wind speed at hub height:

$$\lambda = \frac{\mu(U_h)}{\Gamma(1 + \frac{1}{k})}. \quad (\text{A.11})$$

The vector of shape parameters and the correlation matrix are obtained numerically using hourly data provided by MERRA2 and are assumed to be time-independent. They only vary in space.

III Solar Angles and Tracking Modeling

In this section, we describe the formulas of solar angles (Flow chart A.3) required to calculate the incidence angle for PV fixed-tilted arrays (left panel of figure A.2) and for CSP tracked-horizontal collectors (right panel of figure A.2) which are needed for the solar irradiance decomposition and parametrization (Section IV), and for the CSP solar field modeling (Section 1). All the definitions and formulas have been taken from [178, 267, 497].

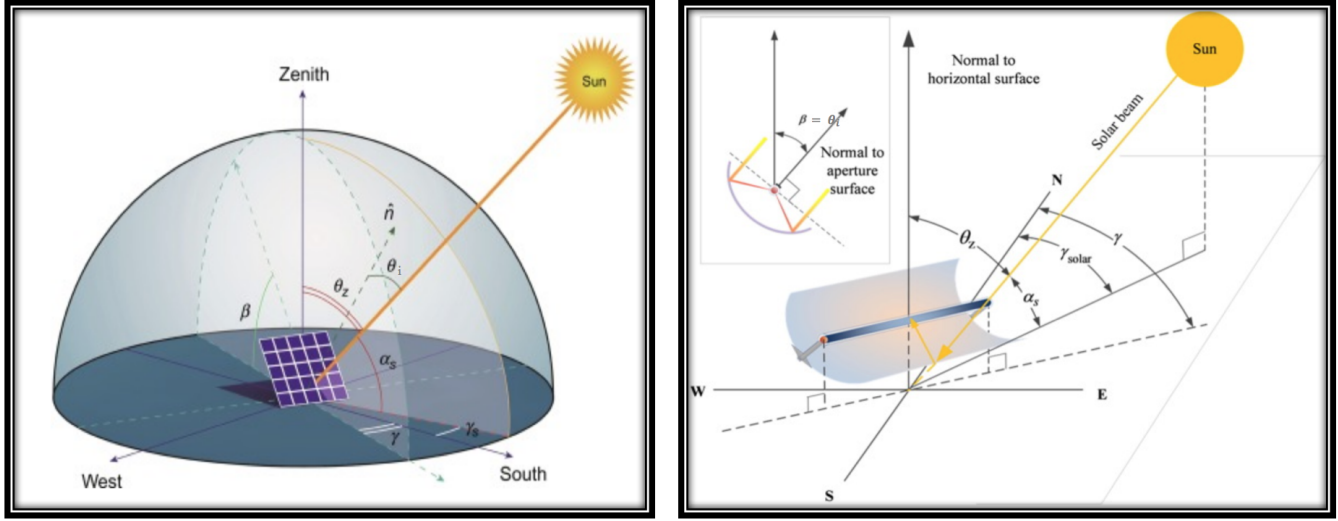


Figure A.2: **Left:** Incidence angle (θ_i), Zenith angle (θ_z), sun elevation (α_s), slope or tilt (β), surface azimuth (γ) and solar azimuth (γ_s) for Photovoltaic (PV) fixed-tilted arrays. **Right:** Same schematic depiction of solar angles for Concentrated Solar Power (CSP) parabolic trough tracked-horizontal collectors.

As illustrated in the flow chart A.3, we first have to compute the angular angles. ϕ is the local latitude. **The solar declination**, δ (A.12), varies seasonally due to earth's tilted axis of rotation (-23.45° in winter solstice; 23.45° in summer solstice; and 0° during the autumn and spring equinoxes). The equation (A.12) assumes that the earth's orbit around the sun is a perfect circle and the factor, $360/365$, converts the day number, n , to a position in the orbit. **The hour angle**, ω (A.13), is the angular displacement of the sun east or west of the local meridian according to the Local Solar Time (LST). The hour angle is negative when the sun is east of the local meridian (in the morning; $LST < 12h$); and positive when the sun is west of the local meridian (afternoon; $LST > 12h$); and zero when the sun is in line with the local meridian (noon; $LST = 12h$). The hour angle converts the LST (h) into the number of degrees in which the sun moves across the sky. Since the earth rotates 15° per hour, each hour away from solar noon corresponds to an angular motion of the sun in the sky of 15° . There is an important distinction between **the LST** (A.14) and the standard time or Local Time (LT). In the solar time, the sun aligns with the local meridian ($\omega = 0$) exactly at 12:00 or "solar noon". However, the standard time is not based on the local meridian, but on the standard meridian for the local time zone. As a result, the standard time must be adjusted to reflect the current time of day in solar time (**the Local Standard Time Meridian (LSTM)** (A.16)). LST varies from LT throughout the year because the earth's orbit velocity varies throughout the year due to the following reasons. First, the length of the day required by the earth to complete one revolution about its own axis is not uniform throughout the year. This variation is due primarily to the fact that the earth follows an elliptical path around the sun [497] (i.e., the orbital eccentricity of the earth). Second, the variation of the distance between the sun and a specific location on the earth's surface also varies because of the axial tilt of the earth (often known as the obliquity of the ecliptic). The third reason is the human adjustments such as time zones and Daylight Saving Time (DST). **The Equation of Time (ET)** (A.17) corrects for the eccentricity of the earth's orbit and the earth's axial [267]. **The Time Correction factor (TC)** (A.15) takes into account the time zones by accounting the longitude lon correction; and the daylight saving time DST . The sun takes 4 min to traverse 1° of longitude ($4 \text{ min}/^\circ$) (A.15).

Then, we have to calculate the position of the sun. **The zenith angle**, θ_z , (A.18) is the angle between the sun's rays and the vertical direction. It complements **the solar elevation or sun altitude**, α_s (A.19). **The solar azimuth**, γ_s (A.20), is the angle of the sun's rays measured in the horizontal plane from due south for the northern hemisphere or due north for the southern hemisphere.

Finally, we compute **the angle of incidence**, θ_i (A.21), which is the angle between the sun's rays and the normal on a surface. It depends on **the tilt** β , **the surface azimuth**, γ , and the solar azimuth, γ_s (Figure A.2). These angles depend on **whether the surface is fixed (without tracking) or tracked** [178] (bottom side of the flow chat A.3).

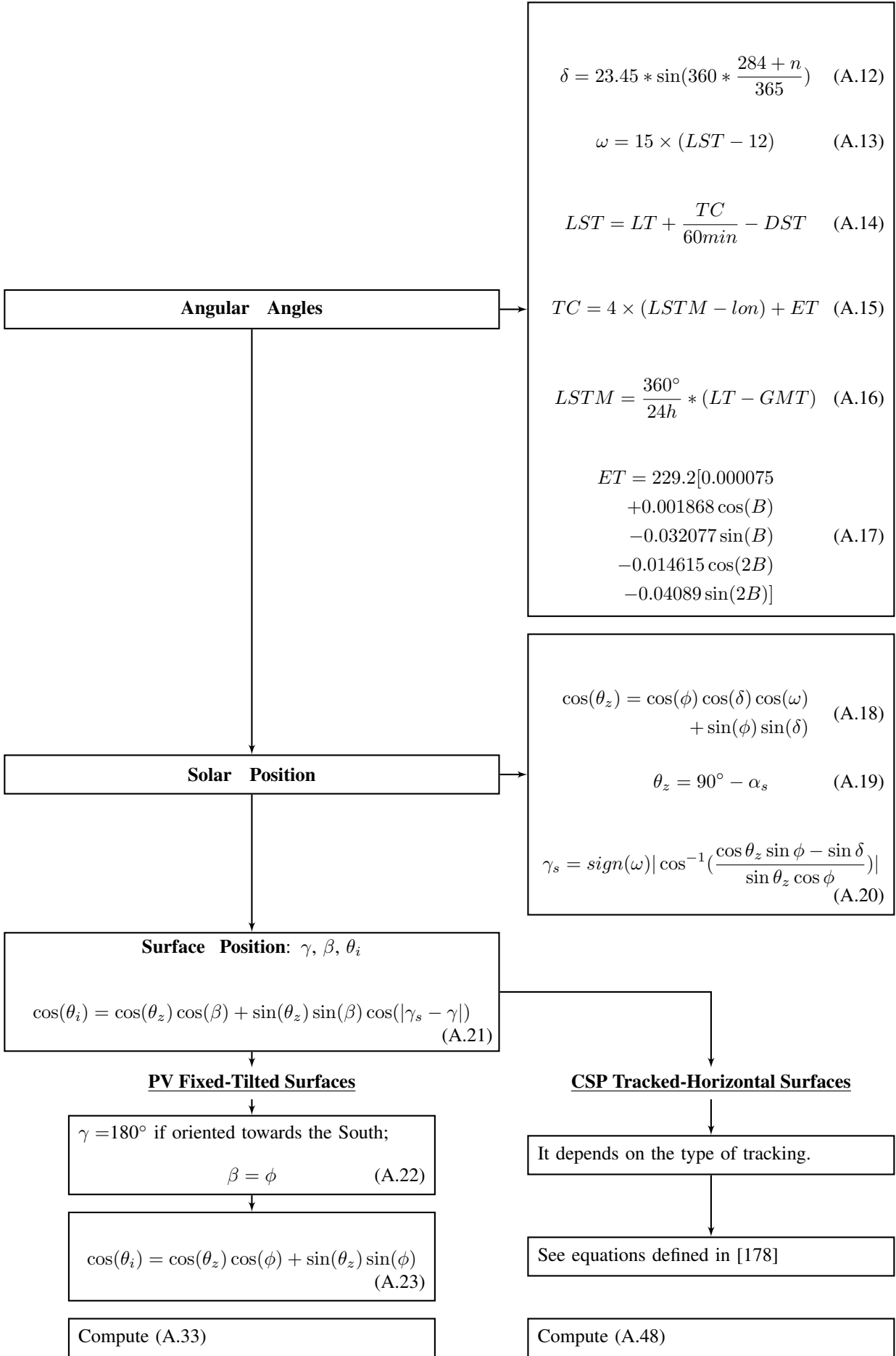


Figure A.3: Mathematical formulation of the solar angles required to calculate the incidence angle (θ_i) for Photovoltaic (PV) fixed-tilted arrays (left panel of figure A.2) and for Concentrated Solar Power (CSP) tracked-horizontal collectors (right panel of figure A.2): Zenith angle (θ_z), sun elevation (α_s), slope or tilt (β), surface azimuth (γ) and solar azimuth (γ_s). δ is the solar declination; ω is the hour angle; LST is the Local Solar Time; LT is the Local Time; TC is the Time Correction factor; DST is the Daylight Saving Time; $LSTM$ is the Local Standard Time Meridian; ET is the equation of time; ϕ is the latitude; lon is the longitude; B is the day angle and n is the day number. Source: Own elaboration based on [178, 267, 497, 350].

IV Solar Irradiance Decomposition and Parametrization

1 Solar Irradiance Decomposition

The solar irradiance usually available from climate data (Section IV, Chapter 2) is the "surface downward irradiance" or the **Global Horizontal Irradiance GHI** (A.24), which is the sum of the direct ($DirHI$) and diffuse components ($DiffHI$) on a horizontal surface:

$$GHI(d, h) = DirHI(d, h) + DiffHI(d, h), \quad (A.24)$$

with h denotes hourly values over a given day d .

To separate the diffuse from the direct component, the model from Reindl et al. [442] is used. **The diffuse horizontal irradiance** is calculated as follows (A.25):

$$DiffHI(d, h) = GHI(d, h) * diffuse_{ratio}(d, h), \quad (A.25)$$

with $diffuse_{ratio}(d, h)$ is the diffuse ratio (A.26).

$$diffuse_{ratio}(d, h) = \begin{cases} 1.4 - 1.749K_T(d, h) + 0.0177 \sin(\alpha_s(d, h)), & \text{if } 0.3 \leq K_T(d, h) \leq 0.78 \\ 1.02 - 0.254K_T(d, h) + 0.0123 \sin(\alpha_s(d, h)), & \text{if } K_T(d, h) < 0.3 \\ 0.486K_T(d, h) - 0.182 \sin(\alpha_s(d, h)), & \text{if } K_T(d, h) > 0.3. \end{cases} \quad (A.26)$$

The clearness index, $K_T(d, h)$ (A.27), is defined as the ratio of the global horizontal irradiance at the surface, $GHI(d, h)$, to the corresponding irradiance available at the top of the atmosphere, $GHI_0(d, h)$, i.e., the extraterrestrial irradiance. if $K_T(d, h) = 1$, it means "clear sky".

$$K_T(d, h) = \frac{GHI(d, h)}{GHI_0(d, h)} \quad (A.27)$$

The global horizontal extraterrestrial solar irradiance, GHI_0 (A.28), depends on the global normal extraterrestrial irradiance, $GHI_{0,n}$ (A.29), and on the zenith angle θ_z (A.18):

$$GHI_0(d, h) = GHI_{0,n}(d, h) * \cos(\theta_z), \quad (A.28)$$

$$GHI_{0,n}(d, h) = S_c * [1.000110 + 0.034221 * \cos(B) + 0.001280 * \sin(B) + 0.000719 * \cos(2B) + 0.000077 * \sin(2B)], \quad (A.29)$$

with $S_c = 1367W/m^2$ is the solar constant; and B is the day angle [178].

Finally, **the direct beam irradiance, $DirHI(d, h)$, on horizontal surface** is computing by subtracting the global (A.24) from the diffuse component (A.25) as stated in equation (A.30):

$$DirHI(d, h) = GHI(d, h) - DiffHI(d, h). \quad (A.30)$$

For solar elevations below 10° , $DirHI(d, h)$ is set to zero as the sun may be behind the Photovoltaic (PV) arrays or Concentrated Solar Power (CSP) collectors.

i PV Global Tilted Irradiance

The Global Tilted Irradiance, $GTI(d, h)$ (A.31), used by PV, is calculated as the sum of the Direct Tilted Irradiance $DirTI(d, h)$, the Diffuse Tilted Irradiance $DiffTI(d, h)$ and the Reflected Tilted Irradiance $RefTI(d, h)$:

$$GTI(d, h) = DirTI(d, h) + DiffTI(d, h) + RefTI(d, h). \quad (A.31)$$

The direct beam irradiance on a sloped surface is calculated as follows (A.32):

$$DirTI(d, h) = DirHI(d, h) * R_{direct}, \quad (A.32)$$

with R_{direct} is the direct transfer ratio (A.33) accounting for the geometric relation between the sun and the solar panel surface. θ_i is the angle of incidence corresponding to fixed PV panels (A.23) and θ_z is the zenith angle (A.18). $DirHI(d, h)$ is the direct beam irradiance on horizontal surface (A.30).

$$R_{direct} = \frac{\cos \theta_i}{\cos \theta_z} \quad (A.33)$$

To get **the diffuse irradiance, $DiffTI(d, h)$, on a sloped surface** (A.34), the anisotropic sky-model of Hay-Davis-Klucher-Reindl (HDKR model) [443] is used:

$$DiffTI(d, h) = DirHI(d, h) * R_{diff}(d, h), \quad (A.34)$$

where R_{diff} is the diffuse transfer factor (A.35):

$$R_{diff}(d, h) = A_i(d, h) * R_{direct} * (1 - A_i(d, h)) * transpo_{iso} * (1 + fR(d, h) * \sin(\frac{\beta}{2}))^3, \quad (A.35)$$

with β is the tilt angle (A.22); $A_i(d, h)$ is the anisotropy index (A.36) with $GHI_0(d, h)$ is the global horizontal extraterrestrial solar irradiance (A.28); $transpo_{iso}$ is the isotropic transposition factor (A.37); and $fR(d, h)$ is the modulating factor (A.38) accounting for cloudiness, expressed as the root of the ratio of direct beam irradiance $DirHI$ and global irradiance $GHI(d, h)$ on horizontal surface.

$$A_i(d, h) = \frac{DirHI(d, h)}{GHI_0(d, h)} \quad (A.36)$$

$$transpo_{iso} = \frac{1 + \cos(\beta)}{2} \quad (A.37)$$

$$fR(d, h) = \sqrt{\frac{DirHI(d, h)}{GHI(d, h)}} \quad (A.38)$$

The reflected component of the tilted irradiance (A.39) follows the usual formula given by [178, Chapter 2], with an albedo of 0.2, since the global tilted irradiance (A.31) tends to be dominated by its direct and diffuse components.

$$RefTI(d, h) = GHI(d, h) * (R_{ref} * albedo) \quad (A.39)$$

$(R_{ref} * albedo)$ is the reflected transfer ratio (A.40):

$$R_{ref} = \frac{(1 - \cos(\beta))}{2}. \quad (A.40)$$

ii CSP Direct Normal Irradiance

The Direct Normal Irradiance, $DirNI(d, h)$ (A.41), used by CSP, represents that portion of solar irradiance reaching the surface of the earth that has not been scattered or absorbed by the atmosphere. The adjective “normal” refers to the direct irradiance as measured on a plane normal to its direction. It depends on the zenith angle θ_z (A.18) and on the direct beam irradiance on horizontal surface $DirHI(d, h)$ (A.30).

$$DirNI(d, h) = \frac{DirHI(d, h)}{\cos(\theta_z)} \quad (A.41)$$

2 Solar Irradiance Intra-daily Parametrization

Contrary to Modern-Era Retrospective Analysis for Research and Applications 2 (MERRA-2) reanalysis, COordinated Regional climate Downscaling EXperiment (CORDEX) climate data only provides mean daily of the global horizontal irradiance, $GHI(d)$. To take into account the diurnal cycle, we assume that **the clearness index is constant throughout the day** (i.e. the fluctuations associated with the intraday variations of the clearness index—associated with the changes in the cloud cover—are ignored) (A.42):

$$K_T(d, h) = \frac{GHI(d, h)}{GHI_0(d, h)} = \frac{GHI(d)}{GHI_0(d)}. \quad (A.42)$$

The hourly global horizontal irradiance, $GHI(d, h)$, is thus computed as follows (A.43):

$$GHI(d, h) = GHI_0(d, h) * \frac{GHI(d)}{GHI_0(d)}, \quad (A.43)$$

with $GHI_0(d) = \frac{1}{24} \sum_1^{24} GHI_0(d, h)$ and $GHI_0(d, h)$ is the global horizontal extraterrestrial solar irradiance (A.28).

With this parametrization, the variance of the solar mean CFs may be underestimated since intra-daily fluctuations of the cloud cover account for most of the daily solar irradiance variance, especially for the direct component used by CSP [313], but this discrepancy may remain limited to the extent that the intraday variations of the clearness index are averaged out at regional level.

V CSP Production Modules

This section describes the modeling of the thermal energy provided by the CSP Solar Field (SF) or/and by the Thermal Energy Storage (TES) for different Solar Multiples (SMs) (Section 1); and the electrical energy provided by the Power Block (PB) (Section 2).

A schematic depiction of the main components of the parabolic trough CSP plant illustrating the main parameters calculated is presented in figure 2.5 and the left panel of figure 2.7 (Chapter 2).

1 Solar Field Modeling

The SF production for given SM, $P_{SF,therm}^{SM}$, to be dispatched to the PB and/or the TES is given by equation (A.44):

$$P_{SF,therm}^{SM} = \eta_{SF} \times A_{SF}^{SM} \times DirNI \quad (A.44)$$

where $DirNI$ (A.41) is estimated from the climate data (Section IV, Chapter 2), A_{SF}^{SM} is the total SF area for a given Solar Multiple (SM) (2.6) and η_{SF} is **the overall SF efficiency** (A.45):

$$\eta_{SF} = \eta_{SF,geo} \times \eta_{SF,opt} \times \eta_{SF,therm} \times \eta_{SF,avail} \quad (A.45)$$

Table A.2: Main characteristics of the 50 MW Concentrated Solar Power with Thermal Energy Storage Andasol 1 power plant, taken as reference for this thesis. Adapted from Silva et al. [483] (Appendix A).

Property	Symbol	Value
Total reference aperture area	A_{SF}^{ref}	510,120 m ²
Row distance between collectors	d_{row}	17.2 m
Collector length	l_{coll}	150 m
Collector aperture width	W_{coll}	5.77 m
Focal length	f	7.1 m
Solar field inlet temperature	$T_{SF,inlet}$	293 °C
Solar field outlet temperature	$T_{SF,outlet}$	393 °C
CSP nominal power	$P_{PB,elec,nom}^{ref}$	50 MW

where $\eta_{SF,geo}$, $\eta_{SF,opt}$, $\eta_{SF,therm}$ and $\eta_{SF,avail}$ are efficiencies respectively associated with geometrical, optical, thermal and **additional losses associated with the collectors' availability**. We set the latter to (A.46):

$$\eta_{SF,avail} = 99.5 \% . \quad (A.46)$$

The overall geometrical efficiency (A.47) is given by the product of the cos-loss efficiency, $\cos(\theta_i)$, the Incidence Angle Modifier-loss efficiency, IAM, the shading-loss efficiency, S , and the row-end-loss efficiency R :

$$\eta_{SF,geo} = \cos(\theta_i) \times IAM \times S \times R . \quad (A.47)$$

The cos-loss occurs when the sun rays are not perpendicular to the aperture area of the collector. The angle, θ_i , is the incidence angle for a plane rotated about a horizontal east-west axis with continuous north-south tracking (A.48), taken as reference tracking option for CSP (Section i, Chapter 2):

$$\cos(\theta_i) = (1 - \cos^2(\delta) \sin^2(\omega))^{1/2}, \quad (A.48)$$

where δ is the solar declination and ω is the hour angle (Section III).

When the sun is not perpendicular to the collector plane, it affects the rays reflection and hence the receiver absorption. **The IAM factor** (A.49) is the variance in output performance of a solar collector as the angle of incidence changes [451]:

$$IAM = \cos(\theta_i) [1 + \sin^3(\theta_i)] . \quad (A.49)$$

The losses due to shading (Figure A.4(a)) occurs at low solar altitude angles until a critical zenith angle, θ_z , is reached and depends on the row distance between collectors, d_{row} , e.g., small distances imply high shading losses. The shading loss, S , is given by equation (A.50) [483, 403]:

$$S = \frac{W_{eff}}{W_{coll}} = \frac{d_{row}}{W_{coll}} \frac{\cos \theta_z}{\cos \theta_i}, \quad (A.50)$$

where W_{eff} is the effective mirror width (that is, the width of the aperture that is not shaded), and W_{coll} is the mirror width (Table A.2). The quantity, S , ranges between 0 (full shading) and 1 (no shading).

Finally, if the sun beam upon a collectors' edges is reflected but does not hit the receiver, a part of the receiver with the length, $f \tan \theta_i$, does not contribute to the heat production (the red part of figure A.4(b)). **The row-end loss factor** (A.51) is thus written as [483, 403]:

$$R = 1 - \frac{f \tan \theta_i}{l_{coll}}, \quad (A.51)$$

where f is the focal length of the collector and l_{coll} is the collector length (Table A.2).

Optical losses are caused by imperfect reflection (due to dirt), transmission and absorption of the collectors [451]. All contributions are assumed constant and we set **the overall optical efficiency of the collectors** to (A.52):

$$\eta_{SF,opt} = 73 \% . \quad (A.52)$$

Thermal losses occur on the receiver, connections and piping. Only the receiver losses are considered (Figure A.4(c)) and are caused by the difference between the average fluid temperature, $T_{fluid} = (T_{SF,inlet} + T_{SF,outlet})/2$, with $T_{SF,inlet}$ and $T_{SF,outlet}$ are the SF inlet and outlet temperatures (Table A.2), and the temperature of the receiver cover, T_{cover} , which is here 37 °C higher than the temperature of the surrounding ambient air, T_{amb} , obtained from the climate data (Section IV, Chapter 2). Conduction losses are neglected. We write **the irradiance loss** as (A.53):

$$q_{rad} = \sigma \epsilon A_{receiver} (T_{fluid}^4 - T_{cover}^4), \quad (A.53)$$

where σ is the Stefan-Boltzmann constant, $A_{receiver} = l_{coll} W_{coll} \pi / C$ is the receiver area, C is the concentration ratio (i.e., $C = A_{SF}^{SM} / A_{receiver}$), and ϵ is the receiver emissivity (equal to 0.08 for absorbing pipes with ceramic-metal material) [451]. **The natural convection losses** between the glass cover and the ambient air can be expressed as (A.54):

$$q_{conv} = h_{conv} A_{receiver} (T_{cover} - T_{amb}), \quad (A.54)$$

where the parameter h_{conv} is the loss coefficient of the receiver.

The incident solar energy collected by the receiver is $\text{DirNI} \times C \times A_{receiver}$. **The total thermal efficiency** is therefore given by equation (A.55):

$$\eta_{SF,therm} = 1 - \frac{q_{conv} + q_{rad}}{\text{DirNI} \times C \times A_{receiver}} = 1 - \frac{h_{conv}(T_{cover} - T_{amb}) + \sigma \epsilon (T_{fluid}^4 - T_{cover}^4)}{C \times \text{DirNI}} . \quad (A.55)$$

We consider the values given by [451], for the same nominal capacity of our reference CSP plant, i.e. $C = 71$ and $h_{\text{conv}} = 2 \text{ W m}^{-2} \text{ K}^{-1}$ which is a low value because of the coating and the vacuum between the absorbing pipe and cover (Figure A.4(c)). The forced convection (i.e. by strong winds) is neglected.

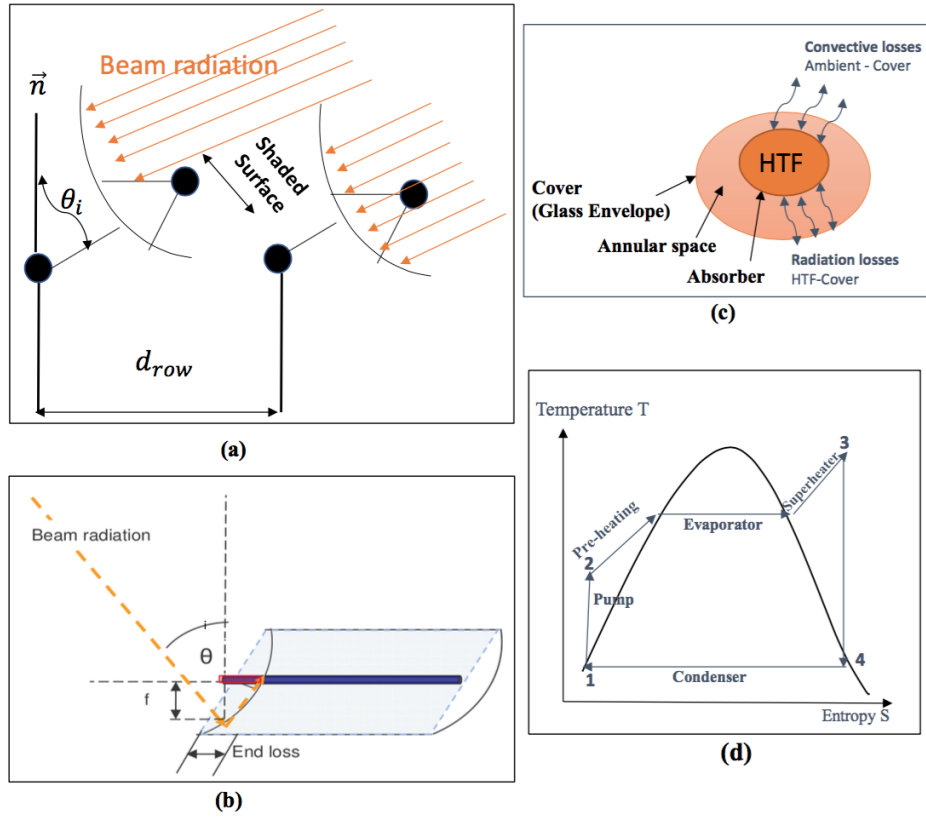


Figure A.4: (a) Shading effect; (b) End losses effect; (c) Thermal losses occurring on the receiver; (d) We refer to "1" as the state of temperature and enthalpy after condensation; "2" after pump; "3" after steam generator (pre-heating, evaporation and superheating); and "4" after turbine (Figure 2.5, Chapter 2). Source: Own elaboration based [403].

2 Power Block Modeling

The CSP net electrical power output, P_{elec}^{SM} , is given by equation (A.56):

$$P_{\text{elec}}^{SM} = P_{\text{in}}^{SM} \eta_{\text{PB}}^{SM}, \quad (\text{A.56})$$

where P_{in}^{SM} is the total available thermal energy for PB (illustrated in the caption of figures 2.5 and 2.9, Chapter 2) and η_{PB} is the overall PB efficiency (A.57):

$$\eta_{\text{PB}}^{SM} = \eta_{\text{turb}} \eta_{\text{gen}}^{SM} (1 - \xi). \quad (\text{A.57})$$

The quantity, ξ , represents the parasitic loss, which corresponds to the electrical needs for the plant operation for example to run heat transfer fluid pumps, tracking systems, transport of cooling water from source to plant (in case of wet cooling) or ventilation (in case of dry cooling), or electrical losses on the generator and on the transformer. It varies roughly between 4 % and 13 % of the nominal gross power output of the plant [451], we set it to (A.58):

$$\xi = 4\%. \quad (\text{A.58})$$

The term (A.59)

$$\eta_{\text{turb}} = (h_3 - h_4) / (h_3 - h_2) \quad (\text{A.59})$$

is the constant thermodynamic efficiency of an ideal Clausius-Rankine cycle (thus, all operating pressures and temperatures are constant). This implies that instead of varying steam temperatures, the mass flow is regulated to reach a constant temperature of the heat transfer fluid. In addition, condensation temperature is assumed to be constant and independent from ambient temperatures. Given the enthalpy $h_2 = 232.0 \text{ kJ/kg}$, $h_3 = 3002 \text{ kJ/kg}$ and $h_4 = 1959 \text{ kJ/kg}$ corresponding to each state of the temperature-entropy diagram of the Rankine cycle (Figure A.4(d)) for dry cooling [451], it is here equal to 37.6 %.

Then, the thermal power of the turbine (Figure 2.5, Chapter 2) is calculated by equation (A.60):

$$P_{\text{turb,therm}}^{SM} = \dot{m}_{\text{steam}} \times (h_3 - h_4) = \frac{P_{\text{in}}^{SM}}{h_3 - h_2} \times (h_3 - h_4). \quad (\text{A.60})$$

The generator efficiency, η_{gen} , is approximated by the following equation (A.61) [451]:

$$\eta_{\text{gen}}^{SM} = \frac{\frac{P_{\text{turb,therm}}^{SM}}{P_{\text{turb,therm,nom}}^{ref}} - (1 - \eta_{\text{gen,nom}}^{ref})}{\frac{P_{\text{turb,therm}}^{SM}}{P_{\text{turb,therm,nom}}^{ref}}}, \quad (\text{A.61})$$

with $P_{\text{turb,therm,nom}}^{ref}$ is $P_{\text{PB,elec,nom}}^{ref}$ (Table A.2). Here, $\eta_{\text{gen,nom}}^{ref}$ is the nominal generator efficiency, which we set to 97%, as in [451]. The nominal PB efficiency is derived from the following formula (A.62):

$$\eta_{\text{PB,nom}}^{ref} = \eta_{\text{turb}} \eta_{\text{gen,nom}}^{ref} (1 - \xi). \quad (\text{A.62})$$

The solar to electricity efficiency is given by equation (A.63):

$$\eta_{\text{solar-to-elec}} = \frac{P_{\text{elec}}^{SM}}{\text{DirNI} \times A_{\text{SF}}^{SM}}. \quad (\text{A.63})$$

VI PV Production Modules

This section describes the modeling of the Direct Current (DC) energy provided by the Solar Panels (SP) or/and by the Battery Energy Storage (BES) for different Inverter Loading Ratios (ILRs) (Section 1); and the Alternating Current (AC) energy provided by the inverter (INV) (Section 2).

A schematic depiction of the main components of the Photovoltaic (PV) plant illustrating the main parameters calculated is presented in the left panel of figure 2.7 (Chapter 2).

1 Solar Panels Modeling

The PV model, used in this thesis, is based on a parametric approach to model the SP efficiency where the effect of the temperature leads to a relation in the form (A.64) [177]:

$$\eta_{SP} = \eta_{SP}^{ref} \left[1 + \beta_{SP}^{ref} (T_{SP} - T_{SP,STC}^{ref}) + \gamma_{SP}^{ref} \log\left(\frac{GTI}{GTI_{STC}}\right) \right], \quad (\text{A.64})$$

where $\eta_{SP}^{ref} = \frac{P_{\text{SP,DC,nom}}^{ref}}{A_{\text{SP}}^{ref} * GTI_{STC}}$ is the SP's electrical efficiency at the reference temperature, $T_{SP,STC}^{ref} = 25^\circ\text{C}$, and at the reference Global Tilted Irradiance, $GTI_{STC} = 1000\text{W}/\text{m}^2$, obtained under Standard Test Conditions (STC). $A_{\text{SP}}^{ref} = 1.675\text{m}^2$ is the reference SP area and $P_{\text{SP,DC,nom}}^{ref} = 250\text{W}$ is the reference DC nominal power. The temperature coefficient, β_{SP}^{ref} , and the solar irradiance coefficient, γ_{SP}^{ref} , are mainly material properties having values of about -0.004K^{-1} and 0.12 respectively for crystalline silicon SPs [382], taken as reference for PV (Section ii, Chapter 2). The latter, however, is usually taken as zero [190] and equation (A.64) reduces to (A.65) which represents the traditional linear expression for the PV electrical efficiency [177]:

$$\eta_{SP} = \eta_{SP}^{ref} \left[1 + \beta_{SP}^{ref} (T_{SP} - T_{SP}^{ref}) \right]. \quad (\text{A.65})$$

The SP temperature (A.66) is calculated as follows [177]:

$$T_{SP} = T_{\text{amb}} + \frac{GTI}{GTI_{NOCT}} * L(U) * (T_{SP,NOCT}^{ref} - T_{\text{amb},NOCT}), \quad (\text{A.66})$$

where $L(U) = \frac{9.5}{5.7+3.8U}$ is the loss ratio, U is the wind speed, T_{amb} is the ambient temperature and GTI is the Global Tilted Irradiance (GTI) (A.31) given by climate data (Section IV, Chapter 2). The Nominal Operating Cell Temperature (NOCT), $T_{SP,NOCT}^{ref} = 319.15\text{K}$, is defined as the temperature reached by the SP under the following conditions: $GTI_{NOCT} = 800\text{W}/\text{m}^2$, $T_{\text{amb},NOCT} = 20^\circ\text{C}$, and $U = 1\text{m}/\text{s}$.

Based on the EVANS model [190], the DC power generated by a PV SP (A.67), for given ILR, is calculated by the product of the total area of the SP A_{SP}^{ILR} (2.6), the number of SPs N_{SP} , the global tilted irradiance GTI (A.31), and the efficiency of the SP η_{SP} (A.65):

$$P_{\text{SP,DC}}^{ILR} = N_{SP} * A_{\text{SP}}^{ILR} * \eta_{SP} * GTI. \quad (\text{A.67})$$

2 Inverter Modeling

The AC electrical production (A.68) is simulated by multiplying the DC power, $P_{\text{SP,DC}}^{ILR}$ (A.67), by the nominal inverter efficiency $\eta_{\text{INV,nom}}^{ref}$:

$$P_{\text{SP,AC}}^{ILR} = P_{\text{SP,DC}}^{ILR} * \eta_{\text{INV,nom}}^{ref}. \quad (\text{A.68})$$

In fact, the inverter efficiency can be simulated using equation (A.69) where y_0 , c_1 , c_2 can be determined using a non linear regression algorithm [332]. However, we found that $\eta_{\text{inv,sim}}$ do not vary a lot with $P_{\text{SP,DC}}^{ILR}$. Therefore, a constant value is used $\eta_{\text{INV,nom}}^{ref} = 97.2\%$ [464].

$$\eta_{\text{inv,sim}} = y_0 + c_1 \left[1 - \exp(-C_2 * P_{\text{SP,DC}}^{ILR}) \right] \quad (\text{A.69})$$

VII Storage Module

1 CSP Solar Multiple and PV Inverter Loading Ratio

The total thermal (resp. Direct Current -DC-) energy supplied by CSP Solar Field-SF- (resp. PV Solar Panel-SP-) or the amount of energy than can be stored in the storage system, during the day, depend on the Solar Multiple-SM- (resp. Inverter Loading Ratio-ILR-) [194]. The latter is a dimensionless parameter that describes the additional CSP SF (resp. PV SP) that are required to produce electricity also in times when the sun does not shine. As illustrated in the right panel of figure 2.7 (Chapter 2), a SM or ILR of 1, for instance, means that the SF (resp. SP) is sized to the rating of the Power Block-PB- (resp. inverter-INV-). Thus, the plant will be used at full capacity only under nominal irradiance conditions. With an increased SM (resp. ILR), because the CSP SF (resp. PV panel) can produce more energy than can be used by the PB (resp. INV), some of the CSP (resp. PV) energy need to be stored. A CSP (resp. PV) plant with SM (resp. ILR) of 2 would have SF (resp. SP) size and TES (resp. BES) capacity large enough so that one SF (resp. SP) will drive the PB (resp. INV) while the other will serve to fill the storage for night operation. SF (resp. SP) size and TES (resp. BES) capacity can be increased with SM (resp. ILR) 3 and 4 and allow to produce more surplus thermal (resp. DC) energy which allow to maintain the production at nominal capacity for several hours [360, 451] (as discussed in section 3, chapter 2).

Figure A.5 details the equations needed to increase the CSP SF (resp. PV SP) size relative to the PB (resp. inverter) size as explained in section 1 (Chapter 2).

$$\diamond A_x^{SM/ILR} ?$$

$$P_{y,x,nom}^{ref} = \frac{P_{y,y,nom}^{ref}}{\eta_{y,nom}^{ref}} = \text{threshold}_{CSP-TES \text{ or } PV-BES}$$

$$SM/ILR^{ref/SMorILR} = \frac{P_{x,x,nom}^{ref/SMorILR}}{P_{y,x,nom}^{ref}} = \frac{P_{x,x,nom}^{ref/SMorILR}}{P_{y,y,nom}^{ref}} \eta_{y,nom}^{ref}$$

❖ Reference case:

$$SM/ILR^{ref} = \frac{P_{x,x,nom}^{ref}}{P_{y,x,nom}^{ref}} = \frac{P_{x,x,nom}^{ref}}{P_{y,y,nom}^{ref}} \eta_{y,nom}^{ref} = \frac{A_x^{ref} * \eta_{x,nom}^{ref} * S}{P_{y,y,nom}^{ref}} \eta_{y,nom}^{ref}$$

Method 1:

$$P_{x,x,nom}^{SM/ILR} = SM/ILR * P_{x,x,nom}^{ref}$$

$$\Rightarrow A_x^{SM/ILR} * \eta_{x,nom}^{ref} * S = SM/ILR * P_{x,x,nom}^{ref}$$

$$A_x^{SM/ILR} = \frac{SM/ILR * P_{x,x,nom}^{ref}}{\eta_{x,nom}^{ref} * S}$$

$$\Rightarrow A_x^{SM/ILR} = \frac{SM/ILR * P_{y,y,nom}^{ref}}{\eta_{x,nom}^{ref} * S * \eta_{y,nom}^{ref}}$$

With: $\mathcal{X}O_{DP/STC} = \eta_{x,nom}^{ref} * S$

$$\mathcal{Y}O_{DP/STC} = \mathcal{X}O_{DP/STC} * \eta_{y,nom}^{ref}$$

Method 2:

$$P_{x,x,nom}^{SM/ILR} = A_x^{SM/ILR} * \eta_{x,nom}^{ref} * S$$

$$\Rightarrow A_x^{SM/ILR} = \frac{P_{x,x,nom}^{SM/ILR}}{\eta_{x,nom}^{ref} * S}$$

and:

$$A_x^{ref} = \frac{P_{x,x,nom}^{ref}}{\eta_{x,nom}^{ref} * S}$$

We divide $A_x^{SM/ILR}$ by A_x^{ref} :

$$\frac{A_x^{SM/ILR}}{A_x^{ref}} = \frac{P_{x,x,nom}^{SM/ILR}}{P_{x,x,nom}^{ref}} = \frac{SM/ILR * P_{y,y,nom}^{SM/ILR}}{SM/ILR^{ref} * P_{y,y,nom}^{ref}}$$

$$\Rightarrow A_x^{SM/ILR} = A_x^{ref} * \frac{SM/ILR}{SM/ILR^{ref}}$$

Figure A.5: Relationship between Concentrated Solar Power-CSP- Solar Multiple-SM- (resp. Photovoltaic-PV- Inverter Loading Ratio-ILR-) and CSP Solar Field-SF- (resp. PV Solar Panels-SP-) area: Depending on the value of the CSP SM (resp. PV ILR), different amount of thermal (resp. Direct Current-DC-) energy is provided by the CSP SF (resp. PV SP) and thus stored in the thermal-TES- (resp. battery-BES-) storage system in order to be used by the Power Block-PB- (resp. Inverter-INV-) to produce electricity whenever it is needed. $X = \{SF, SP\}$; $Y = \{PB, INV\}$; $x = \{therm, DC\}$; and $y = \{elec\}$ (Section 1, Chapter 2). Source: Own elaboration based on [451].

2 Storage Model without Constraints

The storage model without constraints assumes that the energy charged, $P_{X \rightarrow \Theta, x}^{SM/ILR}$, the energy discharged, $P_{\Theta \rightarrow Y, x}^{SM/ILR}$, and the state of charge, $SOC_{E, \Theta}^{SM/ILR}$, are only determined by the energy supplied to and extracted from the storage system (i.e., limited only by the surface of the SF or SP (2.6) and not by the storage constraints of table 2.3 in chapter 2). As shown in figure 2.8 (Chapter 2) illustrating the dispatching conditions at some time spell t , (1) the thermal energy from the SF (resp. SP), $P_{X, x}^{SM/ILR}$, can go directly to the PB (resp. INV) at nominal capacity (during period of high solar irradiance) or operate in partial load whenever the irradiance is high enough to run the PB (resp. INV). So, the production ($P_{X \rightarrow Y, x}^{SM/ILR}$) will be the minimum between the SF output ($P_{X, x}^{SM/ILR}$) and the thermal (resp. DC) nominal capacity ($P_{Y, x, nom}^{ref}$). Then, (2) if the SF (resp. SP) energy is above the maximum thermal (resp. DC) capacity ($P_{Y, x, nom}^{ref}$) during peak solar hours, all the "extra" thermal energy from the SF (resp. SP) (i.e., the difference between the SF (SP) output and the threshold ($P_{X \rightarrow \Theta, x}^{SM/ILR}$)) to be dispatched later (as no constraints on storage are assumed to be in place), and the plant is producing electricity ($P_{X \rightarrow Y, x}^{SM/ILR}$) at nominal thermal (resp. DC) capacity, $P_{Y, x, nom}^{ref}$, at the same time. (3) In times of little or no solar irradiance, the thermal (resp. DC) power provided by the SF (resp. SP) is less than the power required to operate in full load ($P_{Y, x, nom}^{ref}$), the PB (resp. INV) is fueled by energy from the SF (resp. SP) and the TES (resp. BES) system ($P_{X \rightarrow Y, x}^{SM/ILR} + P_{\Theta \rightarrow Y, x}^{SM/ILR}$). This might happen when the sky is cloudy fluctuating the solar irradiance during the day. Without any solar irradiance available (e.g., after sunset), the missing power needed to run the PB (resp. INV) at nominal capacity has to come only from the storage system ($P_{\Theta \rightarrow Y, x}^{SM/ILR}$) until it is completely depleted unless the current state of charge ($SOC_{E, \Theta}^{SM/ILR}$) is not large enough to cover this deficit, in which case the TES (resp. BES) is emptied to inject as much energy to the PB (resp. INV) as possible.

VIII Capacity Factors, Covariances and Bias Correction

1 Observed CSP Solar Multiple and PV Inverter Loading Ratio

In this section, we compare the observed CSP Solar Multiple (SM), SM_p^{obs} (A.70), of each operational CSP plant p (Table A.6) by calculating it as the ratio of the observed Solar Field (SF) capacity, $\omega_{SF,k,p}^{obs}$, divided by the observed Power Block (PB) capacity, $\omega_{k,p}^{obs}$:

$$SM_p^{obs} = \frac{\omega_{SF,k,p}^{obs}}{\omega_{k,p}^{obs}} = \frac{A_{SF,p}^{obs} * DNI_{DP} * \langle \eta_{SF} \rangle}{\omega_{k,p}^{obs}}, \quad (A.70)$$

where $A_{SF,p}^{obs}$ is the observed CSP SF area (depicted in (A.71)) and $\langle \eta_{SF} \rangle = 20.13\%$ is the mean of the SF efficiency (A.45).

$$\begin{cases} p1 = NOOR1; A_{SF,p1}^{obs} = 1308000m^2; \omega_{k,p1}^{obs} = 160MW [22] & \rightarrow SM_{p1}^{obs} = 1.31 \\ p2 = NOOR2; A_{SF,p2}^{obs} = 1779900m^2; \omega_{k,p2}^{obs} = 200MW [22] & \rightarrow SM_{p2}^{obs} = 1.43 \\ p3 = NOOR3; A_{SF,p3}^{obs} = 1321197m^2; \omega_{k,p3}^{obs} = 150MW [22] & \rightarrow SM_{p3}^{obs} = 1.41 \\ p4 = AinBeniMathar; A_{SF,p4}^{obs} = 183120m^2; \omega_{k,p4}^{obs} = 20MW [5] & \rightarrow SM_{p4}^{obs} = 1.47 \end{cases} \quad (A.71)$$

From A.71, we can see that **the difference in the SM of the different CSP plants is very small**. This verification has been done only for CSP plants since **all operational PV plants considered for bias correction are without storage (i.e., ILR1); and onshore wind is assumed without storage** (Table A.6).

2 Bias Correction Approach

The hourly wind, PV/PV-BES and CSP/CSP-TES CFs—obtained from the theoretical renewable production models—and aggregated at regional level are statistically adjusted to observations.

The hourly bias-corrected Capacity Factor (CF) is given by the following expression (A.72):

$$\eta_{h,k}^{corr} = \frac{\eta_{y,k}^{obs}}{\langle \eta_{h,k}^{clim} \rangle} \times \eta_{h,k}^{clim}, \quad (A.72)$$

where η_h and η_y correspond to hourly and yearly CFs. The index k is a multi-index representing a pair $k = (i, j)$ or $k = (i, j, j')$ of region i and technology j or j with storage j' . The brackets correspond to averages over all years available from the climate data (Section IV, Chapter 2). The subscripts "obs" and "clim" denote, respectively, the observations and predictions from climate data. For instance, using COordinated Regional climate Downscaling EXperiment (CORDEX) climate data with future projections, $\langle \eta_{h,k}^{clim} \rangle$ is the mean CF obtained with CORDEX (with parametrization) over the historical experiment (1951 – 2005); and $\eta_{h,k}^{clim}$ is the hourly CFs obtained with CORDEX (with parametrization) over the projection experiment (2006-2100). **The annual observed CF** for the year 2018, $\eta_{y,k}^{obs}$, for given region, i , and power plant p (Table A.6 and table 2.1 in chapter 2) is calculated as follows (A.73):

$$\eta_{y,k}^{obs} = \frac{\sum_p Prod_{y,k,p}^{obs}}{\sum_p \omega_{k,p}^{obs}} = \frac{Prod_{y,k}^{obs}}{\omega_k^{obs}}. \quad (A.73)$$

3 Inter-annual Variability of Predicted Mean CFs and Demand Obtained from Climate Reanalysis

The inter-annual variability of the predicted mean Capacity Factors (CFs) and demand obtained from hourly Modern-Era Retrospective Analysis for Research and Applications 2 (MERRA-2) climate data from 1980 – 2019 is presented in figure A.6.

4 Estimates of Correlations and Covariances

Estimates of the covariances between the predicted CFs and the inverse of the demand for the same region (2.3), over the year 2018, are reported in table A.4. We compute also the correlations between technologies in table A.5.

These covariances and correlations are calculated to analyze the impact of temporal complementarity on the reduction of the adequacy risk (section 2 in Chapter 3 and section 2 in Chapter 4 where we also examine the impact of spatial or spatio-temporal complementarity).

The correlations of CFs with demand can be analyzed by looking at the daily and seasonal cycles of demand and CFs (Figure 3.2, 3.3e, and 3.3d in Chapter 3 ; and figure 4.3 in Chapter 4).

5 Critical Appraisal of the Obtained Profiles of Wind and Solar Capacity Factors

i Wind Speed Extrapolation Approach

Whether the extrapolation of wind speed using the power law is a good approximation of the vertical profile of the wind or not, arbitrarily choosing a value of $\alpha = 1/7$ may lead to large errors in the estimation of the daily and seasonal cycle of the wind speed at hub height.

In fact, the wind Capacity Factor (CF) depends strongly on wind speed (i.e., wind production is the cube of wind speed) and on air density or temperature. Therefore, the approach that should be used to extrapolate wind speed at hub height must consider the influence of surface roughness and thermal stratification (i.e., atmospheric stability).

Table A.3: Bias correction factor $\frac{\eta_{y,k}^{obs}}{\langle \eta_{h,k}^{clim} \rangle}$ by technology j or j' and region i , obtained from hourly (a): Modern-Era Retrospective Analysis for Research and Applications 2 (MERRA-2) climate reanalysis over the year 2018. (b), (c), (d), (e): COordinated Regional climate Downscaling EXperiment (CORDEX) climate data using different climate models (Table 2.2, Chapter 2) over the whole historical period (1951–2005). The name of each climate model is hereafter referred as Global Climate Model (GCM) + Regional Climate Model (RCM): version 4 of the Rossby Centre regional Atmospheric model (RCA4); the version 351 of the Weather Research and Forecasting model (WRF351); Centre National de Recherches Météorologiques-Coupled Model (CNRM-CM5); Earth System Model (EC-EARTH); Geophysical Fluid Dynamics Laboratory’s Earth System Model (GFDL-ESM2M); Community Climate System Model (CCSM4).

Zones	Wind	PV				CSP				
		ILR1	ILR2	ILR3	ILR4	SM1	SM^{ref}	SM2	SM3	SM4
NORTH	3.861	0.927	0.503	0.352	0.263	1.341	0.790	0.746	0.517	0.388
CENTER	2.013	0.854	0.465	0.325	0.243	1.462	0.862	0.814	0.565	0.424
EAST	2.279	0.927	0.503	0.352	0.263	1.219	0.719	0.678	0.470	0.351
SOUTH	0.963	1.001	0.541	0.378	0.283	1.341	0.790	0.746	0.517	0.388

(a) MERRA-2 Reanalysis.

Zones	Wind	PV (ILR1)	CSP	
			SM1	SM2
NORTH	0.929	1.265	1.401	0.760
CENTER	0.876	1.905	1.526	0.828
EAST	0.929	1.587	1.276	0.692
SOUTH	0.982	1.591	1.401	0.760

(b) CORDEX—CNRM-CM5 + RCA4 model.

Zones	Wind	PV (ILR1)	CSP	
			SM1	SM2
NORTH	0.924	1.319	1.382	0.748
CENTER	0.867	2.188	1.508	0.816
EAST	0.924	1.720	1.257	0.680
SOUTH	0.981	1.653	1.382	0.748

(c) CORDEX—EC-EARTH + RCA4 model.

Zones	Wind	PV (ILR1)	CSP	
			SM1	SM2
NORTH	0.944	1.181	1.460	0.784
CENTER	0.892	1.906	1.591	0.855
EAST	0.944	1.576	1.329	0.714
SOUTH	0.995	1.641	1.460	0.784

(d) CORDEX—GFDL-ESM2M + RCA4 model.

Zones	Wind	PV (ILR1)	CSP	
			SM1	SM2
NORTH	0.864	0.959	1.152	0.655
CENTER	0.787	1.488	1.263	0.720
EAST	0.864	1.191	1.040	0.591
SOUTH	0.941	1.124	1.152	0.655

(e) CORDEX—CCSM4 + WRF351 model.

As discussed in section 1, the logarithmic law is used for the vertical profile of the horizontal wind speed in the boundary layer of a neutral fluid. A fluid is neutral if it is not stratified, i.e., if the vertical gradient of (potential) density (or of the potential temperature in the special case of the atmosphere) is zero. Therefore, the logarithmic law does not take into account the thermal stratification. This may not be critical given that we rarely deviate from the neutral stability conditions since current hub heights are beyond the surface layer (right panel of figure 1.5, chapter 1) [287], but the complexity lies in estimating precisely the surface roughness—which does not depend on the atmospheric conditions—and we do not have measurements of wind profiles to derive it experimentally; and it is difficult to determine it for all regions of Morocco from the characteristic values that are usually given for different types of surface.

In addition, the power law with constant α (i.e., Von Karman approach), does not take into account the stability of the atmosphere or the roughness of the surface. In fact, high (resp. low) values of α are associated with a faster (resp. lower) convergence of the wind speed to the upper-level wind speed. A stably stratified air column, with warm air above cold air, prevents turbulent vertical mixing, as energy needs to be spent on rising heavy air parcels on top of lighter air parcels. A weaker stratification then favors vertical mixing. In addition, unstable stratification, with warm air below cold air, leads to convection (i.e., rising air) which facilitate vertical mixing even more. Thus, we are led to hypothesize that stable (resp. unstable) conditions are associated with high (resp. low) values of α . Stable (resp. unstable) conditions are indeed more likely to occur in winter and at night (resp. in summer and during the day). At night, solar irradiance is zero, while blackbody emissions from the ground is positive. This promotes stable stratification by cooling the surface air, while the air aloft remains relatively warm. To the contrary, during the day, solar irradiance heats the ground, resulting in a net heating of the surface air, promoting a destabilization of the air column and possibly convection. A similar argument holds for winter vs. summer. Thus, we expect to find higher values of α at night and during winter than during the day and summer.

Tobin et al. [518] concludes that Justus and Mikhail’s approach, where α varies, does not necessarily provide a better approximation of the vertical profile of the wind speed than the Von Karman approach. To simplify, we choose the power law with constant alpha and compare our simulations with existing studies.

When we look at the daily and seasonal cycle of the wind CF simulated using Modern-Era Retrospective Analysis for Research and Applications 2 (MERRA-2) over the year 2018 (Figure 3.2a, Chapter 3), we can see that the wind CF increases during the day (between 8am and 7pm) with a high intensity in winter and increases in summer; but evenly distributed over the whole day and year. It appears that the daily profile obtained follows the daily variations in the wind speed presented by Nfaoui et al. [380, Figure II.7]; and also follows the seasonal profile of the Weibull parameters shown in [380, Figure II.16] of the same reference which shows that the scale parameter increases in summer and the shape parameter increases in winter (i.e., regular and intense wind in winter).

Zones	ILR1/ Wind	ILR1/ SM1	ILR1/ SM^{ref}	ILR1/ SM2	ILR1/ SM3	ILR1/ SM4	Wind/ SM1	Wind/ SM^{ref}	Wind/ SM2	Wind/ SM3	Wind/ SM4
NORTH	11.38	63.24	36.94	33.71	15.94	5.96	6.89	5.08	3.76	-5.85	-
CENTER	17.29	71.04	38.10	34.33	13.88	2.46	32.88	28.95	26.52	9.84	-0.35
EAST	24.42	63.55	34.71	31.40	13.16	2.84	32.01	21.98	19.7	6.05	-1.36
SOUTH	6.22	73.72	39.23	35.24	13.55	1.49	13.37	9.78	9.41	5.90	1.75

Zones	ILR2/ Wind	ILR3/ Wind	ILR4/ Wind	ILR2/ SM1	ILR3/ SM1	ILR4/ SM1	ILR2/ SM^{ref}	ILR3/ SM^{ref}	ILR4/ SM^{ref}
NORTH	10.52	4.73	-0.64	39.92	20.08	8.24	34.30	20.27	8.31
CENTER	16.19	9.13	2.84	43.39	20.63	6.41	34.47	20.21	6.26
EAST	18.54	9.17	2.69	38.45	18.39	5.91	31.20	18.07	5.79
SOUTH	4.34	2.77	0.65	45.34	21.90	7.32	36.01	21.12	7.08

Zones	ILR2/ SM2	ILR3/ SM2	ILR4/ SM2	ILR2/ SM3	ILR3/ SM3	ILR4/ SM3	ILR2/ SM4	ILR3/ SM4	ILR4/ SM4
NORTH	31.92	20.27	8.32	15.49	14.00	8.27	5.80	5.44	4.70
CENTER	31.62	20.05	6.25	13.02	11.63	5.57	2.26	1.96	1.38
EAST	28.74	17.99	5.78	12.32	10.91	5.32	2.64	2.31	1.71
SOUTH	32.94	20.77	7.01	12.90	11.81	5.55	1.39	1.23	0.85

Table A.4: Estimates of the covariances (10^{-10}) between the predicted capacity factors and the inverse of the demand in the same region obtained from hourly MERRA2 climate data over the year 2018. ILR and SM denotes, respectively, the Inverter Loading Ratio and Solar Multiple. ILR1 or SM1: without storage; ILR>1 or SM>1: with increasing levels of storage from Photovoltaic (PV) or Concentrated Solar Power (CSP).

Zones	ILR1/ Wind	ILR1/ SM1	ILR1/ SM^{ref}	ILR1/ SM2	ILR1/ SM3	ILR1/ SM4	Wind/ SM1	Wind/ SM^{ref}	Wind/ SM2	Wind/ SM3	Wind/ SM4
NORTH	0.11	0.95	0.75	0.72	0.50	0.30	0.04	0.04	0.03	-0.07	-0.22
CENTER	0.33	0.97	0.75	0.71	0.47	0.24	0.30	0.39	0.38	0.23	-0.02
EAST	0.33	0.97	0.76	0.72	0.49	0.25	0.28	0.27	0.26	0.12	-0.07
SOUTH	0.17	0.95	0.73	0.69	0.45	0.18	0.21	0.22	0.23	0.24	0.27

Zones	ILR2/ Wind	ILR3/ Wind	ILR4/ Wind	ILR2/ SM1	ILR3/ SM1	ILR4/ SM1	ILR2/ SM^{ref}	ILR3/ SM^{ref}	ILR4/ SM^{ref}
NORTH	0.14	0.08	-0.01	0.78	0.54	0.35	0.914	0.73	0.48
CENTER	0.42	0.34	0.21	0.81	0.55	0.339	0.92	0.78	0.479
EAST	0.35	0.24	0.13	0.80	0.547	0.337	0.93	0.77	0.472
SOUTH	0.16	0.14	0.06	0.79	0.543	0.329	0.910	0.75	0.459

Zones	ILR2/ SM2	ILR3/ SM2	ILR4/ SM2	ILR2/ SM3	ILR3/ SM3	ILR4/ SM3	ILR2/ SM4	ILR3/ SM4	ILR4/ SM4
NORTH	0.891	0.775	0.505	0.630	0.780	0.732	0.380	0.488	0.671
CENTER	0.902	0.820	0.506	0.612	0.783	0.741	0.302	0.374	0.523
EAST	0.909	0.810	0.498	0.627	0.791	0.739	0.325	0.406	0.576
SOUTH	0.883	0.787	0.483	0.580	0.805	0.640	0.238	0.296	0.371

Table A.5: Estimates of the correlations between the predicted capacity factors and the inverse of the demand in the same region obtained from hourly MERRA2 climate data over the year 2018. ILR and SM denotes, respectively, the Inverter Loading Ratio and Solar Multiple. ILR1 or SM1: without storage; ILR>1 or SM>1: with increasing levels of storage from Photovoltaic (PV) or Concentrated Solar Power (CSP).

In general, the measured or simulated wind speed and wind production, by other studies, is given only in the regions where wind turbines are installed in Morocco. With our regional wind speed simulations (not shown here), we found a maximum in the SOUTH, followed by the EAST. El Khchine et al. shows the monthly variation of wind speed at height 50 m and height 100m [303, Figures 1 and 2] for two Moroccan cities, one in the SOUTH (Dakhla) and one in the EAST (Taza). The figures show a different seasonality depending on the region. In the South, the wind speed increases in summer; while in the EAST, the wind speed increases in winter and decreases in summer. This is consistent with [380,

Figure I.17] for the wind production. This, indeed, corresponds to what we discussed in section 1 and section 2 (Chapter 3) and section 1 (Chapter 4): in scenarios with maximum penetration, wind is installed in EAST while when the variance—and thus the seasonal correlation of wind production with the summer peak—starts to play a role in scenarios with high penetrations—but less than the maximum—or low penetration scenarios, wind capacities are installed in SOUTH.

Unfortunately, we do not have hourly data for several years, or at least for shorter time scales than a year, at our disposition to validate the CF estimations against observations. However, the simulation results show relatively good consistency with the results obtained in the literature.

ii PV Capacity Factors Profiles

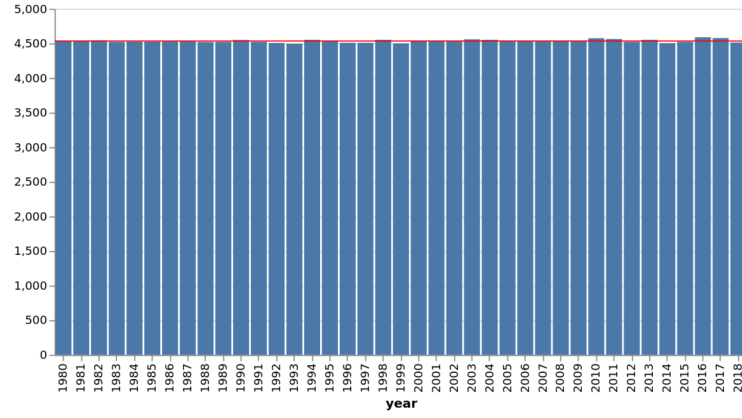
The obtained patterns of the Global Horizontal Irradiance (GHI) (Figure 3.3a, Chapter 3), the Global Tilted Irradiance (GTI) (Figure 3.3b, Chapter 3), and the PV Capacity Factors (CFs) (Figure 3.3d, Chapter 3) are in line with the discussion done in section i (Chapter 1) where the GHI increases in summer while the GTI has two maxima in the vernal and autumnal equinoxes and two minima in the summer and winter solstices, which explains the PV CFs profile; due to the incidence angle that increases—at noon and during sunrise and sunset—in summer more than in winter.

These patterns in the monthly variation of GHI or GTI or PV power output are also found by several sources for Morocco such as the Global Solar Atlas [16]; the simulations of monthly electrical production done by Bousselamti et al. [107, Figure 3 (a)] for PV plants with 70 MW installed in Ouarzazate city and found that its simulations are close to the ones obtained by the System Advisor Model (SAM) simulations; Solar Atlas of MASEN [31] that compute the GTI and the PV output and the performance ratio for a given area in Morocco; Boughamrane et al. [102, Figures 3, 5, 8, 9 and 10] that compare the measures of PV alternating (AC) energy, PV CF and PV efficiency to simulations of PVsyst software in Assa (in the south of Morocco); Attari et al. [69, Figures 2 and 4] that compute the GTI (tilt = 32°), PV production and PV CF; Haibaoui et al. [240, Figures 6 and 8] that compare the monthly AC electricity generation of two PV technologies, monocrystalline vs polycrystalline silicon, in Mohammedia and Casablanca cities; Merrouni et al. [349, Figures 8 and 9] that compute the monthly PV production and PV module efficiency in eastern Morocco; and Nfaoui et al. [381, Figures 7 and 11] that compute the monthly direct, diffuse and global irradiance on horizontal plane in Khouribga city.

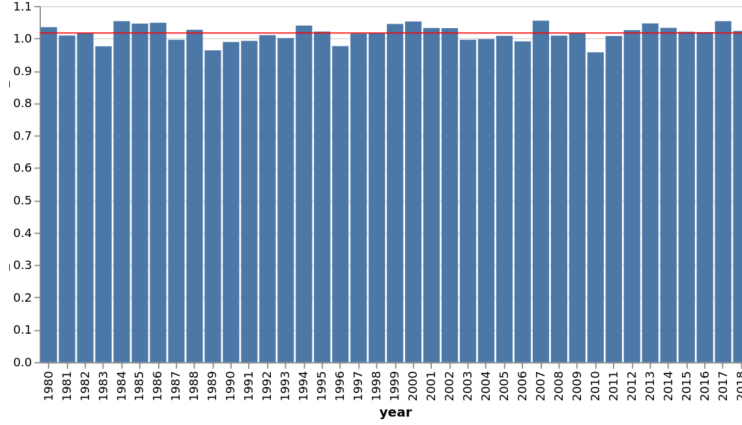
We also verified these patterns by running online simulations in Renewables.ninja software [29]; PVGIS software [20]; PVEducation tool [34] and the Solar Position and Intensity (SOLPOS) calculator of the National Renewable Energy Laboratory (NREL) [32].

iii CSP Capacity Factors Profiles

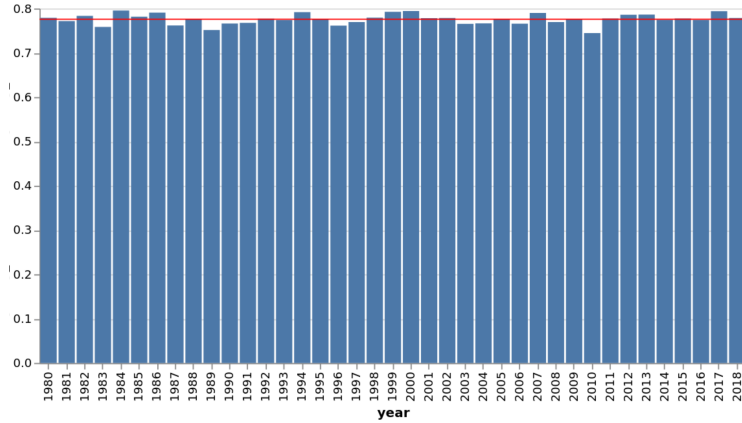
The obtained patterns of CSP CFs (Figure 3.3e, Chapter 3) are also in line with the discussion done in section i (Chapter 1) where the Direct Normal Irradiance (DNI) (Figure 3.3c, Chapter 3) tends to increase in summer, as North-South (N-S) tracking is performant in summer; which explains the CSP CFs profile.



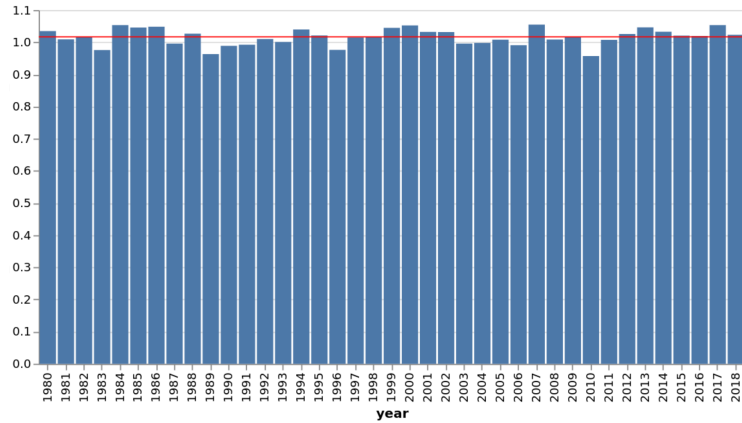
(a) Mean Demand (MW)



(b) Wind Mean Capacity Factors



(c) PV without storage Mean Capacity Factors



(d) CSP without storage Mean Capacity Factors

Figure A.6: Interannual variability of mean-variance optimization inputs over the whole period (1980 – 2019) available from the Modern-Era Retrospective Analysis for Research and Applications 2 (MERRA-2) reanalysis climate data. Photovoltaic (PV) and Concentrated Solar Power (CSP) Capacity Factors are without storage, i.e., PV Inverter Loading Ratio and CSP Solar Multiple of 1.

IX Rental Cost Modeling

This section summarizes the parameters needed in section 1 (Chapter 2).

The coefficient α_j in equation (2.15) is **the yearly-mean CF in (h) of the technology j** . It illustrates the yearly-mean production duration or the amount of time (h) on average that the technology j can produce energy at nominal power of the plant over one year to install ω_k with $k = (i, j)$ (A.74):

$$\alpha_j = \frac{\eta_{(i,j)} \omega_{(i,j)}}{P_{elec,nom,j}^{ref}} = \overline{\eta_{(i,j)}}, \quad (\text{A.74})$$

where: $P_{elec,nom,j}^{ref} = \begin{cases} P_{PB,elec,nom,j}^{ref}, & \text{if } j = \text{CSP} \\ P_{INV,AC,nom,j}^{ref} = P_{INV,DC,nom,j}^{ref} * \eta_{INV,nom}^{ref} = P_{SP,DC,nom,j}^{ref} * \eta_{INV,nom}^{ref} & \text{if } j = \text{PV} \end{cases}$

Similarly to α_j , the coefficients $\alpha'_{j'}$, $\beta'_{j'}$ and $\gamma'_{j'}$ in equation (2.16) illustrate **the yearly-mean storage duration**. They are obtained by determining, respectively, how much energy storage capacity, storage power of charging/discharging and total energy discharged are needed on average to charge/discharge energy at nominal power of the plant over one year to install ω_k with $k = (i, j, j')$:

$$\begin{cases} \alpha_{j'} = \frac{\text{store-capacity}_{j'}^{SM/ILR}}{P_{elec,nom,j}^{ref}} \\ \beta_{j'} = \frac{\text{store-power}_{j'}^{SM/ILR}}{P_{elec,nom,j}^{ref}} \\ \gamma_{j'} = (n\alpha)_{j'} = \frac{\sum E_{discharged}_{j'}^{SM/ILR}}{P_{elec,nom,j}^{ref}} \end{cases}$$

$\gamma_{j'}$ corresponds to the autonomy or the discharge duration. Indeed, all storage systems degrade with use because they are subject to fatigue (during each charge-discharge cycle) and thus must be replaced during the lifetime of the storage system. The cost for that replacement must be taken into account in the variable operating cost of the storage system ($VOM'_{j'}$). However, real cycling processes are often complex and not well defined. A common simplification consists in assuming fixed number of full equivalent cycles equal to one per day (thus 365 per year) over the lifetime of j' (one cycle corresponds to one charge and one discharge). **The number of equivalent full cycles per year** (A.75) and **the Average Discharging Depth** (A.76) are calculated as follows [432]:

$$n_{j'} = 365 * ADD_{j'}^{SM/ILR}, \quad (\text{A.75})$$

$$ADD_{j'-SM/ILR} = \frac{\sum E_{discharged}_{j'}^{SM/ILR}}{365 * \text{store-capacity}_{j'}^{SM/ILR}}. \quad (\text{A.76})$$

All the storage parameters are given in table 2.3 (Chapter 2).

X Optimization Post-Processing Formulas

Here, we derive a few analytical formulas to help understand the behavior of the optimization program.

i At Maximum Penetration

We first consider the case when the penetration is maximized. For that purpose, we leave out the variance term from the cost function. The Lagrangian corresponding to this single-objective maximization problem is given by the expression (A.77):

$$\mathcal{L}(\omega, \lambda, \delta) = \sum_{\mathbf{k}} \mathbb{E} \left[\frac{\eta_{\mathbf{k}}}{\sum_i D_i} \right] \omega_{\mathbf{k}} - \lambda \left(\sum_{\mathbf{k}} c_{\mathbf{k}} \omega_{\mathbf{k}} - C_{\text{tot}} \right) + \sum_{\mathbf{k}} \delta_{\mathbf{k}} \omega_{\mathbf{k}}, \quad (\text{A.77})$$

where non-negative coefficient λ is the Karush-Kuhn-Tucker (KKT) multiplier associated with the maximum-cost constraint and δ is the vector of non-negative KKT multipliers associated with the positive-capacities constraint.

The first-order condition (A.78) is:

$$\mathbb{E} \left[\frac{\eta_{\mathbf{k}}}{\sum_i D_i} \right] + \delta_{\mathbf{k}} = \lambda c_{\mathbf{k}} \quad \text{for all } \mathbf{k}, \quad (\text{A.78})$$

and the slackness conditions (A.79) and (A.80):

$$\delta_{\mathbf{k}} \omega_{\mathbf{k}} = 0 \quad (\text{A.79})$$

$$\lambda \left(\sum_{\mathbf{k}} c_{\mathbf{k}} \omega_{\mathbf{k}} - C_{\text{tot}} \right) = 0. \quad (\text{A.80})$$

Due to the first-order condition and dual feasibility, the case with λ equal to 0 is impossible since this would imply the contradiction $\mathbb{E}[\eta_{\mathbf{k}} / \sum_i D_i] = -\delta_{\mathbf{k}} \leq 0$. Thus, λ is positive (i.e., the maximum-cost constraint is activated) and such that (A.81):

$$\lambda = \frac{\mathbb{E} \left[\frac{\eta_{\mathbf{k}}}{\sum_i D_i} \right] + \delta_{\mathbf{k}}}{c_{\mathbf{k}}} \quad \text{for all } \mathbf{k}, \quad (\text{A.81})$$

and $\sum_{\mathbf{k}} c_{\mathbf{k}} \omega_{\mathbf{k}} = C_{\text{tot}}$.

Let us define the index k_0, k_1, \dots , such that $\delta_{k_0}/c_{k_0} \leq \delta_{k_1}/c_{k_1} \leq \dots$. Then the capacities are ranked by decreasing maximum-penetration ratio, i.e., $\mathbb{E}[\eta_{k_0}/\sum_i D_i] \geq \mathbb{E}[\eta_{k_1}/\sum_i D_i] \geq \dots$.

If $\delta_{k_0} \geq 0$, then $\delta_k \geq 0$ for all k , all capacities are 0, the maximum-cost constraint is not active and so $\lambda = 0$, leading to a contradiction. Thus, $\delta_{k_0} = 0$ and $\lambda = \mathbb{E}[\eta_{k_0}/\sum_i D_i]/c_{k_0}$.

Finally, if $\delta_{k_1} = 0$, then one would exactly have (A.82):

$$\frac{\mathbb{E}\left[\frac{\eta_{k_0}}{\sum_i D_i}\right]}{c_{k_0}} = \frac{\mathbb{E}\left[\frac{\eta_{k_1}}{\sum_i D_i}\right]}{c_{k_1}}, \quad (\text{A.82})$$

which, loosely, has a zero probability.

In conclusion, for all practical purposes, the mean penetration is maximized by installing all the capacity allowed by the maximum-cost constraint in the zone and technology with the highest maximum-penetration ratio (2.19), i.e., $\omega_{k_0} = C_{\text{tot}}/c_{k_0}$ and $\omega_{k_1} = \omega_{k_2} = \dots = 0$.

ii At High Penetrations

We now start from the situation maximizing the mean penetration, as described in the previous section i and start to give some weight to the variance. To proceed, we scalarize the bi-objective problem by introducing a positive weight q . The Lagrangian of the scalarized maximization problem is given by (A.83):

$$\mathcal{L}(\omega, \lambda, \delta) = \sum_k \mathbb{E}\left[\frac{\eta_k}{\sum_i D_i}\right] \omega_k - q \sum_{k,l} \omega_k \text{Cov}\left[\frac{\eta_k}{\sum_i D_i}, \frac{\eta_l}{\sum_i D_i}\right] \omega_l - \lambda \left(\sum_k c_k \omega_k - C_{\text{tot}} \right) + \sum_k \delta_k \omega_k. \quad (\text{A.83})$$

The first-order condition becomes (A.84):

$$\mathbb{E}\left[\frac{\eta_k}{\sum_i D_i}\right] - 2q \sum_l \text{Cov}\left[\frac{\eta_k}{\sum_i D_i}, \frac{\eta_l}{\sum_i D_i}\right] \omega_l + \delta_k = \lambda c_k \quad \text{for all } k, \quad (\text{A.84})$$

and the slackness conditions are the same as in section i.

The solution to this problem for $q = 0$ is that of the previous section i. Increasing q from this situation, we thus assume that ω_{k_0} is positive, so that δ_{k_0} is 0. If all other capacities remain 0, and the covariance between k_0 and k is small, the total-capacity constraint remains active ($\lambda > 0$) as long as (A.85):

$$q < \frac{\mathbb{E}\left[\frac{\eta_{k_0}}{\sum_i D_i}\right]}{2V\left[\frac{\eta_{k_0}}{\sum_i D_i}\right]} := q_c. \quad (\text{A.85})$$

We now increase q from 0, while remaining in the interval $[0, q_c]$, so that $\lambda > 0$, and look for the largest value of q such that all capacities but that of k_0 remain 0. In this case, ω_{k_0} is still equal to C_{tot}/c_{k_0} . In other words, we impose that $\delta_k > 0$ for all k different from k_0 . The first-order condition (A.84) then implies (A.86):

$$\mathbb{E}\left[\frac{\eta_k}{\sum_i D_i}\right] - 2q \text{Cov}\left[\frac{\eta_k}{\sum_i D_i}, \frac{\eta_{k_0}}{\sum_i D_i}\right] \omega_{k_0} < \lambda c_k, \quad (\text{A.86})$$

which is equivalent to, with $\lambda = \mathbb{E}[\eta_{k_0}/\sum_i D_i] - 2qV[\eta_{k_0}/\sum_i D_i]\omega_{k_0}/c_{k_0}$, with (A.87):

$$q < \frac{c_{k_0}}{2C_{\text{tot}}} \frac{\frac{\mathbb{E}\left[\frac{\eta_{k_0}}{\sum_i D_i}\right]}{c_{k_0}} - \frac{\mathbb{E}\left[\frac{\eta_k}{\sum_i D_i}\right]}{c_k}}{\frac{V\left[\frac{\eta_{k_0}}{\sum_i D_i}\right]}{c_{k_0}} - \frac{\text{Cov}\left[\frac{\eta_k}{\sum_i D_i}, \frac{\eta_{k_0}}{\sum_i D_i}\right]}{c_k}}. \quad (\text{A.87})$$

Thus, the first capacity to be installed after k_0 is the one for which the right-hand side of this last expression is the smallest.

iii At Low Penetrations

We now turn to the case for which the variance is small. The extreme case of zero variance corresponds to the situation where all capacities are 0 because no weight is put on the mean penetration.

Let us consider the less trivial situation in which a weight $r > 0$ is put on the mean penetration. That is, we scalarize the mean-variance problem to yield a corresponding Lagrangian given by (A.88):

$$\mathcal{L}(\omega, \lambda, \delta) = r \sum_k \mathbb{E}\left[\frac{\eta_k}{\sum_i D_i}\right] \omega_k - \sum_{k,l} \omega_k \text{Cov}\left[\frac{\eta_k}{\sum_i D_i}, \frac{\eta_l}{\sum_i D_i}\right] \omega_l - \lambda \left(\sum_k c_k \omega_k - C_{\text{tot}} \right) + \sum_k \delta_k \omega_k. \quad (\text{A.88})$$

The first-order condition becomes (A.89):

$$r \mathbb{E}\left[\frac{\eta_k}{\sum_i D_i}\right] - 2 \sum_l \text{Cov}\left[\frac{\eta_k}{\sum_i D_i}, \frac{\eta_l}{\sum_i D_i}\right] \omega_l + \delta_k = \lambda c_k \quad \text{for all } k. \quad (\text{A.89})$$

Since $C_{\text{tot}} > 0$, there is an interval $[0, r_c]$, with $r_c > 0$, such that as long as r stays within this interval, the maximum-cost constraint is inactive, i.e., $c_k \omega_k < C_{\text{tot}}$ and $\lambda = 0$.

Let us consider that r is increased from 0 while remaining in $[0, r_c]$. If some cross-covariances are non-zero, it may be that some capacities are zero. If instead we assume that the covariance matrix is diagonal, i.e., that $\text{Cov}[\eta_{\mathbf{k}}/\sum_i D_i, \eta_{\mathbf{l}}/\sum_i D_i] = 0$ for all \mathbf{k}, \mathbf{l} such that $\mathbf{k} \neq \mathbf{l}$. The first-order condition (A.89) implies (A.90):

$$\omega_{\mathbf{k}} = \frac{r\mathbb{E}\left[\frac{\eta_{\mathbf{k}}}{\sum_i D_i}\right] + \delta_{\mathbf{k}}}{2\text{V}\left[\frac{\eta_{\mathbf{k}}}{\sum_i D_i}\right]} \quad \text{for all } \mathbf{k}. \quad (\text{A.90})$$

Thus, in this case, $\delta_{\mathbf{k}} > 0$ implies that $r = 0$.

As a conclusion, if the covariance matrix is diagonal and for r in $[0, r_c]$, either $r = 0$ and all capacities are 0, or $r > 0$ and all capacities are positive and such that (A.91):

$$\omega_{\mathbf{k}} = r \frac{\mathbb{E}\left[\frac{\eta_{\mathbf{k}}}{\sum_i D_i}\right]}{2\text{V}\left[\frac{\eta_{\mathbf{k}}}{\sum_i D_i}\right]} \quad \text{for all } \mathbf{k}. \quad (\text{A.91})$$

Table A.6: Characteristics of the onshore wind, Photovoltaic (PV) and Concentrated Solar Power (CSP) without or with Thermal Energy Storage (TES) operational plants in Morocco in 2018. PT: Parabolic Trough CSP. ST: Solar Tower CSP. h: expected hours of storage. We ignore the production from auto-producers, except for wind plants since their installed capacity is included in the total wind capacity. Data from: MEME [23], RES4MED [302], Energypedia [13], GEO [14], CSP FOCUS [10], SolarPACES [33] and MASEN [22]. The index k is a multi-index representing a pair $k = (i, j)$ or $k = (i, j, j')$ of region i and technology j or j, j' . $i = \{NORTH, CENTER, EAST, SOUTH\}$; $j = \{PV - ILR1, Wind, CSP - SM1\}$ and $j' = \{BES, TES\}$. ILR and SM denotes, respectively, the Inverter Loading Ratio and Solar Multiple. ILR1 or SM1: PV or CSP without storage.

Power Plant p Name	Techno j or j, j'	Region i	City	$\omega_{k,p}^{obs}$ (MW)	$Prod_{y,k,p}^{obs}$ (GWh/yr)	$\eta_{y,k,p}^{obs}$ (%)	Commissioning	Source
Abdelkhalek Torres/Koudia Al Baida	Wind	NORTH	Tetouan	50	200	45.7	2000	[23]
Abdelkhalek Torres/Koudia Al Baida	Wind	NORTH	Tetouan	3.5	12	39.1	2001	[13]
Lafarge	Wind	NORTH	Tetouan	32	12	4.20	2005	[302]
Tangier1 (Dhar Saadane; Bni Jmel)	Wind	NORTH	Tanger	140	510	41.6	2009	[23]
Haouma	Wind	NORTH	Ksar sghir	50.6	200	45.1	2014	[23]
Jbel Sendouk/Khalladi	Wind	NORTH	Ksar sghir	120	378	36.0	2018	[23]
Amougdoul	Wind	CENTER	Essaouira	60	210	40.0	2007	[23, 302, 14]
CIMAR	Wind	SOUTH	Laayoune	5	16	36.5	2011	[302]
Aftissat	Wind	SOUTH	Boujdour	200	1000	57.1	2018	[23]
Akhfennir1	Wind	SOUTH	Laayoune	102	378	42.4	2014	[23]
Akhfennir2	Wind	SOUTH	Laayoune	102	378	42.4	2017	[23]
Foum El Oued	Wind	SOUTH	Laayoune	50.6	200	45.1	2014	[23]
Tarfaya	Wind	SOUTH	Tarfaya	300	1084	41.2	2014	[23]
Noor 4	PV	CENTER	Ouarzazate	70	120	19.6	2018	[23]
Noor Laayoune1	PV	SOUTH	Laayoune	80	150	21.4	2018	[23]
Noor Boujdour1	PV	SOUTH	Boujdour	20	40	22.8	2018	[23]
Noor 1	CSP (PT, 3 h)	CENTER	Ouarzazate	160	520	37.1	2016	[22, 10, 33]
Noor 2	CSP (PT, 7 h)	CENTER	Ouarzazate	200	699	39.9	2018	[22, 10, 33]
Noor 3	CSP (ST, 7 h)	CENTER	Ouarzazate	150	515	39.2	2018	[22, 10, 33]
Ain Beni Mathar	CSP (PT, 0 h) *	EAST	Jerrada	20	55	31.4	2011	[10, 33]

*The integrated solar combined-cycle power plan Ain Beni Mathar is composed of a 450 MW combined cycle and a 20 MW solar PT system [5]. We consider only the solar part here.

Publication Overview

I Oral Communications (Seminars/ Conferences)

- PhD Students' Day - Scenarios of Energy Transition in Morocco in the Context of Climate Change; **2019**, Ecole Polytechnique, Palaiseau, France.
- Highlight Intro Team - Oral Presentation of the Work of "Renewables" Team; **2020**, Online.
- INTRO Seminar - Sensitivity of the Moroccan Portfolio to Solar Technologies: Impact of Cost and Storage, **2020**, Online.
- Webinar on Renewable Energy and Resources | Longdom cited as:
Ayat-allah Bouramdane; Adequacy of Renewable Energy Mixes with Concentrated Solar Power and Photovoltaic in Morocco: Impact of Thermal Storage and Cost; Renewable Energy 2020; October 26, **2020**; London, UK (Online).
- International E-Conference on Geological and Environmental Sustainability -
Towards a Large-Scale Integration of Designed Concentrated Solar Power and Utility-Scale Photovoltaics in Morocco: Impact of Cost and Storage; **2020**; London, UK (Online).
Available at <https://www.youtube.com/watch?v=ZnHQoYwFvSA&t=1169s>.
- International E-Conference on Renewable Energy and Resources -
Sensitivity of the Moroccan Mix to the Integration of Thermal and Battery Storage Combined with Concentrated Solar Power and Photovoltaic: Impact of Storage and Cost; **2021**; London, UK (Online).
Available at <https://www.youtube.com/watch?v=FjgkHbGVP44&t=15637s>
- EGU General Assembly 2021– Session «Spatial and Temporal Modelling of Renewable Energy Systems» cited as:
Bouramdane, A. Sensitivity of the Moroccan Mix to the Integration of Thermal and Battery Storage Combined with Concentrated

Solar Power and Photovoltaics: Design, Dispatch and Optimal Mix Analysis, EGU General Assembly 2021, online, EGU21-8755, <https://doi.org/10.5194/egusphere-egu21-8755>, **2021**, Vienna, Austria (Online).

- International Meet on Nanotechnology (NANOMEET2021) - Utility-Scale PV-Battery versus CSP-Thermal Storage in Morocco: Storage, Cost and Climate Change Effect under Penetration Scenarios.; **2021**; Porto, Portugal (Online).

II Poster Presentations

- Scientific Conference on Climate Change and Energy Transition in the Mediterranean - An Optimal Recommissioning Study of the Actual (2018) Moroccan Solar-Wind Mix; **2019**, Ecole Polytechnique, Palaiseau, France.
- 6th Edition of the Scientific Days on Climate and Impacts 2020: Adequacy of Renewable Energy Mixes with Concentrated Solar Power and Photovoltaic in Morocco: Impact of Thermal Storage and Cost; **2020**, Campus of Paris-Saclay University, Ecole CentraleSupélec, Orsay (Online).
Available at <https://premc.org/climat-impacts-2020/posters/>.

III Publications in Peer-Reviewed Journal as Main Author

- Bouramdane, A.-A.; Tantet, A.; Drobinski, P. Adequacy of Renewable Energy Mixes with Concentrated Solar Power and Photovoltaic in Morocco: Impact of Thermal Storage and Cost. *Energies* **2020**, 13, 5087 (*accepted for publication*) [105].
- Bouramdane, A.-A.; Tantet, A.; Drobinski, P. Utility-Scale PV-Battery versus CSP-Thermal Storage in Morocco: Storage and Cost Effect under Penetration Scenarios. *Energies* **2021**, 14, 4675 (*accepted for publication*) [106].
- At the time of this writing, the last study of this thesis (Chapter 5)—RCP 8.5 Climate Change Versus Cost Effect on Optimal Scenario Mixes of Variable and Dispatchable Technologies in Morocco: Climate Model Inter-Comparison—*has not been submitted/published*.

Bibliography

- [1] *According to Abdelkader Himdi, Director of Operations and Maintenance at MASEN and Sergio Relloso, Performance Guarantee Manager at SENER, EPC partner to all three Phases of the Ouarzazate Project.* <https://www.solarpaces.org/csp-puts-end-morocco-electricity-blackouts/>.
- [2] *Advanced CSP Teaching Materials Chapter 5 Parabolic Trough Technology.* Available online <https://fddocuments.in/document/chapter-5-parabolic-trough-technology.html> (accessed on June 21st 2021).
- [3] *Advanced CSP Teaching Materials Chapter 9 Thermal Energy Storage.* Available online <https://dokumen.tips/documents/chapter-9-thermal-energy-storage-energy-09advanced-csp-teaching-materials.html> (accessed on June 21st 2021).
- [4] *After a Meeting with the Responsible of the National Planning and Dispatching Department of the National Office of Electricity (ONE) in Casablanca (Morocco).*
- [5] *Ain Beni Mathar: Une Centrale Électrique Thermo Solaire Unique au Maroc.* <https://www.afdb.org/fr/projects-and-operations/selected-projects>.
- [6] *Alternative Energy from Solar, Wind, Biomass, Fuel Cells and More: PV with Batteries: A Threat to CSP?* <https://www.altenergymag.com/article/2014/09/pv-with-batteries-a-threat-to-csp/1500>.
- [7] *CAT (Climate Action Tracker).* <https://climateactiontracker.org>.
- [8] *Climate Vulnerable Forum (2016) Climate Vulnerable Forum Commit to Stronger Climate Action at COP22.* Available online https://unfccc.int/files/meetings/marrakech_nov_2016/application/pdf/cvf_declaration_release_en.pdf (accessed on June 21st 2021).
- [9] *Connecting Countries to Climate Technology Solutions.* <https://www.ctc-n.org/content/morocco-2014>.
- [10] *CSP Focus.* <http://www.cspfocus.cn/en/>.
- [11] *CSP Today (2008), An Overview of CSP in Europe, North Africa and the Middle East, CSP Today, London.*
- [12] *Energy Storage is Key For the Future of the Concentrated Solar Power Market (Power Technology; Last Updated May 9th, 2019).* <https://www.power-technology.com/comment/csp-energy-storage/>.
- [13] *Energypedia.* https://energypedia.info/wiki/Wind_Energy_Country_Analyses_Morocco.
- [14] *Global Energy Observatory (GEO).* <http://globalenergyobservatory.org/>.
- [15] *Global Mean Wind Speed.* <https://dupontconsulting.wordpress.com/tag/wind-power/>.
- [16] *Global Solar Atlas.* <https://globalsolaratlas.info/global-pv-potential-study>.
- [17] *Going Solar Chapter 8 : Know Your Solar PV Cells and Panels – Green Sarawak.* <https://www.going-solar.com/going-solar-chapter-8-know-your-solar-pv-cells-and-panels/>.
- [18] *Green Energy Park (GEP).* <http://www.greenenergypark.ma/>.
- [19] *Introduction to Electricity Markets - Lesson 3: Economics of Power Generation, Transmission and Distribution.* <https://www.e-education.psu.edu/ebf483/node/517>.
- [20] *JRC Photovoltaic Geographical Information System (PVGIS) Software.* https://re.jrc.ec.europa.eu/pvg_tools/fr/#PVP.
- [21] *MEDIA24 | Environnement. Energies renouvelables : 3.685 MW de Puissance Installée à fin 2019.* <https://www.medias24.com/energies-renouvelables-3-685-mw-de-puissance-installee-a-fin-2019-6619.html>.
- [22] *Middle East and North Africa Concentrating Solar Power Knowledge and Innovation Program (MENA CSP KIP).* Available online http://cmimarseille.org/menacskip/wp-content/uploads/2017/08/Youssef_Stitou_MENA_CSP_KIP_Jordan_Workshop_25_July_2017.pdf (accessed on June 21st 2021).
- [23] *Ministère de l'Energie, des Mines et de l'Environnement (MEME).* <https://www.mem.gov.ma/pages/index.aspx>.
- [24] *Moroccan Administrative Regions.* https://en.wikipedia.org/wiki/Regions_of_Morocco.
- [25] *Moroccan Agency for Sustainable Energy (MASEN).* <http://www.masen.ma/fr/projets>.
- [26] *Morocco's Nationally Determined Contribution Under the UNFCCC.* Available online <https://www4.unfccc.int/sites/ndcstaging/PublishedDocuments/Morocco%20First/Morocco%20First%20NDC-English.pdf> (accessed on June 21st 2021).

- [27] Office National de l'Electricité et de l'Eau Potable (ONEE). <http://www.one.org.ma/>.
- [28] PowerFilm Solar - Thin Film. <https://www.powerfilmsolar.com/technology/thin-film/>.
- [29] Renewables.ninja Software. <https://www.renewables.ninja/>.
- [30] SOAS | Climate Change and Development. https://www.soas.ac.uk/cedep-demos/000_P524_CCD_K3736-Demo/module/topindex.htm.
- [31] Solar Atlas of MASEN. <https://solaratlas.masen.ma/lta?c=31.615966;-8.02002:5&s=31.625815;-7.989137>.
- [32] Solar Position and Intensity (SOLPOS) calculator. National Renewable Energy Laboratory (NREL). <https://midcdmz.nrel.gov/solpos/solpos.html>.
- [33] Solar Power And Chemical Energy Systems (SolarPACES). <https://solarpaces.nrel.gov/>.
- [34] Solar Radiation on a Tilted Surface | PVEducation. <https://www.pveducation.org/pvcdrom/properties-of-sunlight/solar-radiation-on-a-tilted-surface>.
- [35] Statistics Portal for Market Data, Market Research and Market Studies (Statista). <https://www.statista.com/>.
- [36] The Engineering ToolBox. https://www.engineeringtoolbox.com/surface-solar-radiation-d_1213.html.
- [37] Top Concentrated Solar Power Producing Countries (NS Energy; Last Updated Apr 26, 2019). <https://www.nsenerybusiness.com/features/concentrated-solar-power-countries/>.
- [38] US Department of Energy. Energy Efficiency and Renewable Energy. The History of Solar. https://www1.eere.energy.gov/solar/pdfs/solar_timeline.pdf.
- [39] World Nuclear Association. How can nuclear combat climate change? <https://www.world-nuclear.org/nuclear-essentials/how-can-nuclear-combat-climate-change.aspx>.
- [40] Yoshiaki Shibata. How can "Solar PV + Battery System" Be Economically Competitive Reliable Power Generation? -Strategies for Post- FIT. IEEEJ: July 2017.
- [41] Wind Energy: Technology and Economics. 12 1993.
- [42] Global hydrogen review 2021. 2021.
- [43] Siham Acharki. *Apports de la Modélisation et de la Télédétection dans l'Étude de l'Impact des Changements Climatiques sur les Ressources en Eau : Application aux Périmètres Irrigués du Loukkos et du Gharb (Maroc)*. PhD thesis, PhD Thesis, Université Abdelmalek Essaâdi : UAE, 2020. Available online <https://hal.archives-ouvertes.fr/tel-03029192/document> (accessed on June 21st 2021).
- [44] Alemayehu Addisu, L. George, P. Courbin, and V. Sciandra. Smoothing of renewable energy generation using Gaussian-based method with power constraints. *Energy Procedia*, 134:171–180, 2017.
- [45] S. Afxentis, N. Chatzigeorgiou, V. Efthymiou, I. Papageorgiou, A. Armenakis, G. Papagiannis, G. Christoforidis, J. Sancho, H. Rodrigues, C. Casimiro, N. Poize, T. Pristovnik, S. Mocci, A. Rubiu, and G. Georgiou. Technical Assessment of Coupled PV and Battery Systems - A Case Study from the Mediterranean Region. *2019 1st International Conference on Energy Transition in the Mediterranean Area (SyNERGY MED)*, pages 1–6, 2019.
- [46] A. Akhil, G. Huff, Aileen B. Currier, Jacquelynne Hernández, D. Bender, Benjamin C. Kaun, Dan Rastler, S. Chen, Andrew L. Cotter, D. Bradshaw, William D. Gauntlett, J. M. Eyer, Todd Olinsky-Paul, Michelle Ellison, and S. Schoenung. DOE/EPRI Electricity Storage Handbook in Collaboration with NRECA. 2016.
- [47] Mohammed H. Albadi. Solar PV Power Intermittency and its Impacts on Power Systems? An Overview. *The Journal of Engineering Research*, 16:142–150, 2019.
- [48] Ahmad Alferidi. Detailed Reliability Models of Integrated Solar Power Technologies in Electric Power Systems. 2018.
- [49] A Alhamwi. Optimal Mix Analyses of Renewable Power Generation in the MENA Region: A Case Study For Morocco. Master's thesis, KASSEL University: Germany, CAIRO university GIZA, Egypt, 2013. Available online https://www.uni-kassel.de/eecs/fileadmin/datas/fb16/remena/theses/batch3/MasterThesis_Alaa_Alhamwi.pdf (accessed on June 21st 2021).
- [50] Alaa Alhamwi, David Kleinhans, Stefan Weitemeyer, and Thomas Vogt. Optimal Mix of Renewable Power Generation in the MENA region as a Basis for an Efficient Electricity Supply to Europe. *EPJ Web of Conferences*, 79:03004, 01 2014.
- [51] Alaa Alhamwi, David Kleinhans, Stefan Weitemeyer, and Thomas Vogt. Moroccan National Energy Strategy Reviewed from a Meteorological Perspective. *Energy Strategy Reviews*, 6:39–47, 03 2015.
- [52] G. Allan, Igor Eromenko, P. McGregor, and J. Swales. The Regional Electricity Generation Mix in Scotland: A Portfolio Selection Approach. 2010.
- [53] R. Allan and B. Soden. Large Discrepancy Between Observed and Simulated Precipitation Trends in the Ascending and Descending Branches of the Tropical Circulation. *Geophysical Research Letters*, 34, 2007.
- [54] R. J. Allen, J. Norris, and M. Wild. Evaluation of Multidecadal Variability in CMIP5 Surface Solar Radiation and Inferred Underestimation of Aerosol Direct Effects Over Europe, China, Japan, and India. *Journal of Geophysical Research*, 118:6311–6336, 2013.
- [55] CSP Alliance. *The Economic and Reliability Benefits of CSP with Thermal Energy Storage: Literature Review and Research Needs*. Report, CSP Alliance, 2014. Available online http://www.inship.eu/docs/TES%20the_economic_and_reliability_benefits_of_csp_with_thermal_storage_2014_09_09_final.pdf (accessed on June 21st 2021).
- [56] A. Aly, A. Bernardos, Carlos M. Fernández-Peruchena, S. S. Jensen, and A. Pedersen. Is Concentrated Solar Power (CSP) a Feasible Option for Sub-Saharan Africa?: Investigating the Techno-Economic Feasibility of CSP in Tanzania. *Renewable Energy*, 135:1224–1240, 2019.

- [57] T. Ambrizzi, M. Reboita, R. P. da Rocha, and M. Llopart. The State of the Art and Fundamental Aspects of Regional Climate Modeling in South America. *Annals of the New York Academy of Sciences*, 1436, 2019.
- [58] Tayeb Amegroud. Morocco's Power Sector Transition: Achievements and Potential. 2015.
- [59] Moises Angeles, J. González, D. Erickson, and J. L. Hernández. The Impact of Climate Changes in the Renewable Energy Resources in the Caribbean Region. *Solar Energy*, pages 467–481, 2006.
- [60] Sophia Antipolis. *Climate Change and Energy in the Mediterranean*. European Investment Bank, 2008. Available online https://www.eib.org/attachments/country/climate_change_energy_mediterranean_en.pdf (accessed on June 21st 2021).
- [61] Mohamed Aoubouazza, Rachid Rajel, and Rachid Essafi. Impact of Extreme Climate Events on Water Resources and Agriculture and Biodiversity in Morocco. *Journal of Climatology and Weather Forecasting*, 1:1–9, 2013.
- [62] R. Arce, R. Mahía, Eva Medina, and G. Escribano. A Simulation of the Economic Impact of Renewable Energy Development in Morocco. *Energy Policy*, 46:335–345, 2012.
- [63] D.J. Arent, R.S.J Tol, E. Faust, J.P. Hella, S. Kumar, K.M. Strzepek, F.L. Tóth, and Yan D. *Key Economics Sectors and Services*. Clim. Chang. 2014 Impacts, Adapt. Vulnerability. Part A Glob. Sect. Asp. Contrib. Work. Gr. II to Fifth Assess. Rep. Intergov. Panel Clim. Chang. Chang., Cambridge, NY: Cambridge University Press, 2014. Available online https://www.ipcc.ch/site/assets/uploads/2018/02/WGIIAR5-Chap10_FINAL.pdf (accessed on June 21st 2021).
- [64] S. Armstrong and W. G. Hurley. A New Methodology to Optimise Solar Energy Extraction Under Cloudy Conditions. *Renewable Energy*, 35:780–787, 2010.
- [65] M. Arnesano, A. Carlucci, and D. Laforgia. Extension of Portfolio Theory Application to Energy Planning Problem – The Italian Case. *Energy*, 39:112–124, 2012.
- [66] R. M. Arroyo and L. J. Miguel. The Role of Renewable Energies for the Sustainable Energy Governance and Environmental Policies for the Mitigation of Climate Change in Ecuador. *Energies*, 13:3883, 2020.
- [67] M. Ashari and C. Nayar. An Optimum Dispatch Strategy Using Set Points For a Photovoltaic (PV)–Diesel–Battery Hybrid Power System. *Solar Energy*, 66:1–9, 1999.
- [68] L I M Asri, Wan Nur Suryani Firuz Wan Ariffin, Aini Syuhada Aini Md Zain, J Nordin, and N S Saad. Comparative study of energy storage systems (esss). *Journal of Physics: Conference Series*, 1962, 2021.
- [69] Kamal Attari, Ali Elyakoubi, and Adel Asselman. Performance analysis and investigation of a grid-connected photovoltaic installation in morocco. *Energy Reports*, 2:261–266, 2016.
- [70] M. Auffhammer. Quantifying Economic Damages from Climate Change. *Journal of Economic Perspectives*, 32:33–52, 2018.
- [71] S. Awerbuch. Investing in Photovoltaics: Risk, Accounting and the Value of New Technology. *Energy Policy*, 28:1023–1035, 2000.
- [72] S. Awerbuch and S. Yang. Efficient Electricity Generating Portfolios For Europe: Maximising Energy Security and Climate Change Mitigation. 2007.
- [73] B. Ayugi, G. Tan, Gnim Tchelim Gnitou, M. Ojara, and Victor Ongoma. Historical Evaluations and Simulations of Precipitation Over East Africa from Rossby Centre Regional Climate Model. *Atmospheric Research*, 232:104705, 2020.
- [74] Alae Azouzoute, Ahmed Alami Merrouni, and Samir Touili. Overview of the Integration of CSP as An Alternative Energy Source in the MENA Region. *Energy Strategy Reviews*, 29:100493, 2020.
- [75] World Bank. *Concentrating Solar Power: Clear Power On Demand 24/7*. World Bank, Washington, DC, 2021. Available online <https://pubdocs.worldbank.org/en/849341611761898393/WorldBank-CSP-Report-Concentrating-Solar-Power-Clean-Power-on-Demand-24-7-FINAL.pdf> (accessed on December 10th 2021).
- [76] F. Bañuelos-Ruedas, C. Angeles-Camacho, and S. Rios-Marcuello. Methodologies Used in the Extrapolation of Wind Speed Data at Different Heights and Its Impact in the Wind Energy Resource Assessment in a Region. 2011.
- [77] I. Barstad, A. Sorteberg, and M. D. Mesquita. Present and Future Offshore Wind Power Potential in Northern Europe based on Down-scaled Global climate Runs with Adjusted SST and Sea Ice Cover. *Renewable Energy*, 44:398–405, 2012.
- [78] B. Bartók. Changes in Solar Energy Availability For South-Eastern Europe with Respect to Global Warming. *Physics and Chemistry of The Earth*, 35:63–69, 2010.
- [79] B. Bartók, M. Wild, D. Folini, D. Lüthi, S. Kotlarski, C. Schär, R. Vautard, S. Jerez, and Z. Imecs. Projected Changes in Surface Solar Radiation in CMIP5 Global Climate Models and in EURO-CORDEX Regional Climate Models For Europe. *Climate Dynamics*, 49:2665–2683, 2016.
- [80] M. Bartos and M. Chester. Impacts of Climate Change on Electric Power Supply in the Western United States. *Nature Climate Change*, 5:748–752, 2015.
- [81] Benedikt Battke, T. Schmidt, David Grosspietsch, and V. H. Hoffmann. A Review and Probabilistic Model of Lifecycle Costs of Stationary Batteries in Multiple Applications. *Renewable & Sustainable Energy Reviews*, 25:240–250, 2013.
- [82] L. Baxter and Kevin Calandri. Global Warming and Electricity Demand: A Study of California. *Energy Policy*, 20:233–244, 1992.
- [83] S. D. Bazyomo, E. Lawin, O. Coulibaly, and A. Ouedraogo. Forecasted Changes in West Africa Photovoltaic Energy Output by 2045. *Climate*, 4:53, 2016.
- [84] Sarah Becker, Bethany A. Frew, G. Andresen, Timo Zeyer, S. Schramm, M. Greiner, and M. Jacobson. Features of a Fully Renewable US Electricity System: Optimized Mixes of Wind and Solar PV and Transmission Grid Extensions. *Energy*, 72:443–458, 2014.
- [85] Sarah Becker, Rolando A. Rodríguez, G. Andresen, S. Schramm, and M. Greiner. Transmission Grid Extensions During the Build-Up of a Fully Renewable Pan-European Electricity Supply. *Energy*, 64:404–418, 2014.

- [86] Henok Ayele Behabtu, Maarten Messagie, Thierry Coosemans, Maitane Berecibar, Kinde Anlay Fante, Abraham Alem Kebede, and Joeri Van Mierlo. A review of energy storage technologies' application potentials in renewable energy sources grid integration. *Sustainability*, 2020.
- [87] Omar Benzohra, Sidi Salah Ech-Charqaouy, F. Fraija, and D. Saifaoui. Optimal Renewable Resources Mix For Low Carbon Production Energy System in Morocco. *Energy Informatics*, 3:1–21, 2020.
- [88] A. Berger, G. Maracchi, and M. Teixeira. Milankovitch Effects on Long-Term Climatic Changes. 1991.
- [89] M. Bessec and Julien Fouquau. The Non-Linear Link Between Electricity Consumption and Temperature in Europe: A Threshold Panel Approach. *Energy Economics*, 30:2705–2721, 2008.
- [90] Juraj Betak, Marek Caltik, Tomas Cebecauer, Daniel Chrkavy, Branislav Erdelyi, Konstantin Rosina, Marcel Suri, and Nada. Suriova. *Global Photovoltaic Power Potential By Country*. Energy Sector Management Assistance Program (ESMAP): World Bank Group, Washington, D.C., 2020. Available online <http://documents1.worldbank.org/curated/en/466331592817725242/pdf/Global-Photovoltaic-Power-Potential-by-Country.pdf> (accessed on June 21st 2021).
- [91] H. Beyer, B. Decker, J. Luther, and R. Steinberger-Willms. Spatial and Temporal Characteristics of Short Term Fluctuations in Solar Radiation for PV-Plant Applications. 1991.
- [92] S. Bhartendu and S. J. Cohen. Impact of CO₂-Induced Climate Change on Residential Heating and Cooling Energy Requirements in Ontario, Canada. *Energy and Buildings*, 10:99–108, 1987.
- [93] A. Bhattacharya and S. Kojima. Power Sector Investment Risk and Renewable Energy: A Japanese Case Study Using Portfolio Risk Optimization Method. *Energy Policy*, 40:69–80, 2012.
- [94] A. Bichet, B. Hingray, G. Évin, A. Diedhiou, C. Kébé, and S. Anquetin. Potential Impact of Climate Change on Solar Resource in Africa for Photovoltaic Energy: Analyses From CORDEX-AFRICA Climate Experiments. *Environmental Research Letters*, 14:124039, 2019.
- [95] H. Bloomfield, D. Brayshaw, A. Troccoli, C. Goodess, M. D. Felice, L. Dubus, P. Bett, and Y. Saint-Drenan. Quantifying the Sensitivity of European Power Systems to Energy Scenarios and Climate Change Projections. *Renewable Energy*, 164:1062–1075, 2021.
- [96] D. Bogdanov and Christian Breyer. The Role of Solar Energy Towards 100% Renewable Power Supply for Israel: Integrating Solar PV, Wind Energy, CSP and Storages. 2015.
- [97] B. Bonin, A. Laureau, G. Krivtchik, Gilles Bordier, H. Safa, E. Merle, J. Miss, Y. Richet, and F. Bréon. Viability Limits of the Renewable Source in an Electricity Mix: The MIXOPTIM analysis methodology. *The European Physical Journal Plus*, 134:1–17, 2019.
- [98] B. Bonin, H. Safa, A. Laureau, E. Merle-Lucotte, J. Miss, and Y. Richet. MIXOPTIM: A Tool for the Evaluation and the Optimization of the Electricity Mix in a Territory. *The European Physical Journal Plus*, 129:1–15, 2014.
- [99] B. Bonin, H. Safa, F. Thais, A. Laureau, E. Merle-Lucotte, J. Miss, Danylo Matselyuk, Y. Richet, and F. Bréon. The Role of Power Sources in the European Electricity Mix. *EPJ Nuclear Sciences & Technologies*, 3:10, 2017.
- [100] B. Borowy and Z. Salameh. Methodology for Optimally Sizing the Combination of a Battery Bank and PV Array in a Wind/PV Hybrid System. *IEEE Transactions on Energy Conversion*, 11:367–375, 1996.
- [101] Arthur Bossavy, Tobias Bossmann, Laurent Fournié, Luc Humberset, and Paul Khallouf. Optimal Flexibility Portfolios for a High-RES 2050 Scenario. 2018. Available online <https://www.artelys.com/wp-content/uploads/2019/04/S1-Optimal-flexibility-portfolios-for-a-high-RES-2050-scenario.pdf> (accessed on June 21st 2021).
- [102] Lahbib Boughamrane, Mohamed Boulaid, Abdellah Tihane, A. Sdaq, Khalid Bouabid, and Ahmed Ihlal. Comparative analysis of measured and simulated performance of the moroccan first mv grid connected photovoltaic power plant of assa , southern morocco. 2016.
- [103] T. E. Boukelia and M. Mecibah. Parabolic trough solar thermal power plant: Potential, and projects development in Algeria. *Renewable & Sustainable Energy Reviews*, 21:288–297, 2013.
- [104] M. Boulakhbar, B. Lebrouhi, T. Kousksou, S. Smouh, A. Jamil, M. Maaroufi, and M. Zazi. Towards a Large-Scale Integration of Renewable Energies in Morocco. *Journal of Energy Storage*, 32:101806 – 101806, 2020.
- [105] A.A. Bouramdane, A. Tantet, and P. Drobinski. Adequacy of Renewable Energy Mixes with Concentrated Solar Power and Photovoltaic in Morocco: Impact of Thermal Storage and Cost. *Energies*, 13:5087, 2020.
- [106] A.A. Bouramdane, A. Tantet, and P. Drobinski. Utility-Scale PV-Battery versus CSP-Thermal Storage in Morocco: Storage, Cost and Climate Change Effect under Penetration Scenarios. *Energies*, 2021.
- [107] L. Bousselamti and M. Cherkaoui. Modelling and Assessing the Performance of Hybrid PV-CSP Plants in Morocco: A Parametric Study. *International Journal of Photoenergy*, 2019:1–15, 2019.
- [108] T. Bowen, Ilya Chernyakhovskiy, and P. Denholm. Grid-Scale Battery Storage: Frequently Asked Questions. 2019.
- [109] W. Braff, J. M. Mueller, and Jessika E. Trancik. Value of Storage Technologies For Wind and Solar Energy. *Nature Climate Change*, 6:964–969, 2016.
- [110] YA Brahim, MEM Saidi, K Kouraiss, A Sifeddine, and L Bouchaou. Analysis of Observed Climate Trends and High Resolution Scenarios For the 21st Century in Morocco. *J Mater Environ Sci* 8, 4:1375–1384, 2017.
- [111] B. Brand and K. Blok. Renewable Energy Perspectives For the North African Electricity Systems: A Comparative Analysis of Model-Based Scenario Studies. *Energy Strategy Reviews*, 6:1–11, 2015.
- [112] B. Brand and Jonas Zingerle. The Renewable Energy Targets of the Maghreb Countries: Impact on Electricity Supply and Conventional Power Markets. *Energy Policy*, 39:4411–4419, 2011.
- [113] Bernhard Brand, Amine Boudghene Stambouli, and Driss Zejli. The Value of Dispatchability of CSP plants in the Electricity Systems of Morocco and Algeria. *Energy Policy*, 47:321–331, 2012.

- [114] Paul B. Breslow and D. Sailor. Vulnerability of Wind Power Resources to Climate Change in the Continental United States. *Renewable Energy*, 27:585–598, 2002.
- [115] Patrick R. Brown and F. O’sullivan. Spatial and Temporal Variation in the Value of Solar Power Across United States Electricity Markets. *Renewable & Sustainable Energy Reviews*, 121:109594, 2020.
- [116] T. Brown, Tobias Bischof-Niemz, K. Blok, C. Breyer, H. Lund, and B. Mathiesen. Response to ‘Burden of proof’: A comprehensive Review of the Feasibility of 100% Renewable-Electricity Systems. *Renewable & Sustainable Energy Reviews*, 92:834–847, 2017.
- [117] L. Buitinck, Gilles Louppe, Mathieu Blondel, Fabian Pedregosa, A. Mueller, O. Grisel, Vlad Niculae, P. Prettenhofer, A. Gramfort, J. Grobler, R. Layton, J. Vanderplas, Arnaud Joly, B. Holt, and G. Varoquaux. API Design for Machine Learning Software: Experiences From the Scikit-Learn Project. *ArXiv*, abs/1309.0238, 2013.
- [118] D. Burnett, E. Barbour, and G. Harrison. The UK Solar Energy Resource and the Impact of Climate Change. *Renewable Energy*, 71:333–343, 2014.
- [119] A. Buttler, Felix Dinkel, S. Franz, and H. Spliethoff. Variability of Wind and Solar Power – An Assessment of the Current Situation in the European Union Based on the Year 2014. *Energy*, 106:147–161, 2016.
- [120] E. Byers, Jim W Hall, J. Amezcaga, G. O’Donnell, and Alex Leathard. Water and Climate Risks to Power Generation with Carbon Capture and Storage. *Environmental Research Letters*, 11:024011, 2016.
- [121] W. Cai, Simon Borlace, M. Lengaigne, P. V. Rensch, M. Collins, G. Vecchi, A. Timmermann, A. Santoso, M. McPhaden, Lixin Wu, M. England, Guojian Wang, E. Guilyardi, and F. Jin. Increasing Frequency of Extreme El Niño Events Due To Greenhouse Warming. *Nature Climate Change*, 4:111–116, 2014.
- [122] Johnston Peter Campbell, Jose Frazier Gomez, and Benoit Laplante. *Climate Risk and Adaptation in the Electric Power Sector*. Asian Development Bank, Manila, Phillippines, 2012. Available online <https://www.adb.org/sites/default/files/publication/29889/climate-risks-adaptation-power-sector.pdf> (accessed on June 21st 2021).
- [123] A. Carr and T. Pryor. A Comparison of the Performance of Different PV Module Types in Temperate Climates. *Solar Energy*, 76:285–294, 2004.
- [124] D. Carvalho, A. Rocha, M. Gómez-Gesteira, and C. S. Santos. Potential Impacts of Climate Change on European Wind Energy Resource Under the CMIP5 Future Climate Projections. *Renewable Energy*, 101:29–40, 2017.
- [125] Shankar Chandramowli and F. Felder. Impact of Climate Change on Electricity Systems and Markets – A Review of Models and Forecasts. *Sustainable Energy Technologies and Assessments*, 5:62–74, 2014.
- [126] D. Chattopadhyay, M. Bánkuti, M. Bazilian, F. D. de Sisternes, S. Oguah, and M. Sánchez. Capacity Planning Model with CSP and Battery. *2018 IEEE Power & Energy Society General Meeting (PESGM)*, pages 1–5, 2018.
- [127] L. Chen, S. Pryor, and D. Li. Assessing the Performance of Intergovernmental Panel on Climate Change AR5 climate models in Simulating and Projecting Wind Speeds Over China. *Journal of Geophysical Research*, 117, 2012.
- [128] M. Chentouf and M. Allouch. Analysis of Environmental Impacts of Renewable Energy on the Moroccan Electricity Sector: A System Dynamics Approach. 2018.
- [129] Mohammed Chentouf and Mohamed Allouch. Renewable and Alternative Energy Deployment in Morocco and Recent Developments in the National Electricity Sector. *Open Access Journal of Photoenergy*, 2, 01 2018.
- [130] H. Chepfer, H. Brogniez, and V. Noel. Diurnal Variations of Cloud and Relative Humidity Profiles Across the Tropics. *Scientific Reports*, 9, 2019.
- [131] M. Chester, M. Bartos, D. Eisenberg, B. Gorman, and N. Johnson. Impacts of Climate Change on Electric Transmission Capacity and Peak Electricity Load in the United States. 2015.
- [132] K. Chhatbar and Dr. Richard Meyer. The Influence of Meteorological Parameters on the Energy Yield of Solar Thermal Power Plants. 2011.
- [133] Bernadette Del Chiaro, Sarah Payne, and Tony Dutzik. Solar Thermal Power and the Fight Against Global Warming. 2008.
- [134] N. Christidis, G. Jones, and P. Stott. Dramatically Increasing Chance of Extremely Hot Summers Since the 2003 European Heatwave. *Nature Climate Change*, 5:46–50, 2015.
- [135] J. Císcar and P. Dowling. Integrated Assessment of Climate Impacts and Adaptation in the Energy Sector. *Energy Economics*, 46:531–538, 2014.
- [136] Seán Collins, P. Deane, B. O. Ó Gallachóir, S. Pfenninger, and I. Staffell. Impacts of Inter-annual Wind and Solar Variations on the European Power System. *Joule*, 2:2076 – 2090, 2018.
- [137] Energy Transitions Commission. *Reaching Net-Zero Carbon Emissions From Harder-To-Abate Sectors By Mid-Century*. The Energy Transitions Commission. Available online [https://www.ieta.org/resources/COP24/Misc%20Media%20Files/Dec7/SE16%20\(3\).pdf](https://www.ieta.org/resources/COP24/Misc%20Media%20Files/Dec7/SE16%20(3).pdf) (accessed on June 21st 2021).
- [138] L. Cradden, D. Burnett, A. Agarwal, and G. Harrison. Climate Change Impacts on Renewable Electricity Generation. 2015.
- [139] Anna Creti and Fulvio Fontini. *Economics of Electricity: Markets, Competition and Rules*. Cambridge University Press, 2019.
- [140] Jennifer Cronin, G. Anandarajah, and O. Dessens. Climate Change Impacts on the Energy System: A Review of Trends and Gaps. *Climatic Change*, 151:79 – 93, 2018.
- [141] J. Crook, Laura A. Jones, P. Forster, and R. Crook. Climate Change Impacts on Future Photovoltaic and Concentrated Solar Power Energy Output. *Energy and Environmental Science*, 4:3101–3109, 2011.
- [142] J. Cunha and Paula F. V. Ferreira. Designing Electricity Generation Portfolios Using the Mean-Variance Approach. *International Journal of Sustainable Energy Planning and Management*, 4:17–30, 2015.

- [143] H. Cutforth and D. Judiesch. Long-Term Changes to Incoming Solar Energy on the Canadian Prairie. *Agricultural and Forest Meteorology*, 145:167–175, 2007.
- [144] G. Czigis and G. Giebel. Realisable Scenarios For a Future Electricity Supply Based 100% on Renewable Energies. 2007.
- [145] Alima Dajuma, S. Yahaya, S. Touré, A. Diedhiou, R. Adamou, A. Konaré, Mariama Sido, and M. Golba. Sensitivity of Solar Photovoltaic Panel Efficiency to Weather and Dust over West Africa: Comparative Experimental Study between Niamey (Niger) and Abidjan (Côte d’Ivoire). 2016.
- [146] M. David, Faly H. Ramahatana Andriamasomanana, and Olivier Liandrat. Spatial and Temporal Variability of PV Output in an Insular Grid: Case of Reunion Island. *Energy Procedia*, 57:1275–1282, 2014.
- [147] Carlos de Castro and Iñigo Capellán-Pérez. Concentrated Solar Power: Actual Performance and Foreseeable Future in High Penetration Scenarios of Renewable Energies. *BioPhysical Economics and Resource Quality*, 3:1–20, 2018.
- [148] Agence de la Transition Écologique (ADEME). Transition(s) 2050 : l’Étude prospective de l’ademe.
- [149] Fernando de Llano Paz, S. I. Antelo, Anxo R. Calvo Silveira, and I. Soares. The Technological and Environmental Efficiency of the EU-27 Power Mix: An Evaluation Based on MPT. *Energy*, 69:67–81, 2014.
- [150] Fernando de Llano Paz, Anxo R. Calvo Silveira, and Martín Portos García. The Problem of Determining the Energy Mix: from the Portfolio Theory to the Reality of Energy Planning in the Spanish Case. *European Research Studies Journal*, 15:3–30, 2012.
- [151] Réseau de Transport d’Électricité (RTE). Futurs Énergétiques 2050. 2021.
- [152] P. Denholm, K. Clark, and M. O’Connell. On the Path to SunShot. Emerging Issues and Challenges in Integrating High Levels of Solar into the Electrical Generation and Transmission System. 2016.
- [153] P. Denholm, E. Ela, B. Kirby, and M. Milligan. Role of Energy Storage with Renewable Electricity Generation. 2010.
- [154] P. Denholm and M. Hand. Grid Flexibility and Storage Required to Achieve Very High Penetration of Variable Renewable Electricity. *Energy Policy*, 39:1817–1830, 2011.
- [155] P. Denholm and M. Hummon. Simulating the Value of Concentrating Solar Power with Thermal Energy Storage in a Production Cost Model. 2012.
- [156] P. Denholm, R. Margolis, and Joshua D. Eichman. Evaluating the Technical and Economic Performance of PV Plus Storage Power Plants: Report Summary. 2017.
- [157] P. Denholm, Joshua Novacheck, J. Jorgenson, and M. O’Connell. Impact of Flexibility Options on Grid Economic Carrying Capacity of Solar and Wind: Three Case Studies. 2016.
- [158] P. Denholm, M. O’Connell, G. Brinkman, and J. Jorgenson. *Overgeneration from Solar Energy in California: A field Guide to the Duck chart*. Report, National Renewable Energy Laboratory, Golden, CO, 2015. Available online <https://www.nrel.gov/docs/fy16osti/65023.pdf> (accessed on June 21st 2021).
- [159] P. Denholm, Y. Wan, M. Hummon, and M. Mehos. Analysis of Concentrating Solar Power with Thermal Energy Storage in a California 33% Renewable Scenario. 2013.
- [160] Paul Denholm, Jennie Jorgenson, Mackay Miller, Ella Zhou, and Caixia Wang. *Methods for Analyzing the Economic Value of Concentrating Solar Power with Thermal Energy Storage*. Technical Report, National Renewable Energy Laboratory, Golden, CO, 2015. Available online <https://www.nrel.gov/docs/fy15osti/64256.pdf> (accessed on June 21st 2021).
- [161] Paul Denholm and M. Mehos. Enabling Greater Penetration of Solar Power via the Use of CSP with Thermal Energy Storage. *Concentrating Solar Power: Data and Directions for an Emerging Solar Technology*, 01 2011.
- [162] J. Després. Development of a Dispatch Model of the European Power System For Coupling with a Long-Term Foresight Energy Model. 2015.
- [163] Francisco Diez, Andrés Martínez-Rodríguez, Luis Manuel Navas-Gracia, Leticia Chico-Santamarta, Adriana Corrêa-Guimarães, and Renato Andara. Estimation of the hourly global solar irradiation on the tilted and oriented plane of photovoltaic solar panels applied to greenhouse production. *Agronomy*, 11:495, 2021.
- [164] DLR. *Concentrating Solar Power for the Mediterranean Region. Report*, 2005. Available online https://www.dlr.de/tt/Portaldata/41/Resources/dokumente/institut/system/publications/MED-CSP_complete_study-small.pdf (accessed on June 21st 2021).
- [165] DLR. *Trans-Mediterranean Interconnection for Concentrating Solar Power.*, 2006. Available online https://www.dlr.de/tt/Portaldata/41/Resources/dokumente/institut/system/projects/WP00_TRANS-CSP-Introduction_and_Summary-Final.pdf (accessed on June 21st 2021).
- [166] M. Dolinar, B. Vidrih, L. Kajfez-Bogataj, and S. Medved. Predicted Changes in Energy Demands For Heating and Cooling Due To Climate Change. *Physics and Chemistry of The Earth*, 35:100–106, 2010.
- [167] Federico Dominio. Techno-Economic Analysis of Hybrid PV-CSP Power Plants. Advantages and Disadvantages of Intermediate and Peak Load Operation. 2014.
- [168] L. Dong and M. McPhaden. The Effects of External Forcing and Internal Variability on the Formation of Interhemispheric Sea Surface Temperature Gradient Trends in the Indian Ocean. *Journal of Climate*, 30:9077–9095, 2017.
- [169] T. Drennen, J. Erickson, and D. Chapman. Solar Power and Climate Change Policy in Developing Countries. *Energy Policy*, 24:9–16, 1993.
- [170] Fatima Driouech. Distribution des Précipitations Hivernales Sur Le Maroc Dans Le Cadre d’un Changement Climatique: Descente d’Échelle et Incertitudes. 2010.
- [171] P. Drobinski. Climate and Environmental Change in the Mediterranean Basin – Current Situation and Risks For the Future. 2020.

- [172] P. Drobinski, P. Carlotti, R. Newsom, R. Banta, R. Foster, and J. Redelsperger. The Structure of the Near Neutral Atmospheric Surface Layer as Observed During the CASES'99 Experiment. 2003.
- [173] P. Drobinski, Nicolas Da Silva, S. Bastin, S. Mailler, C. Muller, B. Ahrens, O. B. Christensen, and P. Lionello. How Warmer and Drier will the Mediterranean Region be at the End of the Twenty-First Century? *Regional Environmental Change*, 20:1–12, 2020.
- [174] Er Du, Ning Zhang, Bri-Mathias Hodge, Qin Wang, Chongqing Kang, Benjamin Kroposki, and Qing Xia. The Role of Concentrating Solar Power Towards High Renewable Energy Penetrated Power Systems. *IEEE Transactions on Power Systems*, PP:1–1, 05 2018.
- [175] Er Du, Ning Zhang, Bri-Mathias Hodge, Qin Wang, Zongxiang Lu, Chongqing Kang, Benjamin Kroposki, and Qing Xia. Operation of a High Renewable Penetrated Power System With CSP Plants: A Look-Ahead Stochastic Unit Commitment Model. *IEEE Transactions on Power Systems*, PP:1–1, 08 2018.
- [176] Ershun Du, N. Zhang, B. Hodge, C. Kang, B. Kroposki, and Q. Xia. Economic Justification of Concentrating Solar Power in High Renewable Energy Penetrated Power Systems. *Applied Energy*, 222:649–661, 2018.
- [177] S. Dubey, J. Sarvaiya, and B. Seshadri. Temperature Dependent Photovoltaic (PV) Efficiency and Its Effect on PV Production in the World – A Review. *Energy Procedia*, 33:311–321, 2013.
- [178] John A. Duffie and William A. Beckman. *Solar Engineering of Thermal Processes*. WILEY, 4 edition, 2013. 944 Pages.
- [179] J. Dunne, J. John, A. Adcroft, Stephen M. Griffies, R. Hallberg, E. Shevliakova, R. Stouffer, W. Cooke, Krista A. Dunne, M. Harrison, J. Krasting, S. Malyshev, P. Milly, P. Philipps, L. T. Sentman, B. Samuels, Michael J. Spelman, M. Winton, A. T. Wittenberg, and N. Zadeh. GFDL's ESM2 Global Coupled Climate–Carbon Earth System Models. Part I: Physical Formulation and Baseline Simulation Characteristics. *Journal of Climate*, 25:6646–6665, 2012.
- [180] Ricardo Dutra and A. Szklo. Assessing Long-Term Incentive Programs For Implementing Wind Power in Brazil Using GIS Rule-Based Methods. *Renewable Energy*, 33:2507–2515, 2008.
- [181] J. Ebinger and W. Vergara. Climate Impacts on Energy Systems: Key Issues for Energy Sector Adaptation. 2011.
- [182] O. Edenhofer, R. P. Madruga, Y. Sokona, K. Seyboth, Patrick R. Matschoss, Susanne Kadner, T. Zwickel, Patrick Eickemeier, Gerrit Hansen, S. Schlömer, and C. V. Stechow. Renewable Energy Sources and Climate Change Mitigation: Special Report of the Intergovernmental Panel on Climate Change. 2011.
- [183] O. Edenhofer, R. Pichs-Madruga, and Y. Sokona. Climate Change 2014 : Mitigation of Climate Change. 2014.
- [184] E. Ela, M. Milligan, and B. Kirby. Operating Reserves and Variable Generation. 2011.
- [185] A. elderbos, E. Delarue, K. Kessels, and W.D. andHaeseleer. The Levelized Cost of Storage Critically Analyzed and Its Intricacies Clearly Explained (KU Leuven). 2016.
- [186] M. Eltawil and Z. Zhao. Grid-Connected Photovoltaic Power Systems: Technical and Potential Problems—A Review. *Renewable & Sustainable Energy Reviews*, 14:112–129, 2010.
- [187] G. Eskeland and Torben K. Mideksa. Electricity Demand in a Changing Climate. *Mitigation and Adaptation Strategies for Global Change*, 15:877–897, 2010.
- [188] Greenpeace et L'Institut Rousseau. Les coûts actuels des Énergies Électriques bas-carbone. 2021.
- [189] Abbetta Evans, Vladimir Strezov, and Tim J. Evans. Comparing the sustainability parameters of renewable, nuclear and fossil fuel electricity generation technologies. 2010.
- [190] D. Evans. Simplified Method for Predicting Photovoltaic Array Output. *Solar Energy*, 27:555–560, 1980.
- [191] L. Fabietti, Tomasz T. Gorecki, Emil Namor, F. Sossan, M. Paolone, and C. Jones. Enhancing the Dispatchability of Distribution Networks through Utility-Scale Batteries and Flexible Demand. *Energy and Buildings*, 172:125–138, 2018.
- [192] C. Fant, C. Schlosser, and K. Strzepek. The Impact of Climate Change on Wind and Solar Resources in Southern Africa. *Applied Energy*, 161:556–564, 2016.
- [193] David Feldham and M. Bolinger. On the Path to SunShot: Emerging Opportunities and Challenges in Financing Solar. 2016.
- [194] D. Feldman, R. Margolis, P. Denholm, and J. Stekli. Exploring the Potential Competitiveness of Utility-Scale Photovoltaics plus Batteries with Concentrating Solar Power, 2015–2030. 2016.
- [195] Paulino Martínez Fernández. An Application of the Modern Portfolio Theory to the Optimization of the European Union Power Generation Mix From An Environmental Perspective. 2019.
- [196] V. J. Fesharaki, M. Dehghani, and J. J. Fesharaki. The Effect of Temperature on Photovoltaic Cell Efficiency. 2011.
- [197] Audun Fidje and T. Martinsen. Effects of Climate Change on the Utilization of Solar Cells in the Nordic Region. 2006.
- [198] C. Field, V. Barros, M. Mastrandrea, K. Mach, Abdrabo, W. Adger, Yury A. Anokhin, O. Anisimov, D. Arent, J. Barnett, V. Burkett, R. Cai, M. Chatterjee, S. Cohen, W. Cramer, P. Dasgupta, D. Davidson, F. Denton, P. Döll, K. Dow, Y. Hijioka, and O. Hoegh-Guldberg. Climate Change 2014: Impacts, Adaptation, and Vulnerability. Part A: Global and Sectoral Aspects. Contribution of Working Group II to the Fifth Assessment Report of the Intergovernmental Panel on Climate Change. 2014.
- [199] S. Filahi, Y. Tramblay, L. Mouhir, and E. Diaconescu. Projected Changes in Temperature and Precipitation Indices in Morocco From High-Resolution Regional Climate Models. *International Journal of Climatology*, 37:4846–4863, 2017.
- [200] C. Fleischer. Minimising the Effects of Spatial Scale Reduction on Power System Models. *Energy Strategy Reviews*, 32:100563, 2020.
- [201] J. Forrester. The Value of CSP with Thermal Energy Storage in Providing Grid Stability. *Energy Procedia*, 49:1632–1641, 2014.
- [202] Gonzalo Escribano Francés, José María Marín-Quemada, and E. González. RES and Risk: Renewable Energy's Contribution to Energy Security. A Portfolio-Based Approach. *Renewable & Sustainable Energy Reviews*, 26:549–559, 2013.
- [203] B. François, B. Hingray, M. Borga, D. Zoccatelli, C. Brown, and J. Creutin. Impact of Climate Change on Combined Solar and Run-of-River Power in Northern Italy. *Energies*, 11:290, 2018.

- [204] Bethany A Frew. 8760-Based Method for Representing Variable Generation Capacity Value in Capacity Expansion Models. 8 2017.
- [205] J. Frunt, W. Kling, and V. Bosch. Classification and Quantification of Reserve Requirements for Balancing. *Electric Power Systems Research*, 80:1528–1534, 2010.
- [206] M. Gaetani, T. Huld, E. Vignati, F. Monforti-Ferrario, A. Dosio, and F. Raes. The Near Future Availability of Photovoltaic Energy in Europe and Africa in Climate-Aerosol Modeling Experiments. *Renewable & Sustainable Energy Reviews*, 38:706–716, 2014.
- [207] M. Gaetani, E. Vignati, F. Ferrario, T. Huld, and A. Dosio. Climate Modelling and Renewable Energy Resource Assessment. 2015.
- [208] Dhruv Gami, R. Sioshansi, and P. Denholm. Data Challenges in Estimating the Capacity Value of Solar Photovoltaics. *IEEE Journal of Photovoltaics*, 7:1065–1073, 2017.
- [209] G. Gaudiosi and C. Borri. Offshore Wind Energy in the Mediterranean Countries. 2010.
- [210] R. Gelaro, W. McCarty, M. Suárez, R. Todling, A. Molod, L. L. Takacs, C. Randles, A. Darmenov, M. Bosilovich, R. Reichle, K. Wargan, L. Coy, R. Cullather, C. Draper, S. Akella, V. Buchard, Austin Conaty, A. D. Silva, W. Gu, Gi-Kong Kim, R. D. Koster, R. Lucchesi, Dagmar Merkova, J. E. Nielsen, Gary Partyka, S. Pawson, W. Putman, M. Rienecker, S. Schubert, M. Sienkiewicz, and Bin Zhao. The Modern-Era Retrospective Analysis for Research and Applications, Version 2 (MERRA-2). *Journal of climate*, Volume 30 Iss 13:5419–5454, 2017.
- [211] P. Gent, G. Danabasoglu, L. Donner, M. Holland, E. Hunke, S. Jayne, D. Lawrence, R. Neale, P. Rasch, M. Vertenstein, P. Worley, Zong-Liang Yang, and M. Zhang. The Community Climate System Model Version 4. *Journal of Climate*, 24:4973–4991, 2011.
- [212] A. Gerlak, Jaron D. Weston, B. McMahan, Rachel L. Murray, and Megan Mills-Novoa. Climate Risk Management and the Electricity Sector. *Climate Risk Management*, 19:12–22, 2017.
- [213] R. Ghedamsi, N. Settou, A. Gouareh, A. Khamouli, N. Saifi, B. Recioui, and Boubekker Dokkar. Modeling and Forecasting Energy Consumption For Residential Buildings in Algeria Using Bottom-Up Approach. *Energy and Buildings*, 121:309–317, 2016.
- [214] C. Giannakopoulos, P. Hadjinicolaou, C. Zerefos, and G. Demosthenous. Changing Energy Requirements in the Mediterranean Under Changing Climatic Conditions. *Energies*, 2:805–815, 2009.
- [215] G. Giebel. A Variance Analysis of the Capacity Displaced By Wind Energy in Europe. *Wind Energy*, 10:69–79, 2007.
- [216] A. Gil, M. Medrano, I. Martorell, A. Lázaro, P. Dolado, B. Zalba, and L. Cabeza. State of the Art on High Temperature Thermal Energy Storage For Power Generation. Part 1—Concepts, Materials and Modellization. *Renewable & Sustainable Energy Reviews*, 14:31–55, 2010.
- [217] V. Gil, M. Gaertner, C. Gutiérrez, and T. Losada. Impact of Climate Change on Solar Irradiation and Variability Over the Iberian Peninsula Using Regional Climate Models. *International Journal of Climatology*, 39:1733–1747, 2018.
- [218] F. Giorgi and X. Bi. A Study of Internal Variability of a Regional Climate Model. *Journal of Geophysical Research*, 105:29503–29521, 2000.
- [219] F. Giorgi and L. Mearns. Introduction to Special Section : Regional Climate Modeling Revisited. *Journal of Geophysical Research*, 104:6335–6352, 1999.
- [220] M. Gitizadeh and H. Fakhrazadegan. Battery Capacity Determination with Respect to Optimized Energy Dispatch Schedule in Grid-Connected Photovoltaic (PV) Systems. *Energy*, 65:665–674, 2014.
- [221] Nacxitl Calva González. Application of the Portfolio Theory to the Power Sector in Mexico. 2016.
- [222] R. Gottschalg, T. Betts, S. R. Williams, D. Sauter, D. Infield, and M. J. Kearney. A Critical Appraisal of the Factors Affecting Energy Production From Amorphous Silicon Photovoltaic Arrays in a Maritime Climate. *Solar Energy*, 77:909–916, 2004.
- [223] I. Graabak and M. Korpås. Variability Characteristics of European Wind and Solar Power Resources—A Review. *Energies*, 9:449, 2016.
- [224] Peter Grant. Climate Change Financing and Aid Effectiveness: Morocco Case Study. *OECD*, 2011. Available online <https://www.oecd.org/environment/environment-development/48458464.pdf> (accessed on June 21st 2021).
- [225] A. Green, C. Diep, and R. Dunn. High Capacity Factor CSP-PV Hybrid Systems. *Energy Procedia*, 69:2049–2059, 2015.
- [226] S. Greene, M. Morrissey, and S. E. Johnson. Wind Climatology, Climate Change, and Wind Energy. *Geography Compass*, 4:1592–1605, 2010.
- [227] Jonathan M. Gregory, Ronald J. Stouffer, Mario J. Molina, Amnat Chidthaisong, Susan Solomon, Graciela B. Raga, Pierre Friedlingstein, Nathaniel L. Bindoff, Hervé Le Treut, Matilde Rusticucci, Ulrike Lohmann, Philip W. Mote, David A. Randall, Jesper Heile Christensen, Brian J. Hoskins, Thomas F. Stocker, Martin R. Manning, Kenneth L. Denman, Peter Lemke, Philip D. Jones, Guy P. Brasseur, Gerald A. Meehl, Neville Nicholls, Julie M. Arblaster, Dahe Qin, Richard A. Wood, Martin Heimann, Gabriele C. Hegerl, David W. Fahey, Richard B. Alley, Terje Koren Berntsen, Piers M. Forster, Vladimir M. Kattsov, Francis W. Zwiers, Jiawen Ren, David Wratt, Penny Whetton, V. Ramaswamy, Eystein Jansen, Bruce Hewitson, Peter Stott, Zhenlin Chen, Taroh Matsuno, Jean Jouzel, Jonathan T. Overpeck, Reto Knutti, Richard C. J. Somerville, Kevin E. Trenberth, Jürgen Willebrand, Fortunat Joos, and Dáithí A. Stone. Climate change 2021—the physical science basis. *Chemistry International*, 2021.
- [228] G. Gualtieri and Sauro Secci. Comparing Methods to Calculate Atmospheric Stability-Dependent Wind Speed Profiles: A Case Study on Coastal Location. *Renewable Energy*, 36:2189–2204, 2011.
- [229] Rafael Guédez, J. Spelling, Björn Laumert, and T. Fransson. Optimization of Thermal Energy Storage Integration Strategies for Peak Power Production by Concentrating Solar Power Plants. *Energy Procedia*, 49:1642–1651, 2014.
- [230] Rafael Guédez, Monika Topel, James Spelling, and Björn Laumert. Enhancing the Profitability of Solar Tower Power Plants through Thermoeconomic Analysis based on Multi-objective Optimization. *Energy Procedia*, 69:1277–1286, 2015.
- [231] C. Gueymard and S. Wilcox. Assessment of Spatial and Temporal Variability in the US Solar Resource From Radiometric Measurements and Predictions From Models Using Ground-Based or Satellite Data. *Solar Energy*, 85:1068–1084, 2011.

- [232] M. Günther, N. Janotte, A. Mezhrab, K. Hennecke, C. Schillings, Stefan Wilbert, and Fabian Wolferstätter. Advanced CSP Teaching Materials Chapter 2 Solar Radiation. 2011.
- [233] C. Gutiérrez, S. Somot, P. Nabat, M. Mallet, M. Gaertner, and O. Perpiñán. Impact of Aerosols on the Spatiotemporal Variability of Photovoltaic Energy Production in the Euro-Mediterranean Area. *Solar Energy*, 174:1142–1152, 2018.
- [234] C. Gutiérrez, A. D. L. Vara, Juan Jesús González-Alemán, and M. Gaertner. Impact of Climate Change on Wind and Photovoltaic Energy Resources in the Canary Islands and Adjacent Regions. *Sustainability*, 13:4104, 2021.
- [235] W. Gutowski, F. Giorgi, B. Timbal, A. Frigon, D. Jacob, Hyun-Suk Kang, K. Raghavan, B. Lee, C. Lennard, G. Nikulin, E. O'Rourke, M. Rixen, S. Solman, Tannecia S. Stephenson, and F. Tangang. WCRP Coordinated Regional Downscaling EXperiment (CORDEX): A Diagnostic MIP For CMIP6. *Geoscientific Model Development*, 9:4087–4095, 2016.
- [236] H. Paeth and B. Mannig. On the Added Value of Regional Climate Modeling in Climate Change Assessment. *Climate Dynamics*, 41:1057–1066, 2012.
- [237] M. Hadjipanayi, Ioannis Koumparou, N. Philippou, V. Paraskeva, A. Phinikarides, G. Makrides, V. Efthymiou, and G. Georghiou. Prospects of Photovoltaics in Southern European, Mediterranean and Middle East Regions. *Renewable Energy*, 92:58–74, 2016.
- [238] N. Haegel, H. Atwater, T. Barnes, C. Breyer, A. Burrell, Y. Chiang, S. Wolf, B. Dimmler, D. Feldman, S. Glunz, J. Goldschmidt, D. Hochschild, R. Inzunza, I. Kaizuka, B. Kroposki, S. Kurtz, S. Leu, R. Margolis, K. Matsubara, A. Metz, W. Metzger, M. Morjaria, S. Niki, S. Nowak, I. M. Peters, S. Philipps, T. Reindl, A. Richter, Doug Rose, K. Sakurai, R. Schlatmann, M. Shikano, W. Sinke, R. Sinton, B. J. Stanbery, M. Topic, W. Tumas, Y. Ueda, J. Lagemaat, P. Verlinden, M. Vetter, E. Warren, M. Werner, M. Yamaguchi, and A. Bett. Terawatt-Scale Photovoltaics: Transform Global Energy. *Science*, 364:836 – 838, 2019.
- [239] J. Haerter, S. Hagemann, C. Moseley, and C. Piani. Climate Model Bias Correction and the Role of Timescales. *Hydrology and Earth System Sciences*, 15:1065–1079, 2010.
- [240] Amine Haibaoui, Bouchaib Hartiti, Abderrazzak Elamim, and A. Ridah. Production study of two grid-connected pv systems in two moroccan cities. *2017 International Renewable and Sustainable Energy Conference (IRSEC)*, pages 1–6, 2017.
- [241] Elaine Hale, Brady Stoll, and Trieu Mai. *Capturing the Impact of Storage and Other Flexible Technologies on Electric System Planning*. Report, National Renewable Energy Laboratory, 2016. Available online <https://www.nrel.gov/docs/fy16osti/65726.pdf> (accessed on June 21st 2021).
- [242] William T. Hamilton, Mark Husted, A. Newman, R. Braun, and M. Wagner. Dispatch Optimization of Concentrating Solar Power with Utility-Scale Photovoltaics. *Optimization and Engineering*, 21:335–369, 2020.
- [243] Kenneth Hansen, Christian Breyer, and H. Lund. Status and Perspectives on 100% Renewable Energy Systems. *Energy*, 175:471–480, 2019.
- [244] Elizabeth Harder and J. M. Gibson. The Costs and Benefits of Large-Scale Solar Photovoltaic Power Production in Abu Dhabi, United Arab Emirates. *Renewable Energy*, 36:789–796, 2011.
- [245] E. Harrison, P. Minnis, B. Barkstrom, V. Ramanathan, R. Cess, and G. Gibson. Seasonal Variation of Cloud Radiative Forcing Derived From the Earth Radiation Budget Experiment. *Journal of Geophysical Research*, 95:18687–18703, 1990.
- [246] Abubakar Sani Hassan, L. Cipcigan, and N. Jenkins. Optimal Battery Storage Operation For PV Systems with Tariff Incentives. *Applied Energy*, 203:422–441, 2017.
- [247] T. Hastie, R. Tibshirani, and J. Friedman. The Elements of Statistical Learning: Data Mining, Inference, and Prediction, 2nd Edition. In *Springer Series in Statistics*, 2009.
- [248] S. E. Haupt, J. Copeland, W. Y. Cheng, Yongxin Zhang, C. Ammann, and P. Sullivan. A Method to Assess the Wind and Solar Resource and to Quantify Interannual Variability Over the United States Under Current and Projected Future Climate. *Journal of Applied Meteorology and Climatology*, 55:345–363, 2016.
- [249] E. Hawkins and R. Sutton. The Potential to Narrow Uncertainty in Regional Climate Predictions. *Bulletin of the American Meteorological Society*, 90:1095–1107, 2009.
- [250] W. Hazeleger, C. Severijns, T. Semmler, Simona Ștefănescu, Shuting Yang, X. Wang, K. Wyser, E. Dutra, J. Baldasano, R. Bintanja, P. Bougeault, R. Caballero, A. Ekman, J. Christensen, B. Hurk, P. Jiménez, C. Jones, P. Kållberg, T. Koenigk, R. McGrath, P. Miranda, T. V. Noije, T. Palmer, J. A. Parodi, T. Schmith, F. Selten, T. Storelvmo, A. Sterl, H. Tapamo, Martin Vancoppenolle, P. Viterbo, and U. Willén. EC-Earth A Seamless Earth-System Prediction Approach in Action. *Bulletin of the American Meteorological Society*, 91:1357–1363, 2010.
- [251] D. Heide, L. V. Bremen, M. Greiner, C. Hoffmann, M. Speckmann, and S. Bofinger. Seasonal Optimal Mix of Wind and Solar Power in a Future, Highly Renewable Europe. *Renewable Energy*, 35:2483–2489, 2010.
- [252] D. Heide, Martin Greiner, L. V. Bremen, and C. Hoffmann. Reduced Storage and Balancing Needs in a Fully Renewable European Power System with Excess Wind and Solar Power Generation. *Renewable Energy*, 36:2515–2523, 2011.
- [253] Detlev Heinemann. *Energy Meteorology - Lecture Notes.*, 2000. Available online https://uol.de/f/5/inst/physik/ag/enmet/download/lectures/Energy_Meteorology_Script.pdf (accessed on June 21st 2021).
- [254] M. Hekkenberg, H. Moll, and A. S. uiterkamp. Dynamic Temperature Dependence Patterns in Future Energy Demand Models in the Context of Climate Change. *Energy*, 34:1797–1806, 2009.
- [255] Catherine Heymans, S. Walker, S. Young, and M. Fowler. Economic Analysis of Second Use Electric Vehicle Batteries For Residential Energy Storage and Load-Levelling. *Energy Policy*, 71:22–30, 2014.
- [256] Lion Hirth, Falko Ueckerdt, and Ottmar Edenhofer. Integration Costs Revisited - An Economic Framework of Wind and Solar Variability. *Renewable Energy*, 74:925–939, 08 2014.
- [257] Samuel Hitz and J. Smith. Estimating Global Impacts From Climate Change. *Global Environmental Change-human and Policy Dimensions*, 14:201–218, 2004.

- [258] J. Holton. An Introduction to Dynamic Meteorology. 1972.
- [259] M. Hosenuzzaman, N. A. Rahim, J. Selvaraj, M. Hasanuzzaman, A. A. Malek, and A. Nahar. Global Prospects, Progress, Policies, and Environmental Impact of Solar Photovoltaic Power Generation. *Renewable & Sustainable Energy Reviews*, 41:284–297, 2015.
- [260] M. K. Hubbert. Energy Resources of the Earth. *Scientific American*, 225:60–70, 1971.
- [261] Isabelle Huber, L. Bugliaro, M. Ponater, H. Garny, C. Emde, and B. Mayer. Do Climate Models Project Changes in Solar Resources. *Solar Energy*, 129:65–84, 2016.
- [262] M. Huber, Desislava Dimkova, and T. Hamacher. Integration of Wind and Solar Power in Europe: Assessment of Flexibility Requirements. *Energy*, 69:236–246, 2014.
- [263] H. Hueging, Rabea Haas, K. Born, D. Jacob, and J. G. Pinto. Regional Changes in Wind Energy Potential over Europe Using Regional Climate Model Ensemble Projections. *Journal of Applied Meteorology and Climatology*, 52:903–917, 2013.
- [264] IEA. Energy Policies Beyond IEA Countries: Morocco 2019. 2019.
- [265] IEA. Snapshot of Global PV Markets 2020. 2020.
- [266] T. Ioannis, Tarvydas Dalius, and Zucker Andreas. *Cost Development of Low Carbon Energy Technologies — Scenario-Based Cost Trajectories to 2050*. 2017 Edition (EUR 29034 EN). Publications Office of the European Union, Luxembourg, 2018. Available online <https://doi.org/10.2760/490059> (accessed on June 21st 2021).
- [267] M. Iqbal. An Introduction to Solar Radiation. 1983.
- [268] IRENA. *Renewable Energy Technologies: Cost Analysis Series - Concentrating Solar Power*. Report, IRENA, Abu Dhabi, UAE, 2012. Available online https://www.irena.org/documentdownloads/publications/re_technologies_cost_analysis-csp.pdf (accessed on June 21st 2021).
- [269] IRENA. *Renewable Energy Technologies: Cost Analysis Series - Solar Photovoltaics*. Report, IRENA, Abu Dhabi, UAE, 2012. Available online https://www.irena.org/-/media/Files/IRENA/Agency/Publication/2012/RE_Technologies_Cost_Analysis-SOLAR_PV.pdf (accessed on June 21st 2021).
- [270] IRENA. *Global Energy Transformation: A Roadmap to 2050*. Report, International Renewable Energy Agency, Abu Dhabi, UAE, 2018. Available online https://www.irena.org/-/media/Files/IRENA/Agency/Publication/2018/Apr/IRENA_Report_GET_2018.pdf (accessed on June 21st 2021).
- [271] IRENA. *Utility-Scale Batteries Innovation Landscape Brief*. Report, IRENA, Abu Dhabi, UAE, 2019. Available online https://www.irena.org/-/media/Files/IRENA/Agency/Publication/2019/Sep/IRENA_Utility-scale-batteries_2019.pdf (accessed on June 21st 2021).
- [272] IRENA. *Renewable capacity highlights*. Report, IRENA, Abu Dhabi, UAE, 2020. Available online https://www.irena.org/-/media/Files/IRENA/Agency/Publication/2020/Mar/IRENA_RE_Capacity_Highlights_2020.pdf?la=en&hash=B6BDF8C3306D271327729B9F9C9AF5F1274FE30B (accessed on December 10th 2021).
- [273] I. James. Introduction to Circulating Atmospheres. 1994.
- [274] J.C. Jansen, L.W.M. Beurskens, and X. Van Tilburg. Application of Portfolio Analysis to the Dutch Generating Mix Reference Case and Two Renewables Cases, Year 2030, SE and GE Scenario. (*ECN-C-05-100*). Netherlands, 2006.
- [275] S. Jerez, Laura Palacios-Peña, C. Gutiérrez, P. Jiménez-Guerrero, J. M. López-Romero, Enrique Pravia-Sarabia, and J. Montávez. Sensitivity of Surface Solar Radiation to Aerosol–Radiation and Aerosol–Cloud Interactions Over Europe in WRFv3.6.1 Climatic Runs with Fully Interactive Aerosols. *Geoscientific Model Development*, 14:1533–1551, 2021.
- [276] S. Jerez, Isabelle Tobin, R. Vautard, J. P. Montávez, J. M. López-Romero, F. Thais, B. Bartók, O. B. Christensen, A. Colette, M. Déqué, G. Nikulin, S. Kotlarski, E. van Meijgaard, C. Teichmann, and M. Wild. The impact of Climate Change on Photovoltaic Power Generation in Europe. *Nature Communications*, 6, 2015.
- [277] S. Jerez, R. Trigo, S. Vicente-Serrano, D. Pozo-Vázquez, R. Lorente-Plazas, J. Lorenzo-Lacruz, F. J. Santos-Alamillos, and J. Montávez. The Impact of the North Atlantic Oscillation on Renewable Energy Resources in Southwestern Europe. *Journal of Applied Meteorology and Climatology*, 52:2204–2225, 2013.
- [278] W. Jewell and T. D. Unruh. Limits on Cloud-Induced Fluctuation in Photovoltaic Generation. *IEEE Transactions on Energy Conversion*, 5:8–14, 1990.
- [279] Jing Jiang and W. Perrie. The Impacts of Climate Change on Autumn North Atlantic Midlatitude Cyclones. *Journal of Climate*, 20:1174–1187, 2007.
- [280] T. Jilbert, G. Reichart, B. Aeschlimann, D. Günther, W. Boer, and G. Lange. Climate-Controlled Multidecadal Variability in North African Dust Transport to the Mediterranean. *Geology*, 38:19–22, 2010.
- [281] P. Jiménez, J. Hacker, J. Dudhia, S. E. Haupt, J. A. Ruiz-Arias, C. Gueymard, G. Thompson, T. Eidhammer, and A. Deng. WRF-Solar: Description and Clear-Sky Assessment of an Augmented NWP Model for Solar Power Prediction. *Bulletin of the American Meteorological Society*, 97:1249–1264, 2016.
- [282] C. Jones, P. Samuelsson, and Erik Kjellström. Regional Climate Modelling at the Rossby Centre. *Tellus A: Dynamic Meteorology and Oceanography*, 63:1 – 3, 2011.
- [283] J. Jorgenson, P. Denholm, and M. Mehos. Estimating the Value of Utility-Scale Solar Technologies in California Under a 40% Renewable Portfolio Standard (Report Summary) (Presentation). 2014.
- [284] J. Jorgenson, M. Mehos, and P. Denholm. Comparing the Net Cost of CSP-TES to PV Deployed with Battery Storage. 2016.
- [285] R. S. José, J. L. Perez, R. M. González, J. Pecci, A. Garzon, and M. Palacios. Impacts of the 4.5 and 8.5 RCP Global Climate Scenarios on Urban Meteorology and Air Quality: Application to Madrid, Antwerp, Milan, Helsinki and London. *J. Comput. Appl. Math.*, 293:192–207, 2016.

- [286] P. Joskow. Comparing the Costs of Intermittent and Dispatchable Electricity Generating Technologies. *The American Economic Review*, 101:238–241, 2011.
- [287] Bénédicte Jourdiér. Ressource Éolienne en France Métropolitaine: Méthodes d’Évaluation du Potentiel, Variabilité et Tendances. 2015.
- [288] Verena Jülch. Comparison of Electricity Storage Options Using Levelized Cost of Storage (LCOS) Method. *Applied Energy*, 183:1594–1606, 2016.
- [289] C. Justus and A. Mikhail. Height Variation of Wind Speed and Wind Distributions Statistics. *Geophysical Research Letters*, 3:261–264, 1976.
- [290] A. Kalair, N. Abas, M. Saleem, and N. Khan. Role of Energy Storage Systems in Energy Transition from Fossil Fuels to Renewables. 2020.
- [291] Dongbum Kang, K. Ko, and J. Huh. Comparative Study of Different Methods for Estimating Weibull Parameters: A Case Study on Jeju Island, South Korea. *Energies*, 11:356, 2018.
- [292] G. Kariniotakis. Renewable Energy Forecasting: From Models to Applications. 2017.
- [293] T. V. Karman. Über Laminare Und Turbulente Reibung. *Zamm-zeitschrift Fur Angewandte Mathematik Und Mechanik*, 1:233–252.
- [294] W. Katzenstein, E. Fertig, and J. Apt. The Variability of Interconnected Wind Plants. *Energy Policy*, 38:4400–4410, 2010.
- [295] Yoichi Kaya and Keiichi Yokobori. Environment, energy and economy: Strategies for sustainability. 1999.
- [296] B. Ke, T. Ku, Y. Ke, C. Chuang, and Hong-Zhang Chen. Sizing the Battery Energy Storage System on a University Campus With Prediction of Load and Photovoltaic Generation. *IEEE Transactions on Industry Applications*, 52:1136–1147, 2016.
- [297] N. A. Kelly and T. Gibson. Improved Photovoltaic Energy Output for Cloudy Conditions with a Solar Tracking System. *Solar Energy*, 83:2092–2102, 2009.
- [298] W. Kempton, F. Pimenta, D. Veron, and B. Colle. Electric Power From Offshore Wind Via Synoptic-Scale Interconnection. *Proceedings of the National Academy of Sciences*, 107:7240 – 7245, 2010.
- [299] J. Kern, T. Fichter, Massimo Moser, F. Trieb, F. Seidel, Klas Heising, and Philippe Lempp. MOREMix - Power Sector Optimization for Morocco. 2016.
- [300] M. R. B. Khan, J. Pasupuleti, Jabbar Al-Fattah, and Mehrdad Tahmasebi. Energy Management System For PV-Battery Microgrid Based on Model Predictive Control. 2019.
- [301] V. Kharin and F. Zwiers. Estimating Extremes in Transient Climate Change Simulations. *Journal of Climate*, 18:1156–1173, 2005.
- [302] N. Khatib. *Country Profile Morocco. Report*. RES4MED&Africa, 2018. Available online <https://www.res4africa.org/wp-content/uploads/2018/06/Country-profile-Marocco-2.pdf> (accessed on June 21st 2021).
- [303] Younes El Khchine, M. Sriti, and Nacer Eddine El Kadri Elyamani. Evaluation of Wind Energy Potential and Trends in Morocco. *Heliyon*, 5, 2019.
- [304] D. Kirschen, J. Ma, V. Silva, and R. Belhomme. Optimizing the Flexibility of a Portfolio of Generating Plants to Deal with Wind Generation. *2011 IEEE Power and Energy Society General Meeting*, pages 1–7, 2011.
- [305] R. Knutti and J. Sedlacek. Robustness and Uncertainties in the New CMIP5 Climate Model Projections. *Nature Climate Change*, 3:369–373, 2013.
- [306] H. Koch, S. Voegelé, F. Hattermann, and Shaochun Huang. The Impact of Climate Change and Variability on the Generation of Electrical Power. *Meteorologische Zeitschrift*, 24:173–188, 2015.
- [307] N. Komendantova, A. Patt, Lucile Barras, and Antonella Battaglini. Perception of Risks in Renewable Energy projects: The Case of Concentrated Solar Power in North Africa. *Energy Policy*, 40:103–109, 2012.
- [308] N. Komendantova, A. Patt, and K. Williges. Solar Power Investment in North Africa: Reducing Perceived Risks. *Renewable & Sustainable Energy Reviews*, 15:4829–4835, 2011.
- [309] Christoph Kost, Benjamin Pfluger, Wolfgang Eichhammer, and Mario Ragwitz. Fruitful symbiosis: Why an Export Bundled with Wind Energy is the Most Feasible Option for North African Concentrated Solar Power. *Energy Policy - ENER POLICY*, 39:7136–7145, 11 2011.
- [310] S. Kozarcanin, H. Liu, and G. Andresen. 21st Century Climate Change Impacts on Key Properties of a Large-Scale Renewable-Based Electricity System. *Joule*, 3:992–1005, 2019.
- [311] C. S. Lai and M. McCulloch. Levelized Cost of Electricity For Solar Photovoltaic and Electrical Energy Storage. *Applied Energy*, 190:191–203, 2017.
- [312] V. Lara-Fanego, J. A. Ruiz-Arias, D. Pozo-Vázquez, F. J. Santos-Alamillos, and J. Tovar-Pescador. Evaluation of the WRF model Solar Irradiance Forecasts in Andalusia (Southern Spain). *Solar Energy*, 86:2200–2217, 2012.
- [313] M. Larrañeta, S. Moreno-Tejera, I. Lillo-Bravo, and M. Silva-Pérez. Impact of the Intra-day Variability of the DNI on the Energy Yield of CSP Plants. 2019.
- [314] Sylvain Lassonde. Potentiels et Limites Météorologiques et Climatiques d’un Foisonnement des Énergies Renouvelables. 2018.
- [315] A. Lawin, Marc Niyongendako, and Célestin Manirakiza. Solar Irradiance and Temperature Variability and Projected Trends Analysis in Burundi. *Climate*, 7:83, 2019.
- [316] Lazard. Lazard’s Levelized Cost of Storage Analysis, [2.0. version]. 2016.
- [317] Haibin Li, A. Robock, and M. Wild. Evaluation of Intergovernmental Panel on Climate Change Fourth Assessment Soil Moisture Simulations For the Second Half of the Twentieth Century. *Journal of Geophysical Research*, 112, 2007.

- [318] P. Lionello, I. Trigo, V. Gil, M. Liberato, K. Nissen, J. G. Pinto, C. Raible, M. Reale, A. Tanzarella, R. Trigo, S. Ulbrich, and U. Ulbrich. Objective Climatology of Cyclones in the Mediterranean Region: A Consensus View Among Methods with Different System Identification and Tracking Criteria. *Tellus A: Dynamic Meteorology and Oceanography*, 68, 2016.
- [319] C. Liousse, E. Assamoi, P. Criqui, C. Granier, and R. Rosset. Explosive Growth in African Combustion Emissions From 2005 to 2030. *Environmental Research Letters*, 9:035003, 2014.
- [320] H. Liu, G. Andresen, and M. Greiner. Cost-Optimal Design of a Simplified Highly Renewable Chinese Electricity Network. *Energy*, 147:534–546, 2018.
- [321] D. Lobell, C. Bonfils, and P. Duffy. Climate Change Uncertainty For Daily Minimum and Maximum Temperatures: A Model Inter-Comparison. *Geophysical Research Letters*, 34, 2006.
- [322] Luciano Losekann, Gustavo A. Marrero, F. Ramos-Real, and E. D. Almeida. Efficient Power Generating Portfolio in Brazil: Conciliating Cost, Emissions and Risk. *Energy Policy*, 62:301–314, 2013.
- [323] K. Lovegrove, G. James, D. Leitch, A. Milczarek, A. Ngo, J. Rutovitz, M. Watt, and J. Wyder. Comparison of Dispatchable Renewable Electricity Options: Technologies for an Orderly Transition. 2018.
- [324] Yuehong Lu, Z. Khan, Manuel S. Alvarez-Alvarado, Y. Zhang, Zhijia Huang, and M. Imran. A Critical Review of Sustainable Energy Policies for the Promotion of Renewable Energy Sources. *Sustainability*, 12:5078, 2020.
- [325] André F. P. Lucena, A. Szklo, R. Schaeffer, and Ricardo Dutra. The Vulnerability of Wind Power to Climate Change in Brazil. *Renewable Energy*, 35:904–912, 2010.
- [326] André F. P. Lucena, A. Szklo, R. Schaeffer, R. Souza, B. Borba, Isabella V.L. Costa, A. Júnior, and S. Cunha. The vulnerability of Renewable Energy to Climate Change in Brazil. *Energy Policy*, 37:879–889, 2009.
- [327] Ben Lumby and A. Miller. Utility Scale Solar Power Plants: A Guide For Developers and Investors. 2011.
- [328] H. Lund and B. Mathiesen. Energy System Analysis of 100% Renewable Energy Systems-The Case of Denmark in Years 2030 and 2050. *Energy*, 34:524–531, 2009.
- [329] D. MacKay. Bayesian Interpolation. *Neural Computation*, 4:415–447, 1992.
- [330] S. H. Madaeni, R. Sioshansi, and P. Denholm. Capacity Value of Concentrating Solar Power Plants. 2011.
- [331] S. H. Madaeni, R. Sioshansi, and P. Denholm. How Thermal Energy Storage Enhances the Economic Viability of Concentrating Solar Power. *Proceedings of the IEEE*, 100:335–347, 2012.
- [332] Siva Ramakrishna Madeti and S. Singh. A Comprehensive Study on Different Types of Faults and Detection Techniques for Solar Photovoltaic System. *Solar Energy*, 158:161–185, 2017.
- [333] G. Makrides, B. Zinsser, G. Georgiou, M. Schubert, and J. Werner. Temperature Behaviour of Different Photovoltaic Systems Installed in Cyprus and Germany. *Solar Energy Materials and Solar Cells*, 93:1095–1099, 2009.
- [334] Monto Mani and R. Pillai. Impact of Dust on Solar Photovoltaic (PV) Performance: Research Status, Challenges and Recommendations. *Renewable & Sustainable Energy Reviews*, 14:3124–3131, 2010.
- [335] J. Manwell, J. G. McGowan, and A. Rogers. Book Review: Wind Energy Explained: Theory, Design and Application. *Wind Engineering*, 30:169 – 170, 2006.
- [336] J. Marcos, L. Marroyo, E. Lorenzo, and M. García. Smoothing of PV Power Fluctuations By Geographical Dispersion. *Progress in Photovoltaics*, 20:226–237, 2012.
- [337] H. Markowitz. Portfolio Selection. *J. Financ.*, 7:77–91, 1952.
- [338] M. Marwali, M. Hai-li, S. M. Shahidehpour, and K. H. Abdul-Rahman. Short Term Generation Scheduling in Photovoltaic-Utility Grid with Battery Storage. *IEEE Transactions on Power Systems*, 13:1057–1062, 1997.
- [339] V. Masson-Delmotte, P. Zhai, H. Pörtner, D. Roberts, J. Skea, P. Shukla, A. Pirani, W. Moufouma-Okia, C. Péan, R. Pidcock, S. Connors, J. B. Matthews, Cheng Yang, Xiaoping Zhou, and L. Steg. Global Warming of 1.5°C: Summary For Policy Makers. 2018.
- [340] Madeleine McPherson, M. Mehos, and P. Denholm. Leveraging Concentrating Solar Power Plant Dispatchability: A Review of the Impacts of Global Market Structures and Policy. *Energy Policy*, 139:111335, 2020.
- [341] G. Meehl, T. Stocker, W. Collins, P. Friedlingstein, T. Gaye, J. Gregory, A. Kitoh, R. Knutti, J. Murphy, A. Noda, S. Raper, I. Watterson, A. Weaver, and Zongci Zhao. Global Climate Projections. 2007.
- [342] G. Meehl and C. Tebaldi. More Intense, More Frequent, and Longer Lasting Heat Waves in the 21st Century. *Science*, 305:994 – 997, 2004.
- [343] M. Mehos, J. Jorgenson, P. Denholm, and C. Turchi. An Assessment of the Net Value of CSP Systems Integrated with Thermal Energy Storage. *Energy Procedia*, 69:2060–2071, 2015.
- [344] P. Meier, M. Vagliasindi, and Imran M. *The Design and Sustainability of Renewable Energy Incentive: An Economic Analysis. Report*. World Bank, Washington, DC, 2015. Available online <http://hdl.handle.net/10986/20524> (accessed on June 21st 2021).
- [345] R. Mendelsohn and M. Schlesinger. Climate-Response Functions. *AMBIO: A Journal of the Human Environment*, 28:362–366, 1999.
- [346] María Mendiluce. Risky Business: Building a Resilient Power Sector. *IEEE Power and Energy Magazine*, 12:34–41, 2014.
- [347] A. A. Merrouni, Ab. Mezrhah, and A. Mezrhah. CSP Sites Suitability Analysis in the Eastern Region of Morocco. *Energy Procedia*, 49:2270–2279, 2014.
- [348] Ahmed Merrouni, Fakhreddine Elalaoui, Abdellatif Ghennioui, and Ahmed Mezrhah. A GIS-AHP Combination for the Sites Assessment of Large-Scale CSP Plants with Dry and Wet Cooling Systems. Case Study: Eastern Morocco. *Solar Energy*, 166:2–12, 05 2018.

- [349] Ahmed Alami Merrouni, Ahmed Mezrhah, Mohammed Amine Moussaoui, and Hanane Ait Lahoussine Ouali. Integration of pv in the moroccan buildings: Simulation of a small roof system installed in eastern morocco. *International Journal of Renewable Energy Research*, 6:306–314, 2016.
- [350] Joseph J. Michalsky. The astronomical almanac’s algorithm for approximate solar position (1950 - 2050). *Solar Energy*, 40:227–235, 1988.
- [351] Torben K. Mideksa and Steffen Kallbekken. The Impact of Climate Change on the Electricity Market: A Review. *Energy Policy*, 38:3579–3585, 2010.
- [352] Kaisa Miettinen. Nonlinear Multiobjective Optimization. In *International Series in Operations Research and Management Science*, 1998.
- [353] M. M. Miglietta, T. Huld, and Fabio Monforti-Ferrario. Local Complementarity of Wind and Solar Energy Resources over Europe: An Assessment Study From a Meteorological Perspective. *Journal of Applied Meteorology and Climatology*, 56:217–234, 2017.
- [354] N. Miller, D. Manz, Jim Roedel, Paul E. Marken, and Erik Kronbeck. Utility Scale Battery Energy Storage Systems. *IEEE PES General Meeting*, pages 1–7, 2010.
- [355] M. Milligan. Modeling Utility-Scale Wind Power Plants Part 2: Capacity Credit. *Wind Energy*, 3:167–206, 2000.
- [356] A. Mills. An Evaluation of Solar Valuation Methods Used in Utility Planning and Procurement Processes. 2014.
- [357] A. Mills. Changes in the Economic Value of Variable Generation at High Penetration Levels: A Pilot Case Study of California. 2014.
- [358] J. Moemken, Mark Reyers, H. Feldmann, and J. Pinto. Future Changes of Wind Speed and Wind Energy Potentials in EURO-CORDEX Ensemble Simulations. *Journal of Geophysical Research*, 123:6373–6389, 2018.
- [359] Azeroual Mohamed, El Aboubakr, Hassan MOUSSAOUI, and Hassane El Markhi. Renewable Energy Potential and Available Capacity for Wind and Solar Power in Morocco Towards 2030. *Journal of Engineering Science and Technology Review*, 11:189–198, 02 2018.
- [360] Sanan T. Mohammad, H. Al-Kayiem, M. Assadi, O. Sabir, and A. K. Khelif. An Integrated Program of a Stand-Alone Parabolic Trough Solar Thermal Power Plant: Code Description And Test. *Case Studies in Thermal Engineering*, 12:26–37, 2018.
- [361] B. Mohandes, L. El-Chaar, and L. Lamont. Application Study of 500 W Photovoltaic (PV) System in the UAE. *Applied Solar Energy*, 45:242–247, 2009.
- [362] H. Mohring, D. Stellbogen, R. Schäffler, S. Oelting, R. Gegenwart, P. Kontinen, T. Carlsson, M. Cendagorta, and W. Herrmann. Outdoor Performance of Polycrystalline Thin Film PV Modules in Different European Climates. 2004.
- [363] A. Monin and A. Obukhov. Basic Laws of Turbulent Mixing in the Ground Layer of Atmosphere. 1954.
- [364] Julián Moral-Carcedo and José Vicéns-Otero. Modelling the Non-Linear Response of Spanish Electricity Demand to Temperature Variations. *Energy Economics*, 27:477–494, 2005.
- [365] Massimo Moser, F. Trieb, and T. Fichter. Potential of Concentrating Solar Power Plants for the Combined Production of Water and Electricity in MENA Countries. *Journal of Sustainable Development of Energy, Water and Environment Systems*, 1:122–140, 2013.
- [366] R. Moss, J. Edmonds, K. Hibbard, M. Manning, S. Rose, D. Vuuren, T. Carter, S. Emori, M. Kainuma, T. Kram, G. Meehl, John F. B. Mitchell, N. Nakicenovic, K. Riahi, Steven J. Smith, R. Stouffer, A. Thomson, J. Weyant, and T. Wilbanks. The Next Generation of Scenarios For Climate Change Research and Assessment. *Nature*, 463:747–756, 2010.
- [367] Mohammed Mraoua and D. Bari. Temperature Stochastic Modeling and Weather Derivatives Pricing: Empirical Study with Moroccan Data. 2009.
- [368] B. Mueller and S. Seneviratne. Systematic Land climate and Evapotranspiration Biases in CMIP5 Simulations. *Geophysical Research Letters*, 41:128 – 134, 2014.
- [369] Björn Müller, M. Wild, A. Driesse, and K. Behrens. Rethinking Solar Resource Assessments in the Context of Global Dimming and Brightening. *Solar Energy*, 99:272–282, 2014.
- [370] Theresa Müller and Steffi Schreiber. How to balance intermittent feed-in from renewable energies? – a techno-economic comparison of flexibility options. 2017.
- [371] P. Nabat, S. Somot, M. Mallet, F. Sevault, M. Chiacchio, and M. Wild. Direct and Semi-Direct Aerosol Radiative Effect on the Mediterranean Climate Variability Using a Coupled Regional Climate System Model. *Climate Dynamics*, 44:1127–1155, 2014.
- [372] Mourad Nachtane. *Énergies Marines Renouvelables et Étude des Performances des Matériaux Composites: Cas d’une Hydrolienne*. PhD thesis, 10 2019.
- [373] Paul Nahmmacher, E. Schmid, M. Pahle, and B. Knopf. Strategies Against Shocks in Power Systems – An Analysis For the Case of Europe. *Energy Economics*, 59:455–465, 2016.
- [374] Nebojsa Nakicenovic, J. Alcamo, G. Davis, B. Vries, J. Fenhann, S. Gaffin, K. Gregory, A. Grubler, T. Jung, T. Kram, E. Rovere, L. Michaelis, S. Mori, T. Morita, William Pepper, H. Pitcher, L. Price, Keywan Riahi, A. Röhrli, H. Rogner, Alexei G. Sankovski, M. Schlesinger, P. Shukla, S. Smith, Ruth Swart, S. V. Rooijen, Nadejda M. Victor, and Z. Da-di. Special Report on Emissions Scenarios: A Special Report of Working Group III of the Intergovernmental Panel on Climate Change. 2000.
- [375] A. Narimani, A. Abeygunawardana, G. Nourbakhsh, G. Ledwich, and G. Walker. Comparing Operational Value of CSP with TES to PV with Battery Storage in Australian National Electricity Market. *2017 Australasian Universities Power Engineering Conference (AUPEC)*, pages 1–5, 2017.
- [376] J. Nelson. The Physics of Solar Cells. 2003.
- [377] J. H. Nelson, J. Johnston, A. Mileva, Matthias Fripp, I. Hoffman, Autumn Petros-Good, Christian Blanco, and D. Kammen. High-Resolution Modeling of the Western North American Power System Demonstrates Low-Cost and Low-Carbon Futures. *Energy Policy*, 43:436–447, 2012.

- [378] G. Nemet. Beyond the Learning Curve: Factors Influencing Cost Reductions in Photovoltaics. *Energy Policy*, 34:3218–3232, 2006.
- [379] H. Nfaoui, J. Buret, and A. Sayigh. Wind Characteristics and Wind Energy Potential in Morocco. *Solar Energy*, 63:51–60, 1998.
- [380] Hassan Nfaoui. Caractéristiques du Gisement Éolien Marocain et Optimisation d’un Système Aérogénérateur/Groupe Électrogène pour l’Électrification des Villages Isolés. 2004.
- [381] Mohamed Nfaoui and Khalil El-hami. Extracting the maximum energy from solar panels. *Energy Reports*, 2018.
- [382] G. Notton, C. Cristofari, M. Mattei, and P. Poggi. Modelling of a Double-Glass Photovoltaic Module Using Finite Differences. *Applied Thermal Engineering*, 25:2854–2877, 2005.
- [383] A. Nottrott, J. Kleissl, and B. Washom. Storage Dispatch Optimization For Grid-Connected Combined Photovoltaic-Battery Storage Systems. *2012 IEEE Power and Energy Society General Meeting*, pages 1–7, 2012.
- [384] A. Nottrott, J. Kleissl, and B. Washom. Energy Dispatch Schedule Optimization and Cost Benefit Analysis For Grid-Connected, Photovoltaic-Battery Storage Systems. *Renewable Energy*, 55:230–240, 2013.
- [385] I. Nygaard and Touria Dafrallah. Utility Led Rural Electrification in Morocco: Combining Grid Extension, Mini-grids, and Solar Home Systems. *Wiley Interdisciplinary Reviews: Energy and Environment*, 5:155–168, 2016.
- [386] Association négaWatt. Synthèse du scénario négawatt 2022.
- [387] Manasseh Obi, S. Jensen, Jennifer B. Ferris, and R. Bass. Calculation of Levelized Costs of Electricity For Various Electrical Energy Storage Systems. *Renewable & Sustainable Energy Reviews*, 67:908–920, 2017.
- [388] A. Odusola and Babatunde O. Abidoye. Effects of Temperature and Rainfall Shocks on Economic Growth in Africa. 2015.
- [389] O. S. Ohunakin, M. Adaramola, O. Oyewola, O. J. Matthew, and R. Fagbenle. The Effect of Climate Change on Solar Radiation in Nigeria. *Solar Energy*, 116:272–286, 2015.
- [390] H. Omrani, P. Drobinski, T. Arsouze, S. Bastin, C. Lebeaupin-Brossier, and S. Mailler. Spatial and Temporal Variability of Wind Energy Resource and Production Over the North Western Mediterranean Sea: Sensitivity to Air-Sea Interactions. *Renewable Energy*, 101:680–689, 2017.
- [391] Janosch Ondraczek, N. Komendantova, and A. Patt. WACC the Dog: The Effect of Financing Costs on the Levelized Cost of Solar PV Power. *Renewable Energy*, 75:888–898, 2015.
- [392] F. Onea, L. Deleanu, L. Rusu, and C. Georgescu. Evaluation of the Wind Energy Potential Along the Mediterranean Sea Coasts. *Energy Exploration & Exploitation*, 34:766 – 792, 2016.
- [393] A. Ouammi, D. Zejli, H. Dagdougui, and R. Benchrif. Artificial Neural Network Analysis of Moroccan Solar Potential. *Renewable & Sustainable Energy Reviews*, 16:4876–4889, 2012.
- [394] M. Oukili, S. Zouggar, M. Seddik, T. Ouchbel, F. Vallée, and Mohamed El Hafiani. Comparative Study of the Moroccan Power Grid Reliability in Presence of Photovoltaic and Wind Generation. *Smart Grid and Renewable Energy*, 4:366–377, 2013.
- [395] M. Oukili, S. Zouggar, M. Seddik, F. Vallée, M. E. Hafyani, and T. Ouchbel. Evaluation of the Moroccan Power Grid Adequacy with Introduction of Concentrating Solar Power (CSP) Using Solar Tower and Parabolic Trough Mirrors Technology. *Energy Procedia*, 42:113–122, 2013.
- [396] Ismail Ouraich and W. Tyner. Moroccan Agriculture, Climate change, and the Moroccan Green Plan: A CGE Qnalysis. *African Journal of Agricultural and Resource Economics*, 13, 2018.
- [397] Özlem Özkizilkaya. Thermosensibilité de la Demande électrique : Identification de la Part Non Linéaire par Couplage d’une Modélisation Bottom-up et de l’Approche Bayésienne. 2014.
- [398] B. Palmintier, R. Broderick, B. Mather, M. Coddington, K. Baker, F. Ding, M. Reno, M. Lave, and Ashwini Bharatkumar. On the Path to SunShot. Emerging Issues and Challenges in Integrating Solar with the Distribution System. 2016.
- [399] Z. Pan, R. Arritt, E. Takle, W. Gutowski, C. J. Anderson, and M. Segal. Altered Hydrologic Feedback in a Warming Climate Introduces A “Warming Hole”. *Geophysical Research Letters*, 31, 2004.
- [400] I. Panagea, I. Tsanis, A. Koutroulis, and M. Grillakis. Climate Change Impact on Photovoltaic Energy Output: The Case of Greece. *Advances in Meteorology*, 2014:85–106, 2014.
- [401] A. Papadopoulou, George Vasileiou, and A. Flamos. A Comparison of Dispatchable RES Technoeconomics: Is There a Niche for Concentrated Solar Power? *Energies*, 13:4768, 2020.
- [402] R. Pasicko, C. Branković, and Z. Simic. Assessment of Climate Change Impacts on Energy Generation From Renewable Sources in Croatia. *Renewable Energy*, 46:224–231, 2012.
- [403] A. Patnode. *Simulation and Performance Evaluation of Parabolic Trough Solar Power Plants*. PhD thesis, PhD Thesis, University of Wisconsin-Madison., 2006. Available online <http://digital.library.wisc.edu/1793/7590> (accessed on June 21st 2021).
- [404] A. Patt, S. Pfenninger, and Johan Lilliestam. Vulnerability of Solar Energy Infrastructure and Output to Extreme Events: Climate Change Implications (Conference paper). 2010.
- [405] A. Patt, S. Pfenninger, and Johan Lilliestam. Vulnerability of Solar Energy Infrastructure and Output to Climate Change. *Climatic Change*, 121:93–102, 2013.
- [406] I. Pawel. The Cost of Storage – How to Calculate the Levelized Cost of Stored Energy (LCOE) and Applications to Renewable Energy Generation. *Energy Procedia*, 46:68–77, 2014.
- [407] Stephen Peake. Renewable energy - power for a sustainable future. 2018.
- [408] J. C. Perez, A. Gonzalez, J. P. Díaz, F. Expósito, and Jonatan Felipe. Climate Change Impact on Future Photovoltaic Resource Potential in an Orographically Complex Archipelago, the Canary Islands. *Renewable Energy*, 133:749–759, 2019.

- [409] R. Perez, M. David, T. Hoff, M. Jamaly, S. Kivalov, J. Kleissl, P. Lauret, and Marc J. R. Perez. Spatial and Temporal Variability of Solar Energy. 2016.
- [410] V. Pérez-Andreu, Carolina Aparicio-Fernández, A. Martínez-Ibernón, and José-L. Vivancos. Impact of Climate Change on Heating and Cooling Energy Demand in a Residential Building in a Mediterranean Climate. *Energy*, 165:63–74, 2018.
- [411] J. Peter. How Does Climate Change Affect Electricity System Planning and Optimal Allocation of Variable Renewable Energy. *Applied Energy*, 252:113397, 2019.
- [412] M. Peters, T. Schmidt, D. Wiederkehr, and M. Schneider. Shedding Light on Solar Technologies—A Techno-Economic Assessment and its Policy Implications. *Energy Policy*, 39:6422–6439, 2011.
- [413] E. Peterson and Joseph P. Hennessey. On the Use of Power Laws for Estimates of Wind Power Potential. *Journal of Applied Meteorology*, 17:390–394, 1978.
- [414] Mario Petrollese and Daniele Cocco. Optimal Design of a Hybrid CSP-PV plant for Achieving the Full Dispatchability of Solar Energy Power Plants. *Solar Energy*, 137:477–489, 11 2016.
- [415] Uwe Pfeifroth, A. Sanchez-Lorenzo, V. Manara, J. Trentmann, and R. Hollmann. Trends and Variability of Surface Solar Radiation in Europe Based On Surface- and Satellite-Based Data Records. 2018.
- [416] R. Philipona, K. Behrens, and C. Ruckstuhl. How Declining Aerosols and Rising Greenhouse Gases Forced Rapid Warming in Europe Since the 1980s. *Geophysical Research Letters*, 36, 2009.
- [417] Nicolas Plain, B. Hingray, and Sandrine Mathy. Accounting For Low Solar Resource Days to Size 100% Solar Microgrids Power Systems in Africa. *Renewable Energy*, 131:448–458, 2019.
- [418] Werner J. Platzer. Combined Solar Thermal and Photovoltaic Power Plants: An Approach to 24h Solar Electricity? *AIP Conference Proceedings*, 2016.
- [419] A. Polman, M. Knight, E. Garnett, B. Ehrler, and W. Sinke. Photovoltaic Materials: Present Efficiencies and Future Challenges. *Science*, 352, 2016.
- [420] A. Possner and K. Caldeira. Geophysical Potential For Wind Energy Over the Open Oceans. *Proceedings of the National Academy of Sciences of the United States of America*, 114:11338 – 11343, 2017.
- [421] A. Poullikkas. A Comparative Overview of Large-Scale Battery Systems for Electricity Storage. *Renewable & Sustainable Energy Reviews*, 27:778–788, 2013.
- [422] Jordan G. Powers, J. Klemp, W. Skamarock, C. A. Davis, J. Dudhia, D. Gill, J. Coen, D. Gochis, R. Ahmadv, S. Peckham, G. Grell, J. Michalakes, S. Trahan, S. Benjamin, C. Alexander, G. Dimego, Wei Wang, C. Schwartz, G. Romine, Z. Liu, C. Snyder, Fei Chen, M. Barlage, W. Yu, and M. Duda. The Weather Research and Forecasting Model: Overview, System Efforts, and Future Directions. *Bulletin of the American Meteorological Society*, 98:1717–1737, 2017.
- [423] D. Pozo-Vázquez, F. J. Santos-Alamillos, V. Lara-Fanego, J. A. Ruiz-Arias, and J. Tovar-Pescador. The Impact of the NAO on the Solar and Wind Energy Resources in the Mediterranean Area. 2011.
- [424] D. Pozo-Vázquez, J. Tovar-Pescador, S. Gámiz-Fortis, M. J. Esteban-Parra, and Y. Castro-Díez. NAO and Solar Radiation Variability in the European North Atlantic Region. *Geophysical Research Letters*, 31, 2004.
- [425] R. Praveen, M. Baseer, A. Awan, and Muhammad Zubair. Performance Analysis and Optimization of a Parabolic Trough Solar Power Plant in the Middle East Region. *Energies*, 11:741, 2018.
- [426] A. Prein, W. Langhans, G. Fossler, A. Ferrone, N. Ban, K. Goergen, Michael Keller, M. Tölle, O. Gutjahr, F. Feser, Erwan Brisson, S. Kollet, J. Schmidli, N. V. van Lipzig, and R. Leung. A Review on Regional Convection-Permitting Climate Modeling: Demonstrations, Prospects, and Challenges. *Reviews of Geophysics (Washington, D.C. : 1985)*, 53:323 – 361, 2015.
- [427] J. Prospero and P. Lamb. African Droughts and Dust Transport to the Caribbean: Climate Change Implications. *Science*, 302:1024 – 1027, 2003.
- [428] S. Pryor and R. Barthelmie. Climate Change Impacts on Wind Energy: A Review. *Renewable & Sustainable Energy Reviews*, 14:430–437, 2010.
- [429] S. Pryor and R. Barthelmie. Assessing the Vulnerability of Wind Energy to Climate Change and Extreme Events. *Climatic Change*, 121:79–91, 2013.
- [430] S. Pryor, R. Barthelmie, and E. Kjellström. Potential Climate Change Impact on Wind Energy Resources in Northern Europe: Analyses Using a Regional Climate Model. *Climate Dynamics*, 25:815–835, 2005.
- [431] S. Pryor, J. Schoof, and R. Barthelmie. Climate Change Impacts on Wind Speeds and Wind Energy Density in Northern Europe: Empirical Downscaling of Multiple AOGCMs. *Climate Research*, 29:183–198, 2005.
- [432] S. Quoilin, K. Kavvadias, A. Mercier, Irene Pappone, and A. Zucker. Quantifying Self-Consumption Linked to Solar Home Battery Systems: Statistical Analysis and Economic Assessment. *Applied Energy*, 182:58–67, 2016.
- [433] E. Radziemska. The Effect of Temperature on the Power Drop in Crystalline Silicon Solar Cells. *Renewable Energy*, 28:1–12, 2003.
- [434] P. Räisänen and H. Järvinen. Impact of Cloud and Radiation Scheme Modifications on Climate Simulated by the ECHAM5 Atmospheric GCM. *Quarterly Journal of the Royal Meteorological Society*, 136:1733–1752, 2010.
- [435] D Ramin Jalilvand. *Renewable Energy for the Middle East and North Africa: Policies for a Successful Transition*. Friedrich Ebert Stiftung, Berlin, Germany, 2012. Available online <http://library.fes.de/pdf-files/iez/08959.pdf> (accessed on June 21st 2021).
- [436] Khalid Raouz. Morocco’s Energy System Forecasted Using LEAP. *ROYAL INSTITUTE OF TECHNOLOGY*, 2015.
- [437] D. Rasmussen, T. Holloway, and G. Nemet. Opportunities and Challenges in Assessing Climate Change Impacts on Wind Energy—A Critical Comparison of Wind Speed Projections in California. *Environmental Research Letters*, 6:024008, 2011.

- [438] A. Razak, Y. Irwan, W. Leow, M. Irwanto, I. Safwati, and M. Zhafarina. Investigation of the Effect Temperature on Photovoltaic (PV) Panel Output Performance. *International Journal on Advanced Science, Engineering and Information Technology*, 6:682–688, 2016.
- [439] J. Redelsperger, C. Thorncroft, A. Diedhiou, T. Lebel, D. Parker, and J. Polcher. African Monsoon Multidisciplinary Analysis: An International Research Project and Field Campaign. *Bulletin of the American Meteorological Society*, 87:1739–1746, 2006.
- [440] J. W. Reed. Wind Power Climatology. *Weatherwise*, 27:236–242, 1974.
- [441] N. Reich, B. Mueller, A. Armbruster, W. V. Sark, K. Kiefer, and C. Reise. Performance Ratio revisited: Are PR>90% Realistic? *Progress in Photovoltaics*, 20:717–726, 2012.
- [442] D. T. Reindl, W. Beckman, and J. Duffie. Diffuse Fraction Correlations. *Solar Energy*, 45:1–7, 1990.
- [443] D. T. Reindl, W. Beckman, and J. Duffie. Evaluation of Hourly Tilted Surface Radiation Models. *Solar Energy*, 45:9–17, 1990.
- [444] J. Remund and S. C. Müller. Trends in Global Radiation Between 1950 and 2100. 2010.
- [445] Ren. Renewables 2019 Global Status Report. 2012.
- [446] REN21. *Renewables 2020 Global Status Report*. REN21, Paris, France, 2020. Available online https://www.ren21.net/wp-content/uploads/2019/05/gsr_2020_full_report_en.pdf (accessed on June 21st 2021).
- [447] REN21. *Renewables 2021 Global Status Report*. REN21, Paris, France, 2020. Available online https://www.ren21.net/wp-content/uploads/2019/05/GSR2021_Full_Report.pdf (accessed on June 21st 2021).
- [448] Mark Meyers, J. Moemken, and J. Pinto. Future Changes of Wind Energy Potentials Over Europe in a Large CMIP5 Multi-Model Ensemble. *International Journal of Climatology*, 36:783–796, 2015.
- [449] S. N. Rezaei, L. Chouinard, S. Langlois, and F. Légeron. Analysis of the Effect of Climate Change on the Reliability of Overhead Transmission Lines. *Sustainable Cities and Society*, 27:137–144, 2016.
- [450] K. Riahi, S. Rao, V. Krey, C. Cho, V. Chirkov, G. Fischer, G. Kindermann, N. Nakicenovic, and P. Rafaj. RCP 8.5— A Scenario of Comparatively High Greenhouse Gas Emissions. *Climatic Change*, 109:33–57, 2011.
- [451] C Richts. The Moroccan Solar Plan: A Comparative Analysis of CSP and PV Utilization Until 2020. Master’s thesis, University of Kassel, Kassel, Germany, 2012. Available online https://inis.iaea.org/search/search.aspx?orig_q=RN:47087488 (accessed on June 21st 2021).
- [452] Y. Riffonneau, S. Bacha, F. Barruel, and S. Ploix. Optimal Power Flow Management for Grid Connected PV Systems With Batteries. *IEEE Transactions on Sustainable Energy*, 2:309–320, 2011.
- [453] L. A. Roberto, Jaeger-Waldau Arnulf, Vellei Marika, Sigfusson Bergur, M. Davide, Jakubcionis Mindaugas, Perez Fortes Maria Del Mar, Lazarou Stavros, Giuntoli Jacopo, Weidner Ronnefeld Eveline, De Marco Giancarlo, S. Amanda, and Gutierrez Moles Carmen. ETRI 2014 - Energy Technology Reference Indicator Projections For 2010-2050. 2014.
- [454] Rolando A. Rodríguez, Sarah Becker, G. Andresen, D. Heide, and M. Greiner. Transmission Needs Across a Fully Renewable European Power System. *Renewable Energy*, 63:467–476, 2014.
- [455] B. Rothstein, S. Mimler, U. Müller, , and L. O’enschläger. The Electricity Industry as Stakeholder of Climate Change. Contribution to the Second National Workshop of EPA, Adaptation to Climate Change in Germany—Regional Scenarios and National Tasks. 2006.
- [456] A. Røyne, C. Dey, and D. Mills. Cooling of Photovoltaic Cells under Concentrated Illumination: A Critical Review. *Solar Energy Materials and Solar Cells*, 86:451–483, 2005.
- [457] E. Rubin, I. Azevedo, P. Jaramillo, and Sonia Yeh. A Review of Learning Rates For Electricity Supply Technologies. *Energy Policy*, 86:198–218, 2015.
- [458] J. A. Ruiz-Arias, C. Arbizu-Barrena, F. J. Santos-Alamillos, J. Tovar-Pescador, and D. Pozo-Vázquez. Assessing the Surface Solar Radiation Budget in the WRF Model: A Spatiotemporal Analysis of the Bias and Its Causes. *Monthly Weather Review*, 144:703–711, 2016.
- [459] J. A. Ruiz-Arias, J. Dudhia, and C. Gueymard. A Simple Parameterization of the Short-Wave Aerosol Optical Properties For Surface Direct and Diffuse Irradiances Assessment in a Numerical Weather Model. *Geoscientific Model Development*, 7:1159–1174, 2014.
- [460] M. Rummukainen. State-of-the-Art with Regional Climate Models. *Wiley Interdisciplinary Reviews: Climate Change*, 1:82–96, 2010.
- [461] Eirik Andre Rye, Arne Lie, and Harald G. Svendsen. Analyzing Large-Scale Renewable Energy Integration and Energy Storage in Morocco using a Flow-based Market Model. *2016 13th International Conference on the European Energy Market (EEM)*, pages 1–5, 2016.
- [462] P. Samuelsson, C. Jones, Ulrika Will’En, A. Ullerstig, Stefan Gollvik, Ulf Hansson, E. Jansson, Christer Kjellström, G. Nikulin, and K. Wyser. The Rossby Centre Regional Climate model RCA3: Model Description and Performance. *Tellus A: Dynamic Meteorology and Oceanography*, 63:23 – 4, 2011.
- [463] A. Sanchez-Lorenzo, Aaron Enriquez-Alonso, M. Wild, J. Trentmann, S. Vicente-Serrano, Alejandro Sanchez-Romero, R. Posselt, and M. Z. Hakuba. Trends in Downward Surface Solar Radiation From Satellites and Ground Observations Over Europe During 1983–2010. *Remote Sensing of Environment*, 189:108–117, 2017.
- [464] M. Sarniak. Researches of the Impact of the Nominal Power Ratio and Environmental Conditions on the Efficiency of the Photovoltaic System: A Case Study for Poland in Central Europe. *Sustainability*, 12:6162, 2020.
- [465] Kelvin Say, W. Schill, and M. John. Degrees of Displacement: The Impact of Household PV Battery Prosumage on Utility Generation and Storage. *ArXiv*, abs/2003.06987, 2020.
- [466] G. Schellekens, A. Battaglini, Johan Lilliestam, J. McDonnell, and A. Patt. *100% Renewable Electricity — A Roadmap to 2050 For Europe and North Africa. Report*, 2010. Available online <https://www.pwc.co.uk/assets/pdf/100-percent-renewable-electricity.pdf> (accessed on June 21st 2021).

- [467] Thomas Schinko, Sönke Bohm, Nadejda Komendantova, El Mostafa Jamea, and Marina Blohm. Morocco's Sustainable Energy Transition and the Role of Financing Costs: A Participatory Electricity System Modeling Approach. *Energy, Sustainability and Society*, 9, 12 2019.
- [468] Thomas Schinko and Nadejda Komendantova. De-risking Investment into Concentrated Solar Power in North Africa: Impacts on the Costs of Electricity Generation. *Renewable Energy*, 92:262–272, 2016.
- [469] Markus Schlott, A. Kies, Tom Brown, S. Schramm, and M. Greiner. The Impact of Climate Change on a Cost-Optimal Highly Renewable European Electricity Network. *Applied Energy*, 230:1645–1659, 2018.
- [470] Oliver Schmidt, Sylvain Melchior, A. Hawkes, and I. Staffell. Projecting the Future Levelized Cost of Electricity Storage Technologies. *Joule*, 3:81–100, 2019.
- [471] W. Schram, I. Lampropoulos, and W. V. Sark. Photovoltaic Systems Coupled with Batteries that are Optimally Sized for Household Self-Consumption: Assessment of Peak Shaving Potential. *Applied Energy*, 223:69–81, 2018.
- [472] C. Schwalm, Spencer Glendon, and P. Duffy. RCP 8.5 Tracks Cumulative CO₂ Emissions. *Proceedings of the National Academy of Sciences of the United States of America*, 117:19656 – 19657, 2020.
- [473] G. Schwerhoff and Mouhamadou Sy. Financing Renewable Energy in Africa – Key Challenge of the Sustainable Development Goals. *Renewable & Sustainable Energy Reviews*, 75:393–401, 2017.
- [474] Michael Scioletti, A. Newman, Johanna K. Goodman, Alexander J. Zolan, and S. Leyffer. Optimal Design and Dispatch of a System of Diesel Generators, Photovoltaics and Batteries For Remote Locations. *Optimization and Engineering*, 18:755–792, 2017.
- [475] L. Sedefian. On the Vertical Extrapolation of Mean Wind Power Density. *Journal of Applied Meteorology*, 19:488–493, 1980.
- [476] M. Segal, Z. Pan, R. Arritt, and E. Takle. On the Potential Change in Wind Power Over the US due to increases of Atmospheric Greenhouse Gases. *Renewable Energy*, 24:235–243, 2001.
- [477] Z. Sen, Abdüsselam Altunkaynak, and T. Erdik. Wind Velocity Vertical Extrapolation by Extended Power Law. *Advances in Meteorology*, 2012:1–6, 2012.
- [478] J. Shi, W. Lee, Y. Liu, Y. Yang, and P. Wang. Forecasting Power Output of Photovoltaic Systems Based on Weather Classification and Support Vector Machines. *IEEE Transactions on Industry Applications*, 48:1064–1069, 2012.
- [479] Behrang Shirizadeh, Q. Perrier, and P. Quirion. *How Sensitive Are Optimal Fully Renewable Power Systems to Technology Cost Uncertainty?* FAERE Policy Paper, CIRED, Paris, France, 2019. Available online http://faere.fr/pub/PolicyPapers/Shirizadeh_Perrier_Quirion_FAERE_PP2019_04.pdf (accessed on June 21st 2021).
- [480] R. Shouman and H. Ezz. Forecasting Transition Electricity Solar Energy From MENA To Europe ENAS. 2016.
- [481] J. P. Sierra, Ricard Castrillo, M. Mestres, C. Möso, P. Lionello, and L. Marzo. Impact of Climate Change on Wave Energy Resource in the Mediterranean Coast of Morocco. *Energies*, 13:2993, 2020.
- [482] J.P.M. Sijm. *Cost and Revenue Related Impacts of Integrating Electricity From Variable Renewable Energy Into the Power System — A Review of Recent Literature*. (ECN–E-14-022). ECN, Petten, 2014.
- [483] Jo Silva and Rui Castro. Modeling and Simulation of a Parabolic Trough Power Plant. *Green*, 2:97–104, 01 2012.
- [484] R. Sioshansi, S. H. Madaeni, and P. Denholm. A Dynamic Programming Approach to Estimate the Capacity Value of Energy Storage. *IEEE Transactions on Power Systems*, 29:395–403, 2014.
- [485] D. Sisterson and P. Frenzen. Nocturnal Boundary-Layer Wind Maxima and the Problem of Wind Power Assessment. *Environmental Science & Technology*, 12:218–221, 1978.
- [486] C. Skamarock, B. Klemp, J. Dudhia, O. Gill, D. Barker, G. Duda, Xiang yu Huang, W. Wang, and G. Powers. A Description of the Advanced Research WRF Version 3. 2008.
- [487] J. R. Snape. Spatial and Temporal Characteristics of PV Adoption in the UK and Their Implications for the Smart Grid. *Energies*, 9:1–18, 2016.
- [488] Kepa Solaun and E. Cerdá. Climate Change Impacts on Renewable Energy Generation. A Review of Quantitative Projections. *Renewable & Sustainable Energy Reviews*, 116:109415, 2019.
- [489] Kepa Solaun and E. Cerdá. Impacts of Climate Change on Wind Energy Power – Four Wind Farms in Spain. *Renewable Energy*, 145:1306–1316, 2020.
- [490] A. A. Solomon, D. Kammen, and D. Callaway. Investigating the Impact of Wind–solar Complementarities on Energy Storage Requirement and the Corresponding Supply Reliability Criteria. *Applied Energy*, 168:130–145, 2016.
- [491] S. Solomon, D. Qin, M. Manning, Z. Chen, M. Marquis, K. Averyt, M. Tignor, and H. L. Miller. Climate Change 2007: The Physical Science Basis. Contribution of Working Group I to the Fourth Assessment Report of the Intergovernmental Panel on Climate Change. Summary for Policymakers. 2007.
- [492] S. Spiecker and C. Weber. The Future of the European Electricity System and the Impact of Fluctuating Renewable Energy – A Scenario Analysis. *Energy Policy*, 65:185–197, 2014.
- [493] R. Stanfield, X. Dong, B. Xi, A. Kennedy, A. Genio, Patrick Minnia, and J. Jiang. Assessment of NASA GISS CMIP5 and Post-CMIP5 Simulated Clouds and TOA Radiation Budgets Using Satellite Observations. Part I: Cloud Fraction and Properties. *Journal of Climate*, 27:4189–4208, 2014.
- [494] M. Stanton, S. Dessai, and J. Paavola. A Systematic Review of the Impacts of Climate Variability and Change on Electricity Systems in Europe. *Energy*, 109:1148–1159, 2016.
- [495] Allan Starke, Jose Cardemil, Rodrigo Escobar, and Sergio Colle. Assessing the Performance of Hybrid CSP + PV Plants in Northern Chile. *Solar Energy*, 138, 11 2016.

- [496] S. Sterl, S. Liersch, H. Koch, N. V. Lipzig, and W. Thiery. A New Approach For Assessing Synergies of Solar and Wind Power: Implications For West Africa. *Environmental Research Letters*, 13:094009, 2018.
- [497] W. B. Stine and R. Harrigan. *Solar Energy Fundamentals and Design : With Computer Applications*. 1985.
- [498] William B. Stine and Michael Geyer. *Power From The Sun*. 4 edition, 2001. <https://www.powerfromthesun.net/book.html>.
- [499] T. Stocker, D. Qin, G. Plattner, M. Tignor, S. Allen, J. Boschung, A. Nauels, Y. Xia, Vincent Bex, P. Midgley, L. Alexander, Nathaniel L. Bindoff, François-Marie Bréon, J. Church, U. Cubasch, S. Emori, P. Forster, P. Friedlingstein, N. Gillett, J. Gregory, D. Hartmann, E. Jansen, B. Kirtman, R. Knutti, K. K. Kanikicharla, P. Lemke, J. Marotzke, V. MASSON-DELMOTTE, G. Meehl, I. Mokhov, S. Piao, Qin Da-he, V. Ramaswamy, D. Randall, M. Rhein, M. Rojas, C. Sabine, D. Shindell, L. Talley, D. Vaughan, S. Xie, M. Allen, O. Boucher, D. Chambers, J. Christensen, P. Ciais, P. Clark, M. Collins, J. C. Comiso, V. V. Menezes, R. Feely, T. Fichet, A. M. Fiore, G. Flato, J. Fuglestad, G. Hegerl, P. Hezel, G. Johnson, G. Kaser, V. Kattsov, J. Kennedy, A. K. Tank, C. L. Quéré, G. Myhre, T. Osborn, A. Payne, J. Perlwitz, S. Power, M. Prather, S. Rintoul, J. Rogelj, Thomas F. RStocker, M. Rusticucci, M. Schulz, J. Sedlacek, P. Stott, R. Sutton, P. Thorne, and D. Wuebbles. *Climate Change 2013. The Physical Science Basis. Working Group I Contribution to the Fifth Assessment Report of the Intergovernmental Panel on Climate Change - Abstract For Decision-Makers*. 2013.
- [500] G. Strandberg, L. Bärring, Ulf Hansson, C. Jansson, C. Jones, E. Kjellström, Marco Kupiainen, G. Nikulin, P. Samuelsson, and A. Ullerstig. CORDEX Scenarios For Europe From the Rossby Centre Regional Climate Model RCA4. 2015.
- [501] Suphachol Suphachalasai, M. Touati, F. Ackerman, A. P. Knight, Devi Glick, Ariel I. Horowitz, John A Rogers, and Tayeb Amegroud. Morocco - Energy Policy MRV : Emission Reductions from Energy Subsidies Reform and Renewable Energy Policy. 2018.
- [502] H. Svendsen, A. A. Shetaya, and K. Loudiyi. Integration of Renewable Energy and the Benefit of Storage From a Grid and Market Perspective - Results From Morocco and Egypt Case Studies. *2016 International Renewable and Sustainable Energy Conference (IRSEC)*, pages 1164–1168, 2016.
- [503] M. Syed, Gregory M. Morrison, and J. Darbyshire. Shared Solar and Battery Storage Configuration Effectiveness For Reducing the Grid Reliance of Apartment Complexes. *Energies*, 13:4820, 2020.
- [504] A. Tantet, M. Stéfanon, P. Drobinski, J. Badosa, Silvia Concettini, A. Créti, C. D’Ambrosio, D. Thomopoulos, and P. Tankov. E4clim 1.0: The Energy for a Climate Integrated Model: Description and Application to Italy. *Energies*, 12:4299, 2019.
- [505] B. Tarroja, F. Mueller, Joshua D. Eichman, J. Brouwer, and S. Samuelsen. Spatial and Temporal Analysis of Electric Wind Generation Intermittency and Dynamics. *Renewable Energy*, 36:3424–3432, 2011.
- [506] K. Taylor, R. Stouffer, and G. Meehl. An Overview of CMIP5 and the Experiment Design. *Bulletin of the American Meteorological Society*, 93:485–498, 2012.
- [507] C. Tebaldi and R. Knutti. The Use of the Multi-Model Ensemble in Probabilistic Climate Projections. *Philosophical Transactions of the Royal Society A: Mathematical, Physical and Engineering Sciences*, 365:2053 – 2075, 2007.
- [508] H. Tennekes. The Logarithmic Wind Profile. *Journal of the Atmospheric Sciences*, 30:234–238, 1973.
- [509] Eric J Tervo, Kenechi A. Agbim, F. DeAngelis, J. Hernandez, H. Kim, and Adewale Odukumaiya. An Economic Analysis of Residential Photovoltaic Systems with Lithium Ion Battery Storage in the United States. *Renewable & Sustainable Energy Reviews*, 94:1057–1066, 2018.
- [510] M. Thatcher. Modelling Changes To Electricity Demand Load Duration Curves As a Consequence of Predicted Climate Change For Australia. *Energy*, 32:1647–1659, 2007.
- [511] D. Thevenard and S. Pelland. Estimating the Uncertainty in Long-Term Photovoltaic Yield Predictions. *Solar Energy*, 91:432–445, 2013.
- [512] G. Thompson and T. Eidhammer. A Study of Aerosol Impacts on Clouds and Precipitation Development in a Large Winter Cyclone. *Journal of the Atmospheric Sciences*, 71:3636–3658, 2014.
- [513] H. Thornton, A. Scaife, B. Hoskins, and D. Brayshaw. The Relationship Between Wind Power, Electricity Demand and Winter Weather Patterns in Great Britain. *Environmental Research Letters*, 12:064017, 2017.
- [514] J. Thornton. The Effect of Sandstorms on PV Arrays and Components. 1992.
- [515] Ijjou Tizgui, Fatima Guezar, Hassane Bouzahir, and A. N. Vargas. Estimation and Analysis of Wind Electricity Production Cost in Morocco. *International Journal of Energy Economics and Policy*, 8:58–66, 05 2018.
- [516] Isabelle Tobin, W. Greuell, S. Jerez, F. Ludwig, R. Vautard, M. Vliet, and François-Marie Bréon. Vulnerabilities and Resilience of European Power Generation to 1.5°C, 2°C and 3°C Warming. *Environmental Research Letters*, 13:044024, 2018.
- [517] Isabelle Tobin, S. Jerez, R. Vautard, F. Thais, E. Meijgaard, A. F. Prein, M. Déqué, S. Kotlarski, C. F. Maule, G. Nikulin, T. Noel, and C. Teichmann. Climate Change Impacts on the Power Generation Potential of a European Mid-Century Wind Farms Scenario. *Environmental Research Letters*, 11:034013, 2016.
- [518] Isabelle Tobin, R. Vautard, I. Balog, François-Marie Bréon, S. Jerez, P. Ruti, F. Thais, M. Vrac, and P. Yiou. Assessing Climate Change Impacts on European Wind Energy From Ensembles High-Resolution Climate Projections. *Climatic Change*, 128:99–112, 2014.
- [519] G. Totschnig, R. Hirner, A. Müller, L. Kranzl, M. Hummel, H. Nachtnebel, P. Stanzel, I. Schicker, and H. Formayer. Climate Change Impact and Resilience in the Electricity Sector: The Example of Austria and Germany. *Energy Policy*, 103:238–248, 2017.
- [520] K. Trenberth and J. Fasullo. Global Warming Due To Increasing Absorbed Solar Radiation. *Geophysical Research Letters*, 36, 2009.
- [521] K. Trenberth and S. Josey. *Observations: Surface and Atmospheric Climate Change*. 2007.
- [522] F. Trieb. AQUA-CSP Concentrating Solar Power for Seawater Desalination - Final Report. 2007. Available online <https://www.artelys.com/wp-content/uploads/2019/04/S1-Optimal-flexibility-portfolios-for-a-high-RES-2050-scenario.pdf> (accessed on June 21st 2021).

- [523] F. Trieb, D. Hess, J. Kern, T. Fichter, Massimo Moser, U. Pfenning, N. Caldez, C. Rúa, A. Türk, D. Frieden, A. E. Gharra, Nicolas Cottret, A. Beneking, Saskia Ellenbeck, and Johan Lilliestam. Bringing Europe and Third Countries Closer Together Through Renewable Energies: D3.5: North Africa Case Study Final Report. 2015.
- [524] F. Trieb, Marlene O’Sullivan, T. Pregger, C. Schillings, and W. Krewitt. Characterisation of Solar Electricity Import Corridors from MENA to Europe. 2009.
- [525] Falko Ueckerdt, R.J. Brecha, and Gunnar Luderer. Analyzing Major Challenges of Wind and Solar Variability in Power Systems. *SSRN Electronic Journal*, 81, 01 2014.
- [526] Falko Ueckerdt, Robert Brecha, Gunnar Luderer, Patrick Sullivan, Eva Schmid, Nico Bauer, Diana Bottger, and Robert Pietzcker. Representing Power Sector Variability and the Integration of Variable Renewables in Long-Term Energy-Economy Models using Residual Load Duration Curves. *Energy (Oxford)*, 90(2), 10 2015.
- [527] Falko Ueckerdt, Robert Pietzcker, Yvonne Scholz, Daniel Stetter, Anastasis Giannousakis, and Gunnar Luderer. Decarbonizing Global Power Supply Under Region-Specific Consideration of Challenges and Options of Integrating Variable Renewables in the REMIND Model. *Energy Economics*, 06 2016.
- [528] Arun Kumar V, Ashu Verma, and Lavleen Singal. An Economic Examination of Solar Energy with Storage Based Supply Options: Solar PV-Battery and CSP with Thermal-Storage. *International Journal of Engineering and Advanced Technology (IJEAT) ISSN: 2249 – 8958, Volume-8, Issue-6S3*, pages 1–5, 2019.
- [529] A. van Stiphout, Kristof De Vos, and Geert Deconinck. The Impact of Operating Reserves on Investment Planning of Renewable Power Systems. *IEEE Transactions on Power Systems*, 32:378–388, 2017.
- [530] John van Zalk and Paul Behrens. The spatial extent of renewable and non-renewable power generation: A review and meta-analysis of power densities and their application in the u.s. *Energy Policy*, 2018.
- [531] A. D. L. Vara, C. Gutiérrez, Juan Jesús González-Alemán, and M. Gaertner. Intercomparison Study of the Impact of Climate Change on Renewable Energy Indicators on the Mediterranean Islands. *Atmosphere*, 11:1036, 2020.
- [532] D. Villanueva, A. Feijóo, and J. Pazos. Multivariate Weibull Distribution for Wind Speed and Wind Power Behavior Assessment. *Resources*, 2:370–384, 2013.
- [533] A. Voldoire, E. Sanchez-Gomez, D. Salas y Mélia, B. Decharme, C. Cassou, S. Sénési, S. Valcke, I. Beau, A. Alias, M. Chevallier, M. Déqué, J. Deshayes, H. Douville, E. Fernandez, G. Madec, E. Maisonnave, M. Moine, S. Planton, D. Saint-Martin, S. Szopa, S. Tyteca, R. Alkama, S. Belamari, A. Braun, L. Coquart, and F. Chauvin. The CNRM-CM5.1 Global Climate Model: Description and Basic Evaluation. *Climate Dynamics*, 40:2091–2121, 2012.
- [534] D. Vuuren, J. Edmonds, M. Kainuma, K. Riahi, A. Thomson, K. Hibbard, G. Hurtt, T. Kram, V. Krey, J. Lamarque, T. Masui, M. Meinshausen, N. Nakicenovic, S. Smith, and S. Rose. The Representative Concentration Pathways: An Overview. *Climatic Change*, 109:5–31, 2011.
- [535] J. Wachsmuth, A. Blohm, S. Gößling-Reisemann, T. Eickemeier, M. Ruth, Rebecca Gasper, and S. Stührmann. How will Renewable Power Generation be Affected by Climate Change? The Case of a Metropolitan Region in Northwest Germany. *Energy*, 58:192–201, 2013.
- [536] L. Wald. Basics in Solar Radiation at Earth Surface. 2018.
- [537] Lucien Wald. Basics in solar radiation at earth surface. 2018.
- [538] Yi-Hui Wang, R. K. Walter, C. White, M. Kehrli, S. Hamilton, Patrick H Soper, and B. Ruttenberg. Spatial and Temporal Variation of Offshore Wind Power and its Value Along the Central California Coast. 2019.
- [539] J. Weber, Fabian Gotzens, and D. Witthaut. Impact of Strong Climate Change on the Statistics of Wind Power Generation in Europe. *Energy Procedia*, 153:22–28, 2018.
- [540] A. Weisheimer and T. Palmer. Changing Frequency of Occurrence of Extreme Seasonal Temperatures Under Global Warming. *Geophysical Research Letters*, 32, 2005.
- [541] S. Weitemeyer, D. Kleinhans, T. Vogt, and C. Agert. Energy System Modelling – Interactions And Synergies in a Highly Renewable Pan-European Power System. 2014.
- [542] J. Weniger, T. Tjaden, and V. Quaschnig. Sizing of Residential PV Battery Systems. *Energy Procedia*, 46:78–87, 2014.
- [543] L. Wenz, A. Levermann, and M. Auffhammer. North–South Polarization of European Electricity Consumption Under Future Warming. *Proceedings of the National Academy of Sciences*, 114:E7910 – E7918, 2017.
- [544] K. V. Weverberg, C. Morcrette, Hsi-Yen Ma, S. Klein, and J. Petch. Using Regime Analysis To Identify the Contribution of Clouds to Surface Temperature Errors in Weather and Climate Models. *Quarterly Journal of the Royal Meteorological Society*, 141:3190–3206, 2015.
- [545] Joakim Widén, Nicole Carpmann, V. Castellucci, David Lingfors, Jon Olauson, Flore Remouit, M. Bergkvist, Mårten Grabbe, and R. Waters. Variability Assessment and Forecasting of Renewables: A Review For Solar, Wind, Wave and Tidal Resources. *Renewable & Sustainable Energy Reviews*, 44:356–375, 2015.
- [546] B. Wielicki, Takmeng Wong, R. Allan, A. Slingo, J. Kiehl, B. Soden, C. Gordon, A. Miller, Shi-Keng Yang, D. Randall, F. Robertson, J. Susskind, and H. Jacobowitz. Evidence For Large Decadal Variability in the Tropical Mean Radiative Energy Budget. *Science*, 295:841 – 844, 2002.
- [547] T. Wilbanks, V. Bhatt, D. Bilello, S. Bull, J. Ekmann, W. Horak, Y. Huang, M. Levine, M. Sale, D. Schmalzer, and M. Scott. Effects of Climate Change on Energy Production and Use in the United States. 2008.
- [548] M. Wild. Global Dimming and Brightening: A Review. *Journal of Geophysical Research*, 114, 2009.
- [549] M. Wild. Enlightening Global Dimming and Brightening. *Bulletin of the American Meteorological Society*, 93:27–37, 2012.

- [550] M. Wild, D. Folini, and Florian Henschel. Impact of Climate Change on Future Concentrated Solar Power (CSP) Production. 2017.
- [551] M. Wild, D. Folini, Florian Henschel, Natalie Fischer, and Björn Müller. Projections of Long-Term Changes in Solar Radiation Based on CMIP5 Climate Models and their Influence on Energy Yields of Photovoltaic Systems. *Solar Energy*, 116:12–24, 2015.
- [552] M. Wild, D. Folini, C. Schär, N. Loeb, E. Dutton, and G. Koenig-Langlo. A New Diagram of the Global Energy Balance. 2013.
- [553] M. Wild, H. Gilgen, A. Roesch, A. Ohmura, C. Long, E. Dutton, B. Forgan, A. Kallis, V. Russak, and A. Tsvetkov. From Dimming to Brightening: Decadal Changes in Solar Radiation at Earth’s Surface. *Science*, 308:847 – 850, 2005.
- [554] M. Wild and B. Liepert. Editorial: The Earth Radiation Balance As Driver of the Global Hydrological Cycle. *Environmental Research Letters*, 2010.
- [555] M. Wild and Edgar Schmucki. Assessment of Global Dimming and Brightening in IPCC-AR4/CMIP3 Models and ERA40. *Climate Dynamics*, 37:1671–1688, 2011.
- [556] Martin Wild. Short-Wave and Long-Wave Surface Radiation Budgets in GCMs : A Review Based on the IPCC-AR4/CMIP3 Models. *Tellus A*, 60:932–945, 2008.
- [557] J. Wohland, Mark Reyers, Juliane Weber, and D. Witthaut. More Homogeneous Wind Conditions Under Strong Climate Change Decrease the Potential for Inter-State Balancing of Electricity in Europe. *Earth System Dynamics Discussions*, 8:1047–1060, 2017.
- [558] F. Woldemeskel, Ashish Sharma, B. Sivakumar, and R. Mehrotra. Quantification of Precipitation and Temperature Uncertainties Simulated by CMIP3 and CMIP5 Models. *Journal of Geophysical Research*, 121:3–17, 2016.
- [559] Xinhai Xu, K. Vignarooban, B. Xu, Keng Hsu, and A. M. Kannan. Prospects and Problems of Concentrating Solar Power Technologies for Power Generation in the Desert Regions. *Renewable & Sustainable Energy Reviews*, 53:1106–1131, 2016.
- [560] Lejiang Yu, S. Zhong, X. Bian, and W. Heilman. Temporal and Spatial Variability of Wind Resources in the United States as Derived from the Climate Forecast System Reanalysis. *Journal of Climate*, 28:1166–1183, 2015.
- [561] T. Zachariadis and P. Hadjinicolaou. The Effect of Climate Change on Electricity Needs – A Case Study From Mediterranean Europe. *Energy*, 76:899–910, 2014.
- [562] Behnam Zakeri and S. Syri. Electrical Energy Storage Systems: A Comparative Life Cycle Cost Analysis. *Renewable & Sustainable Energy Reviews*, 42:569–596, 2015.
- [563] C. Zamuda, B. Mignone, D. Bilello, K. Hallett, C. Lee, J. Macknick, R. Newmark, and D. Steinberg. U. S. Energy Sector Vulnerabilities to Climate Change and Extreme Weather. 2013.
- [564] H. Zhao, Q. Wu, Shuju Hu, H. Xu, and C. Rasmussen. Review of Energy Storage System For Wind Power Integration Support. *Applied Energy*, 137:545–553, 2015.
- [565] A. Zhisheng, W. Guoxiong, L. Jianping, Sun Youbin, Liu Yimin, Z. Weijian, Cai Yan-jun, Duan Anmin, L. Li, Mao Jiangyu, Cheng Hai, Shi Zheng-guo, Tan Liangcheng, Y. Hong, Ao Hong, Chang Hong, and F. Juan. Global monsoon dynamics and climate change. *Annual Review of Earth and Planetary Sciences*, 43:29–77, 2015.
- [566] E. Zhou, W. Cole, and B. Frew. Valuing Variable Renewable Energy for Peak Demand Requirements. *Energy*, 165:499–511, 2018.
- [567] Adriana Zurita, Carlos Mata-Torres, J. Cardemil, and R. Escobar. Evaluating Different Operation Modes of a Hybrid CSP+PV+TES+BESS Plant Varying the Dispatch Priority. 2019.

Titre: Scénarios d'Intégration de l'Énergie Solaire à Grande Échelle avec l'Éolien au Maroc: Impact de Stockage, Coût, Complémentarité Spatio-Temporelle et Changement Climatique.

Mots clés: Énergies Renouvelables, Stockage, Coût, Complémentarité Spatio-Temporelle, Changement Climatique, Scénarios de Mix.

Résumé: Il semble qu'à l'heure actuelle, de nombreux pays ont tendance à privilégier le solaire thermodynamique (CSP) combiné avec son système de stockage thermique (TES)—peu onéreux—par rapport au Photovoltaïque (PV) car il peut améliorer la résilience de leur système énergétique. Cependant, leur interaction dans un mix optimal n'a pas fait l'objet de recherches détaillées et particulièrement pour confirmer cette perception dans un climat futur. Par exemple, si le critère de comparaison n'est que l'argent, PV occupe-t-il une position de leader? Mais il n'est pas juste de justifier ces deux technologies simplement par le coût mais aussi par la corrélation de la production avec la pointe de consommation. Cela suscite une autre question: PV ou son homologue CSP? étant donné qu'elles ont une sensibilité distincte à la température et aux nuages. De plus, si le système de stockage par batterie (BES)—à coût prohibitif—est couplée à une installation PV à grande échelle, cela signifie que CSP-TES sera remplacé par le PV-BES? Cette thèse discute un ensemble de scénarios d'intégration solaire à grande échelle avec l'éolien dans un mix prospectif marocain sous différents niveaux de pénétration, configurations de stockage et combinaisons de technologies renouvelables (REs). Notre objectif est non seulement de maximiser la production RE, mais aussi de réduire sa variabilité. Cette approche de Moyenne-Variance est implémentée dans le modèle E4CLIM, que nous avons adapté aux quatre zones électriques marocaines pour fitter le modèle de demande et corriger les biais dans les facteurs de charge (CF) calculés à partir des données climatiques; ignorant les contraintes du réseau et les échanges d'électricité avec les pays voisins. Nous avons ajouté une contrainte de coût total maximal; et proposons une méthode de calcul de coût de chaque technologie en tenant en compte leur dépendance aux heures de production, qui est conçue dans

le modèle de stockage développé et implémenté au BES et aux modules CSP-TES ajoutés. Nous présentons, pour chaque régime de pénétration, quelques ratios qui contribuent à déterminer dans quelle région une capacité donnée sera affectée; et proposons des diagnostics pour évaluer quelle technologie remplace le mieux la production conventionnelle à coût marginal élevé. La première étude répond aux questions liées à l'intégration de l'éolien/PV/CSP/CSP-TES tandis que la deuxième étude détermine les conditions dans lesquelles les avantages que peut apporter le CSP-TES dépassent ceux du PV-BES afin de faire partie du mix jusqu'à ce qu'une condition plus avantageuse empêche son intégration; en examinant comment l'intégration du CSP et du stockage influencerait les bénéfices des complémentarités spatio-temporelles dans le climat actuel. Nous concluons que contrairement à l'intégration de CSP/CSP-TES avec PV, l'ajout de BES au PV révèle une sensibilité plus élevée des mix aux technologies solaires non seulement à faibles pénétrations en raison de la variabilité réduite mais aussi à des pénétrations élevées en raison des différences dans la capacité de stockage et le coût. Enfin, la troisième étude évalue l'impact du changement climatique sur les ressources et leurs implications sur les CFs et la demande d'ici la fin du 21ème siècle par rapport au forçage historique observé. Nous constatons qu'il y a un impact dans les mix ayant une forte pénétration mais qui est insignifiant devant l'effet éventuel de réduction des coûts. Cependant, il est peu probable que le changement climatique ait un effet perceptible sur les mix optimaux avec une faible pénétration, mais le message clé est que le futur impact sur chaque technologie est incertain. Nous discutons les sources d'incertitude et les principales options pour avoir des mix REs résilients au climat.

Title: Scenarios of Large-Scale Solar Integration with Wind in Morocco: Impact of Storage, Cost, Spatio-Temporal Complementarity and Climate Change.

Keywords: Renewable Energies, Storage, Cost, Spatio-Temporal Complementarity, Climate Change, Scenario Mixes.

Abstract: It appears that at the moment, many countries tend to favor Concentrated Solar Power (CSP) combined with its low-cost Thermal Energy Storage (TES) system over Photovoltaic (PV) as it can enhance the resilience of their energy system. However, their interplay in optimal mixes has not yet been addressed deeply enough by any study and particularly to confirm this perception in future warming climate. For instance, if the judging criteria is only money, does PV stand at a leading position? but, it is not fairly to justify those two technologies merely by cost but also by the correlation of production with peak consumption. Here comes another question: PV or its counterpart CSP? as they have distinct sensitivity to temperature and clouds. Moreover, if PV is coupled with expensive Battery Energy Storage (BES), does this mean CSP-TES will be replaced by PV-BES? This thesis discusses a set of scenarios of large-scale solar integration with wind in optimal Moroccan prospective mix under different penetration levels, storage configurations and combinations of renewable (RE) technologies. We take as objective not only to maximize the RE production, but also to reduce its variability. This Mean-Variance approach is implemented in the E4CLIM model, which we have adapted to the four Moroccan electricity zones to fit the demand model and correct biases in the Capacity Factors (CFs) calculated using climate data; ignoring the grid constraints and exchanges of electricity with neighboring countries. We add a maximum-total cost constraint to the optimization problem; and propose a method to define the rental cost of each production technology taking their dependence on the hours of production into account, which is designed in the developed storage model implemented to BES and to the added CSP-TES mod-

ules. We present, for each penetration regime, some ratios that contribute to determine what region a given capacity will be assigned to; and propose some production-demand adequacy diagnostics to evaluate which technology displaces more expensive fossil fuel generators during peak, mid and base load hours; and which one increase or reduce the curtailment. The first study addresses the questions associated with wind/PV/CSP/CSP-TES integration while the second study determines the conditions under which CSP-TES can provide an advantage against PV-BES so as to be part of the mix until a more advantageous condition prevents its integration; by examining how the integration of CSP and storage would influence the benefits from time-space complementarity in the actual climate. We conclude that contrary to the integration of CSP/CSP-TES with PV, the addition of BES to PV reveals a higher sensitivity of the mixes to solar technologies not only at low penetrations due to the reduced variability but also at high penetrations due to the differences in the storage capacity and cost. Finally, the third study assesses the impact of climate change on the resources and their implications on CFs and demand by the end-21st century relative to the historical observed forcing. We find that there are some indications of a potential impact in mixes with high penetrations but which are trivial with the eventual cost reduction effect on capacity pathways projected by climate models. However, climate change is unlikely to have a discernible effect on optimal mixes with low proportions of REs, but the key message is that the future impact on each technology is considered to be highly uncertain. We discuss the sources of uncertainty and the main options for climate-resilient RE mixes.